Journal of the Brazilian Chemical Society

# JBCS

The ***Journal of the Brazilian Chemical Society*** is published twelve issues per year by the *Sociedade Brasileira de Química* (*Brazilian Chemical Society*).
***SBQ Periodicals Coordinator:*** Cesar Zucco

***Editorial and Publishing Office:***
Instituto de Química, Unicamp, CP 6154, 13083-970 Campinas - SP, Brazil
Tel/Fax: +55 19 3521-3151; E-mail: office@jbcs.sbq.org.br

***Subscriptions and Advertising Office:***
Sociedade Brasileira de Química, CP 26037, 05513-970 São Paulo - SP, Brazil
Tel: +55 11 3032-2299; Fax: +55 11 3814-3602; E-mail: sbqsp@iq.usp.br

The ***Journal of the Brazilian Chemical Society*** serves its readers as a forum for information related to the advancement of Chemistry. The *Journal* is devoted to the publication of research papers in all fields of Chemistry, except education, philosophy and history of Chemistry

***Information for authors***: Full details of how to submit material for publication in the ***Journal of the Brazilian Chemical Society*** are given in the link **Instructions for Authors** http://jbcs.sbq.org.br/jbcs/authorinfo.html

***Galley proofs*** are sent by the Editorial Office to the author who submitted the manuscript. Proofs should be checked and returned as soon as possible (preferably within 48 hours)

***Subscription Rates - 2012***. Members of the Sociedade Brasileira de Química: R$80,00 (Brazil) and US$80 (other countries). Non-members: R$200,00 (Brazil), US$80 (Latin America) and US$148 (other countries). Institutions: R$200,00 (Brazil) and US$220 (other countries). See also World Wide Web http://www.sbq.org.br/portal2/formularios/JBCSBR.doc

***Back issues***. Back issues of all previously published volumes are available directly from the Subscriptions Office



*The Item-Fee Code for this publication is: 0103-5053 $6.00 + 0.00*

*Printed on acid-free paper*

***Indexed in the following databases:*** *Science Citation Index®, Science Citation Index expanded (SciSearch®), ISI Alerting Services, Chemical Abstracts-CA Plus, Chemistry Citation Index®, Current Contents®/Physical, Chemical and Earth Sciences, IndexCopernicus, Portal de Periódicos da Capes, SciELO and SCOPUS*

*Financial support:*

CNPq · CAPES · Ministério da Educação · Ministério da Ciência e Tecnologia · FAPESP (online version)

*Printed in Brazil*

***Desktop Publishing:*** *Hermano - Phone: +55 11 5571-8937*
***Printed by:*** *Print Master - Phone: +55 19 3223-1044*

JBCS

Journal of the Brazilian Chemical Society

ISSN 0103-5053

Vol. 23, No. 1, January, 2012

## Cover Picture

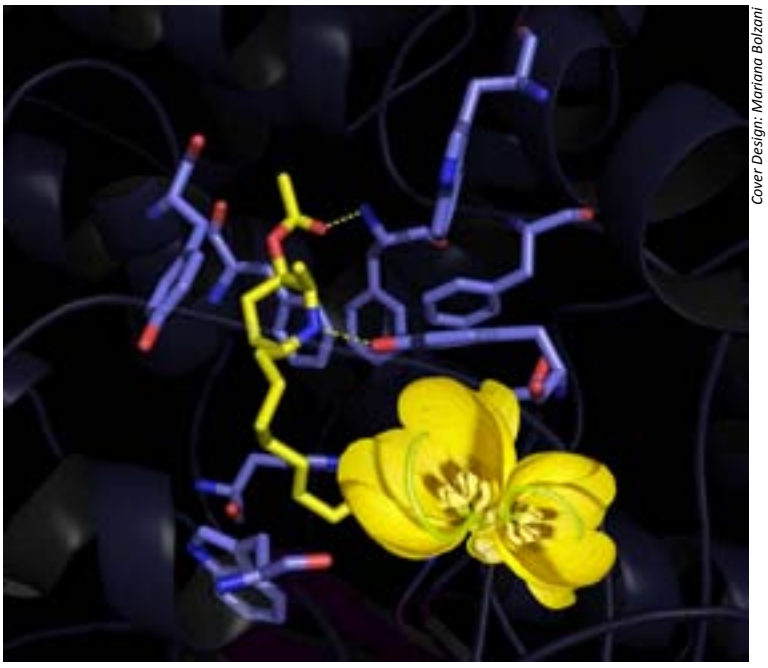

Cover Design: Mariana Bolzani

This cover figure was inspired in the rare alkaloids (-)-spectaline and (-)-cassine accumulated in the beautiful yellow flowers of *Senna spectabilis*. This creative art simulates the best docking pose obtained for (-)-*O*-acetyl-cassine in active site of acetylcholinesterase. Details are discussed in the Article **Molecular Docking and Molecular Dynamic Studies of Semi-Synthetic Piperidine Alkaloids as Acetylcholinesterase Inhibitors** by *Amanda Danuello, Nelilma C. Romeiro, Guilherme M. Giesel, Marcos Pivatto, Claudio Viegas Jr., Hugo Verli, Eliezer J. Barreiro, Carlos A. M. Fraga, Newton G. Castro and Vanderlan S. Bolzani* on page 163.

## Contents

### Editorial

1 **???????????**
*???????????/*

## Communications

5 **Asymmetric Organocatalytic Synthesis of β-Hydroxyynones with a Quaternary Carbon Center under Aqueous Conditions**
*Guowei Kang, Jun Jiang, Hongxin Liu and Huayue Wu*
SI online

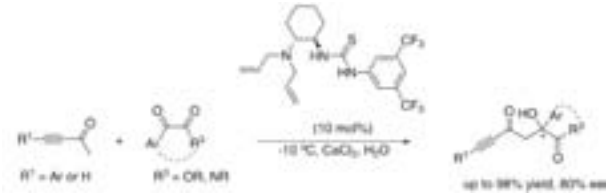

**Graphical Abstract**
The chiral thiourea catalyzed direct aldol reaction of unmodified methyl ynones under aqueous conditions is described. This procedure afforded β-hydroxyynones bearing a quaternary carbon center with moderate to good yields and enantioselectivities

11 **A Polyether Glycol Derived from Cashew Nutshell as a Kinetic Inhibitor for Methane Hydrate Formation**
*Jorge Cesar Ferreira, Adriana Teixeira and Pierre M. Esteves*
SI online

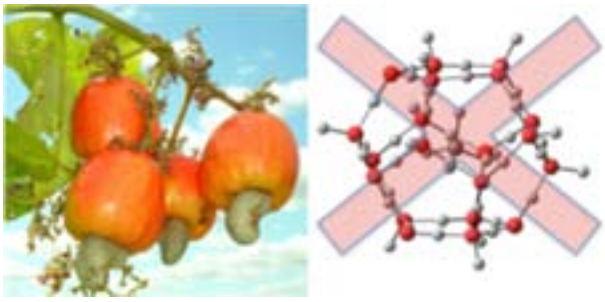

**Graphical Abstract**
A polyether glycol obtained from cardanol presented significant ability to the inhibition of methane hydrate

## Review

14 **Biomedical Applications of Nanobiosensors: the State-of-the-Art**
*Mahendra Rai, Aniket Gade, Swapnil Gaikwad, Priscyla D. Marcato and Nelson Durán*

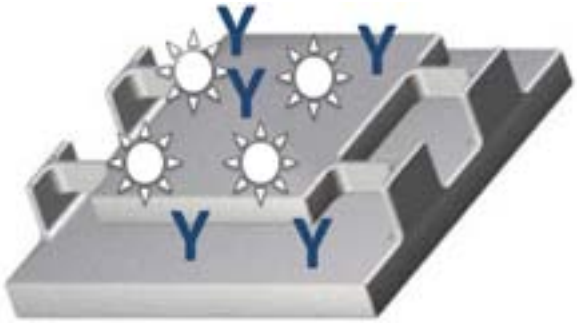

**Graphical Abstract**
Optical nanobiosensors with nanometric-sized dimensions opened new researches for intracellular monitoring leading to develop sensitive robust and reproducible nanobiosensors. The sensors are equipped with immobilized bio-receptor probes, *e.g.* antibodies, enzyme substrate etc and these probes will revolutionize the future of disease diagnosis

## Articles

25 **Synthesis, Characterization and Photophysical Properties of ESIPT Reactive Triazine Derivatives**
*Marcelo D. Kuplich, Fábio S. Grasel, Leandra F. Campo, Fabiano S. Rodembusch and Valter Stefani*
SI online

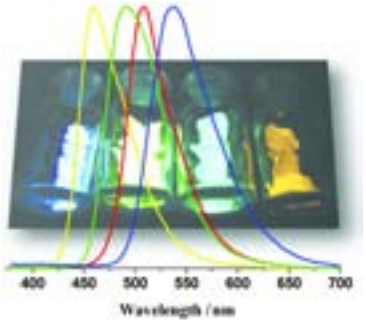


**Graphical Abstract**
We present four reactive ESIPT fluorescent 1,3,5-triazine derivatives from nucleophilic aromatic substitution of cyanuric chloride. The dyes are fluorescent by an intramolecular proton transfer mechanism in the blue-orange region with a large Stokes shift. The incorporation of the dyes into cellulose fibers could be done successfully

32 **Pt $L_{2,3}$ - Edge X-ray Absorption Spectroscopy Investigation of Zerovalent $[Pt(PPh_3)_2(\eta^2\text{-}L)]$ {L = $C_2H_4$, $C_{60}$ and $C_2(CN)_4$} Compounds**
*Gilson H. M. Dias, Nazareth F. da Fonseca and Marcelo H. Herbst*

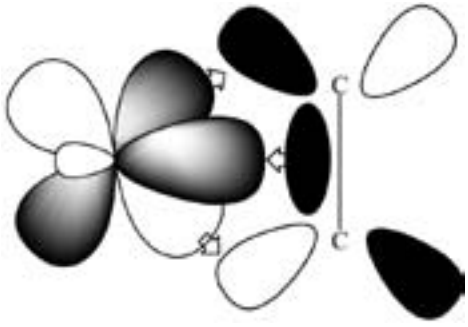

**Graphical Abstract**
The $d_\pi$-orbital energy of three $[Pt(PPh_3)_2(\eta^2\text{-}L)]$ compounds {L = $C_2H_4$, $C_{60}$ and $C_2(CN)_4$}, quantitatively determined by Pt $L_{2,3}$ X-ray absorption spectroscopy (XAS), follows the order $[Pt(PPh_3)_2(\eta^2\text{-}C_2H_4)]$ < $[Pt(PPh_3)_2(\eta^2\text{-}C_{60})]$ < $[Pt(PPh_3)_2\{\eta^2\text{-}C_2(CN)_4\}]$, in line with the π-acidity of the olefin ligands

**39** **Tributyltin in Crustacean Tissues: Analytical Performance and Validation of Method**
*Joyce Cristale, Dayana M. dos Santos, Bruno S. Sant'Anna, Daniela C. Sandron, Sara Cardoso, Alexander Turra and Mary Rosa R. de Marchi*

**Graphical Abstract**
Gas chromatography with pulsed flame photometric detector (GC-PFPD) has proved to be an advantageous technique for tributyltin (TBT) quantification in crustacean tissues when performed after extraction with an apolar solvent (toluene) followed by Grignard derivatization

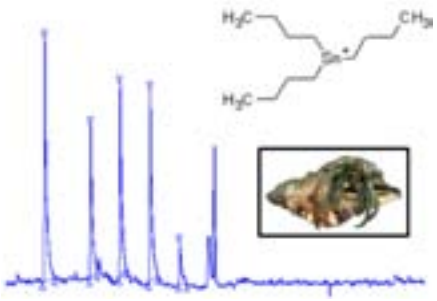

**46** **Layered Metal Laurates as Active Catalysts in the Methyl/Ethyl Esterification Reactions of Lauric Acid**
*Fábio da Silva Lisboa, José Eduardo F. da Costa Gardolinski, Claudiney S. Cordeiro and Fernando Wypych*
SI online

**Graphical Abstract**
The work describes the catalytic activity of layered laurates in the methyl (ethyl) esterification reactions of lauric acid, for which conversions between 75 and 90% were observed. The catalysts were reused in three consecutive reaction cycles and some of them preserved the structure and retained the catalytic activity close to those observed in the first cycle

**57** **Evaluation of Solid-Phase Microextraction using a Polythiophene Film and Liquid Chromatography with Spectrophotometric Detection for the Determination of Antidepressants in Plasma Samples**
*Juciene A. Caris, Andréa R. Chaves and Maria Eugênia C. Queiroz*

**Graphical Abstract**
Polythiophene films were electropolymerized on the surface of metal (stainless steel) wires for the development of solid-phase microextraction (SPME). These polymeric films were evaluated as SPME phases for the liquid chromatography (LC) analysis of antidepressants in plasma samples for toxicological analysis purpose

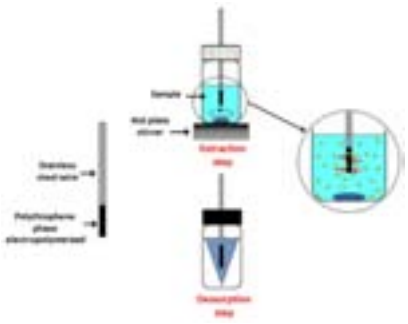

**65** **Electrospray Ionization Tandem Mass Spectrometry of the Two Main Antimalarial Drugs: Artemether and Lumefantrine**
*Vanessa G. dos Santos, Ricardo J. Alves, Marcos N. Eberlin, Gerson A. Pianetti and Isabela C. César*
SI online

**Graphical Abstract**
ESI(+)-MS/MS spectra of protonated lumefantrine (*m*/*z* 528), showing rich dissociation chemistry. Water loss is the most favored initial dissociation forming the major fragment ion of *m*/*z* 510. This elimination is likely favored due to the formation of a highly stable, fully delocalized, resonance stabilized benzyl-like cation, which may rearranges to a tropylium-like ion

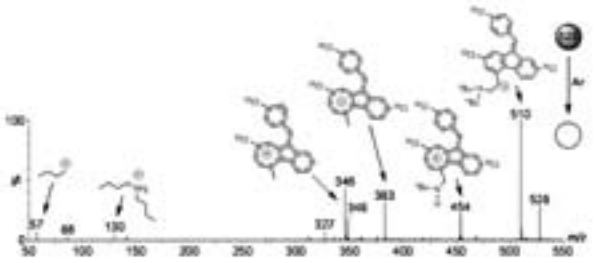

**72** **Migration of Phthalate-based Plasticizers from PVC and non-PVC Containers and Medical Devices**
*Marlei Veiga, Denise Bohrer, Paulo C. Nascimento, Adrian G. Ramirez, Leandro M. Carvalho and Regina Binotto*

**Graphical Abstract**
Migration of phthalate-based plasticizers from hemodialyzers

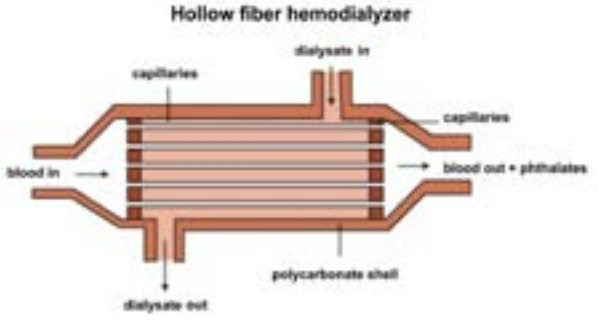

**78** ***In Situ* Solvent Formation Microextraction based on Ionic Liquids and 1-(2-Hydroxynaphtalene-1-yl)ethane Oxime for Determination of Zinc**
*Mehdi Hosseini, Nasser Dalali, Saeid Mohammad Nejad and Rostam Jamali*

**Graphical Abstract**
Schematic diagram for preconcentration and determination of zinc by *in situ* solvent formation microextraction based on use of ionic liquid (IL) ) as an extractant solvent, sodium hexafluorophosphate ($NaPF_6$) as an ion-pairing agent, 1-(2-hydroxynaphtalene-1-yl) ethane oxime as complexing agent and detection by flame atomic absorption spectrometry

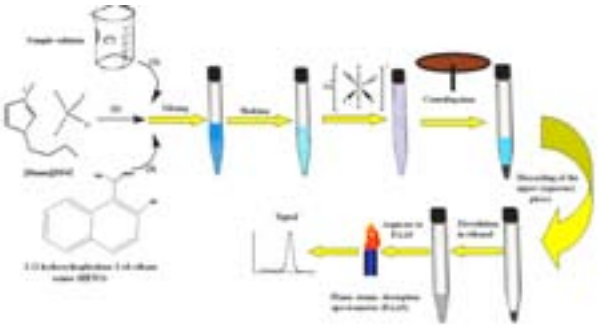

**85** **Advanced QSAR Studies on PPARδ Ligands Related to Metabolic Diseases**
*Vinícius G. Maltarollo, Danielle C. Silva and Káthia M. Honório*
SI online

**Graphical Abstract**
Docking, HQSAR, CoMFA and ESP maps for the most potent compound of the series

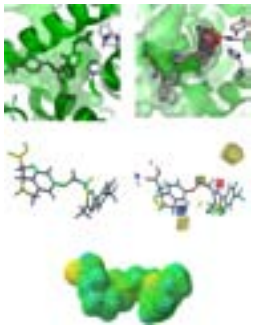

**96** **HPLC Determination of Histamine, Tyramine and Amino Acids in Shrimp By-Products**
*Carolina Bueno-Solano, Jaime López-Cervantes, Dalia I. Sánchez-Machado and Olga N. Campas-Baypoli*

**Graphical Abstract**
In seafood products is possible the conversion of free amino acid to biogenic amines by microbial decarboxylation, therefore, the proposed HPLC method here may be useful for evaluation of the sanitary quality of various shrimp by-products

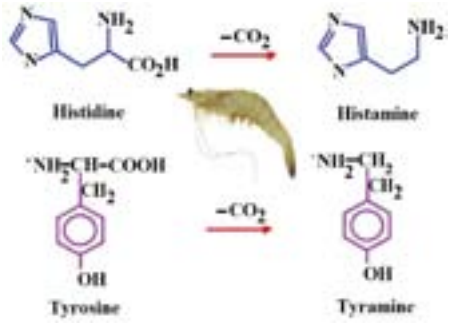


**103** **Simultaneous Extraction and Detection of Ochratoxin A and Citrinin in Rice**
*Helen C. S. Hackbart, Luciana Prietto, Ednei G. Primel, Jaqueline Garda-Buffon and Eliana Badiale-Furlong*

**Graphical Abstract**
This study compared four extraction procedures for the simultaneous determination of mycotoxins ochratoxin A and citrinin in samples of rice

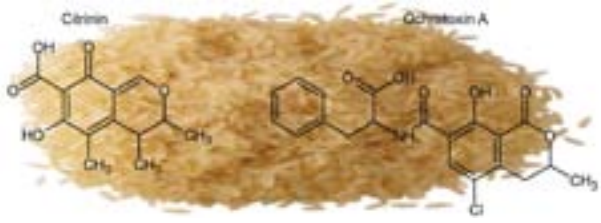


**110** **Direct Electrochemical Analysis of Dexamethasone Endocrine Disruptor in Raw Natural Waters**
*Thiago M. B. F. Oliveira, Francisco W. P. Ribeiro, Jefferson M. do Nascimento, Janete E. S. Soares, Valder N. Freire, Helena Becker, Pedro de Lima-Neto and Adriana N. Correia*

**Graphical Abstract**
Square-wave voltammograms and the corresponding analytical curve for various concentrations of DMZ in raw natural waters on the HMDE under optimum conditions

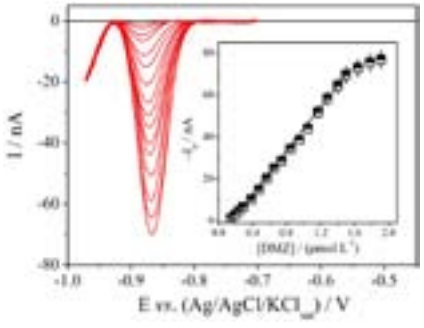

**120** **Morphology, Microstructure and Electrocatalytic Properties of Activated Copper Surfaces**
*Juan C. M. Gamboa, Denise F. S. Petri, Tânia M. Benedetti, Vinicius R. Gonçales and Mauro Bertotti*

**Graphical Abstract**
The electrochemical reduction of nitrate and nitrite is facilitated at copper cathodes after activation of the surface in acidic medium. To understand in more details the morphologic change of the surface during the activation process and its correlation with electrochemical properties, images of the copper surface were obtained by scanning electron microscopy (SEM) and atomic force microscopy (AFM)

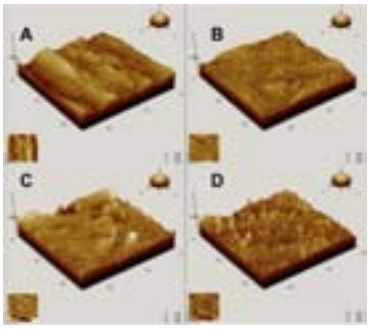


**124** **Total Synthesis and Allelopathic Activity of Cytosporones A-C**
*Charles E. M. Zamberlam, Alisson Meza, Carla Braga Leite, Maria Rita Marques, Dênis P. de Lima and Adilson Beatriz*

*SI online*

**Graphical Abstract**
The preparation of cytosporones A-C from the same starting material through a short synthetic route, with good yields, is reported. All compounds were tested for allelopathic activity on lettuce seeds. Cytosporone A and its methylated precursor showed remarkable allelopathic activity, inhibiting seed germination and seedling growth

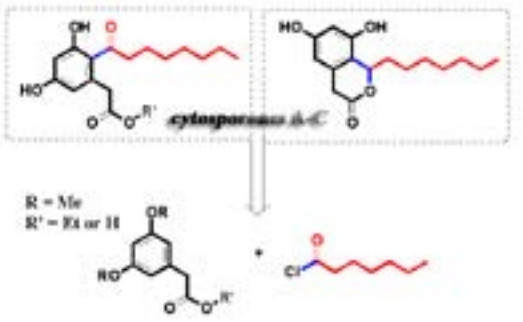


**132** **Determination of Polychlorinated Biphenyls in Seawater using Headspace Solid-Phase Microextraction Coupled with Gas Chromatography-Mass Spectrometry with the Aid of Experimental Design**
*Xingliang Song, Jinhua Li, Lingxin Chen, Zongwei Cai, Chunyang Liao, Hailong Peng and Hua Xiong*

**Graphical Abstract**
Polychlorinated biphenyls were highly sensitively determined in seawater containing large amounts of humic substances by combining $KMnO_4$ treatment and headspace solid-phase microextraction coupled with gas chromatography-mass spectrometry with the aid of experimental design

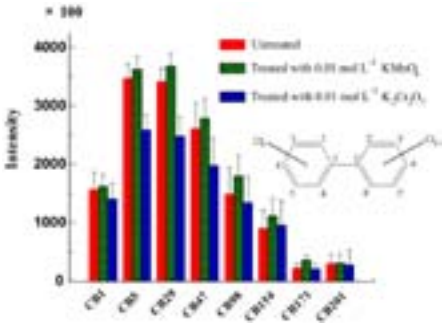


**142** **A Method for Determination of Ammonia in Air using Oxalic Acid-Impregnated Cellulose Filters and Fluorimetric Detection**
*Erika P. Felix and Arnaldo A. Cardoso*

**Graphical Abstract**
An easy method of application was developed for the determination of ammonia in ambient air. The samples are collected using cellulose filters impregnated with oxalic acid, followed of fluorimetric detection. The method is reliable for measuring low concentrations of ammonia and where there are rapid fluctuations in their concentrations

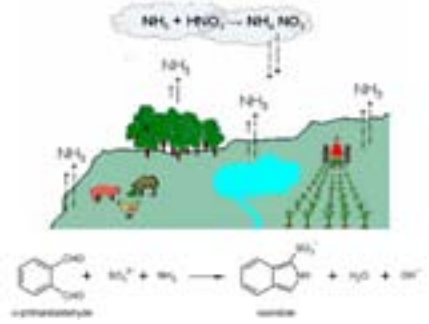

**148** **Ultra-Performance Liquid Chromatographic Method for Measurement of Voriconazole in Human Plasma and Oral Fluid**
*Paula Boeira, Marina V. Antunes, Huander F. Andreolla, Alessandro C. Pasqualotto and Rafael Linden*

**Graphical Abstract**
A new and extensively validated ultra-performance liquid chromatographic method for voriconazole measurement in plasma and oral fluid is presented. Run time was 4 min, with mobile phase comsuption of 2.2 mL *per* analysis. Panel **A** shows a chromatogram of a plasma sample and panel **B** shows the chromatogram of an oral fluid sample, both from the same patient

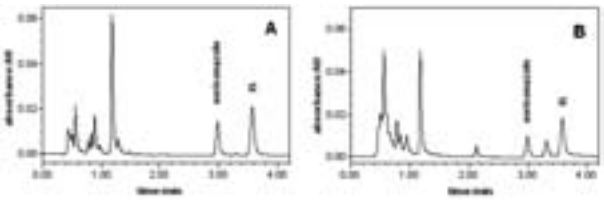

**156** **Cooking Effects on Iron and Proteins Content of Beans (*Phaseolus Vulgaris* L.) by GF AAS and MALDI-TOF MS**
*Juliana Naozuka and Pedro V. Oliveira*


**Graphical Abstract**
The domestic cooking effect of beans in the Fe, proteins and organic compounds distribution was evaluated by GF AAS, Bradford method and MALDI-TOF MS

**163** **Molecular Docking and Molecular Dynamic Studies of Semi-Synthetic Piperidine Alkaloids as Acetylcholinesterase Inhibitors**
SI online
*Amanda Danuello, Nelilma C. Romeiro, Guilherme M. Giesel, Marcos Pivatto, Claudio Viegas Jr., Hugo Verli, Eliezer J. Barreiro, Carlos A. M. Fraga, Newton G. Castro and Vanderlan S. Bolzani*

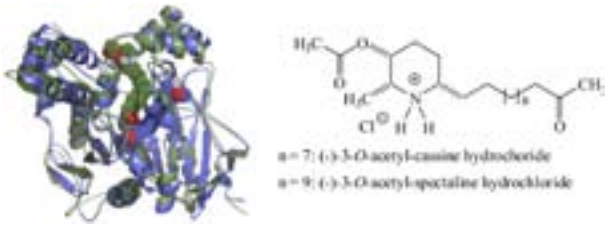

**Graphical Abstract**
Molecular modeling studies were carried out aiming to elucidate the molecular basis of the differential acetylcholinesterase inhibition profiles of the semi-synthetic derivatives (-)-3-*O*-acetyl-cassine hydrochloride (**9**) and (-)-3-*O*-acetyl-spectaline hydrochloride (**10**)

## Short Reports

**171** **Metal Chloride Hydrates as Lewis Acid Catalysts in Multicomponent Synthesis of 2,4,5-Triarylimidazoles or 2,4,5-Triaryloxazoles**
SI online
*Marcelo V. Marques, Marcelo M. Ruthner, Luiz A. M. Fontoura and Dennis Russowsky*


**Graphical Abstract**
A series of metal halide hydrates was proved to be efficient Lewis acid catalysts promoting the multicomponent Radziszewski reaction for the triarylimidazole synthesis in alcoholic media. In absence of aldehyde, triaryloxazoles were obtained in good yields

**180** **Effects of the Essential Oil from Fruits of *Schinus terebinthifolius* Raddi (Anacardiaceae) on Reproductive Functions in Male Rats**
*Cristiano R. G. Affonso, Rozeverter M. Fernandes, Jamylla M. G. de Oliveira, Maria do Carmo de Carvalho e Martins, Sidney G. de Lima, Gustavo R. de Sousa Júnior, Maria Zenaide de Lima C. Moreno Fernandes and Surama F. Zanini*

**Graphical Abstract**
Essential oils extracted from fruits of *Schinus terebinthifolius* Raddi were analyzed by GC and GC-MS, and evaluated for their reproductive toxicity on male rats. The results showed there are no toxic effects on male reproduction after treatment with essential oil at the tested doses

**186** **Biomimetic Hydrogen Generation Catalyzed by Triironnonacarbonyl Disulfide Cluster**
*Charles A. Mebi, Kyra E. Brigance and Robert B. Bowman*

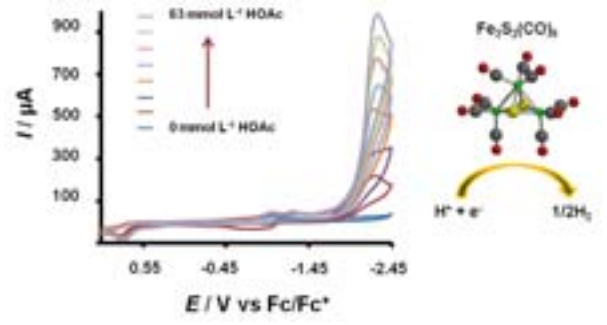


**Graphical Abstract**
$Fe_3S_2(CO)_9$ catalyzes the electrochemical reduction of acetic acid to produce $H_2$; it mimics the [Fe-Fe] hydrogenase enzyme

*J. Braz. Chem. Soc.*, Vol. 23, No. 1, 5-10, 2012.
Printed in Brazil - ©2012 Sociedade Brasileira de Química
0103 - 5053 $6.00+0.00

# Communication

## Asymmetric Organocatalytic Synthesis of β-Hydroxyynones with a Quaternary Carbon Center under Aqueous Conditions

***Guowei Kang, Jun Jiang,* Hongxin Liu and Huayue Wu****

*College of Chemistry and Materials Engineering, Wenzhou University, Chashan University Town, Wenzhou, Zhejiang Province 325035, People's Republic of China*

A reação aldólica direta de metil inonas não-modificadas sob condições aquosas catalisada pela amina terciária quiral de tiouréia é descrita. Este procedimento evitou a reação retroaldólica dos produtos β-hidroxinonas, e admite as isatinas (1H-indol-2,3-diona) e os menos ativos ésteres α-ceto acíclicos como aceptores, oferecendo um arranjo estruturalmente diverso de β-hidroxinonas tendo um centro de carbono quaternário, com rendimentos de moderado a bom e enancioseletividade.

The chiral tertiary amine thiourea catalyzed direct aldol reaction of unmodified methyl ynones under aqueous conditions is described. This procedure avoided the retro-aldol reaction of the β-hydroxyynone products, and tolerated both the isatin (1H-indole-2,3-dione) and the less active acyclic α-keto esters as acceptors, affording a structurally diverse array of β-hydroxyynones bearing a quaternary carbon center with moderate to good yields and enantioselectivities.

**Keywords:** β-hydroxyynones, chiral thiourea, aldol reaction, aqueous condition

## Introduction

Enantioriched β-hydroxyynones are highly functionalized building blocks for the synthesis of biologically active compounds and natural products, such as fostriecin[1] and maitotoxin.[2] Although the aldol reaction is the most efficient way to construct β-hydroxy carbonyl structures, the β-hydroxyynone products are usually synthesized via the addition of alkynyllithium or alkynylmagnesium halide to the corresponding β-hydroxylated Weinreb amides.[3-12] This is due to the fact that ynones are good Michael acceptors and the ynone-derived β-hydroxy ketones tend to undergo retro-aldol reactions.[13,14] Thus, direct catalytic asymmetric aldol reactions involving ynones are highly desirable. In 2004, Trost *et al.*[13] reported the first enantioselective aldol additions of methyl ynones to α-ketal aldehydes using a chiral dinuclear zinc catalyst. Subsequently, Silva *et al.*[14] found that proline derived sulfonamide could efficiently catalyze the aldol reaction of the methoxymethyl ether (MOM)-protected ynones and aldehyde with good yields and enantioselectivities.[14] However, the unmodified simple methyl ynones are not good substrates under proline-sulfonamide catalysis conditions with low yields because of several side products.[14] More importantly, no example of the asymmetric catalytic synthesis of β-hydroxyynones resulting in a quaternary carbon center has been reported. Since List *et al.*[15] reported the proline catalyzed cross-aldol reaction between ketones and aldehydes,[15] many amine derivatives such as proline-amide type catalysts[16-18] have been developed for such transformations,[19-22] being most of which based on the enamine-activiation mechanism.[19-22] However, in comparison with simple ketones, the formation of enamine intermediates with primary or secondary amine catalysts and inactive unmodified ynones remains a great challenge. Based on the fact that DABCO can efficiently catalyze the direct aldol reaction between simple methyl ynone and isatin (1H-indole-2,3-dione) in our pilot experiment, it was envisioned the developing of the chiral tertiary amine catalysts in order to realize this asymmetric transformation. During the preparation of this study, Guo *et al.*[23] and Allu *et al.*[24] reported chiral tertiary amine thiourea and urea catalyzed enantioselective aldol reactions of ketones with excellent results. Herein, we report our preliminary results with chiral tertiary amine thiourea[25] catalyzed direct aldol reactions of methyl ynones, affording β-hydroxyynones with a quaternary carbon center under aqueous conditions[26] with moderate to good yields and enantioselectivites (Figure 1).

*e-mail: junjiang@wzu.edu.cn; huayuewu@wzu.edu.cn

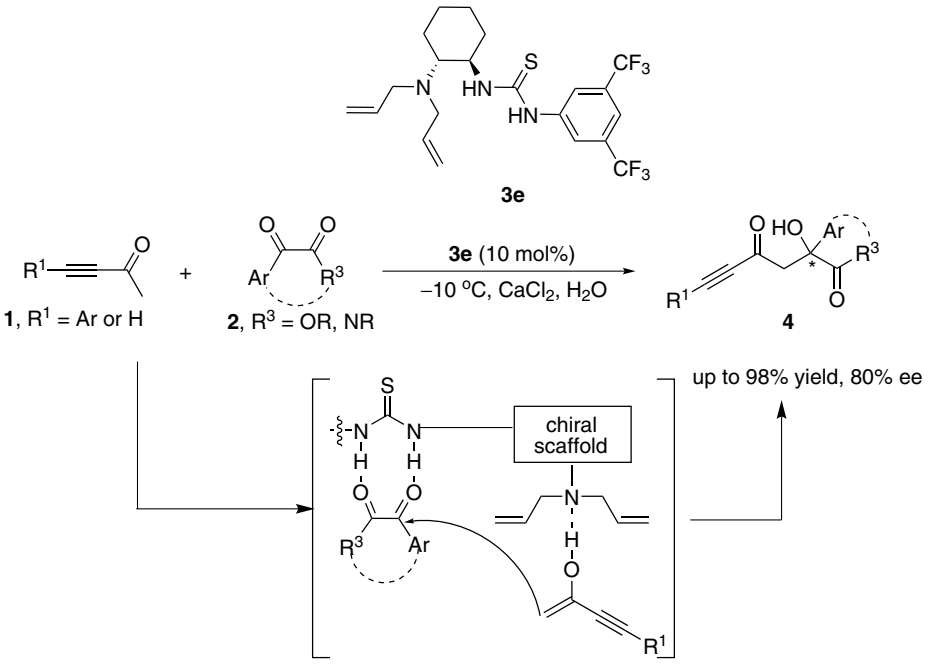


**Figure 1**. Thiourea catalyzed direct aldol reaction of methyl ynone and active ketones.

## Results and Discussion

The organocatalyzed asymmetric aldol reactions between simple ketones or aldehydes and isatins have been intensely studied,[27-37] as these chiral 3-alkyl-3-hydroxyindolin-2-one products are important building blocks in both natural products and medicinal compound syntheses.[38,39] However, the asymmetric aldol reactions between ynones and isatins remain a synthetic challenge since the products tend to undergo retro-aldol reaction in organic solvents. For example, 42% of product **4a** converted to starting materials after stirring with 20 mol% DABCO in $CH_2Cl_2$ for 24 h, and a similar result was obtained when $CHCl_3$ was used as solvent. Moreover, ynones have the ability to act as both electrophile and nucleophile under certain conditions, such as base catalysis. Initially, our investigation began with the reaction of ynone **1a** with *N*-butyl substituted isatin **2a** by using 20 mol% of DABCO as the catalyst. To our delight, the reaction catalyzed by DABCO gave the desired product with 80% yield in 3 days at room temperature in $CHCl_3$. Several solvents were then tested (Table 1, entries 1-6), and water was found to dramatically enhance the reaction rate with 88% yield in 1 h (Table 1, entry 6). Because this β-hydroxyynone product was stable in water, it was supposed that using water as the solvent may not only increase the reaction concentration but also avoid the retro-aldol reaction.

In the sequence, it was examined the asymmetric catalytic ability of chiral thiourea catalysts (Figure 2) at 0 °C with 5 equivalents of ynone **1a**, using brine as solvent instead of water to avoid freezing (Table 1, entries 7-13). The reactions catalyzed by quinine and cinchonidine proceeded smoothly but with very low enantioselectivities (ee) (Table 1, entries 7-8). Better results were obtained when tertiary amine thioureas were used as catalysts (Table 1, entries 9-13). The screening studies revealed that catalyst **3e** was the best choice in terms of enantioselectivity, which gave the desired product with 82% yield and 71% ee after 10 h. The variation of the group bonded to nitrogen of the isatin heterocycle did not increase the enantioselectivity (Table 1, entries 13-17). For example, *N*-hexyl isatin or *N*-phenyl isatin led to slightly lower enantioselectivities (Table 1, entries 16-17), while the use of *N*-methyl isatin afforded the corresponding product **4ab** in relatively low ee (Table 1, entry 14), and *N*-Boc isatin was found inactive when used in this reaction under aqueous condition. Next, several solvents were screened at 0 °C with 5 equivalents of ynone **1a** to improve the enantioselectivity (Table 2). The reactions in these screened organic solvents either led to long reaction time and low yield or decreased the enantiocontrol (Table 2, entries1-5). Further experiments investigated the influence of additives. It was shown that salts affect the enantioselectivity. The best result was obtained when $CaCl_2$ was used as the additive, gaving the desired product with 93% yield and 73% ee at 0 °C. Finally, the enantioselectivity was improved to 80% ee by cooling the reaction to −10 °C. Further cooling (−20 °C) was tried, but did not improve the enantioselectivity. The reaction was then performed on a 1 mmol scale of **2a** and 5 mmol of **1a** in 5mL of solvent under the optimal conditions (Table 2, entry 13).

**Table 1**. Catalyst screening on the direct aldol reaction between ynone and isatin[a]

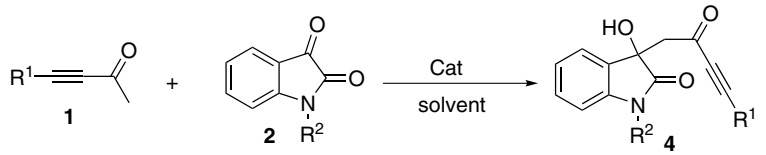


**1a**: $R^1$ = Ph
**1b**: $R^1$ = 4-Me-$C_6H_4$
**1c**: $R^1$ = H

**2a**: $R^2$ = n-Butyl
**2ab**: $R^2$ = Me
**2ac**: $R^2$ = Allyl
**2ad**: $R^2$ = n-$C_6H_{13}$
**2ae**: $R^2$ = Ph

**4a**: $R^1$ = Ph, $R^2$ = n-Butyl
**4ab**: $R^1$ = Ph, $R^2$ = Me
**4ac**: $R^1$ = Ph, $R^2$ = Allyl
**4ad**: $R^1$ = Ph, $R^2$ = n-$C_6H_{13}$
**2ae**: $R^1$ = Ph, $R^2$ = Ph

| entry | Catalyst | 2 | Solvent | 4 | Yield / %[d] | ee / %[e] |
|---|---|---|---|---|---|---|
| 1[b] | DABCO | **2a** | dioxane | **4a** | 24 | – |
| 2[b] | DABCO | **2a** | $CH_2Cl_2$ | **4a** | 18 | – |
| 3[b] | DABCO | **2a** | $CHCl_3$ | **4a** | 10 | – |
| 4[b] | DABCO | **2a** | THF | **4a** | 19 | – |
| 5[b] | DABCO | **2a** | toluene | **4a** | 21 | – |
| 6[b] | DABCO | **2a** | $H_2O$ | **4a** | 88 | – |
| 7[c] | quinine | **2a** | brine | **4a** | 91 | 6 |
| 8[c] | cinchonidine | **2a** | brine | **4a** | 87 | 12 |
| 9 | **3a** | **2a** | brine | **4a** | 89 | 38 |
| 10 | **3b** | **2a** | brine | **4a** | 92 | 56 |
| 11 | **3c** | **2a** | brine | **4a** | 95 | 50 |
| 12 | **3d** | **2a** | brine | **4a** | 96 | 45 |
| 13 | **3e** | **2a** | brine | **4a** | 82 | 71 |
| 14 | **3e** | **2ab** | brine | **4ab** | 98 | 56 |
| 15 | **3e** | **2ac** | brine | **4ac** | 95 | 65 |
| 16 | **3e** | **2ad** | brine | **4ad** | 91 | 69 |
| 17 | **3e** | **2ae** | brine | **4ae** | 97 | 68 |

[a]Unless otherwise noted, reactions were carried out with 0.5 mmol **1a**, 0.1 mmol of **2** and 10 mol% of catalyst in 0.5 mL solvent at 0 °C for 10 h; [b]reactions were carried out with 0.2 mmol **1a**, 0.1 mmol of **2** at room temperature for 1 h; [c]reactions were carried out for 3 h; [d]isolated yield; [e]ee: enantioselectivity determined by chiral HPLC.

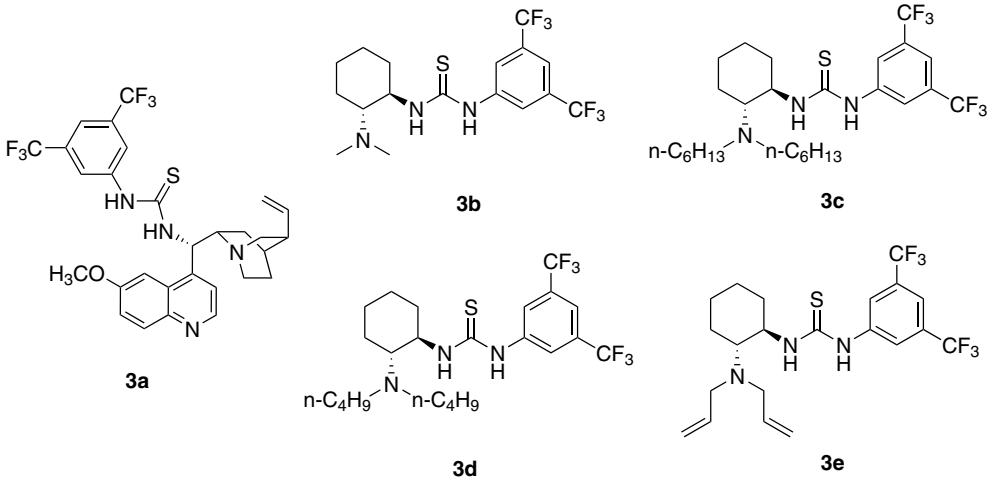


**Figure 2**. Chemical structure of screened catalysts.

However, decreased enantioselectivity was observed (85% yield, 53% ee).

With the optimal reaction conditions in hand, it was then examined the scope of the direct aldol reactions between ynones and active ketones. The reactions were generally conducted in saturated $CaCl_2$ solution at −10 to 20 °C for 9-72 h. The results are summarized in Table 3. All of the isatins showed high reactivities and

**Table 2.** Effects of reaction condition on the direct aldol reaction between ynone and isatin[a]

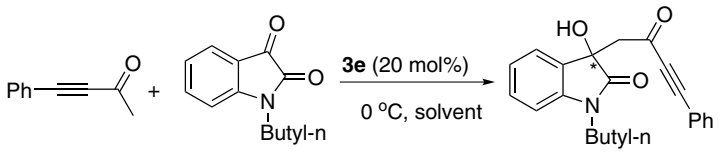


**1a** **2a** **4a**

| entry | Solvent | time / h | Temperature / °C | Yield / %[b] | ee / %[c] |
|---|---|---|---|---|---|
| 1 | $CHCl_3$ | 48 | 0 | 77 | 59 |
| 2 | Toluene | 48 | 0 | 90 | 57 |
| 3 | THF | 48 | 0 | 25 | 66 |
| 4 | $CH_3CN$ | 48 | 0 | 66 | 64 |
| 5 | MeOH | 48 | 0 | 80 | 24 |
| 6 | AcONa/$H_2O$ | 9 | 0 | 96 | 68 |
| 7 | KF/$H_2O$ | 9 | 0 | 62 | 58 |
| 8 | $NH_4Cl$/$H_2O$ | 9 | 0 | 97 | 65 |
| 9 | LiF/$H_2O$ | 9 | 0 | 97 | 66 |
| 10 | KBr/$H_2O$ | 9 | 0 | 97 | 67 |
| 11 | $CaCl_2$/$H_2O$ | 9 | 0 | 93 | 73 |
| 12 | $CaCl_2$/$H_2O$ | 14 | −10 | 95 | 80 |
| 13[d] | $CaCl_2$/$H_2O$ | 12 | −10 | 85 | 53 |

[a]Unless otherwise noted, reactions were carried out with 0.5 mmol of **la**, 0.1 mmol of **2a** and 10 mol% of catalyst **3e** in 0.5 mL solvent; [b]isolated yield; [c]ee: enantioselectivity determined by chiral HPLC; [d]reaction was performed on a 1 mmol scale of **2a** and 5 mmol of **1a** in 5 mL solvent.

afforded the β-hydroxyynones containing a quaternary carbon center with excellent yields and moderate to good ees. The position of the substituent on the isatin had an obvious influence on the enantioselectivity. For example, 4-substituted isatins afforded products with low ees (Table 3, entries 2-3, 46-54% ee), while substituents at other positions on the isatin heterocycle led to higher enantioselectivities (Table 3, entries 4-11, 57-78% ee). The electronic nature of the substituents also plays an important role on the enantiocontrol. Isatins with an electron-donating group on the aromatic ring gave similar results to **2a** (Table 3, entries 1, 4 and 9), whilst the presence of an electron-withdrawing group resulted in reduced enantioselectivity (such as Table 3, entry 8). Next, other ynones were also tested. Because both of the reactants are solid, the reaction involving **1b** was carried out in $CH_3CN$ instead of $CaCl_2$ solution, and led to the product **4ba** with 53% yield and 78% ee (Table 3, entry 12). When but-3-yn-2-one **1c** was used as the donor in this reaction, the racemic product was obtained (Table 3, entry 13). Notably, besides isatins, less active acyclic α-keto esters **2l-2o** can also be applied in this reaction, but only under aqueous conditions. The reaction of α-keto esters with ynone **1a** led to the desired products with moderate yields and enantioselectivities (Table 3, entries 14-17, 34-44% yield, 47-63% ee). The ester group will affect the yield and ee as the result of steric hindrance. For example, more sterically congested **2m** and **2n** afforded the β-hydroxyynones with relatively low yields and moderate ees (Table 3, entries 15-16).

## Conclusion

In conclusion, we have developed the chiral tertiary amine thiourea catalyzed direct aldol reactions of unactivated methyl ynones, efficiently resulting in β-hydroxyynones containing a quaternary carbon center as the only product with moderate to good yields and enantioselectivities (34-98% yield, 46-80% ee). Importantly, aqueous conditions were found to not only dramatically enhancing the reaction rate, but also increase the enantioselectivity. Notably, besides isatins, less active acyclic α-keto esters can also be used as substrates in this reaction under standard conditions, albeit in lower yields.

## Experimental

Nuclear magnetic resonance (NMR) spectra were recorded on a Bruker-500 MHz spectrometer. High-resolution mass spectrometry (HRMS, Micromass GCT-MS) spectra were recorded on a P-SIMS-Gly from

**Table 3**. Direct aldol reaction of ynones and active ketones[a]

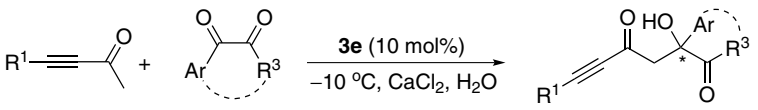


**1** **2** **4**

| entry | $R^1$ | **2** | | time / h | Yield of **4** / %[e] | ee / %[f] |
|---|---|---|---|---|---|---|
| 1 | **1a** | 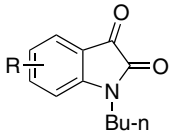 R = H | **2a** | 14 | **4a**, 90 | 80 |
| 2 | **1a** | R = 4-Cl | **2b** | 12 | **4b**, 86 | 46 |
| 3 | **1a** | R = 4-Br | **2c** | 10 | **4c**, 97 | 54 |
| 4 | **1a** | R = 5-Me | **2d** | 22 | **4d**, 90 | 77 |
| 5 | **1a** | R = 5-F | **2e** | 12 | **4e**, 98 | 70 |
| 6 | **1a** | R = 5-Cl | **2f** | 18 | **4f**, 90 | 66 |
| 7 | **1a** | R = 5-Br | **2g** | 16 | **4g**, 90 | 66 |
| 8 | **1a** | R = 5-$NO_2$ | **2h** | 9 | **4h**, 89 | 57 |
| 9 | **1a** | R = 5-MeO | **2i** | 13 | **4i**, 94 | 78 |
| 10 | **1a** | R = 6-Br | **2j** | 10 | **4j**, 97 | 70 |
| 11 | **1a** | R = 7-F | **2k** | 11 | **4k**, 95 | 65 |
| 12[b] | **1b** | | **2a** | 50 | **4ba**, 53 | 78 |
| 13[c] | **1c** | | **2a** | 46 | **4ca**, 70 | 2 |
| 14[d] | **1a** | 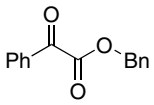 | **2l** | 72 | **4l**, 42 | 47 |
| 15[d] | **1a** | 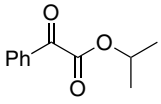 | **2m** | 72 | **4m**, 36 | 63 |
| 16[d] | **1a** | 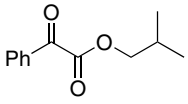 | **2n** | 72 | **4n**, 34 | 62 |
| 17[d] | **1a** | 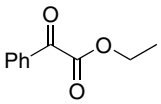 | **2o** | 72 | **4o**, 44 | 60 |

[a]Unless otherwise noted, reactions were carried out with 0.5 mmol of **1**, 0.1 mmol of **2** and 10 mol% of catalyst **3e** at −10 °C in 0.5 mL saturated $CaCl_2$ solution; [b]reaction was carried out in $CH_3CN$ at −5 °C; [c]reaction was carried out at 10 °C; [d]reaction was carried out at 20 °C; [e]isolated yield; [f]ee: enantioselectivity determined by chiral HPLC.

Bruker Daltonics Inc. Infrared (IR) spectra were recorded on a Nicolet MX-1E FT-IR spectrometer. High performance liquid chromatography (HPLC) analysis was performed on a Shimadzu LC-20AT series HPLC. Chiralpak AS, AD, OD and IA were purchased from Daicel Chemical Industries, Ltd. Optical rotation data were acquired on a PolAAr 3005 automatic polarimeter. Solvents for the column chromatography were distilled before use.

### General procedure for the asymmetric organocatalytic synthesis of β-hydroxyynones with a quaternary carbon center under aqueous conditions

Active ketone (0.1 mmol) and catalyst **3e** (10 mol%) were added to the saturated $CaCl_2$ solution (0.5 mL) in a tube and the mixture was stirred at the corresponding temperature for 15 min, then the ynone (0.5 mmol) was

added and the resulting mixture was stirred for 9-72 h at the determined temperature (monitored by thin layer chromatography (TLC)). The reaction mixture was extracted with $CH_2Cl_2$ (3 × 0.5 mL) and the organic phase was purified by flash column chromatography on silica gel (eluent: petroleum ether/ethyl acetate = 5/1-3/1) to yield pure products.

## Supplementary Information

Supplementary data are available free of charge at http://jbcs.sbq.org.br as a PDF file.

## Acknowledgements

We are grateful for the financial support from NSFC (21002071 and 21072153), Department of Education of Zhejiang Province (Y201017083) and Science and Technology Department of Zhejiang Province (2009R50002).

## References

1. Trost, B. M.; Frederiksen, M. U.; Papillon, J. P. N.; Harrington, P. E.; Shin, S.; Shireman, B. T.; *J. Am. Chem. Soc.* **2005**, *127*, 3666.
2. Nicolaou, K. C.; Aversa, R. J.; Jin, J.; Rivas F.; *J. Am. Chem. Soc.* **2010**, *132*, 6855.
3. Chavez, D. E.; Jacobsen, E. N.; *Angew. Chem., Int. Ed.* **2001**, *40*, 3667.
4. Marshall, J. A.; Ellis, K.; *Tetrahedron Lett.* **2004**, *45*, 1351.
5. Evans, D. A.; Starr, J. T.; *J. Am. Chem. Soc.* **2003**, *125*, 13531.
6. Fujii, K.; Maki, K.; Kanai, M.; Shibasaki, M.; *Org. Lett.* **2003**, *5*, 733.
7. Funel, J-A.; Prunet, J.; *J. Org. Chem.* **2004**, *69*, 4555.
8. Shin, Y.; Fournier, J.-H.; Balachandran, R.; Madiraju, C.; Raccor, B. S.; Zhu, G.; Edler, M. C.; Harnel, E.; Day, B. W.; Curran, D. P.; *Org. Lett.* **2005**, *7*, 2873.
9. Handa, M.; Scheidt, K. A.; Bossart, M.; Zheng, N.; Roush, W. R.; *J. Org. Chem.* **2008**, *73*, 1031.
10. O'Neil, G. W.; Fürstner, A.; *Chem. Commun*. **2008**, 4294.
11. Shimp, H.; Micalizio, G. C.; *Tetrahedron* **2009**, *65*, 5908.
12. Cook, C.; Guinchard, X.; Liron, F.; Roulland, E.; *Org. Lett.* **2010**, *12*, 744.
13. Trost, B. M.; Fettes, A.; Shireman, B. T.; *J. Am. Chem. Soc.* **2004**, *126*, 2660.
14. Silva, F.; Sawicki, M.; Gouverneur, V.; *Org. Lett.* **2006**, *8*, 5417.
15. List, B.; Lerner, R. A.; Barbas III, C. F.; *J. Am. Chem. Soc.* **2000**, *122*, 2395.
16. Tang, Z.; Jiang, F.; Yu, L.-T.; Cui, X.; Gong, L.-Z.; Mi, A.-Q.; Jiang, Y.-Z.; Wu, Y.-D.; *J. Am. Chem. Soc.* **2003**, *125*, 5262.
17. Tang, Z.; Jiang, F.; Cui, X.; Gong, L.-Z.; Mi, A.-Q.; Jiang, Y.-Z.; Wu, Y.-D.; *Proc. Natl. Acad. Sci.* U. S. A. **2004**, *101*, 5755.
18. Tang, Z.; Yang, Z.-H.; Chen, X.-H.; Cun, L.-F.; Mi, A.-Q.; Jiang, Y.-Z.; Gong, L.-Z.; *J. Am. Chem. Soc.* **2005**, *127*, 9285.
19. List, B.; *Acc. Chem. Res.* **2004**, *37*, 548.
20. Notz, W.; Tanaka, F.; Barbas III, C. F.; *Acc. Chem. Res.* **2004**, *37*, 580.
21. List, B.; *Tetrahedron* **2002**, *58*, 5573.
22. Pellissier, H.; *Tetrahedron* **2007**, *63*, 9267.
23. Guo, Q.; Bhanushali, M.; Zhao,C.-G.; *Angew. Chem., Int. Ed.* **2010**, *49*, 9460.
24. Allu, S.; Molleti, N.; Panem, R.; Singh, V. K.; *Tetrahedron Lett.* **2011**, *52*, 4080.
25. Doyle, A. G.; Jacobsen, E. N.; *Chem. Rev.* **2007**, *107*, 5713.
26. Paradowska, J.; Stodulski, M.; Mlynarski, J.; *Angew. Chem., Int. Ed.* **2009**, *48*, 4288.
27. For a review see: Zhou, F.; Liu, Y.-L.; and Zhou, J.; *Adv. Synth. Catal.* **2010**, *352*, 1381.
28. Chen, J.-R.; Liu, X.-P.; Zhu, X.-Y.; Li, L.; Qiao, Y.-F.; Zhang, J.-M.; Xiao, W.-J.; *Tetrahedron* **2007**, *63*, 10437.
29. Malkov, A. V.; Kabeshov, M. A.; Bella, M.; Kysilka, O.; Malyshev, D. A.; Pluhackova, K.; Kocovsky, P.; *Org. Lett.* **2007**, *9*, 5473.
30. Nakamura, S.; Hara, N.; Nakashima, H.; Kubo, K.; Shibata, N.; Toru, T.; *Chem. Eur. J.* **2008**, *14*, 8079.
31. Itoh, T.; Ishikawa, H.; Hayashi, Y.; *Org. Lett.* **2009**, *11*, 3854.
32. Angelici, G.; Corrêa, R. J.; Garden, S. J.; Tomasini, C.; *Tetrahedron Lett.* **2009**, *50*, 814.
33. Raj, M.; Veerasamy, N.; Singh, V. K.; *Tetrahedron Lett.* **2010**, *51*, 2157.
34. Chen, W.-B.; Du, X.-L.; Cun, L.-F.; Zhang, X.-M.; Yuan, W.-C.; *Tetrahedron* **2010**, *66*, 1441.
35. Hara, N.; Nakamura, S.; Shibata, N.; Toru, T.; *Adv. Synth. Catal.* **2010**, *352*, 1621.
36. Luppi, G.; Monari, M.; Corrêa, R. J.; Violante, F. D.; Pinto, A. C.; Kaptein, B.; Broxterman, Q. B.; Garden, S. J.; Tomasini, C.; *Tetrahedron* **2006**, *62*, 12017.
37. Corrêa, R. J.; Garden, S. J.; Angelici, G.; Tomasini, C.; *Eur. J. Org. Chem.* **2008**, *4*, 736.
38. Goehring, R. R.; Sachdeva, Y. P.; Pisipati, J. S.; Sleevi, M. C.; Wolfe, J. F.; *J. Am. Chem. Soc.* **1985**, *107*, 435.
39. Tokunaga, T.; Hume,W. E.; Nagamine, J.; Kawamura, T.; Taiji, M.; Nagata, R.; *Bioorg. Med. Chem. Lett.* **2005**, *15*, 1789.

*Submitted: September 15, 2011*
*Published online: November 17, 2011*

*J. Braz. Chem. Soc.*, Vol. 23, No. 1, 11-13, 2012.
Printed in Brazil - ©2012 Sociedade Brasileira de Química
0103 - 5053 $6.00+0.00

# Communication

## A Polyether Glycol Derived from Cashew Nutshell as a Kinetic Inhibitor for Methane Hydrate Formation

***Jorge Cesar Ferreira,[a] Adriana Teixeira[a,b] and Pierre M. Esteves*[*,a]***

*[a]Instituto de Química, Universidade Federal do Rio de Janeiro, CP 68545, 21945-970 Rio de Janeiro-RJ, Brazil*

*[b]Centro de Pesquisa e Desenvolvimento Leopoldo Américo Miguez de Mello, PETROBRAS, Av. Horácio Macedo No. 950, 21941-915 Rio de Janeiro-RJ, Brazil*

O polieterglicol derivado do líquido da casca da castanha do caju (CNSL) inibiu a formação de hidrato de metano. O polímero mostrou-se mais eficiente que o copolímero poli(vinilpirrolidona)-poli-(*N*-vinilcaprolactama)(PVP-PVCap) nas condições testadas ($CH_4$, 1470 psi e 4 °C), sendo esse último um dos melhores inibidores de hidratos comercialmente disponíveis.

The polyether glycol derived from cashew nutshell liquid (CNSL) inhibited the formation of methane hydrate. The polymer proved to be more efficient than the polyvinyl pyrrolidone-poly(*N*-vinyl) caprolactam (PVP-PVCap) co-polymer under tested conditions ($CH_4$, 1470 psi and 4 °C), being the latter one of the best commercially available hydrate inhibitors.

**Keywords:** methane hydrate, flow assurance, kinetic inhibitor

## Introduction

Clathrates of natural gas have been studied since 1890 when the first guest-host system was discovered.[1-3] Hydrate structures I (SI) and II (SII) formed by the building blocks (Figure 1), frequently occur and are formed by methane or natural gas. The formation of such clathrates represents a problem for the oil and gas industry since the plug formation of hydrate crystals can reduce or even interrupt the production.

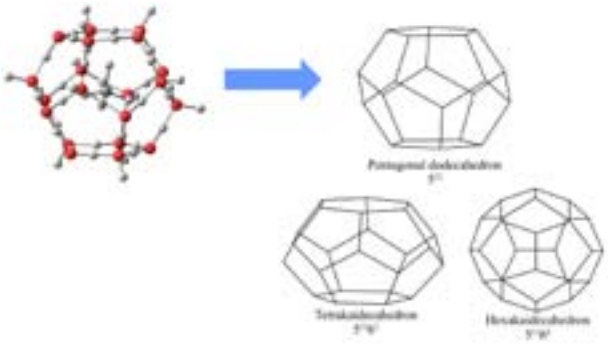

**Figure 1.** Different cavities of hydrate crystal structures: structure I (SI) contains $5^{12}$ and $5^{12}6^2$ cavities and structure II (SII) contains $5^{12}$ and $5^{12}6^4$ cavities. On the top left side, a whole atom representation of the $5^{12}$ cavity is shown.

*e-mail: pesteves@iq.ufrj.br

Alcohol solutions with 10-60 wt.% are often used as thermodynamic inhibitors of such clathrates and about 500,000,000 US dollars are annually spent on hydrate prevention and flow assurance. Methanol and ethanol are the most frequently used alcohols for such goal.[2] Another class of hydrate inhibitors is the low dosage hydrate inhibitors (LDHI). Polymers as polyvinyl pyrrolidone (PVP) and poly(*N*-vinyl) caprolactam (PVCap) have been applied as kinetic hydrate inhibitors.

Cashew nut is a fruit from a native Brazilian tree. The liquids obtained from the nut processing for feeding are by-products and are mostly waste material.[4] The cashew nutshell liquid is found in mesocarp spongy (Figure 2).[4]

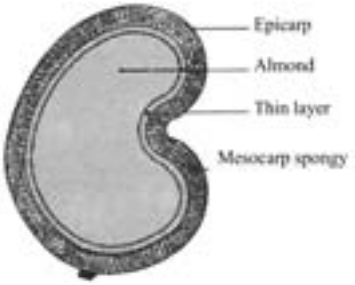


**Figure 2.** Longitudinal section of cashew nuts.[4]

Cardanols are decarboxylated derivatives obtained by thermal decomposition of any naturally occurring anacardic

acids, which are the major components present in the cashew nutshell oil (Figure 3).

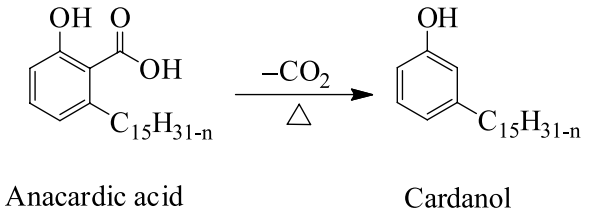


**Figure 3.** Structure of the anacardic acids and cardanol present in cashew nutshell liquid where n = 0, 2, 4, 6.

A chemical modification in a side chain of the cardanol produces a highly soluble polyether glycol in water (Figure 4).[5] Due to the high water solubility of this polymer and its easy availability in our laboratory, we have decided to evaluate it for the inhibition of gas hydrate formation, and our results are presented below.

## Experimental

The polymer obtained from cardanol and used in this work was prepared according to a procedure previously described.[5] Figure 4 briefly describes this procedure.[5] PVP/PVCap co-polymer was used as received and was tested to evaluate the inhibition of hydrate formation. All tests were carried out in a 316 inox steel autoclave produced by Autoclave Engineers (290 $cm^3$ volume), under pressures of 14.7 MPa (1470 psi). A preparation of a typical test run consisted of 200 $cm^3$ of solution at low polymer concentration (0.5 wt.% PVP/PVCap co-polymer, as recommended, or 0.025 wt.% to polyether glycol from cardanol prepared in distilled water). Then, the reactor was sealed and cooled at 277 K. The void volume was then purged with methane (99.99% purity from White Martins (Brazil), used as received) and the reactor was pressurized at 14.7 MPa. The system was stirred at 500 rpm[6,7] with a 6-blade stirrer and was considered an NVT ensemble. Data acquisition for temperature and pressure was obtained at one-second intervals. Pressure decrease indicates that the gas is being consumed due to methane hydrate formation, *i.e.*, $CH_4 + nH_2O = CH_4 \cdot (H_2O)_n$ (methane hydrate). These experiments were carried out in triplicates (additional results in the Supplementary Information section, SI). Characterization of the polymer was made through $^1H$ and $^{13}C$ nuclear magnetic resonance (NMR) and infrared (IR) spectroscopy.

## Results and Discussion

Figure 5 shows the results for the cardanol derived polyether glycol solution and, to compare its performance, a commercial PVP/PVCap co-polymer was employed. Typical plots of pressure over time were observed, and can be compared with data from literature.[8] The blank test started to form hydrate from the very beginning, being discerned from the drop in the pressure. It is observed that for both polyether glycol and PVP/PVCap polymer cases, there is a small decrease in the pressure, which can be associated to methane solubilization and to growth of a small portion of hydrate, before eventual drastic hydrate formation. The PVP/PVCap co-polymer led to the catastrophic hydrate formation (see the drastic drop in gas pressure) after 27 h, about 1 day. On the other hand, the cashew nutshell derived polymer maintained the high pressure in the cell for several days, when the tests were interrupted (see results for triplicates of this experiment in the SI section). Figure 6 shows the methane consumption as a function of time.

The cardanol derived polyether glycol solution therefore reveals a better inhibitor behavior, delaying the catastrophic formation of the gas hydrate for a longer time, compared to the commercial PVP/PVCap co-polymer. This one retarded the methane catastrophic hydrate formation for only about 1 day. The impressive performance of the cashew nutshell liquid derived polymer from renewable resource (biomass) and its low cost (*ca.* 1.00 US dollar *per* g of pure polymer, using research grade reactants, equivalent to 0.25 US dollar *per* L of solution 0.025 wt.%) should make it an attractive option for methane hydrate inhibition in

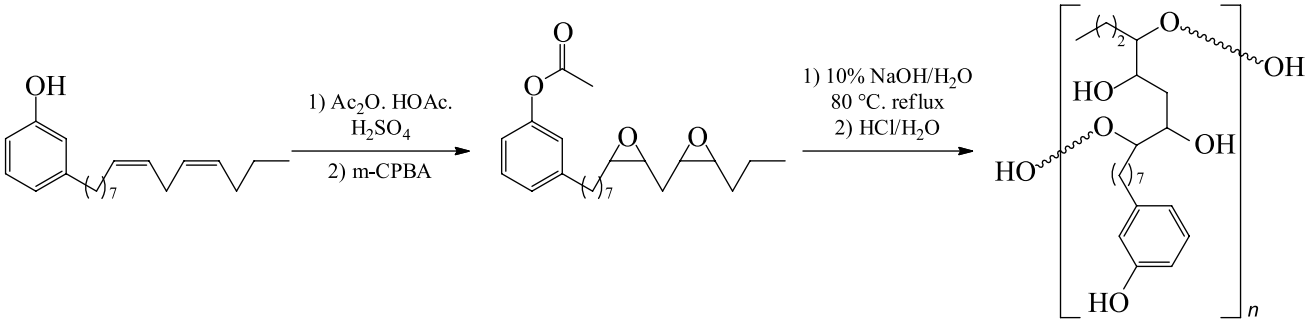


**Figure 4.** Preparation of the polyether glycol from anacardic acid.[5]

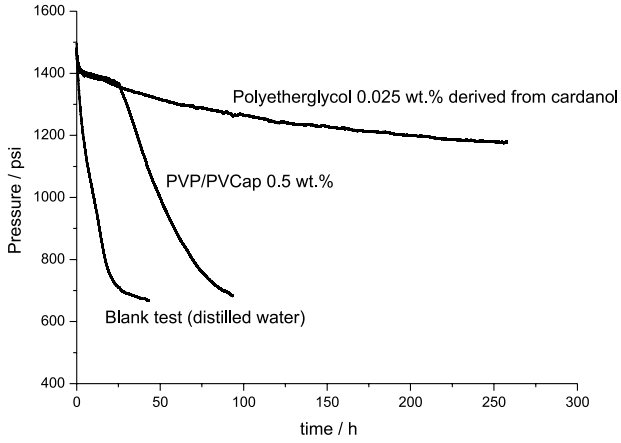


**Figure 5.** Inhibition performance of polyether glycol derived from cardanol compared with PVP/PVCap co-polymer and a blank test.

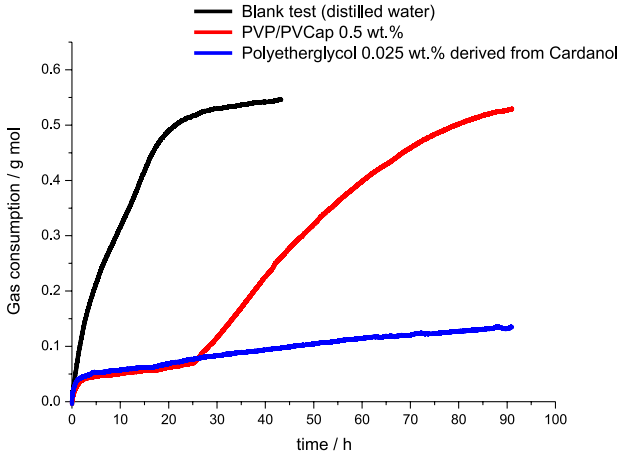


**Figure 6.** Consumption of methane gas using solution of polyether glycol derived from cardanol compared with PVP/PVCap co-polymer solution and a blank test (distilled water).

the oil industry. Further studies in this direction are being carried out in our laboratory.

## Conclusions

We showed that this polymer derived from cashew nutshell oil works as an inhibitor of the catastrophic methane hydrate formation, being more efficient (under the present experimental conditions: $CH_4$, 1470 psi and 4 °C) than the commercial PVP-PVCap co-polymer. This polymer derived from biomass can be used as an option for commercial inhibitors with advantages for oil exploitation and flow assurance.

## Supplementary Information

Data concerning the triplicates of the inhibition experiments with the polyether glycol and blank tests, IR and $^{1}H$ and $^{13}C$ NMR characterizations of the polymer, together with simulated $^{1}H$ and $^{13}C$ spectra of the monomer, are available free of charge at http://jbcs.sbq.org.br as pdf file.

## Acknowledgements

The authors thank to Conselho Nacional de Desenvolvimento Científico e Tecnológico (CNPq), Coordenação de Aperfeiçoamento de Pessoal de Nível Superior (CAPES) and Fundação de Amparo à Pesquisa do Estado do Rio de Janeiro (FAPERJ) by the financial support, and Prof. Simon J. Garden for helpful discussion.

## References

1. Lederhos, J. P.; Long, J. P.; Sum, A.; Christiansen, R. L.; Sloan Jr., E. D.; *Chem. Eng. Sci.* **1996**, *51*,1221.
2. Ripmeester, J. A.; Ratcliffe, C. I.; *J. Phys. Chem.* **1990**, *94*, 8773.
3. Sloan, E. D.; Koh, C. A.; *Clathrate Hydrates of Natural Gases*, 3rd ed.; CRC Press: New York, 2008.
4. Soares, J. B.; *O Caju Aspectos Tecnológicos*; Banco do Nordeste do Brasil: Fortaleza, CE, Brasil, 1986.
5. Ferreira, J. C.; Visconte, Y. L. L.; Guimarães, P. I. C.; *Br PI 0403145-8*, **2004**
6. Natajaran, V.; Bishinoi, P. R.; Kalogerakis, N.; *Chem. Eng. Sci.* **1994**, *49*, 2075.
7. Vysniauskas, A.; Bishnoi, P. R.; *Chem. Eng. Sci.* **1983**, *38*, 1061.
8. Yang, J.; Tohidi, B.; *Chem. Eng. Sci.* **2011**, *66*, 278.

*Submitted: July 21, 2011*
*Published online: November 29, 2011*

*J. Braz. Chem. Soc.*, Vol. 23, No. 1, 14-24, 2012.
Printed in Brazil - ©2012 Sociedade Brasileira de Química
0103 - 5053 $6.00+0.00

Review

# Biomedical Applications of Nanobiosensors: the State-of-the-Art

***Mahendra Rai,[a] Aniket Gade,[a] Swapnil Gaikwad,[a] Priscyla D. Marcato[b] and Nelson Durán*[b,c]***

[a]*Department of Biotechnology, Sant Gadge Baba Amravati University, Amravati-444 602, Maharashtra, India*

[b]*Biological Chemistry Laboratory, Chemistry Institute, Universidade Estadual de Campinas, CP 6154, 13083-970 Campinas-SP, Brazil*

[c]*Center of Natural and Human Sciences, Universidade Federal do ABC (UFABC), 09210-170 Santo André-SP, Brazil*

O desenvolvimento de nanobiosensores é um dos avanços mais recentes no campo da nanotecnologia. A investigação sobre nanobiosensores ópticos com dimensões submicrométricas tem aberto novos horizontes para as medições intracelulares. Aproveitando as propriedades únicas dos nanomateriais, nanobiosensores mais rápidos e sensíveis podem ser desenvolvidos. Além de serem sensíveis e rápidos, os estudos de nanobiosensores têm voltado seus esforços para o desenvolvimento de sensores baseados em nanomateriais que são acessíveis, robustos e reprodutíveis. Os nanobiosensores estão equipados com sondas biorreceptoras imobilizadas, por exemplo, anticorpos, substrato de enzima. A excitação por laser é transmitida para o sistema fotométrico na forma de sinal óptico (fluorescência). Os nanobiosessores poderão revolucionar no futuro o diagnóstico de doenças. A presente revisão discute os conceitos básicos, a evolução e as aplicações biomédicas de nanobiosensores.

Development of nanobiosensor is one of the most recent advancement in the field of Nanotechnology. Research on optical nanobiosensors with submicron-sized dimensions has opened new horizons for intracellular measurements. Taking advantage of the unique properties of the nanomaterials, faster and sensitive nanobiosensors can be developed. Apart from being sensitive and fast, the studies related to nanobiosensors have geared their efforts towards the development of nanomaterial-based sensors that are affordable, robust and reproducible. The nanobiosensors are equipped with immobilized bioreceptor probes, *e.g.*, antibodies, enzyme substrate. Laser excitation is transmitted to photometric system in the form of optical signal (fluorescence). Nanobiosensors will revolutionize the future of disease diagnosis. The present review discusses the basic concepts, developments and the biomedical applications of nanobiosensors.

**Keywords:** nanobiosensor, biomedical, nanotechnology, nanoparticles

## 1. Introduction

The terms ''nanoscience'' or 'nanotechnology'' are best used for phenomenon associated with structures approximately 1-100 nm in size where the properties of interest are due to the size of the structure. However, another definition seems more practical and unconstrained by any arbitrary size limitations: "The design, characterization, production, and application of structures, devices and systems by controlled manipulation of size and shape at the nanometer scale that produces structures, devices and systems with at least one novel/superior characteristic or property".[1] There have been renewed interest and activity in the synthesis, characterization and application of metallic nanoparticles as a novel system. Developments in organization of nanoscale structures into predefined super structures ensure that nanotechnology will play crucial role in many key technologies in the present millennium. It is gaining importance in areas such as catalysis, optics, biomedical sciences, mechanics, magnetic and energy science. The silver and certain other noble metal nanoparticles have many important applications in the

*e-mail: duran@iqm.unicamp.br

field of biolabelling,[2] drug delivery system,[3-6] filters and also antimicrobial drugs,[4,7] sensors.[8]

Metallic and inorganic nanoparticles at the nanoscale demonstrate novel properties and functions that differ significantly from those reported in the bulk. The small size, larger surface area, improved solubility and multifunctionality of nanoparticles open many new research avenues for scientists. Nanoparticles reveal unique properties in terms of particle aggregation, photoemission, electrical, magnetic, luminescent, heat conductivity and catalytic activity. These properties have recently been applied in different biological studies like disease diagnosis, bio-molecule detection, sample separation, purification and concentration, signal transduction and amplification (sensors).[9] These nanoparticles further enhance the detection sensitivity of microbial monitoring, degradation and recovery efficiency of chemicals.[10,11]

Metals are essential components in biological environments, participating in functions as diverse as electron transport, maintenance of structural integrity, enzymatic catalysis and neuronal communication.[12] For biological measurements, it has been known that sensors of the nanosize regime are essential for minimally invasive cellular monitoring. Nanosensors have been prepared by using various metals for many analytes, including calcium,[13] oxygen,[14] potassium,[15] zinc[16] and magnesium.[17]

The devices that take advantage of the high specificity of biological reactions for detecting target analytes are known as biosensors. It is a combination of a biological recognition element (specific to the target analyte) with a physical transducer that translates the bio-recognition event into a measurable effect, such as an electrical signal, an optical emission or a mechanical motion (Figure 1). Bioreceptors are important components, which provide specificity to biosensor technologies. They allow for binding of the specific analyte of interest to the sensor for the quantification with minimum interference from other factors in complex sampling mixtures.

In 1960s, Clark and Lyons,[18] Updike and Hicks[19] developed the first biosensor based on the specific catalytic interaction of the glucose oxidase enzyme with glucose.

A good definition of a biosensor was published by Topal[20] and by Pathak *et al.*:[21] "A biosensor is a measurement system for the detection of an analyte that combines a biological component with a physicochemical detector, and a nanobiosensor is a biosensor that works on the nano-scale size as described before".

The biosensor components are divided in the biological elements that are the sensitive part and can be tissues, microorganisms, organelles, cell receptors, enzymes, antibodies, nucleic acids, synthetic receptors and organs.[22]

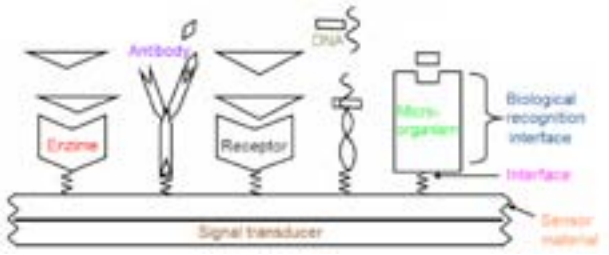


**Figure 1.** Schematic representation of nanobiosensor components (modified from Topal).[20]

The other important components are the transducer that measures the physical change that occurs with the reaction at the bioreceptor then transforming that energy into measurable electrical output.The latter one is the detector system in which the signals from the transducer are passed to a detector where they are amplified and analyzed and converted to concentration units and transferred to a display or/and data storage device.

The process of detection and amplification is possible to describe as: analyte-bio-receptor-transducer-biocatalyst-the output from the transducer is amplified, processed and displayed.

Over the years, new techniques in biosensing have set the stage for great advances in the field of biological research.[23-26]

The quantitative analysis of single components from complex biological and environmental samples has traditionally been achieved by the time-consuming and expensive combination of highly sophisticated chromatographic and spectroscopic techniques. Most recent advances in the field of biosensors include the development of optical nanobiosensors. The development in the nanotechnology leading to the fabrication of optical fibers with submicron-sized dimensions has opened new avenues for intracellular measurements. The application of submicron fiber-optic chemical probes has been developed by Kopelman *et al.*,[21-24,27-30] who has developed chemical nanoprobes for monitoring pH and nitric oxide. The use of nanobiosensors for given analytes in medical,[31] industrial[8] and environmental[32-36] applications has meant that alternatives to bulky laboratory-based procedures, especially in the case of *in vivo* analysis.[27,28]

The photonic explorer for bioanalysis with biologically localized embedding (PEBBLE) scheme has decisive advantages over most means of cellular measurement in terms of the small device size (*ca.* 20-200 nm spheres) that causes minimal physical perturbation, compared to fibers or electrodes.[17,30,37-39] The class of devices involves fiber-optic sensors that can be fabricated to have extremely small sizes, making them suitable for monitoring

intracellular physiological and biological parameters in microenvironments.

## 2. State-of-the-Art

Biosensors, which are devised to integrate a biological probe and a transducer, have been received increasing interest for environmental, industrial and biomedical diagnostics.[8,31,35,36] The combination of near field scanning optical microscopy (NSOM) and surface-enhanced Raman scattering (SERS) has been used to detect chemicals on solid substrates with sub-wavelength (100 nm) special resolution.[40] Nanostructured electrochemical biosensors are prepared by immobilizing the biorecognition elements on the polycarbonate (PC) surrounding gold nanodisks (approximately, 30 nm in diameter) in nanoelectrode ensembles (NEEs) made in track-etched commercial membranes. A suitable redox mediator is added to the sample solution to shuttle electrons from the nanoelectrodes to the biorecognition layer, both elements being in strict spatial proximity. In this way, one can exploit the highly improved signal-to-background current ratio which is peculiar of NEEs with respect to other electrochemical transducers. Two detection schemes were tested: one based on the direct immobilization of the target protein on the PC of the NEE and other based on the immobilization on PC of an antibody to capture the target protein. In both cases, the biorecognition process was completed by adding a primary antibody and a secondary antibody with horse radish peroxidase (HRP) as enzyme label; methylene blue was the redox mediator added to the electrolyte solution.[41]

Song *et al.*[42] reported that the detection of cytochrome *c* probed in a single cell using the optical nanobiosensor having mouse anticytochrome *c* antibodies. They proved that the combination of nanobiosensor with the ELISA immunoassay (enzyme-linked immunosorbent assay) improved the detection sensitivity of the nanobiosensor due to enzymatic amplification. Microcantilevers, such as those used in atomic force microscopes, have been recently employed as this new class of biosensors.[43] Nanomechanical biosensors have demonstrated that they are capable of detecting single base mismatches in oligonucleotide hybridization without labeling,[44,45] as well as performing protein recognition[46] with extreme sensitivity. Other DNA detection schemes have been reported, for example, one which is used as a capture oligonucleotide combined with a DNA probe attached to a gold nanoparticle.[47] This method can detect a single mismatch measured by resonance. Wu *et al.*[48] reported the effect of different phosphate buffer concentrations suggesting that electrostatic repulsive forces between neighboring DNA molecules must play a role in cantilever motion and demonstrating that configurational entropy changes and the intermolecular interactions can control the direction of motion in nanomechanical sensors.

The substrate, a three-carbon compound, is immobilized onto gold nanoparticles. The resulting compound is expected to diminish steric hindrances that can hamper the access of the substrate to the active center of the enzyme, thus favoring an improvement in the interaction force.[43,49] Lechuga *et al.*[50] found that, fabricated devices by standard Silicon CMOS microelectronics technology according to a precise design for achieving a high sensitivity for biosensing applications in genomic and proteomics. They have developed three types of nanobiosensors: (*i*) a surface plasmon resonance biosensor, (*ii*) an integrated, Mach-Zehnder nano interferometer device based on optical waveguides and (*iii*) nanomechanical biosensors based on microcantilevers. Interestingly, the rapid response of enzymatic biosensors based on immobilizing bioactive enzymes and related materials have been attractive and popular field for research.[51]

Nanopore sensor reagent-less electrochemical biosensor was designed, which involves immobilization within Au-coated nanopores of bacterial periplasmic binding proteins (bPBP) for glucose detection.[52] Some applications of nanosensors, developed for single-cell analysis and applications of biochips for biological sensing of pathogenic agents and medical diagnostics.[53,54] A biochip system constructed for bacteria detection was compact and sensitive. This portable biochip system is expected to contribute significantly to environmental sensing and medical diagnosis.[55] Current developments in nanoelectronics, biochemistry and information technology are providing feasible development pathways to allow the creation of nanorobots.[56-59] Nanorobots are considered a new possibility for the health sector to improve medical instrumentation, diagnosis and therapeutic treatments.[60] Medical nanorobot manufacturing includes embedded and integrated devices, which can comprise the main sensing, actuation, data transmission, remote control uploading and coupling power supply subsystems addressing the basics to biomedical instrumentation.[61-65]

Self-assembling process serves as a powerful tool to generate molecular films of biological molecules on a wide variety of substrates. The ease and simplicity of self assembled monolayers (SAMs) and the ability to control biomolecule surface orientation allow SAMs to play crucial role in the design of artificial biomolecular recognition devices. The SAMs are exploited in many areas of science including biotechnology, material science, microelectronics and superlattices, chemical sensing and molecular recognition, particularly in the future design of

biosensors.[66] Biosensor devices, based on the conversion of molecular recognition reactions into useful response signals, offer considerable promise for biological analysis.

## 3. Biomedical Applications of Nanobiosensors

Current developments in nanoelectronics, biochemistry and information technology are providing feasible development pathways to allow the creation of nanorobots.[56-58,67,68] The design of medical nanorobot will include embedded and integrated devices, which consists of the main sensing, actuation, data transmission, remote control uploading and coupling power supply subsystems.[61-64,69,70] A first series of nanotechnology prototypes for molecular machines is being investigated in different ways,[71-74] and some interesting devices for propulsion and sensing have been presented.[75-78] Sensors for biomedical applications are advancing through tele-operated surgery.[79-83] More complex molecular machines, or nanorobots, having embedded nanoscopic features should provide new tools for common medical treatments.[63,84,85]

### 3.1. Detection of diabetes

Patients with diabetes must take small blood samples many times a day to control glucose levels. Such procedures are extremely uncomfortable and inconvenient. To avoid this problem, the level of sugar in the body can be observed via constant glucose monitoring using medical nanorobotics. To envisage how actual and upcoming stages of nanotechnology can be applied in medicine, numerical analysis and computational nanotechnology, to illustrate the proposed nanorobot performance in the bloodstream, using a 3D vessel as test bed for diabetes control. The nanorobot sensor activation used proteomic-based information to detect biochemical changes associated with hyperglycemia.[86]

The nanorobot exterior consists of carbon metal nanocomposites, which are a diamond-like carbon thin film and possess atomic smoothness, chemical inertness and hardness properties close to those of diamond.[87] It have an artificial glycocalyx surface which minimizes adsorption and bioactivity in relation to fibrinogen as well as other blood proteins, ensuring sufficient biocompatibility to avoid immune system attack.[80,81] Typically, the favorable characteristics (such as large mobilities and high transconductance) of carbon promote it as an ideal component for integrated nanoelectronics, providing the suitable properties for successful radiofrequency (RF) applications.[88-90] The nanorobot uses a radiofrequency identification device (RFID) CMOS transponder system for *in vivo* positioning.[91,92]

The generated information by nanorobots will help doctors and specialists to provide a real-time health care and the medication regimen of the patient. It also reduces the time lost of the patient on suffering from hyperglycemia. A multiplicity of blood-borne nanorobots should allow glucose monitoring from different locations simultaneously throughout the body, thus permitting the physician to assemble a whole-body map of serum glucose concentrations. This will have diagnostic utility in detecting anomalous glucose uptake rates, which can assist in determining the tissues that may have suffered diabetes-related damage, and to what extent. Onboard sensors can also measure and report diagnostically relevant observations such as patient blood pressure, early signs of tissue gangrene or changes in local metabolism related to diabetes.[65,86] The application of new materials has demonstrated a wide range of possibilities for use in manufacturing better sensors and actuators with nanoscale sizes.[77,93] These developments along with 3D simulation should assist the design and manufacturing of nanorobots with integrated embedded nanoelectronics and circuits.

Nanorobots should enable a more effective diabetes treatment, helping patients to achieve a healthier and more comfortable life-style. The hardware structural design has provided the greater details on nanorobot safety and durability, with sensing capabilities to monitor diabetes. The nanorobot sensor detection system used proteomic-based information to sense biochemical changes associated with hyperglycemia. The model design, with integrated nanocircuit architecture, deal with major control interface requirements, describing the key parameters for telemetric control and inside-body retrieving information. With reference to integrated architecture, cell phones may play an important role in bringing lives of people into the therapeutic application of medical nanorobotics.[94-96]

### 3.2. Immunoassay (detection of Ab-Ag reaction)

It is well well-known that the peak extinction wavelength of the localized surface plasmon resonance (LSPR) spectrum is reliant upon the size, shape and interparticle spacing of the nanoparticles as well as its own dielectric properties and those of its local environment including substrate, solvent and adsorbates.[97,98] The high sensitivity of the LSPR spectrum of non spherical nanoparticles to adsorbate induced changes in the local dielectric constant (*viz.*, refractive index) are now being used to develop a different class of nanoscale chemosensors and nanobiosensors. This sensor detects changes in the refractive index induced by molecules near the surface of noble metal thin films.[99,100]

Riboh *et al.*[101] demonstrated LSPR nanobiosensor study on the prototypical immunoassay involving biotin (B) and anti-biotin (AB). The optical biosensors detect change in local refractive index by monitoring the LSPR extinction maximum with UV-Visible spectroscopy.

The maximum LSPR wavelength shift observed for AB binding to biotinylated nanoparticles caused a +38 nm red-shift in the LSPR $\lambda_{max}$. These results indicated that the LSPR nanobiosensor reacts minimally to nonspecific binding,[102] offering an exciting application of nanoscience to medical diagnostics and biomedical research.[103] The LSPR nanobiosensor developed in this study expected to demonstrate a wide range of biomedical and environmental applications. The LSPR biosensor may be an alternative to currently existing immunosensors. The sensor designed would be completely noninvasive and capable of organelle specific sensing. LSPR biosensors offer a variety of advantages over traditional flat surface SPR due to the short electromagnetic field decay length (5-6 nm)[101] of noble metal nanoparticles. Other kinds of nanobiosensors were also described.[104-106]

### 3.3. Application in cancer

Telomerase is a specialized reverse transcriptase, which is composed of an essential catalytic subunit and an RNA component[107,108] that, together with telomere-associated proteins, maintains telomere length and function.[109,110] In normal cells, a critical telomere length is eventually reached, thereby inducing cellular senescence and finally leading to apoptosis. Elevated levels of telomerase activity are found in the majority of malignancies and are believed to play a critical role in tumorgenesis.[111-116] Telomere dysfunction also results in genetic instability with complex cellular and molecular responses involving the retinoblastoma gene/p53 gene checkpoints and apoptosis pathways.[117-119]

A novel nanobiosensor (based on magnetic nanoparticles) has been developed by Grimm *et al.*[120] for rapid screening of telomerase activity in biological samples.[121] The technique makes use of nanoparticles which, upon annealing to telomerase-synthesized telomeric repeats (TTAGGG), change their magnetic state (a phenomenon readily detectable by magnetic readers). A high throughput version of this technique and the use of magnetic resonance imaging for the purpose of detection allow processing of hundreds of samples within tens of minutes with ultrahigh sensitivities. Nanoparticle assembly formation leads to change in the relaxation time (T2) of surrounding water, which can be readily measured by benchtop magnetic resonance (MR) relaxometers or imaging systems. The developed magnetic nanosensors can be utilized to determine telomerase activity in a variety of applications. The sensitivity of the method ranges from potential single molecule detection (*e.g.*, magnetic force microscopy) to 10-100 attomole levels using Benchtop read-outs (relaxometers). The assay permitted the detection of *ca.* 10 attomoles of telomerase-synthesized DNA by MR imaging, which competes well with other PCR (polymerase chain reaction) independent assay methodologies.[120]

Recently, an optical fiber nanobiosensor was constructed to detect efficiently a general cancer biomarker, telomerase at single cell level with its nanoscale tip.[122]

The number of significant advantages shown by developed technique has over other methods are as follows: (*i*) assay is quantitative, (*ii*) method is easy and fast (approximately 150 min for an entire determination and only a minute for actual measurements), (*iii*) does not requires solid phase, (*iv*) method can be extended to a high-throughput screening format and (*v*) achieves high degree of sensitivity without PCR and therefore avoids PCR-related artifacts and difficulties in quantification.

Wang[123] reported miniaturized devices that enable rapid and direct analysis of the specific binding of small molecules to proteins using silicon nanowire (SiNW) field-effect transistor (FET) devices. Detection of small-molecule inhibitors of long form ATP (adenosine triphosphate) binding to Abl (tyrosine kinase) with constitutive expression that was responsible for chronic myelogenous leukemia. In addition, concentration-dependent inhibition of ATP binding was analyzed for four additional small molecule inhibitors. This study demonstrated that this methodology efficiently distinguishes among the affinities of distinct, small-molecule inhibitors, therefore, useful as platform for drug discovery.

A simple and low cost device to fabricate polySiNW-FET (poly-crystalline silicon nanowire field-effect transistor) for biosensing application was recently published.[124] Recently, it was also reported a detection method for vascular endothelial growth factor (VEGF) for cancer diagnoses using an anti-VEGF aptamer.[125]

The field of biosensor development for DNA detection can benefit from the advances produced on the synthesis of artificial nucleic acid analogues peptide nucleic acid (PNA) having alluring properties.[126] PNA is an achiral and uncharged DNA mimic, where the sugar phosphate backbone has been replaced with a peptide like *N*-(2-aminoethyl) glycine polyamide structure, to which the nucleobases are connected by methylene carbonyl linkages.

Standard surface characterization techniques can be employed providing a complement to biochemical analyses due to the small thickness of DNA films (< 10 nm). Thus, recently, the formation of self assembled monolayers

(SAMs) of thiol-derivatized single stranded forms PNA (ssPNA) chains on gold surfaces has been characterized by surface science techniques, as reflection absorption infrared spectroscopy (RAIRS), X-ray photoelectron spectroscopy (XPS) and atomic force microscopy (AFM).[127] The molecular orientation of PNAs was strongly dependent on the surface coverage ability. The property of ssPNA to form locally ordered SAMs on gold nanoparticles, which are stabilized by intermolecular interactions of the adjacent nucleotides, provides new challenges for the development of functionalized surfaces with specific recognition properties.

Mateo-Marti *et al.*[128] investigated surface science techniques, the potential of Bio-SAMs of PNA to detect specific hybridization of complementary sequences of DNA. They have reported on efficient ssDNA recognition capability of ssPNA molecules on gold surfaces. They used two powerful label-free techniques for surface characterization and DNA detection, synchrotron radiation based X-ray photoemission spectroscopy and polarization modulation RAIRS (PM-RAIRS), presenting a detailed spectroscopic characterization of the process of these techniques. PM-RAIRS are surface specific infrared techniques ideally suited for the study of biomolecule SAMS deposited on a metal surface, RAIRS determines the presence of self-assembled biomolecules on the metal. The technique can also be used to determine the outcome of biomolecular recognition phenomena occurring at SAM surfaces due to its excellent capability for chemical group identification. With the thorough analysis of the N 1s XPS core-level peak, it is possible to identify each of the chemical components involved in the process and to understand the changes observed in the lineshape of the N 1s core-level peak due to hybridization of PNA-DNA BioSAMS.

A new methodology by nanostructuring the sensing electrodes creates nucleic acid sensors that have a large sensitivities and that are capable of rapid analysis. This methodology stated that only highly branched electrodes with fine structuring attained molar sensitivity. Planar chips with multiple electrically independent gold leads were passivated with silicon dioxide and at the tip of each lead were apertures with diameters sizes. Using metal electrodeposition under a wide range of plating conditions, it was generated different nanostructured palladium electrodes in the apertures to complete a microelectrode array. The strong binding affinity of palladium for thiols enabled them to functionalize and to attach biomolecular probes on the nanostructured microelectrodes, which were reproducible, robust and programmable. The authors suggested that an intimate link between nanoscale sensor structure and biodetection sensitivity will aid the development of high performance diagnostic tools diseases diagnosis.[129]

Song *et al.*[42] demonstrated the intracellular measurement of cytochrome *c* using an optical nanobiosensor. Cytochrome *c* is an important protein in the process which produces cellular energy. Moreover, cytochrome *c* is well-known as the protein involved in apoptosis, or programmed cell death. α-Aminolevulinic acid (5-ALA) was used to induce apoptosis in MCF-7 human breast carcinoma cells. 5-ALA, a photodynamic therapy (PDT) drug in cells was activated by a laser beam (He-Ne). On photoactivation of PDT, the release of cytochrome *c* from the mitochondria into the cytoplasm of a MCF-7 cell was monitored by the optical nanobiosensor, inserted inside the single cell and also by an enzyme-linked immunosorbent assay (ELISA) outside the cell.[69,130] The amalgamation of the nanobiosensor with the ELISA immunoassay helped in the improved detection of the nanobiosensor. The above results lead to the investigation of an apoptotic pathway at the single cell level.

Zamuner *et al.*[41] has used the polycarbonate capped gold nanodisks (*ca.* 30 nm) for electrochemical sensors using biorecognition elements in a nanoelectrode ensembles (NEEs) in track-etched commercial membranes. In order to shuttle electrons in the system, a redox mediator was added. They tested two different detection systems, first based on direct immobilization of the protein on polycarbonate of the NEE and second based on the immobilization on polycarbonate of an antibody to interact with the protein. In both cases, primary antibody was added and a secondary antibody with horse radish peroxidase (HRP) as enzyme label; methylene blue was the redox mediator in the electrolyte solution. Typical target analytes as single chain fragment variable protein and transtuzumab (Herceptin) were used in both systems, respectively. These sensors were used on a receptor protein HER2 in biological samples. A novel amperometric immunosensor for determination of human serum chorionic gonadotrophin (hCG) was constructed by Yanga *et al.*[131] by immobilizing hCG antibody with nano-gold and chitosan (CHIT) hybrid film electrochemically co-deposited on a glassy carbon electrode.

Nagarth *et al.*[132] have reported a pioneering and promising method for isolation of circulating tumor cells (CTCs) in peripheral blood from cancer patients using a microfluidic device.

### 3.4. Detection of pathogenic bacteria

Traditionally, the identification of bacteria is based on morphology in culture and biochemical tests. But, these methods are tedious and sometimes all bacteria do not grow in

culture and therefore, there is a need to develop fast, sensitive and reliable detection method for the bacteria in clinical samples. Kaittanis *et al.*[133] has used superparamagnetic iron oxide nanoparticles for identification of *Mycobacterium avium* spp. *paratuberculosis* (MAP) through magnetic relaxation. By application of nanosensors direct detection of pathogenic agent can be done. On the other hand, indirect detection is possible through the assessment of the metabolic activity of the pathogen, for example, the monitoring of the consumption rate of nutrients in solution, where nanosensors will be able to assess the metabolic activity of the microbial pathogen.[134] Moreover, it will also helped to determine whether the pathogen can reproduce in presence of an antibiotic. Nath *et al.*[135] have reported a novel gold nanoparticle-based technique for the assessment of bacterial susceptibility via surface plasmon resonance shifts. In 2008, Fu *et al.*[136] developed a novel gold/silicon hetero-structured nanorod-based detection method for *Salmonella*. The dye molecules attached to silicon nanorods produced fluorescence after coming in contact with *Salmonella*. The method has tremendous potential in biomedical diagnostics.

A recent and excellent review emphasized the application of bioconjugated quantum dots for the detection of food contaminants such as pathogenic bacterial toxins like botulinum toxin, enterotoxins produced by *Staphylococcus aureus*, *Escherichia coli*.[137]

## 4. Conclusions

Nanobiosensors have been emerging with fast pace in the field of biomedical, agricultural and environmental sciences[138,139] and with special emphasis with layer-by-layer films[140-142] and with the pioneer research of Brolo and co-workers.[143]

The applications in the field of detection of fatal diseases like cancer and diabetes have brought nanobiosensors in the fore front of research. Rapid assessment of telomerase activity is useful and can be performed by nanobiosensor. A novel nanobiosensor based on magnetic nanoparticles can be utilized for rapid screens of telomerase activity in biological samples. In detection and monitoring of diabetes, traditional methods are often tedious and lack sensitivity. To avoid this problem, the nanorobot sensor can be used since it generates proteomic-based information to detect biochemical changes associated with hyperglycemia. This will also enable more rapid and effective treatment of diabetes. The detection of microbial pathogens and their toxins in patients is now possible by nanobiosensors.

Nanobiosensor can open new avenues towards the development of miniaturized arrays of nanolectrodes, for multi-protein determinations. Nanobiosensor shows the significant improvements in sensitivity, specificity and parallelity in order to meet the future needs of a variety of fields ranging from *in vitro* medical diagnostics, pharmaceutical discovery and pathogen detection. The use of nanobiosensors in other diseases like tuberculosis, malaria and AIDS will certainly open up new vistas in biomedical research by making the diagnosis quick, accurate, cost-effective and painless. However, the nanobiosensor should be evaluated and approved as medical devices before its marketing.

## Acknowledgments

Fundação de Apoio a Pesquisa do Estado de São Paulo (FAPESP), Conselho Nacional de Desenvolvimento Científico e Tecnológico (CNPq, Binational Project Brazil-India), DST (India) and INOMAT (CNPq-Brazil) are acknowledged for supporting.

***Mahendra Rai*** *is a Professor and Head at the Department of Biotechnology of the Sant Gadge Baba Amravati University (Amravati City, India). He was a Visiting Scientist at the Department of Bioenergetics of the University of Genèva (Genèva City, Switzerland) in 2004 and at the Department of Plant Protection of Debrecen University (Debrecen City, Hungary) in 2005 and 2008. His area of expertise includes microbial biotechnology and nanobiotechnology. His present research interests are nanobiotechnology in medicine and agriculture, in particular the use of metallic nanoparticles as new generation of antimicrobials. He is the Director of Internal Quality Assurance Cell (IQAC) of the Sant Gadge Baba Amaravti University. He has published more than 200 research papers in India and abroad. In addition, he has edited/authored more than 20 books.*

***Aniket Gade*** *is an Assistant Professor in the Department of the Biotechnology of Sant Gadge Baba Amravati University (Amravati City, India), where also has submitted his PhD in Biotechnology in 2011, working with mycofabrication of silver nanoparticles by different Phoma sp. and their antimicrobial potential. His interests include mycofabrication of metallic nanoparticles, their functionalization with biomolecules and bioinformatics.*

***Swapnil C. Gaikwad*** *completed his MSc in 2008 and pursuing the PhD, both degrees in Biotechnology from the Sant Gadge Baba Amravati University (Amravati City (MS), India) under the supervision of Professor Mahendra K. Rai. His area of interest is myconanotechnology. His work is focused on mycosynthesis of silver nanoparticles, characterization and their application as potential antimicrobial agent.*

***Priscyla D. Marcato*** *received her PhD in Science from the Universidade Estadual de Campinas (UNICAMP, Campinas City, Brazil) in the group of Professor Nelson Durán in 2009, working with nanostructured pharmaceuticals and cosmetics carriers. Her work is focused on the production, characterization and application of biodegradable polymers, solid lipid nanoparticles and biogenic silver nanoparticles.*

***Nelson Durán*** *is a Professor at the Chemistry Institute of the Universidade Estadual de Campinas (UNICAMP, Campinas City, Brazil). He received his PhD at the University of Porto Rico (USA) in the group of Professor W. Adam in 1972, working on photolysis and thermolysis of 1,2-dioxolanes. He was an Associate Professor at the Universidad Catolica de Valparaiso (Valparaiso City, Chile) from 1973 to 1975 and carried out a Visiting Professorship at the Universidade de São Paulo (USP, São Paulo State, Brazil) in 1975, investigating enzymatic generation of excited states intermediates. In 1978, he jointed the Chemistry Institute of the Universidade Estadual de Campinas working in biological chemistry and biotechnology. His present research interests are nanobiotechnology in cosmetics and in pharmaceuticals, besides metallic nanoparticles as antibiotics carriers.*

## References


1. Bawa, R.; Bawa, S. R.; Maebius, S. B.; Flynn, T.; Wei, C.; *Nanomedicine: NBM* **2005**, *1*, 150.
2. Kulesza, A.; Mitrić, R.; Bonačić-Koutecký, V.; *Eur. Phys. J. D* **2009**, *52*, 203.
3. Marcato, P. D.; Durán, N.; *J. Nanosci. Nanotechnol.* **2008**, *8*, **2216**.
4. Durán, N.; Marcato, P. D.; De Conti, R.; Alves, O. L.; Costa, F. T. M.; Brocchi, M.; *J. Braz. Chem. Soc*. **2011**, *21*, 949.
5. Bawaskar, M.; Gaikwad, S.; Ingle, A.; Rathod, D.; Gade, A.; Durán, N.; Marcato, P.D.; Raí, M.; *Curr. Nanosci.* **2011**, *6*, 376.
6. Lv, Y.; Liu, H.; Wang, Z.; Liu, S.; Hao, L.; Sang, Y.; Liu, D.; Wang, J.; Boughton, R. I.; *J. Membr. Sci.* **2009**, *331*, 50.
7. Rai, M.; Yadav, A.; Gade, A.; *Biotechnol. Adv*. **2009**, *27*, 76.
8. Baruah, S.; Dutta, J.; *Environ. Chem. Lett.* **2009**, *7*, 191.
9. Jain, K. K.; *Clin. Chem.* **2007**, *53*, 2002.
10. Shtykov, S. N.; Rusanova, T. Y.; *Russ. J. Gen. Chem.* **2008**, *78*, 2521.
11. Urban, G. A.; *Meas. Sci. Technol*. **2009**, *20*, 012001.
12. Kidd, P.; Barceló, J.; Bernal, M. P.; Navari-Izzo, F.; Poschenrieder, C.; Shilev, S.; Clemente, R.; Monterroso, C.; *Environ. Exper. Bot*. **2009**, *67*, 243.
13. Asif, M. H; Nur, O.; Willander, M.; Danielsson, B.; *Biosens. Bioelectron*. **2009**, *24*, 3379.
14. Henderson, J. R.; Fulton, D. A.; McNeil, C. J.; Manning, P.; *Biosens. Bioelectron*. **2009**, *24*, 3608.
15. Oberleithner, H.; Callies, C.; Kusche-Vihrog, K.; Schiller, H.; Shahin, V.; Riethmueller, C.; MacGregor, G. A.; de Wardener, H. E.; *Proc. Natl. Acad. Sci. U. S. A.* **2009**, *106*, 2829.
16. Teolato, P.; Rampazzo, E.; Arduini, M.; Mancin, F.; Tecilla, P.; Tonellato, U.; *Chem. Eur. J*. **2007**, *13*, 2238.
17. Park, E. J.; Brasuel, M.; Behrend, C.; Philbert, M. A.; Kopelman, R.; *Anal. Chem.* **2003**, *75*, 3784.
18. Clark, L.; Lyons, C.; *Ann. N. Y. Acad. Sci.* **1962**, *102*, 29.
19. Updike, S. J.; Hicks, G. P.; *Nature* **1967**, *214*, 986.
20. Topal, C. O.; *Fundamentals of Nanotechnology: From Synthesis to Self-Assembly Course* (at Oklahoma State University), 2007, http://frontpage.okstate.edu/nanotech/Reports/2007/Presentations/Cagri%20 Ozge%20Topal.ppt#256,1,NANOBIOSENSORS, accessed in March 2011.
21. Pathak, P.; Katiyar, V. K.; Giri, S.; *J. Nanotechnol. Online*. **2007**, DOI: 10.2240/azojono0116.
22. Shana, A.; Rogers, K. R.; *Meas. Sci. Technol*. **1994**, *5*, 461.
23. Jain, K. K.; *Clin. Chem*. **2007**, *53*, 2002.
24. Alfinito, E.; Pennetta, C.; Reggiani, L.; *Sens. Actuators, B* **2010**, *146*, 554.
25. Shi, H., Yeh, J. I.; *Nanomedicine* **2007**, 2, 587.
26. Shi, H.; Xia, T.; Nel, A. E.; Yeh, J. I.; *Nanomedicine (Philadelphia, PA, U. S.)* **2007**, *2*, 599.
27. Tan, W.; Shi, Z. Y.; Kopelman, R.; *Anal. Chem.* **1992**, *64*, 2985.
28. Tan, W.; Shi, Z. Y.; Smith, S.; Birnbaum, D.; Kopelman, R.; *Science* **1992**, *258*, 778.
29. Xu, H.; Aylott, J. W.; Kopelman, R.; Miller, T. J.; Philbert, M. A.; *Anal. Chem.* **2001**, *73*, 4124.
30. Sumner, J. P.; Aylott, J. W.; Monson, E.; Kopelman, R.; *Analyst* **2002**, *127,* 11.

31. Kerman, K.; Saito, M.; Yamamura, S.; Takamura, Y.; Tamiya, E.; *TrAC, Trends Anal. Chem.* **2008**, *27*, 585.
32. Santos, A. S.; Pereira, A. C.; Durán, N.; Kubota, L. T.; *Electrochim. Acta* **2006**, *52*, 215.
33. Santos, A. D.; Pereira, A. C.; Sotomayor, M. D. R. T.; Tarley, C. R. T.; Durán, N.; Kubota, L. T.; *Electroanalysis* **2007**, *19*, 549.
34. Pereira, A. C.; Kisner, A.; Durán, N.; Kubota, L. T. In *Nanostructureed Materials in Electrochemistry*; Eftekhari, A, ed.; Wiley-VCH: Weinheim, 2008, p. 243.
35. Bogue, R.; *Sensor Rev*. **2009**, *29*, 310.
36. Sadik, O. A.; Zhou, A. L.; Kikandi, S.; Du, N.; Wang, Q.; Varner, K.; *J. Environ. Monit.* **2009**, *11*, 1782.
37. Clark, H. A.; Hoyer, M.; Parus, S.; Philbert, M. A.; Kopelman, R.; *Mikrochim. Acta* **1999**, *131*, 121.
38. Clark, H. A.; Kopelman, R.; Tjalkens, R.; Philbert, M. A.; *Anal. Chem.* **1999**, *71*, 4837.
39. Lee, Y. E. K.; Smith, R.; Kopelman, R.; *Annu. Rev. Anal. Chem*. **2009**, *2*, 57.
40. Jiang, Y.; Wang, A.; Ren, B.; Tian, Z. Q.; *Langmuir* **2008**, *24,* 12054.
41. Zamuner, M.; Mucelli, S. P.; Tormen, M.; Stanta, G.; Ugo, P.; *Eur. J. Nanomed*. **2008**, *1*, 33.
42. Song, J. M.; Kasili, P. M.; Griffin, G. D.; Vo-Dinh, T.; *Anal. Chem.* **2004**, *76*, 2591.
43. Ansari, M.; Cho, C.; *Sensors* **2009**, *9*, 6046.
44. Lee, C. K.; Radhakrishnan, R.; Chen, C. C.; Li, J.; Thillaigovindan, J.; Balasubramanian, N.; *J. Lightw. Technol*. **2008**, *26*, 839.
45. Zhang, N. H.; Chen, J. Z.; *J Biomech.* **2009**, *42*, 1483.
46. Xiang, W.; Lee, C. K.; *IEEE J. Sel. Top. Quantum Electr.* **2009**, *15*, 1323.
47. Kim, J. Y.; Lee, J. S.; *Nano Lett.* **2009**, *12,* 4564.
48. Wu, G.; Ji, H.; Hansen, K.; Thundat, T.; Datar, R.; Cote, R.; Hagan, M. F.; Chakraborty, A. K.; Majumdar, A.; *Proc. Natl. Acad. Sci. U. S. A.* **2001**, *98*, 1560.
49. Frey, B. L.; Corn, R. M.; *Anal. Chem.* **1996**, *68*, 3187.
50. Lechuga, L. M.; Tamayo, J.; Calle, A.; Dominguez, C.; *Rev. Mexicana Física* **2006**, *52*, 94.
51. Wang, H.; Wang, X.; Zhang, X.; Quin, X.; Zhao, Z.; Miao, Z.; Huang, N.; Chen, Q.; *Biosens. Bioelectron*. **2009**, *25*, 142.
52. Tripathi, A.; Wang, J.; Luck, L. A.; Suni, II.; *Anal. Chem.* **2007**, *79*, 1266.
53. Vo-Dinh, T.; Brian, M.; Cullum, D.; Stokes, L.; *Sens. Actuators, B* **2001**, *74*, 2.
54. Pierstorff, E.; Ho, D.; *J. Nanosci. Nanotechnol*. **2007**, *7*, 2949.
55. Song, J. M.; Culha, M.; Kasili, P. M.; Griffin, G. D.; Vo-Dinh, T.; *Biosens. Bioelectron*. **2005**, *20*, 2203.
56. Freitas Jr., R. A.; *Nanomedicine: Basic Capabilities*, vol. 1; Landes Bioscience: Georgetown, Texas, 1999.
57. Appenzeller, J.; Martel, R.; Derycke, V.; Rodasavljevic, M.; Wind, S.; Neumayer, D.; *Microelectron. Eng.* **2002**, *64*, 391.
58. Liu, J. Q.; Shimohara, K.; *IEEE Trans. Syst. Man Cybern. Part C* **2007**, 37, 325.
59. Khataee, H. R.; Khataee, A. R.; *Digest J. Nanomater. Biostruct.* **2009**, *4*, 613.
60. Couvreur, P.; Vauthier, C.; *Pharm. Res*. **2006**, *23*, 1417.
61. LaVan, D. A.; McGuire, T.; Langer, R.; *Nat. Biotechnol*. **2003**, *21*, 1184.
62. Cuschieri, A.; *Surgeon* **2005**, *3*, 125.
63. Leary, S. P.; Liu, C. Y.; Apuzzo, M. L. I.; *Neurosurgery* **2006**, *58*, 1009.
64. Hede, S.; Huilgol, N.; *J. Cancer Res. Ther*. **2006**, *2*, 182.
65. Cavalcanti, A.; Shirinzadeh, B.; Zhang, M.; Kretly, L. C.; *Sensors* **2008**, *8*, 2932.
66. Varatharajan, S.; Berchmans, S.; Yegnaraman, V.; *J. Chem. Sci. (Bangalore, India)* **2009**, *121*, 665.
67. Vaughn, J. R.; *Over the Horizon: Potential Impact of Emerging Trends in Information and Communication Technology on Disability Policy and Practice*; National Council on Disability: Washington (DC), 2006.
68. Lim, T. C.; Ramakrishna, S.; *Z. Naturforsch., A.: Phys. Sci.* **2006**, *61*, 402.
69. Shi, H.; Xia, T.; Nel, A. E.; Yeh, J. I.; *Nanomedicine* **2007**, *2*, 599.
70. Cavalcanti, A.; Shirinzadeh, B.; Freitas Jr., R. A.; Hogg, T.; *Nanotechnology* **2008**, *19*, 015103.
71. Mathieu, J. B.; Martel, S.; Yahia, L.; Soulez, G.; Beaudoin, G.; *Biomed. Mater. Eng*. **2005**, *15*, 367.
72. Jiang, H. W.; Wang, S. G.; Xu, W.; Zhang, Z. Z.; He, L.; *Jiqiren/Robot (China)* **2005**, *27*, 569.
73. Cavalcanti, A.; Freitas Jr., R. A.; *IEEE Trans. Nanobiosci.* **2005**, *4*, 133.
74. Behkam, B.; Sitti, M. J.; *Dyn. Syst. Meas. Control Trans. ASME* **2006**, *128*, 36.
75. Li, W. J.; Xi, N.; Fung, W. K.; Wong, T. S.; *Encyclopedia Nanosci. Nanotechnol.* **2004**, *7*, 351.
76. Xi, J.; Schmidt, J. J.; Montemagno, C. D.; *Nat. Mater.* **2005**, *4*, 180.
77. Villar, I. D.; Matias, I. R.; Arregui, F. J.; Claus, R. O.; *IEEE Trans. Nanotechnol.* **2005**, *4*, 187.
78. Ding, B.; Seeman, N. C.; *Science* **2006**, *314*, 1583.
79. Reuss, J. L.; Kirchner, R. S.; *US pat. 6364834* **2002**.
80. Freitas Jr., R. A.; *Nanomedicine: NBM.* **2005**, *1*, 2.
81. Freitas Jr., R. A.; *Int. J. Surg*. **2005**, *3*,1.
82. Nowlin, W. C.; Guthart, G. S.; Younge, R. G.; Cooper, T. G.; Gerbi, C.; Blumenkranz, S. J.; *US pat. 687988* **2005**.
83. Andrews, R. J.; *Ann. N. Y. Acad. Sci*. **2007**, *1122*, 169.
84. Patel, G. M.; Patel, G. C.; Patel, R. B.; Patel, J. K.; Patel, M.; *J. Drug. Target.* **2006**, *14*, 63.
85. Cavalcanti, A.; Shirinzadeh, B.; Freitas Jr., R. A.; Kretly, L. C.; *Recent Pat. Nanotechnol.* **2007**, *1*,1.
86. Cavalcanti, A.; Shirinzadeh, B.; Kretly, L. C.; *Nanomedicine* **2008**, *4*, 127.

87. Narayan, R. J.; *Diam. Relat. Mat.* **2005**, *14*, 1319.
88. Musa, G.; Mustata, I.; Ciupina, V.; Vladoiu, R.; Prodan, G.; Vasile, E.; *Diam. Relat. Mat.* **2004**, *13,* 1398.
89. Gannon, C. J.; Cherukuri, P.; Yakobson, B. I.; Cognet, L.; Kanzius, J. S.; Kittrell, C.; *Cancer* **2007**, *110*, 2654.
90. Rutherglen, C.; Burke, P.; *Nano Lett.* **2007**, *7*, 3296.
91. Ricciardi, L.; Pitz, I.; Sarawi, S. F. A.; Varadan, V.; Abbott, D.; *Proc. SPIE-Int. Soc. Opt. Eng.* **2003**, *5119*, 199.
92. Ricci, A.; Grisanti, M.; De Munari, I.; Ciampolini, P.; *IEEE Trans. Very Large Scale Integrated (VLSI) Systems* **2009**, *17*, 1719.
93. Goicoechea, J.; Zamarreño, C. R.; Matias, I. R.; Arregui, F. J.; *Sens. Actuators, B* **2007**, *126*, 41.
94. Gordijo, C. R.; Koulajian, K.; Shuhendler, A. J.; Bonifacio, L. D.; Huang, H. Y.; Chiang, S.; Ozin, G. A.; Giacca, A.; Wu, X. Y.; *Adv. Funct. Mater*. **2011**, *21*, 73.
95. Cash, K. J.; Clark, H. A.; *Trends Mol. Med*. **2010**, *16*, 584.
96. Samuel, D.; Bharali, D.; Mousa, S. A.; *Int. J. Nanotechnol*. **2011**, *8*, 53
97. Kreibig, U. In *Handbook of Optical Properties*, vol. 2; Hummel, R. E.; Wissmann, P., eds.; CRC Press: Boca Raton, 1997, p. 145.
98. Baida, H.; Billaud, P.; Marhaba, S.; Christofilos, D.; Cottancin, E.; Crut, A.; Lerme, J.; Maioli, P.; Pellarin, M.; Broyer, M.; Del Fatti, N.; Vallee, F.; *Nano Lett.* **2009**, *9*, 3463.
99. Brockman, J. M.; Nelson, B. P.; Corn, R. M.; *Annu. Rev. Phys. Chem*. **2000**, *51*, 41.
100. Huang, C.; Bonroy, K.; Reekman, G.; Verstreken, K.; Lagae, L.; Borghs, G.; *Microelectron. Eng.* **2009**, *86*, 2437.
101. Riboh, J. C.; Haes, A. J.; McFarland, A. D.; Yonzon, C. R.; Van Duyne, R. P.; *J. Phys. Chem*. **2003**, *107*, 1772.
102. Haes, A. J.; Van Duyne, R. P.; *J. Am. Chem. Soc.* **2002**, *124*, 10596.
103. Kim, H. M.; Jin, S. M.; Lee, S. K.; Kim, M. G.; Shin, Y. B.; *Sensors* **2009**, *9*, 2334.
104. Choi, J. W.; Oh, B. K.; Kim, Y. K.; Min, H. J.; *J. Microbiol. Biotechnol*. **2007**, *17*, 5.
105. Suprun, E.; Bulko, T.; Lisitsa, A.; Gnedenko, O.; Ivanov, A.; Shumyantseva, V.; Archakov, A.; *Biosens. Bioelectron*. **2010**, *25*, 1694.
106. Xiao, G.; Cai, J. Y.; *Prog.Chem*. **2010**, *22*, 194.
107. Greider, C. W.; Blackburn, E. H.; *Cell* **1985**, *43*, 405.
108. Greider, C. W.; *Proc. Natl. Acad. Sci. U. S. A*. **1998**, *95*, 90.
109. Van Steensel, B.; de Lange, T.; *Nature* **1997**, *385*, 740.
110. Van Steensel, B.; Smogorzewska, A.; de Lange, T.; *Cell* **1998**, 92, 401.
111. Kim, N. W.; Piatyszek, M. A.; Prowse, K. R.; Harley, C. B.; West, M. D.; Ho, P. L.; Coviello, G. M.; Wright, W. E.; Weinrich, S. L.; Sahy, J. W.; *Science* **1994**, *266*, 2011.
112. Shay, J. W.; Bacchetti, S.; *Eur. J. Cancer* **1997**, *33*, 787.
113. Bodnar A. G.; Ouellette, M.; Frolkis, M.; Holt, S. E.; Chiu, C. P.; Morin, G. B.; Harley, C. B.; Shay, J. W.; Lichtsteiner, S.; Woodring E.; Wright, W. E.; *Science* **1998**, 279, 349.
114. Counter, C. M.; Meyerson, M.; Eaton, E. N.; Ellisen, L. W.; Caddle, S. D.; Haber, D. A.; Weinberg, R. A.; *Oncogene* **1998**, *16*, 1217.
115. Vaziri, H.; Benchimol. S.; *Curr. Biol.* **1998**, *8*, 279.
116. Chang, S.; Khoo, C. M.; Naylor, M. L.; Maser, R. S.; DePinho, R. A.; *Genes Dev*. **2003**, *17*, 88.
117. Artandi, S. E.; DePinho, R. A.; *Curr. Opin. Genet. Dev.* **2000**, *10*, 39.
118. Lan, J.; Xiong, Y. Y.; Lin, Y. X.; Wang, B. C.; Gong, L. L.; Xu, H. S.; *World J. Gastroenterol.* **2003**, *9*, 54.
119. Leri, A.; Franco, S.; Zacheo, A.; Barlucchi, L.; Chimenti, S.; Limana, F.; Nadal-Ginard, B.; Kajstura, J.; Anversa, P.; Blasco, M. A.; *EMBO J.* **2003**, *22*, 131.
120. Grimm. J.; Perez, M.; Josephson, L.; Weissleder, R.; *Cancer Res*. **2004**, *64*, 639.
121. Kaittanis, C.; Santra, S.; Perez, J. M.; *J. Amer. Chem. Soc.* **2009**, *131*, 12780.
122. Zheng, X. T.; Li, C. M.; *Biosens. Bioelectron*. **2010**, *25*, 1548.
123. Wang, W. U.; *Proc. Natl. Acad. Sci. U. S. A.* **2005**, *102*, 3208.
124. Hsiao, C. V.; Lin, C. H.; Hung, C. H.; Su, C. J.; Lo, Y. R.; Lee, C. C.; Lin, H. C.; Ko, F. H.; Huang, T. Y.; Yang, Y. S.; *Biosens. Bioelectron.* **2009**, *24*, 1223.
125. Lee, H. S.; Kim, K. S.; Kim, C. J.; Hahn, S. K.; Jo, M. H.; *Biosens. Bioelectron*. **2009**, *24*, 1801.
126. Eschenmoser, A.; *Chimia* **2005**, *59*, 836.
127. Mateo-Martí, E.; Briones, C.; Roman, E.; Briand, E.; Pradier, C. M.; Martın-Gago, J. A.; *Langmuir* **2005**, *21*, 9510.
128. Mateo-Martí, E.; Briones, C.; Pradier, C. M.; Martín-Gago, J. A.; *Biosens. Biolectron.* **2007**, *22*, 1926.
129. Soleymani, L.; Fang, Z.; Sargent, E. H.; Shana, O.; Kelley, S. O.; *Nature Nanotechnol* **2009**, *4*, 844.
130. Shi, H.; Yeh, J. I.; *Nanomedicine* **2007**, *2*, 587.
131. Yang, G. M.; Chang, Y. B.; Yang, H.; Tan, L; Wu, Z. S.; Lu, X. X.; Yang, Y. H.; *Anal. Chim. Acta* **2009**, *644*, 72.
132. Nagrath, S.; Sequist, L. V.; Maheswaran, S.; Bell, D. W.; Irimia, D.; Ulkus, L.; Smith, M. R.; Kwak, E. L.; Digumarthy, S.; Muzikansky, A.; Ryan, P.; Balis, U. J.; Tompkins, R. G.; Haber, D. A.; Toner, M.; *Nature* **2007**, *450*, 1235.
133. Kaittanis, C.; Naser, S. A.; Perez, J. M.; *Nano Lett.* **2007**, *7*, 380.
134. Kaittanis,C.; Nath, S.; Perez, J. M.; *PLoS ONE*, **2008**, *3*, e3253, doi:10.1371/journal.pone.0003253.
135. Nath, S.; Kaittanis, C.; Tinkham, A.; Perez, J. M.; *Anal. Chem.* **2008**, *80*, 1033.
136. Fu, J.; Park, B.; Siragusa, G.; Jones, L.; Tripp, R.; Zhao, Y.; Cho, Y. J.; *Nanotechnology* **2008**, *19*, DOI: 10.1088/0957-4484/19/15/155502.
137. Vinayaka, A. C.; Thakur, M. S.; *Anal. Bioanal. Chem*. **2010**, *397*, 1445.
138. Vidotti, M.; Carvalhal, R. F.; Mendes, R. K.; Ferreira, D. C. M.; Kubota, L. T.; *J. Braz. Chem. Soc.* **2011**, *22*, 3.

139. Pereira, A. C.; Kisner, A.; Durán, N.; Kubota, L. T.; *J. Nanosci. Nanotechnol.* **2010**, *10*, 651.
140. Moraes, M. L.; de Souza, N. C.; Hayasaka, C. O.; Ferreira, M.; Rodrigues Filho, U. P.; Riul Jr., A.; Zucolotto, V.; Oliveira Jr., O. N.; *Mat. Sci. Eng. C* **2009**, *29*, 442.
141. Moraes, M. L.; Rodrigues Filho, U. P.; Oliveira Jr., O. N.; Ferreira, M. J.; *Solid State Electrochem.* **2007**, *11*, 489.
142. Perinoto, A. C.; Maki, R. M.; Colhone, M. C.; Santos, F. R.; Migliaccio, V.; Daghastanli, K. R.; Stabeli, R. G.; Ciancaglini, P.; Paulovich, F. V.; de Oliveira, M. C. F.; Oliveira Jr., O. N.; Zucolotto, V.; *Anal. Chem.* **2010**, *82*, 9763.
143. Gordon, R.; Sinton, D.; Kavanagh, K. L.; Brolo, A. G.; *Acc. Chem. Res.* **2008**, 41, 1049.

*Submitted: May 5, 2011*
*Published online: October 18, 2011*

**FAPESP has sponsored the publication of this article.**

Article

*J. Braz. Chem. Soc.*, Vol. 23, No. 1, 25-31, 2012.
Printed in Brazil - ©2012 Sociedade Brasileira de Química
0103 - 5053 $6.00+0.00

# Synthesis, Characterization and Photophysical Properties of ESIPT Reactive Triazine Derivatives

***Marcelo D. Kuplich, Fábio S. Grasel, Leandra F. Campo, Fabiano S. Rodembusch and Valter Stefani****

*Laboratório de Novos Materiais Orgânicos, Instituto de Química, Universidade Federal do Rio Grande do Sul, Av. Bento Gonçalves 9500, CP 15003, 91501-970 Porto Alegre-RS, Brazil*

Uma série de quatro compostos fotoativos derivados da triazina foi obtida a partir da substituição nucleofílica aromática no cloreto cianúrico. Os compostos foram caracterizados por espectroscopia de infravermelho (IR) e ressonância magnética nuclear (NMR de $^{1}H$ e $^{13}C$), além de espectrometria de massas de alta resolução (HRMS MALDI). A espectroscopia de absorção na região do UV-Vis e a emissão de fluorescência (no estado sólido e em solução) foram também utilizadas para estudar o comportamento fotofísico destes compostos. Os derivados obtidos são fluorescentes na região do azul-laranja por um mecanismo de transferência protônica intramolecular no estado excitado e apresentam um grande deslocamento de Stokes (6365-10290 $cm^{-1}$). Os derivados sintetizados neste trabalho reagiram com sucesso com fibras de celulose para dar novos compostos celulósicos fluorescentes.

Four new reactive fluorescent triazine derivatives were obtained from nucleophilic aromatic substitution of cyanuric chloride. The compounds were characterized by infrared spectroscopy (IR), nuclear magnetic resonance ($^{13}C$ and $^{1}H$ NMR) and high resolution mass spectrometry (HRMS MALDI). UV-Vis and steady-state fluorescence (in solution and in solid state) spectroscopies were also applied to characterize the photophysical behavior. The dyes are fluorescent by an intramolecular proton transfer mechanism (ESIPT) in the blue-orange region, with a large Stokes shift between 6365-10290 $cm^{-1}$. The fluorescent cyanuric derivatives could successfully react with cellulose fibers to give new fluorescent cellulosic materials.

**Keywords:** triazine, benzazoles, cyanuric chloride, ESIPT, reactive dyes, cellulose

## Introduction

The 2,4,6-trichloro-1,3,5-triazine (TCT), so-called cyanuric chloride, is an important triazine derivative and a well-known precursor in organic synthesis.[1-11] This precursor have become a very attractive field of research by virtue of the applications that can be envisaged with the obtained products, such as polymers,[12-15] non-linear optical materials[16-18] and new photoactive materials.[19-23] A particular interest has been reported on the use of cyanuric chloride in reactive dyes[24] since they are able to bond hydroxy groups from the cellulose and amino or thiol from proteins or polyamides.[25] In this way, several structures have been reported using TCT as molecular link between the chromophore or fluorescent dye and the organic matrix.[26-29]

On the other hand, the benzazoles often show a large Stokes shift due to an excited state intramolecular proton transfer (ESIPT) mechanism.[30] This phenomenon has widespread implications as optical sensors,[31-34] photoactive hybrid materials[35,36] and new polymeric materials.[37]

Despite of the great attention of ESIPT-exhibiting dyes and the versatile applications of cyanuric chloride in organic synthesis as starting material to produce dyes, herbicides, polymers and compounds of pharmaceutical interest,[38] this paper presents the synthesis and the photophysical characterization of new ESIPT reactive dyes based on the triazine moiety. Additionally, the obtained derivatives were tested as fluorophores for cellulosic materials.

## Experimental

### Materials and methods

2,4,6-Trichloro-1,3,5-triazine were purchased from ACROS Organics. All the solvents were used as received or

*e-mail: vstefani@iq.ufrgs.br

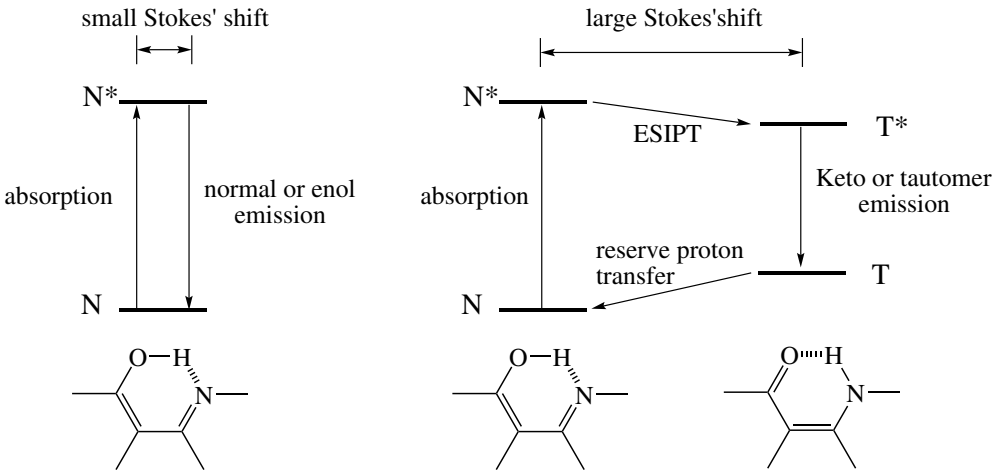


**Figure 1.** Photophysical pathways from ESIPT-exhibiting dyes: normal (or enol) emission (left) and ESIPT (or tautomer) emission (right).

purified using standard procedures. Spectroscopic grade solvents (Merck) were used for fluorescence and UV-Vis measurements. Melting points (mp) were measured with a Gehaka PF 1000 apparatus and are uncorrected. Infrared spectra were recorded on a Shimadzu FTIR8300 in KBr pellets. $^{1}$H and $^{13}$C NMR spectra were performed on a VARIAN INOVA YH300 using tetramethylsilane (TMS) as the internal standard and DMSO-$d_6$ (Aldrich) as the solvent at room temperature. UV-Vis absorption spectra were performed on a Shimadzu UV-1601PC spectrophotometer. Steady state fluorescence spectra were measured with a Hitachi spectrofluorometer model F-4500. Spectrum correction was performed to enable measuring a true spectrum by eliminating instrumental response such as wavelength characteristics of the monochromator or detector using Rhodamine B as a standard (quantum counter). For the photophysical measurements in the solid state, the photoactive cellulose fibers were measured in bulk using a solid sample holder. In this device, the light beam was irradiated to the sample at an angle of *ca.* 30°, and the light beam from the sample was reflected at an angle of *ca.* −60°. All experiments were performed at room temperature in a concentration of $10^{-6}$ mol $L^{-1}$. HRMS spectra were recorded with a Bruker Reflex III spectrometer.

### Synthesis of the triazine derivatives

The dyes **1a**-**d** were prepared using a previously described methodology.[39] The triazine benzazole derivatives **3a**-**d** were prepared according to Figure 2. In a typical experiment, an equimolar amount of the amino derivative **1a**-**d** and 2,4,6-trichloro-1,3,5-triazine were both dissolved in acetone. The dye solution was added dropwise into the triazine solution, cooled up to 0 ºC, followed by addition of a $Na_2CO_3$ solution (10%). The final solution was mixed for 1 h. The crude product, which precipitates, was washed with water and cold acetone and dried at room temperature. The purification was made by recristallization using dioxane/water. The final yields were from 70 to 96%.

#### 2-[4'-(*N*-4,6-Dichloro-1,3,5-triazin-2-yl)-2'-hydroxyphenyl] benzoxazole (**3a**)

Yield: 70%; mp > 350 ºC; IR (KBr) $\nu_{max}$/cm$^{-1}$ 3296 ν(N-H), 3059 $\nu_{arom}$(C-H), 1618 ν(C=N), 1537 and 1501 $\nu_{arom}$(C=C), 1238 ν(Ar-O), 1188 ν(C-N), 748 ν(C-Cl); $^{1}$H NMR (300 MHz, DMSO-$d_6$) δ/ppm 10.96 (s, 1H, OH), 7.98 (d, 1H, $H_{6'}$, $J_o$ 8.7 Hz), 7.88-7.76 (m, 2H, $H_4$ and $H_7$), 7.66 (d, 1H, $H_{3'}$, $J_m$ 2.0 Hz), 7.50-7.38 (m, 2H, $H_5$ and $H_6$), 7.21 (dd, 1H, $H_{5'}$, $J_m$ 2.0 Hz and $J_o$ 8.7 Hz); $^{13}$C NMR (75.4 MHz, DMSO-$d_6$) δ/ppm 162 ($C_2$), 158 ($C_{4'a}$), 154 ($C_{4'b}$ and $C_{4'c}$), 153 ($C_{2'}$), 149 ($C_8$), 142 ($C_{4'}$), 139 ($C_9$), 128 ($C_5$), 126 ($C_6$ or $C_{6'}$), 125 ($C_{6'}$ or $C_6$), 119 ($C_4$), 112 ($C_{3'}$ or $C_7$), 111 ($C_7$ or $C_{3'}$), 108 ($C_{5'}$), 106 ($C_{1'}$); exact mass: 373.0133 g mol$^{-1}$; the exact molecular mass for $C_{16}H_9Cl_2N_5O_2$ *m/z* 373.012 was found by HRMS (MALDI).

#### 2-[4'-(*N*-4,6-Dichloro-1,3,5-triazin-2-yl)-2'-hydroxyphenyl] benzothiazole (**3b**)

Yield: 80%; mp > 350 ºC; IR (KBr) $\nu_{max}$/cm$^{-1}$ 3331 ν(N-H), 3069 $\nu_{arom}$(C-H), 1612 ν(C=N), 1566 and 1481 $\nu_{arom}$(C=C), 1238 ν(Ar-O), 1186 ν(C-N), 752 ν(C-Cl); $^{1}$H NMR (300 MHz, DMSO-$d_6$) δ/ppm 11.19 (s, 1H, OH), 8.24 (d, 1H, $H_{3'}$, $J_m$ 2.7 Hz), 7.94-7.80 (m, 2H, $H_4$ and $H_7$), 7.72 (dd, 1H, $H_{5'}$, $J_m$ 2.7 Hz and $J_o$ 9.0 Hz), 7.54-7.42 (m, 2H, $H_5$ and $H_6$), 7.19 (d, 1H, $H_{6'}$, $J_o$ 9.0 Hz); $^{13}$C NMR (75.4 MHz, DMSO-$d_6$) δ/ppm 170 ($C_2$), 164 ($C_{4'a}$), 162 ($C_{4'b}$ and $C_{4'c}$), 155 ($C_{2'}$), 149 ($C_9$), 140 ($C_{4'}$), 129 ($C_8$),

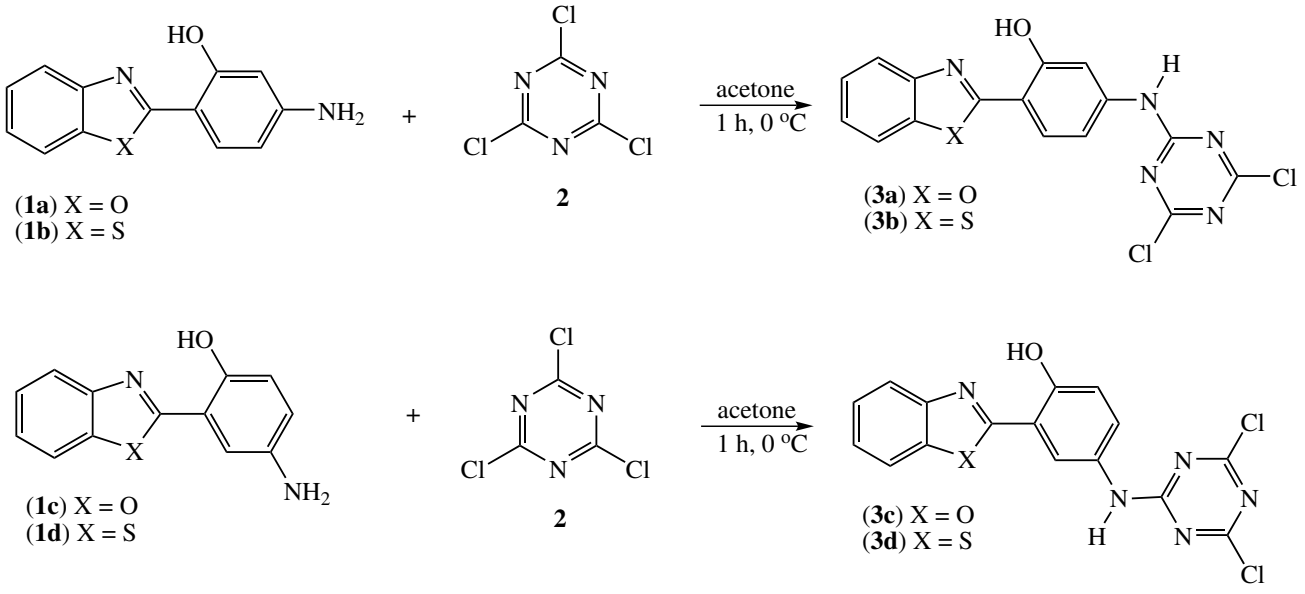


**Figure 2.** Synthesis of the triazine derivatives **3a**-**d**.

128 ($C_4$), 126 ($C_5$ or $C_6$), 125 ($C_5$ or $C_6$), 121 ($C_{6'}$), 119 ($C_7$ or $C_{3'}$), 118 ($C_{3'}$ or $C_7$), 111 ($C_{5'}$), 110 ($C_{1'}$); exact mass: 388.9905 g mol$^{-1}$; the exact molecular mass for $C_{16}H_9Cl_2N_5OS$ *m/z* 388.990 was found by HRMS (MALDI).

### 2-[5'-(*N*-4,6-Dichloro-1,3,5-triazin-2-yl)-2'-hydroxyphenyl] benzoxazole (**3c**)

Yield: 83%; mp > 350 ºC; IR (KBr) $\nu_{max}$/cm$^{-1}$ 3302 ν(N-H), 3065 $\nu_{arom}$(C-H), 1616 ν(C=N), 1587 and 1501 $\nu_{arom}$(C=C), 1238 ν(Ar-O), 1167 ν(C-N), 739 ν(C-Cl); $^1$H NMR (300 MHz, DMSO-$d_6$) $\delta$/ppm 10.98 (s, 1H, OH), 8.23 (d, 1H, $H_{6'}$, $J_m$ 2.7 Hz), 7.94-7.84 (m, 2H, $H_4$ and $H_7$), 7.61 (dd, 1H, $H_{4'}$, $J_m$ 2.7 Hz and $J_o$ 9.0 Hz), 7.54-7.44 (m, 2H, $H_5$ and $H_6$), 7.17 (d, 1H, $H_{3'}$, $J_o$ 9.0 Hz); $^{13}$C NMR (75.4 MHz, DMSO-$d_6$) $\delta$/ppm 170 ($C_2$), 164 ($C_{4'a}$), 162 ($C_{4'b}$ and $C_{4'c}$), 155 ($C_{2'}$), 149 ($C_8$), 140 ($C_9$), 129 ($C_{4'}$), 126 ($C_5$ or $C_6$), 125 ($C_5$ or $C_6$), 121 ($C_4$), 119 ($C_{6'}$ or $C_{3'}$), 118 ($C_{3'}$ or $C_{6'}$), 111 ($C_7$), 110 ($C_{1'}$); exact mass: 373.0133 g mol$^{-1}$; the exact molecular mass for $C_{16}H_9Cl_2N_5O_2$ *m/z* 373.012 was found by HRMS (MALDI).

### 2-[5'-(*N*-4,6-Dichloro-1,3,5-triazin-2-yl)-2'-hydroxyphenyl] benzothiazole (**3d**)

Yield: 96%; mp > 350 ºC; IR (KBr) $\nu_{max}$/cm$^{-1}$ 3285 ν(N-H), 3063 $\nu_{arom}$(C-H), 1556 and 1501 $\nu_{arom}$(C=C), 1238 ν(Ar-O), 1198 ν(C-N), 758 ν(C-Cl); $^1$H NMR (300 MHz, DMSO-$d_6$) $\delta$/ppm 11.09 (s, 1H, OH); 8.41 (d, 1H, $H_{6'}$, $J_m$ 2.7 Hz). 8.15 (d, 1H, $H_4$ or $H_7$), 8.05 (d, 1H, $H_7$ or $H_4$), 7.60 (dd, 1H, $H_{4'}$, $J_m$ 2.7 Hz and $J_o$ 9.0 Hz), 7.54 (t, 1H, $H_5$ or $H_6$), 7.45 (t, 1H, $H_6$ or $H_5$), 7.13 (d, 1H, $H_{3'}$, $J_o$ 9.0 Hz); $^{13}$C NMR (75.4 MHz, DMSO-$d_6$) $\delta$/ppm 170 ($C_2$), 169 ($C_{5'a}$), 164 ($C_{5'b}$ or $C_{5'c}$), 154 ($C_{2'}$), 151 ($C_9$), 135 ($C_{5'}$), 129 ($C_8$), 127 ($C_5$ or $C_6$), 127 ($C_5$ or $C_6$), 125 ($C_4$), 122 ($C_7$ or $C_{4'}$), 122 ($C_{4'}$ or $C_7$), 122 ($C_{6'}$), 118 ($C_{1'}$), 117 ($C_{3'}$); exact mass: 388.9905 g mol$^{-1}$; the exact molecular mass for $C_{16}H_9Cl_2N_5OS$ *m/z* 388.989 was found by HRMS (MALDI).

### Dye incorporation into the cellulose fibers

In a typical experiment, the cellulose was stained by addition of the cotton (100 mg) into an aqueous solution of $Na_2SO_4$ (0.05 mol L$^{-1}$) and 0.2 ml of sodium hydroxide (10% m/v) followed by the addition of the fluorescent dye (1 mg mL$^{-1}$ in DMSO). The reaction mixture was allowed to react for 1 h at 45 ºC. The crude stained cotton was washed several times with water, followed by Soxhlet extraction using acetone for 3 h in order to remove the unreacted fluorescent dye. The percentages of the triazine dye incorporation were evaluated using the absorption data from UV-Vis spectroscopy. Since the extinction coefficients of the dyes are well-known, the percentages of the triazine dye incorporation, which were from 80 up to 95%, were determined by the reactive dye extinction coefficients at a specific wavelength from UV-Vis data of the washing solutions (Lambert-Beer Law).

## Results and Discussion

### Photophysical characterization

Figures 3 and 4 show the normalized UV-Vis absorption spectra of the triazine derivatives (**3a**-**d**) in

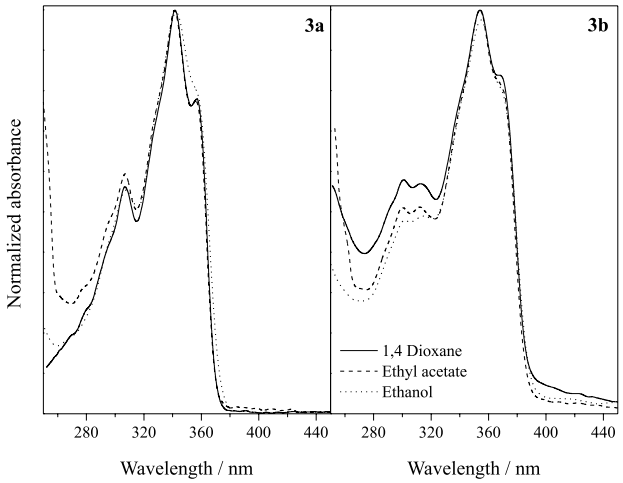


**Figure 3.** Normalized absorption spectra of **3a**-**b**.

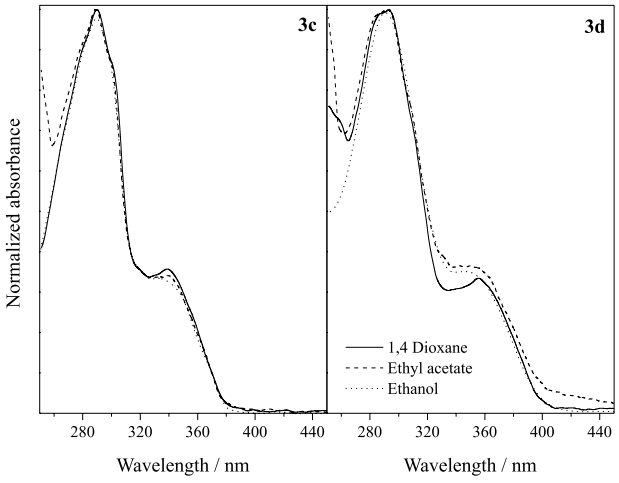


**Figure 4.** Normalized absorption spectra of **3c**-**d**.

1,4-dioxane, ethyl acetate and ethanol. The relevant UV-Vis data are summarized in Table 1.

An absorption band maxima ($\lambda_{max}$) located around 358 and 368 nm (with molar extinction coefficient values ($\varepsilon_{max}$) in agreement with $\pi$-$\pi^*$ transitions) could be observed for the derivatives **3a** and **3b**, respectively. A small solvatochromic effect could be observed for these dyes (*ca.* 4 nm). The absorption maximum of **3b** is red shifted in relation to **3a**, which can be explained by the better electron delocalization. This is allowed by the sulfur atom in relation to the oxygen. The same photophysical behavior was observed for derivatives **3c** and **3d**, with an absorption maximum located *ca.* 338 and 352 nm, respectively.

The intense absorption bands observed at 280-310 nm for derivatives **3c**-**d** indicate that the substitution in the phenolic ring is decisive for the photophysics of these dyes and can be associated to a difference of planarity of the dyes.[40] A non-planar structure does not allow a more effective electronic delocalization among the two $\pi$ systems (phenolic and benzoxazolic rings). In this way, the *para* derivative showed to be less planar than their *metha* analogue. The intense bands at 280-310 nm are related to the oxazole chromophore.[41,42] The difference between the molecular planarity of these dyes is confirmed taking the molar extinction coefficient values into account (see Table 1). A less planar structure usually presents a lower probability for the $\pi$-$\pi^*$ transition.

Figures 5 and 6 present the normalized fluorescence emission spectra of these dyes. The curves were obtained using the absorption maxima as the excitation wavelengths. The relevant data are also summarized in Table 1.

The derivatives **3a**-**d** present one main band located at *ca.* 471, 506, 514 and 546 nm, respectively. In solution, these dyes are fluorescent in the blue-green (**3a**-**b**) and green-yellow (**3c**-**d**) regions. The fluorescence emission bands are ascribed to the ESIPT band (T* emission) since

**Table 1.** Relevant UV-Vis data of the triazine derivatives **3a**-**d**

| Dye | Solvent | $\lambda_{abs}$ / nm | $\varepsilon_{max} \times 10^4$ / (mol$^{-1}$ L cm$^{-1}$) | $\lambda_{em}$ / nm | $\Delta\lambda_{ST}$ / (nm/cm$^{-1}$) |
|---|---|---|---|---|---|
| **3a** | 1,4-dioxane | 358 | 4.4 | 474 | 116/6836 |
| | ethyl acetate | 356 | 3.1 | 471 | 115/6859 |
| | ethanol | 360 | 5.6 | 467 | 107/6365 |
| **3b** | 1,4-dioxane | 370 | 5.2 | 510 | 140/7419 |
| | ethyl acetate | 366 | 4.4 | 505 | 139/7520 |
| | ethanol | 367 | 4.9 | 504 | 137/7407 |
| **3c** | 1,4-dioxane | 339 | 1.4 | 515 | 176/10081 |
| | ethyl acetate | 341 | 1.4 | 515 | 174/9908 |
| | ethanol | 335 | 1.3 | 513 | 178/10358 |
| **3d** | 1,4-dioxane | 356 | 1.2 | 547 | 191/9809 |
| | ethyl acetate | 350 | 1.9 | 547 | 197/10290 |
| | ethanol | 350 | 1.1 | 544 | 194/10189 |

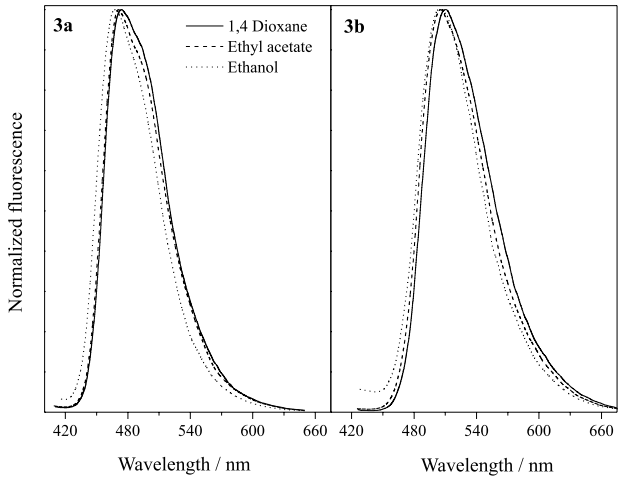


**Figure 5.** Normalized fluorescence emission spectra of **3a**-**b**.

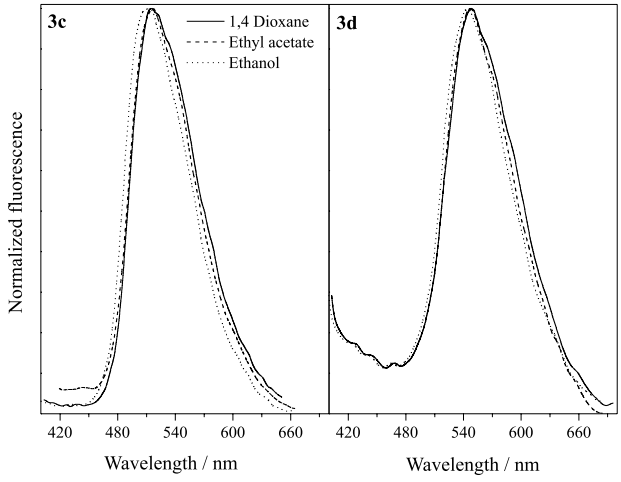


**Figure 6.** Normalized fluorescence emission spectra of **3c**-**d**.

a Stokes shift higher than 100 nm could be detected for all dyes.[43]

Figure 7 shows the normalized fluorescence emission spectra in the solid state of the dyes **3a**-**d**, as well as the dyes covalently bounded into the cellulose matrix. The absorption maxima in solution were used as excitation wavelength in the solid state measurements. As already observed in solution, the derivatives **3a**-**d** present one main band located from 459 to 537 nm, which comprises the blue-orange region.

Concerning the location of the fluorescence emission maxima in solution (Table 1), the dyes in the solid state present blue shifted bands (**3a**: 459 nm, **3b**: 508 nm, **3c**: 491 nm and **3d**: 536 nm), indicating that the studied solvents can better stabilize the keto tautomer in the excited state. Additionally, comparing dyes **3a**-**c** in the solid state and the cellulosic material after the staining process, it can be observed small changes in the fluorescence emission maxima due to the interaction with the cellulose matrix.

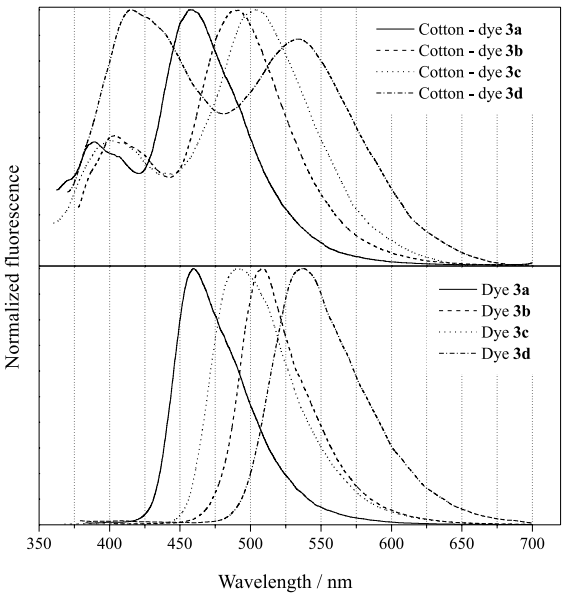


**Figure 7.** Normalized solid-state fluorescence emission spectra of the derivatives **3a**-**d** (bottom) and covalently bounded into cellulose fibers (top). This measurement treats the fibers in bulk using a solid sample holder with the light beam irradiated to the sample at an angle of *ca.* 30º, and the light beam from the sample reflected at an angle of *ca.* −60º.

However, after the staining process using dye **3d**, a dual fluorescence emission can be observed in the cellulose. The band located at higher wavelengths is ascribed to the ESIPT band and, the blue shifted one is ascribed to the normal relaxation (N* emission).[44] This photophysical behavior confirms a conformational equilibrium in the ground state for this dye. Since the hydroxyl moieties in the cellulose matrix could stabilize through intermolecular hydrogen bond, additional conformers can be related to the normal emission.[44] A pictorial scheme with the inter (left) and intramolecular (right) hydrogen bonds between the ESIPT dye and the cellulose is presented in Figure 8. Although the synthesized triazine dyes present two reactive chlorine atoms, the reactive dye is shown with only one replaced chlorine atom by the cellulose matrix. This is because the used temperature for the incorporation of the triazine derivatives into the cellulose fibers was below the needed temperature to replace the last chlorine atom.[24]

## Conclusions

Four new fluorescent cotton reactive dyes were synthesized, purified and characterized by infrared spectroscopy, nuclear magnetic resonance ($^{13}C$ and $^{1}H$ NMR), high resolution mass spectrometry (HRMS MALDI), UV-Vis and steady-state fluorescence spectroscopies (in solution and in the solid state). The triazine derivatives are fluorescent in the blue-orange region with a Stokes shift between 6365-10290 $cm^{-1}$. The fluorescent cyanuric derivatives could

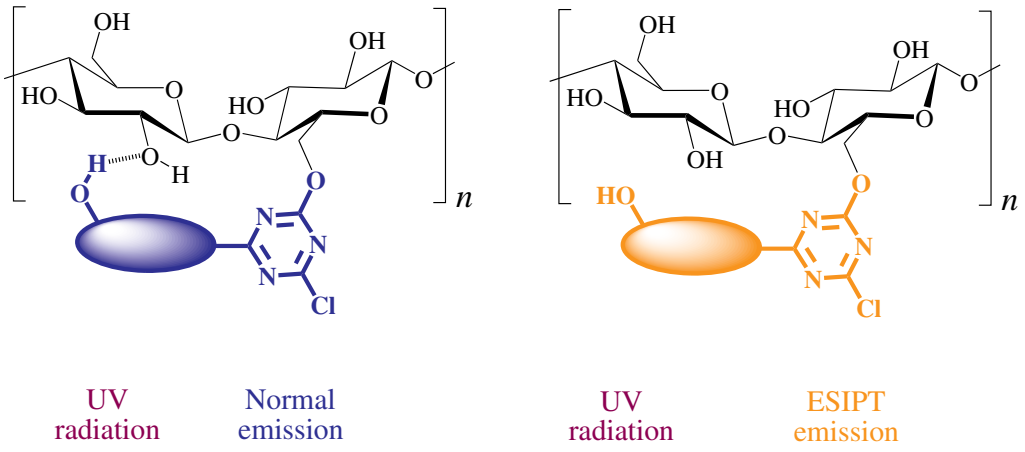


**Figure 8.** Scheme of interaction between the ESIPT dyes and the cellulose.

successfully react with cellulose fibers to produce new ESIPT fluorescent cellulosic materials. A dual fluorescence emission could be observed in the stained cotton using the dye **3d**, which indicates a conformational equilibrium in solution in the ground state. The emission at long wavelength (ESIPT band) is related to the ESIPT band and, the blue shifted ones are due to conformational forms with a normal relaxation.

## Supplementary Information

A color picture of the new ESIPT fluorescent cellulose fibers, as well as the dyes in solid state, are shown in the Supplementary Information (Figure S1), and other data free of charge at http://jbcs.sbq.org.br as pdf file.

## Acknowledgements

We are grateful for financial support and scholarships from the Brazilian agencies CNPq (Conselho Nacional de Desenvolvimento Científico e Tecnológico) and Fundação de Amparo à Pesquisa do Estado do Rio Grande do Sul (FAPERGS).

## References

1. Blotny, G.; *Tetrahedron* **2006**, *62*, 9507
2. Blotny, G.; *Tetrahedron Lett*. **2003**, *44*, 1499.
3. Zhang, P.; Yu, Y.-D.; Zhang, Z.-H.; *Synth. Commun*. **2008**, *38*, 4474.
4. Haval, K. P.; *Synlett* **2006**, *13*, 2156.
5. Giacomelli, G.; Porcheddu, A.; De Luca, L.; *Curr. Org. Chem*. **2004**, *8*, 1497.
6. Duan, H. D.; Wang, L. Z.; Qin, D. W.; Li, X. M.; Wang, S. X.; Zhang, Y.; *Synth. Commun.* **2011**, *41*, 380.
7. Mikhaylichenko, S. N.; Patel, S. M.; Dalili, S.; Chesnyuk, A. A.; Zaplishny, V. N.; *Tetrahedron Lett*. **2009**, *50*, 2505.
8. Matloobi, M.; Schramm, H. W.; *J. Heterocycl. Chem*. **2010**, *47*, 724.
9. Courme, C.; Gresh, N.; Lenoir, C.; Vidal, M.; Garbay, C.; Florent, J. C.; Bertounesque, E.; *Heterocycles* **2010**, *81*, 867.
10. Bork, J. T.; Lee, J. W.; Khersonsky, S. M.; Moon, H. S.; Chang, Y. T.; *Org. Lett*. **2003**, *5*, 117.
11. Moral, M.; Ruiz, A.; Moreno, A.; Diaz-Ortiz, A.; Lopez-Solera, I.; de la Hoz, A.; Sanchez-Migallon, A.; *Tetrahedron* **2010**, *66*, 121.
12. Jan, J. Z.; Huang, B. H.; Lin, J.-J.; *Polymer* **2003**, *44*, 1003.
13. Ren, S. J.; Zeng, D. L.; Zhong, H. L.; Wang, Y.; Qian, S.; Fang, Q.; *J. Phys. Chem. B* **2010**, *114*, 10374.
14. Liu, B.; Qian, D. J.; Chen, M.; Wakayama, T.; Nakamura, C.; Miyake, J.; *Chem. Commun.* **2006**, *30*, 3175.
15. Zhong, H. L.; Xu, E. J.; Zeng, D. L.; Du, J. P.; Sun, J.; Ren, S. J.; Jiang, B.; Fang, Q.; *Org. Lett*. **2008**, *10*, 709.
16. Van Cott, K. E.; Amos, T.; Gibson, H. W.; Davis, R. M.; Heflin, J. R.; *Dyes Pigm.* **2003**, *58*, 145.
17. Mahler, J.; Rafler, G.; *Opt. Mater*. **1999**, *12*, 363.
18. Zhong, H. L.; Lai, H.; Fang, Q. A.; *J. Phys. Chem. C* **2011**, *115*, 2423.
19. Omer, K. M.; Ku, S. Y.; Chen, Y. C.; Wong, K. T.; Bard, A. J.; *J. Am. Chem. Soc*. **2010**, *132*, 10944.
20. Iijima, T.; Lee, C. H.; Fujiwara, Y.; Shimokawa, M.; Suzuki, H.; Yamane, K.; Yamamoto, T.; *Opt. Mater*. **2007**, *29*, 1782.
21. Cai, Y.-Q.; Wu, W.; Wang, H.; Miyake, J.; Qian, D.-J.; *Surf. Sci*. **2011**, *605*, 321.
22. Chen, H. F.; Yang, S. J.; Tsai, Z. H.; W. Y. Hung, Wang, T. C.; Wong, K. T.; *J. Mater. Chem*. **2009**, *19*, 8112.
23. Rothmann, M. M.; Haneder, S.; Da Como, E.; Lennartz, C.; Schildknecht, C.; Strohriegl, P.; *Chem. Mater*. **2010**, *22*, 2403.
24. De Hoog, P.; Gamez, P.; Driessen, W. L.; Reedijk, J.; *Tetrahedron Lett*. **2002**, *43*, 6783.
25. Gorensek, M.; *Dyes Pigm.* **1999**, *40*, 225.
26. Taylor, J. A.; Pasha, K.; Phillips, D. A. S.; *Dyes Pigm.* **2001**, *51*, 145.

27. Um, S. I.; Lee, J. K.; Kang, Y.; Baek, D. J.; *Dyes Pigm.* **2006**, *70*, 84.
28. Son, Y. A.; Hong, J. P.; Lim, H. T.; Kim, T. K.; *Dyes Pigm.* **2005**, *66*, 231.
29. Czajkowski, W.; Paluszkiewicz, J.; Stolarski, R.; Kaźmierska, M.; Grzesiak, E.; *Dyes Pigm.* **2006**, *71*, 224.
30. Seo, J.; Kim, S.; Park, S. Y.; *J. Am. Chem. Soc*. **2004**, *126*, 11154.
31. Jung, H. S.; Kim, H. J.; Vicens, J.; Kim, J. S.; *Tetrahedron Lett*. **2009**, *50*, 983.
32. Yang, C.-C.; Tian, Y.; Chen, C.-Y.; Jen, A. K.-Y.; Chen, W.-C.; *Macromol. Rapid Commun*. **2007**, *28*, 894.
33. Wu, Y. K.; Peng, X. J.; Fan, J. L.; Gao, S.; Tian, M. Z.; Zhao, J. Z.; Sun, S.; *J. Org. Chem*. **2007**, *72*, 62.
34. Klymchenko, A. S.; Demchenko, A. P.; *J. Am. Chem. Soc*. **2002**, *124*, 12372.
35. Rodembusch, F. S.; Campo, L. F.; Rigacci, A.; Stefani, V.; *J. Mater. Chem*. **2005**, *15*, 1537.
36. Kober, U. A.; Campo, L. F.; Costa, T. M. H.; Stefani, V.; Gallas, M. R.; *J. Photochem. Photobiol., A* **2007**, *186*, 24.
37. Rodembusch, F. S.; Leusin, F. P.; Bordignon, L. B.; Gallas, M. R.; Stefani, V.; *J. Photochem. Photobiol., A* **2005**, *153*, 81.
38. Joule, J. A.; Mills, K.; *Heterocyclic Chemistry*, 4th ed.; Blackwell Science: Cambridge, 2000.
39. Campo, L. F.; Corrêa, D. S.; Araújo, M. A.; Stefani, V.; *Macromol. Rapid Commun*. **2000**, *21*, 832.
40. Douhal, A.; Amat-Guerri, F.; Lillo, M. P.; Acuña, A. U.; *J. Photochem. Photobiol., A* **1994**, *78*, 127.
41. Nagaoka, S. I.; Kusunoki, J.; Fujibuchi, T.; Hatakenaka, S.; Mukai, K.; Nagashima, U.; *J. Photochem. Photobiol., A* **1999**, *122*, 151.
42. Guallar, V.; Moreno, M.; Lluch, J. M.; Amat-Guerri, F.; Douhal, A.; *J. Phys. Chem*. **1996**, *100*, 19789.
43. Santra, S.; Dogra, S. K.; *Chem. Phys*. **1998**, *226*, 285.
44. Rodembusch, F. S.; Campo, L. F.; Leusin, F. P.; Stefani, V.; *J. Lumin*. **2007**, *126*, 728.

*Submitted: August 1, 2011*
*Published online: October 11, 2011*

*J. Braz. Chem. Soc.*, Vol. 23, No. 1, 32-38, 2012.
Printed in Brazil - ©2012 Sociedade Brasileira de Química
0103 - 5053 $6.00+0.00

Article

# Pt $L_{2,3}$ - Edge X-ray Absorption Spectroscopy Investigation of Zerovalent $[Pt(PPh_3)_2(\eta^2\text{-}L)]$ {L = $C_2H_4$, $C_{60}$ and $C_2(CN)_4$} Compounds

***Gilson H. M. Dias,[a] Nazareth F. da Fonseca[b] and Marcelo H. Herbst*[*,b]***

[a]*Instituto de Química, Universidade Estadual de Campinas, CP 6154, 13083-970 Campinas-SP, Brazil*

[b]*Departamento de Química, Universidade Federal Rural do Rio de Janeiro, 23890-000 Seropédica-RJ, Brazil*

Espectros de absorção de raios X nas bordas $L_{2,3}$ da platina (Pt) de três compostos $[Pt(PPh_3)_2(\eta^2\text{-}L)]$ {L = $C_2H_4$, $C_{60}$ and $C_2(CN)_4$} foram obtidos. As bandas de absorção observadas são efetivas para mensurar a força $\pi^*$-ácida dos ligantes olefínicos (L) coordenados ao fragmento $Pt(PPh_3)_2$. As energias dos orbitais $d_\pi$, determinadas quantitativamente pela diferença entre os deslocamentos das inflexões das bordas e de seus máximos nas linhas brancas $L_{2,3}$ nas segundas derivadas dos espectros, seguem a ordem $[Pt(PPh_3)_2(\eta^2\text{-}C_2H_4)] < [Pt(PPh_3)_2(\eta^2\text{-}C_{60})] < [Pt(PPh_3)_2\{\eta^2\text{-}C_2(CN)_4\}]$. Essas energias dos orbitais $d_\pi$ estão em concordância com as alterações nos comprimentos de ligação das olefinas livres e coordenadas, e com os deslocamentos químicos de coordenação no espectro de RMN de $^{31}P$ dos compostos. Além disso, os valores experimentais concordam com resultados teóricos obtidos para as energias de interação de orbitais $d_\pi$ calculados no nível de funcional de densidade para compostos modelo $[Pt(PH_3)_2(\eta^2\text{-}L)]$.

X-ray absorption spectra at the Pt $L_{2,3}$-edges have been measured for three $[Pt(PPh_3)_2(\eta^2\text{-}L)]$ {L = $C_2H_4$, $C_{60}$ and $C_2(CN)_4$} compounds. The spectral features are effective for measuring the $\pi^*$-acid strength of ligands (L) coordinated to the $Pt(PPh_3)_2$ fragment. The energies of the $d_\pi$-orbitals are quantitatively determined using the difference between the edge jumping and the edge maximum shifts of the $L_{2,3}$-white lines in the second derivatives of the spectra. The $d_\pi$-orbital energies follow the order $[Pt(PPh_3)_2(\eta^2\text{-}C_2H_4)] < [Pt(PPh_3)_2(\eta^2\text{-}C_{60})] < [Pt(PPh_3)_2\{\eta^2\text{-}C_2(CN)_4\}]$. These $d_\pi$-orbital energies are in good agreement with the changes in the bound olefinic carbon bond lengths and the $^{31}P$ NMR chemical shifts of the coordinated phosphines. Furthermore, the experimental values are in good agreement with available $d_\pi$-orbital interaction energy terms calculated using density functional theory for model $[Pt(PH_3)_2(\eta^2\text{-}L)]$ compounds.

**Keywords**: Pt $L_{2,3}$-edge XAS, zerovalent platinum compounds, π back-donation energy, spectral decomposition

## Introduction

X-ray absorption spectroscopy (XAS) is a powerful tool for characterising the electronic and structural properties of coordination complexes. Modern synchrotron radiation facilities make XAS an attractive experimental method for studying several absorbing transition metals.[1] XAS has the ability to probe both occupied and unoccupied 5d valence orbitals through studying the region of the Pt $L_{2,3}$ edges. Two absorption peaks (white lines) are observed at $L_3$- and $L_2$-edges and are split largely due to spin-orbit coupling. The $L_{2,3}$-edges identify the valence 5d-charges of the Pt center in accordance with the selection rules for the photoabsorption process ($\Delta l = \pm 1$ and $\Delta J = 0, \pm 1$). Because electrons are ejected from the 2p, $J = 3/2$, inner orbitals, the $L_2$ edge probes only the d-final orbitals that are characterised by $J = 3/2$, whereas the $L_3$ edge probes those d orbitals with $J = 3/2$ and 5/2. The allowed $2p \rightarrow 6s$ electric dipole transition is not observed because of the small spatial overlap between the 2p and the 6s wave functions.[2] For metals with a closed shell $d^{10}$ configuration, the spectrum is a simple arctangent curve, which reflects the ejection of the electrons restricted to the core orbitals of the continuum Fermi-Sommerfeld levels.[3] A very nearly filled $5d_{3/2}$ state at the $L_2$ edge of Pt metal and its small clusters results in an insignificant d valence band contribution.[4] Consequently, the resultant spectrum can be also treated as an arctangent curve. In addition to metals with unoccupied 5d valence

*e-mail: herbst@ufrrj.br

orbitals, the valence-charge redistribution of a closed-shell $d^{10}$-metal upon alloy formation results in the emergence of prominent white lines at the L-edges. These absorptions provide useful signatures for d-charge depletions from the metal sites.[5] Therefore, these white lines are a key feature for interpreting the Pt $L_{2,3}$ XAS spectra of zerovalent platinum compounds.

Because the Pt L-edges directly probe the unoccupied 5d valence orbitals, assembling the correct information regarding the molecular orbitals would be useful, particularly considering that the coordination of side-on unsaturated ligands to a metal results in vacant d-orbitals on the metal center. The classical Dewar-Chatt-Duncanson model,[6] shown in Scheme 1, states that the occupied π orbitals on the ligands donate electron density to the unoccupied s- or d-orbitals (or sd-hybrids) of the metal (σ-donation) simultaneously with back-donation of electron density from occupied metal d orbitals to the empty π* orbital of the ligand (π back-donation). As a consequence, the carbon-carbon bond distance of the alkene ligand increases as a result of both decreased electron density in the bonding π-orbital and increased electron density in the antibonding π*-orbital.


**Scheme 1.** Ligand σ donation to metal ($a_1 \leftarrow \pi$) and metal to ligand π back-donation ($b_2 \rightarrow \pi^*$), according to the orbital interactions in the Dewar-Chatt-Duncanson model.

The compounds $[M(PH_3)_2(\eta^2\text{-}L)]$ {M = Ni, Pd, Pt; L = $C_2H_4$, $C_{60}$, $C_2(CN)_4$}, which are model compounds for $[Pt(PPh_3)_2(\eta^2\text{-}L)]$, have been the subject of study by several theoretical approaches.[7-9] The upper valence levels of the bent $C_{2v}$ $Pt(PH_3)_2$ fragment have two available filled $b_1$ and $b_2$ platinum orbitals of $d_\pi$ character. The π back-donation to the lowest unoccupied orbital (LUMO) of the ligand, which has π* character, mainly involves the highest occupied (HOMO) $b_2$ orbital. The HOMO lies in the $PtC_2$ plane, whereas the electron density donation from the filled HOMO π orbital of the ligand flows mainly into the 6s-6$p_z$ platinum LUMO of $a_1$ symmetry (σ donation). Previous studies on $[Pt(PH_3)_2(\eta^2\text{-}L)]$ have identified that the major part of the covalent bonding energy term stems from π back-donation to the alkene ligand, which is particularly dependent on the position of the ligand π* energy level and the relativistic destabilisation of the Pt 5d valence orbitals.[9]

The rather unexpected experimental result of prominent white lines at $L_{2,3}$-edges within the structurally similar compounds $[Pt(PPh_3)_2(\eta^2\text{-}L)]$, shown in Scheme 2, allowed us to gain further insight into their chemistry.

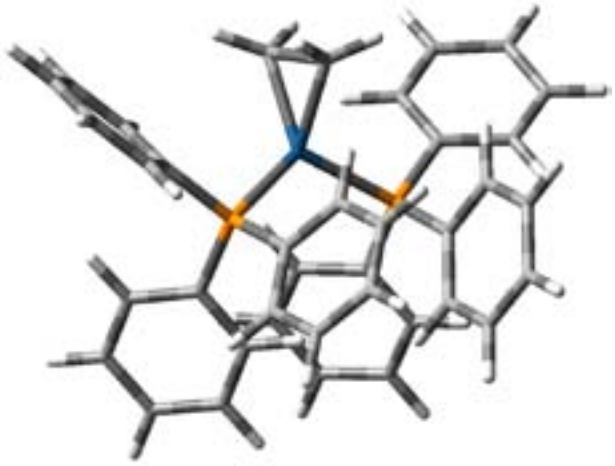

**Scheme 2.** Typical structure of the $[Pt(PPh_3)_2(\eta^2\text{-}L)]$ compounds, showing the crowd of triphenylphosphine ligands. Atom code: Pt (blue), P (orange), C (light gray), H (white).

We concentrate our study on the bond energy differences that result in the white lines in XAS spectra as a contribution to the development of a more efficient method in predicting the relative magnitude of the electronic density in such metal centers.[10] This method is based on the decomposition of the second derivative XAS spectra by using a rather simple model formed by an arctangent step function added to a Lorentzian function. Our results demonstrate that in analysing XAS spectra of organometallic compounds, in which electronic changes at the metal center are usually small, addressing only the absorption spectra is not sufficient; the second derivative provides a better means for accessing reliable data.

## Results and Discussion

The white lines at the absorption edges are especially sensitive to the lifetime of the core holes as well as the localisation and hybridisation of the valence d orbitals. The absorption area, which stems from white lines, is often used for developing semi-quantitative estimations of the unoccupied levels of open d-shell metals. The usual method to obtain the area is by integrating the difference between the white lines and arctangent curves.[11] The arctangent background spectrum of a closed-shell $d^{10}$-metal, or a metal with an insignificant d valence band contribution to the white line, partially minimises the uncertainty that arises from the calibration using the EXAFS (extended X-ray absorption fine structure) oscillations. Another reliable

method for analysing XAS spectra is the decomposition of the white line into an absorption curve (usually a Lorentzian or a Voigt function) and an arctangent function, although this method can produce more than one result that matches the experimental data. In the refinement of nonlinear functions, white lines are fit to a combination of Lorentzian functions to model the absorption curve of the localised states and the remaining step-like arctangent function for the oscillatory components of the continuous states.[12] Thus, the decomposition method corresponds to the non-linear least-square fitting of the experimental data to a combination of a Lorentzian (or Voigt) and an arctangent functions. However, one must be aware that peak fitting is an empirical analysis method, and that the line shapes used to fit the experimental spectrum have little physical meaning. Thus, peak fitting should be used for semi-quantitative purposes, such as the relative variation of spectral features of similar compounds. Instrumental limitations, such as the thickness effect,[13] and the absence of a genuine arctangent function are other factors that can affect the results adversely in both methods. In this work we have used both the decomposition method and the subtraction of metallic gold XAS spectrum method. The decomposition method was best suited, concerning the fitting of the edge jumping ($E_0$) and the possibility of obtaining the fit of the second derivative of the spectra.

Figure 1 shows that the Pt $L_3$-XAS spectra of $[Pt(PPh_3)_2(\eta^2\text{-L})]$ compounds share similar features. Relatively strong and narrow white lines arise at the edge and are followed by deep EXAFS oscillations. In addition to the $L_3$ white line, a pronounced $L_2$ white line (not shown) was also observed, reflecting an unfilled $d_{3/2}$ characteristic for this edge. The proportional broadening of both edges was estimated by the $L_3/L_2$ area ratio, which reflects the contribution of the $J$ = 3/2 and 5/2 hole populations.[14] This ratio is calculated by taking the integrated areas underneath the full Lorentzian peaks fit to the $L_3$ and $L_2$ edge spectra and dividing them in the form $AL_3/AL_2$. The values of $AL_3$ and $AL_2$ and of the area ratios are listed in Table 1. The area ratios are related to the d count in the sequence $[Pt(PPh_3)_2(\eta^2\text{-}C_2H_4)] < [Pt(PPh_3)_2(\eta^2\text{-}C_{60})] < [Pt(PPh_3)_2\{\eta^2\text{-}C_2(CN)_4\}]$ (Table 1). As a consequence of a large contribution of $d_{3/2}$ state to both edges, the $L_3$ edge was used in conjunction with $L_2$ to obtain more reliable values in the next stage.[15]

The spectral interpretation of the white lines, consistent with a quantitative description for the binding energy, was guided by the edge jumping energy ($E_0$), located in the inflection point at the rising edge, and the edge maximum ($E_{max}$) of the white line. For most typical complexes, it has been assumed that only the HOMO is involved at the

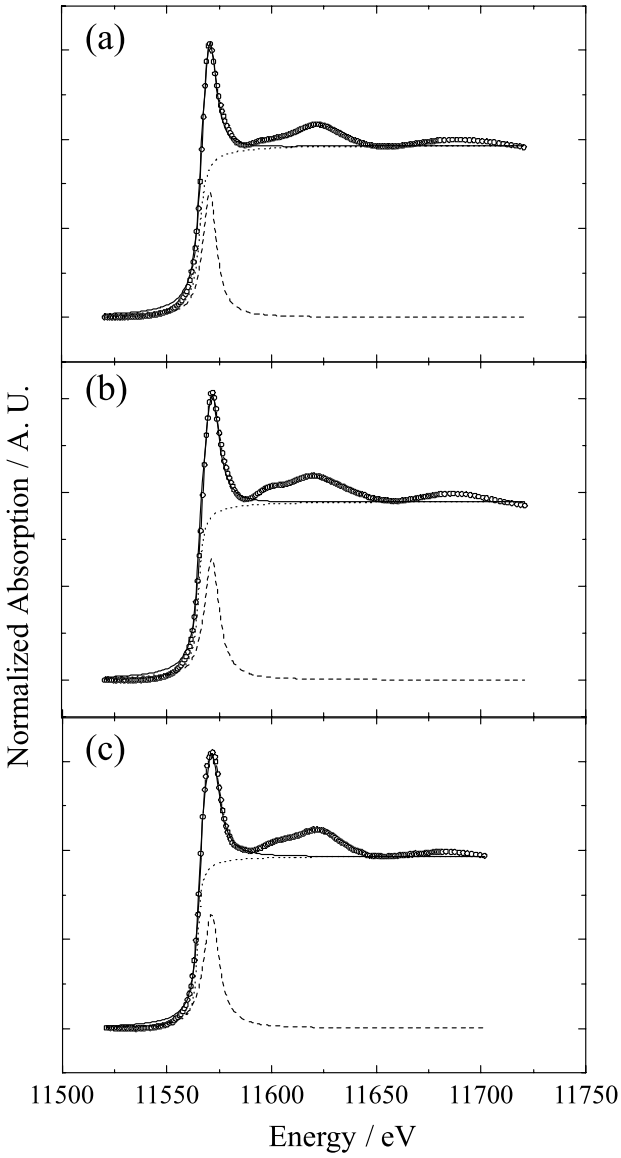


**Figure 1.** Experimental normalised Pt $L_3$-edge XAS absorption spectra of $[Pt(PPh_3)_2(\eta^2\text{-L})]$ compounds (small circles) plotted with the decomposed model spectra (solid line) and the model component curves (dashed line, Lorentzian curve; dotted line, arctangent curve). (a) $[Pt(PPh_3)_2(\eta^2\text{-}C_2H_4)]$, (b) $[Pt(PPh_3)_2(\eta^2\text{-}C_{60})]$ and (c) $[Pt(PPh_3)_2\{\eta^2\text{-}C_2(CN)_4\}]$.

$E_0$, whereas the $E_{max}$ reflects the LUMO holes in an MO description.[16] Moreover, the $E_{max}$ shifts to a higher energy concomitantly with the white line broadening. As a result, the difference between $E_{max}$ and $E_0$ has an approximate value of the half-width of the raising edge.[17] The HOMO is naturally located in the $E_0$ for the particular case of $[Pt(PR_3)_2L]$ compounds, while the $E_{max}$ reflects the holes created mainly on the $b_2$-hybrid orbital by back-bonding into the relatively localised LUMO. Therefore, the $\Delta E_\pi = E_{max} - E_0$ can be related to the $d_\pi$-orbital interaction energy. The main edge feature of $[Pt(PPh_3)_2(\eta^2\text{-L})]$ compounds is the broadening of the white-line in the XAS spectra (Figure 1), which is more

**Table 1.** Selected results of the Pt $L_{2,3}$-edges XAS and the relevant ancillary data for $[Pt(PPh_3)_2(\eta^2\text{-}L)]$ {L = $C_2H_4$, $C_{60}$, $C_2(CN)_4$}

| Compound | $AL_3$ [a] | $AL_2$ [a] | R [b] | $\Delta E_\pi$ $L_3$ | $\Delta E_\pi$ $L_2$ | $\Delta E_\pi$ [c] | $\Delta E_t$ [d] | $\Delta R$ [e] | $\Delta P$ [f] |
|---|---|---|---|---|---|---|---|---|---|
| $[Pt(PPh_3)_2(\eta^2\text{-}C_2H_4)]$ | 8.28 | 4.61 | 1.8 | 3.5 | 3.3 | 3.40 | 3.19 | 0.095 | 39.6 |
| $[Pt(PPh_3)_2(\eta^2\text{-}C_{60})]$ | 8.42 | 3.81 | 2.2 | 4.9 | 4.8 | 4.85 | 4.60 | 0.119 | 31.8 |
| $[Pt(PPh_3)_2(\eta^2\text{-}C_2(CN)_4)]$ | 8.72 | 3.47 | 2.5 | 6.7 | 6.3 | 6.50 | 5.81 | 0.180 | 20.9 |

[a]Areas at $L_3$ (mean ± 0.2) and $L_2$ (mean ± 0.4) edges in eV *per* cm$^2$. [b]Area ratio $AL_3/AL_2$. [c]Average $L_{2,3}$ edges energy $\Delta E_\pi = E_{max} - E_0$ (mean ± 0.03) in eV. [d]Sum $\Delta E_t = E_{B2} + E_{B1}$ in eV from Nunzi *et al.*[8] [e]Elongation parameter ΔR. Difference between the carbon-carbon bond lengths of coordinated and free molecules in angstroms. [f]Difference between the chemical shifts of $^{31}P$ coordinated and $^{31}P$ of free $PPh_3$ in ppm.

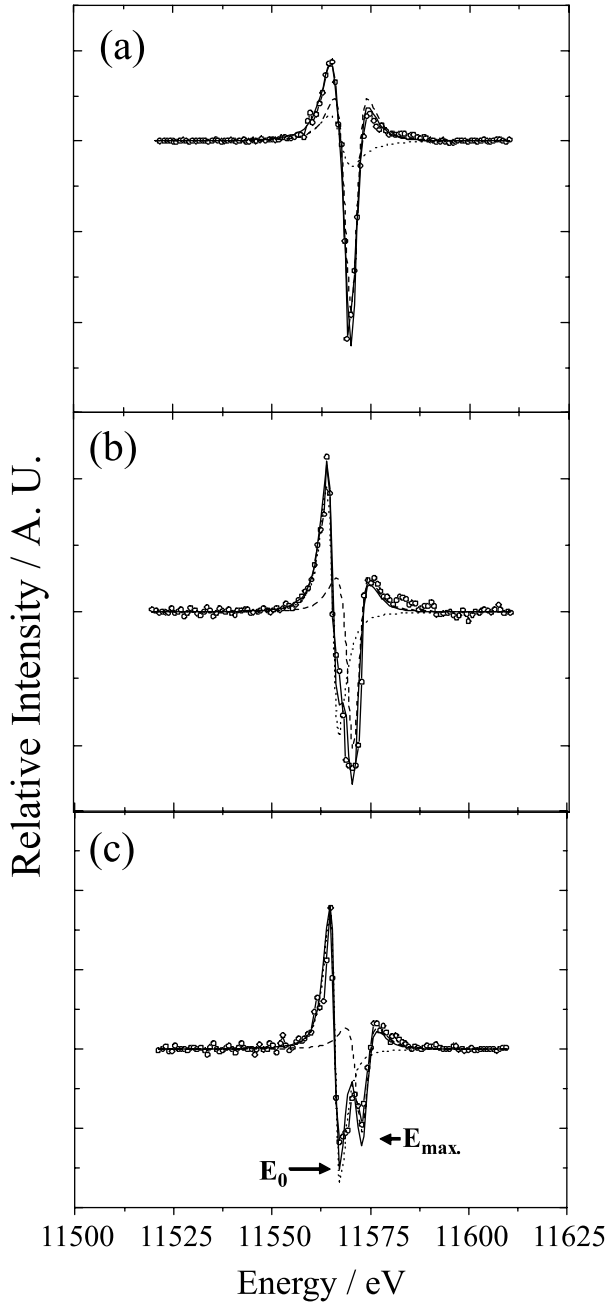


**Figure 2.** Second derivatives of the normalised Pt $L_3$-edge XAS spectra of $[Pt(PPh_3)_2(\eta^2\text{-}L)]$ compounds (small circles) plotted with the decomposed second derivatives spectra (solid line). The symbols for lorentzian and arctangent curves are the same of those in Figure 1. (a) $[Pt(PPh_3)_2(\eta^2\text{-}C_2H_4)]$, (b) $[Pt(PPh_3)_2(\eta^2\text{-}C_{60})]$ and (c) $[Pt(PPh_3)_2\{\eta^2\text{-}C_2(CN)_4\}]$.

distinguishable as a doublet growth in the second derivative spectra shown in Figure 2.

The splitting observed in the second derivative of the XAS spectrum is influenced by the degree of vacancy in 5d levels. With regard to this spectral pattern, the experimental and deconvoluted second derivatives were used as guides in determining the energy positions of peaks more accurately.[18] Table 1 presents selected results for the Pt $L_{2,3}$-edges XAS and relevant ancillary data for the $[Pt(PPh_3)_2(\eta^2\text{-}L)]$ compounds.

The energy values listed in Table 1 are as expected, where $\Delta E_\pi$ is related to both the elongation parameter (ΔR) and the coordination chemical shift (ΔP), calculated from literature data for free and coordinated ligands listed in Table 2.

**Table 2.** Collected literature data for free and coordinated ligands

| Molecule | C-C bond distance / Å | $\delta$ $^{31}P$ NMR / ppm | Reference |
|---|---|---|---|
| $C_2H_4$ | 1.339(5) | - | 19 |
| $C_{60}$ | 1.383(4) | - | 20 |
| $C_2(CN)_4$ | 1.67 | - | 21 |
| $PPh_3$ | - | –5.6 | 22 |
| $[Pt(PPh_3)_2(\eta^2\text{-}C_2H_4)]$ (**1**) | 1.434(13) | 34.0 ($CD_2Cl_2$) | 23 |
| $[Pt(PPh_3)_2(\eta^2\text{-}C_{60})]$ (**2**) | 1.502(30) | 26.2 ($CD_2Cl_2$) | 28 |
| $[Pt(PPh_3)_2\{\eta^2\text{-}C_2(CN)_4\}]$ (**3**) | 1.49(5) | 26.2 ($CD_2Cl_2$) | 24 |

In Figure 3, significant trends are observed. The plot of $\Delta E_\pi$ against ΔR follows the usual order $[Pt(PPh_3)_2(\eta^2\text{-}C_2H_4)] < [Pt(PPh_3)_2(\eta^2\text{-}C_{60})] < [Pt(PPh_3)_2\{\eta^2\text{-}C_2(CN)_4\}]$, which can be explained by the strength of the $d_\pi$ back-donation interaction.

The progressive destabilisation of the $b_2$-type $d_\pi$ donor orbital level, as the energy level of the olefin LUMO in $Pt(PPh_3)_2$ moiety decreases, will decrease the $d_\pi - \pi^*$ energy gap. Because ΔP is inversely proportional to $\Delta E_\pi$, the $^{31}P$ chemical shift of the bonded $PPh_3$, which is upfield relative to the free molecule, indicates that the energy of the HOMO $b_2$ orbital increases. This fact is expected in view of the σ-donor properties of the lone pair orbital on the ancillary $PPh_3$ ligands, which mixes in an antibonding manner with

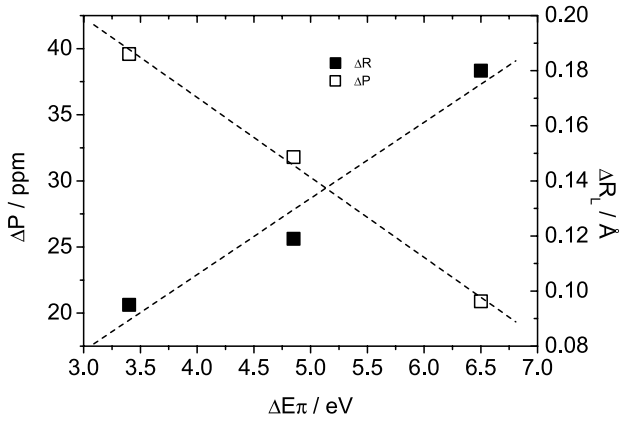


**Figure 3.** Plot of the energy, $\Delta E_\pi$, *versus* $\Delta P$ and $\Delta R$. Experimental uncertainties in bond distances are in the 0.01 Å range, in $^{31}P$ chemical shifts are 0.1 ppm, following the original reports. Uncertainties in $\Delta E_\pi$ are 0.03 eV. The dashed lines indicate the trend in the data.

the antisymmetric $b_2$ combination. The predicted amount of charge withdrawn from the $Pt(PPh_3)_2$ fragment by back-donation is greater for the tetracyanoethylene ligand in $[Pt(PPh_3)_2(\eta^2\text{-L})]$ complexes. The ethylene ligand removes approximately half the amount of tetracyanoethylene, whereas fullerene-60 withdraws an intermediate amount.

It is noteworthy that the XAS data are in good agreement with the results of a density functional theory calculation that has been performed on model complexes.[25] Theoretical procedures decompose part of the total binding energy of $[(PH_3)_2Pt(\eta^2\text{-L})]$ complexes into the orbital interaction term energy $E_{orb} = E_{A1} + E_{B2} + E_{B1}$. The energy contributions from the two synergistic bonding modes originate from stabilising interactions between occupied and virtual orbitals of separate $(PH_3)_2Pt$ and L fragments, corresponding to $\sigma$ donation ($E_{A1}$) and to $\pi$ back-donation ($\Delta E_t = E_{B2} + E_{B1}$).[26] The theoretical contribution of the sum of the d-hybrid orbitals, which are depopulated upon coordination, $\Delta E_t$, was plotted against the experimental $\Delta E_\pi$ in Figure 4.

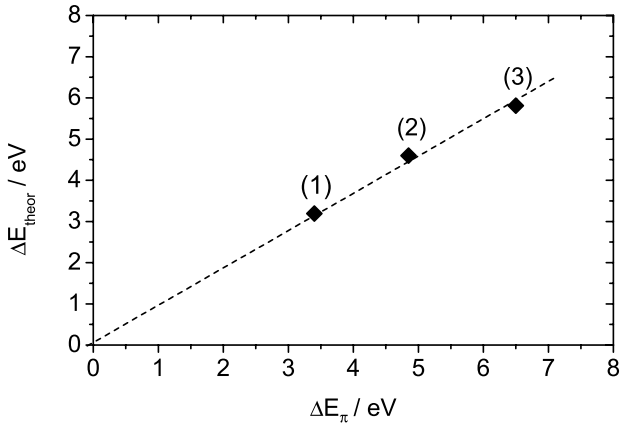


**Figure 4.** The relationship between $\Delta E_\pi$ and $\Delta E_{theor}$. Extrapolation of the line to the zero intercept indicates the trend in the data.

The convergence of the resulting line and the hypothetical zero point energy suggests that this point would fall in the line. Because $PH_3$ is used as model for $PPh_3$ in the $\Delta E_t$ calculation, the $\pi$-acceptor properties of the phosphine ligand are neglected. Energy values between the experimental $\Delta E_\pi$ and the theoretical $\Delta E_t$, which are smaller than 1 eV in Table 1, can be related to back-donation to the d orbital of the phosphorus atom.

## Experimental

### Preparation of complexes

The $[Pt(PPh_3)_2(\eta^2\text{-}C_2H_4)]$ (**1**),[27] $[Pt(PPh_3)_2(\eta^2\text{-}C_{60})]$ (**2**)[28] and $[Pt(PPh_3)_2\{\eta^2\text{-}C_2(CN)_4\}]$ (**3**)[29] complexes were synthesised as described elsewhere and stored under argon prior to use.

### X-ray absorption spectroscopy measurements and data analysis

The experimental spectra at the Pt $L_{2,3}$ edges were recorded at the National Synchrotron Light Laboratory (LNLS, Campinas, SP, Brazil), using the synchrotron radiation at an energy of 1.37 GeV with an average ring current of 120 mA. The Pt $L_{2,3}$-edge XAS spectra were measured on the XAFS I station equipped with a double crystal Si(220) monochromator in transmission mode and two silicon crystals that were slightly detuned to avoid higher harmonics. The XAS data were collected with a 1s accumulation time per point and an energy increment of 0.5 eV in transmission mode at room temperature by using two ionisation chambers filled with argon and measuring the incident (monitor) and transmitted (detector) beam intensity. The powder samples were pasted on a grid carved on a lead metal sheet and capped with Kapton tape. The spectrum of a 7.5 μm platinum metal foil was recorded before and after each XAS spectrum to check energy calibration. All spectra were normalised to unity in the continuum absorption across the absorption edges, such that the step heights coincide.

## Conclusions

Pt $L_{2,3}$ XAS proved to be a powerful quantitative tool for probing the energy of vacant d-orbitals in the triad of compounds $[Pt(PPh_3)_2(\eta^2\text{-L})]$ {L = $C_2H_4$, $C_{60}$, $C_2(CN)_4$}, determining the $d_\pi$-orbital interaction energy term and reinforcing the underlying concepts of the Dewar-Chatt-Duncanson model. The charge withdrawn in terms of energy from the $Pt(PPh_3)_2$ fragments to the alkene

ligands increases in the order $[Pt(PPh_3)_2(\eta^2\text{-}C_2H_4)]$ < $[Pt(PPh_3)_2(\eta^2\text{-}C_{60})]$ < $[Pt(PPh_3)_2(\eta^2\text{-}C_2(CN)_4)]$. It is important to note that for obtaining reliable data from the XAS spectra of organometallic compounds, it is more appropriate to employ the second derivative spectral decomposition than the absorption spectrum itself, due to the usually small changes in electronic density upon complex formation. Finally, the XAS data act as a good reference for the density functional theory data, showing that the differences in the entire binding energy resulting from the approximation of $PPh_3$ with $PH_3$ are not negligible.

## Acknowledgments

We thank the Fundação de Amparo à Pesquisa do Estado de São Paulo (FAPESP) for support of this research (grant 97/11567-7). This work was also partially supported by LNLS. Authors are grateful to an anonymous referee for valuable suggestions.

## References

1. Bianconi, A.; Garcia, J.; Benfatto, M.; *Top. Curr. Chem.* **1988**, *145*, 29; Bianconi, A. In *X-Ray Absorption: Principles, Applications, Techniques of EXAFS, SEXAFS and XANES*; Koningsberger, D. C.; Prins, R., eds.; Wiley: New York, 1988; Penner-Hahn, J. E.; *Coord. Chem. Rev*. **1999**, *192*, 1101.
2. Pantelouris, A.; Küper, G.; Hormes, J.; Feldmann, C.; Jansen, M.; *J. Am. Chem. Soc*. **1995**, *117,* 11749; Brown, M.; Peierls, R. E.; Stern, E. A.; *Phys. Rev. B: Condens. Matter Mater. Phys.* **1977**, *15*, 738; Hitchcock, A. P.; Wen, A. T.; Rühl, E.; *Chem. Phys*. **1990**, *147*, 51.
3. Richtmyer, F. K.; Barnes, S. W.; Ramberg, E.; *Phys. Rev.* **1934**, *46*, 843.
4. Ramaker, D. E.; Mojet, B. L.; Oostenbrink, M. T. G.; Miller, J. T.; Koningsberger, D. C.; *Phys. Chem. Chem. Phys.* **1999**, *1*, 2293.
5. Behrens, P.; Assmann, S.; Bilow, U.; Linke, C.; Jansen, M.; *Z. Anorg. Allg. Chem*. **1999**, *625*, 111; Behrens, P.; *Solid State Commun*. **1992**, *81*, 235; Naftel, S. J.; Bzowski, A.; Sham, T. K.; *J. Alloys Compd.* **1999**, *283*, 5; Drube, W.; Treusch, R.; Sham, T. K.; Bzowski, A.; Soldatov, A. V.; *Phys. Rev. B: Condens. Matter Mater. Phys.* **1998**, *58*, 6871; Jeon, Y.; Qi, B. Y.; Lu, F.; Croft, M.; *Phys. Rev. B: Condens. Matter Mater. Phys.* **1989**, *40*, 1538.
6. Dewar, M. J. S.; *Bull. Soc. Chim. Fr*. **1951**, *18*, C79; Chatt, J.; Duncanson, L. A.; *J. Chem. Soc*. **1953**, 2939.
7. Albright, T. A.; Hoffmann, R.; Thibeault, J. C.; Thorn, D. L.; *J. Am. Chem. Soc*. **1979**, *101*, 3801; Ziegler, T.; *Inorg. Chem*. **1985**, *24*, 1547; Morokuma, K.; Borden, W. T.; *J. Am. Chem. Soc*. **1991**, *113*, 1912; Nunzi, F.; Sgamellotti, A.; Re, N.; Floriani, C.; *J. Chem. Soc., Dalton Trans*. **1999**, 3487; Uddin, J.; Dapprich, S.; Frenking, G.; Yates, B. F.; *Organometallics* **1999**, *18*, 457.
8. Fujimoto, H.; Nakao, Y.; Fukui, K.; *J. Mol. Struct*. **1993**, *300*, 425; Koga, N.; Morokuma, K.; *Chem. Phys. Lett*. **1993**, *202*, 330; Lichtenberger, D. L.; Wright, L. L.; Gruhn, N. E.; Rempe, M. E.; *J. Organomet. Chem*. **1994**, *478*, 213; López, J. A.; Mealli, C.; *J. Organomet. Chem*. **1994**, *478*, 161; Nunzi, F.; Sgamellotti, A.; Re, N.; Floriani, C.; *Organometallics* **2000**, *19*, 1628; Craciun, R.; Vincent, A. J.; Shaughnessy, K. H.; Dixon, D. A.; *Inorg. Chem*. **2010**, *49*, 5546.
9. Li, J.; Schreckenbach, G.; Ziegler, T.; *Inorg. Chem*. **1995**, *34*, 3245.
10. $C_{60}$ is herein treated as an electron-deficient polyalkene.
11. Jeon, Y.; Chen, J.; Croft, M.; *Phys. Rev. B: Condens. Matter Mater. Phys.* **1994**, *50*, 6555; Benfield, R. E.; Grandjean, D.; Kröll, M.; Pugin, R.; Sawitowski, T.; Schmid, G.; *J. Phys. Chem. B* **2001**, *105*, 1961.
12. Outka, D. A.; Stöhr, J.; *J. Chem. Phys*. **1988**, *88*, 3539; Mansour, A. N.; Cook Jr., J. W.; Sayers, D. E.; *J. Phys. Chem*. **1984**, *88*, 2330.
13. Choy, J. -H.; Kim, D. -K.; Demazeau, G.; Jung, D. -Y.; *J. Phys. Chem*. **1994**, *98*, 6258.
14. Pease, D. M.; Fasihuddin, A.; Daniel, M.; Budnick, J. I.; *Ultramicroscopy* **2001**, *88*, 1.
15. Sham, T. K.; *Phys. Rev. B: Condens. Matter Mater. Phys.* **1985**, *31*, 1888; Sham, T. K.; *Solid State Commun*. **1987**, *64*, 1103; de Groot, F. M. F.; Hu, Z. W.; Lopez, M. F.; Kaindl, G.; Guillot, F.; Tronc, M.; *J. Chem. Phys.* **1994**, *101*, 6570.
16. Qi, B.; Perez, I.; Ansari, P. H.; Lu, F.; Croft, M.; *Phys. Rev. B: Condens. Matter Mater. Phys.* **1987**, *36*, 2972.
17. Sham, T. K.; *Phys. Rev. B: Condens. Matter Mater. Phys.* **1985**, *31*, 1903.
18. Lytle, F. W.; Greegor, R. B.; *Appl. Phys. Lett*. **1990**, *56*, 192; Wang, W. -C.; Chen, Y.; Hu, T. -D.; *Phys. Status Solidi B* **1994**, *186*, 545.
19. Costain, C. C.; Stoicheff, B. P.; *J. Chem. Phys*. **1959**, *30*, 777.
20. Fedurco, M.; Olmstead, M. M.; Fawcett, W. R.; *Inorg. Chem*. **1995**, *34*, 390.
21. Bekoe, D. A.; Trueblood, K. N.; *Z. Kristallogr*.**1960**, *113*, 1.
22. Asaro, F.; Lenarda, M.; Pellizer, G.; Storaro, L.; *Spectrochim. Acta, Part A* **2000**, *56*, 2167; Pellizer, G.; Graziani, M.; Lenarda, M.; *Polyhedron* **1983**, *2*, 657; Berger, S.; Braun, S.; Kalinnowski, H. -O.; *NMR Spectroscopy of the Non-Metallic Elements*; Wiley: Chichester, 1977, p. 709.
23. Cheng, P. -T.; Nyburg, S. C.; *Can. J. Chem*. **1972**, *50*, 912.
24. Bombieri, G.; Forselli, E.; Panattoni, C.; Graziani, R.; Bandoli, G.; *J. Chem. Soc. A* **1970**, 1313.
25. Karhánek, D.; Kacer, P.; Kuzma, M.; Splíchalová, J.; Cervený, L.; *J. Mol. Model*. **2007**, *13*, 1009.

26. Frenking, G.; Fröhlich, N.; *Chem. Rev*. **2000**, *100*, 717 and references therein.
27. Nagel, U.; *Chem. Ber*. **1982**, *115*, 1998.
28. Fagan, P. J.; Calabrese, J. C.; Malone, B.; *Science* **1991**, *252*, 1160.
29. Baddley, W. H.; Venanzi, L. M.; *Inorg. Chem*. **1966**, *5*, 33.

*Submitted: January 25, 2011*
*Published online: October 13, 2011*

**FAPESP has sponsored the publication of this article.**

Article

*J. Braz. Chem. Soc.*, Vol. 23, No. 1, 39-45, 2012.
Printed in Brazil - ©2012 Sociedade Brasileira de Química
0103 - 5053 $6.00+0.00

# Tributyltin in Crustacean Tissues: Analytical Performance and Validation of Method

***Joyce Cristale,[a,#] Dayana M. dos Santos,[b] Bruno S. Sant'Anna,[c] Daniela C. Sandron,[a] Sara Cardoso,[a] Alexander Turra[d] and Mary Rosa R. de Marchi*[,a]***

[a]*Department of Analytical Chemistry, Institute of Chemistry, São Paulo State University (UNESP), CP 355, 14800-900 Araraquara-SP, Brazil*

[b]*Department of Chemical and Geological Oceanography, Oceanographic Institute, University of São Paulo, 05508-900 São Paulo-SP, Brazil*

[c]*Department of Zoology, Institute of Biosciences, São Paulo State University (UNESP), 13506-900 Rio Claro-SP, Brazil*

[d]*Department of Biological Oceanography, Oceanographic Institute, University of São Paulo, 05508-120 São Paulo-SP, Brazil*

O ermitão *Clibanarius vittatus* é um organismo típico de regiões intertidais estuarinas sendo considerado um possível bioindicador da presença de tributilestanho (TBT) nesses ambientes. Por esta razão, este estudo apresenta o desempenho analítico e a validação do método para quantificação de TBT em tecidos de *C. vittatus* por cromatografia gasosa com detector fotométrico de chama pulsante (GC-PFPD), após extração com solvente apolar (tolueno) e derivatização com reagente de Grignard. Os limites de detecção do método (LOD) foram 2,0 e 2,8 ng $g^{-1}$ para TBT e DBT (dibutil estanho), respectivamente, e seus limites de quantificação (LOQ) 6,6 e 8,9 ng $g^{-1}$ para TBT e DBT, respectivamente. O método foi aplicado em amostras do Estuário de Santos, Estado de São Paulo, Brasil. As concentrações de TBT e DBT variaram de 26,7-175,0 ng $g^{-1}$ a 46,2-156,0 ng $g^{-1}$, respectivamente. As concentrações encontradas saopreocupantes uma vez que efeitos tóxicos (tais como a alteração endócrina) têm sido relatados em outros organismos, mesmo em níveis inferiores aos registrados no presente estudo.

The hermit crab *Clibanarius vittatus* is a typical organism from intertidal regions being considered as a good bioindicator of tributyltin presence at these environments. Thus this study presents the analytical performance and validation method for TBT quantification in tissues of *C. vittatus* by gas chromatography with pulsed flame photometric detector (GC-PFPD) after extraction with an apolar solvent (toluene) and Grignard derivatization. The limits of detection of the method (LOD) were 2.0 and 2.8 ng $g^{-1}$ for TBT and DBT (dibutyltin), respectively, and its limits of quantification (LOQ) were 6.6 and 8.9 ng $g^{-1}$ for TBT and DBT, respectively. The method was applied to samples from Santos Estuary, São Paulo State, Brazil. TBT and DBT concentrations ranged from 26.7 to 175.0 ng $g^{-1}$ and from 46.2 to 156.0 ng $g^{-1}$, respectively. These concentrations are worrisome since toxic effects (such as endocrine disruption) have been reported for other organisms even under lower levels of registred at this study.

**Keywords:** crustaceans, organotin, tributyltin (TBT), gas chromatography

## Introduction

Butyltin compounds (BTs), members of the class of organometallic contaminants, are found in coastal regions worldwide because they were used in antifouling paints for many years.[1-3] In spite of the total worldwide ban proposed by the International Maritime Organization (IMO) in January 2008, these compounds are still found in different environmental compartments of aquatic systems.[4] Their toxic effects are observed in many species because tributyltin (TBT) can induce an endocrine disruption process known as imposex.[5] This effect in mollusks has been well documented.[6-8] Other effects caused by TBT include shell malformation in the Pacific oyster *Crassostrea gigas*, suppressed

*e-mail: mssqam@iq.unesp.br
[#]Current address: Department of Environmental Chemistry, IDAEA-CSIC, Jordi Girona 18-26, 08034 Barcelona, Catalonia, Spain

growth in the centric diatoms *Skeletonema costatum* and *Thalassiosira pseudonana* and increased mortality in the sabellid *Sabellastarte sanctijosephi*, among other marine organisms affected.[9]

Considering many studies involving abiotic matrices, only few works have quantified organotin compounds in the biota. This is mainly a result of the lack of appropriate analytical methods for these complex matrices. Methods for analysis of BTs have been developed for mollusks[9] and for vertebrates, such as fish and dolphins.[10,11] In crustaceans, besides the observed toxicity in contaminated areas where imposex is detected, there are few published reports for analysis of BTs in these organisms and none involving estuarine hermit crabs.[12] Hermit crabs commonly inhabit coastal and estuarine regions near sources of BT contamination, such as harbors.[13,14] They are scavengers, consuming both dead animals and algae, and have relatively restricted mobility.[15] For these reasons, hermit crabs may be a more accurate sentinel organism than the predatory marine mollusks, the highly mobile fish and other crustaceans that are generally used as environmental indicators of this kind of pollution.

In consequence of the low environmental concentrations of BTs, analytical approaches need to be refined in order to develop methods with high recovery and accuracy. Most studies analyzing BTs used gas chromatography with flame photometric detection (GC-FPD)[10,16] and gas chromatography coupled to tandem mass spectrometry (GC-MS/MS).[17-19] In Brazil, some recent studies have used gas chromatography with pulsed flame photometric detection (GC-PFPD) to analyze BTs in both biotic and abiotic samples.[4,20-22] For analysis of BTs by GC, it is necessary a derivatization step, for which the main used agents are Grignard reagent and sodium tetraethylborate.[2,23,24] In addition to the derivatization, the analytical procedure involves extraction using an apolar solvent (hexane or toluene) and a clean-up step using Florisil and silica.[21] In order to develop a safe and reliable method, validation procedures are necessary.[25] The validation process involves the use of certified reference materials to evaluate the accuracy and precision of the method, as well as the limits of detection (LOD) and quantification (LOQ) of the procedure.

For crustaceans, Guérin *et al.*[12] proposed a method using $NaBEt_4$. However, in Brazil, it is difficult to obtain this reagent because it is not authorized to be transported overland. An alternative for such studies is an adaptation of the used method by Limaverde *et al.*[20] for mollusks, which uses Grignard reagent. Another study[16] successfully used Grignard reagent for analysis of BTs in mussel tissues. Therefore, we aimed to develop a method for the determination of TBT in hermit-crab tissues using Grignard reagent as a derivatizating agent, with the western-Atlantic hermit crab *Clibanarius vittatus* as a biological model.

## Experimental

### Chemicals

TBT (96% tributyltin chloride), DBT (96% dibutyltin dichloride), MBT (95% monobutyltin trichloride), TPrT as surrogate (98% tripropyltin chloride) and TeBT as internal standard (96% tetrabutyltin) were purchased from Sigma-Aldrich (Milwaukee, WI, USA), as well as neutral aluminum oxide and Grignard reagent (2 mol $L^{-1}$ pentyl magnesium bromide in diethyl ether). Methanol, hydrochloric acid, sulfuric acid, sodium hydroxide and anhydrous sodium sulfate were purchased from JT Baker (Xalostoc, Mexico). Hexane and toluene were acquired from Mallinckrodt (Xalostoc, Mexico). Ammonium pyrrolidine dithiocarbamate (98% APDC) was purchased from Fluka (St. Gallen, Switzerland). The certified reference material ERM-CE477 (mussel tissue) was purchased from European Reference Materials.

The butyltin chloride stock solutions were prepared in hexane at concentrations of 5 μg $mL^{-1}$ (MBT), 6 μg $mL^{-1}$ (DBT) and 4 μg $mL^{-1}$ (TBT). Working standard solutions were obtained by dilution of stock solutions and were used for a one-month period.

### Apparatus

Extracts were analyzed by gas chromatography: Varian 3800 (Walnut Creek, CA, USA) equipped with a pulsed flame photometric detector (PFPD) using a tin filter (390 nm) and a VF5 capillary column (30 m × 0.25 mm; Varian, Walnut Creek, CA, USA) using an initial temperature program at 50 °C (hold for 0.50 min), followed by a ramp at 15 °C $min^{-1}$ until 170 °C and then at 10 °C $min^{-1}$ until 280 °C, remaining for 0.50 min. The injector and detector temperatures were 250 and 300 °C, respectively. The injection volume was 2 μL (splitless, 1 min) and the carrier gas (hydrogen) was used at a flow rate of 1.7 mL $min^{-1}$. Since the PFPD response is closely dependent on several detector parameters, the optimization of the conditions for BT analysis included a purge flow closed for 60 s.[21] Chromatograms and area values were calculated by means of Varian Star 5.5 software.

### Sample collection and preparation

Twenty hermit crabs were used for the validation of the method. The crabs were captured by hand during low

tide on Pescadores Beach (23º 58' 21'' S; 46º 23' 35'' W) in the São Vicente Estuary. A pool of these organisms was used in the BT recovery study and in the determination of the limits of detection of the method (LOD).

The used crabs to apply the method were collected at three locations (location 1: 23° 59' 27.8'' S and 46° 18' 15.2'' W, location 2: 23° 59' 13.9'' S and 46° 17' 39.8'' W and location 3: 23° 55' 53.6'' S and 46° 18' 19.4'' W) in Santos Estuary, Southeastern Brazil in São Paulo State. At each of these locations, 15 hermit crabs were collected and pooled in three groups of five crabs to provide a triplicate analysis for each sampling site.

In the laboratory, the specimens were identified according to Melo[26] and stored frozen until analysis. After the hermit crabs were removed from their shells, the dorsal portion of the abdomen was dissected and the gonads and digestive gland were removed, forming a pool of several specimens of *C. vittatus* from each location for the chemical analysis. This pool was stored in aluminum containers at −20 ºC until analysis. Prior to sample processing, each pool was homogenized by vortex.

### Butyltin extraction

The tissue extraction is a modification of the proposed method by Limaverde *et al.*[20] for organotin extractions in mussel tissue. The extraction was performed by adding 3.5 mL of hydrochloric acid and 5 mL of methanol, homogenizing in vortex for 1 min for digestion. After 10 min rest, 1 g of sodium chloride was added to saturate the solution (salting-out effect). The extraction was performed with toluene, replacing ethyl ether-hexane proposed by Limaverde *et al.*[20] A volume of 8 mL of toluene was added, followed by vortex agitation for 1 and 10 min of extraction in an ultrasonic bath, and then centrifugation for 5 min at 2000 rpm. This procedure was repeated three times, and the combined extracts were transferred to a separation funnel, where 10 mL APDC (0.1% v/v in water) was added to complex the TBT and to reduce its water solubility. Then, the organic phase was dried by passing through anhydrous sodium sulfate and transferred to a pear-shaped flask, for concentration in a rotary evaporator (40-50 ºC) to 2 mL. The BT standards have low volatility, so these standards were derivatized with Grignard reagent, following a derivatization method for TBT analysis in sediment samples by GC-PFPD, as reported in other studies on organotin analysis in Brazilian marine sediments.[4,21,27,28] For derivatization, 3 mL of Grignard reagent were added to 2 mL of the concentrated extract. The reaction was stopped after 20 min by adding 20 mL of ultrapure water, in an ice bath. Following solubilization of the white precipitate with a few drops of sulfuric acid, the solution was transferred to a separation funnel and the aqueous phase was discarded. The organic phase was then reconcentrated to 2 mL, dried with sodium sulfate and passed through an aluminum oxide (1 g) column for clean-up with hexane as eluent (6 mL). Final extracts were again concentrated to 0.1 mL with $N_2$ and then TeBT corresponding to 1000 ng $mL^{-1}$ was added as an internal standard (IS).

### Validation of the method

The limits of instrumental detection (iLOD) were experimentally obtained by injecting standard dilutions until the compounds cannot be detected. The standard solutions were submitted to a derivatization step (previously described) before injection into the GC system. The limits of instrumental quantification (iLOQ) and the linear interval were obtained by a linearity curve according to the Huber test.[29] For the determination of the linear interval, it was calculated the area/concentration (A/C) ratios for each compound at each level of the calibration and determined the median (md) of these values. Then, it was calculated the difference between the A/C and the md, and the median of these differences (mad) was determined. The confidence interval (IC) was obtained by multiplying the mad by a constant that varies from 2 to 8. This factor gives the width of the confidence interval, and lower values result in narrower intervals. Thus, for narrower data dispersion, the number 3 is chosen as this factor. A/C values which were above or below this confidence interval were rejected. The first value within this interval was considered to be the iLOQ. The iLOD and iLOQ were also determined for MBT and DBT.

Spiked samples were used for the BT recovery studies and to determine the limits of detection and quantification of the method. 1 g portions from a pool of 20 organisms were used for spiking. From the same pool of 20 organisms, three 1 g samples were analyzed and the found amounts of TBT, DBT and MBT in these samples were subtracted from the results for the spiked samples.

For the recovery study, samples spiked with 66, 89 and 82 ng $g^{-1}$ of TBT, DBT and MBT, respectively, were used. The LOD and LOQ were determined using a sample spiked with 6.6, 8.9 and 33 ng $g^{-1}$ for TBT, DBT and MBT, respectively. The LOD was determined as 3 times of the signal/noise ratio that was obtained by the injection of the spiked sample extract. The LOQ was the smallest amount of the extracted TBT from spiked samples that could be detected and quantified with a recovery higher than 60% and a relative standard deviation (RSD) less than 20%.

The accuracy of the method was determined using 250 mg of the certified reference material (mussel tissue, ERM- CE477, EC-JRC-IRMM, Geel, Belgium), following the described butyltin extraction procedure in the previous section. The certified amounts of TBT, DBT and MBT in the CRM were 2.20 ± 0.19, 1.54 ± 0.12 and 1.5 ± 0.28 mg $kg^{-1}$, respectively.

## Results and Discussion

### Validation of the method

The standard solutions were submitted to a derivatization step before injection into the GC system. A study of the linearity was performed to define the linear interval and the iLOQ for the GC-PFPD system, using the linearity curve according to the Huber test (previously described). Table 1 shows the obtained values of iLOD, iLOQ, linear equation, linear interval and linear regression ($r^2$).

TBT, DBT and MBT were detected and measured in the pool of 20 crabs that were used for the recovery study and for the LOD and LOQ determinations. Three 1 g portions of this pool were analyzed, and the amounts of TBT and DBT in these samples (non-spiked) were 18.6 ng $g^{-1}$ with a RSD of 20% and 18.9 ng $g^{-1}$ with a RSD of 18%, respectively. MBT was not quantified in these samples because the obtained results were unsatisfactory for this compound, as discussed below. The chromatograms for the spiked and non-spiked samples are shown in Figure 1. These amounts were subtracted from the obtained values in the recoveries.

The obtained LOD was 2.0 ng $g^{-1}$ tissue for TBT and 2.8 ng $g^{-1}$ for DBT. In the recovery study, the spiked samples at 66 ng $g^{-1}$ for TBT, 89 ng $g^{-1}$ for DBT and 82 ng $g^{-1}$ for MBT were used, and the recoveries for TBT, DBT and MBT were 97 ± 12%, 107 ± 2% and 92 ± 8%, respectively. The mean recovery of the spiked samples (n = 3) at the level of 6.6 ng $g^{-1}$ tissue for TBT was 62 ± 12%. For DBT

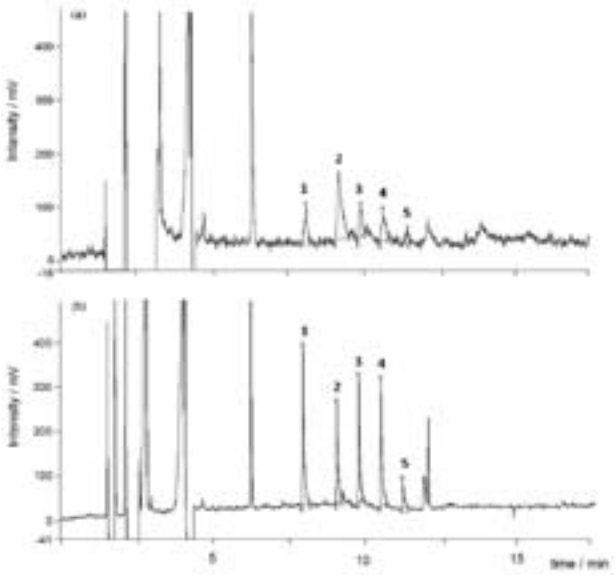

**Figure 1**. Gas chromatograms of (a) testimony and (b) spiked samples: (1) TPrT (surrogate), (2) TeBT (internal standard), (3) TBT, (4) DBT and (5) MBT obtained by GC-PFPD analysis.

(4.4 ng $g^{-1}$ tissue), the recovery from these spiked samples was acceptable (79 ± 11%), whereas for MBT (33 ng $g^{-1}$ tissue) the recovery was unacceptable (10 ± 3%). For TBT and DBT, 6.6 and 4.4 ng $g^{-1}$ were considered as the LOQ, respectively. Table 2 summarizes the obtained results for TBT, DBT and MBT in the method-validation study.

For the evaluation of the accuracy and precision of the method, it was used 250 mg of ERM-CE477 (mussel tissue). The TBT results for the certified reference material (n = 3) were similar to those for the spiked samples (Table 2), with mean recoveries of 98 ± 12%. The recoveries of DBT and MBT were 61 ± 18% and 32 ± 6%, respectively. Because of the unacceptable results that were obtained for MBT at low concentrations in the spiked samples and in the reference material, only TBT and DBT were quantified in the mussel samples, as discussed below. In this study, toluene was used as the extraction solvent, replacing ethyl

**Table 1.** Analytical curve parameters and limits of instrumental detection (iLOD) and instrumental quantification (iLOQ) for the GC/PFPD system for organotin compounds. Values expressed as mass injected into the GC system

| Compound | iLOD / pg | iLOQ / pg | Linear equation | Linear interval / pg | Linear regression ($r^2$) |
|---|---|---|---|---|---|
| TBT | 33 | 66 | y = 0.0009x + 0.0565 | 66-1320 | 0.9398 |
| | | | y = 0.0008x + 0.2823 | 1320-14784 | 0.9693 |
| DBT | 44 | 396 | y = 0.0007x + 0.0208 | 396-1980 | 0.9990 |
| | | | y = 0.0007x + 0.2123 | 1980-22176 | 0.9837 |
| MBT | 165 | 660 | y = 0.0002x – 0.0249 | 660-2310 | 0.9505 |
| | | | y = 0.0011x – 1.1971 | 1980-18480 | 0.9822 |
| TPrT[a] | 41 | 168 | y = 0.001x + 0.0203 | 168-1650 | 0.9656 |
| | | | y = 0.0005x + 0.6479 | 1650-2310 | 0.9344 |

[a]Used as surrogate.

**Table 2.** Summary data for the TBT, DBT and MBT method validation processes for hermit crab (*Clibanarius vittatus)* tissues

| Recovery study | | LOQ study | | Accuracy and precision | |
|---|---|---|---|---|---|
| Spiked samples (n = 3) | | Spiked samples (n = 3) | | Reference material[a] (n = 3) | |
| TBT mass added / (ng $g^{-1}$ tissue) | TBT recovery / % | TBT mass added / (ng $g^{-1}$ tissue) | TBT recovery / % | TBT certified value / (mg $kg^{-1}$ tissue) | TBT recovery / % |
| 66 | 97 ± 12 | 6.6[b] | 62 ± 12 | 2.20 ± 0.19 | 98 ± 12 |
| DBT mass added / (ng $g^{-1}$ tissue) | DBT recovery / % | DBT mass added / (ng $g^{-1}$ tissue) | DBT recovery / % | DBT certified value / (mg $kg^{-1}$ tissue) | DBT recovery / % |
| 89 | 107 ± 2 | 4.4[b] | 79 ± 11 | 1.54 ± 0.12 | 61 ± 18 |
| MBT mass added / (ng $g^{-1}$ tissue) | MBT recovery / % | MBT mass added / (ng $g^{-1}$ tissue) | MBT recovery / % | MBT certified value / (mg $kg^{-1}$ tissue) | MBT recovery / % |
| 82 | 92 ± 8 | 33 | 10 ± 3 | 1.5 ± 0.28 | 32 ± 6 |

[a]ERM-CE477 (mussel tissue); [b]accepted values as limit of quantification of the method (LOQ).

ether-hexane as proposed by Limaverde *et al.*[20] This led to better recovery results, with an increase from 30% to 98 ± 12% for TBT from the ERM-CE477.

Table 3 compares the results that were obtained in this study and those obtained for TBT analyses in other organisms by other authors, showing results comparable to those obtained in this study. The proposed method proved to be suitable for the analyzed samples in this study, as described below. The LOQ could not be compared with other studies because of the lack of this information in the published data. BT levels in a crustacean that were analyzed by GC-FPD and derivatized with Grignard reagent were previously reported.[30] The authors proposed a method involving the addition of Grignard reagent to the mussel extract and shaking for 1 h under controlled temperature at 40 °C. In this study, the reaction time for TBT analysis in the hermit crab *Clibanarius vitattus* was 20 min at ambient temperature. Another advantage of this method is the use of aluminum oxide for clean-up. This is less expensive than Florisil, which is used by many authors for biotic samples.[17,30,31] This method resulted in clean extracts, with good reproducibility (RSD < 20%) and the use of GC-PFPD can contribute for the major sensitivity and selectivity of organotin compounds in complex environmental matrices by using a tin filter.

**Table 3.** Data for TBT in different biotic matrices, taken from literature references and the present study

| Organism | Sample treatment | Analytical system | LOD | Reference |
|---|---|---|---|---|
| *Nassarius nitidus* (mollusk) | extraction: hexane<br>derivatization: Grignard reagent (methyl magnesium bromide)<br>clean-up: Florisil | GC-MS/MS | 4 ng Sn $g^{-1}$ (TBT) | 17 |
| *Stramonita haemastoma* (mollusk) | extraction: hexane<br>derivatization: Grignard reagent (pentyl magnesium bromide)<br>clean-up: silica | GC-PFPD | 0.39 ng Sn $g^{-1}$ (TBT) | 20 |
| *Thais clavigera* (mollusk) | extraction: acetone<br>derivatization: Grignard reagent (n-propyl magnesium bromide)<br>clean-up: Florisil | GC-FPD | 0.02-0.05 ng $g^{-1}$ (MBT, DBT and TBT) | 31 |
| Crustaceans (shrimp, crab, lobster) | extraction: acetic acid<br>derivatization: NaBEt4 | GC-AES | 0.08 ng Sn $g^{-1}$ (TBT) | 12 |
| *Caprella* spp. (crustacean) | extraction: 0.1% v/v tropolone-acetone<br>derivatization: Grignard reagent (n-propyl magnesium bromide)<br>clean-up: Florisil | GC-FPD | 2.0, 1.0 and 0.5 ng $g^{-1}$ (MBT, DBD and TBT) | 30 |
| *Clibanarius vittatus* (crustacean) | extraction: toluene<br>derivatization: Grignard reagent (pentyl magnesium bromide)<br>clean-up: aluminum oxide | GC-PFPD | 2 and 2.8 ng $g^{-1}$ (TBT and DBT)* | this study |

* equivalent to 0.8 ng Sn $g^{-1}$ for TBT and 1.4 ng Sn $g^{-1}$ for DBT.

### Application of the method

Following the validation procedure, the method was applied to the collected samples in Santos Estuary, where the largest harbor in Brazil is located. In addition to the presence of this harbor, the area is also heavily impacted by industrial and urban contaminants. In a previous study,[21] organotin contamination was detected in surface sediments, with a mean concentration of 482 ng Sn $g^{-1}$ dry weight (1205 ng $g^{-1}$ dry weight) for TBT. Based on these data, organisms from this region are suitable for assessments of toxicological risk. Application of this method to hermit crabs can help to understand how this contamination may affect the biota.

The proposed method showed to be suitable for the samples, and TBT and DBT were quantified in all the analyzed samples. The TBT and DBT quantities in the samples were similar among the studied areas, with concentrations ranging from 26.7 to 175 ng $g^{-1}$ for TBT and from 46.2 to 156 ng $g^{-1}$ for DBT. The results of the TBT quantification of these samples are shown in Table 4.

**Table 4.** TBT and DBT data for tissues of hermit crabs collected at three sites in the Santos estuary, southeastern Brazil. Three sample pools (five crabs) from each site were analyzed. The values are expressed as ng $g^{-1}$ wet tissue

| Site | TBT range (n = 3) (ng $g^{-1}$) | DBT range (n = 3) (ng $g^{-1}$) |
|---|---|---|
| 1 | 26.7-155 | 61.4-110 |
| 2 | 103-147 | 46.2-156 |
| 3 | 72.0-175 | 56.4-120 |

Although MBT was detected in the samples, it was not possible to quantify it because the validation procedure was not completed for this compound. Therefore, the comparison between the amounts of TBT and degradation products was made only with DBT. In sediments, it is common to determine the degradation index (which helps to determine if the contamination is recent or old) from the ratio of TBT to DBT + MBT.[32] However, for living organisms, this determination is not applicable because the degradation compounds can be directly assimilated from the abiotic/biotic source.

The lack of data for organotin in the sediment, which was sampled at the same time as the hermit-crab samples, makes difficult the discussion of the assimilation index. However, as in other studies, the amount of bioaccumulation appeared to be similar for these organisms, even in different sampling areas. Abiotic factors including tides, currents, oxyreduction state and salinity, which are frequently used for interpretation of BTs in sediments, are not related to the concentrations of these compounds in organisms. However, data for lipid content, maturation stage and sex could help to interpret the results.

TBT is the most important BT, since it has strong toxic effects. It can accumulate more in animals at lower trophic levels because they have a poor capacity to degrade this compound.[33] The results of this study can be compared with those obtained by Limaverde *et al.*[20] using the gastropod *Stramonita haemastoma* and the bivalve *Perna perna* as bioindicators, with TBT concentrations ranging from < LOD to 62 ng Sn $g^{-1}$ (155 ng TBT $g^{-1}$) for *S. haemastoma* and < LOD to 110 ng Sn $g^{-1}$ (275 ng TBT $g^{-1}$) for *P. perna.* For crustaceans, Takeuchi *et al.*[30] quantified TBT in amphipods (*Caprella* spp.) with a mean TBT concentration of 32 ng $g^{-1}$.

The wide range of concentrations that were found in samples from the same site may be related to different rates of assimilation of this pollutant by organisms, or to their different maturation stages. However, although it was variable, even the lowest concentration of recorded TBT in the study area (26.7 ng $g^{-1}$ wet weight) can cause toxic effects in organisms,[1] since concentrations of 1 ng $g^{-1}$ are usually sufficient to produce these effects.[2] In some cases the effects can be irreversible or even lethal.

## Conclusions

A method was developed for analysis of TBT and DBT (degradation product) in tissues of *Clibanarius vittatus*. This is the first method that is reported for the determination of organotins in this group of crustaceans. The studies of accuracy and precision were carried out with certified reference material and spiked samples. Good results were obtained, with recoveries higher than 60% and RSD lower than 20%. The method proved to be appropriate for TBT and DBT determination in samples from Pescadores Beach (São Paulo State, Brazil). It was possible to quantify these compounds in all samples, and TBT was recorded at concentrations that may cause toxic effects in the biota.

## Acknowledgements

Fundação de Amparo à Pesquisa do Estado de São Paulo (FAPESP, Grant 2006/57007-3) and scholarship to B. S. S. (Grant 2006/61589-8)), Conselho Nacional de Desenvolvimento Científico e Tecnológico (CNPq, research scholarship to A. T., Grant 301240/2006-0, and undergraduate scholarship to S. C. S. and D. C. S.), Fundação de Apoio à Ciência, Tecnologia e Educação (FACTE). Dr. Janet W. Reid revised the English text.

## References


1. Fent, K.; *Toxicol. Lett.* **2003**, *140*, 353.
2. Hoch, M.; *Appl. Geochem.* **2001**, *16*, 719.
3. Antizar-Ladislao, B.; *Environ. Int.* **2008**, *34*, 292.
4. Santos, D. M.; Araújo, I. P.; Machado, E. C.; Carvalho-Filho, M. A. S.; Fernandez, M. A.; Marchi, M. R. R.; Godoi, A. F. L.; *Mar. Pollut. Bull.* **2009**, *58*, 1926.
5. Cao, D.; Jiang, G.; Zhou, Q.; Yang, R.; *J. Environ. Manage.* **2009**, *90*, S16.
6. Gibbs, P. E.; Bryan, G. W.; Pascoe, P. L.; *Mar. Environ. Res.* **1991**, *32*, 79.
7. Bettin, C.; Oehlmann, J.; Stroben, E.; *Helgolander Meeresuntersuchungen* **1997**, *50*, 299.
8. Oehlmann, J.; Fioroni, P.; Stroben, E.; Markert, B.; *Sci. Total Environ.* **1996**, *188*, 205.
9. Bryan, G. W.; Gibbs, P. E.; Newman, M. C.; McIntosh, A. W.; *Metal Ecotoxicology: Concepts & Applications*; Lewis Publishers: Michigan, 1991, p. 323.
10. Kannan, K.; Corsolini, S.; Focardi, S.; Tanabe, S.; Tatsukawa, R.; *Arch. Environ. Con. Tox.* **1996**, *31*, 19.
11. Dorneles, P. R.; Lailson-Brito, J.; Fernandez, M. A. S.; Vidal, L. G.; Barbosa, L. A.; Azevedo, A. F.; Fragoso, A. B. L.; Torres, J. P. M. O.; *Environ Pollut.* **2008**, *156*, 1268.
12. Guérin, T.; Sirot, V.; Volatier, J. L.; Leblanc, J. C.; *Sci. Total Environ.* **2007**, *388*, 66.
13. Turra, A.; *J. Mar. Biol. Assoc. U. K.* **2004**, *84*, 757.
14. Sant'anna, B. S.; Reigada, Á. L. D.; Pinheiro, M. A. A.; *J. Mar. Biol. Assoc. U. K.* **2009**, *89*, 761.
15. Hazlett, B. A.; *Annu. Rev. Ecol. Syst.* **1981**, *12*, 1.
16. Horiguchi, T.; Li, Z.; Uno, S.; Shimizu, M.; Shiraishi, H.; Morita, M.; Thompson, J. A. J.; Levings, C. D.; *Mar. Environ. Res.* **2004**, *57*, 75.
17. Berto, D.; Giani, M.; Boscolo, R.; Covelli, S.; Giovanardi, O.; Massironi, M.; Grassia, L.; *Mar. Pollut. Bull.* **2007**, *55*, 425.
18. Boscolo, R.; Cacciatore, F.; Berto, D.; Marin, M. G.; Giani, M.; *Appl. Organomet. Chem.* **2004**, *18*, 614.
19. Rato, M.; Gaspar, M. B.; Takahashi, S.; Yano, S.; Tanabe, S.; Barroso, C.; *Mar. Pollut. Bull.* **2008**, *56*, 1323.
20. Limaverde, A. M.; Wagener, A. L. R.; Fernandez, M. A.; Scofield, A. L.; Coutinho, R.; *Mar. Environ. Res.* **2007**, *64*, 384.
21. Godoi, A. F. L.; Favoreto, R.; Santiago-Silva, M.; *Quim. Nova* **2003**, *26*, 708.
22. Felizzola, J. F.; Wagener, A. D. L. R.; Almeida, A. C.; Wie, O. L.; *Quim. Nova* **2008**, *31*, 89.
23. Morabito, R.; Massanisso, P.; Quevauviller, P.; *TrAC, Trends Anal. Chem.* **2000**, *19*, 113.
24. Cassi, R.; Tolosa, I.; Bartocci, J.; de Mora, S.; *Appl. Organomet. Chem.* **2002**, *16*, 355.
25. http://www.eurachem.org/guides/pdf/valid.pdf accessed in December 2010.
26. Melo, G. A. S.; *Manual de Identificação dos Crustacea Decapoda do Litoral Brasileiro: Anomura, Thalassinidea, Palinuridea, Astacidea*; Plêiade: São Paulo, Brasil, 1999.
27. de Oliveira, C. R.; dos Santos, D.; Madureira, L. A. S.; de Marchi, M. R. R.; *J. Hazard. Mater.* **2010**, *181*, 851.
28. Santos, D. M. D.; Sant'Anna, B. S.; Sandron, D. C.; de Souza, S. C.; Cristale, J.; Marchi, M. R. R. D.; Turra, A.; *Estuar. Coast. Shelf S.* **2010**, *88*, 322.
29. Huber, L.; *LC GC Eur.* **1998**, *11*, 96.
30. Takeuchi, I.; Takahashi, S.; Tanabe, S.; Miyazaki, N.; *Mar. Environ. Res.* **2004**, *57*, 397.
31. Leung, K. M. Y.; Kwong, R. P. Y.; Ng, W. C.; Horiguchi, T.; Qiu, J. W.; Yang, R.; Song, M.; Jiang, G.; Zheng, G. J.; Lam, P. K. S.; *Chemosphere* **2006**, *65*, 922.
32. Díez, S.; Ábalos, M.; Bayona, J. M.; *Water Res.* **2002**, *36*, 905.
33. Godoi, A. F. L.; Favoreto, R.; Santiago-Silva, M.; *Quim. Nova* **2003**, *26*, 708.


*Submitted: May 22, 2011*
*Published online: October 13, 2011*

**FAPESP has sponsored the publication of this article.**

*J. Braz. Chem. Soc.*, Vol. 23, No. 1, 46-56, 2012.
Printed in Brazil - ©2012 Sociedade Brasileira de Química
0103 - 5053 $6.00+0.00

Article

# Layered Metal Laurates as Active Catalysts in the Methyl/Ethyl Esterification Reactions of Lauric Acid

***Fábio da Silva Lisboa,[a] José Eduardo F. da Costa Gardolinski,[b] Claudiney S. Cordeiro[a] and Fernando Wypych*[,a]***

*[a]Centro de Pesquisas em Química Aplicada (CEPESQ), Departamento de Química, CP 19081 and [b]Laboratório de Análise de Minerais e Rochas (LAMIR), Departamento de Geologia, CP 19062, Universidade Federal do Paraná, 81531-980 Curitiba-PR, Brazil*

No presente trabalho são reportadas as sínteses, caracterizações e investigações das atividades catalíticas de lauratos lamelares de cobre(II), manganês(II), lantânio(III) e níquel(II) nas reações de esterificação metílica e etílica do ácido láurico. Nas reações de esterificação metílica, conversões entre 80 e 90% foram observadas para todos os catalisadores, ao passo que, para a esterificação etílica, somente o laurato de manganês mostrou atividade catalítica razoável, com conversões próximas de 75%. Reações de reuso dos lauratos de cobre e lantânio em três ciclos de reação foram investigadas; nelas, ambos os catalisadores preservaram a sua estrutura e mantiveram a atividade catalítica próxima daquela observada para o primeiro ciclo de reação.

In this work we report the synthesis, characterization and investigation of the catalytic activity of layered copper(II), manganese(II), lanthanum(III) and nickel(II) laurates in the methyl and ethyl esterification reactions of lauric acid. In the methyl esterification, conversions between 80 and 90% were observed for all catalysts, while for the ethyl esterification only manganese laurate showed reasonable catalytic activity, with conversions close to 75%. Reuse of copper and lanthanum laurates in three cycles of reaction was also investigated and both catalysts preserved the structure and retained catalytic activity close to that observed for the first reaction cycle.

**Keywords**: metal carboxylates, layered laurates, biodiesel, lauric acid esterification

## Introduction

There has been much recent discussion regarding alternative sources of energy to replace fossil fuels derived from petroleum. One such alternative is the biodiesel,[1] which is usually obtained through transesterification of vegetable oils and animal fats or esterification of free fatty acids (FFA).[2] In both processes, a catalyst needs to be used. Sodium or potassium methoxide or their precursors (sodium or potassium hydroxide) are currently used for the transesterification reactions and inorganic acids are used for the esterification process.[3]

In transesterification reactions, sodium hydroxide is one of the most common homogeneous catalytic precursors due to its low cost. During homogeneous catalysis, many steps are necessary to produce biodiesel and, as a consequence, the price of the final product increases. This process has many disadvantages, both from economic and ecological standpoints, which can be briefly summarized as: (*i*) it is conducted in batch reactors that limit the large scale production; (*ii*) the catalyst needs to be neutralized and cannot be recovered for reuse; (*iii*) inorganic salts are formed and need to be washed out from the fatty acid methyl esters; (*iv*) soaps are formed when the raw material has some acidity, lowering the reaction yield and inhibiting the separation of the esters from glycerol (a byproduct of the transesterification reaction); (*v*) contaminated glycerine is obtained; (*vi*) the water formed during the saponification reaction retards the transesterification reaction by hydrolysis; (*vii*) the alkaline medium is very aggressive to the equipment, just to cite some drawbacks.

A way to minimize the costs of these processes is to use catalysts that can operate in heterogeneous media, such as transition metal oxides, zeolites and ionic exchange resins, among others. The biodiesel market is expected to grow rapidly due to the environmental benefits and

*e-mail: wypych@ufpr.br

government directives that will come into effect in the near future. Increasing biodiesel consumption requires optimized production processes, simplified operations, high reaction yields and high purity products. Low-cost solid heterogeneous catalysts can help solving some of these problems.

When zinc hydroxide nitrate ($Zn_5(OH)_8(NO_3)_2{\cdot}2H_2O$) was used as catalyst in the methyl/ethyl transterification reaction of soybean or palm oil and esterification of commercial lauric acid, zinc hydroxide nitrate was transformed into zinc carboxylate.[4] This was observed during isolation of the solid after the esterification reactions. Zinc carboxylate was then synthesized and tested, showing to be very active in the production of alkyl monoesters, which were obtained by the esterification reactions of fatty acids and/or transesterification of triacylglycerols (triglycerides).

Similar results were obtained when layered double hydroxides (LDH), also known as hydrotalcite-like compounds, were employed as catalysts in esterification reactions. The use of LDHs or their nanostructured oxides (obtained from the calcination of different LDHs under mild conditions) in esterification reactions only led to the isolation of metal carboxylates after the reactions.[5]

Since in previous studies only zinc laurates were synthesized and evaluated, the objective of the present work was to synthesize and characterize layered copper, manganese, lanthanum and nickel laurates as well as to evaluate their catalytic activity in the methyl and ethyl esterification reactions of commercial lauric acid. Tests of reuse of the copper and lanthanum laurates were performed, in which the structures and respective catalytic activities were investigated up to the third use cycle.

## Experimental

### Catalysts synthesis

Layered metal laurates were synthesized through precipitation or metathesis in alcoholic medium,[4] starting by neutralization of lauric acid with sodium hydroxide and followed by precipitation of each compound through slow addition of an aqueous solution containing the metal ions of interest.

It the first step, 4.33 g (21.6 mmol) of lauric acid P.A. (Vetec, 98%) were totally dissolved in 20 mL of methanol P.A. (ACS, 99.8%) and neutralized by a stoichiometric amount of sodium hydroxide (Vetec, 98%). The white precipitate of sodium laurate obtained was then separated and dissolved in 30 mL of distilled water at room temperature and under vigorous stirring.

In the second step, metal salt solutions were added dropwise to the aqueous/alcoholic sodium laurate solution. After addition, each system was submitted to magnetic stirring for 1 h. The amounts used in the syntheses were: (*i*) for manganese(II) laurate, 10.8 mmol of $Mn(NO_3)_2{\cdot}4H_2O$ (Vetec, 97.0%) were dissolved in 100 mL of distilled water; (*ii*) for copper(II) laurate, 10.8 mmol of $Cu(NO_3)_2{\cdot}3H_2O$ (Synth, 98.0%) were dissolved in 100 mL of distilled water; (*iii*) for lanthanum(III) laurate, 15.0 mmol of $La_2O_3$ (Vetec, 99.5%) were dissolved in 50 mL of 10% $HNO_3$ (Quimex, 65%) in an ice bath and (*iv*) for nickel(II) laurate, 10.8 mmol of $NiCl_2{\cdot}6H_2O$ (Vetec, 97.0%) were dissolved in 100 mL of distilled water.

The washing of the solids was performed first with ethanol P.A. (ACS, 99.5%) to eliminate the possible presence of unreacted lauric acid and later with distilled water to eliminate the residues of the metal salt used in the precipitation, or even sodium laurate formed *in situ*.

The number of washing steps with the organic solvent was considered ideal when the supernatant after centrifugation was visually limpid. About three washing steps were sufficient and this number was also applied to the distilled water washing.

### Esterification reactions

The catalytic activity of the layered metal laurates was investigated in the methyl (ethyl) esterification reaction of lauric acid. The experiments were performed in a 100 mL capacity steel reactor (Büchiglass miniclave drive) equipped with an internal magnetic type hurricane stirring system, applying a standard rotation of 500 rpm. The temperature was controlled with an external thermostated mineral oil bath (Julabo model HE-4).

For the tests in the reactor, the reaction conditions were established starting from a factorial design ($2^3$) with two levels and three variables,[6] in which the influence of temperature, molar ratio (M.R. = alcohol/acid) and catalyst amount were investigated. The high and low levels for each variable were respectively 140 and 100 ºC for temperature (central point of 120 ºC), 14:1 and 6:1 for molar ratio alcohol/acid (central point of 10:1) and 10 and 2% for catalyst percentage in relation to the mass of lauric acid used in the reaction (central point of 6%). Eleven experiments were performed for each catalyst, three of them at the central point.

The reactions were carried out as follows: the lauric acid, alcohol and catalyst were introduced into the reactor, which was tightly closed and heated, reaching the reaction temperature in approximately 15, 25 and 45 min for temperatures of 100, 120 and 140 ºC, respectively.

The reactions were conducted for 2 h[7] and, at the end of the programmed period, the content of the reactor was transferred to a 100 mL round bottom flask, from which the excess alcohol was removed by rotary evaporation with reduced pressure at 65 ºC for methanol and 80 ºC for ethanol. The pressure of the reactor was controlled by the vapor pressure of the most volatile component of the reaction medium, methanol or ethanol. For the reaction temperatures of 100, 120 and 140 ºC using methanol, the pressures registered by the barometer were respectively 4, 6 and $8 \times 10^5$ Pa, while for ethanol, whose experiments were only conducted at 140 ºC, the pressure was $6 \times 10^5$ Pa. The conversion of lauric acid to the respective ester was measured by quantification of free fatty acids, according to the method Ca-5a-40 of the American Oil Chemists' Society (AOCS).[8]

Since the reactions can also proceed due to the influence of temperature,[9] tests of thermal conversion were performed following a factorial design with two levels and two studied variables, temperature and molar ratio, in the absence of the catalyst. The catalytic activity of the tested solids was verified by comparing the results of methyl/ethyl esters conversion, obtained under each condition, for the catalyzed reactions and the respective thermal conversions without catalyst addition.

Catalyst reuse tests were performed to verify the possible maintenance of catalytic activity and structure after the first reaction cycle. Only copper and lanthanum laurates were evaluated. The reuse procedure was accomplished starting from the recovery of the solids, which were washed with acetone and dried in a vacuum stove at 60 ºC until constant mass. As the recovery was not complete, due mainly to physical losses (around 95%), the amount of the reagents (alcohol and lauric acid) and catalyst were adjusted to maintain the same proportions of the first reaction cycle. Based on the proportions and recoveries, the solids were tested in more reaction cycles, resulting in three experiments for each catalyst.

### Characterizations

X-ray diffraction (XRD) patterns were recorded with a Shimadzu XDR-6000 instrument using $CuK_\alpha$ radiation ($\lambda = 1.5418$ Å), dwell time of 2° $min^{-1}$, current of 30 mA and tension of 40 kV. The samples were placed and oriented by hand pressing after filling top-loading aluminum or neutral glass sample holders.

The Fourier transform infrared (FTIR) spectra were recorded with a Bio-Rad FTS 3500GX instrument, using approximately 1% of sample in 100 mg of spectroscopic grade KBr, the pellets being pressed at 10 tonnes. The measurements were performed by transmission mode with accumulation of 32 scans and recorded with a nominal resolution of 4 $cm^{-1}$.

Thermal analysis (thermogravimetry (TGA) and differential thermal analysis (DTA)) measurements were performed in 150 µL alumina crucibles with a Mettler-Toledo TG/SDTA 851e thermoanalyzer under a 50 mL $min^{-1}$ oxygen flow, at a heating rate of 10 °C $min^{-1}$, in the range of 30-1000 °C.

## Results and Discussion

The X-ray powder diffraction patterns (Figure 1) show that the compounds have a layered structure, as can be seen from the typical basal peak sequence between 3 and 20° and absence of non-basal peaks due to the crystals orientation in the sample holder.

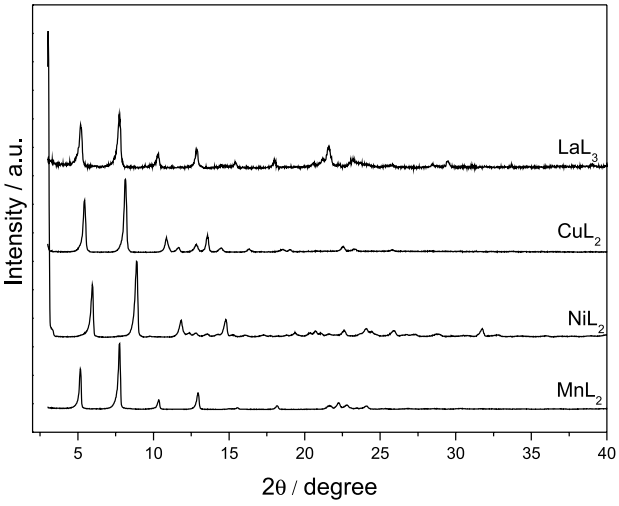


**Figure 1.** X-Ray powder diffraction patterns of the layered laurates.

The stacking direction is along the "a" axis (h00 direction) and the diffraction profile is very similar for all compounds, suggesting that probably all of them are isostructural with anhydrous zinc octanoate.[10] The basal spacings calculated for each of the synthesized laurates are consistent with the organic chains being arranged as tilted bilayers between the zinc layers (Figure 2).[10-12] The model used to represent the laurates structure is based on the structure of anhydrous zinc octanoate, due to the similarity of the XRD patterns with the above described layered metal laurates. The basal spacing values calculated by using the highest order basal peak possible were 29.97 Å, 32.63 Å, 34.16 Å and 34.53 Å for nickel, copper, manganese and lanthanum laurates, respectively. The basal distances for the laurates are coherent with an increase in the ionic radii of the metals present in the structures, $Ni^{2+}$ (0.69 Å),

$Cu^{2+}$ (0.72 Å), $Mn^{2+}$ (0.91 Å) and $La^{3+}$ (1.22 Å). However, the increased radius is not the only factor that contributes to this increase in basal distance. The organic chains are oriented with specific angles, and the coordination of the metal centers and the M–O distances can also influence the basal distance (Figure 2).[13]

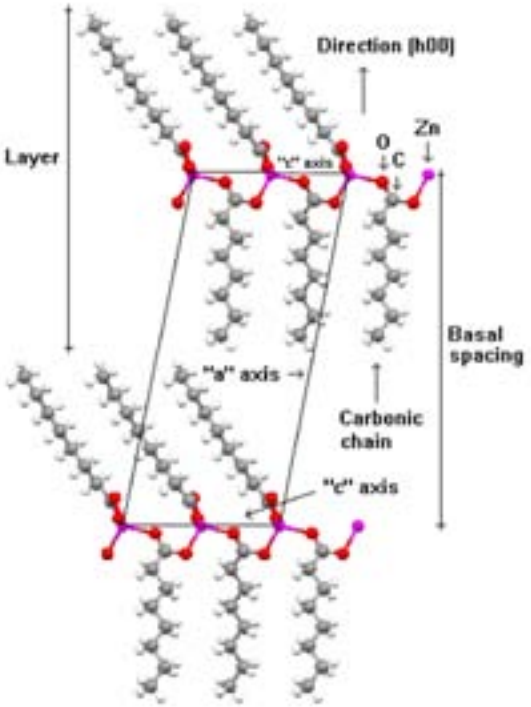


**Figure 2.** Schematic representation of the zinc octanoate structure: view along the "b" axis (adapted from references 10-12).

The FTIR spectra of the compounds (Figure 3) present vibration modes characteristic of saturated fatty acid salts and of the way the carboxylate groups are connected to the metals building the layers. The coordination of the laurate to the metals can be verified by the presence of stretching bands between 430 and 540 $cm^{-1}$, which can be attributed to M–O bonds.[14] All products present vibrations due to O–H bonds, indicating the presence of moisture or of structural water in the composition of the synthesized laurates. For the manganese and lanthanum laurates, the broad band of the O–H bond vibration was attributed to the presence of moisture. For the nickel compounds, on the other hand, there is a low intensity sharp peak, indicating the possibility that water is connected structurally to the inorganic layer. The vibrational groups that undergo the highest variations are those closest to the metal centers, as can be seen in Table 1, which shows the values for the vibrations of the most significant bands in each compound, supplying information about the structure of each layered laurate.

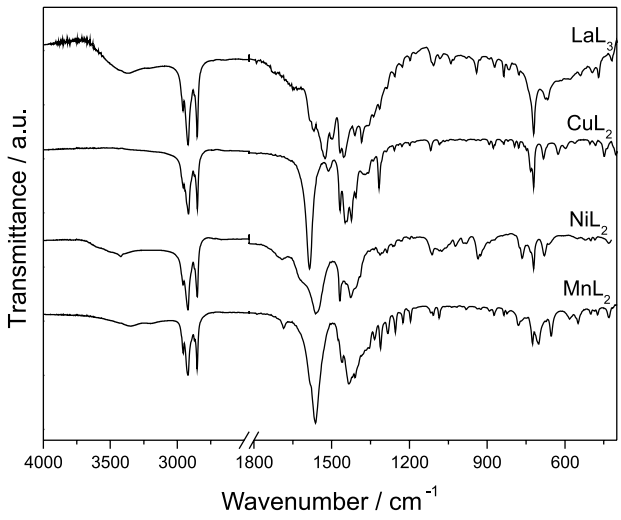


**Figure 3.** FTIR spectra of the layered laurates.

The asymmetric and symmetric stretchings of the methyl groups between 2956 and 2850 $cm^{-1}$ and the angular deformation at 721 $cm^{-1}$ of the methylenic groups have very close energy values for all compounds and are characteristic of saturated chain fatty acids. In many cases these vibrations are taken as a fingerprint of the class of compounds. In the region of 1200 and 1300 $cm^{-1}$, it was possible to verify the presence, in all compounds, of a group of $CH_2$ stretching bands related to the all-*trans* conformation of these groups in the layered carboxylate structure.[15] The weak bands in the region of 750 and 1350 $cm^{-1}$ are attributed to coupling of scissoring, wagging and twisting modes.[13] The profile of the vibrational spectrum indicates that the compounds may really be isostructural, as seen from the XRD analysis. The splitting of the antisymmetric and symmetric vibrational modes of the carboxylate groups, with values of $\Delta\nu$ between 137 and 164 $cm^{-1}$, is typical of compounds with two carboxylates bridging metal centers,[12,14,16] consistent

**Table 1.** Peak positions (in $cm^{-1}$) for the vibrational modes of the layered metal laurates

| Compound | ν M–O | ν O–H | $\nu_{ass}CH_3$ | $\nu_{(s)}CH_3$ | $\delta$ $CH_2$ | $\nu_{ass}$ $COO^-$ | $\nu_{(s)}$ $COO^-$ | $\Delta\nu_{(COO^-)}$ |
|---|---|---|---|---|---|---|---|---|
| $MnL_2$ | 499 | 3344 | 2954 | 2850 | 725 | 1562 | 1409 | 153 |
| $CuL_2$ | 449 | - | 2954 | 2848 | 721 | 1585 | 1421 | 164 |
| $NiL_2$ | 430 | 3423 | 2956 | 2848 | 721 | 1562 | 1425 | 137 |
| $LaL_3$ | 540 | 3375 | 2956 | 2850 | 721 | 1525 | 1384 | 141 |

**Table 2.** Thermal processes of layered metal laurates obtained from the TGA/DTA curves (in °C)

| Compound | Melting point | Burning of the organic matter | Exothermic peak | Oxide formation |
|---|---|---|---|---|
| $MnL_2$ | 81 | 228-356 | 284 | 356 |
| $LaL_3$ | 66 | 326-400 | 370 | 1000 |
| $NiL_2$ | 81 | 318-440 | 365 | 834 |
| $CuL_2$ | 113 | 221-378 | 285; 320 | 425 |

with the layered zinc octanoate structure (Figure 2). The thermal analysis curves (TGA/DTA) of the laurates show very characteristic organic carboxylate decomposition profiles (Figure 4).[17] Table 2 summarizes the processes attributed from the thermal analysis curves.

The compounds $MnL_2$, $LaL_3$, $NiL_2$ and $CuL_2$ presented endothermic melting events at temperatures of 81, 66, 81 and 113 °C, respectively. The melting process occurs in a single thermal event, as observed for zinc carboxylates with different chain lengths.[13] The proximity of the melting point

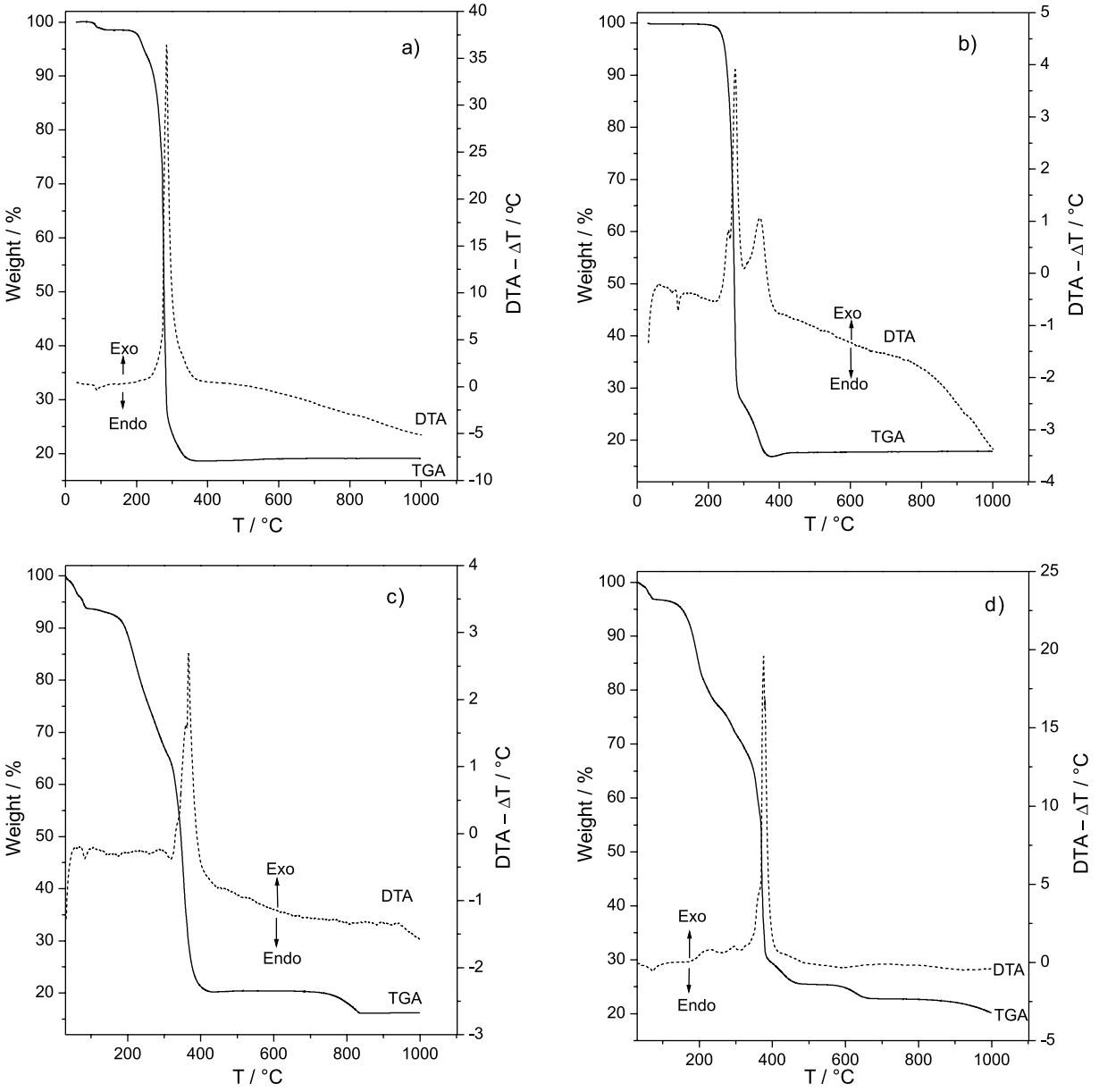


**Figure 4.** Thermal analysis curves (TGA/DTA) of the layered laureates: manganese (a), copper (b), nickel (c) and lanthanum (d).

values can also be another indication of the compounds similar structures. As reported in the literature,[13] in which the melting of the alkyl chains in the saturated fatty acid zinc carboxylates was investigated by XRD, FTIR and DSC, about 30% of the all-*trans* conformation of the methylenic groups present in the structure is lost during melting and a mixture of fragments of the structure is obtained, in which the carboxylate group is coordinated to the metal in the bridge bidentade and the monodentade modes. The laurates of manganese, nickel and lanthanum presented mass losses between 60 and 180 °C, attributed to the loss of physisorbed water in the first compound and structural water in the last two compounds. Even though the water removal temperature of the structure is low, the low melting point of the solids can facilitate removal of the molecules from the structure.

This class of compounds behaves like ionic liquids, especially during the melting observed in the catalytic reactions medium. The organic matter oxidation is accompanied by intense exothermic peaks in the region of 150 and 400 °C in the DTA curves and, after this, it is possible to see the start of formation of stable metal oxides. From the thermal analysis curves and the purity of the compounds, attested by the XRD and FTIR analysis, the compositions of the laurates could be estimated as follows: $Mn\{CH_3(CH_2)_{10}COO\}_2$, $Ni\{CH_3(CH_2)_{10}COO\}_2{\cdot}2H_2O$, $Cu\{CH_3(CH_2)_{10}COO\}_2$ and $La\{CH_3(CH_2)_{10}COO\}_3{\cdot}3H_2O$, where the oxide amounts obtained after the analysis are in agreement with the theoretical values, in the range of 1 to 5%.

## Methyl esterification reactions of lauric acid

The results obtained for the thermal conversion of lauric acid to the respective ester, used as control for comparison with the reactions in which the catalyst was added, can be observed in Table 3. Only ester and water are formed in the reactions. All the tested catalysts melted in the reaction medium and were reconstructed as the temperature decreased, being recovered almost completely, with only small physical losses.

The largest conversion into ester was 67% at 140 ºC, using a molar ratio of 6:1, and the smallest was 12% at 100 ºC, using the molar ratio of 14:1. The results of the central point were very similar, close to 39%, indicating the reproducibility of the assays. The values obtained served as parameters to verify that the addition of the catalysts to the reaction medium increases the conversion of acid into ester. The final results were calculated by subtraction of the values obtained without catalysts (thermal conversion "T") from those where the catalysts were present (catalyzed reaction "C"). These data are compiled in the column "C – T" of Table 4 (and Supplementary Information - Tables S1 to S3) and are given as ester in percentage points (ester p.p.). The subtraction gave positive values for all the evaluated catalysts, except for experiment 8, indicating a contribution of the layered laurates to increase the conversion of lauric acid into ester, and attesting the catalytic activity of the evaluated compounds.

The highest conversions obtained with the catalyzed reactions were observed in experiments 9 (83%) and 14 (90%) for $MnL_2$ (Table 4); 20 (81%) and 25 (77%) for $NiL_2$ (Table S1); 31 (78%) and 36 (82%) for $CuL_2$ (Table S2); and 42 (79%) and 47 (90%) for $LaL_3$ (Table S3). These values represent the largest conversions of lauric acid into ester, but they do not reflect the largest increases in relation to the control. In experiment 15, for example, the conversion was 79%, the third largest conversion value. However, the gain in relation to the thermal conversion was 25 p.p., a larger value than the 16 p.p. of experiment 9. This was also observed for experiments 22, 24, 26, 30, 32 and 33.

**Table 3.** Methyl esterification due to thermal conversion

| | Variable | | Reaction conditions | | Results | |
|---|---|---|---|---|---|---|
| Exp. | M.R. | T | M.R. (alcohol: acid) | T / ºC | Remaining lauric acid / % | Ester / % |
| 1 | –1 | –1 | 6:1 | 100 | 77 | 23 |
| 2 | –1 | +1 | 6:1 | 140 | 33 | 67 |
| 3 | +1 | –1 | 14:1 | 100 | 88 | 12 |
| 4 | +1 | +1 | 14:1 | 140 | 46 | 54 |
| 5 | 0 | 0 | 10:1 | 120 | 60 | 40 |
| 6 | 0 | 0 | 10:1 | 120 | 61 | 39 |
| 7 | 0 | 0 | 10:1 | 120 | 61 | 39 |

Exp = experiment; M.R. = molar ratio; T = temperature. Standard deviation of the central point (Exp. 5, 6 and 7): ± 0.67.

**Table 4.** Methyl esterification using $MnL_2$ as catalyst

| Exp | Variable | | | Reaction conditions | | | Results | |
|---|---|---|---|---|---|---|---|---|
| | M.R | CAT | T | M.R. | Catalyst / % | T / ºC | Ester / % | C – T (Ester p.p.) |
| 8 | –1 | –1 | –1 | 6:1 | 2 | 100 | 20 | –3 |
| 9 | –1 | –1 | +1 | 6:1 | 2 | 140 | 83 | 16 |
| 10 | –1 | +1 | –1 | 6:1 | 10 | 100 | 24 | 1 |
| 11 | +1 | –1 | –1 | 14:1 | 2 | 100 | 18 | 6 |
| 12 | +1 | –1 | +1 | 14:1 | 2 | 140 | 69 | 15 |
| 13 | +1 | +1 | –1 | 14:1 | 10 | 100 | 19 | 7 |
| 14 | –1 | +1 | +1 | 6:1 | 10 | 140 | 90 | 23 |
| 15 | +1 | +1 | +1 | 14:1 | 10 | 140 | 79 | 25 |
| 16 | 0 | 0 | 0 | 10:1 | 6 | 120 | 47 | 7 |
| 17 | 0 | 0 | 0 | 10:1 | 6 | 120 | 47 | 8 |
| 18 | 0 | 0 | 0 | 10:1 | 6 | 120 | 47 | 8 |

Exp = experiment; M.R. = molar ratio (alcohol:acid); CAT = catalyst; T = temperature; C – T = Catalyzed conversion – thermal conversion. Standard deviation of the central point (Exp. 16, 17 and 18): ± 1.62. Reaction time: 2 h.

In general, the factors that most influenced the conversion were temperature and molar ratio (alcohol:acid). The temperature increased positively the conversion and the increase in molar ratio had a negative influence (Table 5). Since the catalyzed path requires lower activation energy, more molecules have sufficient energy to react effectively than in the non-catalyzed path, and the reaction rate and conversion efficiency increase with increasing temperature. In the case of molar ratio (alcohol:acid), the greater amount of alcohol difficults the access of the substrate to the catalyst active site, reducing the reaction rate and consequently changing the equilibrium of the esterification reaction. In order to verify which catalyst had the best catalytic behavior, the percentage of conversion into ester *versus* results of experiments conducted under the same conditions was plotted in a graph (Figure 5). We grouped the experimental conditions in which the variables temperature, molar ratio and catalyst percentage were fixed and the experiments were varied from 1 to 11; then, we verified which catalyst behaved best under each condition. It was surprising that the same catalyst did not

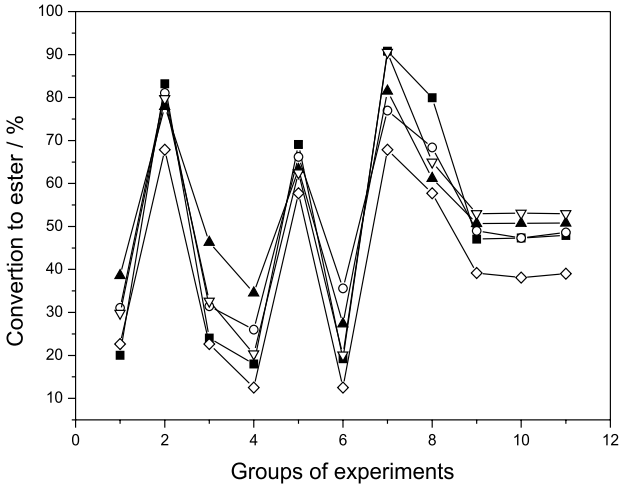


**Figure 5.** Comparison of the conversions to ester obtained in each experimental condition employed for the catalysts in the esterification of lauric acid. (◇) thermal conversion; (▽) $LaL_3$; (▲) $CuL_2$; (○) $NiL_2$; (■) $MnL_2$. Groups of experiments: 1 = 8, 19, 30, 41; 2 = 9, 20, 31, 42; 3 = 10, 21, 32, 43; 4 = 11, 22, 33, 44; 5 = 12, 23, 34, 45; 6 = 13, 24, 35, 46; 7 = 14, 25, 36, 47; 8 = 15, 26, 37, 48; 9* = 16, 27, 38, 49; 10* = 17, 28, 39, 50; 11* = 18, 29, 40, 51 (* = central point; experiments performed in triplicate).

**Table 5.** Variable influences in the methyl esterification reactions of lauric acid

| Compound | 1st order interactions | | | 2nd order interactions | | |
|---|---|---|---|---|---|---|
| | T / ºC | Catalyst | M.R. | Catalyst/M.R. | Catalyst/T | T/M.R. |
| $MnL_2$ | 60.42 | 5.93 | –7.95 | 4.65 | 3.31 | –4.54 |
| $NiL_2$ | 44.94 | 4.83 | –3.27 | 6.68 | –0.16 | –2.84 |
| $CuL_2$ | 37.43 | 0.50 | –11.37 | –5.15 | 0.22 | 2.15 |
| $LaL_3$ | 48.74 | 3.96 | –16.19 | –2.82 | 2.69 | –5.21 |

M.R. = molar ratio (alcohol:acid). All values are expressed as percentage points (p.p.).

always provide the highest conversion under the different experimental conditions. In some cases the conversion was better at lower temperatures; in others, it was better at higher ones.

Since the catalyst percentage used in the reactions was always calculated in relation to the mass of lauric acid, there was a variation in the amount of metal centers present in the reaction medium, due to the different molar weights of each compound, as estimated by thermal analysis. To verify if the molar weight had an influence on the catalyst performance, we analyzed the conversion into ester in function of the metal sites in each case (turnover number - TN). However, this correlation was not observed. Different catalysts performed differently depending on the experimental conditions.

During the melting process, only part of the structure is fragmented and the resulting structural "clusters" (metal site connected to some organic carboxylates) are responsible for the catalytic behavior. To support that, manganese(II), copper(II) and nickel(II) nitrates were used as catalysts to verify the influence only of the cation, and the catalytic activities were similar to those given by thermal conversion (MR of 6:1; 2% of catalyst and 100 °C).

### Ethyl esterification reactions of lauric acid

A factorial design for the ethyl esterification reactions of each laurate was also performed. The tests were based on the best results obtained with the methyl esterification, due to the lower reactivity of ethanol when compared to methanol. The results are shown in Table 6. In the case of transesterification under homogeneous conditions, as the length of carbon chain of the alcohol increases, the nucleophilicity of the alkoxide anions decreases leading to a decrease in the reactivity.[18] The effect is probably similar in the present case.

The only compound that presented relevant catalytic activity when the catalyzed reaction and the thermal conversion were compared was manganese laurate; the reason for this behavior is still under investigation. For the three reactions performed with manganese laurate, the conversions were 63, 70 and 75%, with gains in relation to thermal conversion of 1, 8 and 16 p.p., respectively.

Under similar conditions, when raw halloysite was used as catalyst, the higher gains in relation to the thermal conversion were of 13.95% (M.R. = 6:1 methanol:lauric acid; 160 °C, 2 h and 12% of catalyst) and 19.41% (M.R. = 12:1 methanol:lauric acid; 160 °C, 2 h and 12% of catalyst).[19] When metakaolins were used as catalysts, conversion gains of 54.2% (M.R. = 60:1 methanol:oleic acid, 130 °C, 2 h and 5% of catalyst) and 11.1% (M.R. = 60:1 methanol:oleic acid, 130 °C, 2 h and 5% of catalyst) were recently reported for calcined and sulfuric acid activated standard Kga-1b and Kga-2 kaolinites, respectivelly.[20]

In general, lower conversion gains are reported for the layered laurates (see Tables 4, 6 and Tables S1-S3) but this kind of comparison is difficult to be made due to the completely different behavior of the layered laurates in comparison to traditional heterogeneous catalysts.

**Table 6.** Results for ethyl esterification

| Exp. | Catalyst | Reaction conditions | | | Results | |
|---|---|---|---|---|---|---|
| | | M.R. | Catalyst / % | T / ºC | Ester / % | C – T (Ester p.p.) |
| 52 | - | 6:1 | - | 140 | 62 | - |
| 53 | - | 14:1 | - | 140 | 59 | - |
| 54 | $MnL_2$ | 6:1 | 2 | 140 | 63 | 1 |
| 55 | $MnL_2$ | 6:1 | 10 | 140 | 70 | 8 |
| 56 | $MnL_2$ | 14:1 | 10 | 140 | 75 | 16 |
| 57 | $NiL_2$ | 6:1 | 2 | 140 | - | - |
| 58 | $NiL_2$ | 6:1 | 10 | 140 | - | - |
| 59 | $NiL_2$ | 14:1 | 10 | 140 | - | - |
| 60 | $CuL_2$ | 6:1 | 2 | 140 | 60 | –2 |
| 61 | $CuL_2$ | 6:1 | 10 | 140 | 59 | –3 |
| 62 | $CuL_2$ | 14:1 | 10 | 140 | 41 | –18 |
| 63 | $LaL_3$ | 6:1 | 2 | 140 | 62 | 0 |
| 64 | $LaL_3$ | 6:1 | 10 | 140 | 62 | 0 |

Exp = experiment; M.R. = molar ratio (alcohol: acid); C – T = Catalysed conversion – thermal conversion; (-) without catalyst.

As expected, conversion values were lower for ethyl esterification than for methyl esterification.

### Catalysts reusability tests

Based on the catalysis results for the esterification of lauric acid to methyl laurate obtained for each catalyst, and the observed structure reconstruction or transformation of the catalysts after the reactions, we performed reuse tests to verify the catalytic activity after the first cycle as well as the structure of the re-isolated solid. In these analyses, lanthanum and copper laurates were evaluated, because they were the ones that presented the fastest and best structure reconstruction. Manganese oxide was isolated after rotary evaporation as a dark solid and nickel laurate was reconstructed very slowly. Consequently, both materials were not evaluated in further cycles. The conditions in which the reusability tests were performed were those under which the highest conversion percentages were observed in the first use, following the factorial design.

For copper laurate, the conditions of experiments 31 and 36 presented in Table S2 were used. The values obtained for the second and third cycle in experiment 31 were 80.95 and 82.68%, respectively (Figure 6). These results, when compared with the first use, presented a conversion of 77.94%, representing a small increase in the production of ester. The values obtained for the reuses regarding experiment 36 were respectively 83.40 and 85.42%, demonstrating similar behavior, that is, a slight increase in the ester percentage compared to the first reaction cycle, in which the result was 81.48% conversion (Figure 6).

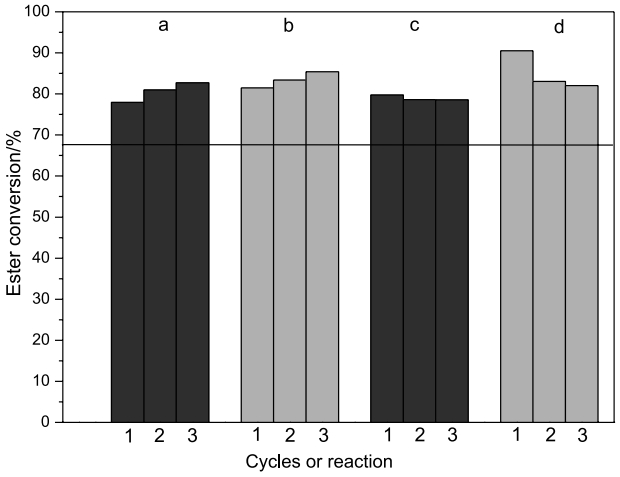


**Figure 6.** Conversions into ester using layered laurates in three reaction cycles. The black line that crosses the graph represents the thermal conversion. a = $CuL_2$, MR 6:1, 2% catalyst, 140 °C; standard deviation: ± 1.38% (Exp. 31); b = $CuL_2$, MR 6:1, 10% catalyst, 140 °C; standard deviation: ± 1.14% (Exp. 36); c = $LaL_3$, MR 6:1, 2% catalyst, 140 °C; standard deviation: ± 0.38% (Exp. 42); d = $LaL_3$, MR 6:1, 10% catalyst, 140 °C; standard deviation: ± 2.68% (Exp. 47).

The results obtained with the first and second reuse under the condition reported in experiment 42 were 78.59 and 78.54%, respectively, values that are comparable with the first reaction (79.73%) (Table S3 and Figure 6). However, for the condition of experiment 47, whose first reaction resulted in a conversion into ester of 90.50%, the values were slightly lower (83.03 and 82.01% for the first and second reuse, respectively). This reflects a slight loss of catalytic activity for the lanthanum laurate. Knowing that losses during recovery were significant, the decrease in activity can be attributed to a volume effect, since the proportions of reactants and catalyst were maintained, but the total volume of the mixture was smaller. This implied in larger evaporation to maintain the reactor pressure constant and in artificial reduction of the molar ratio, thus negatively affecting the ester conversion.

### Characterization of the compounds after the esterification of lauric acid

The solids were characterized by XRD and FTIR after the methyl esterification reactions of lauric acid (Figure 7). The main peaks of the XRD patterns can be indexed in the original structure, although sometimes small transient peaks could be observed. As the time of crystallization was not controlled, the changes in the intensities of the XRD peaks can be attributed to small variations in the crystallization degree. Also, the bands of the FTIR spectra can be attributed to the original structure, not showing any new functional group from any possible impurity. This information let us conclude that the main structures of both catalysts were maintained after three consecutive uses.

Figure 8 displays a schematic representation of the structure of the zinc octanoate and the proposed mechanism for the esterification of lauric acid using melted layered laurates. It should be noted that the laurates were added to the reactor in the solid state and were submitted to melting in the reaction medium, resulting in the partial fragmentation of the structure. The resulting structure fragments (clusters) were responsible for the catalytic activity, since only part of the bonds of the carboxylate ion-metal, in the form of a bidentade bridge, are broken.[13] The coordination of the carboxylates in the monodentade form leaves the metal ions only partially coordinated, probably being the active center, as proposed in the mechanism based on the model of Langmuir-Hinshelwood of Figure 8.[21,22] After cooling, the catalyst is reconstructed and can be recovered for subsequent reuses. This is similar to the behavior of ionic liquids.[23-26]

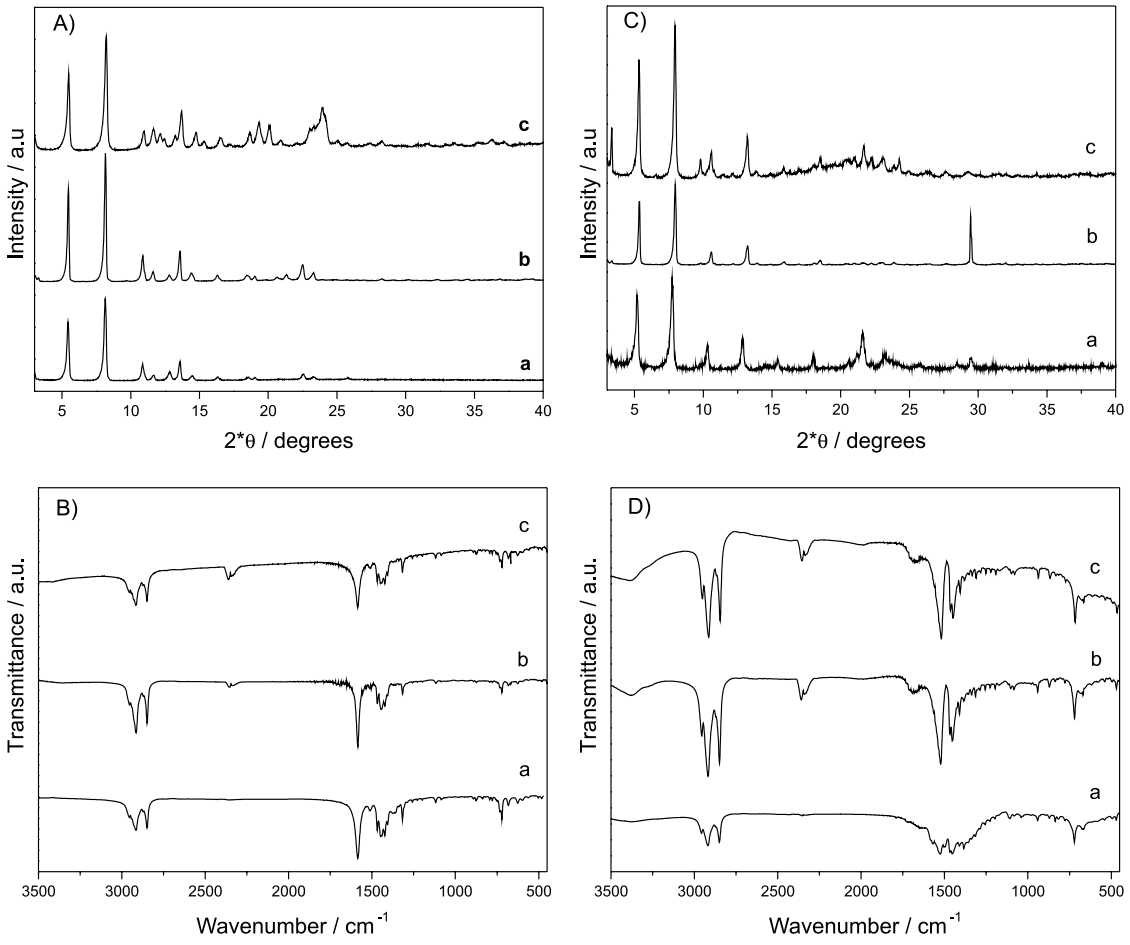


**Figure 7.** XRD patterns (A, C) and FTIR spectra (B, D) of the laurates before (a) and after two reactions of reuse (b, c). A and B copper laurate; C and D lanthanum laurate.

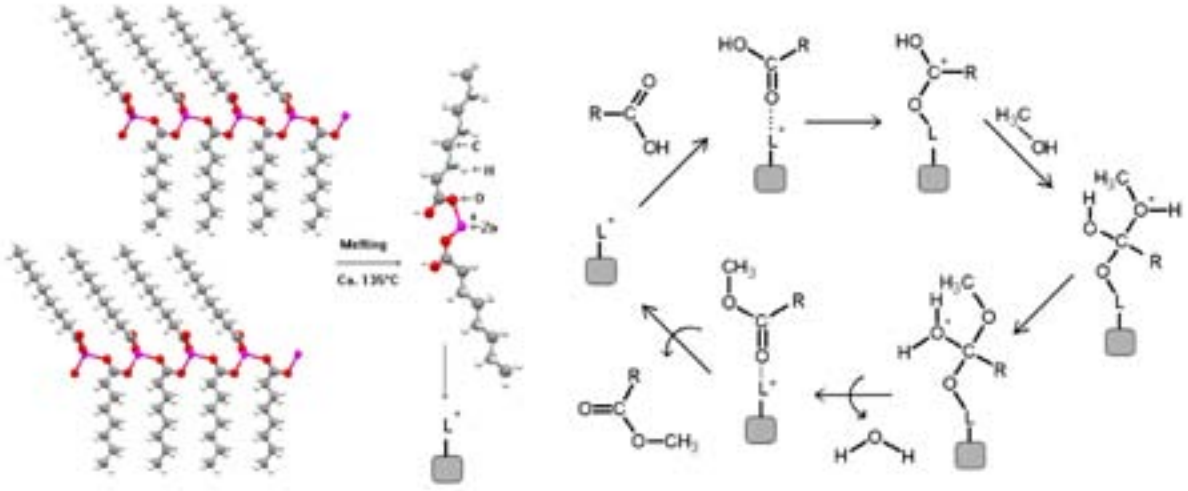


**Figure 8.** Schematic representation of the zinc octanoate structure and the proposed catalytic mechanism involving layered metal laurates (adapted from references 10-12, 21 and 22).

## Conclusions

The synthesized compounds presented layered structures and basal spacings in agreement with the presence of alkyl chains arranged as tilted bilayers between the inorganic layers. The X-ray powder diffraction profiles showed that the compounds are probably isostructural and that the structuring of the layers is obtained by coordination

of the carboxylate groups to different metal centers in a bridge bidentade arrangement.

The compounds melted in the reaction medium and, after cooling, the original structures could be re-isolated. After melting the catalysts behaved as homogeneous catalysts or ionic liquid-like catalysts; consequently, the activity is independent of the surface area of the crystal obtained during synthesis.

The possibility of reusing the copper and lanthanum laurates in the methyl esterification reactions was also verified by tests, which roughly presented conversion values very close to the initial ones.

In the comparison of reactivities, based on the conversion results, all the catalysts showed very similar profiles. This also corroborates the evidence that all compounds have similar or identical structures. As observed in the melted state and supposedly in the reaction medium, all the metals are still partially coordinated to the carboxylate ligands and the activity in similar conditions originates from intrinsic properties of each metal cation with the synergistic effect of the carboxylate and the coordination mode.[13]

The tests of catalytic activity in the methyl esterification of lauric acid demonstrated that in all cases the compounds promoted catalysis when compared with the thermal control, reaching conversions between 80% and 90% in some conditions. However, only manganese laurate demonstrated the ability to catalyze the ethyl esterification reactions of lauric acid, presenting conversions close to 75%.

To the best of our knowledge, this is the first systematic study in which a class of layered metal laurates was evaluated in the methyl and ethyl esterification of lauric acid. Further studies are in progress to evaluate layered carboxylates in the esterification of other fatty acids and complex mixtures of fatty acids and the transesterification of vegetable oils and animal fats.

## Supplementary Information

Supplementary data are available free of charge at http://jbcs.sbq.org.br as PDF file.

## Acknowledgments

We gratefully acknowledge CNPq, CAPES and FINEP for the financial support of this work.

## References

1. Pereira, R. G.; Oliveira, C. D.; Oliveira, J. L.; Oliveira, P. C. P.; Fellows, C. E.; Piamba, O. E.; *Renew. Energ.* **2007**, *32*, 2453.
2. Gerpen, J. V.; *Fuel Process. Technol.* **2005**, *86*, 1097.
3. Ma, F.; Hanna, M. A.; *Bioresour. Technol.* **1999**, *10*, 1.
4. Cordeiro, C. S.; Arizaga, G. G. C.; Ramos, L. P.; Wypych, F.; *Catal. Commun.* **2008**, *9*, 2140.
5. http://dspace.c3sl.ufpr.br/dspace/bitstream/handle/1884/18854/CLAUDINEY%20SOARES%20CORDEIRO%20-%20TESE%20DE%20DOUTORADO.pdf?sequence=1 accessed in August, 2011.
6. Markley, K. S.; *Fats and Oils: A Series of Monographs on the Chemistry and Technology of Fats, Oils and Related Products*; Interscience Publishers Inc.: New York, 1961.
7. Bruns, R. E.; Scarminio, I. S.; Neto, B. B.; *Planejamento e Otimização de Experimentos*; Unicamp: Campinas , São Paulo, Brasil, 1995.
8. AOCS - Official methods and recommended practices of the American Oil Chemists' Society, AOCS Press; Champaign, 2004.
9. Aranda, D. A. G.; Santos, R. T. P.; Tapanes, N. C. O.; Ramos, A. L. D.; Antunes, O. A. C.; *Catal. Lett.* **2008**, *122*, 20.
10. http://cod.ibt.lt/ Crystallographic Open Database, accessed in October, 2010.
11. http://www.ccdc.cam.ac.uk/products/mercury accessed in October, 2010.
12. Lacouture, F.; Peultier, J.; François, M.; Steinmetz, J.; *Acta Crystallogr., Sect. C: Cryst. Struct. Commun.* **2000**, *56*, 556.
13. Barman, S.; Vasudevan, S.; *J. Phys. Chem. B* **2006**, *110*, 22407.
14. Nakamoto, K.; *Infrared and Raman Spectra of Inorganic and Coordination Compounds*, 4th ed.; John Wiley & Sons: New York, 1986.
15. Deacon, G. B.; Phillips, R. J.; *Coord. Chem. Rev*. **1980**, *33*, 227.
16. Alcock, N. W.; Tracy, V. M.; Waddington, T. C.; *J. Chem. Soc., Dalton Trans.* **1976**, 2243.
17. Akanni, M. S.; Okoh, E. K.; Burrows, H. D.; Ellis, H. A.; *Thermochim. Acta* **1992**, *208*, 1.
18. Sridharan, R.; Mathai, I. M.; *J. Sci. Ind. Res.* **1974**, *22*, 178.
19. Zatta, L.; Gardolinski, J. E. F. C.; Wypych, F.; *Appl. Clay Sci*. **2011**, *51*, 165.
20. Nascimento, J. R.; Angelica, R. S.; Costa, C. E. F.; Zamian, J. R.; Rocha Filho, G. N.; *Appl. Clay Sci*. **2011**, *51*, 267.
21. Cordeiro, C. S.; Silva, F. R.; Wypych, F.; Ramos, L. P.; *Quim. Nova* **2011**, *34*, 477.
22. Yan, S.; Salley, S. O.; Simon, K. Y. N.; *Appl. Catal., A* **2009**, *353*, 203.
23. Earle, M. J.; Plechkova, N. V.; Seddon, K. R.; *Pure Appl. Chem.* **2009**, *81*, 2045.
24. Domingos, J. B.; Dupont, J.; *Catal. Commun.* **2007**, *8*, 1383.
25. Himmler, S.; Hormann, S.; Van Hal, R.; Schulz, P. S.; Wasserscheid, P.; *Green Chem.* **2006**, *8*, 887.
26. Lisboa, F. S.; Arizaga, G. G. C.; Wypych, F.; *Top. Catal.* **2011**, *54*, 474.

*Submitted: March 15, 2011*
*Published online: October 18, 2011*

Article

*J. Braz. Chem. Soc.*, Vol. 23, No. 1, 57-64, 2012.
Printed in Brazil - ©2012 Sociedade Brasileira de Química
0103 - 5053 $6.00+0.00

# Evaluation of Solid-Phase Microextraction using a Polythiophene Film and Liquid Chromatography with Spectrophotometric Detection for the Determination of Antidepressants in Plasma Samples

***Juciene A. Caris, Andréa R. Chaves and Maria Eugênia C. Queiroz****

*Departamento de Química, Faculdade de Filosofia Ciências e Letras de Ribeirão Preto, Universidade de São Paulo, 14040-903 Ribeirão Preto-SP, Brazil*

A fase extratora de politiofeno (PTh), desenvolvida por eletropolimerização em haste de aço inox, foi avaliada para microextração em fase sólida (SPME) e análise por cromatografia líquida com detecção espectrofotométrica (LC-UV) de antidepressivos inibidores seletivos da recaptação de serotonina (citalopram, paroxetina, fluoxetina e sertralina) em amostras de plasma. A influência das variáveis da eletropolimerização (velocidade de varredura de potencial, potencial e ciclos de varredura) foi avaliada no desempenho SPME. As variáveis SPME (tempo de extração, temperatura, pH da matriz, força iônica e procedimento de dessorção), assim como a influência das proteínas do plasma no mecanismo de sorção, foram também avaliadas. O método SPME-PTh/LC-UV desenvolvido para a determinação de antidepressivos em amostras de plasma apresentou faixa linear de resposta do limite de quantificação (LOQ, 200-250 ng $mL^{-1}$) a 4000 ng $mL^{-1}$ e precisão interensaio com coeficiente de variação no intervalo de 11 a 15%. O método proposto poderá ser utilizado para a determinação de antidepressivos em amostras de plasma humano para análises toxicológicas de urgência, após a ingestão acidental ou suicida de doses altas de medicamentos.

Polythiophene (PTh) phase electropolymerized on the stainless steel wire was evaluated as solid-phase microextraction (SPME), and analysis by liquid chromatography with spectrophotometric detection (LC-UV) for determination of new-generation antidepressants, selective serotonin reuptake inhibitors (SSRIs) (citalopram, paroxetine, fluoxetine and sertraline), in plasma samples. The influence of electropolymerization variables (scan rate, potential range and scan cycles) was evaluated on SPME performance. The SPME variables (extraction time, temperature, matrix pH, ionic strength and desorption procedure), as well as the influence of plasma proteins on sorption mechanisms were also evaluated. The SPME/LC-UV method developed for determination of antidepressants in plasma sample presented a linear range between the limit of quantification (LOQ, 200-250 ng $mL^{-1}$) to 4000 ng $mL^{-1}$, and interday precision with coefficient of variation (CV) ranged from 11 to 15%. The proposed method can be a useful tool for the determination of antidepressants in human plasma samples in urgent toxicological analysis after the accidental or suicidal intake of higher doses of medications.

**Keywords:** solid-phase microextraction, polythiophene, antidepressants, liquid chromatography

## Introduction

Mood disorders represent a considerable portion of the diseases prevailing worldwide, with high suicide rates. The World Health Organization (WHO) estimates that depressive disorders will become the second most prevalent cause of illness-produced disability by 2020.[1]

Depressive disorders have been found to be significant risk factors for suicide. The use of drugs, like antidepressants (AD), for the treatment of mood disorders has a relatively short history and is still under rapid development. However, in the same way that antidepressants are used in the treatment of depressive disorders, they can also become the underlying cause of suicide. Although there has been significant decrease in suicide rates with the increased use of antidepressants, suicides have augmented due to the use of antidepressants. Therefore, toxicological surveillance of individuals who attempted suicide regarding the presence of AD medications is important for monitoring correlations between the use of AD and suicide rates in populations.[2-7]

*e-mail: mariaeqn@ffclrp.usp.br

The development of highly efficient analytical instrumentation for the endpoint determination of drugs from biological samples involves sample pretreatment, which is usually necessary for the extraction, isolation and concentration of drugs encountered in complex matrices. This is because most analytical instruments cannot handle sample matrices directly.[8]

In the last decade, Arthur and Pawliszyn[9] introduced the solid-phase microextraction (SPME) technique. This solventless technique combines analyte extraction and concentration in a single step, thereby reducing the required time for sample preparation. SPME has been successfully applied to the extraction of volatile and semi-volatile drugs from various sample matrices.[8-10] However, the application of SPME to ionizable drug species is limited due to the neutral charge of commercial SPME coatings. This results in low coating/sample partition coefficient and poor analyte recovery. One promising alternative for the extraction of polar and ionic compounds is the use of conductive polymers as extraction phases.[10,11]

The conducting polymer coatings as polythiophene films[12-16] presented multifunctional properties. Thus, their polymerization on metal wires by electrochemical or chemical methods has been described as a promising alternative for the development of new phases for the SPME technique, therefore expanding the potential application of this method.[17]

In the present work, polythiophene films were electropolymerized (cyclic voltammetry) on the surface of metal (stainless steel) wires, for the development of SPME phases. These polymeric films were evaluated as SPME phases for the liquid chromatography (LC) analysis of selective serotonin reuptake inhibitor (SSRI) antidepressants (Figure 1) in plasma samples for toxicological analysis purposes. The influence of plasma protein on the SPME process was also evaluated.

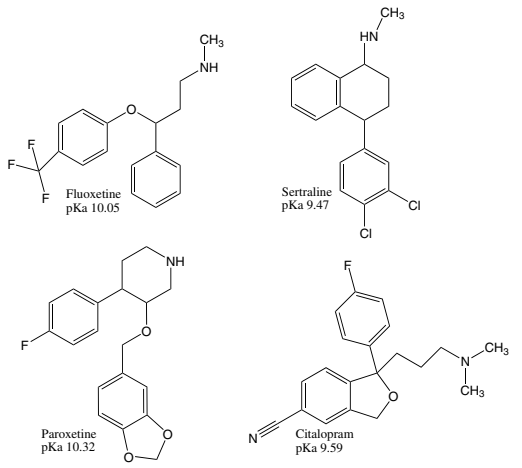


**Figure 1.** Structure and pKa of selected SSRI antidepressants.

## Experimental

### Reagents and analytical standards

The fluoxetine and paroxetine analytical standards were donated by Eli Lilly Co. (Indianapolis, IN, USA) and Libbs Farmacêutica Ltda. (São Paulo-SP, Brazil), respectively. Citalopram and sertraline were acquired from F. Hoffmann-La Roche Ltd. (Basel, Switzerland).

The diluted standard solutions of antidepressants were prepared considering the therapeutic range. For this purpose, their respective stock solutions (1 mg $mL^{-1}$) were diluted in methanol. These solutions remained stable for 45 days when they were stored at –20 °C. The water used to prepare the mobile phase was previously purified in a Milli-Q system (Millipore, Bedford, MA, USA).

Methanol, acetonitrile (both, HPLC grade), anhydrous dibasic sodium phosphate 99.4% and hydrochloric acid 38% were purchased from J. T. Baker Chemical Co. (Phillipsburg, NJ, USA). Monobasic monohydrate sodium phosphate 99.6% and sodium borate 99.5% were acquired from Mallinckrodt Baker Inc. (Phillipsburg, NJ, USA). Sodium perchlorate ($NaClO_4$) and tetrabutylammonium tetrafluoroborate (TBATFB) both 98% were provided by Acros Organics (Morris Plains, NJ, USA). The thiophene monomer 99% electrochemical grade was purchased from Sigma-Aldrich (St.Louis, MO, USA).

### Plasma samples

The blank plasma (drug-free) with negative serology for hepatitis B and C, Chagas disease, HTLV I/II, TGP and syphilis was kindly supplied by Hospital das Clínicas de Ribeirão Preto (University of São Paulo, Ribeirão Preto-SP, Brazil).

The synthetic plasma sample was prepared by using sodium chloride (145 mmol $L^{-1}$), potassium chloride (4.5 mmol $L^{-1}$), calcium chloride (32.5 mmol $L^{-1}$), magnesium chloride (0.8 mmol $L^{-1}$), urea (2.5 mmol $L^{-1}$) and d-glucose (4.7 mmol $L^{-1}$).[18] The pH of synthetic plasma solution was adjusted to 7.4 using sodium hydroxide solution (1 mol $L^{-1}$).

### Chromatographic conditions

All the analyses were performed on a Varian ProStar 230 liquid chromatograph (Palo Alto, CA, USA) with UV detector ($\lambda$ = 230 nm). The drugs were separated in a LiChrospher®60 RP-Select B (5 μm, 250 × 4 mm i.d.) column equipped with an RP-Select B, LiCroCART®4-4 pre-column. The mobile phase consisted of methanol and phosphate buffer solution (0.05 mol $L^{-1}$, pH 4.5) (60:40, v/v).

Elution was carried out in the isocratic mode at room temperature (25 °C) and flow rate of 1.0 mL $min^{-1}$. The mobile phase was filtered and degassed prior to use.

### Electropolymerization process

For the development of SPME polythiophene phase, the cyclic voltammetry experiments were performed using a three-electrode system (Potentiostat/Galvanostat model PG Omnimetra 3901, coupled to a microcomputer operating with the software PG 3901). A platinum wire was utilized as the counter electrode, a silver/silver chloride (Ag/AgCl) electrode was used as reference and a cylindrical stainless steel 316 [1 cm × 2.32 mm i.d., composed of iron, nickel (7 to 20%) and chromium (17 to 25%)] was employed as the working electrode. Initially, the stainless steel was polished with steel wool and washed with ultra-pure water in an ultrasonic bath for 30 min. These electrodes were kept in acetone.

For the electrodeposition of thiophene, 0.1 mol $L^{-1}$ $NaClO_4$ (electrolyte) in an acetonitrile solution containing 0.3 mol $L^{-1}$ of the monomer was evaluated at a scan rate of 50 mV $s^{-1}$, within the –0.2 to 1.7 V potential range. Furthermore, TBATFB (0.5 mol $L^{-1}$) in acetonitrile solution containing 0.3 mol $L^{-1}$ of the monomer was also evaluated at a scan rate of 100 mV $s^{-1}$, within the –0.2 and 2.2 V potential range.

The influence of the film thickness on the SPME performance was evaluated with 20 and 50 scan cycles for polythiophene electropolymerization in $NaClO_4$ (0.1 mol $L^{-1}$) solution, and with 10, 15, 20 and 30 cycles in TBATFB (0.5 mol $L^{-1}$) solution.

### Scanning electron microscopy (SEM) of PTh coated SS surfaces

The surface of the polythiophene film coated on SS wire was cut into a 1 cm-long piece and then analyzed on a Zeiss EVO50 scanning electron microscope (20 kV accelerating potential).

### Optimization of the SPME process

The SPME (electropolymerized polythiophene phase) variables such as time, temperature, matrix pH, sample volume and ionic strength were optimized in human plasma samples and investigated in triplicate assays. The stirring speed and polythiophene film dimension were kept constant during the optimization.

The influence of the matrix pH on the SPME performance was evaluated by the following procedure: in a glass vial (5 mL) sealed with a silicone septum, 3.0 mL buffer solution [0.05 mol $L^{-1}$, phosphate buffer (pH 4.0 and 7.0) and borate buffer (pH 9.0)] were added to 250 µL of a sample spiked with the drug standard solutions, which resulted in a drug concentration of 500 ng $mL^{-1}$. The polythiophene electropolymerized electrode was immersed into the sample and the extractions were performed under magnetic stirring at a rate of 1200 rpm for 40 min at 25 °C. Then, the polythiophene electrode was inserted into a conical vial containing the mobile phase (static mode, 250 µL) for 15 min at 25 °C. 20 µL of this extract were injected into the LC-UV system.

The volume of the plasma sample (250, 500 and 1000 µL), extraction time (10, 20, 30 and 40 min) and temperature (25, 40 and 50 °C) were optimized to establish the sorption equilibrium between the drugs and the extraction phase. The influence of ionic strength on the SPME performance was also examined by addition of NaCl (0, 5 and 10% m/v).

For the desorption process, different solvents were evaluated (water, methanol and mobile phase). After the desorption process, the electrode was washed with methanol/water (1:1, v/v) solution for 20 min to ensure total removal of the analytes and plasma endogenous compounds.

## Results and Discussion

### Electropolymerization process

Cyclic voltammetry is a convenient tool for the coating of metallic electrodes. The one-step production of films, the fiber-to-fiber reproducibility and the control of fiber thickness by changing the number of scan cycles must be highlighted among its advantages.[19-21]

Some organic solvents and supporting electrolytes have been used in the electropolymerization of polythiophene film and its derivatives.[15,16,20] The electrochemical properties of polythiophene films largely depend on the supporting electrolyte, especially on the type of anion.[22-25] According to Wu and Pawliszyn,[26] the use of different electrolytes enables manipulation of the functionality of the resulting polymers. Therefore, two electrolyte solutions (namely TBATFB and $NaClO_4$) in acetonitrile were evaluated for the electrodeposition of polythiophene in order to increase the selectivity and efficiency of the extraction phase.[12,27]

The polythiophene phase electropolymerized in TBATFB/acetonitrile 0.5 mol $L^{-1}$ electrolyte solution gave the best results. Different numbers of scan cycles (10, 15, 20 and 30) were evaluated in order to improve the SPME-polythiophene extraction performance. The polythiophene phase electropolymerized in TBATFB

by mean of 20 scan cycles resulted in homogenous and more stable films, as well as higher SPME efficiency. The polythiophene phase electropolymerized using over 20 scan cycles resulted in a morphologically unstable film regarding the SPME process.

The obtained cyclic voltammogram using the prepared electrode under the optimal electrodeposition conditions is shown in Figure 2.

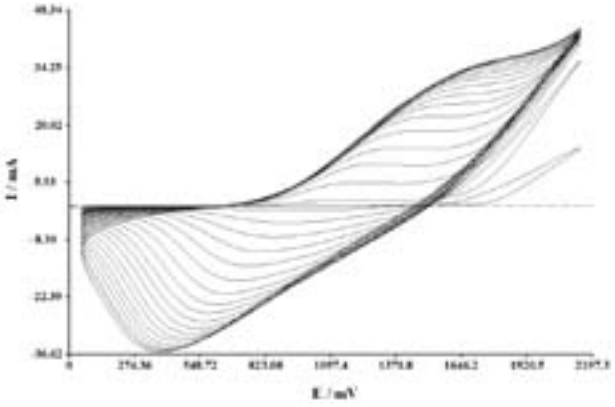

**Figure 2.** Cyclic voltammogram for the electrodeposition of polythiophene (SS electrode) in TBATFB/acetonitrile solution (0.5 mol $L^{-1}$) at a scan rate of 100 mV $s^{-1}$, during 20 cycles.

The shape and the peak positions observed in the cyclic voltammograms can reflect the properties of the polymer.[28] The increasing current on successive cycles shows that the thickness polymer is increasing. The regular increase of the current on successive cycles also illustrates that the polymer is regularly increasing into a packed structure (Figure 2).

The morphology of the polythiophene phase (optimized electropolymerization conditions) was investigated by scanning electron micrography (SEM) (Figure 3). According to the SEM images, these films presented porous structure, which resulted in larger surface areas and favored the extractive capacity of the polymeric phase (Figure 3a and b). The thickness of the polythiophene coating (*ca.* 180.6 μm) was also estimated by SEM (Figure 3c).

According to the SS wire geometry (surface area 0.771 $cm^2$) and the polythiophene coating average thickness (180.6 μm), the developed polythiophene film presented an approximate volume of 14 μL.

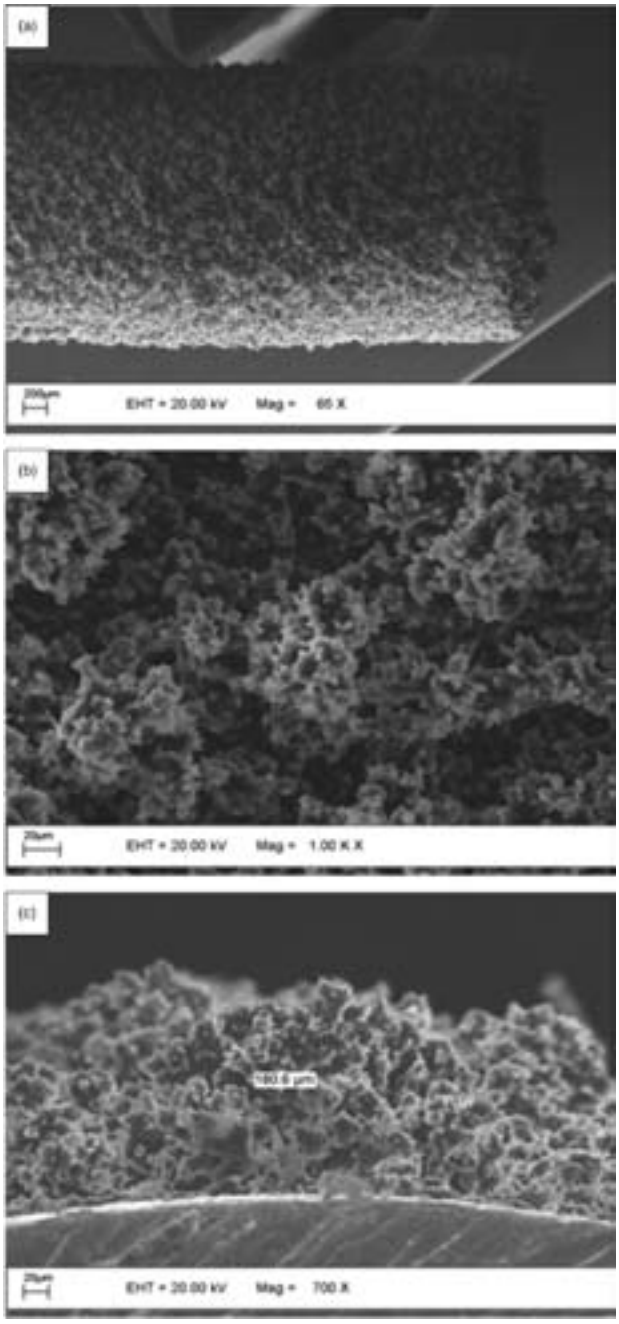


**Figure 3.** Scanning electron micrographs of the polythiophene phase: (a) 65-fold view, (b) 1000-fold view and (c) 700-fold view.

## Optimization of SPME variables

Drug ionization is related to the pH of the matrix (biological fluid), so the this variable could affect SPME performance. Thus, the pH adjustment could improve the sensitivity of the method.[29] As shown in Figure 4a, the dilution of the plasma sample with phosphate buffer 0.05 mol $L^{-1}$ pH 9.0 increased the efficiency of the SPME procedure. In this condition, the drugs were partially ionizable, according to the pKa of the antidepressants (9.47 to 10.32).[10,30] Plasma dilution with buffer solution at pH values higher than 9.0 resulted in precipitation of the proteins, thus, pH values above pH 9.0 were not evaluated.

The increase in the extraction temperature from 25 to 50 °C decreased the average peak area of the extracted drugs (Figure 4b). With a temperature increase, diffusion coefficients and Henry`s constants are increased and partition coefficients to the extraction phase are decreased.[31]

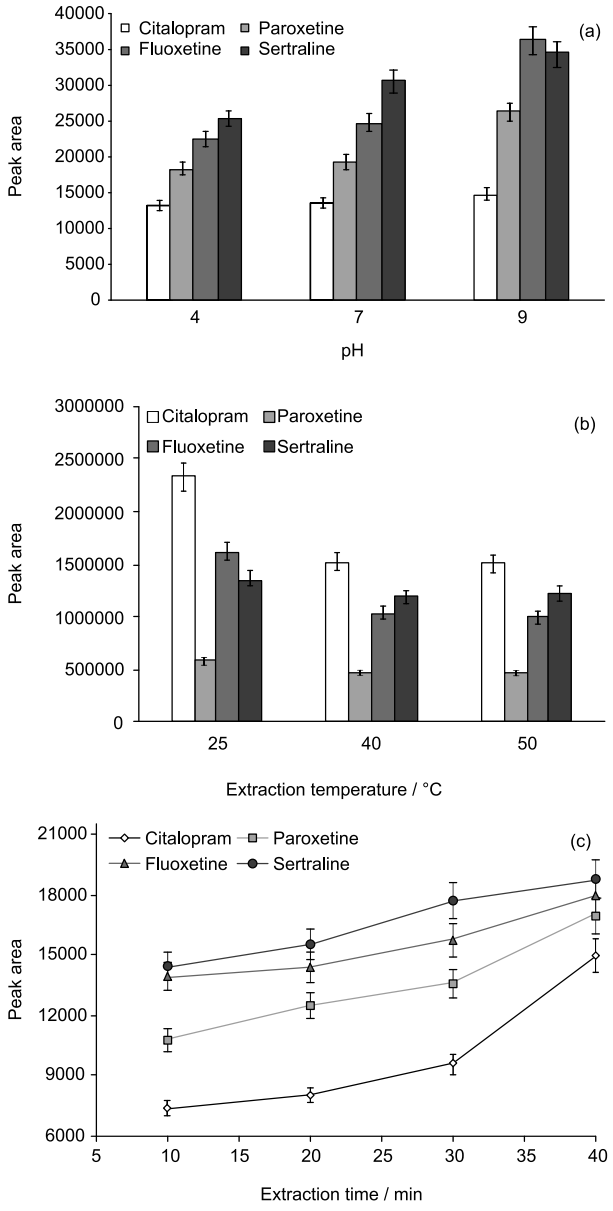


**Figure 4.** The effect of pH of plasma samples (a), temperature (b) and time (c) on SPME performance.

Thus, the subsequent extraction was carried out at room temperature (25 °C) to ensure stability and robustness of the polythiophene films.

Representative extraction time profiles (10-40 min) at 25 °C are shown in Figure 4c. Although the sorption equilibrium had not been reached at 40 min, this time was selected for subsequent analysis to save time. However, the extraction time and mass transfer conditions were strictly controlled to ensure good precision.[29]

Olszowy *et al.*[16] compared the extraction efficiency of SPME-PTh phases to adrenolytic drug analysis in aqueous and plasma medium. The equilibrium time for this analysis had not been found until 16 min for both samples (aqueous and plasma). So, the authors conducted extractions out of equilibrium time (10 min) to improve the total time analysis.[16]

In the selected condition (pH 9.0, 40 min and 25 ºC), the proposed SPME-polythiophene/LC method displayed precision and accuracy for analysis of antidepressants. In agreement with Figure 4c, the competitive process among drugs and polythiophene phase was not observed up to 40 min.

The influence of the ionic strength on the extraction process was evaluated by adding NaCl to the plasma sample (0, 5 and 10%) (data not shown). The polythiophene phase exhibited reduced extraction efficiency in saline solution because of the competition among the salt cations and the analytes. Probably, this happened due to electrostatic or ion-pairing interactions. This likely reduced the ability of the drugs to move into the fiber coating.[8] In low saline concentration, there was no change in the extraction performance.

Among the evaluated solvents for the desorption process (water, methanol and mobile phase), the mobile phase (phosphate buffer 0.05 mol $L^{-1}$, pH 4.5 and methanol 40:60, v/v) gave the best SPME performance (data not shown). The polythiophene phase showed to be stable in mobile phase.

Since the SPME process based on equilibrium sorption is not exhaustive (i.e., only a fraction of the sample is extracted),[31,32] the volume of the plasma sample was also optimized. Different sample volumes (250, 500 and 1000 µL) were subjected to SPME-PTh/LC-UV analysis (Figure 5). According to the obtained results, a plasma sample volume above 250 µL slightly increases the efficiency of the polythiophene fiber on SPME performance. However, a small plasma volume, which was diluted with buffer solution, decreased the matrix viscosity and increased the diffusion

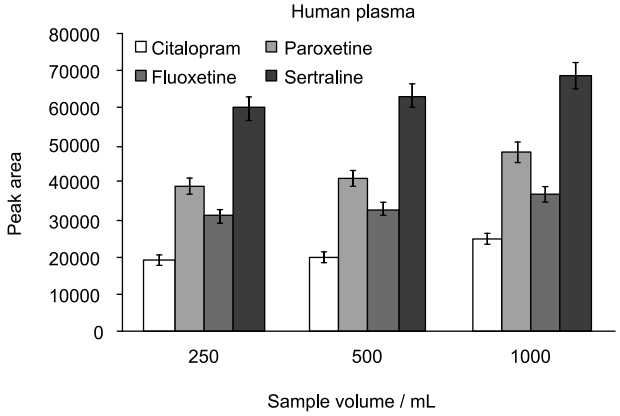


**Figure 5.** The effect of plasma sample volume on SPME performance: plasma sample spiked with antidepressants at a concentration of 1000 ng $mL^{-1}$ and diluted in 3.0 mL phosphate buffer, pH 9.0, 0.05 mol $L^{-1}$ under stirring (1200 rpm).

coefficients. This could reduce the extraction time and increase the lifetime of the polythiophene phase.

The optimized results, among those evaluated for direct SPME-PTh, were obtained under the conditions: 250 μL plasma sample diluted with 3.0 mL borate buffer solution (0.05 mol $L^{-1}$, pH 9.0), followed by immersion of the polythiophene electropolymerized electrode into the sample. The extractions were performed under magnetic stirring at a rate of 1200 rpm for 40 min at 25 °C. For the desorption process, the polythiophene electrode was inserted into a conical vial containing the mobile phase (static mode, 250 μL) for 15 min at 25 °C.

### Analytical validation of the SPME-PTh/LC method

The selectivity of the SPME/LC method can be demonstrated by the chromatograms of (i) blank plasma spiked with antidepressants at 500 ng $mL^{-1}$ and (ii) blank plasma (Figure 6). These chromatograms do not present interfering peaks at the retention time of the antidepressants. The synthetic plasma consisted of a solution with ionic strength and viscosity similar to that of the human plasma, but without the presence of human plasma proteins.[18]

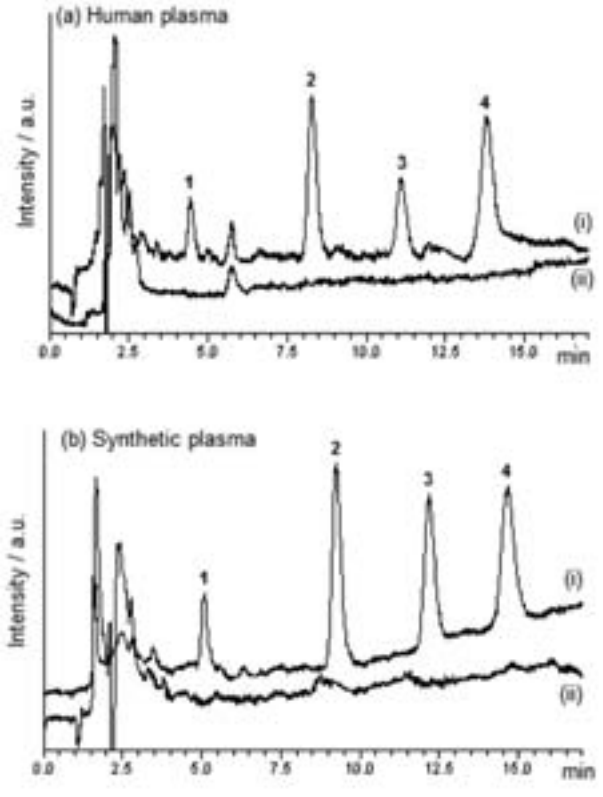


**Figure 6.** SPME/LC chromatograms of (i) blank plasma spiked with antidepressants at 500 ng $mL^{-1}$ and (ii) blank plasma, for analysis of (a) human plasma and (b) synthetic plasma, containing (1) citalopram, (2) paroxetine, (3) fluoxetine and (4) sertraline.

Antidepressants may be prescribed in combination with different psychotropic agents and other drugs. Consequently, an evaluation of the interference (co-elution) of potential co-administered drugs was required. Different drug standards were injected in the LC-UV system to evaluate the co-elution with the analytes in the applied chromatographic conditions (Table 1). On the basis of the retention times, other drugs do not co-elute with the analytes.

**Table 1.** Retention time of the studied drugs as possible interferents

| Drugs | Retention time / min |
|---|---|
| Ascorbic acid | 1.05 |
| Primidone | 1.95 |
| Caffeine | 2.58 |
| Phenacetine | 3.14 |
| Diclofenac | 3.67 |
| Moclobemide | 3.73 |
| Diazepam | 4.19 |
| Propanolol | 5.04 |
| Citalopram | 5.21 |
| Clonazepam | 5.85 |
| Carbamazepine | 5.97 |
| Phenytoin | 6.13 |
| Mirtazapine | 7.34 |
| Paroxetine | 9.72 |
| Fluoxetine | 13.06 |
| Sertraline | 16.30 |

The linearity and limit of quantification (LOQ) of the proposed SPME-PTh/LC method for human and synthetic plasma samples are illustrated in Table 2. The evaluated intervals for both plasma samples were linear, with correlation coefficients greater than 0.998. The LOQ was determined as the lowest concentration of the calibration curve, with CV lower than 15%, and chromatographic signal ten times greater than the signal-to-noise ratio.

The angular coefficients of the calibration curve (method sensitivity) and LOQ values of the SPME-PTh/LC method obtained for the synthetic plasma are lower than those obtained for the human plasma, Table 2.

The sensitivity of the SPME-PTh/LC method in human plasma samples could be improved using a fluorescence detector, which presented LOQ values in the order of 50 ng $mL^{-1}$ (data not shown).

Table 3 lists the values of interassay precision and accuracy of the SPME-PTh/LC method for determination of antidepressants in synthetic and human plasma samples.

Although the sensitivity of the method were reduced due to adsorption of plasma endogenous compounds onto the SPME phase (matrix effect), the polythiophene phase presented selectivity for extraction of antidepressants from the plasma sample.

**Table 2.** Linearity and limit of quantification (LOQ) of SPME-PTh/LC for simultaneous analysis of antidepressants in plasma samples

| | Drug | Linear regression[a] | $r^2$ | LOQ / (ng $mL^{-1}$) |
|---|---|---|---|---|
| Synthetic plasma [a](LOQ: 1000 ng $mL^{-1}$) | citalopram | y = 3066.4 + 35.9 x | 0.998 | 50 |
| | paroxetine | y = 3539.3 + 125.0 x | 0.999 | 25 |
| | fluoxetine | y = 4235.2 + 113.4 x | 0.999 | 25 |
| | sertraline | y = 2454.18 + 8.94 x | 0.998 | 25 |
| Human plasma [a](LOQ: 4000 ng $mL^{-1}$) | citalopram | y = 6059.5 + 2.49 x | 0.998 | 250 |
| | paroxetine | y = 17862.0 + 4.79 x | 0.998 | 200 |
| | fluoxetine | y = 16777.6 + 2.15 x | 0.999 | 250 |
| | sertraline | y = 28259.3 + 9.66 x | 0.999 | 200 |

**Table 3.** Accuracy and inter-assay precision (coefficient of variation, CV) of the SPME-PTh/LC-UV method for analysis of plasma samples

| | Drugs | Added concentration / (ng $mL^{-1}$) | Accuracy / % (n = 5) | CV / % (n = 5) |
|---|---|---|---|---|
| Synthetic plasma | citalopram | 50 | 101 | 5.6 |
| | paroxetine | 25 | 98 | 3.7 |
| | fluoxetine | 25 | 112 | 3.9 |
| | sertraline | 25 | 92 | 6.8 |
| Human plasma | citalopram | 250 | 82 | 13 |
| | paroxetine | 200 | 76 | 15 |
| | fluoxetine | 250 | 87 | 11 |
| | sertraline | 200 | 79 | 14 |

In addition, the relative recovery (Table 4) of drugs from human plasma compared with drug recovery from synthetic plasma was also calculated by using the mean slopes of the constructed curves for the human and synthetic plasma samples (equation 1). The relative recovery correlates the analytical sensitivity of the method in different matrices, human and synthetic plasma samples, thus illustrating the effect of the endogenous compounds on the SPME process.

$$\text{Relative recovery (\%)} = \frac{\text{Slope of the calibration curve in human plasma}}{\text{Slope of the calibration curve in synthetic plasma}} \times 100 \quad (1)$$

The recovery rates of the plasma samples of the SPME/LC method using polythiophene phase for determination of adrenolytic drugs (metoprolol, oxprenolol, mexiletine, propranolol and propaphenon) were lower than those obtained for aqueous samples. The authors did not obtain enough sensitivity for therapeutic drug monitoring analysis (LC-UV method), but according to them, some modifications could improve the method sensitivity.[16]

The fiber-to-fiber reproducibility, or rather, the reproducibility of the electrochemical coating procedure, was also investigated. The average results (n = 5) from the SPME-PTh/LC determination carried out with three different fibers were very similar, with coefficients of variation (CV) ranging from 7 to 13%. These assays were carried out with human plasma samples spiked with drugs (500 ng $mL^{-1}$).

**Table 4.** Ratio between the slopes of the SPME/LC calibration curves obtained for the human and synthetic plasma samples, and recovery, as estimated by equation 1

| Drugs | Ratio between the slopes | Relative recovery / % |
|---|---|---|
| Citalopram | 0.25 | 25 |
| Paroxetine | 0.19 | 19 |
| Fluoxetine | 0.39 | 39 |
| Sertraline | 0.29 | 29 |

## Conclusion

The developed PTH film electropolymerized in acetonitrile solution containing TBATFB is an inexpensive promising alternative for the development of new phases for the SPME technique.

Although the sensitivity of the method was reduced due to adsorption of plasma endogenous compounds onto the SPME phase (matrix effect), the polythiophene phase presented selectivity for extraction of antidepressants from the plasma sample. The competitive process (limited number of surface sites) among drugs and polythiophene phase was not observed.

The sensitivity of the SPME-PTh/LC method in human plasma samples could be improved using a fluorescence detector, which presented LOQ values in the order of 50 ng $mL^{-1}$.

The proposed method can be a useful tool for the determination of antidepressants in human plasma samples in urgent toxicological analysis after the accidental or suicidal intake of medication in higher doses.

## Acknowledgments

This work was supported by grants from Fundação de Amparo à Pesquisa do Estado de São Paulo (FAPESP) and Conselho Nacional de Desenvolvimento Científico e Tecnológico (CNPq).

## References

1. Feldmann Jr., R. E.; Sawa, A.; Seidler, G. H.; *J. Psychiatr. Res.* **2007**, *41*, 713.
2. Nash, J.; Nutt, D.; *Psychiatry* **2007**, *6*, 289.
3. Frey, R.; Schreinzer, D.; Stimpfl, T.; Vycudilik, W.; Berzlanovich, A.; Kasper, S.; *Eur. Neuropsychopharmacol.* **2000**, *10*, 133.
4. Ohberg, A.; Vuori, E.; Klaukka, T.; Lonnqvist, J.; *J. Affect. Disord.* **1998**, *50*, 225.
5. Jick, S. S.; Dean, A. D.; Jick, H.; *Br. Med. J.* **1995**, *310*, 215.
6. Rubino, A.; Roskell, N.; Tennis, P.; Mines, D.; Weich, S.; Andrews, E.; *Br. Med. J.* **2007**, *334*, 242.
7. Malmvik, J.; Liiwenhielm, C. G. P.; Melander, A.; *Eur. J. Clin. Pharmacol.* **1994**, *46*, 291.
8. Kataoka, H.; *Trends Analyt. Chem.* **2003**, *22*, 232.
9. Arthur, C. L.; Pawliszyn, J.; *Anal. Chem.* **1990**, *62*, 2145.
10. Chaves, A. R.; Chiericato Jr., G.; Queiroz, M. E. C.; *J. Chromatogr., B: Anal. Technol. Biomed. Life Sci.* **2009**, *877*, 587.
11. Wu, J.; Pawliszyn, J.; *Anal. Chim. Acta* **2004**, *520*, 257.
12. Gbatu, T. P.; Ceylan, O.; Sutton, K. L.; Rubinson, J. F.; Galal, A.; Caruso, J. A.; Mark Jr., H. B.; *Anal. Commun.* **1999**, *36*, 203.
13. Yates, B. J.; Temsamani, K. R.; Ceylan, O.; Oztemiz, S.; Gbatu, T. P.; La Rue, R. A.; Tamer, U.; Mark Jr., H. B.; *Talanta* **2000**, *58*, 739.
14. Tamer, U.; Yates, B.; Galal, A.; Gbatu, T.; LaRue, R.; Schmiesing, C.; Temsamani, K.; Ceylan, O.; Mark Jr., H.; *Microchim. Acta* **2003**, *143*, 205.
15. Olszowy, P.; Szultka, M.; Fuchs, P.; Kegler, R.; Mundkowski, R.; Miekisch, W.; Schubert, J.; Buszewski, B.; *J. Pharm. Biomed. Anal.* **2010**, *53*, 1022.
16. Olszowy, P.; Szultka, M.; Ligor, T.; Nowaczyk, J.; Buszewski, B.; *J. Chromatogr., B: Anal. Technol. Biomed. Life Sci.* **2010**, *878*, 2226.
17. Mehdinia, A.; Ghassempour, A.; Rafati, H.; Heydari, R.; *Anal. Chim. Acta* **2007**, *587*, 82.
18. Holme, S.; Heaton, W. A.; *Transfus. Sci.* **1994**, *15*, iv.
19. Bagheri, H.; Babanezhad, E.; Es-haghi, A.; *J. Chromatogr., A* **2007**, *1152*, 168.
20. Li, X.; Li, C.; Chen, J.; Li, C.; Sun, C.; *J. Chromatogr., A* **2008**, *1198-1199*, 7.
21. Huang, M.; Jiang, G.; Cai, Y.; *J. Sep. Sci.* **2005**, *28*, 2218.
22. Kabasakaloglu, M.; Kiyak, T.; Toprak, H.; Aksu, M. L.; *Appl. Surf. Sci.* **1999**, *152*, 115.
23. Shen, L.; Xu, J.; Wei, Z.; Xiao, Q.; Pu, S.; *Eur. Polym. J.* **2005**, *41*, 1738.
24. Abou-Elenien, G. M.; El-Maghraby, A. A.; El-Abdallah, G. M.; *Synth. Met.* **2004**, *146*, 109.
25. Vignali, M.; Edwards, R. A. H.; Serantoni, M.; Cunnane, V. J.; *J. Electroanal. Chem.* **2006**, *591*, 59.
26. Wu, J.; Pawliszyn, J.; *J. Chromatogr., A* **2001**, *909*, 37.
27. Sarac, A. S.; Geyik, H.; Parlak, E. A.; Serantoni, M.; *Prog. Org. Coat.* **2007**, *59*, 28.
28. Zhou, M.; Heinze, J.; *Electrochim. Acta* **1999**, *44*, 1733.
29. Mester, Z.; Sturgeon, R.; *Spectrochim. Acta, Part B* **2005**, *60*, 1243.
30. Vasskog, T.; Berger, U.; Samuelsen, P. J.; Kallenborn, R.; Jensen E.; *J. Chromatogr., A* **2006**, *1115*, 187.
31. Lord, H.; Pawliszyn, J.; *J. Chromatogr., A* **2000**, *902*, 17.
32. Theodoridis, G.; Koster, E. H. M.; de Jong, G. J.; *J. Chromatogr., B: Anal. Technol. Biomed. Life Sci.* **2000**, *745*, 49.

*Submitted: December 20, 2010*
*Published online: October 18, 2011*

**FAPESP has sponsored the publication of this article.**

Article

*J. Braz. Chem. Soc.*, Vol. 23, No. 1, 65-71, 2012.
Printed in Brazil - ©2012 Sociedade Brasileira de Química
0103 - 5053 $6.00+0.00

# Electrospray Ionization Tandem Mass Spectrometry of the Two Main Antimalarial Drugs: Artemether and Lumefantrine

*Vanessa G. dos Santos,[a] Ricardo J. Alves,[b] Marcos N. Eberlin,[a] Gerson A. Pianetti[b] and Isabela C. César*[,b]*

[a]*Instituto de Química, Universidade Estadual de Campinas, Cidade Universitária Zeferino Vaz, 13083-970 Campinas-SP, Brazil*

[b]*Faculdade de Farmácia, Universidade Federal de Minas Gerais, Av. Pres. Antônio Carlos 6627, 31270-901 Belo Horizonte-MG, Brazil*

Ionização por electrospray no modo de íons positivos, e espectrometria de massas de alta resolução e exatidão, e em tandem, realizadas em espectrômetro de massas híbrido quadrupolo e tempo de vôo, foram utilizadas para investigar a dissociação química das moléculas intactas dos dois antimaláricos mais amplamente utilizados: artemeter e lumefantrina. As rotas de dissociação das formas cationizadas e protonadas foram claramente estabelecidas via determinações de massas de alta resolução e distribuição isotópica. Os resultados obtidos podem auxiliar a monitorização e a quantificação de artemeter e lumefantrina por LC-MS/MS, assim como de novos derivados ou outros fármacos antimaláricos estruturalmente relacionados.

Electrospray ionization in the positive ion mode and high resolution and high accuracy tandem mass spectrometry performed in a hybrid quadrupole time-of-flight mass spectrometer were used to investigate the dissociation chemistry of the intact molecules of two most widely used antimalarial drugs: artemether and lumefantrine. The dissociation pathways of their cationized and protonated forms were rationalized based on high accuracy mass measurements and isotopic distributions. The obtained results should benefit LC-MS/MS monitoring and quantitation by mass spectrometry of the artemether and lumefantrine molecules, as well as of new derivatives or other structurally related antimalarial drugs.

**Keywords**: artemether, lumefantrine, ion dissociation, tandem mass spectrometry, ESI-MS/MS

## Introduction

Artemether-lumefantrine is a drug association currently of wide use for malaria treatment. The registered fixed dose combination is commercialized in tablets that contain 20 mg of artemether and 120 mg of lumefantrine.[1] The World Health Organization (WHO) recommends this association as first line therapy for *falciparum* malaria in endemic areas, mainly when cases of resistance against traditional drugs are reported.[2] Artemether (Scheme 1) is a semisynthetic derivative of artemisinin, a natural product of the Chinese herb *Artemisia annua*,[3] whereas lumefantrine (Scheme 1) is a synthetic racemic fluorene derivative originally named benflumetol.[4]

Counterfeiting or drugs with substandard antimalarial doses are however major problems of worldwide occurrence that dramatically affects the efficacy of malarial treatment. Ineffective or poor quality drugs is of great concern since their use may contribute to the development of plasmodium resistance in malaria endemic areas, due to the exposition to subtherapeutic doses.[5,6] The development of useful and reliable methods for the identification of antimalarials is therefore essential to evaluate the quality of the antimalarial pharmaceutical preparations.

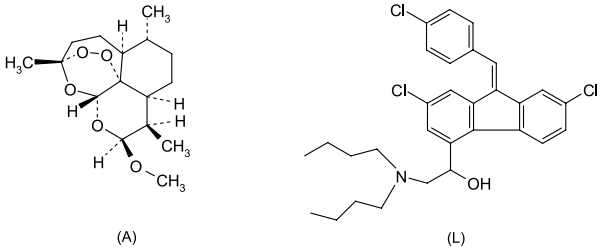


**Scheme 1.** Chemical structures of artemether (A) and lumefantrine (L).

*e-mail: isaccesar@bol.com.br

Chromatographic methods for the analysis of artemether and lumefantrine have been reported, focusing on the quantitation of these drugs in pharmaceutical products[7] or biological matrices.[8,9] HPLC with UV detection is the most common analytical method employed for lumefantrine,[10,11] whereas for artemether, electrochemical[12,13] or ultraviolet detection after acid hydrolysis[14] have been reported. Studies employing mass spectrometry (MS) to quantify these drugs have used electrospray ionization for lumefantrine[9,15,16] and atmospheric pressure chemical ionization for artemether.[17,18] Quantitation was the main focus of these studies, therefore product ions and dissociation routes of these drugs by tandem mass spectrometry were not thoughtfully evaluated.

The determination of the dissociation pathways of these main antimalarial drugs should benefit their monitoring by MS techniques in pharmaceutical products and biological fluids and the proper identification of artemether and lumefantrine derivatives and analogues. Herein we described our results of an investigation via electrospray ionization and tandem mass spectrometry performed in a high resolution and high accuracy hybrid quadrupole time-of-flight mass spectrometer of the dissociation chemistry of the protonated or cationized molecules of artemether and lumefantrine.

## Experimental

### Materials

Artemether and lumefantrine reference standards were purchased from Dafra Pharma (Turnhout, Belgium). Ultrapure water was obtained from a Millipore system (Bedford, MA, USA). Methanol (HPLC grade) was purchased from Tedia (Fairfield, OH, USA) and formic acid (analytical grade) was from J. T. Baker (Phillipsburg, NJ, USA).

### Mass spectrometry

The mass spectrometry experiments were performed using a hybrid quadrupole time-of-flight (Q-TOF) mass spectrometer (Micromass, Manchester, UK). The ionization technique used was electrospray ionization (ESI) in the positive ion mode. Typical MS conditions were: capillary voltage of 3 kV, cone voltage of 30 V, source temperature of 100 °C, desolvation temperature of 100 °C.

Acidic solutions of the drugs were prepared in water/methanol (1:1) containing 0.1% formic acid. These solutions were infused using a syringe pump (Harvard Apparatus) at a flow rate of 5 μL $min^{-1}$. ESI-MS were acquired along the 50-1000 *m/z* range. ESI-MS/MS experiments were done by selecting the ion of interest using the first mass analyzing quadrupole. The selected ion was in turn subjected to 5-40 eV collisions with argon in the collision cell whereas the orthogonal TOF mass analyzer was used to acquire the ESI-MS/MS data. External calibration with a phosphoric acid solution was employed.

## Results and Discussion

### Artemether

Previous reports on the MS detection of the artemether molecule[18,19] have reported on the failure to observe the intact protonated molecule and used therefore only fragments and secondary dissociations for its quantitation. We also found that ESI-MS of an acid methanolic solution of artemether detects none of its protonated molecule $[M + H]^+$ and only fragments were observed. A minor ion of *m/z* 281, $[M + H - H_2O]^+$, has been detected probably due to dissociation by water loss of the protonated molecule $[M + H]^+$ of *m/z* 299. Secure quantitation of drugs is ideally performed via ions formed from the intact molecule. We therefore dissolved the artemether molecule in methanol and doped the resulting solution with lithium chloride hoping to favor the detection of the intact molecule in its cationized form $[M + Li]^+$. Figure 1 shows the resulting ESI(+)-MS for this methanolic solution. The protonated molecule $[M + H]^+$ of *m/z* 299 is again absent. The main ions are $[M + Li]^+$ of *m/z* 305, $[M + Na]^+$ of *m/z* 321 and $[M + K]^+$ of *m/z* 337 as well as the corresponding dimers

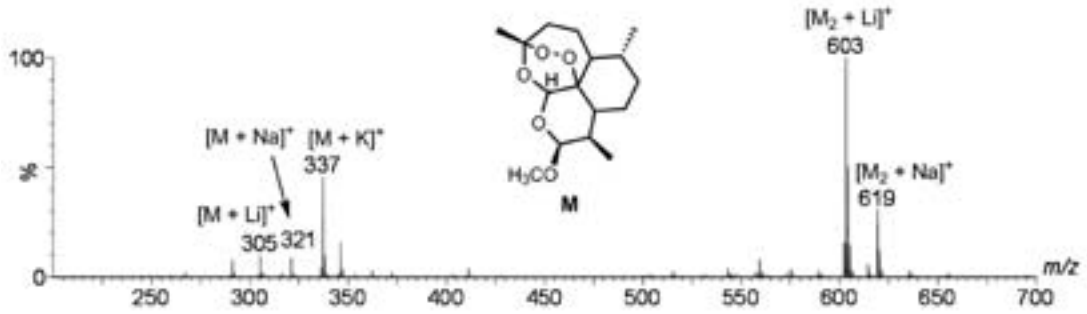


**Figure 1.** ESI(+)-MS of a methanolic solution of artemether doped with LiCl.

$[M_2 + Li]^+$ of *m/z* 603 and $[M_2 + Na]^+$ of *m/z* 619. $Na^+$ and $K^+$ are likely therefore present due to solvent contaminants or from the original sample. Multiple cationization is not ideal for quantitation but allowed us to study, for the first time, the dissociation chemistry of the intact molecule in several of its cationized forms, as well as to double check the proposed routes, see below. The $[M + Li]^+$ ion of *m/z* 305, $[M + Na]^+$ of *m/z* 321 and $[M + K]^+$ of *m/z* 337 were therefore selected and dissociated by collisions with argon (Figure 2). Scheme 2 rationalizes the main dissociation routes for $[M + Li]^+$ of *m/z* 305. The first process is likely isomerization of the $Li^+$ adduct via the rupture of the labile artemether peroxide ring. Loss of $H_2O$ and CO then occurs to produce the fragment ion of *m/z* 259. Subsequently, loss

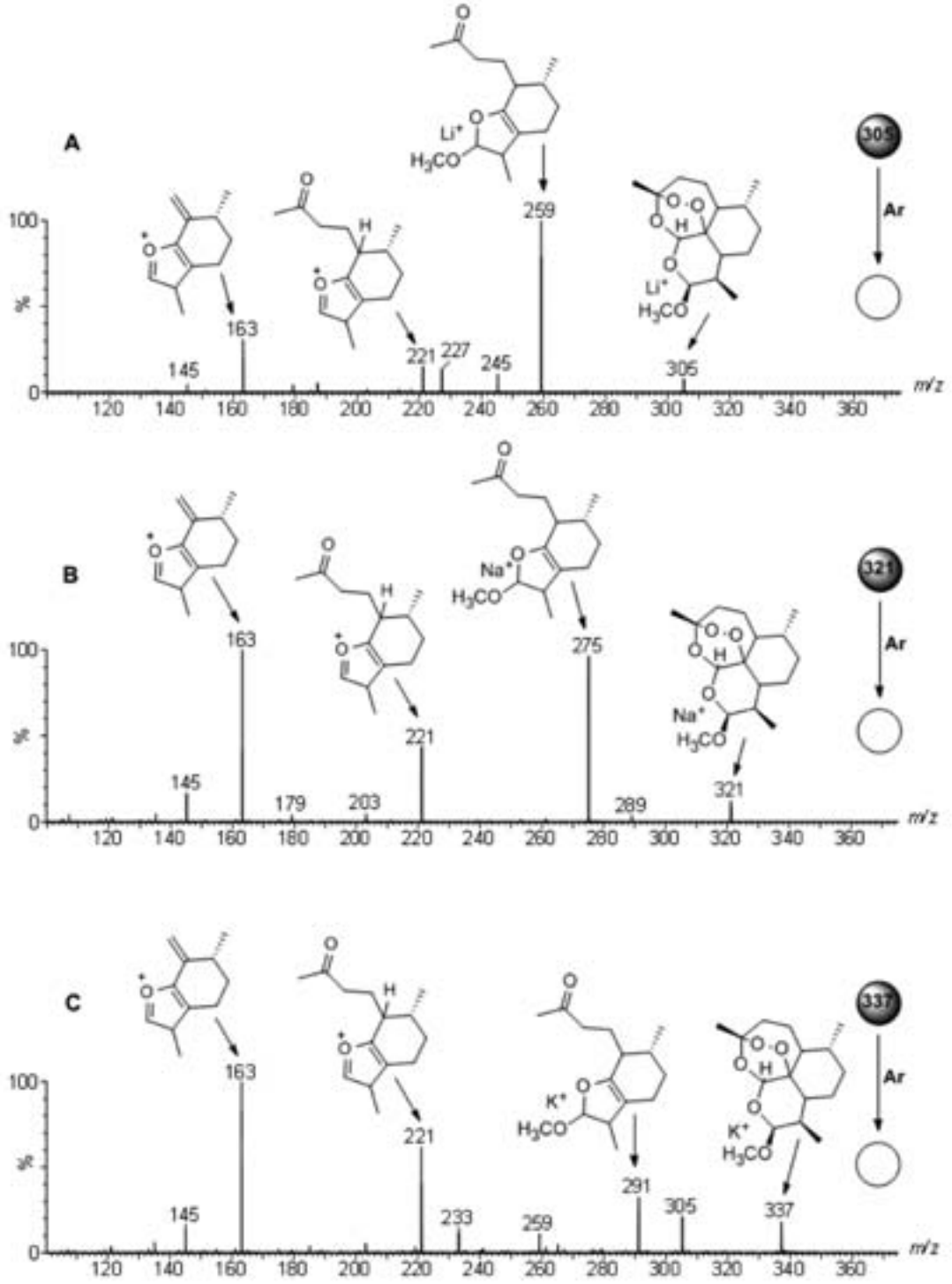


**Figure 2.** ESI(+)-MS/MS of the (A) $[M + Li]^+$, (B) $[M + Na]^+$ and (C) $[M + K]^+$ aducts of artemether.

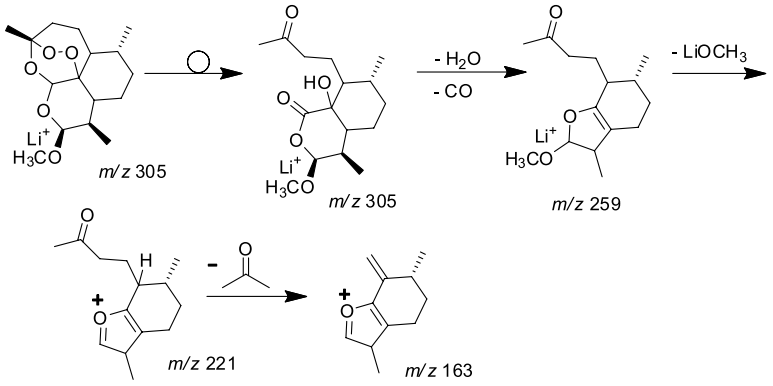


**Scheme 2.** Proposed fragmentation pathway for the cationized forms of artemether, as exemplified for $[M + Li]^+$.

of a neutral $LiOCH_3$ forms the product ion of *m/z* 221, which dissociates in turn by the loss of acetone to form the ion of *m/z* 163. Shi *et al.*[18] and Xing *et al.*[19] also found an ion of *m/z* 163 for the ESI-MS of artemether and proposed a distinct chemical structure for it based on a different mechanistic rationalization. We however favor the routes outlined in Scheme 2.

The concomitant formation via ESI of the $Li^+$, $K^+$ and $Na^+$ adducts of the intact artemether molecule was beneficial since it permits us to double check the accuracy of our proposed dissociation routes (Scheme 2). Indeed, the dissociation observed in the ESI-MS/MS of the $Na^+$ (Figure 2B) and $K^+$ adducts (Figure 2C) were analogous and fully consistent with the proposed routes. The fragments of *m/z* 163 and 221 were, as expected, shared by the three cationized molecules whereas the major cationized fragments in Figure 2 (of *m/z* 259 for $Li^+$ and *m/z* 275 for $Na^+$) display the corresponding *m/z* shifts (16 units from $Li^+$ to $Na^+$). In LC-MS/MS monitoring of this drug, therefore, extensive cationization (by either $Li^+$, $Na^+$ or $K^+$) is recommended whereas the fragment ions of *m/z* 259 (for $Li^+$) and 163 appears to be ideal for the quantitation and confirmation MRM transitions, respectively. The source conditions should also be tuned to reduce the abundance of the dimers such as $[M_2 + Li]^+$ via in-source CID.

## Lumefantrine

Contrary to the artemether molecule, the protonated molecule of lumefantrine seems to be of high stability since an acidic water/methanol (1:1) solution of this drug (0.1% of formic acid) yielded a ESI(+)-MS dominated by an abundant and nearly exclusive set of the $[M + H]^+$ splitted in its expected isotopologue ions (Figure 3). Note in the insert of Figure 3 the quite characteristic isotopologue distribution due to the presence of three chlorine atoms with $^{35}Cl$ and $^{37}Cl$ isotopes. The ions of *m/z* 560 and 592 correspond to the methanol adducts $[M + CH_3OH + H]^+$ and $[M + 2CH_3OH + H]^+$, respectively.

The ESI-MS/MS for protonated lumefantrine, as represented in Figure 4 for its isotopologue ions of *m/z* 528 and 530, showed rich dissociation chemistry. Water loss is the most favored initial dissociation forming (for the ion of *m/z* 528, Figure 4A) the major fragment ion of *m/z* 510. This elimination is likely favored due to the formation of a highly stable, fully delocalized, resonance stabilized

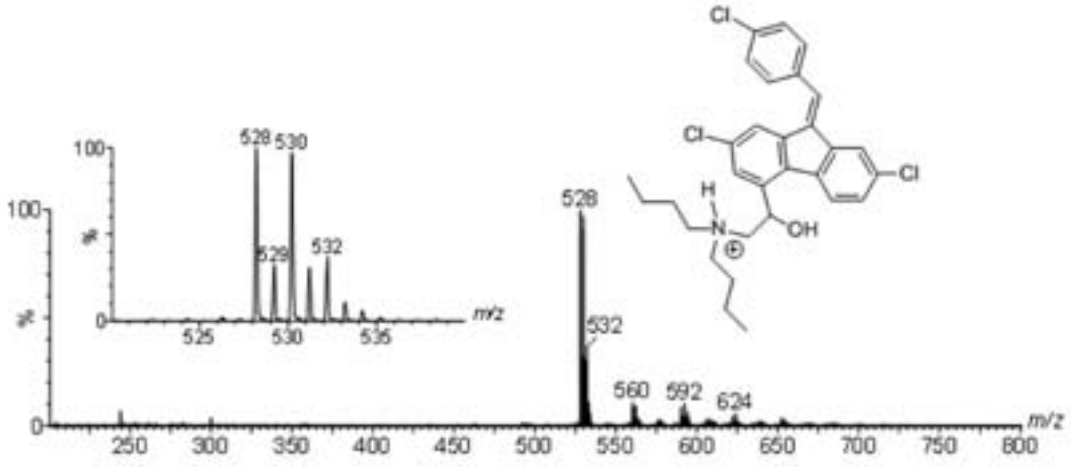


**Figure 3.** ESI(+)-MS of an acidified water:methanol solution of lumefantrine.

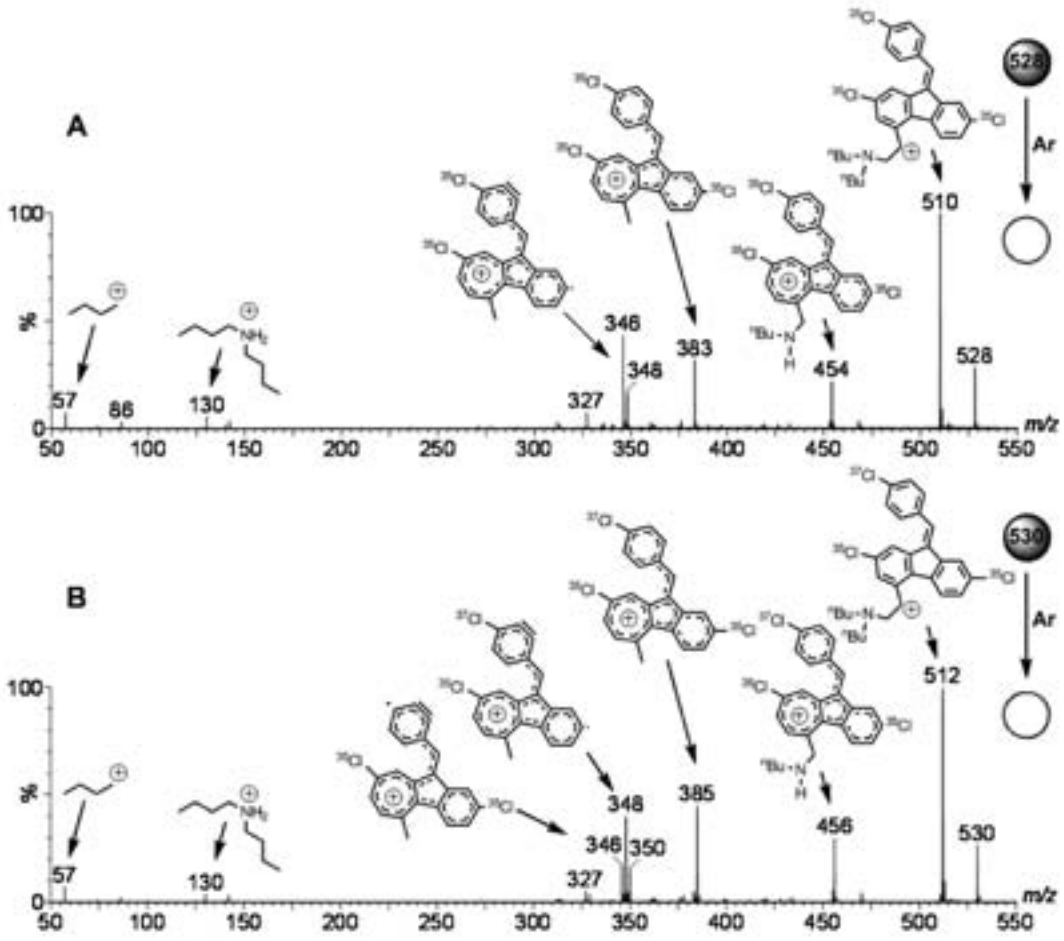


**Figure 4.** ESI(+)-MS/MS of the isotopologue ions of protonated lumefantrine of (A) *m/z* 528 and (B) *m/z* 530.

benzyl-like cation, which may rearranges to a tropylium-like ion (Scheme 3).[20] Dissociation then proceeds at the side chains and the next loss occurs by the elimination of a neutral butene molecule to form the ion of *m/z* 454, and then by the loss of an imine (1-butanimine) to form the ion of *m/z* 383. With apparently no favored route available for the elimination of a neutral molecule, dissociation then proceeds against the even-electron rule[21] by the loss of a chlorine radical (*m/z* 348) and then by the loss of a $H_2$ molecule (*m/z* 346).

The set of $^{35}Cl/^{37}Cl$ isotopologue ions for protonated lumefantrime (Figure 3) also permitted us to double check the proposed dissociation route (Scheme 4) using "natural" isotopic labeling via the selection and dissociation of the ions of *m/z* 528 ($^{35}Cl_3$), 530 ($^{35}Cl_2{}^{37}Cl$) and 532 ($^{35}Cl^{37}Cl_2$). The ESI-MS/MS data fully confirmed the proposed routes via the observation of the corresponding *m/z* shifts due to the presence (or loss) of species bearing $^{37}Cl$ or $^{35}Cl$ atoms, as exemplified for the ion of *m/z* 530 in Figure 4B. Note that all structural assignments of fragment ions have been corroborated by the *m/z* values measured with high accuracy (Table S1- Supplementary Information).

Therefore, for the LC-MS/MS quantitation of lumefantrine, MRM seems to be ideal via the selection of the pair of abundant isotopolgue ions of *m/z* 528 and 530 and the monitoring of the transition due to water loss (*m/z* 510 and 512, respectively) while using the dissociation by water plus butene plus Cl (*m/z* 383 and 385, respectively) for confirmation.

## Conclusions

Using ESI(+) and high-resolution and high accuracy MS/MS performed in a hybrid quadrupole time-of-flight mass spectrometer, the dissociation chemistry of the cationized ($Li^+$, $Na^+$ and $K^+$) molecule of artemether and of protonated isotopologue molecules of lumefantrine were established via high accuracy *m/z* measurements and natural isotopic labeling. These results should benefit secure LC-MS/MS monitoring and quantitation of the artemether and lumefantrine molecules in pharmaceutical formulations or biological fluids as well as new derivatives or other structurally related antimalarial drugs.

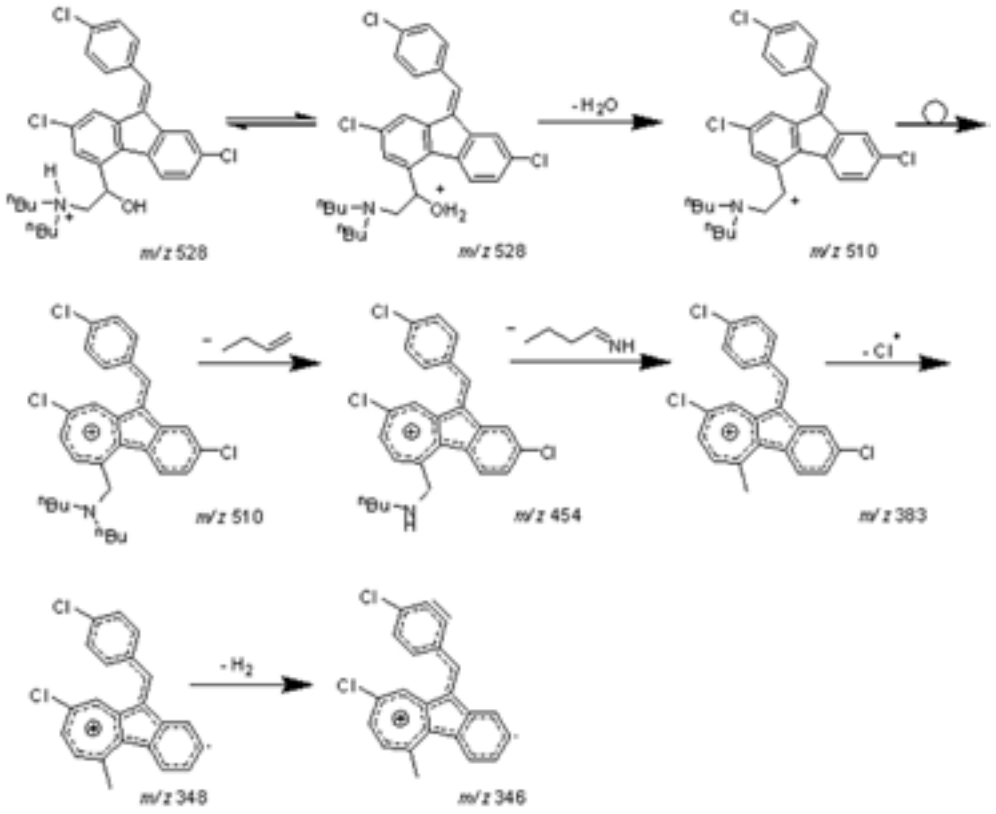


**Scheme 3.** Proposed fragmentation pathway for protonated lumefantrine.

## Supplementary Information

Supplementary data are available free of charge at http://jbcs.sbq.org.br as PDF file.

## Acknowledgments

We thank the following Brazilian Science foundations, FAPESP, FAPEMIG, and CNPq, for financial assistance.

## References

1. Omari, A. A.; Gamble, C.; Garner, P.; *Trop. Med. Int. Health* **2004**, *9*, 192.
2. World Health Organization; *Antimalarial Drug Combination Therapy*, Report of a WHO Technical Consultation, WHO: Geneva, 2001.
3. Hien, T. T.; Davis, T. M.; Chuong, L. V.; Ilett, K. F.; Sinh, D. X.; Phu, N. H.; Agus, C.; Chiswell, G. M.; White, N. J.; Farrar, J.; *Antimicrob. Agents Chemother*. **2004**, *48,* 4234.
4. White, N. J.; Van Vugt, M.; Ezzet, F.; *Clin. Pharmacokinet.* **1999**, *37,* 105.
5. Green, M. D.; Mount, D. L.; Wirtz, R. A.; *Trop. Med. Int. Health* **2001**, *6,* 980.
6. Atemnkeng, M. A.; De Cock, K.; Plaizier-Vercammen, J.; *Trop. Med. Int. Health* **2007**, *12,* 68.
7. César, I. C.; Nogueira, F. H. A.; Pianetti, G. A.; *J. Pharm. Biomed. Anal.* **2008**, *48,* 951.
8. Hodel, E. M.; Zanolari, B.; Mercier, T.; Biollaz, J.; Keiser, J.; Olliaroc, P.; Gentona, B.; Decosterd, L. A.; *J. Chromatogr., B: Anal. Technol. Biomed. Life Sci.* **2009**, *877,* 867.
9. César, I. C.; Ribeiro, J. A. A.; Teixeira, L. S.; Bellorio, K. B.; Abreu, F. C.; Moreira, J. M.; Chellini, P. R.; Pianetti, G. A.; *J. Pharm. Biomed. Anal.* **2011**, *54,* 114.
10. Mansor, S. M.; Navaratnam, V.; Yahaya, N.; Nair, N. K.; Wernsdorfer, W. H.; Degen, P. H.; *J. Chromatogr., B: Anal. Technol. Biomed. Life Sci.* **1996**, *682,* 321.
11. Zeng, M.; Lu, Z.; Yang, S.; Zhang, M.; Liao, J.; Liu, S.; Teng, X.; *J. Chromatogr., B: Anal. Technol. Biomed. Life Sci.* **1996**, *681,* 299.
12. Navaratnam, V.; Mansor, S. M.; Chin, L. K.; Mordi, M. N.; Asokan, M.; Nair, N. K.; *J. Chromatogr., B: Anal. Technol. Biomed. Life Sci.* **1995**, *669,* 289.
13. Karbwang, J.; Na-Bangchang, K.; Molunto, P.; Banmairuroi, V.; Congpuong, K.; *J. Chromatogr., B: Anal. Technol. Biomed. Life Sci.* **1997**, *690,* 259.
14. Thomas, C. G.; Ward, S. A.; *J. Chromatogr., B: Anal. Technol. Biomed. Life Sci.***1992**, *583,* 131.
15. Wahajuddin; Singh, S. P.; Jain G. K.; *J. Chromatogr., B: Anal. Technol. Biomed. Life Sci.* **2009**, *877,* 1133.
16. Liu, T. ; Du, F. ; Wan, Y. ; Zhu, F. ; Xing, J.; *J. Mass Spectrom.* **2011**, *46*, 725.

17. Souppart, C.; Gauducheau, N.; Sandrenan, N.; Richard, F.; *J. Chromatogr., B: Anal. Technol. Biomed. Life Sci.* **2002**, *774,* 195.
18. Shi, B.; Yu, Y.; Li, Z.; Zhang, L.; Zhong, Y.; Su, S.; Liang, S.; *Chromatographia* **2006**, *64,* 523.
19. Xing, J.; Yan, H.; Zhang, S.; Ren, G.; Gao, Y.; *Rapid Commun. Mass Spectrom.* **2006**, *20,* 1463.
20. Mendes, M. A.; Rittner, R.; Suwinski, J.; Szczepankiewicz, W.; Eberlin, M. N.; *Eur. J. Mass Spectrom.* **2002**, *8,* 27.
21. Karni, M.; Mandelbaum, A.; *Org. Mass Spectrom.* **1980**, *15,* 53.

*Submitted: May 25, 2011*
*Published online: October 18, 2011*

**FAPESP has sponsored the publication of this article.**

*J. Braz. Chem. Soc.*, Vol. 23, No. 1, 72-77, 2012.
Printed in Brazil - ©2012 Sociedade Brasileira de Química
0103 - 5053 $6.00+0.00

Article

# Migration of Phthalate-based Plasticizers from PVC and non-PVC Containers and Medical Devices

***Marlei Veiga, Denise Bohrer,* Paulo C. Nascimento, Adrian G. Ramirez, Leandro M. Carvalho and Regina Binotto***

*Departamento de Química, Universidade Federal de Santa Maria, Av. Roraima No. 1000, 97105-900 Santa Maria-RS, Brazil*

A presença de cinco plastificantes derivados de ftalatos em equipamentos para administração intravenosa de soluções e em hemodialisadores (HD), que são feitos tanto de policloreto de vinila (PVC) quanto de outros materiais poliméricos, foi investigada. Destes ftalatos, o único autorizado por agências reguladoras é o di-(2-etilhexil) ftalato (DEHP) em equipamentos de PVC. A determinação foi feita por chromatografia líquida de alta eficiência (HPLC) com detecção UV. Os resultados mostraram que as bolsas para infusão que são feitas tanto de PVC quanto de etil vinil acetato (EVA) contêm apenas DEHP. Entretanto, as mangueiras dos equipos de infusão e dos HD, bem como as fibras capilares dos HD feitas de celulose, contêm não só DEHP, mas também ftalato de dibutila (DBP). Todos os cinco ftalatos investigados foram encontrados nos capilares dos HD feitos de polisulfona. A migração de DEHP para soluções (aminoácidos, glicose e salina) armazenadas em bolsas ocorreu com taxas diferentes para os dois polímeros. Enquanto que para as bolsas de PVC o DEHP foi encontrado em soluções já nos primeiros dias de contato, para as bolsas de EVA a migração iniciou após aproximadamente 6 meses de armazenamento. Como os dispositivos analisados, com exceção das bolsas, contém, além do DHEP, outros ftalatos, o risco posto aos pacientes deve ser motivo de preocupação.

The presence of five plasticizer phthalates in bags and sets for intravenous administration and hemodialyzers (HD), which are made of polyvinyl chloride (PVC) and of other polymeric materials, was investigated. Di-(2-ethylhexyl) phthalate (DEHP) in PVC is the only authorized phthalate by regulatory agencies. Phthalate determination was carried out by high resolution liquid chromatograph (HPLC) with UV detection. The results showed that the infusion bags that are made of both PVC and ethylene vinyl acetate (EVA) contained only DEHP. In contrast, the tubing of infusion sets and of HD (as well as the cellulose capillaries of HD) contained not only DEHP but also dibutyl phthalate (DBP). Moreover, all five investigated phthalates were found in HD polysulfone capillaries. Migration of DEHP into the stored solutions (amino acids, glucose and saline) in bags occurred at different rates from one polymer to another. While DEHP from PVC bags was found in solutions within the first days of contact, the migration from EVA bags started only after approximately 6 months of solution storage. Since PVC and non-PVC devices (as well as capillaries of HD sets) contain DEHP and other phthalate-based plasticizers, the extent of the risk that they pose to patients remains a matter of concern.

**Keywords**: phthalates, infusion sets, hemodializers, PVC bags, EVA bags

## Introduction

It is well known that medical devices that are made of polyvinyl chloride (PVC) may leach di-(2-ethylhexyl) phthalate (DEHP). DEHP is a plasticizer that is used to make the polymer flexible, depending on the substance in contact with the plastic material. Because of this, transfer tubing, transfusion sets and blood bags have been intensively examined as sources of DEHP[1-7] and other kinds of polymers have been proposed as packaging material for pharmaceutical formulations.[8,9] The presence and the release of DEHP have been also investigated in extracorporeal circulation circuits such as hemodialyzers[10] and extracorporeal membranes of oxygenation circuits.[11,12] Concerns are related to the potential health hazards that are associated with the release of DEHP from devices made of

*e-mail: ndenise@quimica.ufsm.br

PVC. DEHP and its metabolites are known to impair the fertility of male rodents, and therefore it is assumed that they will affect human fertility as well.[13]

DEHP is an authorized additive for PVC and its concentration in the polymer mass is limited by Pharmacopoeias[14,15] to 40%. In spite of this, limits for DEHP in formulations that are stored in PVC bags are not establish in the pharmacopeial compendia. The only prescribed test is for DEHP that was extracted by the action of ether on PVC and proposes not to exceed 40% of the polymer mass.

Although PVC is the only allowed polymer to contain DEHP as a plasticizer, studies have shown that non-PVC plastic containers and devices also contain the plasticizer, resulting in the release of some DEHP. Sautou-Miranda *et al.*[16] showed that DEHP rapidly leaches from co-extruded and triple-layered IV tubing into etoposide infusion solution. In this case, the external layer of the tubing material was of PVC and the internal part (in contact with the infusion) of polyethylene. While 51.67 ± 3.63 μg $mL^{-1}$ of DHEP were leached from the PVC tubing in 1 h of contact, only a slightly lower amount (39.85 ± 0.49 μg $mL^{-1}$) was leached from the triple-layered tubing.

The U. S. Food and Drug Administration (US-FDA) launched a non-regulatory publication,[17] in which concerns about DEHP toxicity are discussed. The study concluded that there is little to no risk for patients that are exposed to the amount of released DEHP from PVC bags following the infusion of salts (normal saline or Ringer's solution). However, there is a small risk when considered the exposition to DEHP released from PVC bags which are used to store and administer drugs and require vehicle for solubilization.

In fact, other studies have shown that, depending on the constituents in the formulation, the extractable DEHP can be much higher than expected. The migration process is governed by the nature of the formulation because of the apolar character of DEHP and the absence of chemical bonds between the polymer and the plasticizer. While DEHP concentration was not higher than 24 μg $L^{-1}$ in 14 months in saline solutions, the DEHP amount reached over 300 μg $L^{-1}$ in 2 h in oily vehicles.[18]

Although DEHP is the only allowed plasticizer for PVC, other phthalates may have been used either in PVC or non-PVC medical devices. Diethyl phthalate (DEP)[19] is used as plasticizer for cellulose ester plastic films and sheets, also in adhesive plasticizers and surface lubricants that are used in food and pharmaceutical packaging. Butyl benzyl phthalate (BBP) is a plasticizer for polymers such as polyvinyl acetate, polyurethane and cellulose,[20] to cite only three among a family of more than 10 members.

Wahl *et al.*[21] identified DEHP, dihexyl phthalate (DHP), diisobutyl phthalate (DIBP), dibutyl phthalate (DBP) and butyl 2-ethylhexyl phthalate (BEP) in infusion and dialysis tubing and infusion bags, being DEHP the most abundant plasticizer in all devices. However, while blood storage bags contained only DEHP, at least three different phthalates (DEP, DBP and DIBP) were detected in all other studies.

More recently, the European Chemical Agency (ECHA) recommended that seven chemical substances of very high concern should not be used without specific authorization. They are all used in products to which consumers and workers are exposed. Among them, three phthalates (DEHP, BBP and DBP) were selected due to their impairment of reproduction.[22] The Scientific Committee on Health and Environmental Risks (SCHER) of the European Union launched non-regulatory publications on the presence of phthalates in school supplies.[23] They concluded that phthalates in school supplies are below the tolerable daily intake (TDI), but DEHP may exceed the TDI in other population groups, as those exposed to other plastic apparatus such as medical devices.[23]

In this study, we compared PVC and EVA bags, as well as the tubing of the administration set, in their capability of leaching DEHP, and four other parent phthalates into the solutions of parenteral nutrition components. We also investigated the possibility of hemodialyzers (tubing and capillaries) as a source of DEHP and other phthalates for patients undergoing hemodialysis. For both devices, the concern was not only the presence of the phthalates in the packaging material but also the role of the time of contact during shelf-life and use on the leaching of the plasticizers.

## Material and Methods

### Chromatographic separation

The chromatographic equipment consisted of a DX-300 gradient chromatographic system (Dionex, Sunnyvale, USA) with UV detector (Shimadzu, Kyoto, Japan) and a C-R6A data processor (Shimadzu), and a Supercosil LC-18 (150 × 4.6 mm, 5μm) column. Two different chromatographic conditions were used: one for the determination of the five phthalates and another for the determination of DEHP alone. For the separation of the five phthalates, the eluent consisted of acetonitrile:water in a proportion of 94:6 (v/v) and a flow rate gradient was used. The system started at 0.5 mL $min^{-1}$ and this flow rate was kept for 15 min. After this, it increased to 1.0 mL $min^{-1}$ and stayed at this level up to the end of the chromatographic run. The measurement was carried out at 202 nm and a sample loop of 25 μL was used. For the determination of

DEHP alone, the mobile phase was acetonitrile:methanol (9:1, v/v) at a flow rate of 0.8 mL $min^{-1}$ without gradient.[24,25] The measurement was carried out at 220 nm and a sample loop of 20 µL was used. A blank sample (hexane) was injected 6 times to calculate the limit of detection (LOD).

### Reagents

Standard solutions of diethylhexyl phthalate (DEHP), dibutyl phthalate (DBP), dimethyl phthalate (DMP), diethyl phthalate (DEP) and butylbenzyl phthalate (BBP) (Sigma, St. Louis, USA) were prepared by convenient dilution of a stock solution containing 1mg $mL^{-1}$ in methanol. Acetonitrile, methanol and n-hexane were all from Merck HPLC grade (Darmstadt, Germany). NaCl, KCl, $CaCl_2.2H_2O$, $MgCl_2.6H_2O$, $NaHCO_3$, sodium acetate, glucose and albumin were all from Merck. The water was distilled, de-ionized and further purified using a Milli-Q high-purity water device (Millipore, Bedford, USA).

To avoid contamination, only laboratory glassware was used, previously washed with an ethanolic solution of 10% $HNO_3$ in ethanol (v/v).

### Samples

Samples consisted of new (empty) plastic infusion sets: PVC and EVA bags (Baxter) and burette (B. Braun), and hemodialyzers made of cellulose diacetate (CAHP/DICEA 150, Baxter) and polysulfone (Hemoflow FHHPS, Fresenius). CAPD bags (Baxter) were also analyzed, but in this case, the samples were collected from filled bags. Besides being used to test phthalate migration into the different solutions, these containers or devices were analyzed to determine the concentration of phthalates in the material itself.

Individual solutions of the amino acids, which are usually present in formulations for parenteral nutrition in a concentration of 0.5% (m/v), were stored in new PVC and EVA bags (250 mL). Purified water, 0.9% NaCl and 10% glucose were also individually stored in both kinds of bags. The bags were let to stand at room temperature and aliquots of 1 mL were taken at time intervals of 15, 45, 75, 105, 165, 225 and 365 days through the rubber septum using a glass syringe with a stainless steel needle. The samples were treated as described for the determination of DEHP.

Commercial dialysis concentrates and solutions for parenteral nutrition (all stored in plastic containers) were also analyzed for the determination of their level of contamination by DEHP. At least three samples from the same lot were analyzed. The analyzed samples were: 50% glucose, 0.9% NaCl, two 10% amino acid solutions, two lipid emulsions and two saline concentrates for hemodialysis (one acid and one basic). Pure hexane was used as a blank sample.

### Sample treatment

Samples were prepared as described in the European Pharmacopoeia.[7] For the analysis of solid samples (containers and devices), *ca.* 0.1 g of the material, which was previously cut into small pieces, was mixed with 2 mL hexane and shaken for 15 min in a horizontal shaker (Edmund Bühler, Hechingen, Germany).

Liquid samples were collected in glass tubes and stored at 4 °C until analysis. To 1 mL of each sample, 1 mL hexane was added and the mixture was vortexed for 10 min. The organic layer was transferred to glass tubes and 20 or 25 µl aliquot was injected into the chromatograph.

The extraction procedure was carried out with an aqueous sample that was spiked with the 5 analytes (2.5 mg $L^{-1}$ each) and this was repeated five times with new portions of hexane and all aliquots of hexane were injected into the chromatograph.

An extra test was carried out with the internal capillary of the HD. The dialyzers were dismounted and an amount of *ca.* 1 g of the capillary material was submersed in the pure dialysis solution (synthetic, made by dissolving the components in the usual concentration) and in the dialysis solution spiked with 4.86 mg $L^{-1}$ DEHP. Aliquots of the fluids were collected after 1 h and 5 days of the submersion and analyzed for DEHP.

## Results and Discussion

The chromatogram in Figure 1 shows that the separation of the phthalates (using the optimized conditions) occurred within a running time of 25 min. The analytical curves for each phthalate and the respective figures of merit are given in Table 1. The method demonstrated to be well suited for the simultaneous determination of the 5 phthalates.

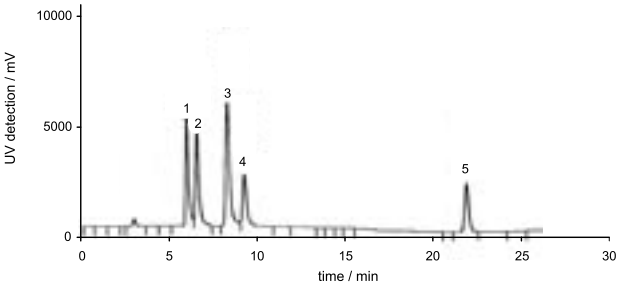


**Figure 1.** Chromatogram of a standard solution containing the phthalates: (1) DMP, (2) DEP, (3) DBP, (4) BBP, in a concentration of 0.25 mg $L^{-1}$, and (5) DEHP in a concentration of 0.50 mg $L^{-1}$.

**Table 1.** Figures of merit of the simultaneous chromatographic determination of the four phthalates and of DEHP alone

| Parameter | Phthalate | | | | |
|---|---|---|---|---|---|
| | DEHP | DMP | DEP | DBP | BBP |
| Range / (mg $L^{-1}$) | 0.50-10.00 | 0.25-5.00 | 0.25-5.00 | 0.25-5.00 | 0.25-5.00 |
| Analytical curve y (peak area) x (conc.) / (mg $L^{-1}$) | y = 6013x – 108 | y = 22833x + 2434 | y = 22649x + 577 | y = 29198x + 232 | y = 11247x + 1619 |
| $R^2$ | 0.994 | 0.998 | 0.998 | 0.999 | 0.997 |
| LOD / (mg $L^{-1}$) | 0.05 | 0.01 | 0.01 | 0.01 | 0.03 |
| Repeatability[a] / % | 1.4 | 1.5 | 0.7 | 0.9 | 1.6 |
| Reproducibility[b] / % | 4.1 | 3.4 | 2.2 | 2.1 | 3.3 |

[a]n = 6; [b]n = 3; $R^2$: linear correlation.

The yield of the extraction of spiked samples showed that more than 95% of the analytes are extracted in the first portion of hexane. Therefore, the procedure was carried out with one extraction step only.

Since only DEHP was found in some samples, the chromatographic system was set in order to determine DEHP only, in a shorter analysis time.[24]

Table 2 presents the amount of plasticizers in the investigated materials. Only DEHP was found in the obtained extracts from the bags. Although in low amounts, EVA bags also presented DEHP in their composition. On the other hand, the tubing material coupled to the bags and the burette presented DBP as well, although in much lower concentrations. Because the HD set contains two types of tubing, one softer than the other, both were analyzed. It is interesting to observe that the amount of DEHP in the softer tubing is at least five times higher than in the harder one. This is an expected result since plasticizers are added to make PVC more flexible. Surprisingly, both HD capillaries presented DEHP and DBP. Moreover, all other phthalates were found in the polysulfone capillary. However, while the sum of all extracted phthalates reached 5 mg $g^{-1}$ in the polysulfone capillary, it was more than double (11.4 mg $g^{-1}$) in the cellulose capillary.

Since the usual shelf-life of infusion solutions is two years, migration rates of DEHP from PVC and EVA bags were measured for a period of 1 year using water and the solutions of NaCl, amino acids and glucose as extractors. Attempts to store the pure components of the lipid emulsion were unsuccessful as the bag was damaged leading to the leak of the content.

Given that phthalates are very soluble in lipophylic vehicles, water soluble constituents were selected, but some apolar species were included. The results are presented in Figure 2. DEHP leached from EVA bags as much as for the PVC bags. Very low amounts were extracted by water and saline solutions from both kinds of bags. Among amino acids, differences were observed. For both kinds of polymers, histidine and threonine amino acids promoted the highest extraction rates. However a difference was observed in the kinetics of the migration. While the extraction for PVC gradually increased over time, the extraction rates for

**Table 2.** Amount of extracted phthalates from plastic materials used for intravenous infusion administration and from hemodialysis sets

| Product | Origin | Supplier | Phthalate ± SD[a] / (mg $g^{-1}$) | | | | |
|---|---|---|---|---|---|---|---|
| | | | DEHP | DMP | DEP | DBP | BBP |
| PVC bag (500 mL) | new empty bag | Baxter | 154 ± 22 | n.d. | n.d. | n.d. | n.d. |
| EVA bag (500 mL) | new empty bag | Baxter | 2.86 ± 0.44 | n.d. | n.d. | n.d. | n.d. |
| PVC bag (1000 mL) | lipid emulsion | Fresenius-Kabi | 170 ± 25 | n.d. | n.d. | n.d. | n.d. |
| PVC bag (2000 mL) | CAPD dialysate | Baxter | 115 ± 23 | n.d. | n.d. | n.d. | n.d. |
| Flexible tubing | infusion set (bag) | Baxter | 82.3 ± 9.7 | n.d. | n.d. | n.d. | n.d. |
| Flexible tubing | burette | B. Braun | 73.3 ± 8.7 | n.d. | n.d. | 0.015 ± 0.003 | n.d. |
| Flexible tubing | dialyzer | Baxter | 135 ± 17 | n.d. | n.d. | 0.024 ± 0.005 | n.d. |
| Flexible tubing | dialyzer | Fresenius-Kabi | 163 ± 21 | n.d. | n.d. | 0.008 ± 0.004 | n.d. |
| Rigid tubing | dialyzer | Baxter | 23.7 ± 1.9 | n.d. | n.d. | 0.055 ± 0.009 | n.d. |
| Rigid tubing | dialyzer | Fresenius-Kabi | 17.8 ± 2.0 | n.d. | n.d. | n.d. | n.d. |
| Capillary (cellulose) | dialyzer | Baxter | 11.3 ± 2.3 | n.d. | n.d. | 0.109 ± 0.021 | n.d. |
| Capillary (polysulfone) | dialyzer | Fresenius-Kabi | 4.75 ± 0.71 | 0.031 ± 0.011 | 0.053 ± 0.009 | 0.022 ± 0.010 | 0.088 ± 0.017 |

[a]SD: standard deviation (n = 3); n.d.: not detected (below the limit of detection).

EVA bags during the first 6 months were very low but after that increased considerably.

Despite the fact that the capillaries contain phthalates, it was supposed that they could also adsorb the circulating DEHP (from the PVC tubing) due to the nature of the capillary material. To confirm the presence of DEHP in the capillaries and also their ability to adsorb the phthalate, the dialyzers were dismounted and an amount of *ca.* 1 g of the capillary material was submersed in the pure dialysate and in the dialysate spiked with DEHP. The results in Figure 3 clearly show that the phthalate can migrate from the capillary into the fluid or *vice versa*, depending on the concentration of DEHP in both phases. Being adsorbed on the capillary, it can be leached anytime thereafter depending on the concentration ratio between the solid and liquid phases.

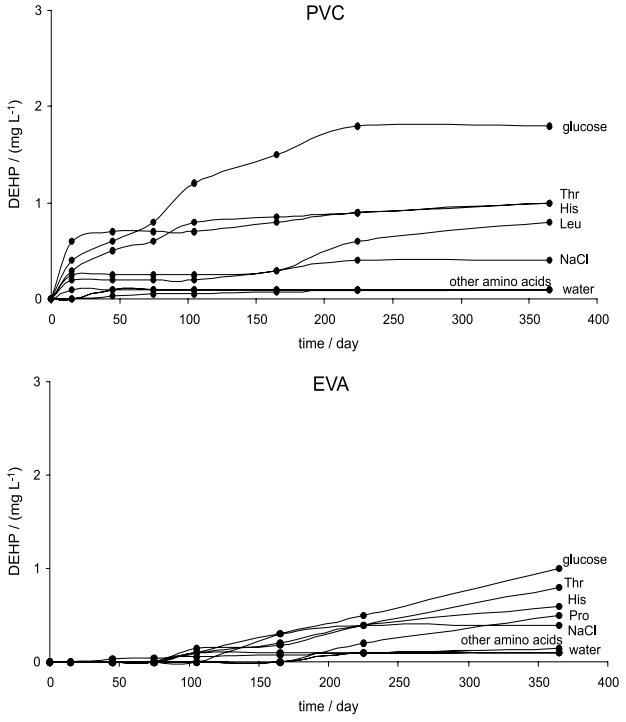


**Figure 2**. Extraction rates of DEHP from PVC and EVA bags in solutions of amino acids, NaCl, glucose and pure water during a period of contact of a year.

Since the HD capillaries present a huge surface purposely to enhance the contact between blood and dialysate, a rough calculation was made to determine the amount of phthalates in the total mass of the capillary in the HD. Considering that each dialyzer contained *ca.* 25 g of the capillary material, the total amount of phthalates was 282 mg in the cellulose dialyzers and 123 mg in the polysulfone dialyzers.

To finalize this study, it was measured the concentration of phthalates in some commercial formulations. Table 3 presents the results for DEHP, as it was the only phthalate found in these samples. It is interesting to see that concentrates for hemodialysis, saline and glucose solutions (even stored in containers supposedly free of phthalates (polyethylene)) presented DEHP at some level. This contamination is probably not from the flasks or bottles where they are stored but from the tubing material that are used in their industrial preparation.

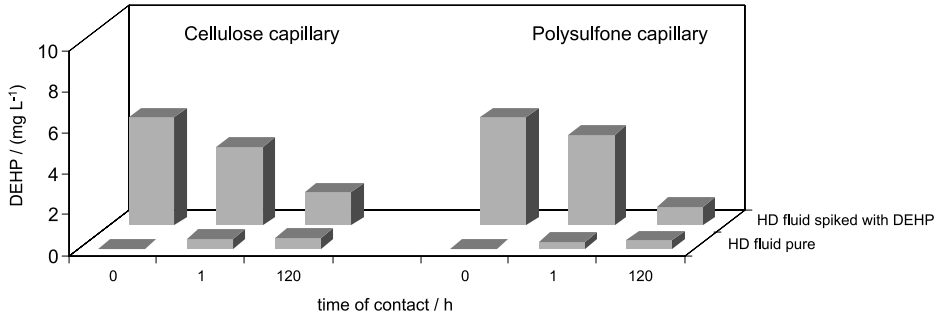


**Figure 3**. DEHP concentration in solution in which 1 g HD capillaries were submersed for 1 h and 5 days. Measurements were carried out using pure HD solution and a solution spiked with 4.86 mg $L^{-1}$ DEHP.

**Table 3** DEHP concentrations in products for parenteral administration and hemodialysis concentrates

| Sample | Packaging | Supplier | DEHP ± SD[a] / (mg $L^{-1}$) |
|---|---|---|---|
| Amino acids | PVC bag | Fresenius-Kabi | 1.65 ± 1.93 |
| Glucose 50% | PVC bottle | Fresenius-Kabi | 0.72 ± 0.05 |
| NaCl 0.9% | PVC bottle | Fresenius-Kabi | 1.04 ± 0.37 |
| Saline concentrate for hemodialysis (acid) | polyethylene bottle | Salbego | 0.91 ± 0.05 |
| Saline concentrate for hemodialysis (basic) | polyethylene bottle | Salbego | 1.03 ± 0.05 |

[a]SD: standard deviation (n = 3).

## Conclusions

Although it was not expected, EVA bags also presented DEHP in their constitution. The other investigated phthalates were found neither in PVC nor in EVA bags. DEHP migration rates by the action of some amino acid, NaCl and glucose occurred to a larger extent than in pure water. The migration from EVA bags required a longer time of contact than from PVC bags since significant amounts of DEHP were found in solutions only after 6 months of storage. Although in low concentration, DBP was also found in the tubing material coupled to bags and burettes. Hemodialysis sets presented phthalates in all parts. The tubing material mostly contains DEHP, but the capillaries contained DEHP and other phthalates. Cellulose diacetate contained only DBP, but polysulfone all four. The possibility of DEHP migration through the capillary membranes into patient blood is difficult to evaluate, the reasons are: firstly, the internal tubing for blood circulation is also made of PVC and secondly, the capillaries themselves contain DEHP and other phthalate-based plasticizers. The risk extent that DEHP and other phthalates pose to patients is still a matter of concern. On the other hand, considering the frequency with which dialysis is used by chronic renal patients and the presence of these plasticizers in all parts of the HD set, physicians must be aware of adverse reactions to the patients.

## Acknowledgement

The authors are grateful to the Brazilian agency CNPq (Conselho Nacional de Desenvolvimento Científico e Tecnológico) for scholarships.

## References

1. Allwood, M. C.; Martin, H.; *Int. J. Pharm.* **1996**, *127*, 65.
2. Jenke, D.; *PDA J. Pharm. Sci. Technol.* **2002**, *56*, 332.
3. Loff, S.; Kabs, F.; Subotic, U.; Schaible, T.; Reinecke, R.; Langbein, M.; *JPEN J. Parenter. Enteral Nutr.* **2002**, *26*, 305.
4. Kambia, K.; Dine, T.; Gressier, B.; Bah, S.; Germe, A.-F.; Luyckx, M.; Brunet, C.; Michaud, L.; Gottrand, F.; *Int. J. Pharm.* **2003**, *262*, 83.
5. Jenke, D.; *PDA J. Pharm. Sci. Technol.* **2006**, *60*, 191.
6. Takehis, H.; Naoko, E.; Masahiko, S.; Katsuhide, T.; Moriyuki, O.; Keizoh, S.; Mutsuko, T.; Kenji, K.; Shinichiro, N.; Toshio, O.; *Int. J. Pharm.* **2005**, *297*, 30.
7. Loff, S.; Hannmann, T.; Subotic, U.; Reinecke, F. M.; Wischmann, H.; Brade, J.; *J. Pediatr. Gastroenterol. Nutr.* **2008**, *47*, 81.
8. Christensson, L.; Junggren, L.; Nilsson-Thorell, C.; Arge, B.; Diehl, U.; Hagstam, K. E.; Lundberg, M.; *Int. J. Artif. Organs* **1991**, *14*, 407.
9. Ito, R.; Miura, N.; Iguchi, H.; Nakamura, H.; Ushiro, M.; Wakui, N.; Nakahashi, K.; Iwasaki, Y.; Saito, K.; Suzuki, T.; Nakazawa, H.; *Int. J. Pharm.* **2008**, *360*, 91.
10. Faouzi, M. A.; Dine, T.; Gressier, B.; Kambia, K.; Luyckx, M.; Pagniez, D.; Brunet, C.; Cazin, M.; Belabed, A.; Cazin, J. C.; *Int. J. Pharm.* **1999**, *180*, 113.
11. Haishima, Y.; Matsuda, R.; Hayashi, Y.; Hasegawa, C.; Yagami, T.; Tsuchiya, T.; *Int. J. Pharm.* **2004**, *274*, 119.
12. Burkhart, H. M.; Joyner, N.; Niles, S.; Ploessl, J.; Everett, J.; Iannettoni, M.; Richenbacher, W.; *ASAIO J*. **2007**, *53*, 365.
13. Directorate General for Health & Consumer Protection (DG SANCO) - European Commission; *Opinion on Medical Devices containing DEHP Plasticized PVC: Neonates and other groups possibly at Risk from DEHP Toxicity*, Doc. No. SANCO/SCMPMD/2002/0010 Final, Europe, 2002.
14. *European Pharmacopoeia*, European Directorate for the Quality of Medicines (EDQM), 4th ed., Strasbourg: France, 2004.
15. The United States Pharmacopeia Convention, *The United States Pharmacopeia*, USP 30, Rockville, 2008.
16. Sautou-Miranda, V.; Brigas, F.; Vanheerswynghels, S.; Chopineau, J.; *Int. J. Pharm.* **1999**, *178*, 77.
17. The U. S. Food and Drug Administration (US-FDA), Center for Devices and Radiological Health, *Safety Assessment of Di-2-ethylhexylphthalate (DEHP) Released from PVC Medical Devices*, Rockville, 1999.
18. Arabin, A.; Jacobsson, S.; Hagman, A.; Östelius, J.; *Int. J. Pharm*. **1986**, *28,* 211.
19. World Health Organization (WHO), *Diethyl Phthalate*, Concise International Chemical Assessment Document 52, Geneva, 2003.
20. World Health Organization (WHO), *Butyl Benzyl Phthalate*, Concise International Chemical Assessment Document 17, Geneva, 1999.
21. Wahl, H. G.; Hoffmann, A.; Häring, H.-U.; Liebich, H. M.; *J. Chromatogr., A* **1999**, *874*, 1.
22. http://echa.europa.eu/doc/press/ni_09_07_first_svhc_20090526.pdf accessed in March 2011.
23. Scientific Committee on Health and Environmental Risks (SCHER) - European Commission; *Opinion on Phthalates in School Supplies*, 2008
24. Aignasse, M. F.; Prognon, P.; Stachowicz, M.; Gheyouche, R.; Pradeau, D.; *Int. J. Pharm.* **1995**, *113*, 241.
25. Kambia, K.; Dine, T.; Gressier, B.; Germe, A.-F.; Luyckx, M.; Brunet, C.; Michaud, L.; Gottrand, F.; *J. Chromatogr., B: Anal. Technol. Biomed. Life Sci.* **2001**, *755*, 297.

*Submitted: April 30, 2011*
*Published online: October 18, 2011*

*J. Braz. Chem. Soc.*, Vol. 23, No. 1, 78-84, 2012.
Printed in Brazil - ©2012 Sociedade Brasileira de Química
0103 - 5053 $6.00+0.00

Article

# *In Situ* Solvent Formation Microextraction based on Ionic Liquids and 1-(2-Hydroxynaphtalene-1-yl)ethane Oxime for Determination of Zinc

***Mehdi Hosseini,*[a] Nasser Dalali,[a] Saeid Mohammad Nejad[a] and Rostam Jamali[b]***

*[a]Phase Separation & FIA Lab., Department of Chemistry, Faculty of Science, University of Zanjan, 45195-313, Zanjan, Iran*

*[b]Analytical Chemistry Advanced Laboratory, Department of Chemistry, University of Razi, Kermanshah, Iran*

Um método simples de microextração com formação de solvente *in situ* (ISFME) baseado no uso de líquido iônico (IL) como solvente extrator e hexafluorofosfato de sódio ($NaPF_6$) como agente par-iônico foi proposto para a concentração de níveis de traço de zinco. Neste método, o íon zinco foi complexado com 1-(2-hidroxinaftaleno-1-il)etano oxime (HNEO) e extraído em uma fase líquida iônica. Após a separação, o analito enriquecido na fase final foi determinado por espectrometria de absorção atômica de chama (FAAS). ISFME é um método rápido, simples e adequado para extração e concentração de inorgânicos tais como íons metálicos em soluções contendo uma elevada concentração de sal. As influências dos parâmetros analíticos na eficiência da microextração foram investigadas e otimizadas. Sob condições otimizadas, o limite de detecção e o fator de enriquecimento foram 0,05 μg $L^{-1}$ and 81, respectivamente. O desvio padrão relativo (R.S.D.) obtido foi 0,8%. A exatidão do método foi confirmada pela análise de materiais de referência certificados. O método apresentado foi aplicado com êxito na determinação de zinco em amostras de zinco.

A simple *in situ* solvent formation microextraction (ISFME) method based on use of ionic liquid (IL) as extractant solvent and sodium hexafluorophosphate ($NaPF_6$) as ion-pairing agent was proposed for the concentration of trace levels of zinc. In this method, zinc ion was complexed with 1-(2-hydroxynaphtalene-1-yl)ethane oxime (HNEO) and extracted into an ionic liquid phase. After phase separation, the enriched analyte in the final solution was determined by flame atomic absorption spectrometry (FAAS). ISFME is a fast, simple and suitable method for extraction and concentration of inorganic such as metal ions from sample solutions containing a high concentration of salts. The influences of the analytical parameters on the microextraction efficiency were investigated and optimized. Under the optimum conditions, the limit of detection and the enhancement factor were 0.05 μg $L^{-1}$ and 81, respectively. The relative standard deviation (R.S.D.) was obtained 0.8%. The accuracy of the method was confirmed by analyzing certified reference materials. The presented method was successfully applied for the determination of zinc in water samples.

**Keywords:** zinc, *in situ* solvent formation microextraction, ionic liquid, flame atomic absorption spectrometry

## Introduction

The determination of heavy metals in foods, and drinking and irrigation waters has become an important part of most studies concerned with environmental pollution and occupational health hazards. Although it is difficult to classify trace metals into essential and toxic groups, yet it is well known that an essential metal becomes toxic at sufficiently high intakes.[1] Even though zinc is an essential requirement for a healthy body, excess of zinc can be harmful and causes zinc toxicity.[2] Excessive absorption of zinc can suppress copper and iron absorption. The free zinc ion in solution is highly toxic to plants, invertebrates and even vertebrate fish. The free ion activity model (FIAM) is well-established in the literature, and shows that just micromolar amounts of the

*e-mail: mehdihosseini_znu@yahoo.com

free ion kill some organisms. A recent example showed 6 μmol $L^{-1}$ killing 93% of all daphnia in water. The free zinc ion is also a powerful Lewis acid up to the point of being corrosive. Stomach acid contains hydrochloric acid, in which metallic zinc readily dissolves to give corrosive zinc chloride. Swallowing a post-1982 American one cent piece (97.5% zinc) can cause damage to the stomach lining due to the high solubility of the zinc ion in the acidic stomach.[3] Therefore, a precise, accurate and rapid measurement of zinc is much interesting. Different analytical techniques have been reported to determine zinc in various samples including flame atomic absorption spectrometry (FAAS), graphite furnace atomic absorption spectrometry (GFAAS), inductively coupled plasma optical emission spectrometry (ICP OES), inductively coupled plasma mass spectrometry (ICP-MS) differential pulse stripping voltammetry, ion chromatography and molecular absorption spectrophotometry.[4]

From the analytical tools above listed, flame atomic absorption spectrometry is widely used because of low costs, operational facility and high sample throughput.[5-8] However, conventional FAAS has a limit of detection that is not low enough to determine zinc at trace levels in several types of matrix. Therefore, a preconcentration and separation steps are needed prior to analyte determination by flame atomic absorption spectrometry.

In inorganic trace analysis, preconcentration of desired trace elements is frequently required prior to the instrumental determination to lower the limits of detection, improve the precision and accuracy of the analytical results, and to widen the scope of the determination techniques.[9] The continuous quest for novel sample preparation and preconcentration procedures has led to the development of new methods such as solid-phase microextraction (SPME),[10] stir bar sorptive extraction (SBSE),[11] single drop microextraction (SDME),[12] hollow fiber-liquid phase microextraction (HF-LPME),[13] cloud point extraction (CPE),[14] solid phase extraction (SPE),[15] dispersive liquid-liquid microextraction (DLLME)[16] and cold-induced aggregation microextraction (CIAME).[17]

The main advantages of the mentioned techniques are their high speed and negligible volume of the used solvent. However, in the presence of high content of salts their performance decreases, significantly.[18] Room-temperature ionic liquids (RTILs) are being recently considered as replacement solvents in the sample preparation because of their unique chemical and physical properties such as negligible vapor pressure, non-flammability, good extractability for various organic compounds and metal ions as a neutral or charged complexes, as well as tunable viscosity and miscibility with water and organic solvents.[19] By definition, ionic liquids are known as solvents entirely consisting of ionic species and do have melting points close or below room temperature. Ionic liquids consist of a salt where one or both the ions are large, and the cations have low degree of symmetry.[20] Ionic liquids (ILs) are proving to be increasingly interesting fluids for application in soft-matter material systems from electrochemistry to energetic materials, and are also studied as potential solvents in separation processes.[21,22] Properties, including low melting points, wide liquid ranges and negligible vapor-pressure, have encouraged researchers to explore the uses of ILs to replace volatile organic solvents (VOCs).

This paper is aimed at developing a microextraction technique against very high content of salts. Among the different sample preparation methods, a new mode of homogeneous liquid-liquid microextraction (HLLME) based on ILs, termed *in situ* solvent formation microextraction (ISFME), was developed in the present research. In ISFME, there is no interface between water and extractant phases. During the formation of fine droplets of the extractant phase, the extractant molecules collect the hydrophobic species, and the extraction process is complete after formation of the droplets. As a result, mass transfer from aqueous phase into separated phase has no significant effect on the extraction step. In the presence of high content of salt, the solubility of ILs increases and the phase separation cannot occur. However, according to the common ion effect, the solubility of ILs decreases in the presence of common ion. Consequently, the volume of the extractant phase does not alter. Because of high density of ILs, even in the saturated solutions (40%, w/v), the fine droplets of extractant phase can settle. Due to very low solubility of water in the hydrophobic ILs, the residual salinity from the matrix is negligible. Rather than the other technique that are used for concentration of heavy metal ions, ISFME is faster and simpler and is applicable for solutions containing higher concentration of salts. For evaluating the performance of ISFME, zinc was selected as a test analyte and determined in water samples using atomic detection.

## Experimental

### Instrumentation

The measurements of zinc ions were performed with a Varian specterAA-220 flame atomic absorption spectrometer equipped with a hollow cathode lamp and a deuterium background corrector. The hollow cathode lamp of zinc was operated at 4 mA, using the wavelength at 213.9 nm, slit of 0.2 nm, burner height of 8 mm and

acetylene gas flow rate of 1.5 L $min^{-1}$. All measurements were carried out in peak area mode (measurement time of 3 s). A HERMLE centrifuge equipped with a swing out rotor (4-place, 6000 rpm, Cat. No. Z 360) was obtained from Hettich (Kirchlengern, Germany). A Metrohm digital pH-meter (model 692, Herisau, Switzerland), equipped with a glass-combination electrode, was used for pH adjustment.

### Reagents

All the used reagents in this work were of analytical grade of Merck (Darmstadt, Germany). Sodium hexafluorophosphate ($NaPF_6$) was purchased from ACROS (Geel, Belgium). All aqueous solutions were prepared in double-distilled water. Working standard solutions were obtained by appropriate stepwise dilution of the stock standard solution (1000 mg $L^{-1}$ solution of zinc in 0.1 mol $L^{-1}$ nitric acid). Working solutions (ILs), 1-hexyl-3-methylimidazolium tetrafluoroborate [Hmim][$BF_4$], 0.6 mg $\mu L^{-1}$, were prepared in ethanol. A solution of 100 mg $NaPF_6$ was prepared by dissolving an appropriate amount of $NaPF_6$ in doubly distilled water. A solution of HNEO (Figure 1) that was synthesized as literatures[23-25] ($2.0 \times 10^{-2}$ mol $L^{-1}$) was prepared by dissolving an appropriate amount of this chelating agent in ethanol. The water certified reference material (GBW07602) was purchased from National Research Center for Certified Reference Materials (Beijing, China).

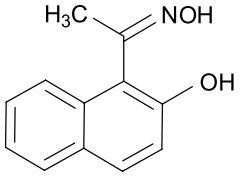


**Figure 1.** Chemical structure of 1-(2-hydroxynaphtalene-1-yl)ethane oxime (HNEO).

### ISFME procedure

A 5 mL of the sample solution (or standard solution) containing zinc ion, HNEO ($2.0 \times 10^{-2}$ mol $L^{-1}$), and [Hmim][$BF_4$] (30 mg) was transferred to 10 mL screw-cap conical-bottom glass centrifuge tube. After shaking, 0.6 mL $NaPF_6$ (100 mg) was added to the solution and a cloudy solution was formed. Then, the mixture was centrifuged for 5 min at 4000 rpm. As a result, the fine droplets of IL settled at the bottom of the centrifuge tube. Aqueous phase was simply removed by inverting the tubes. Subsequently, IL-phase was dissolved in 50 µL ethanol solution and it was aspirated to the flame atomic absorption spectrometer.

## Results and Discussion

### Effect of pH

pH plays an important role on the metal-chelate formation and subsequent extraction. The separation of metal ions in aqueous phase into IL-phase by ISFME involves prior complex formation with sufficient hydrophobicity to be extracted. The influence of pH of the sample solutions on the extraction efficiency was studied in the pH range of 2.0-8.0. The pH of sample solution was adjusted using HCl, acetate/acetic acid and NaOH. According to the obtained results (Figure 2), the absorbance was relatively constant in the pH range of 4.0-6.0. Thus, a pH value of 5.0 was chosen for further experiments.

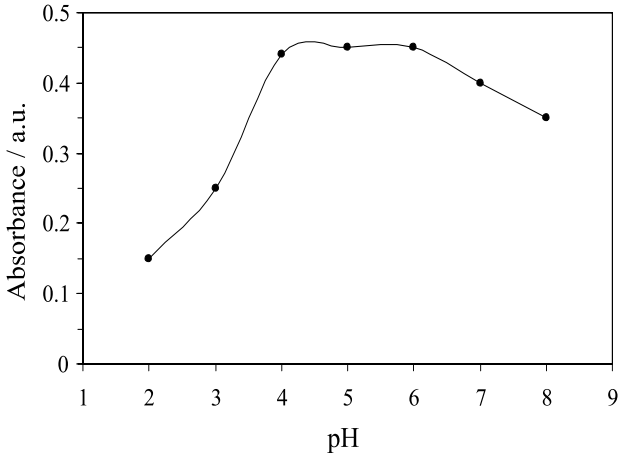


**Figure 2.** Effect of pH on the absorbance of the Zn-HENO complex. Conditions: zinc 10 µg $L^{-1}$, HENO $2.0 \times 10^{-2}$ mol $L^{-1}$, [Hmim][$BF_4$] 30 mg, $NaPF_6$ 100 mg and diluting solvent 50 µL.

### Selection of the diluting solvent

In order to decrease the viscosity of IL-phase, it must be diluted, thus different solvents were tested. The diluting solvent must completely dissolve IL and the complex. The solvents such as acetone (20-90%), acetonitrile (20-70%) and ethanol (40-90%) were examined. As shown in Figure 3, in the presence of 80% ethanol, the solution was clear and the maximum absorbance was obtained. Therefore, ethanol 80% was chosen as the diluting solvent. In the presence of 30% acetone and acetonitrile, IL-phase could not be completely dissolved, and the solution was turbid. In order to enhance the sensitivity and the enrichment factor, the effect of the volume of the diluting solvent was investigated. The absorbance decreased by increasing the volume of the diluting solvent (Figure 4). Therefore, a volume of 50 µL ethanol 80% was chosen to dilute the IL-phase.

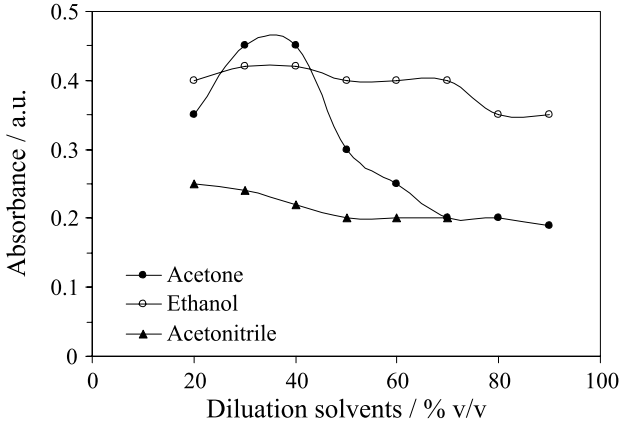


**Figure 3.** Effect of the type of the diluting solvent on the absorbance of Zn-HENO complex. Conditions: zinc 10 μg $L^{-1}$, HENO 2.0 × $10^{-2}$ mol $L^{-1}$, [Hmim][$BF_4$] 30 mg, $NaPF_6$ 100 mg and diluting solvent 50 μL.

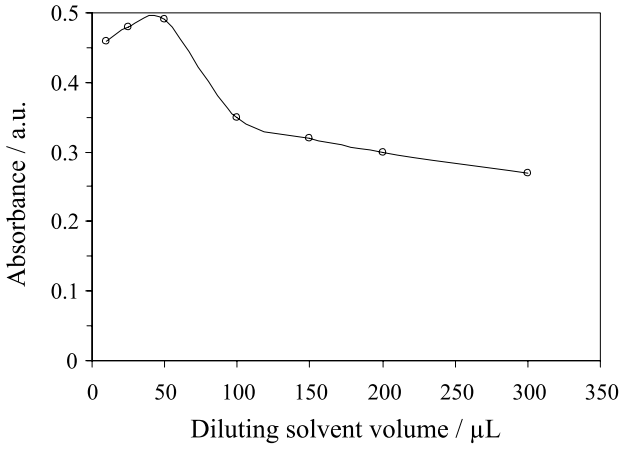


**Figure 4.** Effect of the volume of the diluting solvent (ethanol 80%) on the absorbance of the Zn-HENO complex. Conditions: zinc 10 μg $L^{-1}$, HENO 2.0 × $10^{-2}$ mol $L^{-1}$, [Hmim][$BF_4$] 30 mg and $NaPF_6$ 100 mg.

### Effect of the salt content

In the presence of high content of salts, the solubility of ILs increases and the phase separation cannot occur. However, according to the common ion effect, the solubility decreases in the presence of common ion. $Na_2SO_4$ was chosen in order to study the salt effect. As shown in Figure 5, in excess of $NaPF_6$, the phase separation successfully occurred up to 30% $Na_2SO_4$. At higher salt content, the density of the solution became higher than that of IL so, the extract ant phase did not settle.

### Effect of $NaPF_6$

In order to decrease the solubility of IL-phase in brines, $NaPF_6$ was added to the sample solutions as an ion-pairing agent. As a consequence of the reaction between the water-miscible IL and the ion-pairing agent, a water-immiscible IL with very low solubility must be

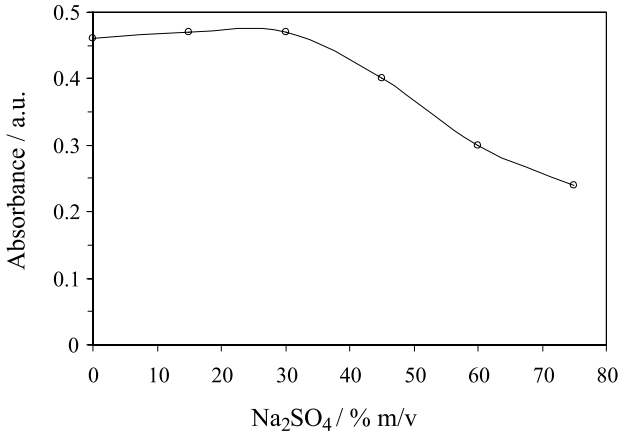


**Figure 5.** Effect of $Na_2SO_4$ on the absorbance of the Zn-HENO complex. Conditions: Zinc 10 μg $L^{-1}$, HENO 2.0 × $10^{-2}$ mol $L^{-1}$, [Hmim][$BF_4$] 30 mg, $NaPF_6$ 100 mg and diluting solvent 50 μL.

formed. Ion-pairing agent must have no interference in the extraction system. The solubility of IL decreases according to the common ion effect so, the phase separation can successfully occur. The effect of $NaPF_6$ was investigated in the range of 25-200 mg in the presence of 30 mg [Hmim][$BF_4$] and the results are shown in Figure 6. By adding $NaPF_6$, [Hmim][$PF_6$] was formed and according to the common ion effect by increasing the amount of $NaPF_6$, the solubility of [Hmim][$PF_6$] decreased and the absorbance subsequently increased. Thus, the amount of 100 mg $NaPF_6$ was chosen for the subsequent experiments.

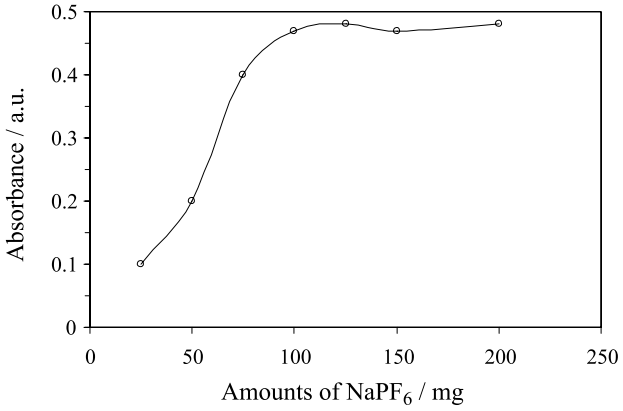


**Figure 6.** Effect of the amount of $NaPF_6$ on the absorbance of the Zn-HENO complex. Conditions: zinc 10 μg $L^{-1}$, HENO 2.0 × $10^{-2}$ mol $L^{-1}$, [Hmim][$BF_4$] 30 mg and diluting solvent 50 μL.

### Effect of the ionic liquid amount

The amount of [Hmim][$BF_4$] that is used in this preconcentration procedure is a critical factor to obtain high recovery. Therefore, the extraction system was carefully studied in order to define the lowest IL-phase volume that is necessary for achieving the highest recovery. The effect of [Hmim][BF4] was studied in the range of 5-60 mg in

the presence of 100 mg $NaPF_6$. As can be seen in Figure 7, the absorbance increased by increasing the amount of [Hmim][$BF_4$], and then, gradually decreased due to the increase in the volume of the settled phase. Thus, the amount of 30 mg [Hmim][$BF_4$] was chosen for the subsequent experiments.

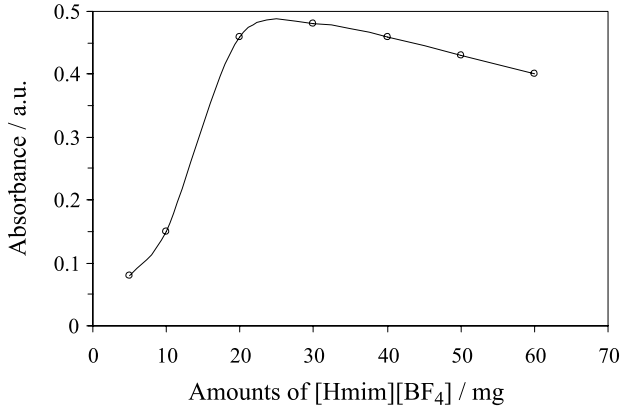


**Figure 7.** Effect of [Hmim][$BF_4$] on the absorbance of the Zn-HENO complex. Conditions: zinc 10 μg $L^{-1}$, HENO 2.0 × $10^{-2}$ mol $L^{-1}$, $NaPF_6$ 100 mg and diluting solvent 50 μL.

### Effect of the HENO concentration

The effect of HENO on the absorbance of the complex was studied in the range of 5.0 × $10^{-4}$-5.0 × $10^{-2}$ mol $L^{-1}$. The absorbance increased by increasing of the HENO concentration up to 2.0 × $10^{-2}$ mol $L^{-1}$ and then, remained constant (Figure 8). Therefore, a concentration of 2.0 × $10^{-2}$ mol $L^{-1}$ was chosen as the optimum concentration.

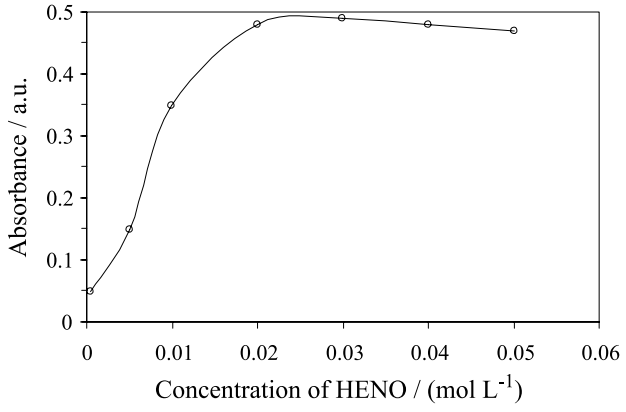


**Figure 8.** Effect of the HENO concentration on the absorbance of the Zn-HENO complex. Conditions: zinc 10 μg $L^{-1}$, [Hmim][$BF_4$] 30 mg, $NaPF_6$ 100 mg and diluting solvent 50 μL.

### Effect of the centrifuge rate

The effect of the centrifugation rate on the absorbance was studied in the range of 500-5000 rpm. It was found that over 3500 rpm, IL-phase completely settled, hence 4000 rpm was selected as the optimum point. At the optimum rate, absorbance was investigated as a function of centrifugation time. The absorbance was constant beyond 5 min, indicating the complete transfer of IL-phase to the bottom of centrifuge tube. So, the optimum centrifugation time of 6 min was chosen.

### Effect of foreign ions

To assess the possible applications of the present procedure, the effect of foreign ions which may interfere with the determination of zinc or/and often coexisting in various real samples was examined. The interferences were studied by analyzing 10 mL of a solution containing 20 μg $L^{-1}$ Zn(II) and other ions at different concentrations, according to the recommended extraction procedure. Table 1 shows the tolerance limits of the interfering ions. An ion was considered to interfere when its presence produced a variation of more than ± 5% in the absorbance of the analyte. Commonly encountered ions such as alkali and some alkaline earth elements do not form stable complexes with HENO. However, $Cu^{2+}$ interfered with the determination of $Zn^{2+}$ in a maximum ratio of 20. This interference was eliminated using an excess of HENO reagent in sample solutions or by masking it with a suitable reagent, such as thiourea.

**Table 1.** Tolerance limits of interfering in the determination of 20 μg $L^{-1}$ $Zn^{2+}$

| Ions | Tolerance limits (mol ratio) | Recovery / % |
|---|---|---|
| $Na^+$, $K^+$, $Ca^{2+}$, $Mg^{2+}$, $Ba^{2+}$ | > 100000 | 99.8 |
| $Fe^{2+}$ | 200 | 98.5 |
| $Fe^{3+}$ | 1000 | 100.1 |
| $Mn^{2+}$ | 250 | 98.5 |
| $Cd^{2+}$, $Pb^{2+}$ | 500 | 98.4 |
| $Ni^{2+}$ | 50 | 99.3 |
| $Co^{2+}$ | 50 | 99.2 |
| $NO_3^-$, $Cl^-$, $SO_4^{2-}$ | 500 | 98.2 |
| $Br^-$ | 1000 | 99.6 |
| $Cu^{2+}$ | 20 | 99.1 |

### Figures of merit

The sensitivity of the developed method is reflected by the limit of detection (LOD) studies, being defined as the lowest concentration of metal ions below which the quantitative sorption of the metal ion by basic alumina is not perceptibly seen. Table 2 summarizes the analytical characteristics of the optimized method, including limit of detection, reproducibility and enhancement factor. The limit of detection (LOD = 0.05 μg $L^{-1}$) was calculated as $3S_b/m$

($S_b$ is the standard deviation of the blank signals and m is the slope of calibration curve after preconcentration). The precision of the method for the determination of 10 μg $L^{-1}$ zinc was investigated for 8 replicate measurements and, a relative standard deviation of 0.8% was obtained. The calibration curve was investigated between 5.0-500.0 μg $L^{-1}$ which was linear. Enhancement factor (EF = 81) was obtained from the slope ratio of the calibration curve after and before preconcentration.

**Table 2.** Analytical figures of merit of the method

| Parameter | Optimized value |
|---|---|
| linear range / (μg $L^{-1}$) | 5.0-500.0 |
| limit of detection (LOD) / (μg $L^{-1}$)[a] | 0.05 |
| R.S.D. / % (n = 6)[b] | 0.8 |
| enhancement factor[c] | 81 |

[a]Determined as $3S_b/m$ (where $S_b$ and m are the standard deviation of the blank signal and the slope of the calibration graph, respectively); [b]values in parentheses are the Zn concentration (μg $L^{-1}$) for which the R.S.D. was obtained; [c]calculated as the slope ratio of the calibration graph obtained with and without preconcentration.

### Analysis of real and reference samples

The feasibility of the methodology for the determination of zinc in water samples (Zanjan City, Iran) was explored by the standard addition method. The results for this study are presented in Table 3 for water samples. The recovery of spiked samples is reasonably satisfactory and was confirmed using the standard addition method which indicates the capability of the system in determining Zn. A good agreement was obtained between the added and measured analyte amounts. The recovery values that were calculated for the added standards were always higher than 96%, thus confirming the accuracy of the procedure and its independence from the matrix effects. In order to establish the validity of the proposed procedure, the method was applied to the determination of the content of the studied analyte Zn(II) in a standard reference material. Portions (0.5 g) of GBW07602 bush twigs and leaves (reference) were transferred into beakers, 10 mL of concentrated $HNO_3$ and 3 mL of $H_2O_2$ (30%) were added. It was heated until the solution became transparent, continuously heated to near dryness and the residue was dissolved in 0.1 mol $L^{-1}$ HCl. After adjustment of the pH to 8.0, the solution was made up to 50 mL with distilled water. The content of the studied elements was determined according to the recommend procedure. The results are presented in Table 3. As can be seen, the results are in agreement with reference values.

## Conclusions

[Hmim][$BF_4$] was chosen as a green medium and an alternative to the traditional volatile organic solvents for this extraction system. The determination was carried out by flame atomic absorption spectrometry (FAAS). The *in situ* solvent formation microextraction (ISFME) technique was successfully used for the preconcentration of trace amount of zinc in saline samples. The relative standard deviation, the limit of detection and the linear range of this procedure are also satisfactory. This method is fast, simple, safe and robust against very high content of salt (up to 30%). Therefore, ISFME is a powerful sample preparation technique for saline solutions and salt products that are used in food and pharmaceutical industries. The preconcentration method was successfully applied to the zinc determination in water samples and reference material, with good accuracy and reproducibility.

## Acknowledgement

The authors express their appreciation to the Graduate School and Research Council of Zanjan University (Iran) for financial support of this work.

**Table 3.** Determination of $Zn^{+2}$ in reference material, mineral, rain and tap water samples and the relative recoveries of spiked samples (n = 3)

| Samples | Certified value / (μg $L^{-1}$) | Added $Zn^{+2}$ / (μg $L^{-1}$) | Found / (μg $L^{-1}$) | R.S.D. / % | Recovery / % |
|---|---|---|---|---|---|
| Tap water | | 0 | 8.5 ± 0.2 | 0.8 | |
| | | 10 | 18.7 ± 0.6 | 1.0 | 101.0 |
| | | 50 | 57.4 ± 0.5 | 0.6 | 96.10 |
| Mineral water | | 0 | n.d. | 0.9 | |
| | | 10 | 11.5 ± 0.9 | 0.4 | 115.0 |
| | | 50 | 51.1 ± 1.5 | 0.6 | 105.5 |
| Rain water | | 0 | 8.0 ± 0.3 | 0.5 | |
| | | 10 | 19.2 ± 0.9 | 1.0 | 106.6 |
| | | 50 | 58.5 ±1.2 | 0.9 | 101.7 |
| GBW07602 | 40.0 ± 3.0 | | 38.0 ± 2.0 | 0.4 | 97.0 |

All values are in μg $L^{-1}$; n.d.: not detected.

## References


1. Sattar, A.; Ahmad, B.; Jamshaid, M.; *Pak. J. Agric. Sci.* **1990**, *27*, 156.
2. Fosmire, G. J.; *Am. J. Clin. Nutr.* **1990**, *51*, 225.
3. Brita, T. A. M.; Karel, A. C. S.; Colin, R. J.; *Aquat. Toxicol.* **2006**, *77*, 393.
4. Ferreira, S. L. C.; Andrade, J. B.; Korn, M. G. A.; Pereira, M. G.; Lemos, V. A.; Santos, W. N. L.; Rodrigues, F. M.; Souza, A. S.; Ferreira, H. S.; Silva, E. G. P.; *J. Hazard. Mater.* **2007**, *145*, 358.
5. Anthemidis, A. N.; Zachariadis, G. A.; Stratis, J.A.; *Talanta* **2001**, *54*, 935.
6. Hosseini, M.; Dalali, N.; Karimi, A.; Dastanra, K.; *Turk. J. Chem.* **2010**, *38*, 805.
7. Divrikli, U.; Akdogan, A.; Soylak, M.; Elci, L.; *J. Hazard. Mater.* **2007**, *149*, 331.
8. Ghaedi, M.; Niknam, K.; Taheri, K.; Hossainian, H.; Soylak, M.; *Food Chem. Toxicol.* **2010**, *48*, 891.
9. Tuzen, M.; Soylak, M.; Elci, L.; Dogan, M.; *Anal. Lett.* **2004**, *37*, 1185.
10. Guidotti, M.; *J. AOAC Int.* **2000**, *83*, 1082.
11. Kole, P. L.; Millership, J.; McElnay, J. C.; *J. Pharm. Biom. Anal.* **2011**, *54*, 701.
12. Gil, S.; Loos-Vollebregt, M. T. C.; Bendicho, C.; *Spectrochim. Acta, Part B* **2009**, *64*, 208.
13. Jiang, H.; Hu, B.; Chen, B.; Zu, W.; *Spectrochim. Acta, Part B* **2008**, *63*, 770.
14. Kulichenko, S. A.; Doroschuk, V. O.; Lelyushok, S. O.; *Talanta* **2003**, *59*, 767.
15. Tuzen, M.; Melek, E.; Soylak, M.; *J. Hazard. Mater.* **2008**, *159*, 335.
16. Liang, P.; Sang, H.; *Anal. Biochem.* **2008**, *380*, 21.
17. Gharehbaghi, M.; Shemirani, F.; Davudabadi Farahani, M.; *J. Hazard. Mater.* **2009**, *165*, 1049.
18. Mahpishanian, S.; Shemirani, F.; *Talanta* **2010**, *82*, 471.
19. Abdolmohammad-Zadeh, H.; Sadeghi, G. H.; *Anal. Chim. Acta* **2009**, *649*, 211.
20. Rogers, R. D.; Seddon, K. R.; *Ionic Liquids as Green Solvents: Progress and Prospects*, ACS Symposium Series 856; American Chemical Society: Washington, DC, 2003.
21. Welton, T; *Chem. Rev.* **1999**, *99*, 2071.
22. Visser, A. E.; Swatloski, R. P.; Reichert, W. M.; Griffin, S. T.; Rogers, R. D.; *Ind. Eng. Chem. Res*. **2000**, *39*, 3596.
23. Fischer, H.; *Org. Synth. Coll.* **1955**, *3*, 513.
24. Semon, W. L.; Damerell, V. R.; *Org. Synth., Coll.* **1943**, *2*, 204.
25. Hartung, W. H., Crossley, F.; *Org. Synth., Coll.* **1943**, *2*, 363.


*Submitted: July 8, 2011*
*Published online: October 18, 2011*

*J. Braz. Chem. Soc.*, Vol. 23, No. 1, 85-95, 2012.
Printed in Brazil - ©2012 Sociedade Brasileira de Química
0103 - 5053 $6.00+0.00

Article

# Advanced QSAR Studies on PPARδ Ligands Related to Metabolic Diseases

*Vinícius G. Maltarollo,[a] Danielle C. Silva[a] and Káthia M. Honório*[*,a,b]*

[a]*Universidade Federal do ABC, Santo André-SP, Brazil*

[b]*Escola de Artes, Ciências e Humanidades, Universidade de São Paulo, São Paulo-SP, Brazil*

PPARδ é um receptor nuclear que, quando ativado, regula o metabolismo de carboidratos e lipídios, e está relacionado com diversas enfermidades, tais como síndrome metabólica e diabetes tipo 2. Para entender as principais interações entre alguns ligantes bioativos e o receptor PPARδ, modelos de QSAR 2D e 3D foram obtidos e comparados com mapas de potencial eletrostático (MEP) e dos orbitais de fronteira (HOMO e LUMO), assim como resultados de docagem molecular. Os modelos de QSAR obtidos apresentaram bons resultados estatísticos e foram utilizados para predizer a atividade biológica de compostos do conjunto-teste (validação externa), e os valores preditos estão em concordância com os resultados experimentais. Além disso, todos mapas moleculares foram utilizados para avaliar as possíveis interações entre os ligantes e o receptor PPARδ. Portanto, os modelos de QSAR 2D e 3D, assim como os mapas de HOMO, LUMO e MEP, podem fornecer informações sobre as principais propriedades necessárias para o planejamento de novos ligantes do receptor PPARδ.

PPARδ is a nuclear receptor that, when activated, regulates the metabolism of carbohydrates and lipids and is related to metabolic syndrome and type 2 diabetes. To understand the main interactions between ligands and PPARδ, we have constructed 2D and 3D QSAR models and compared them with HOMO, LUMO and electrostatic potential maps of the compounds studied, as well as docking results. All QSAR models showed good statistical parameters and prediction outcomes. The QSAR models were used to predict the biological activity of an external test set, and the predicted values are in good agreement with the experimental results. Furthermore, we employed all maps to evaluate the possible interactions between the ligands and PPARδ. These predictive QSAR models, along with the HOMO, LUMO and MEP maps, can provide insights into the structural and chemical properties that are needed in the design of new PPARδ ligands that have improved biological activity and can be employed to treat metabolic diseases.

**Keywords**: *diabetes mellitus,* PPARδ, HQSAR, 3D-QSAR, quantum chemistry, molecular modeling

## Introduction

Peroxisome proliferator-activated receptor delta (PPARδ) is a nuclear receptor that, when activated by specific ligands, promotes the transcription of genes that control the metabolism of lipids and carbohydrates. These receptors are expressed in several types of tissues and cells, but are significantly found in the brain, cardiac and skeletal muscles, adipose tissue and skin. Natural ligands of PPARδ include fatty acids and eicosanoids.[1-3] Figure 1 shows the structure of PPARδ and an endogenous ligand in its active site.

Some effects of PPARδ activation involve the decrease of glucose oxidation, the increase of lipid utilization into the muscle tissues, insulin sensibility and oxidation of fatty acids. Based on these effects, substances that activate the PPARδ receptor can be used to treat two chronic diseases: type 2 *diabetes mellitus* (DM) and metabolic syndrome.[4-7] DM is a disease of carbohydrate metabolism that is related to hyperglycemia and insulin resistance.[8-11] Metabolic syndrome is a disease of lipid metabolism and is consequently involved in obesity and insulin resistance. The two diseases can arise from similar causes, such as sedentary lifestyle, inadequate nutrition, genetics, and oxidative stress.[6,12,13] In the 1990s, DM affected 4% of the global population and some studies have estimated that this number will increase by 1.5% in 2025. Type 2 DM is the most common type of diabetes and represents 90% of DM cases.[14] Therefore, there is an urgency of developing

*e-mail: kmhonorio@usp.br

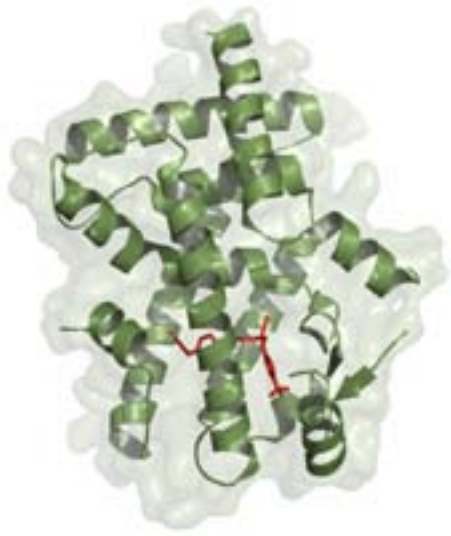

**Figure 1.** Structure of PPARδ and the natural ligand D32 (red). See online for color image.

new safe and effective agents to treat DM and metabolic syndrome, and several authors have been studied PPAR as a potential target to treat these diseases.[15-18]

Structure and ligand-based approaches have been successfully employed in the development of new drugs. Two and three-dimensional quantitative structure-activity relationships (2D and 3D QSAR) and quantum chemical descriptors have been used to understand the main interactions between drugs and biological receptors, as well as in designing new classes of drugs for many diseases.[19-27] Therefore, the main objective of this study is to construct reliable HQSAR, CoMFA and CoMSIA models and utilize them in combination with quantum chemical maps to understand the main interactions between a set of bioactive ligands and the PPARδ receptor.

## Methodology

### Data set

In general, PPAR ligands have a polar head (e.g., a COOH group), a linker group (e.g., a benzene ring–O–$(CH_2)_2$–) and a hydrophobic tail (see general structure in Table 1). Our compound set consists of indanylacetic acid derivatives that have very similar structures to the generic model of PPAR ligands.[28-32] From the indanylacetic acid derivatives synthesized by Wickens *et al.*,[29] we have selected 51 compounds to constitute the entire data set. A training set was formed using 41 of the compounds, and the remaining 10 comprised the test set (external validation). The selection of training and test sets was based on cluster analyses, and the chemical diversity of the two sets is very significant.

Table 1 displays the chemical structures and the values of biological activity ($EC_{50}$) for all compounds studied. These values were all measured under the same experimental conditions,[29] converted to corresponding $pEC_{50}$ value (–log $EC_{50}$) and used as dependent variables in the QSAR analyses. Figure 2 displays the distribution of $pEC_{50}$ values for the training and test sets.

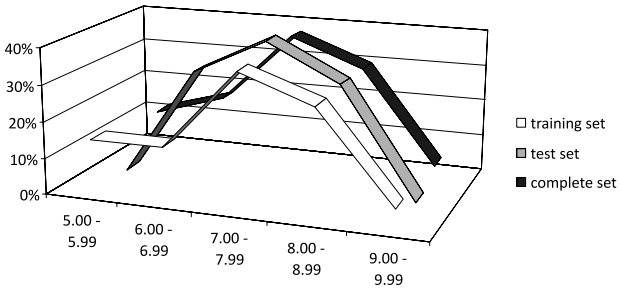


**Figure 2.** Distribution of $pEC_{50}$ values for the training, test and complete data sets.

### Protein structure

To perform the molecular alignment of the data set, docking studies were necessary. We selected the protein structure from the Protein Data Bank (PDB) with regard to the characteristics that showed good correlation with the biological system. First, eight structures of PPARδ with the best resolution (≤ 2.40Å) were chosen; then, the RMS fit for all structures were calculated using the Pymol[33] software. The alignment error was 0.464Å, and Figure 3 shows the alignment of all protein structures selected.

The PPARδ structures did not show significant differences when compared with each other. Therefore, we have selected the protein structure with the PDB code 3GZ9[34] in order to perform the molecular alignment of the compound set. This PPARδ structure has the better resolution (2.00 Å), and its ligand is structurally similar to the compounds in our data set. The PPAR ligand binding domain has a polar pocket with three main amino acids (His323, His449 and Tyr473), as well as a Y shaped hydrophobic cavity.[3,33,35,36] Before molecular alignment was performed on all the compound sets, redocking and crossdocking processes were carried out to validate the methodology selected. For the docking analyses, the crystallographic ligand and water molecules were removed and hydrogen atoms were added using the Biopolymer module, implemented in Sybyl 8.1.[37] Some aminoacid residues in the binding site (e.g. histidine, glutamine and asparagines) were manually checked for possible flipped orientation, protonation, and tautomeric states using the Pymol 1.0 program (DeLano Scientific, San Carlos, USA). The docking process was flexible with respect to the ligands.

**Table 1.** Structure of compounds studied and $EC_{50}$ values

| Compound | General structure | $R^1$ | $R^2$ | X | Y | $EC_{50}$ / (nmol $L^{-1}$) |
|---|---|---|---|---|---|---|
| | | Training set | | | | |
| **1** | 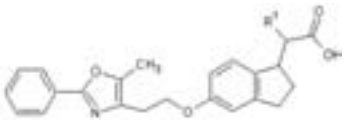 | H | - | - | - | 27 |
| **2** | | $CH_2CH_3$ | - | - | - | 590 |
| **3** | | $OCH_3$ | - | - | - | 4400 |
| **4** | | 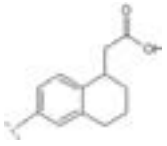 | - | - | - | 3140 |
| **5** | 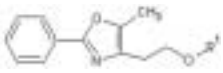 | 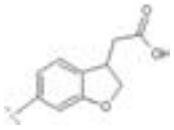 | - | - | - | 10000 |
| **6** | | 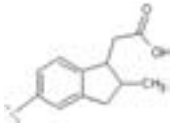 | - | - | - | 883 |
| **7** | | 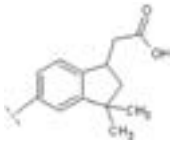 | - | - | - | 6480 |
| **8** | | 4-$OCH_3$ | - | - | - | 3 |
| **9** | | 3-$OCH_3$ | - | - | - | 18 |
| **10** | | 4-Et | - | - | - | 3 |
| **11** | | 4-t-Bu[a] | - | - | - | 21 |
| **12** | | 4-i-Pr[b] | - | - | - | 1 |
| **13** | 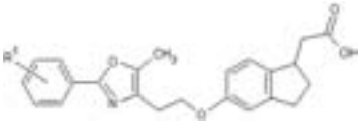 | 4-F | - | - | - | 7 |
| **14** | | 4-Ph | - | - | - | 6 |
| **15** | | 4-$CH_3$ | - | - | - | 4 |
| **16** | | 3-$CH_3$ | - | - | - | 64 |
| **17** | | 4-CN | - | - | - | 35 |
| **18** | | 3-CN | - | - | - | 73 |
| **19** | | H | - | S | N | 11 |
| **20** | | 4-$CH_3$ | - | S | N | 0.8 |
| **21** | | 3,4-$OCH_2O$ | - | S | N | 5 |
| **22** | | 4-$OCH_3$ | - | S | N | 4 |
| **23** | | 3-$OCH_3$ | - | S | N | 61 |
| **24** | | 4-F | - | S | N | 7 |
| **25** | | 2-F | - | S | N | 116 |
| **26** | | 3-$OCH_3$ | - | S | N | 272 |
| **27** | 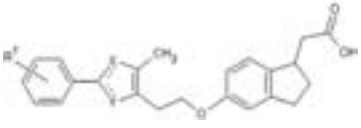 | 3-Me | - | S | N | 272 |
| **28** | | 3-$CF_3$ | - | S | N | 30 |
| **29** | | 4-$OCF_3$ | - | S | N | 2 |
| **30** | | 4-Ph[c] | - | S | N | 13 |
| **31** | | 4-Ph | - | N | $NCH_3$ | 28 |
| **32** | | 4-Ph | - | $NCH_3$ | N | 309 |
| **33** | | 4-Et[d] | - | N | $NCH_3$ | 31 |
| **34** | | 4-Et | - | $NCH_3$ | N | 347 |
| **35** | | 4-$OCH_3$ | - | N | $NCH_3$ | 86 |
| **36** | | 4-$OCH_3$ | - | $NCH_3$ | N | 10000 |
| **37** | | H | - | $NCH_3$ | N | 10000 |
| **38** | 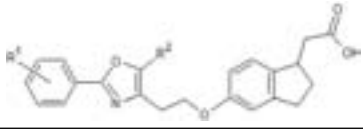 | H | Et | - | - | 7 |
| **39** | | 4-$CH_3$ | Et | - | - | 5 |
| **40** | | 4-Et | Et | - | - | 11 |
| **41** | | H | Pr | - | - | 10 |

**Table 1.** continuation

| Compound | General structure | $R^1$ | $R^2$ | X | Y | $EC_{50}$ / (nmol $L^{-1}$) |
|---|---|---|---|---|---|---|
| | | Test set | | | | |
| **42** | 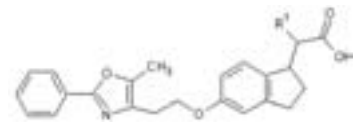 | $CH_3$ | - | - | - | 120 |
| **43** | 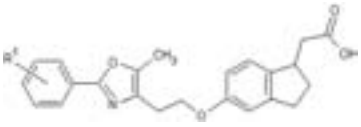 | H | - | - | - | 14 |
| **44** | | 3-F | - | - | - | 13 |
| **45** | | 3-Cl | - | - | - | 13 |
| **46** | | 4-Cl | - | - | - | 3 |
| **47** | 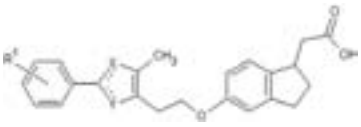 | 4-i-Pr | - | S | N | 5 |
| **48** | | 3-F | - | S | N | 47 |
| **49** | | 4-Cl | - | S | N | 1.5 |
| **50** | | H | - | N | $NCH_3$ | 257 |
| **51** | 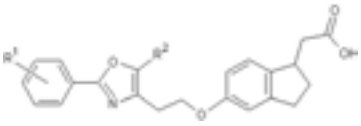 | H | $(CH_2)_2$-Ph | - | - | 10000 |

[a]t-Bu = $C(CH_3)_3$; [b]i-Pr = $CH(CH_3)_3$; [c]Ph = $C_6H_{11}$; [d]Et = $CH_2CH_3$.

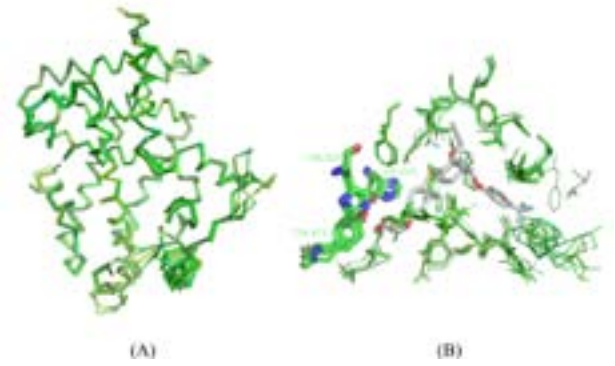


**Figure 3.** Alignment of PPARδ structures with resolution ≤ 2.40Å from Protein Data Bank. (A) Backbone view of aligned structures; (B) aligned residues into the binding site. See online for color image.

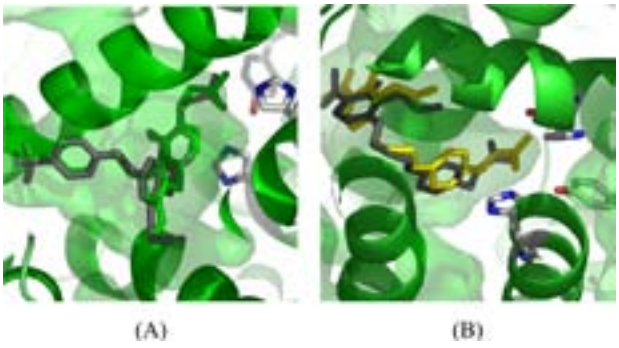


**Figure 4.** (A) Redocking and (B) crossdocking results. Both crystallographic ligands are shown in gray and the docked ligands are in green (D32) and yellow (L41), respectively. See online for color image.

### Redocking and crossdocking

Using Surflex docking implemented in Sybyl 8.1,[37] we docked the natural ligand of PPARδ found in the 3GZ9[34] structure, called D32 or (2,3-dimethyl-4-phenyl] sulfanyl} phenoxy) acetic acid. The redocking results were compared with the crystallographic structure of the ligand. The redocking process was also performed using the same receptor structure (3GZ9), but with the ligand from the 3D5F structure called L41 or (4-[3-(4-acetyl-3-hydroxy-2-propylphenoxy)propoxy] phenoxy) acetic acid. The results obtained from redocking and crossdocking are shown in Figure 4.

From Figure 4, we can observe that the selected methodology reproduces the geometries and the positioning of molecules into the binding site accurately. Therefore, Surflex docking can be used to dock all compound sets to create reliable 3D QSAR models.

### 2D and 3D QSAR studies

All 2D and 3D QSAR analyses, calculations and visualizations were performed using the Sybyl 8.1 package (Tripos, St. Louis, USA), running on Linux workstations.

The 2D QSAR analyses were performed using a specialized fragment-based method to develop a predictive quantitative structure-activity relationship. This method is known as hologram QSAR (HQSAR) and permits the visualization of the positive and negative contributions of each molecular fragment to the biological activity. The HQSAR models can be affected by a number of parameters concerning hologram generation, such as hologram length,

fragment size and fragment distinction. Initially, each molecule in the data set was energetically minimized by the Tripos force field; the Gasteiger-Huckel charges were calculated and the molecular holograms were generated using the standard parameters implemented in Sybyl 8.1.

Comparative molecular field analysis (CoMFA) and comparative molecular similarity indices analysis (CoMSIA) are two methods based on molecular force fields that reproduce some interactions between ligands and their biological receptors. In combination with HQSAR maps, 3D QSAR results can show a complete understanding of electrostatic, stereochemical, hydrophobic, and H-bond donor and acceptor features of bioactive ligands. Structural alignment is an important parameter in developing reliable 3D QSAR models, and in this case, we have employed a docking methodology to align all the compounds of the data set. For this, we used the Surflex module of Sybyl 8.1 (scoring function: ChemScore)[37] on the PPARδ structure with PDB code 3GZ9. Figure 5 displays the molecular alignment of the compound set obtained from this methodology.

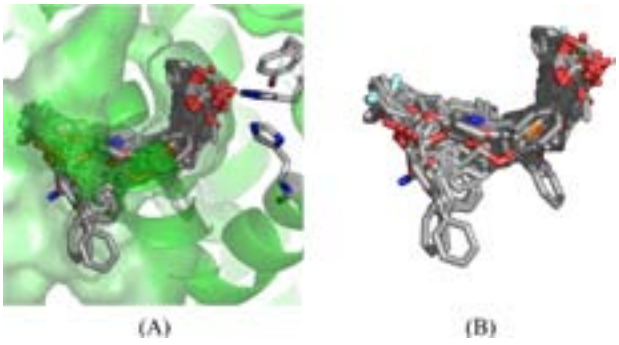


**Figure 5.** Molecular alignment of all compounds studied. See online for color image.

After aligning all compounds in the PPARδ structure, we have constructed several models based on CoMFA and CoMSIA. Initially, we calculated the atomic charges using the PM3 method,[38,39] implemented in the MOPAC package, as this method contains many of the same AM1 parameters, but these ones were derived more systematically.[40] These CoMFA models were based on the relationship between the values of biological activity and the values of the force fields based on the stereochemical (according to Lennard-Jones potential) and electrostatic (Coulomb potential) interactions. All CoMFA and CoMSIA models were investigated using full leave-one-out cross-validation ($q^2$) and no validation ($r^2$) methods, as well as CoMFA and CoMSIA standard options for variable scaling. The values of $pEC_{50}$ were used as the dependent variable in all QSAR analyses.

For CoMSIA analyses, stereochemical, electrostatic, hydrophobic, H bond acceptor and H bond donor similarity indices were evaluated using the standard indices implemented in Sybyl 8.1. A CoMFA and CoMSIA region focusing method was applied to increase the resolution of the 3D QSAR models. The statistical evaluation for the CoMSIA analyses was performed in the same way as described for CoMFA.

### Quantum chemical maps

Based on previous QSAR studies[41-44] using quantum chemical descriptors, we can note that the energy of the lowest unoccupied molecular orbital (LUMO), the charge of a carbon atom and the value of the dipole moment of a class of PPARδ ligands are important properties in describing the biological activity. Therefore, we decided to calculate the HOMO, LUMO and ESP (electrostatic surface potential) maps for some of the compounds studied. The calculations were performed with the DFT method implemented in the Gaussian09 software,[45] using the B3LYP[46,47] functional and DGDZVP[48,49] basis sets, since this functional is appropriated for organic molecules and this set of functional and basis set was employed in a previous study, providing good results when compared to crystallographic data.[50]

## Results and Discussion

### HQSAR analyses

The first 2D QSAR analyses employed several combinations of molecular parameters, such as the screening of the 12 default series of hologram length (ranging from 53 to 401 bins), fragment distinction (atoms, bonds, connections, hydrogen atoms, chirality, donor and acceptor atoms) and fragment size. All results from the PLS analyses, using several fragment distinction combinations and different fragment sizes, are displayed in Table 2.

Analyzing the results from Table 2 using the default fragment size (4-7), we can observe that the models 2, 3 and 8 have presented the best statistical parameters. Afterwards, we varied the fragment size for the three models selected in order to assess the influence of the length of the fragments to be included in the hologram fingerprint. From Table 2, we can see that the best statistical results among all models were obtained for model 28 ($r^2$ = 0.863 and $q^2$ = 0.656). This model was derived using a combination of A, B, C and H, with 5 being the optimum number of PLS components with a fragment size of 7-10. It is interesting to note that the best model contains hydrogen atoms as the fragment distinction, indicating the importance of possible hydrogen bonds between the ligands and the binding site of the biological receptor.

**Table 2.** HQSAR results using several fragment distinction combinations and fragment sizes

| Model | Fragment size | Distinction | $q^2$ | SEP | $r^2$ | SEE | HL | N |
|---|---|---|---|---|---|---|---|---|
| 1 | 4-7 | A/B | 0.488 | 0.881 | 0.799 | 0.552 | 151 | 5 |
| 2 | 4-7 | A/B/C | 0.577 | 0.812 | 0.869 | 0.451 | 83 | 6 |
| 3 | 4-7 | A/B/C/H | 0.555 | 0.833 | 0.878 | 0.437 | 59 | 6 |
| 4 | 4-7 | A/B/C/H/Ch | 0.496 | 0.849 | 0.759 | 0.588 | 401 | 3 |
| 5 | 4-7 | A/B/C/H/Ch/DA | 0.545 | 0.818 | 0.805 | 0.535 | 61 | 4 |
| 6 | 4-7 | A/B/H | 0.434 | 0.939 | 0.880 | 0.432 | 151 | 6 |
| 7 | 4-7 | A/B/C/Ch | 0.546 | 0.829 | 0.851 | 0.475 | 83 | 5 |
| **8** | **4-7** | **A/B/DA** | **0.607** | **0.783** | **0.834** | **0.509** | **53** | **6** |
| 9 | 4-7 | A/B/C/DA | 0.533 | 0.841 | 0.862 | 0.458 | 199 | 5 |
| 10 | 4-7 | A/B/H/DA | 0.497 | 0.861 | 0.780 | 0.569 | 53 | 4 |
| 11 | 4-7 | A/B/C/Ch/DA | 0.448 | 0.914 | 0.866 | 0.451 | 199 | 5 |
| 12 | 4-7 | A/B/C/H/DA | 0.490 | 0.866 | 0.781 | 0.568 | 61 | 4 |
| 13 | 4-7 | A/B/H/Ch/DA | 0.533 | 0.829 | 0.823 | 0.511 | 307 | 4 |
| 14 | 2-5 | A/B/DA | 0.412 | 0.957 | 0.748 | 0.627 | 307 | 6 |
| 15 | 3-6 | A/B/DA | 0.433 | 0.926 | 0.792 | 0.56 | 151 | 5 |
| 8 | 4-7 | A/B/DA | 0.607 | 0.783 | 0.834 | 0.509 | 53 | 6 |
| 16 | 5-8 | A/B/DA | 0.499 | 0.871 | 0.867 | 0.449 | 257 | 5 |
| 17 | 6-9 | A/B/DA | 0.489 | 0.879 | 0.884 | 0.419 | 257 | 5 |
| 18 | 7-10 | A/B/DA | 0.476 | 0.903 | 0.888 | 0.418 | 97 | 6 |
| 19 | 2-5 | A/B/C | 0.466 | 0.912 | 0.789 | 0.573 | 199 | 6 |
| 20 | 3-6 | A/B/C | 0.579 | 0.810 | 0.86 | 0.466 | 257 | 6 |
| 2 | 4-7 | A/B/C | 0.577 | 0.812 | 0.869 | 0.451 | 83 | 6 |
| 21 | 5-8 | A/B/C | 0.634 | 0.745 | 0.870 | 0.443 | 61 | 5 |
| 22 | 6-9 | A/B/C | 0.491 | 0.877 | 0.892 | 0.404 | 151 | 5 |
| 23 | 7-10 | A/B/C | 0.496 | 0.861 | 0.825 | 0.507 | 151 | 4 |
| 24 | 2-5 | A/B/C/H | 0.426 | 0.946 | 0.781 | 0.584 | 257 | 6 |
| 25 | 3-6 | A/B/C/H | 0.490 | 0.891 | 0.850 | 0.484 | 401 | 6 |
| 3 | 4-7 | A/B/C/H | 0.555 | 0.833 | 0.878 | 0.437 | 59 | 6 |
| 26 | 5-8 | A/B/C/H | 0.526 | 0.847 | 0.876 | 0.433 | 353 | 5 |
| 27 | 6-9 | A/B/C/H | 0.560 | 0.804 | 0.834 | 0.495 | 353 | 4 |
| **28** | **7-10** | **A/B/C/H** | **0.656** | **0.722** | **0.863** | **0.456** | **61** | **5** |

$q^2_{LOO}$, leave-on-out cross-validated correlation coefficient; SEP, cross-validated standard error; $r^2$, noncross-validated correlation coefficient; SEE, noncross-validated standard error; HL, hologram length; N, optimal number of components. Fragment distinction: A, atoms; B, bonds; C, connections; H, hydrogen atoms; Ch, chirality; DA, donor and acceptor.

After the HQSAR model construction, the next step was employing an external validation process, in which the compounds in the test set were completely excluded during the training of the model, and the best model generated was used to predict the values of the biological property of the new compounds. Thus, the predictive power of the best HQSAR model (derived using the molecules from the training set; fragment distinction A/B/C/H; fragment size 7-10, Table 2) was assessed by predicting the $pEC_{50}$ values for the test set (**42**-**51**, Table 1). The prediction results are listed in Table S1 (Supplementary Information) and Figure 6. It is possible to see that the test set compounds, which represent the different structural features incorporated within the training set, were well predicted by the best HQSAR model. From the low residual values, we can say that the HQSAR model obtained is robust and can be used in further medicinal chemistry studies.

### 3D QSAR analyses

After several analyses, the best CoMFA model was obtained by a focusing process using a weight of 0.5 and a distance of 1.0. This model shows $q^2 = 0.714$ and $r^2 = 0.993$, with steric and electrostatic proportions of 34% and 66%, respectively. Table S2 displays the statistical results from all CoMFA analyses. It is interesting to note that the electrostatic contribution for the CoMFA model is more important than the contributions from the steric data. This fact indicates that electrostatic interactions (*e.g.*, hydrogen bonds) are important in describing and improving biological activity. According to experimental evidence, PPARδ has a polar cavity with 3 main amino acids (His323, His449 and Tyr473) to which activating ligands must bind.[3] Therefore, the electrostatic forces are more important than the steric ones because of the large

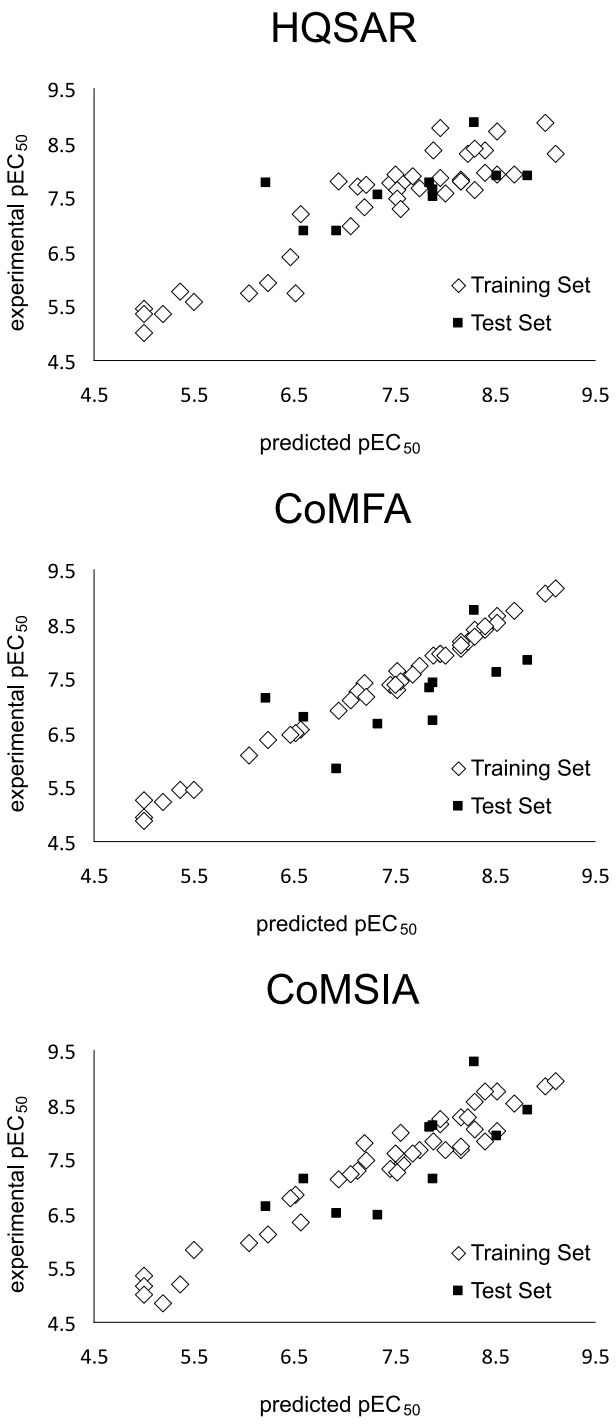


**Figure 6.** Plots of experimental *versus* predicted $pEC_{50}$ using HQSAR, CoMFA and CoMSIA models.

size of the active site. In theory, many molecules can bind to the site in many positions.

Next, for the CoMFA model construction, we employed the compounds from the test set (**42**-**51**, Table 1) in order to validate this model. The prediction results are listed in Table S1 and Figure 6. The analysis of the outcomes showed that the compounds in the test set were well predicted by the best CoMFA model, indicating that this model has a high predictive power and can be used to obtain the interaction fields of new compounds.

To construct the CoMSIA model, we calculated several molecular fields (steric-S, electrostatic-E, hydrophobic-H, H-bond acceptor-A and donor-D) without using the focusing option, and the results are summarized in Table S3. From the best initial model (model 8, $q^2 = 0.229$) based on electrostatic and hydrophobic contributions, we employed the region focusing method to improve the predictive power of the model. The main results obtained after the focusing are shown in Table S4; it can be seen that the best CoMSIA model ($q^2 = 0.620$ and $r^2 = 0.941$) is composed by electrostatic and hydrophobic fields (60.9 and 39.1%, respectively) and was obtained by a focusing process with a weight of 0.5 and a distance of 1.5. It is interesting to note that this model, as well as CoMFA one, has high electrostatic contribution. Furthermore, hydrophobic interactions are also important. PPARδ has a large active site that presents a small cavity with polar character; however, the other amino acids of the active site can participate in hydrophobic interactions. Therefore, the polar cavity is responsible for activating the receptor, and the hydrophobic pocket is responsible for stabilizing the ligands in the binding site. Because the polar interactions (*e.g.*, hydrogen bonds) involve high energy, when compared to the hydrophobic interactions (*e.g.*, van der Waals), it is expected that electrostatic effects have a high proportion on the obtained CoMSIA model.

Next, we used the compounds from the test set (**42**-**51**, Table 1) to validate the generated CoMSIA model, and the prediction results are listed in Table S1 and Figure 6. After analyzing the outcomes, it was possible to conclude that the compounds from the test set were well predicted by the best CoMSIA model, indicating that this model is robust and can be used to plan new compounds.

## Physicochemical discussion

After the construction of 2D and 3D QSAR models, we performed theoretical calculations of some molecular properties, such as the maps of molecular orbitals (highest occupied molecular orbital - HOMO and lowest unoccupied molecular orbital - LUMO) and electrostatic surface potential (ESP), and correlated them to the 2D and 3D contribution maps obtained from the HQSAR, CoMFA and CoMSIA models. Figures 7 and 8 show all contribution maps obtained for the most (**20**) and the least potent (**36**) compounds, respectively.

From Figures 7(A) and 8(A), we can observe that both molecules display polar contacts with the three main

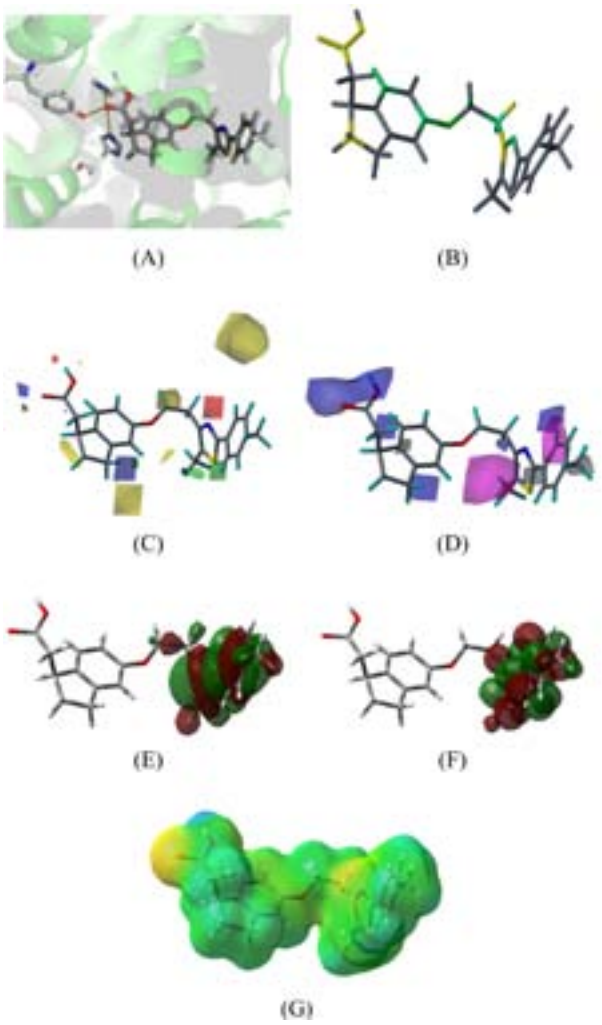


**Figure 7.** Contribution maps for the most potent compound (**20**). (A) molecule docked into the active site; (B) HQSAR, (C) CoMFA, (D) CoMSIA, (E) HOMO, (F) LUMO and (G) ESP maps. See online for color image.

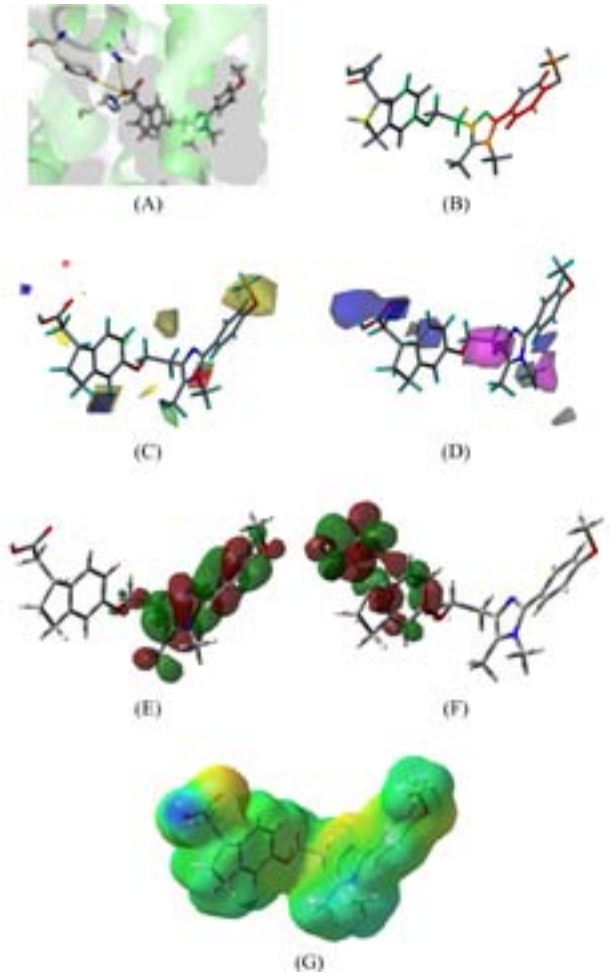


**Figure 8.** Contribution maps for the least potent compound (**36**). (A) molecule docked into the active site; (B) HQSAR, (C) CoMFA, (D) CoMSIA, (E) HOMO, (F) LUMO and (G) ESP maps. See online for color image.

polar amino acids (His323, His449 and Tyr473), shown in yellow dotted lines. From the other maps calculated, we can note the following findings: (*i*) HQSAR maps show positive (green and yellow) and negative (orange and red) contributions. The central N atom from the five-atom ring contributes positively in both compounds. For the HQSAR map of compound **20** (the most potent), the COOH group shows a positive contribution, indicating the importance of polar contacts to biological activity. For the 2D map of compound **36** (the less potent), the benzene ring and *o*-methyl terminal group show a negative contribution. This may possibly be related to their steric hindrance. (*ii*) In our previous HQSAR study,[22] we have noted that polar groups linked to hydrophobic groups (*m*-methyl anthranilic acid) have influence on PPARδ affinity, but this can be improved using small polar groups. The most potent compound of previous study has $pEC_{50}$ = 7.9 and the most potent compound of this work (compound **20**) has $pEC_{50}$ = 8.3. Therefore, this outcome corroborates our HQSAR study. (*iii*) CoMFA electrostatic maps show positive (blue) and negative (red) contributions; CoMFA steric maps display positive (green) and negative (yellow) contributions. Analyzing the CoMFA maps for the least potent compound (**36**), it is possible to observe that the steric contributions confirm the negative influence of the benzene ring and *o*-methyl group for biological activity. Therefore, this confirmed the HQSAR evidence for the negative contribution of these groups. The steric hindrance of these groups can possibly block the polar groups from approaching polar residues. From the docking of compound **36**, we can note that the COOH group is more distant from the polar residues than the polar group of compound **20**. Furthermore, the COOH group in both molecules has a positive electrostatic contribution, indicating the importance of the polar contacts. The substitution of the N atom on the imidazole ring (compound **36**) by the S atom (compound **20**) causes an increase in electrostatic

contribution, demonstrating the role of electronegative atoms in this position in improving the biological activity. (*iv*) CoMSIA maps show the same color systems as the electrostatic contributions used in the CoMFA analysis. Hydrophobic positive contributions are represented in white and negative contributions represented in magenta. For the most potent compound (**20**), the benzene and methyl groups have positive hydrophobic contributions to the biological activity. Both molecules have a negative hydrophobic contribution in regards to the linker region [–O–$(CH_2)_2$–] and a positive electrostatic contribution to the COOH region, which is in agreement to the HQSAR and CoMFA maps. (*v*) According Huang *et al.*,[51] we note that polar groups (consequently, hydrogen bond donors and acceptors) as COOH head are important to PPARδ affinity. Huang *et al.*[51] have performed a tridimensional QSAR based on ligand alignment and they have obtained very similar results of electrostatic properties. So, in order to develop new PPARδ modulators, it is important to keep a COOH group or to use a bioisosterism technique to preserve electrostatic requirements. (*vi*) After analysis of the HOMO maps, we observe no difference among the compounds studied. However, the LUMO maps indicate a significant variation in the atomic contributions for this orbital, which can explain the differences in biological activity. For the most potent compound (**20**), the main atomic LUMO contributions are located at hydrophobic tail while the least potent compound (**36**) has the main LUMO contribution located at the COOH group. Since this orbital (LUMO) indicates the capacity to accept electrons,[52] we can identify the possible sites involved in charge transfer reactions between the ligand and the protein. (*vii*) ESP maps show the charge distribution into the molecular surfaces. There is a large difference of charge among the two compounds mainly in the region of polar contacts (COOH group). Compound **20** has the most negative surface and compound **36** has the most positive surface located at the COOH group. This may represent a low ability to accept H-bond in this region.

PPARδ activation depends on specific interactions, and the main ones involve hydrogen bonds with polar residues. As the polar interactions are the most energetic, they can better stabilize the ligand-receptor complex. Therefore, regardless of which residues are involved in the polar contacts, it is important that these interactions are strong, as well as hydrophobic, in order to stabilize the ligand in the binding site, which can be realized by the hydrophobic tail and the linker group.

In order to obtain more detailed information on the main interactions into the binding site, we decided to calculate its volume and hydrophobic profile. The volume of the active site was determined with FPocket package[53,54] (available on http://bioserv.rpbs.univ-paris-diderot.fr/fpocket/index.html) and Computed Atlas of Surface Topography of proteins (CASTp),[55] available on http://sts.bioengr.uic.edu/castp/index.php. The FPocket and CASTp packages provided a volume of 1896.2 Å$^3$ and 1896.7 Å$^3$, respectively. This data indicates that the PPAR cavity is very large and can accommodate a large variety of ligands. From spheres generated by FPocket, we can plot the surface of active site colored by hydrophobic profile, by employing USFC Chimera program.[56] Figure 9 shows the surface of binding site, where blue color indicates polar areas and orange represents hydrophobic regions.

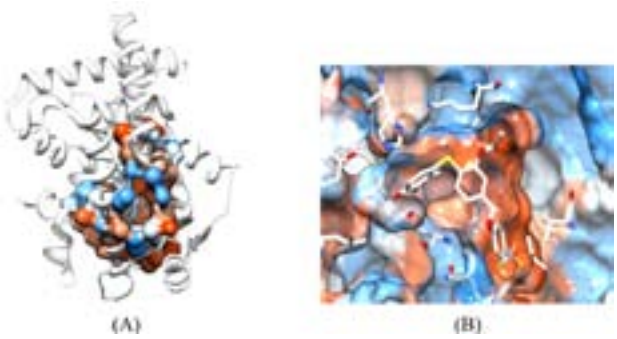


**Figure 9.** (A) Cavity obtained from FPocket package; (B) binding site surface with natural ligand D32. See online for color image.

From Figure 9, it is possible to observe that the region near to COOH group of ligands (His323, His449 and Tyr473) has a polar surface and the entire cavity has a hydrophobic surface. In addition to QSAR studies, the results obtained from volume and hydrophobic profile of binding site provide an insight on the electrostatic and hydrophobic interactions with the main residues of the binding site, which are important to PPARδ activation.

## Conclusions

The 2D and 3D QSAR models obtained in this work present good internal and external consistency (HQSAR: $r^2$ = 0.863 and $q^2$ = 0.656; CoMFA: $q^2$ = 0.714 and $r^2$ = 0.993; CoMSIA: $q^2$ = 0.620 and $r^2$ = 0.941). Besides, an external validation process has yielded a good correlation between experimental and predicted $pEC_{50}$ values for the test set compounds. Furthermore, CoMFA and CoMSIA maps as well as quantum chemical plots show a good physicochemical interpretation of the possible protein-ligand interactions. In addition to the generated maps, we can note the importance of the COOH group in the ligands with the polar contacts in the binding site and the influence of the linker group and the hydrophobic

tail used to stabilize the ligand in the active site. The presence of more electronegative atoms than nitrogen on the imidazole ring of hydrophobic tails increases the electrostatic positive contribution and significantly favors the biological activity. In order to obtain more detailed information on the main interactions into the binding site, we calculate its volume and hydrophobic profile, which indicate that the PPAR cavity is very large and can accommodate a large variety of ligands, as well as the entire cavity has a hydrophobic surface. From the findings of this study, we can conclude that the combination of QSAR studies with molecular modeling techniques is a powerful tool to propose molecular modifications in order to obtain new structural-based ligands for PPARδ, which can be used to treat diabetes, cardiovascular diseases and metabolic syndrome.

## Supplementary Information

Supplementary data (Tables S1-S4) are available free of charge at http://jbcs.sbq.org.br, as PDF file.

## Acknowledgments

The authors would like to thank FAPESP, CNPq and CAPES (Brazilian agencies) for their funding.

## References

1. Berger, J.; Moller, D. E.; *Annu. Rev. Med.* **2002**, *53*, 409.
2. Robinson, E.; Grieve, D. J.; *Pharmacol. Ther.* **2009**, *122*, 246.
3. Xu, H. E.; Lambert, M. H.; Montana, V. G.; Parks, D. J.; Blanchard, S. G.; Brown, P. J.; Sternbach, D. D.; Lehmann, J. M.; Wisely, G. B.; Willson, T. M.; Kliewer, S. A.; Milburn, M. V.; *Mol. Cell* **1999**, *3*, 397.
4. Miller, A. R.; *Drug Dev. Res.* **2006**, *67*, 574.
5. Shi, Y.; *Drug Discov. Today* **2007**, *12*, 440.
6. Cameron, A. J.; Shaw, J. E.; Zimmet, P. Z.; *Endocrinol. Metab. Clin.* **2004**, *33*, 351.
7. Billin, A. N.; *Expert Opin. Invest. Drugs* **2008**, *17*, 1465.
8. Patrick, J. B.; *Am. J. Med.* **2007**, *120*, S12.
9. McLellan, K. C. P.; Barbalho, S. M.; Cattalini, M.; Lerario, A. M.; *Rev. Nutr.* **2007**, *20*, 515.
10. Araújo, L. M. B.; Britto, M. M. D. S.; Porto da Cruz, T. R.; *Arq. Bras. Endocrinol. Metab.* **2000**, *44*, 509.
11. Azevedo, A. P. D.; Papelbaum, M.; D'Elia, F.; *Rev. Bras. Psiquiatr.* **2002**, *24*, 77.
12. Lombo, B.; Satizábal, C.; Villalobos, C.; Tique, C.; Kattah, W.; *Acta Med. Colomb.* **2007**, *32*, 9.
13. Eckel, R. H.; Grundy, S. M.; Zimmet, P. Z.; *Lancet* **2005**, *365*, 1415.
14. King, H.; Aubert, R. E.; Herman, W. H.; *Diabetes Care* **1998**, *21*, 1414.
15. Luquet, S.; Gaudel, C.; Holst, D.; Lopez-Soriano, J.; Jehl-Pietri, C.; Fredenrich, A.; Grimaldi, P. A.; *BBA-Mol. Basis Dis.* **2005**, *1740*, 313.
16. Fredenrich, A.; Grimaldi, P. A.; *Diabetes Metab.* **2005**, *31,* 23.
17. Gross, B.; Staels, B.; *Best. Pract. Res. Cl. En.* **2007**, *21*, 687.
18. Shearer, B. G.; Billin, A. N.; *BBA-Mol. Cell Biol. L.* **2007**, *1771,* 1082.
19. Honório, K. M.; Garratt, R. C.; Polikatpov, I.; Andricopulo, A. D.; *J. Mol. Graphics Modell.* **2007**, *25*, 921.
20. Honório, K. M.; Garratt, R. C.; Polikatpov, I.; Andricopulo, A. D.; *Lett. Drug Des. Discovery* **2006**, *3*, 261.
21. Da Silva, S. L.; Da Silva, A.; Honório, K. M.; Marangoni, S.; Toyama, M. H.; Da Silva, A. B. F.; *THEOCHEM* **2004**, *684*, 1.
22. Garcia, T. S.; Honorio, K. M.; *J. Braz. Chem. Soc.* **2011**, *22*, 65.
23. Alves, C. N.; Pinheiro, J. C.; Camargo, A. J.; Ferreira, M. M. C.; Romero, R. A. F.; Da Silva, A. B. F.; *THEOCHEM* **2001**, *541*, 81.
24. Camargo, A. J.; Mercadante, R.; Honorio, K. M.; Alves, C. N.; Da Silva, A. B. F.; *THEOCHEM* **2002**, *583*, 105.
25. Molfetta, F. A.; Bruni, A. T.; Honorio, K. M.; Da Silva, A. B. F.; *Eur. J. Med. Chem.* **2005**, *40*, 329.
26. Alves, C. N.; Macedo, L. G. M.; Honorio, K. M.; Camargo, A. J.; Santos, L. S.; Jardim, I. N.; Barata, L. E. S.; Da Silva, A. B. F., *J. Braz. Chem. Soc.* **2002**, *13*, 300.
27. Calgarotto, A. K.; Miotto, S.; Honorio, K. M.; Da Silva, A. B. F.; Marangoni, S.; Silva, J. L.; Comar, M.; Oliveira, K. M. T.; da Silva, S. L.; *THEOCHEM* **2007**, *808*, 25.
28. Rudolph, J.; Chen, L.; Majumdar, D.; Bullock, W. H.; Burns, M.; Claus, T.; Dela Cruz, F. E.; Daly, M.; Ehrgott, F. J.; Johnson, J. S.; Livingston, J. N.; Schoenleber, R. W.; Shapiro, J.; Yang, L.; Tsutsumi, M.; Ma, X.; *J. Med. Chem.* **2007**, *50*, 984.
29. Wickens, P.; Zhang, C.; Ma, X.; Zhao, Q.; Amatruda, J.; Bullock, W.; Burns, M.; Cantin, L. D.; Chuang, C. Y.; Claus, T.; Dai, M.; Dela Cruz, F.; Dickson, D.; Ehrgott, F. J.; Fan, D.; Heald, S.; Hentemann, M.; Iwuagwu, C. I.; Johnson, J. S.; Kumarasinghe, E.; Ladner, D.; Lavoie, R.; Liang, S.; Livingston, J. N.; Lowe, D.; Magnuson, S.; Mannelly, G.; Mugge, I.; Ogutu, H.; Pleasic-Williams, S.; Schoenleber, R. W.; Shapiro, J.; Shelekhin, T.; Sweet, L.; Town, C.; Tsutsumi, M.; *Bioorg. Med. Chem. Lett.* **2007**, *17*, 4369.
30. Havranek, M.; Sauerberg, P.; Mogensen, J. P.; Kratina, P.; Jeppesen, C. B.; Pettersson, I.; Pihera, P.; *Bioorg. Med. Chem. Lett.* **2007**, *17*, 4144.
31. Sierra, M. L.; Beneton, V. R.; Boullay, A. B. N. D.; Boyer, T.; Brewster, A. G.; Donche, F. D. R.; Forest, M. C.; Fouchet, M. H. I. N.; Gellibert, F. O. J.; Grillot, D. A.; Lambert, M. H.; Laroze, A.; Le Grumelec, C.; Linget, J. M.; Montana, V. G.; Nguyen, V. L.; Nicodme, E.; Patel, V.; Penfornis, A.; Pineau, O.; Pohin,

D.; Potvain, F.; Poulain, G. R.; Ruault, C. C. B.; Saunders, M.; Toum, J. R. M.; Xu, H. E.; Xu, R. X.; Pianetti, P. M.; *J. Med. Chem.* **2007**, *50*, 685.

32. Cantin, L. D.; Liang, S.; Ogutu, H.; Iwuagwu, C. I.; Boakye, K.; Bullock, W. H.; Burns, M.; Clark, R.; Claus, T.; dela Cruz, F. E.; Daly, M.; Ehrgott, F. J.; Johnson, J. S.; Keiper, C.; Livingston, J. N.; Schoenleber, R. W.; Shapiro, J.; Town, C.; Yang, L.; Tsutsumi, M.; Ma, X.; *Bioorg. Med. Chem. Lett.* **2007**, *17*, 1056.
33. The PyMOL Molecular Graphics System, v0.99; DeLano Scientific LLC: South San Francisco, California, 2006.
34. Connors, R. V.; Wang, Z.; Harrison, M.; Zhang, A.; Wanska, M.; Hiscock, S.; Fox, B.; Dore, M.; Labelle, M.; Sudom, A.; Johnstone, S.; Liu, J.; Walker, N. P. C.; Chai, A.; Siegler, K.; Li, Y.; Coward, P.; *Bioorg. Med. Chem. Lett.* **2009**, *19*, 3550.
35. Nascimento, A. S.; *Biochimie* **2010**, *92*, 499.
36. Pochetti, G.; Godio, C.; Mitro, N.; Caruso, D.; Galmozzi, A.; Scurati, S.; Loiodice, F.; Fracchiolla, G.; Tortorella, P.; Laghezza, A.; Lavecchia, A.; Novellino, E.; Mazza, F.; Crestani, M.; *J. Biol. Chem.* **2007**, *282*, 17314.
37. *Sybyl 8.1*; Tripos Inc.: St. Louis, MO, USA, 2008.
38. James, J. P. S.; *J. Comput. Chem.* **1989**, *10*, 209.
39. James, J. P. S.; *J. Comput. Chem.* **1989**, *10*, 221.
40. Gotwals, R. R.; Sendlinger, S. C.; *A Chemistry Educator's Guide to Molecular Modeling*; The North Carolina School of Science and Mathematics: Durham, 2007.
41. Maltarollo, V. G.; Homem-de-Mello, P.; Honório, K. M.; *J. Mol. Model.* **2010**, *16*, 799.
42. Honorio, K. M.; da Silva, A. B. F.; *J. Mol. Model.* **2005**, *11*, 200.
43. Weber, K. C.; Honório, K. M.; Da Silva, S. L.; Mercadante, R.; Da Silva, A. B. F.; *Int. J. Quantum Chem.* **2005**, *103*, 731.
44. Weber, K. C.; Honório, K. M.; Bruni, A. T.; Andricopulo, A. D.; da Silva, A. B. F.; *Struct. Chem.* **2006**, *17*, 307.
45. Frisch, M. J.; Trucks, G. W.; Schlegel, H. B.; Scuseria, G. E.; Robb, M. A.; Cheeseman, J. R.; Scalmani, G.; Barone, V.; Mennucci, B.; Petersson, G. A.; Nakatsuji, H.; Caricato, M.; Li, X.; Hratchian, H. P.; Izmaylov, A. F.; Bloino, J.; Zheng, G.; Sonnenberg, J. L.; Hada, M.; Ehara, M.; Toyota, K.; Fukuda, R.; Hasegawa, J.; Ishida, M.; Nakajima, T.; Honda, Y.; Kitao, O.; Nakai, H.; Vreven, T.; Montgomery, Jr., J. A.; Peralta, J. E.; Ogliaro, F.; Bearpark, M.; Heyd, J. J.; Brothers, E.; Kudin, K. N.; Staroverov, V. N.; Kobayashi, R.; Normand, J.; Raghavachari, K.; Rendell, A.; Burant, J. C.; Iyengar, S. S.; Tomasi, J.; Cossi, M.; Rega, N.; Millam, N. J.; Klene, M.; Knox, J. E.; Cross, J. B.; Bakken, V.; Adamo, C.; Jaramillo, J.; Gomperts, R.; Stratmann, R. E.; Yazyev, O.; Austin, A. J.; Cammi, R.; Pomelli, C.; Ochterski, J. W.; Martin, R. L.; Morokuma, K.; Zakrzewski, V. G.; Voth, G. A.; Salvador, P.; Dannenberg, J. J.; Dapprich, S.; Daniels, A. D.; Farkas, Ö.; Foresman, J. B.; Ortiz, J. V.; Cioslowski, J.; Fox, D. J.; *Gaussian 09, Revision*, Gaussian, Inc.: Wallingford CT, 2009.
46. Becke, A. D.; *J. Chem. Phys.* **1993**, *98*, 1372.
47. Lee, C.; Yang, W.; Parr, R. G.; *Phys. Rev. B: Condens. Matter Mater. Phys.* **1988**, *37*, 785.
48. Sosa, C.; Andzelm, J.; Elkin, B. C.; Wimmer, E.; Dobbs, K. D.; Dixon, D. A.; *J. Phys. Chem.* **1992**, *96*, 6630.
49. Godbout, N.; Slahub, D. R.; Andzelm, J.; Wimmer, E.; *Can. J. Chem.* **1992**, *70*, 560.
50. Maltarollo, V. G.; Mello, P. H.; Honório, K. M.; *J. Mol. Model.* **2011**, *17*, 2549.
51. Huang, H.-J.; Lee, K.-J.; Yu, H. W.; Chen, H.-Y.; Tsai, F.-J.; Chen, C. Y.-C.; *J. Biomol. Struc. Dyn.* **2010**, *28,* 187.
52. Arroio, A.; Honório, K. M.; da Silva, A. B. F.; *Quim. Nova* **2010**, *33*, 694.
53. Schmidtke, P.; Le Guilloux, V.; Maupetit, J.; Tuffery, P.; *Nucleic Acids Res.* **2010**, *38*, W582.
54. Le Guilloux, V.; Schmidtke, P.; Tuffery, P.; *BMC Bioinformatics* **2009**, *10,* 168.
55. Dundas, J.; Ouyang, Z.; Tseng, J.; Binkowski, A.; Turpaz, Y.; Liang, J.; *Nucleic Acid Res.* **2006**, *34,* W116.
56. Pettersen, E. F.; Goddard, T. D.; Huang, C. C.; Couch, G. S.; Greenblatt, D. M.; Meng, E. C.; Ferrin, T. E.; *J. Comput. Chem.* **2004**, *13,* 1605.

*Submitted: April 5, 2011*
*Published online: October 20, 2011*

**FAPESP has sponsored the publication of this article.**

*J. Braz. Chem. Soc.*, Vol. 23, No. 1, 96-102, 2012.
Printed in Brazil - ©2012 Sociedade Brasileira de Química
0103 - 5053 $6.00+0.00

Article

# HPLC Determination of Histamine, Tyramine and Amino Acids in Shrimp By-Products

***Carolina Bueno-Solano, Jaime López-Cervantes, Dalia I. Sánchez-Machado* and Olga N. Campas-Baypoli***

*Departamento de Biotecnología y Ciencias Alimentarias, Instituto Tecnológico de Sonora, 5 de Febrero 818 Sur, Cd. Obregón, MX-85000 Sonora, México*

Aminas biogênicas em alta concentração podem afetar a qualidade dos alimentos e causar várias doenças, pois estão presentes em produtos como frutos do mar, vinhos e outros produtos fermentados. Subprodutos do camarão são uma fonte rica de proteína hidrolisada que podem ser usadas como suplemento alimentar. Amostras (de subprodutos de camarão) de proteína seca em pó, proteínas hidrolisadas líquidas e farinha da cabeça de camarão foram analisadas para avaliar o conteúdo de histamina e tiramina. As aminas foram extraídas com ácido tricloroacético 5% e posteriormente derivatizadas com *o*-ftaldialdeído. A separação cromatográfica foi realizada em uma coluna analítica, Chrom SEP C18 SS 5 mm (4,6 mm × 150 mm) com eluição por gradiente, os comprimentos de onda foram $\lambda_{ex}$ = 335 nm e $\lambda_{em}$ = 440 nm. A fase móvel utilizada foi uma mistura de tetrahidrofurano, metanol e tampão fosfato a uma vazão de 0,6 mL $min^{-1}$. Sob essas condições, a repetibilidade (desvio padrão relativo < 6,55%), reprodutibilidade (< 5,60%) e exatidão foram satisfatórias. Os valores de recuperação foram 84,51, 90,75, 95,37, 98,68 e 84,29% para L-tirosina, L-triptofano, L-lisina, tiramina e histamina, respectivamente. Este método tem sido aplicado com sucesso para a quantificação de aminoácidos precursores e aminas biogênicas em matrizes diversas.

Biogenic amines in high concentration can affect the quality of foods and cause several diseases since they are present in products like seafood, wines, and other fermented products. Shrimp by-products are a rich source of protein hydrolysate that can be used as dietary supplements. Samples (from shrimp by-products) of dry protein powder, liquid protein hydrolysate and flour of shrimp head were analyzed to evaluate the histamine and tyramine contents. Amines were extracted with trichloroacetic acid 5% and derivatized with *o*-phthaldialdehyde. The chromatographic separation was performed in an analytical column, Chrom SEP SS C18 5 μm (4.6 mm × 150 mm) and a fluorescence detector was used with wavelengths at $\lambda_{ex}$ = 335 nm and $\lambda_{em}$ = 440 nm. The mobile phase was a mixture of tetrahydrofuran, methanol and phosphate buffer at a flow rate of 0.6 mL $min^{-1}$ using elution gradient. Under these conditions, the repeatability (relative standard deviation, RSD < 6.55%), reproducibility (< 5.60%) and accuracy were of satisfying quality. The recovery values were 84.51, 90.75, 95.37, 98.68 and 84.29% for L-tyrosine, L-tryptophan, L-lysine, tyramine and histamine, respectively. This method has been successfully applied for the quantification of precursor amino acids and biogenic amines in different matrices.

**Keywords:** biogenic amines, *o*-phtaldialdehyde, shrimp by-products, HPLC, protein hydrolysate

## Introduction

Biogenic amines are organic bases of low molecular weight that can be formed or degraded as a result of normal metabolic activity of animals, plants and microorganisms.[1] In some food products, such as fish, seafood, cheese, meat, wine, and other fermented foods, they are produced as a result of the descarboxylation from corresponding free amino acids by microbial activity.[2-4] In reference to these food products, high concentrations of biogenic amines may cause headaches, respiratory distress, heart palpitation, hypertension or hypotension, and several allergenic disorders.[5] Nevertheless, natural polyamines, as putrescine, cadaverine, spermine and spermidine, in low concentration have multiple functions in living organisms, such as growth factors, antioxidants,

*e-mail: dalia.sanchez@itson.edu.mx

stabilizers of DNA and RNA, metabolic regulators and nutrients.[6]

The estimation of high concentrations of histamine, tyramine, putrescine and cadaverine is of great importance, not only from a toxicity point of view, but as indicators of the degree of freshness or spoilage in food that is associated with inadequate sanitary conditions during the production procedures.[7,8] The most widely used analytical methods for identification and quantification of biogenic amines and amino acids are high performance liquid chromatography (HPLC) and capillary electrophoresis which are combined with different detection techniques like spectrophotometry, fluorometric, electrochemical and mass spectrometric.[9-11] Due to the fact that most biogenic amines and amino acids have do not fluoresce properties, it is necessary to perform a chemical derivatization prior to fluorescence detection.[12] Different derivatization reagents have been tested, *o*-phthaldialdehyde (OPA) in combination with a thiol compound, such as 2-mercaptoethanol (MCE) that is the most employed.[3-5] 9-Fluorenylmethyl chloroformate (FMOC-Cl) is another compound used for the detection of primary and secondary biogenic amines, but there are generation of undesirable compounds.[10,13] Other chemical derivatizing agents are phenyl isothiocyanate (PITC), dansylchloride and *N*-(9-fluorenylmethoxycarbonyloxy) succinimide.[6] The response of some agent during the analysis by HPLC is affected by the reaction time of the sample with the chemical derivatizing agent. This makes impossible to create sequences of injections in which the sample had been previously prepared. For this reason, it is necessary to develop automated methods in which an auto-sampler is responsible for carrying out the procedure of derivatization some minutes before the analysis, providing better accuracy.

Shrimp is one of the most consumed seafood in the world. In Sonora (Mexico), the shrimp production by aquaculture was 68500 tons in 2008. Only 65% of the shrimp is edible, the other 35% (cephalothorax and exoskeleton) is discarded and this can generate an environmental problem. This waste (the 35%) is a good source of protein and chitin. Several techniques have been developed to process the discarded parts, such as enzymatic and acid hydrolyzation, sun-drying and lactic fermentation. Lactic acid fermentation has been reported to be a workable and economical technique which will stabilize and retain the nutritional quality of the waste[14]. With this technique, protein hydrolysate, chitin and lipids can be recovered. Several studies have reported the analysis of biogenic amines in seafood, for example, tuna,[15] sardine,[16] cold smoked salmon,[17] and fermented fish products.[18] However, there is no reported study concerning the biogenic amine content in shrimp waste. The purpose of the present study is to develop and validate an automated method for the determination of biogenic amines and amino acids in powdered protein hydrolysate from shrimp waste using an HPLC method with *o*-phthaldialdehyde and 2-mercaptoetanol.

## Results and Discussion

### Biogenic amine and amino acid extractions

For the extraction of biogenic amines and their amino acid precursors, numerous reagents have been employed. For example, methanol 75%,[3] perchloric acid 1 mol $L^{-1}$ and 0.6 mol $L^{-1}$,[1,10,13] and tricholoroacetic acid (TCA) 5 and 10%.[19-21] The preliminary assays show that the best extraction was with TCA 5%. The volume of TCA 5% (5 and 10 mL), the time of vortex (60 and 90 s), sonication (1, 3 and 6 min) and centrifugation (15, 20 and 25 min) were recorded. The optimal results were achieved using 10 mL of TCA 5%, 90 s in vortex, sonication for 6 min and centrifugation for 15 min. For the determination of the amount of used sample in the extraction, different concentrations of protein hydrolysate powder (15, 30 and 50 mg) were applied. The assays indicated that 15 mg of dry powder was adequate for the analysis.

### Derivatization procedure

In the derivatization of the biogenic amines and amino acids, a mixture of OPA/MCE was employed. The most important advantage of OPA over other derivatization reagents is that it quickly reacts with amines and enables the biogenic amines to be detected at low levels. The negative point here is that OPA reacts only with primary amines and leads to poorly stable compounds.[7] OPA derivatization does not show the presence of excess reagent (interfering with the analyte resolutions), which are detected when using FMOC derivatization methods.[6] The OPA derivatives are not stable, so, it was necessary to performer an automated precolumn derivatization. This was carried out prior to the injection in the auto-sampler.

### Identification and separation

To determine the optimal chromatographic conditions for the determination of biogenic amines and amino acids, preliminary trials with standards were performed, as recommended by several researchers.[1,2,6] The trials were performed using different proportions of the eluent from proposed mobile phases by other research.[22] With a mobile phase of (A) tetrahydrofuran:methanol:phosphate

buffer (10 mmol $L^{-1}$) (1:8:91) and mobile phase (B) methanol:phosphate buffer (10 mmol $L^{-1}$) (80:20), the biogenic amines and amino acid peaks showed good separation. Additionally, in trials of three flow rates of the mobile phase (0.6, 0.9 and 1.0 mL $min^{-1}$) and four different column temperatures (35, 38, 40 and 42 °C), the better resolution of biogenic amines and amino acids was obtained at 38 °C with a flow rate of 0.6 mL $min^{-1}$.

Biogenic amines and amino acids were identified through the comparison of their retention times with those times from stock standard solutions. Figure 1 shows the chromatograms of standard of biogenic amines and free amino acids (a) and shows chromatograms of the analytes in dry powder (b). Peak standards were observed at 26.24 ± 0.09 min for L-tyrosine, 32.45 ± 0.02 min for L-tryptophan, 28.84 ± 0.05 min for histamine, and 34.79 ± 0.02 min for L-lysine, while tyramine peaked at 35.29 ± 0.02 min, for an average of 10 injections. Peaks in dry powder were observed at 26.57 ± 0.09 min for L-tyrosine, 32.40 ± 0.02 min for L-tryptophan, 28.92 ± 0.05 min for histamine and 34.70 ± 0.02 min for L-lysine, while tyramine peaked at 35.20 ± 0.02 min, for an average of 10 injections.

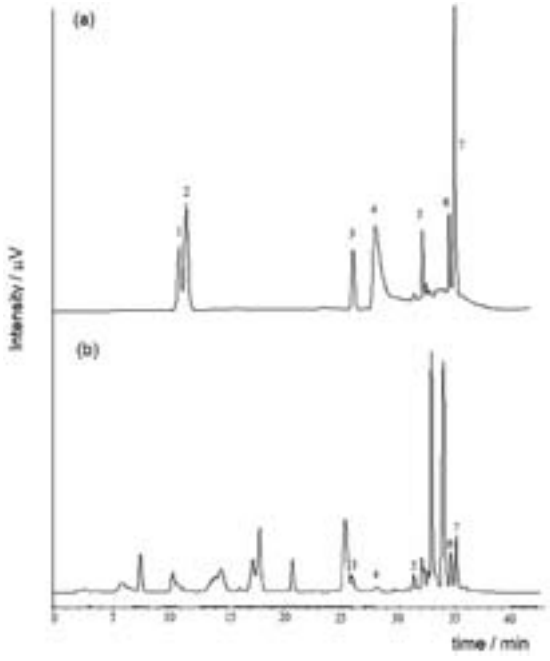


**Figure 1.** HPLC chromatograms of standard of biogenic amines and free amino acids (a) and dry powder (b). Peaks identified: (1) histidine, (2) glutamine, (3) L-tyrosine, (4) histamine, (5) L-tryptophan, (6) L-lysine and (7) tyramine.

## Method validation

With this method, it is also possible to determine histidine, glutamine, tryptamine, cadaverine and putrescine (information not shown), however, histidine and glutamine cannot be quantified due to the presence of interference in the sample, and the others biogenic amines are not present in the sample.

Quantification was performed by the external standard method based on the peak height of the eluted biogenic amines and amino acids. The linearity was evaluated using standard stock solutions of L-tyrosine, L-tryptophan, L-lysine, tyramine and histamine. The calibration curves were constructed for each amino acid and biogenic amine. In all cases, the relationships between concentrations and peak height were linear, with coefficients of determination greater than 0.999. The regression equations for the calibration plots for L-tyrosine, L-tryptophan, L-lysine, tyramine and histamine are shown in Table 1.

The repeatability and reproducibility of the method were evaluated. For repeatability, a total of eight injections of the same sample was performed by duplicate under optimum conditions during a working day, and three replicate analyses of the same sample were made on three different days to determine reproducibility. The relative standard deviations (RSD) were less than 7% for all compounds, for both reproducibility and repeatability. Considering these RSD values, the reproducibility and repeatability are satisfactory. These results indicate that this method can be applied as quantitative analyses of L-tyrosine, L-tryptophan, L-lysine, tyramine and histamine in a protein hydrolysate from the fermentation of shrimp waste. The limits of detection (LOD, defined as three times the basis of signal-to-noise ratio, as American Chemical Society Guidelines)[23] for L-tyrosine, L-tryptophan, L-lysine, tyramine and histamine were 52, 70, 88, 58 and 6.28 ng $mL^{-1}$, respectively. Table 2 shows the results of the test for repeatability, reproducibility and LOD.

**Table 1.** Calibrations curves of L-tyrosine, L-tryptophan, L-lysine, tyramine and histamine

| Compound | Range / (µg $ml^{-1}$) | Equation | $r^2$ |
|---|---|---|---|
| L-Tyrosine | 1.9-47.6 | $y = 139860x - 5628.6$ | 0.9995 |
| L-Tryptophan | 2.8-64.4 | $y = 127676x - 10247$ | 0.9990 |
| L-Lysine | 3.2-80.4 | $y = 77813x - 4290.8$ | 0.9995 |
| Tyramine | 2.2-32.4 | $y = 498923x + 37931$ | 0.9994 |
| Histamine | 0.6-9.6 | $y = 107963x - 2358.6$ | 0.9990 |

$x$: amount (µg $ml^{-1}$); $y$: peak area; $r^2$: determination coefficient; samples were injected by duplicate.

The accuracy was estimated by means of recovery assays. For the recovery, eight samples of dry powder were spiked with a known concentration of the five components prior to extraction, derivatization and quantification. Table 3 shows the recovery of L-tyrosine, L-tryptophan, L-lysine,

**Table 2.** Precision of the method for determination of L-tyrosine, L-tryptophan, L-lisyne, histamine and tryramine

| Compound | Retention times / min | Repeatability ($n$ = 8) | | Reproducibility ($n$ = 3) | | LOD / (ng ml$^{-1}$) |
|---|---|---|---|---|---|---|
| | | Mean ± SD[a] / (mg g$^{-1}$ dry mass) | RSD / % | Mean ± SD[a] / (mg g$^{-1}$ dry mass) | RSD / % | |
| L-Tyrosine | 26.57 | 3.10 ± 0.05 | 1.65 | 3.25 ± 0.10 | 3.01 | 52 |
| L-Tryptophan | 32.40 | 11.54 ± 0.50 | 4.29 | 12.04 ± 0.67 | 5.60 | 70 |
| L-Lysine | 34.70 | 21.32 ± 0.56 | 2.65 | 22.33 ± 1.16 | 5.21 | 88 |
| Tyramine | 35.20 | 1.54 ± 0.08 | 5.77 | 1.79 ± 0.06 | 3.55 | 58 |
| Histamine | 28.92 | 0.98 ± 0.07 | 6.55 | 1.04 ± 0.05 | 4.87 | 6 |

tyramine and histamine. These results are similar to those reported in previous works of biogenic amines and amino acids in meat and meat products,[1] honey and wines.[22]

### Concentration of histamine, tyramine and free amino acids in shrimp protein hydrolysate and flour of shrimp head

The quantity of L-tyrosine, L-tryptophan, L-lysine, histamine and tyramine in dry powder, liquid protein hydrolysate and the flour of shrimp heads were determined in separate preparations and analyzed from 5 different batches of each of the three samples. In the samples of liquid protein hydrolysate and dry powder, the free amino acid in the highest concentration was L-lysine. Meanwhile, for flour of shrimp heads, L-tyrosine was greater (Table 4). The mean contents of L-lysine were 10.36 ± 1.82 and 11.53 ± 1.09 mg g$^{-1}$ dry matter in liquid protein hydrolysate and dry powder, respectively. For flour of shrimp heads, the content of L-lysine was 9.64 ± 1.10 mg g$^{-1}$dry matter. The sample that presented the highest content of L-tyrosine was the flour of shrimp heads and the least was liquid protein hydrolysate. L-tyrosine is the direct precursor of tyramine, thus, a low level of L-tyrosine can be attributed to high level in tyramine.[24] The highest content of free L-tryptophan was in the flour of shrimp head and the smallest one was in liquid protein hydrolysate with a concentration of 8.95 ± 0.33 mg g$^{-1}$dry matter. The content of free L-tryptophan in hydrolysates principally depends on the fermentation process, because during fermentation, the shrimp by-products are deproteinized by the produced proteolytic enzymes by the microorganism,[25] the flour of shrimp head was also produced with all the shrimp, not only the heads. These results are higher than the reports in other publications.[26] The concentration of these amino acids varies with the specie of shrimp and the type of production process.

The highest content of histamine was in the flour of shrimp head, meanwhile in liquid protein hydrolysate was not detected. In dry powder, the mean concentration of histamine was 663 mg kg$^{-1}$ dry matter. The production of high levels of histamine is dependent on temperature and level of the availability of free histidine.[3] The values of histamine in this research are similar to that reported in other publication,[27] in which a concentration of 579 mg kg$^{-1}$ in fermented fish was found. Other authors analyzed shrimp paste for the concentration of histamine and found 1180 mg kg$^{-1}$.[18] The highest content of tyramine was in the liquid protein hydrolysate, but the flour of shrimp head did not present this biogenic amine. Among biogenic amines in food, histamine is potentially hazardous and is the agent causing histaminic intoxication.[1] The established limit of the histamine level for fish is 50 mg kg$^{-1}$ for the U. S. Food and Drug Administration (US FDA) and 100 mg kg$^{-1}$ for the European Union. However, there are no established levels for histamine and tyramine for by-products from shrimp waste. Also, there is no reported study for the biogenic amine content in protein hydrolysate from fermented shrimp waste.

**Table 3.** Recovery of free amino acid, histamine and tryramine from spiked dry powder

| Compound | Mean value / (mg g$^{-1}$ dry mass) | Amount addition / (mg g$^{-1}$ dry mass) | Amount found / (mg g$^{-1}$ dry mass) | Recovery / %[b] | RSD / % |
|---|---|---|---|---|---|
| L-Tyrosine | 3.02 | 6.16 | 8.18 | 84.51 ± 2.08 | 2.46 |
| L-Tryptophan | 10.60 | 8.45 | 18.25 | 90.75 ± 2.99 | 3.29 |
| L-Lysine | 20.45 | 10.55 | 30.72 | 95.37 ± 4.74 | 4.97 |
| Tyramine | 1.61 | 0.68 | 2.30 | 98.68 ± 5.68 | 5.76 |
| Histamine | 0.98 | 3.05 | 4.03 | 84.29 ± 4.09 | 4.85 |

[a]Percent recovery = (amount found − mean value) / (amount addition) × 100.

**Table 4.** Histamine, tryramine and free amino acid content in shrimp by-products

| Sample | L-tyrosine / (mg $g^{-1}$)[a] | L-tryptophan / (mg $g^{-1}$)[a] | L-lysine / (mg $g^{-1}$)[a] | Tyramine / (mg $kg^{-1}$)[a] | Histamine / (mg $kg^{-1}$)[a] |
|---|---|---|---|---|---|
| Liquid protein hydrolysate | | | | | |
| 1 | 4.88 | 8.62 | 11.39 | 5830 | nd |
| 2 | 5.37 | 8.49 | 10.53 | 4530 | nd |
| 3 | 4.10 | 9.25 | 11.42 | 4770 | nd |
| 4 | 3.91 | 9.27 | 12.09 | 4850 | nd |
| 5 | 4.80 | 9.01 | 9.71 | 4200 | nd |
| Dry powder | | | | | |
| 1 | 4.63 | 11.09 | 10.19 | 770 | 810 |
| 2 | 4.62 | 9.01 | 11.61 | 1690 | 590 |
| 3 | 4.61 | 13.72 | 13.51 | 1870 | 590 |
| 4 | 4.29 | 8.93 | 11.13 | 950 | nd |
| 5 | 4.56 | 9.09 | 11.28 | 630 | nd |
| Flour of shrimp heads | | | | | |
| 1 | 12.71 | 11.44 | 9.43 | nd | 1310 |
| 2 | 12.98 | 9.61 | 9.46 | nd | 1380 |
| 3 | 11.55 | 10.53 | 9.23 | nd | 1420 |
| 4 | 8.65 | 9.96 | 11.75 | nd | 1300 |
| 5 | 11.05 | 11.27 | 9.43 | nd | 1470 |

[a]Results expressed as mg $g^{-1}$ and mg $kg^{-1}$ dry matter; nd = non-detected.

## Conclusions

The conditions of transport and storage, thus as during the fermentation, can occur a protein hydrolysis, generating the amino acids that are more availability for a descarboxylation reaction. This HPLC method makes possible the identification of biogenic amines and amino acids in shrimp by-products and also promotes a sensitive, precise and accurate procedure for their quantification. The method would be very useful for the analysis of other foods and by-products fermented like measure of their sanitary and nutritional quality.

## Experimental

### Chemicals

*O*-phthaldialdehyde (OPA), 2-mercaptoetanol (MCE), sodium phosphate monobasic monohydrate, biogenic amines (histamine and tyramine) and amino acid standards (kit, LAA-21) were purchased from Sigma (St. Louis, MO, USA). HPLC-grade methanol (EDM, Darmstadt, Germany), hydrochloric acid and ethanol were from Fermont (Monterrey, Nuevo León, Mexico). Trichloroacetic acid (TCA) was obtained from Fluka (Seelze, Germany). All aqueous solutions were prepared with ultrapure water purified with a NANOpure Diamond UV system (Barnstead International, Dubuque, Iowa, USA). All reagents were of analytical grade and the purity of the reference standards were > 98%.

### Preparation of standard solutions and OPA/MCE solution

Stock standard solutions of L-tyrosine (476 μg $mL^{-1}$), L-tryptophan (644 μg $mL^{-1}$), L-lysine (804 μg $mL^{-1}$), histamine (100 μg $mL^{-1}$) and tyramine (540 μg $mL^{-1}$) were prepared in 0.1 mol $L^{-1}$ hydrochloric acid. All stock solutions were stored in dark and refrigerated at 4 °C, the stock standard solutions were prepared every two weeks. Working solutions were prepared from those solutions and diluted with 0.1 mol $L^{-1}$ hydrochloric acid. Calibration curves were constructed using six different concentrations of the standard solutions that were based in the level of the compounds in the dried protein hydrolysate.

The specific procedure for the solution preparation involved the dissolution of 250 mg of reagent in 1.5 mL of ethanol and the addition of 200 μl of 2-mercaptoethanol in a 10 mL volumetric flask. Then, this was diluted with 0.4 mol $L^{-1}$ borate buffer solution (pH 10.5). The reagent solution rested for 90 min before being used or stored at 4 °C.[22]

### Sample preparation

For the method validation, a powder protein hydrolysate was employed, and for the assay of the method applicability

powder protein, liquid protein hydrolysate and flour of shrimp heads.

The production of the liquid protein and dry powder was performed following the developed methodology by Bueno-Solano *et al.*[14] Briefly, for the production of liquid protein hydrolysate, shrimp (*Penaeus* spp.) remnant samples (heads and cephalothoraxes) were used. Slightly thawed and minced remnants were fermented at 30 °C for 36 h. The silage was centrifuged (5 °C) at 1250 rpm for 15 min to obtain the chitin-rich fraction (sediment), the liquid protein hydrolysate and the lipid fraction.

For the dry powder production, the liquid hydrolysate rich in protein was dehydrated using a spray dryer SD-04 Lab Scale Spry Drier (LabPlant, Huddersfield, West Yorkshire, England). The liquid hydrolysate was transferred to a conical flask and placed in an electric grill at a constant 80 °C. The temperature of the air inlet was 180 °C and the air outlet was 140 °C. The speed of the peristaltic pump was minimized to produce a slow flow of fluid input (1 L $h^{-1}$), the flow of air in the chamber was 100%. The dry sample was collected in glass bottles with lids. For the production of the flour of shrimp heads, shrimp heads were dried on an electric oven (75 °C) overnight, then were milled and homogenized.

### Extraction of biogenic amines and amino acids

Samples were triturated and homogenized. The flour of shrimp heads (15 mg), powder protein (15 mg) and liquid hydrolysate (50 mg) were each placed in a 10 ml volumetric flask, diluted with 5% of TCA, mixed for 90 s and sonificated for 6 min. Then, 300 µL of the solution were diluted to 5 mL with methanol:water (50:50) in a volumetric flask. Finally, 1 mL of this solution was filtered with a 0.45 µm membrane. The derivatization was performed in the sample vial using an auto-sampler program. A description of the full auto-sampler program is shown in Table 5.

**Table 5.** Auto-sampler program for derivatization

| Step | Description |
|---|---|
| 1 | collect OPA reagent (100 µl) from reagent vial |
| 2 | inject to sample vial |
| 3 | mix in sample vial |
| 4 | wait for reaction time (5 min) |
| 5 | wash needle |
| 6 | collect required quantity of derivatized sample |
| 7 | inject onto column (5 µL) |

### Equipment

The HPLC system (Varian, Melbourne, Victoria, Australia) was equipped with an auto injector 410, a Meta Chem solvent degasser, a system controller with the Galaxie Workstation for chromatography data analysis, a pump 230 and a fluorescence detector 363, all of Varian. The chromatographic analysis was performed using an analytical scale (4.6 mm × 150 mm, 5 µm) Chromsep SS C18 column with a Chromsep guard column SS 10 × 3 mm and a particle size of 5 µm (Varian, Melbourne, Victoria, Australia).

### Chromatographic conditions

The mobile phase was similar to those used by Pereira *et al.*,[22] mobile phase (A) tetrahydrofuran:methanol:phosphate buffer (10 mmol $L^{-1}$) (1:8:91) and mobile phase (B) methanol:phosphate buffer (10 mmol $L^{-1}$) (80:20), filtered through a 0.45 µm membrane and degassed. The HPLC conditions were flow rate of 0.6 ml $min^{-1}$, column temperature of 38 °C and volume of injection of 5 µL for all standard solutions. The gradient program was (min/A%/B%): 0/75/25, 8/75/25, 12/67/33, 25/50/50, 30/0/100, 35/67/33 and 43/75/25. For the detection of amino acids and biogenic amines, the optimal wavelengths were $\lambda_{ex}$ = 335 nm and $\lambda_{em}$ = 440 nm, with a total time of the analyses of 43 min.

### Statistical analysis

The SPSS 11.0 Windows program constructed the statistical analyses, (SPSS Inc., Chicago, IL). The relative standard deviation (RSD) is the ratio standard deviation/average, expressed as percentage.

## Acknowledgements

This research was financed under project No. SON-2004-C03-016 with mixed funds from Government of the State of Sonora and the National Council for Science and Technology (FOMIX-CONACYT). Michael A. Bryan, M. B. A. and Native English Professor offered suggestions and improvements in the wording of this manuscript.

## References

1. Hernández-Jover, T.; Izquierdo-Pulido, M.; Veciana-Nogués, M. T.; Mariné-Font, A.; Vidal-Carou, M. C.*; J. Agric. Food Chem.* **1996**, *44*, 2710.
2. Kirschbaum, J.; Luckas, B.; Beinert, W. D.; *J. Chromatogr., A* **1994**, *661*, 193.
3. Antoine, F. R.; Wei, C. I.; Littell, R. C.; Quinn, B. P.; Hogle, A. D.; Marshall, M. R.; *J. Food Sci.* **2001**, *66*, 72.
4. Landete, J. M.; Ferrer, S.; Polo, L.; Pardo, I.; *J. Agric. Food Chem.* **2005**, *53*, 1119.

5. Kalkan Y, H.; Üren, A.; Yücel, U.; *Food Technol. Biotechnol.* **2007**, *45*, 62.
6. Lozanov, V.; Petrov. S.; Mitev, V.; *J. Chromatogr., A* **2004**, *1025*, 201.
7. Alberto, M. R.; Arena, M. F.; Nadra, M. C. M. In *Public Health Microbiology Methods and Protocols*; Spencer, J. F. T.; Spencer, A. L. R., eds.; Editorial Humana Press Inc.: New Jersey, 2004, p. 481-487.
8. Galgano, F.; Favati, F., Bonadio, M.; Lorusso, V.; Romano, P.; *Food Res. Int.* **2009**, *42*, 1147.
9. Shakila, R. J.; Vasundhara, T. S.; Kumudavally, K. V.; *Food Chem.* **2001**, *72*, 255.
10. Lozanov, V.; Benkova, B.; Mateva, L.; Petrov, S.; Popov, E.; Slavov, C.; Mitev, V.; *J. Chromatogr., B: Anal. Technol. Biomed. Life Sci.* **2007**, *860*, 92.
11. Cortacero-Ramírez, S.; Arráez-Román, D.; Segura-Carretero, A.; Fernández-Gutiérrez, A.; *Food Chem*. **2007**, *100*, 383.
12. Borboa, B. M.; Rohrer, J. S.; *J. Chromatogr, A* **2007**, *1155*, 22.
13. Bauza, T.; Blaise, A.; Daumas, F.; Cabanis, J. C.; *J. Chromatogr, A* **1995**, *707*, 373.
14. Bueno-Solano, C.; López-Cervantes, J.; Campas-Baypoli, O. N.; Lauterio-García, R.; Adan-Bante, N. P.; Sánchez-Machado, D. I.; *Food Chem.* **2009**, *112*, 671.
15. Veciana-Nogués, M. T.; Mariné-Font, A.; Vidal-Carou, M .C.; *J. Agric. Food Chem.* **1997**, *45*, 2036.
16. Gökoglu, N.; Cengiz, E.; Yerlikaya, P.; *Food Chem.* **2004**, *15*, 1.
17. Dondero, M.; Cisternas, F.; Carvajal, L.; Simpson, R.; *Food Chem.* **2004**, *87*, 543.
18. Tsai, Y.; Lin, C.; Chien, L.; Lee, T.; Wei, C.; Hwang, D.; *Food Chem.* **2006**, *98*, 64.
19. Rezaei, M.; Jafari, H.; Sahari, M .A.; Hosseini, H.; Montazeri, N.; Parviz, M.; Nazarinia, A.; *J. Food Biochem.* **2006**, *31*, 541.
20. Katikou, P.; Georgantelis, D.; Paleologos, E. K.; Ambrosiadis, I.; Kontominas, M. G.; *Food Chem.* **2006**, *54*, 4277.
21. Marks, H. I.; Anderson, C. R.; *J. Chromatogr., A* **2005**, *1094*, 60.
22. Pereira, V.; Pontes, M.; Câmara, J. S.; Marques, J. C.; *J. Chromatogr., A* **2008**, *1189*, 435.
23. American Chemical Society (ACS), Subcommitee of Environmental Analytical Chemistry; *Anal. Chem.* **1980**, *52*, 2242.
24. Izquierdo Cañas, P. M.; García, R. E.; Gómez, A. S.; Fernández, G. M.; Palop, H. M. L. L.; *J Food Compos. Anal*. **2008**, *21*, 731.
25. Rao, M. S.; Muñoz, J.; Stevens, W. F.; *Appl Microbiol. Biotechnol*. **2000**, *54*, 808.
26. Sánchez-Machado, D. I.; Chavira-Willys; B.; López-Cervantes, J.; *J. Chromatogr., B: Anal. Technol. Biomed. Life Sci.* **2008**, *863*, 88.
27. Mah, J.; Han, H.; Oh, Y.; Kim, M.; Hwang, H.; *Food Chem.* **2002**, *79*, 239.

*Submitted: October 22, 2010*
*Published online: October 25, 2011*

*J. Braz. Chem. Soc.*, Vol. 23, No. 1, 103-109, 2012.
Printed in Brazil - ©2012 Sociedade Brasileira de Química
0103 - 5053 $6.00+0.00

Article

# Simultaneous Extraction and Detection of Ochratoxin A and Citrinin in Rice

***Helen C. S. Hackbart,* Luciana Prietto, Ednei G. Primel, Jaqueline Garda-Buffon and Eliana Badiale-Furlong***

*Escola de Química e Alimentos, Fundação Universidade Federal do Rio Grande, CP 474, 96201-900 Rio Grande-RS, Brazil*

Este estudo comparou quatro procedimentos de extração para a determinação simultânea das micotoxinas citrinina e ocratoxina A em amostras de arroz. Os procedimentos de Soares e Rodriguez-Amaya, Tanaka e os métodos de extração QuEChERS (Quick, Easy, Cheap, Effective, Rugged and Safe) e por ultrassom foram comparados em termos de geração de resíduos, limite de detecção, limite de quantificação e recuperação simultânea de micotoxinas. O procedimento de Soares e Rodriguez-Amaya e a extração por ultrassom apresentaram as menores recuperações, 83 e 55% para a ocratoxina A (OTA) e 55 e 48% para citrinina (CIT), respectivamente. O procedimento de Tanaka e a extração QuEChERS tiveram recuperações de 98 e 105% para OTA e 64 e 78% para CIT, respectivamente. Este último permitiu a extração simultânea das duas micotoxinas com uma redução de até 25 vezes na quantidade de solventes.

This study compared four extraction procedures for the simultaneous determination of mycotoxins ochratoxin A and citrinin in samples of rice. Soares and Rodriguez-Amaya and Tanaka procedures and the extraction methods QuEChERS (Quick, Easy, Cheap, Effective, Rugged and Safe) and by ultrasound were compared in terms of residue generation, limit of detection, limit of quantification and simultaneous recovery of mycotoxins. Soares and Rodriguez-Amaya and the method by ultrasound presented the lowest recoveries, 83 and 55% for ochratoxin A (OTA) and 48 and 55% for citrinin (CIT), respectively. Tanaka procedure and QuEChERS method presented the highest recoveries, 98 and 105% for OTA and 64 and 78% for CIT, respectively. The latter enabled the simultaneous extraction of the two mycotoxins, with a reduction of up to 25 times of the amount of the involved solvent.

**Keywords:** rice, occurrence, ochratoxin A, citrinin, extraction method

## Introduction

Fungi produce a large variety of toxic secondary metabolites called mycotoxins.[1] These compounds comprise several chemical structures including some relatively simple ones,[1] which occur in mycelium of filamentous fungi, normally after a period of balanced growth followed by stress conditions.[2,3] *Aspergillus*, *Penicillium* and *Fusarium* are among the fungal genera that occur in food and that have toxigenic species, such as *Aspergillus ochraceus* and *Penicillium citrinum*, the main producers of ochratoxin A and citrinin, respectively.[4,5]

Ochratoxin A (OTA) (N-{[(3*R*)-5-chloro-8-hydroxy-3-methyl-1-oxo-3,4-dihydro-1*H*-isochromen-7-yl]carbonyl}-L-phenylalanine, Figure 1) is classified by the International Agency for Research on Cancer (IARC from World Health Organization (WHO)) as a probably carcinogenic agent for humans (Group 2B, IARC).[6] It has been also correlated to the Balkan endemic nephropathy (BEN).[7] Its presence was detected in many stored and dry foods,[8,9] such as corn, wheat, oats, beans, nuts, peanuts, rice, barley, sorghum, cotton seed, coffee beans, cocoa and spices.[10-13]

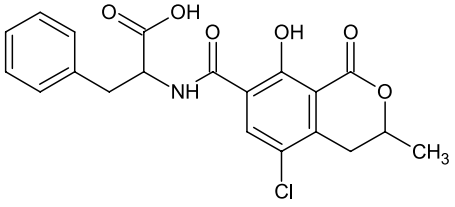


**Figure 1.** Chemical structure of ochratoxin A.

Citrinin (CIT) [(3*R*,4*S*)-8-hydroxy-3,4,5-trimethyl-6-oxo-4,6-dihydro-3*H*-isochromene-7-carboxylic acid,

*e-mail: hhackbart@hotmail.com

Figure 2] has been known since 1931, when it was isolated from *Penicillium citrinum* and, afterwards, from the Australian plant *Crotolaria crispata*.[14,15] This mycotoxin is associated with cases of porcine nephropathy and has been found as a contaminant in corn, rice, wheat and other grains,[16,17] cheese[18] and fruits during senescence.[19] The adverse effects caused by CIT on the human body are chronic rather than acute. It has been demonstrated that its intake may cause hepatic and renal failure in the long run.[4]

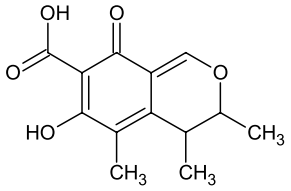


**Figure 2.** Chemical structure of citrinin.

The development of methodologies that allows the simultaneous extraction of these mycotoxins[20] in different matrices has been encouraged since the toxicity was determined.[21] Extractions in the liquid phase were largely studied for the determination of ochratoxin A,[22] and most of the validated methods were based on the extraction of ochratoxin A and citrinin through the solubility of these compounds in organic solvents[23] or alkaline solutions.[24] These methods were satisfactory for the extraction from liquid matrices, but not from solid samples.[25] The organic solvent mixtures that were used for solid matrices have shown low recoveries and high amount of solvent residues.[26]

The most difficult task for the determination of mycotoxins in solid matrices happens in the extraction phase because they can produce emulsions and foams with the matrices during this process.[27,28] One of the phases of the extraction process must remove the lipids and proteins before the chromatographic analysis. The extraction with acetonitrile has been traditionally used[27] because it enables the precipitation of proteins and the addition of hexane removes the soluble interference.[28]

The development of new extraction techniques that could decrease the time of extraction, the consumption of solvents, the exposure of the analyst, the generation of residue and the costs would be ideal for the extraction of these contaminants from food and would make it easier to guarantee food safety. Methods such as Soares and Rodriguez-Amaya[27] and Tanaka[28] are commonly used for the determination of mycotoxins in different matrices with adequate analytical efficiency. However, their disadvantage is the large amount of needed solvents for the extraction. This fact makes difficult to establish an analytical routines which can be accessible to most laboratories that are involved in the extraction of mycotoxins since both the discharge of residues and the cost of solvents are challenges to be faced.

The QuEChERS (Quick, Easy, Cheap, Effective, Rugged and Safe)[29] method is a procedure that has been adopted for the extraction of pesticides[30-32] due to its quickness and accessible cost. Another interesting feature is that it is efficient for the extraction of analytes with different polarities in trace level in complex samples with some reliability.[33-35] The extraction of mycotoxin that uses solvents under the operation of ultrasound is also being considered interesting, once it provides the extraction of compounds with distinct polarities, imputed the optimization of the solute-solvent contact.[36]

This study aims at comparing the phase of extraction and purification of four methods regarding its ability to simultaneously extract ochratoxin A and citrinin in rice, by using high performance liquid chromatography with a photodiode array detector (HPLC-PDA). Soares and Rodriguez-Amaya[27] and Tanaka[28] procedures and the extractions which use modified QuEChERS (applied with some modifications, Anastassiades *et al.*)[29] and ultrasound (Liazid *et al.*[36]) were compared in terms of residue generation, limit of detection (LOD), limit of quantification (LOQ) and simultaneous recovery of mycotoxins.

## Experimental

### Samples

Rice bran was used to evaluate the extraction and purification phases of the different methods. The applicability was evaluated by a study of the simultaneous occurrence of the mycotoxins in rice (*Oryza sativa, L.*) samples. The samples were from experimental fields at Instituto Riograndense do Arroz (IRGA) in Cachoeirinha City (Rio Grande do Sul State, Brazil). After the harvest, the grains were milled and 36 samples were sorted out: (n = 6) rough rice, (n = 6) parboiled rough rice, (n = 6) polished rice, (n = 6) white polished rice, (n = 6) bran and (n = 6) parboiled bran. Samples (n = 2) of rough rice and bran which had been stored in silos for 18 months were also collected. The 38 samples were grounded in a knife grinder and sieved separating the 0.5 mm fractions.

### Reagents and solvents

Ochratoxin A and citrinin were purchased from Sigma-Aldrich (São Paulo, Brazil) purity > 98%. The reagents methanol and acetonitrile of chromatographic grade were purchased from Mallinckrodt (Phillipsburg, NJ, USA).

Phosphoric acid (85%) of analytical grade, glacial acetic acid, hexane and benzene were purchased from Merck (Darmstadt, Germany). Chloroform and potassium chloride, sodium chloride, ammonium sulfate and magnesium sulfate were purchased from Synth (São Paulo, Brazil). Sodium acetate was purchased from Vetec (Rio de Janeiro, Brazil) and diatomaceous earth from Nuclear (Celite 545, São Paulo, Brazil). Ultrapure water was produced by Direct-Q UV3® system (Millipore, Bedford, MA, USA).

### Preparation of standard solution of ochratoxin A and citrinin

Analytical and storage standard solutions were individually prepared from commercial containers containing 5 mg of mycotoxins and each mycotoxin was dissolved in 100 mL of benzene:acetonitrile (98:2, v/v). The storage solutions were diluted in order to produce standard solutions, whose concentrations were determined by the mass in the container and the final volume of the solution. The concentrations were spectrophotometrically confirmed in a Cary 100 equipment from Varian (USA). The concentration of the values of molar absorptivity (ε) 5440 and 5490 mol $cm^{-1}$ and the wavelength of maximum absorbance 333 and 321 nm for OTA and CIT, respectively, were considered for the estimative.[6] The solutions were stored in an amber container and chilled at 4 ºC, until use.

### Extraction and purification

The phases of the extraction and purification, which were described in validated methods by four authors, were compared.

The method of extraction and purification described by Soares and Rodriguez-Amaya[27] (procedure 1) used 50.00 g of sample, homogenized in a blender for 5 min with 300 mL of methanol:potassium chloride at 4%, (9:1 v/v). After filtration, 150 mL was collected and mixed with 150 mL of ammonium sulfate at 30% (clarifying) with 50 mL of diatomaceous earth. The mixture rested for 5 min and was filtrated. Then, 150 mL of distilled water was added to 150 mL of filtrated solution in a separatory funnel. Three partitions with 10 mL of chloroform were performed. The collected organic extracts were separated in three portions, the solvent was evaporated and the containers were stored at −20 ºC in order to perform the screening, the confirmation and the quantification of the mycotoxins.

The modified method of extraction and cleaning of the extract described by Tanaka *et al.*[28] (procedure 2) consisted of weighing 10.00 g of sample with 100 mL of acetonitrile:water (3:1 v/v). The extraction was carried out in an orbital shaking table at 200 rpm at 25 ºC for 30 min. The liquid fraction was separated by filtration, the extract was defatted by liquid partition with 20 mL of hexane under slow shaking for 3 min and the acetonitrile:water phase was collected, this operation was performed twice. 4 g of sodium chloride were added to the defatted extract for the water removal. The acetonitrile was collected in a flat-bottomed flask evaporated at 70 ºC in a rotary evaporator. The dry flask was washed with 30 mL of chloroform:methanol (9:1 v/v), homogenized in ultrasonic bath for 1 min, and then, the extract was transferred to a centrifuge tube. After the centrifugation, the organic phase (chloroform) was collected and dried under a nitrogen stream and the flasks were stored in a freezer.

The QuEChERS method (procedure 3) was developed by Anastassiades *et al.*[29] and applied with some modifications. A sample of 10.00 g was weighed in a centrifuge flask and 20 mL of water were added. 20 mL of acidified acetonitrile with 0.2 mL of glacial acetic acid were added, followed by orbital shaking table at 200 rpm at 25 ºC for 10 min. Changes from the original methodology were due to the addition of salts and clean up. 1.5 g of magnesium sulfate was added, besides 0.85 g of sodium acetate, followed by orbital shaking table at 200 rpm at 25 ºC for 10 min. The material was centrifuged at a rotation speed of 3220 × *g* for 8 min and 0.3 g of magnesium sulfate and 0.2 g of diatomaceous earth were added to the liquid phase, followed by manual shaking for 1 min and separation by centrifugation at 3220 × *g* for 8 min. The liquid phase was dried in a concentrator under a nitrogen stream.

The method was described by Liazid *et al.*[36] (procedure 4) and applied with some modifications. It consisted in weighing of 5.00 g of sample in a centrifuge flask, for which 40 mL of acetonitrile:water (3:1 v/v) was added. The mixture was submitted to ultrasound for 30 min at 60 kHz. The extract was filtered after the addition of 2 g of sodium chloride to the defatted extract for water removal. The acetonitrile phase was collected in a separatory funnel and defatted with 10 mL of hexane extract by slow shaking. The operation was carried twice. The defatted extract was dried in a water bath at 50 °C under a nitrogen stream.

The dry residues that were obtained after the extractions were resuspended in benzene P.A. and shaken in ultrasound bath for 30 s before the chromatographic analysis.

### Operational conditions in high performance liquid chromatography

The features of the liquid chromatograph were (Waters, Miliford, MA, USA) equipped with a photodiode array detector, PDA 2996, with quaternary pump model

600, injector Rheodyne 7725i, loop injection of 20 µL, analytic column Synergi Fusion-RP 80 Å, Phenomenex® (250 × 4.60 mm, 4 µm) with data collecting system Empower PDA Software, isocratic elution system, with acetonitrile and purified water, acidified with phosphoric acid until pH 3.0 (50:50 v/v), flow of 1 mL $min^{-1}$ with 20 min of run time.

Linearity covered the range from 1.5 to 7.5 µg $mL^{-1}$ of each mycotoxin, in a total of six points and the record of the answering signal was outlined with the help of the data collecting system, which provided the coefficient of determination ($r^2$) and the equation of concentration *versus* signal, providing the limits of detection and quantification.[37] Each concentration was injected three times and the values of the area averages were used to calculate the coefficients of variation for the accuracy analysis. The recovery was determined by the fortification of the sample in three different levels 3, 4 and 6 µg $kg^{-1}$ for citrinin and 8, 10 and 15 µg $kg^{-1}$ for ochratoxin A.

## Results and Discussion

The retention times in the best operation conditions were 10.8 and 13.4 min for CIT and OTA, respectively, and the total run time was 20 min. Figure 3 shows the chromatogram of the two mycotoxins under study in a 254 nm wavelength, ideal to simultaneously detect the mycotoxins.

The readings of the maximum for the absorption spectrum were at 216 nm for ochratoxin A and 330 nm for citrinin. The spectral profiles were used to confirm the identity of both mycotoxins and to quantify them by the peak areas.

The LOD and LOQ values were 0.7 and 2.4 µg $kg^{-1}$ for citrinin and 1 and 3 µg $kg^{-1}$ for ochratoxin A, respectively, and the analytical curves were linear in the range from 1.5 to 7.5 µg $mL^{-1}$, being described by the equations $y = 8 \times 10^3 x + 3.54 \times 10^{-3}$ for citrinin and $y = 4.9 \times 10^3 x + 1.78 \times 10^{-3}$ for ochratoxin A. Tokusoglu and Bozoglu[38] used the HPLC-FL (high performance liquid chromatography with fluorescence detection) to determine citrinin and ochratoxin A in olive samples, the obtained LOD value was 0.05 µg $kg^{-1}$ for both CIT and OTA.

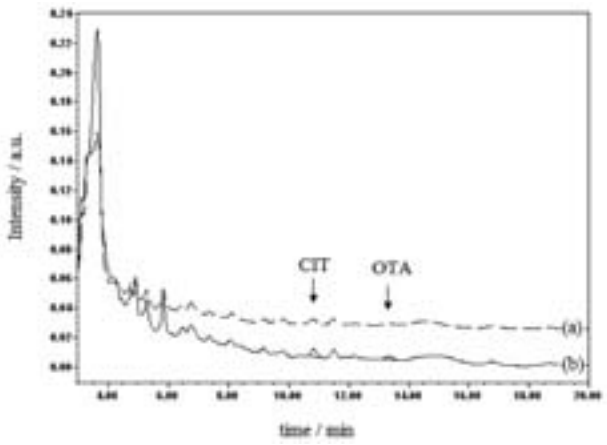


**Figure 3.** HPLC-PDA chromatograms in a 254 nm wavelength obtained from rice with the QuEChERS extraction procedure: (a) a rice non-fortified sample extract and (b) fortified with 3 µg $kg^{-1}$ of CIT and OTA. Arrows indicates the retention times of the mycotoxins.

Ibáñez-Vea *et al.*[39] used the UHPLC-FL for determining aflatoxins ($B_1$, $B_2$, $G_1$ and $G_2$), ochratoxin A and zearalenone in breakfast cereal samples. The LOD and LOQ values were 0.062 and 0.2 µg $kg^{-1}$ for ochratoxin, respectively.[39]

The determination coefficients ($r^2$) were 0.998 for both mycotoxins. The analytical curve for the relation between the concentration and the absorption of mycotoxin proved that the models are appropriate. This statement was achieved since a determination coefficient ($r^2$) higher than 0.999 was considered an ideal adjustment of the data for the regression line.[37] After determining the best chromatographic conditions for the separation and the quantification of the mycotoxins under study, different aspects that were taken into consideration to compare the methods were evaluated, according to Table 1. The most important data for the selection of the procedure were the sample mass, the number of phases and the amount of used solvents. Regarding these aspects, the QuEChERS method stood out.

According to Table 1, Soares[27] and Tanaka[28] extraction phases (in comparison with the ultrasound[36] and QuEChERS)[29] show that a minimum number of phases and low consumption of solvents and materials turn QuEChERS into an attractive method. This is even if there is no difference in relation to the quantity of sample. Besides, because of

**Table 1.** Operational characteristics of the four extraction procedures under study

| Procedure | Soares | Tanaka | QuEChERS | Ultrasound |
|---|---|---|---|---|
| Sample mass / g | 50 | 10 | 10 | 5 |
| Extraction phase | 300 mL MeOH:KCl | 100 mL $C_2H_3N$:$H_2O$ | 40 mL $C_2H_3N$:$H_2O$ | 40 mL $C_2H_3N$:$H_2O$ |
| Clean up - phase 1 | 150 mL $H_2O$ distilled | 40 mL $C_6H_{14}$ | 3 g $MgSO_4$; 1.7 g $CH_3COONa$; 1 g $Na_3C_6H_5O_7$ | 20 mL $C_6H_{14}$ |
| Clean up - phase 2 | 30 mL ($CHCl_3$) | 27 mL (MeOH:$CHCl_3$) | 3 mL ($C_2H_3N$) | 30 mL ($C_2H_3N$) |
| Residue / mL | 600 | 160 | 15 | 40 |

the reduced volume in comparison with the other extraction systems, QuEChERS eliminates phases. The difference is in the extract cleaning which is carried out with salts and diatomaceous earth, thus, considerably decreasing the amount of solvents and the analyst exposure to them. Figure 3 shows the HPLC-PDA chromatogram obtained following the QuEChERS extraction procedure.

The recommended criteria for the evaluation by FAO (Food and Agriculture Organization) in Worldwide Regulation for Mycotoxins[8] includes the percentage of recoveries for trace analysis (μg $kg^{-1}$), such as the case of mycotoxin determination. The results of the interval of recoveries for each extraction procedure under study are presented in Table 2.

The modified QuEChERS method was used to evaluate the occurrence of ochratoxin A and citrinin in rice (*Oryza sativa, L.)* samples. Considering all 38 samples, ochratoxin A was found in the sample of rough rice which was stored in silos with 560 μg $kg^{-1}$ of contamination. This amount is higher than the recommended one by the Commission of the European Communities (the European Union regulatory agency),[40] which establishes a maximum limit of 5 μg $kg^{-1}$ and, by the Agência Nacional de Vigilância Sanitária (ANVISA, Brazilian regulatory agency)[41] that recommends a maximum limit of 10 μg $kg^{-1}$ for grains.

The citrinin occurred in one of the samples of parboiled rough rice with 120 μg $kg^{-1}$ of contamination. Table 3 shows the quantified amounts by high performance liquid chromatography with a photodiode array detector (HPLC-FDA). The concentration that was determined for citrinin can also be considered high in comparison with the maximum limits established by the same legislation for mycotoxins that have similar effect to ochratoxin A.

The QuEChERS method was applied to the extraction of several analytes, such as mycotoxins. Sospedra *et al.*[42] improved this methodology by using a mixture of

**Table 2.** Recoveries of ochratoxin and citrinin of the four extraction procedures studied by HPLC-PDA

| Procedure | Mycotoxins | Fortification level / (μg $kg^{-1}$) | Recovery[a] / % | CV[a] / % |
|---|---|---|---|---|
| Soares and Rodriguez-Amaya | ochratoxin A | 8 | 71.6 | 2.8 |
| | | 15 | 82.7 | 3.2 |
| | citrinin | 3 | 55.5 | 1.8 |
| | | 6 | 52.9 | 2.4 |
| Tanaka | ochratoxin A | 8 | 89.0 | 2.2 |
| | | 15 | 98.3 | 1.6 |
| | citrinin | 3 | 64.0 | 3.4 |
| | | 6 | 62.7 | 2.8 |
| QuEChERS | ochratoxin A | 8 | 76.8 | 2.4 |
| | | 15 | 105.3 | 4.8 |
| | citrinin | 3 | 77.8 | 3.1 |
| | | 6 | 75.9 | 1.8 |
| Ultrasound | ochratoxin A | 8 | 54.7 | 2.5 |
| | | 15 | 53.4 | 1.8 |
| | citrinin | 3 | 48.3 | 3.3 |
| | | 6 | 45.7 | 0.9 |

CV: coefficient of variation; [a]n = 3.

**Table 3.** Incidence and concentration of ochratoxin A and citrinin in rice samples analyzed by QuEChERS modified method

| Samples | No. of analyzed samples | No. of positive samples | Mycotoxins / (μg $kg^{-1}$) | |
|---|---|---|---|---|
| | | | OTA LOD (1.0) | CIT LOD (0.7) |
| Rough rice | 6 | nd | nd | nd |
| Parboiled rough rice | 6 | 1 | nd | 120 |
| Polished rice | 6 | nd | nd | nd |
| White polished rice | 6 | nd | nd | nd |
| Bran | 6 | nd | nd | nd |
| Parboiled bran | 6 | nd | nd | nd |
| Rough rice stored in silos | 1 | 1 | 560 | nd |
| Bran stored in silos | 1 | nd | nd | nd |

LOD: limit of detection; nd: non-detected.

methanol:acetonitrile (85:15 v/v) for the extraction of trichothecenes in wheat flour samples from Spain. High performance liquid chromatography with a mass detector (HPLC-MS) was used for determining these compounds, the recovery amounts ranged from 86 to 108%, the values of the coefficients of variation were lower than 7% and the LOQ values varied from 4 to 100 μg $kg^{-1}$. Zanella *et al.*[32] performed a review of the QuEChERS method for the extraction of pesticide multiresidue in distinct food matrices. 52 pesticides were analyzed by gas chromatography with a mass detector (GC-MS) and 169 pesticides and 26 mycotoxins were analyzed by liquid chromatography with a mass detector (LC-MS). For simultaneous extraction, their recovery percentages ranged from 70 to 120% in the case of 100% of the pesticides and 80% of the mycotoxins. The LOQ values for the mycotoxins ranged from 1 to 100 μg $kg^{-1}$.[32]

The QuEChERS method has shown efficient results when applied with mass spectrometry, but can also be applied with other detectors with satisfactory results. Hajslova *et al.*[43] used ultra-high performance liquid chromatography with a mass spectrometry utilizing an orbitrap (UHPLC/Orbitrap-MS) and time of flight (UPLC-TOF-MS) for the detection of mycotoxins of the group *Fusarium*, which were extracted from grain samples and products derived from grains. In order to extract them, the authors modified and adapted the QuEChERS method. The LOQ values ranged from 10 to 100 μg $kg^{-1}$, the recoveries from 94 to 108% and the coefficients of variation were lower than 7% for UPLC-TOF-MS. The UHPLC/Orbitrap-MS technique was used for raw extract analysis.[43]

The coexistence of multimycotoxins in grains is also mentioned by other authors. Pfohl-Leszkowiez *et al.*[44] reported the occurrence of aflatoxin $B_1$, ochratoxin A and citrinin in rice sold in five provinces in the center Vietnam. The co-occurrence of ochratoxin A, citrinin and fumonisin $B_1$ was also reported by authors in grain samples sold in France.[12] Villa and Markaki[45] also used HPLC-FL in order to analyze the presence of aflatoxin $B_1$ and ochratoxin A in 55 grain samples and, 19 out of 55 were contaminated with both mycotoxins.

In Brazil, many publications have reported the increase in the occurrence of mycotoxins in food and rations,[46] resulting in a new legislation for mycotoxins in food and feed. The contamination with zearalenone (ZEN), ochratoxin A (OTA), citrinin (CIT) and trichothecenes is still low when compared to contaminations that are caused by aflatoxins (AFA $B_1$, $B_2$, $G_1$ and $G_2$).[46] Sylos *et al.*[11] used Soares and Rodriguez-Amaya method and, added a partition with cyclohexane to find evidence of the presence of ochratoxin A and aflatoxins in 68 rice samples (in São Paulo State, Brazil), but ochratoxin A was not found in any sample. Simas *et al.*[47] analyzed the occurrence of aflatoxins and ochratoxins in grains used for feeding dairy cattle (in Bahia State, Brazil). 80 samples were analyzed, but ochratoxins were not detected. However, the aflatoxins were detected in 33.75% of the samples with contamination levels ranging from 1 to 3 μg $kg^{-1}$.[47]

Nunes *et al.*[48] detected OTA in rice samples (in Rio Grande do Sul State, Brazil), as well as the presence of *Penicillium* in non-positive samples due to the conditions of the analytical method. Dors *et al.*[49] evaluated the occurrence of aflatoxin $B_1$, $B_2$, deoxynivalenol, ochratoxin A and zearalenone in rice samples and only aflatoxin $B_1$ was found.

These data show the importance of developing an accessible and reliable methodology for mycotoxins evaluation in grain and foods. It should lead to smaller residue volumes for the constant monitoring of important grains in the world agribusiness. Therefore, it is possible to prevent damage to public health without causing much impact on the environment. It is important to mention that this procedure is also more economical. Thus, the determination of mycotoxins becomes more accessible for the control of grain contamination. Besides, food safety may be improved.

## Conclusion

The results of this study show that the method of extraction and purification QuEChERS (modified) enables the simultaneous extraction of ochratoxin A and citrinin with reliable performance and a significant reduction in the volume of solvents (about 25 times). The importance of simple and accessible methodology was confirmed by the verification of contaminated samples by ochratoxin A and citrinin, even in a reduced number of samples, demonstrating the importance of assessing the presence of these mycotoxins.

## Acknowledgments

The authors thank Conselho Nacional de Desenvolvimento Científico e Tecnológico (CNPq) for the sponsorships given to the Master's program and Instituto Riograndense do Arroz (IRGA) for providing the samples and for funding this study.

## References

1. Richard, J. J.; *Int. J. Food Microbiol.* **2007**, *119*, 3.
2. Taniwaki, M.; Martins C.; Iamanaka B.; Leite R.; Vicente E.; Okazaki M.; *REVNET-DTA* **2004**, *4*, 1.

3. Rupollo, G.; Gutkoski, L. C.; Martins, I. R.; Elias, M. C.; *Ciênc. Agrotec.* **2006**, *30*, 118.
4. Knasmuller, S.; Cavin, C.; Chakraborty, A.; Darroudi, F.; Majer, B. J.; Huber, W. W.; Ehrlich, B. A. *Nutr. Cancer* **2004**, *50*, 190.
5. Elmholt, S.; Rasmussenp, H.; *Mycopathologia* **2005**, *150*, 421.
6. World Health Organization (WHO); *Some Naturally Occurring Substances: Food items and Constituents, Heterocyclic Aromatic Amines and Mycotoxins*, vol. 56; International Agency for Research on Cancer (IARC): Lyon, France, 1993, p. 489.
7. Castegnaro, M.; Canadas, D.; Vrabcheva, T.; Petkova-Bocharova, T.; Chernozemsky, I. N.; Pfohl-Leszkowicz, A.; *Mol. Nutr. Food Res.* **2005**, *50*, 519.
8. Food and Agriculture Organization (FAO); *Worldwide Regulations for Mycotoxins 1995. A Compendium*, FAO Food and Nutrition Paper, No. 64, Rome.
9. Dilkin, P.; *Biológico* **2002**, *64*, 187.
10. Furlong, E. B.; Soares, L. A. S.; Vieria, A. P.; Dadalt, G.; *Rev. Inst. Adolfo Lutz* **1999**, *58*, 105.
11. Sylos, C. M.; Simionato, E. M. R. S.; Astray, R. M.; *Rev. Inst. Adolfo Lutz* **2003**, *62*, 123.
12. Molinié, A.; Faucet, M.; Castegnaro, M.; Pfohl-Leszkowicz, A.; *Food Chem.* **2005**, *92*, 391.
13. Costa, T. P.; Germano, P. M. L.; Germano, M. I. S.; *Higiene Alimentar* **2005**, *19*, 39.
14. Berndt, W. O. In *Ochratoxin-Citrinin as Nephrotoxins*; Llewellyn, G. C.; O'Rear; P. C., eds.; Plenum Press: New York, 1990, p. 55-56.
15. Chagas, G. M.; Oliveira, M. B. M; Campello, A. P.; Kluppel, M. L. W.; *J. Appl. Toxicol*. **1995**, *15*, 91.
16. Heber, D.; Lembertas, A.; Lu, Q. Y.; Bowerman, S.; Go, V. L. W.; *J. Altern. Complement. Med.* **2001**, *7*, 133.
17. Meister, U.; *Eur. Food Res. Technol.* **2004**, *218*, 394.
18. Bailly, J. D.; Querin, A.; Le Bars-bailly, S.; Benard, G.; Guerre, P.; *J. Food Prot.* **2002**, *65*, 1317.
19. Aziz, N. H.; Moussa, L. A. A.; *Food Control* **2002**, *13*, 281.
20. Madhyastha, M. S.; Marquardt, R. R.; Mais, A.; Borsa, J.; Frohlich, A. A.; *J. Food Prot.* **1994**, *57*, 48.
21. Treucksess, M. W. In *Official Methods of Analysis of AOAC International*; Horwitz, W., ed.; AOAC International: Gaithersburg, Md., 2003, p. 56B.
22. Monaci, L.; Palmisano, F.; *Anal. Bioanal. Chem.* **2004**, *378*, 1777.
23. González-Peñas, E.; Leache, C.; Bizcarte, M.; Obanos A. P.; *J. Chromatogr., A* **2004**, *1025*, 163.
24. Senyuva, H. Z.; Gilbert, J.; Ozcan, S.; Ulken, U.; *J. Food Prot.* **2005**, *68*, 1512.
25. Goldberg, D. M.; Soleas, G. S.; Yan, J.; *J. Agric. Food Chem.* **2001**, *49*, 2733.
26. Pfohl-Leszkowicz, A.; Molinié, A.; Castegnaro, M.; *Revista Mexicana de Micologia* **2004**, *19*, 7.
27. Soares, L. M. V.; Rodriguez-Amaya, D. B.; *J. Assoc. Off. Anal. Chem.* **1989**, *72*, 22.
28. Tanaka, T.; Yoneda, A.; Inoue, S.; Sugiura, Y.; Ueno, Y.; *J. Chromatog., A*. **2000**, *882*, 23.
29. Anastassiades, M.; Lehotay, S. J.; Stajnbaher, D.; Schenck, F. J.; *J. AOAC Int.* **2003**, *86*, 412.
30. Sulyok, M.; Berthiller, F.; Krska, R.; Schuhmacher, R.; *Mass Spectrom.* **2006**, *20*, 2649.
31. van Der Lee, M. K.; van Der Weg, G.; Traag, W. A.; Mol, H. G. J.; *J. Chromatogr., A*. **2008**, *1186*, 325.
32. Zanella, R.; Adaime, M. A.; Friggi, C. A.; Prestes, D. O.; *Quim. Nova* **2009**, *32*, 1620.
33. Schenck, F. J.; Hobbs J. E.; *Bull. Environ. Contam. Toxicol.* **2004**, *73*, 24.
34. Mol, H. G. J.; Plaza-Bolaños, P.; Zomer, P.; Rijk, T.; Stolker, A. A. M.; Mulder, P. P. J.; *Anal. Chem.* **2008**, *80*, 9450.
35. Spanjer, M.; Rensen, P.; Scholten, J. M.; *Food Addit. Contam., Part A* **2008**, *25*, 472.
36. Liazid, A.; Palma, M.; Brigui, J.; Barroso, C. G.; *Talanta* **2007**, *71*, 976.
37. Ribani, M.; Bottoli, C. B. G.; Collins, C. H.; Jardim, I. C. S. F.; Melo, L. F. C.; *Quim. Nova* **2004**, *27*, 771.
38. Tokusoglu, Ö.; Bozoglu, F.; *Ital. J. Food Sci.* **2010**, *22*, 284.
39. Ibáñez-Vea, M.; Martínez, R.; González-Peñas, E.; Lizarraga, E.; Cerain, A. L.; *Food Control* **2011**, *22*, 1949.
40. The Commission of the European Communities; *Commission Regulation (EC) No. 472/2002* amending Regulation (EC) No. 466/2001, Official Journal of the European Communities, 2002, L75/18-20.
41. Agência Nacional de Vigilância Sanitária (ANVISA); *Dispõe sobre Limites Máximos Tolerados (LMT) para Micotoxinas em Alimentos*, Resolução RDC No. 7, Brasil, 2011.
42. Sospedra, I.; Blesa, J.; Soriano, J. M.; Mañes, J.; *J. Chromatogr., A* **2010**, *1217*, 1437.
43. Hajslova, J.; Zachariasova, M.; Lacina, O.; Malachova, A.; Kostelanska, M.; Poustka, J.; *Anal. Chim. Acta* **2010**, *662*, 51.
44. Pfohl-Leszkowicz, A.; Nguyen, M. T.; Tozlovanu, M.; Tran, T. L.; *Food Chem.* **2007**, *105*, 42.
45. Villa, P.; Markaki, P.; *Food Control* **2009**, *20*, 455.
46. Sabino, M.; Rodriguez-Amaya, D. B.; *Braz. J. Microb.* **2002**, *33*, 1.
47. Simas, M. S.; Botura, M. B.; Correa, B.; Sabino, M.; Mallmann, A. C.; Bitencourt, C. B. S. C.; Batatinha, J. M.; *Food Control* **2007**, *18*, 404.
48. Nunes, I. L.; Magagni, G.; Bertolin, T. E.; Badiale-Furlong, E.; *Ciênc. Tecnol. Aliment.* **2003**, *23*, 190.
49. Dors, G. C.; Pinto, L. A. A.; Badiale-Furlong, E.; *LWT Food Sci. Technol.* **2009**, *42*, 433.


*Submitted: February 3, 2011*
*Published online: October 25, 2011*

*J. Braz. Chem. Soc.*, Vol. 23, No. 1, 110-119, 2012.
Printed in Brazil - ©2012 Sociedade Brasileira de Química
0103 - 5053 $6.00+0.00

Article

# Direct Electrochemical Analysis of Dexamethasone Endocrine Disruptor in Raw Natural Waters

***Thiago M. B. F. Oliveira,[a] Francisco W. P. Ribeiro,[a] Jefferson M. do Nascimento,[a] Janete E. S. Soares,[b] Valder N. Freire,[c] Helena Becker,[a] Pedro de Lima-Neto[a] and Adriana N. Correia*[,a]***

*[a]Departamento de Química Analítica e Físico-Química and [c]Departamento de Física, Centro de Ciências, Universidade Federal do Ceará, Campus do Pici, 60455-760 Fortaleza-CE, Brazil*

*[b]Departamento de Farmácia, Faculdade de Farmácia, Odontologia e Enfermagem, Universidade Federal do Ceará, Rua Capitão Francisco Pedro, 1210, Rodolfo Teófilo, 60430-370 Fortaleza-CE, Brazil*

Este trabalho descreve uma metodologia eletroanalítica, utilizando voltametria adsortiva de onda quadrada, que foi aplicada com êxito na determinação direta de resíduos de dexametasona em águas naturais brutas utilizadas no abastecimento público do Estado do Ceará, Brasil. Os limites de detecção obtidos variaram entre $7{,}47 \times 10^{-9}$ e $1{,}80 \times 10^{-8}$ mol $L^{-1}$ para as três matrizes de águas naturais brutas avaliadas. Os valores percentuais médios de recuperação (98,86% ± 0,72), repetibilidade (0,32% ± 0,05) e reprodutibilidade (0,91% ± 0,20) foram significativos, reafirmando a sensibilidade do procedimento. A energia dos orbitais LUMO e as cargas atômicas de Mülliken foram calculadas usando o funcional BLYP/DNP. Os resultados teóricos, aliados aos critérios de diagnóstico da voltametria de onda quadrada, indicam que o mecanismo redox da dexametasona está associado a processos de redução quase-reversível e irreversível dos grupos cetona localizados em C-20 e C-3, respectivamente.

This paper describes an electroanalytical methodology using square-wave adsorptive voltammetry, which has been successfully applied for the direct determination of dexamethasone residues in raw natural waters used for the public supply of the Ceará State, Brazil. The obtained detection limits ranged from $7.47 \times 10^{-9}$ to $1.80 \times 10^{-8}$ mol $L^{-1}$ for the three matrices of raw natural waters evaluated. High percentages of average recovery (98.86% ± 0.72), repeatability (0.32% ± 0.05) and reproducibility (0.91% ± 0.20) were obtained in these samples, reaffirming the sensitivity of the procedure. Energy of the LUMO orbitals and Mülliken's atomic charges were calculated using the functional BLYP/DNP. The theoretical results allied to the diagnostic criteria of the square-wave voltammetry indicate that the dexamethasone redox mechanism is associated to the quasi-reversible and irreversible reduction process of the ketone groups located at C-20 and C-3, respectively.

**Keywords**: dexamethasone, raw natural waters, direct analysis, square-wave adsorptive voltammetry

## Introduction

The absence of a sustainable planning during the process of land occupation, intensified in Brazil from the 60's, caused serious impacts on society as a whole, due to various environmental disequilibra caused, such as contamination of drinking water supplies, constituting a strong threat to national economy and public health.[1] This, associated to difficulty of access, seasonal vulnerability and irregular distribution, has forced the population to survive under intense rationing policy.[2]

To overcome part of these problems, in the State of Ceará, a region with semi-arid climate in Northeastern Brazil, the drinking water supply is maintained by the dams that store it in sufficient quantities to meet the needs of the population. However, this trick has become very limited due to the irregular rainfall season and sometimes to the low accumulated volume.[3] In addition, the combination

*e-mail: adriana@ufc.br

of impermeable crystalline rocks in the soil, high rates of evapotranspiration, long period of dry season and low levels of water retention still has left many victims of drought in the countryside.

Beyond the problems of scarcity, the water reservoirs have been continually contaminated for a variety of micropollutants (μg $L^{-1}$ to ng $L^{-1}$), from discharge of domestic and/or industrial effluents, which persist in the aquatic environment, even after passing through the processes employed in water and sewage treatment plants.[4] This problem has been observed in many reservoirs of the Ceará, such as Gavião and Ayres de Souza dams, responsible for the water public supply of Fortaleza and Sobral cities, respectively, which shows evidence of the evolutionary framework of eutrophication, due to the discharge of these wastes without any treatment, alerting the population to a possible status of public calamity.[5]

Many of these substances are of great scientific interest due to their ability to interfere with the endocrine system of humans and other animals, as well as their offspring, blocking, mimicking, stimulating and/or inhibiting the production of natural hormones.[4,6,7] These natural or synthetic contaminants are known as endocrine disruptors (EDs) and have been one of the most relevant topics in environmental chemistry in terms of water quality.[2,4,6,7]

Dexamethasone, 9-fluoro-11β,17,21-trihydroxy-16α-methylpregna-1,4-diene-3,20-dione, represented by DMZ (Figure 1), is an important catabolic steroid that has a 40-fold greater potency than natural glucocorticoids, such as cortisol and corticosterone, with strong anti-inflammatory and immunosuppressive action.[8]

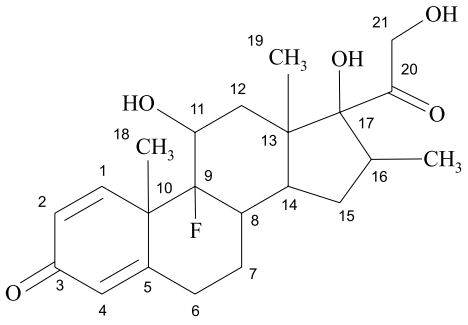


**Figure 1.** Molecular structure of dexamethasone.

Despite its usefulness in the human and veterinary medicine, special care has been dedicated to this drug due to its characteristics as an endocrine disruptor. *In vitro* studies have shown that by acting directly on the granulosa cell, it stimulated progesterone production or could disrupt ovarian steroidogenesis by inhibiting luteinizing hormone (LH) secretion.[9,10] Some authors have reported that it may produce irreversible morphological alterations on the female reproductive tract through changes in the ovarian steroidogenic enzymes, and by inhibiting gonadotrophin secretion/action, which in turn caused infertility.[11] In addition, Illera *et al.*[8] have stated that a single dose of DMZ may disrupt gonadal function in adult female rats even after dexamethasone is undetectable by conventional assay methods, consequently disturbing reproductive function and possibly leading to infertility. Complementing this discussion, Skinner *et al.*[12] reported that extremely low doses of EDs may be capable of inducing adverse effects in animals and, in the precautionary principle, the contact of these substances on humans should be avoided to the maximum.

Thus, the development of precise methods for quantification of residues of these compounds in different environmental matrices allowed the adoption of necessary providence for the control and management of pollution sources.[13-15] Electroanalytical methods can be interesting alternatives for this purpose, due to their sensitivity, selectivity, and relatively short time of analysis in comparison with traditional analytical procedures.[15-18] Square-wave adsorptive voltammetry (SW-AdsV) is a well-established and fast electroanalytical technique and has been applied in the analysis of DMZ in different matrices, such as pharmaceutical preparations and biological fluids.[13,16,17] It has the advantages of allow low detection and quantification limit, high sensitivity, wide spectrum of the test material and analytes with insignificant matrix effect, speed, and relatively low cost of analysis.[15,16] To our knowledge, there are no studies available in the literature concerning the determination of residues of this drug in trace concentration in natural waters, especially regarding direct application in raw waters with different levels of organic matter, and several other dissolved contaminants.

Thus, the aim of this study was to develop an electroanalytical methodology employing SW-AdsV, for the direct determination of DMZ residues in trace concentrations present in raw natural waters, using the Gavião and Ayres de Souza dams, without any step of clean up or extraction procedure.

## Experimental

### Equipments and reagents

A potentiostat (Autolab PGSTAT 30, Metrohm-Eco Chemie) was used to acquire the electrochemical results. It was controlled by a computer, using GPES version 4.9 software (General Purpose Electrochemical System, Metrohm-Eco Chemie). A conventional cell with a three-electrode system, consisting of an Ag/AgCl/$KCl_{sat}$ system as the reference electrode, a graphite rod as the auxiliary

electrode, and a hanging mercury drop electrode (HMDE, 663 VA Stand, Metrohm-Eco Chemie) with a surface area of 0.52 $mm^2$ as a working electrode. A Micronal B474 pH meter equipped with a $Ag/AgCl/KCl_{sat}$ combined electrode was used to adjust the pH values. All solutions were prepared with water purified by a Milli-Q system (Millipore Corp.).

A $1.0 \times 10^{-5}$ mol $L^{-1}$ standard aqueous stock solution of DMZ (CAS: 2392-39-4) was prepared using USP-grade DMZ; it was stored in a dark flask and under refrigeration. Other standard solutions were obtained by diluting a certain amount of stock standard solution with purified water to the desired concentration. The 0.04 mol $L^{-1}$ Britton-Robinson (BR) buffer solutions, used as the supporting electrolyte, were prepared as described in the literature and the pH was adjusted to the desired value by adding appropriate amounts of 0.2 mol $L^{-1}$ NaOH stock solution.[19] All reagents used were analytical grade.

### Electroanalytical procedure

Before each experiment, a stream of high-purity $N_2$ was passed through the solution for 10 min. Negative scans were then performed from 0.0 V to −1.4 V, using cyclic voltammetry (CV) and SW-AdsV techniques. After selecting the best conditions of the pH electrolyte, the effect of analyte preconcentration onto the HMDE surface was evaluated, varying accumulation potential and time. The optimisation of the analytical procedure for SW-AdsV was also carried out following a systematic study of the other experimental parameters that affect the responses, such as pulse potential frequency (f), amplitude of the pulse (a), and height of the potential step ($\Delta E_s$), in relation to peak current and maximum selectivity (half-peak width). Then, analytical curves were performed in purified water in order to assess the sensitivity of the method and its possible application to evaluate the levels of DMZ in natural waters. The recovery experiments were carried out by standard additions of the DMZ stock solution to the supporting electrolytes. All measurements were taken in triplicate, and the value $[DMZ]_{found}$ refers to the concentration obtained by extrapolation of the analytical curves. The standard deviation of the mean intercept measured, for ten replicates, at the reduction potential of the DMZ compound was used together with the slope of the straight lines of the analytical curves in the determination of the limit of detection (LOD) and limit of quantification (LOQ). The accuracy of the procedure was evaluated based on recovery efficiencies (recovery %), which was calculated from the ratio between the found concentration value and the previously added concentration. In case of precision, it was performed based on repeatability experiments realised with ten measurements with the same DMZ standard solution (intraday) and with five measurements in different days with different DMZ standard solutions in the same concentration (interday).[20,21] All measurements were made at room temperature.

### Sampling and physicochemical analysis of the raw natural waters

The raw natural water samples were collected at three different sampling points located in two dams: the Gavião dam (points GD1 and GD2) and the Ayres de Souza dam (point ASD) in the State of Ceará, Brazil. These dams are used for fishing, recreational activities and, primarily, the supply of water to the cities of Fortaleza and Sobral. The strategic sampling points were selected in areas close to the discharge of untreated domestic and industrial sewage, in order to compare the robustness of the procedure. The quality of these waters has been evaluated for simultaneous physicochemical analysis, based on standard methodologies described by APHA,[22] which are discussed later. Water samples were collected in amber glass bottles, transported to the laboratory in charge and kept under refrigeration (± 5 °C) until the time of analyse, following the range of recommended storage time for each parameter.

### Application of the electroanalytical procedure in raw natural waters

Once constructed the analytical curve, the sensitivity, accuracy and precision of the procedure, and the interference of matrix components from raw natural waters in comparison to purified water, were evaluated. For this, electrochemical measurements were performed without any pre-treatment of samples, so that even water from dams was used in preparing the supporting electrolyte, similarly to the procedure employed in purified water. The recovery experiments were carried out by standard additions of the DMZ stock solution to the supporting electrolytes and all experiments were taken in triplicate.

## Results and Discussion

### Effect of pH in the electrochemical behaviour of DMZ

Firstly, a study of the electrochemical behaviour of $2.91 \times 10^{-5}$ mol $L^{-1}$ DMZ solution, from 0.0 to −1.4 V, was carried out by square-wave voltammetry over the pH range of 2.0 to 12.0 in the 0.04 mol $L^{-1}$ BR buffer solution. This compound was found to give two well-defined reduction

processes up to pH 7.0. For the first peak, the peak current ($I_p$) increased up to pH 5.0 and decreased at higher values. For the second peak, the most significant peak current was recorded at pH 2.0, gradually decreasing with increasing pH, as can be seen in Figure 2A for peak 1, and Figure 2B for peak 2.

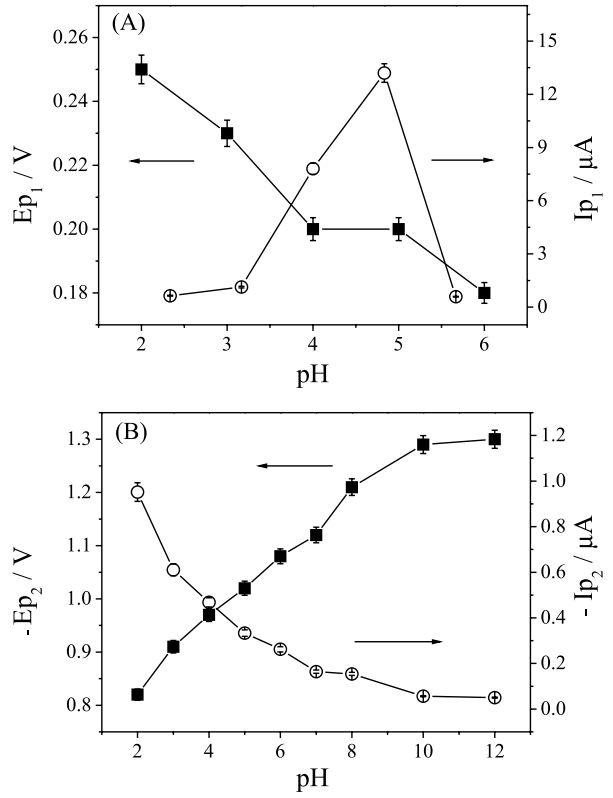


**Figure 2.** Behaviour of peak current and peak potential regarding to the corresponding pH, for peak 1 (A) and peak 2 (B), using $2.91 \times 10^{-5}$ mol $L^{-1}$ of DMZ in BR buffer pH 2.0, on the HMDE with $f = 100$ $s^{-1}$, $a = 50$ mV and $\Delta E_s = 2$ mV.

From pH 7.0, the first peak completely disappears and the second peak undergoes a deformation in the voltammetric profile. This deformation in peak 2 may be related to a transitional state among protonated, neutral and unprotonated DMZ derivatives. Some researchers have reported the difficulties in observing these intermediaries separately, due to the electrochemical properties being quite similar.[16,23]

A linear shift was observed in peak 2 to more negative peak potential ($E_p$) values with increasing pH, suggesting a reaction with the participation of protons. It can be expressed by the following regression expression:

$$- E_p\ (mV) = 718.8 + 58.9\ pH \qquad (1)$$

As can be observed, the value of $\partial E_p/\partial pH$ was close to 60 mV/pH, an ideal value for reactions with the same number of protons and electrons involved in redox reactions. Recently, Goyal *et al.*[17] have shown that this process involves two protons and two electrons *per* DMZ molecule, employing $^1H$ NMR. In addition, DMZ has two $pK_a$ values, so that the first protonation of this molecule should occur in the conjugated ketone group, *i.e.*, another evidence of the strong dependence of this reactive site with the protons concentration. In the case of peak 1, $E_p$ values remain virtually constant with a variation in pH, showing that it is independent of proton concentration in the solution.

The value of $I_p$ for peak 1 at pH 2.0 is already quite significant. This information, together with the fact that the increase in pH causes a shift of peak 2 to more negative $E_p$ values, was used as criteria for the choice of pH 2.0 as the optimum condition for the development of this methodology. A DMZ square-wave voltammogram with net, forward and backward components for both peaks in this same pH is represented in Figure 3, so that the peak 1 was recorded at –0.21 V and peak 2 at –0.83 V.

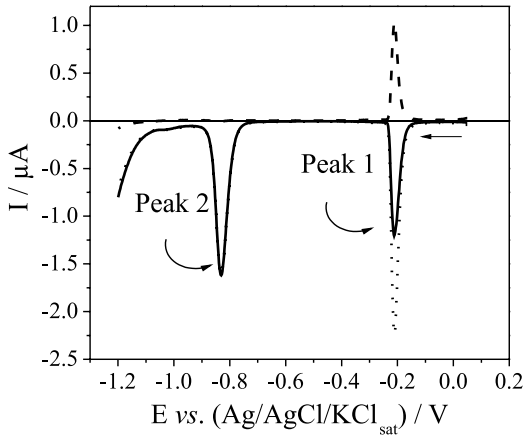


**Figure 3.** Square-wave voltammograms for $2.91 \times 10^{-5}$ mol $L^{-1}$ of DMZ on the HMDE in BR buffer, pH 2.0, with a scan potential ranging from 0.0 V to –1.2 V, $f = 100$ $s^{-1}$, $a = 50$ mV and $\Delta E_s = 2$ mV. Resultant component (—), forward component (---) and backward component (···).

## Mechanistic aspects

From the cyclic voltammetric results, it is possible to observe that both DMZ reduction processes are independent, since different scans exhibit isolated processes; 0.0 to –0.5 V for peak 1 and –0.5 to –1.4 V for peak 2; or both processes simultaneously, 0.0 to –1.4 V; without a decrease in the intensity of peak currents or an alteration in $\Delta E_{p/2}$. Analysing the DMZ molecule as a whole, it was observed that resonance effects at C-3 gives much greater stability to this reactive site if compared to the steric effect observed at C-20. Therefore, it is expected that one reduction process will be observed for each particular ketone group. Thus,

the electrochemical signal associated with C-20 (peak 1) should appear at potentials less negative than C-3 (peak 2).

The reversibility of the processes was also evaluated by cyclic voltammetry. In the case of peak 1, the presence of anodic and cathodic peaks with different intensities and a slope close to the unit were found, from the relationship between log $I_p$ and log $v$, according to equation 2, representing a quasi-reversible system controlled by adsorption.

$$\log (I_p / A) = -8.811 + 0.873 \log (v / mV\ s^{-1}) \quad (2)$$

The cyclic voltammogram for peak 2 showed only one well-defined cathodic peak, which was an indication of an irreversible process. A straight line between $I_p$ and $v$ was observed according to following equation:

$$-I_p (A) = 9.257\times10^{-9} + 2.334\times10^{-9}\ v\ (mV\ s^{-1}) \quad (3)$$

Moreover, no linear displacement of $E_p$ to more negative values with an increase of $v$ was observed. These data characterised an irreversible process with the redox mechanism controlled by adsorption of reagents and products.[24] Due to adsorptive character of the DMZ reduction processes, we chose to work with SW-AdsV as analytical technique.

## Quantum-chemical studies

Theoretical and experimental studies have shown the importance of quantum-chemical studies to understand the electrochemical mechanistic aspects of numerous organic compounds.[25] Here, this information was used to determine the probable sites of reduction of the DMZ, considering its protonated form, because the studies were conducted at pH 2. In this case, the effect of protonation is an aspect that should be considered. The data presented below were obtained from DMOL 3 quantum-chemical software package of the Materials Studios, employing the method of generalized gradient approximation, using the functional BLYP and DNP basis set.

Initially, we performed the calculation of frontier molecular orbital HOMO (highest occupied molecular orbital) and LUMO (lowest unoccupied molecular orbital) of the DMZ before and after the first reduction process. The HOMO orbital indicates the region of the molecule where the oxidation process would be more likely, while the LUMO orbital is responsible for the entry of electrons in the molecule, indicating its site of reduction. Thus, for the DMZ reduction process, only the data for LUMO orbital will be emphasized. From Figure 4A, regarding the protonated molecule of DMZ before the first reduction process, it is observed that the atoms C-13, C-16, C-20 and C-21 are those that present the greatest contribution to the formation of LUMO orbitals. In case of the second reduction process (Figure 4B), the largest contribution is observed from C-1 to C-5, C-9 and C-18.

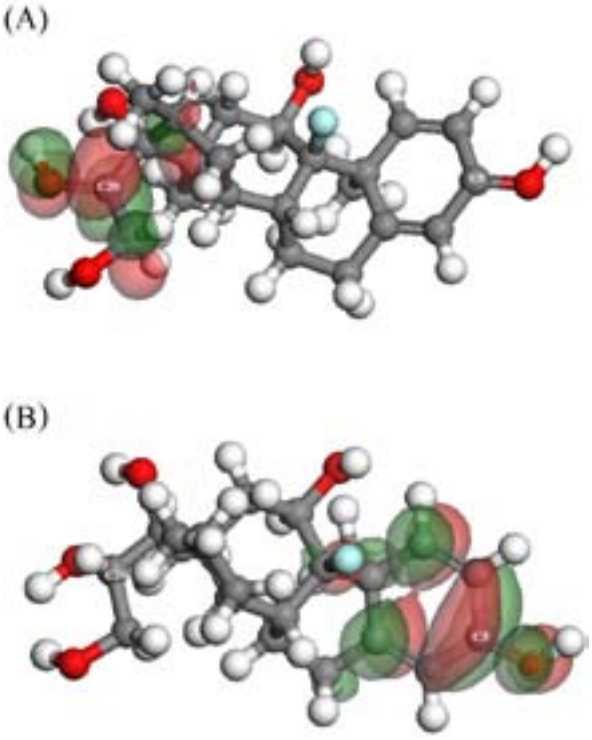


**Figure 4.** Graphic representation of the LUMO orbitals of the protonated DMZ molecule, before of the first (A) and second (B) reduction processes. Carbon (gray ball), hydrogen (white ball), oxygen (red ball), fluor (blue ball) and electronic clouds of the LUMO orbitals (red and green). See online for color image.

After this, the Mülliken's charges for these atoms were calculated, based on three conformers of lowest energy, to investigate where the first and second reduction processes are more probable. The results are described in Table 1. According to the theoretical model, the more positive the value obtained, the greater the tendency to accept electrons and the greater the possibility of the occurrence of the reduction reaction. The results showed that the more positive values for Mülliken's charges were observed in C-20 (charge = 0.466), before of the first reduction process, and in C-3 (charge = 0.399) before the second reduction process. Thus, from the quantum-chemical point of view, the peaks 1 and 2 are related to reduction processes occoring in C-20 and C-3, respectively.

These results were in agreement with previous discussion and corroborated by data recently published in the literature, which indicate that the ketone groups at positions C-3 and C-20 are probable sites of reduction

**Table 1.** Mülliken's charges in the DMZ molecule before of the first (BFR) and before of the second (BSR) reduction processes with the corresponding standard deviation

| Atom | Mülliken's charges | | | |
|---|---|---|---|---|
| | BFR | $SD_{BFR}$ | BSR | $SD_{BSR}$ |
| C-1 | 0.089 | ± 0.0006 | 0.052 | ± 0.0012 |
| C-2 | –0.041 | ± 0.0006 | –0.027 | 0.0 |
| C-3 | 0.391 | 0.0 | 0.399 | ± 0.0015 |
| C-4 | –0.044 | ± 0.0015 | –0.040 | ± 0.0006 |
| C-5 | 0.132 | 0.0 | 0.082 | ± 0.0006 |
| C-6 | –0.115 | ± 0.0006 | –0.096 | 0.0 |
| C-7 | –0.133 | 0.0 | –0.104 | 0.0 |
| C-8 | –0.104 | ± 0.0015 | –0.080 | ± 0.0012 |
| C-9 | 0.292 | 0.0 | 0.289 | ± 0.0006 |
| C-10 | –0.243 | ± 0.0006 | –0.180 | 0.0 |
| C-11 | 0.152 | ± 0.0006 | 0.205 | 0.0 |
| C-12 | –0.123 | 0.0 | –0.058 | ± 0.0015 |
| C-13 | –0.145 | ± 0.0012 | –0.133 | ± 0.0006 |
| C-14 | –0.096 | 0.0 | –0.063 | ± 0.0006 |
| C-15 | –0.097 | ± 0.0006 | –0.078 | ± 0.0012 |
| C-16 | –0.125 | ± 0.0006 | –0.072 | 0.0 |
| C-17 | 0.105 | 0.0 | 0.224 | ± 0.0006 |
| C-18 | –0.134 | 0.0 | –0.120 | 0.0 |
| C-19 | –0.159 | ± 0.0015 | –0.165 | ± 0.0015 |
| C-20 | 0.466 | 0.0 | 0.136 | ± 0.0006 |
| C-21 | 0.095 | ± 0.0006 | 0.168 | 0.0 |

of the DMZ, where the reduction at C-20 generates a corresponding hydroxy compound and at C-3, a pinacol.[16] The proposed mechanism was based on well-defined theoretical model related to electrochemical mechanisms of steroidal anti-inflammatory, focusing in electrochemical reduction of conjugated and unconjugated ketone groups.[26,27]

### Effect of accumulation of potential and time

The influence of the accumulation potential ($E_{acc}$) was investigated on the HMDE in BR buffer pH 2.0 by applying different potentials between –0.10 and –0.93 V by SWV measurements with $f$ = 100 $s^{-1}$, $a$ = 50 mV and $\Delta E_s$ = 2 mV. For peak 1, the best condition was obtained at –0.60 V, due to the higher peak current observed. In the case of peak 2, the current remained practically constant at –0.70 V, reducing substantially at higher values. In relation to accumulation time ($t_{acc}$), both processes maintained practically constant values after 15 s. Therefore, $E_{acc}$ = –0.60 V and $t_{acc}$ = 15 s were chosen and employed in the development of the electroanalytical methodology.

### Voltammetric parameters

The SWV parameters were studied to determine the optimal values to provide the best analytical signal. For both peaks, the frequency was evaluated from 10 to 500 $s^{-1}$. At peak 1, no linear relationship was obtained between $I_p$ and $f$, and the $E_p$ values remained practically constant. The amplitude showed a linear correlation between $I_p$ and $a$, from 5 to 50 mV. The obtained results with the scan increment variations show that $\Delta E_s$ > 2mV does not seem to offer a significant contribution to the peak currents. Thus, the optimized conditions for peak 1 were $f$ = 100 $s^{-1}$, $a$ = 50 mV and $\Delta E_s$ = 2 mV.

For peak 2, a linear dependence between $I_p$ and $f$ was observed up to 100 $s^{-1}$. For the amplitude of pulse values above 15 mV, no linear relationship occurred. The $I_p$ values showed a linear dependence with $\Delta E_s$ variation (from 1 to 7 mV), but above 2 mV an increase of half-peak width was observed, which can decrease the selectivity of the procedure. Therefore, $f$ = 100 $s^{-1}$, $a$ = 15 mV and $\Delta E_s$ = 2 mV were employed as optimized conditions for peak 2.

### Analytical curves

In an attempt to use peak 1 for analytical applications, it was found that the linearity range obtained between $I_p$ and [DMZ] was very small, ranging only from 5.00 × $10^{-6}$ to 1.03 × $10^{-5}$ mol $L^{-1}$, which would imply low values of LOD and LOQ in comparison to other works.[12,13,17] Moreover, the $I_p$ values obtained for [DMZ] > 7.94 × $10^{-6}$ mol $L^{-1}$ had a significant loss of reproducibility, which negatively affected the values of recovery, precision and accuracy of the proposed methodology.

On the other hand, using the linearity range between 4.98 × $10^{-8}$ and 6.10 × $10^{-7}$ mol $L^{-1}$ for peak 2, it was possible to calculate LOD (2.54 × $10^{-9}$ mol $L^{-1}$) and LOQ (8.47 × $10^{-9}$ mol $L^{-1}$) values in the same order of magnitude as those already published.[12,13,17] The repeatability and reproducibility of the measurements were higher than those obtained for peak 1, showing that peak 2 should be considered as the most adequate proposal for analytical applications. Previously, our group reported the development of an electroanalytical procedure to determine DMZ in multicomponent commercial pharmaceutical formulations.[16] The linear regression equation obtained from the analytical curve is represented by:

$$-I_p\,(A) = -1.58\times10^{-9} + 0.09\,[DMZ] \quad (4)$$

As can be observed, the intercept of the analytical curves was negative. Therefore, an evaluation of the

presence of random errors was performed by a significance test in order to determine if the difference between the interception obtained in these analytical curves and the standard values originated from random error.[28] The *t*-test was used, according to equation 5, where $\bar{x}$ is the average from obtained interception values, μ is the standard value expected in the case of the interception being zero, n is the number of determinations, and s is the standard deviation of the current responses.

$$t = (\bar{x} - \mu)\frac{\sqrt{n}}{s} \quad (5)$$

The calculated t value was 4.01, which was lower than the critical value ($t_{critical}$ = 4.30) at an assurance level of 95%, indicating that no considerable difference occurred from the calculated mean value to the standard expected value, and the negative interception was free from random errors. Thus, the obtained sensitivity and precision combined with the simplicity and low cost of the electroanalytical procedure, in comparison to other traditional analytical procedures, reaffirm that the proposal developed here can be successfully employed for practical applications, such as the electroanalytical determination of DMZ in complex samples.

## Application of the method in raw natural waters

The developed electroanalytical procedure was applied to natural water samples, without any previous extraction or clean-up steps that could hinder direct determination, collected at different dams in the State of Ceará, Brazil. These water samples were used to prepare 0.04 mol $L^{-1}$ BR buffer solutions, with pH adjusted to 2.0 by addition of the appropriate quantities of 1.0 mol $L^{-1}$ NaOH solution, and used as supporting electrolyte. These samples were then spiked with known concentrations of DMZ stock solutions and analytical curves were performed by SW-AdsV on the HMDE to evaluate the voltammetric responses and the influence of possible interferences. An example of the analytical curves obtained in raw natural waters from Gavião dam 1 is represented at Figure 5.

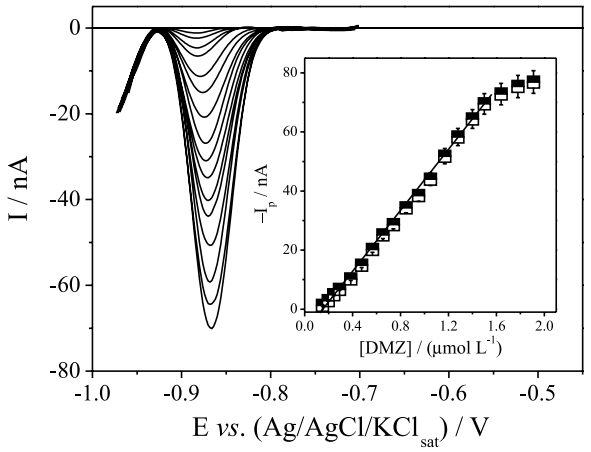


**Figure 5.** (A) Square-wave voltammograms for DMZ in raw natural waters from Gavião dam 1 on the HMDE, buffer solution at pH 2.0, employing $f$ = 100 $s^{-1}$, $a$ = 15 mV, $\Delta E_s$ = 2 mV, $E_{acc}$ = –0.60 V, $t_{acc}$ = 15 s and concentrations in the interval from $1.48\times10^{-7}$ to $1.50\times10^{-6}$ mol $L^{-1}$ of DMZ. (B) Average analytical curve obtained from voltammograms presented in A, including error bar.

The results of the linear regression equation, and figures of merit obtained in purified water and different raw natural waters samples, are shown in Table 2. For concentration ranging from $4.98\times10^{-8}$ and $6.10\times10^{-7}$ mol $L^{-1}$, LOD and LOQ values in the supporting electrolyte and natural waters

**Table 2.** Analytical parameters obtained for DMZ determination employing SW-AdsV on HMDE. PW = purified water; GD1: Gavião dam 1; GD2: Gavião dam 2; ASD: Ayres de Souza dam; r: correlation coefficient; $CI_a$: confidence interval of the intercept; $CI_b$: confidence interval of the slope; $SE_a$: standard error of the intercept; $SE_b$: standard error of the slope; LOD: limit of detection; LOQ: limit of quantification; RSD: relative standard deviation

| Parameter | PW | GD1 | GD2 | ASD |
|---|---|---|---|---|
| Concentration Range / (mol $L^{-1}$) | $4.98\times10^{-8}$ to $6.10\times10^{-7}$ | | $1.48\times10^{-7}$ to $1.50\times10^{-6}$ | |
| Intercept (A) | $-1.58\times10^{-9}$ | $-8.26\times10^{-9}$ | $-9.72\times10^{-9}$ | $-9.99\times10^{-9}$ |
| Slope / (A $mol^{-1}$ L) | 0.09 | 0.05 | 0.07 | 0.07 |
| R | 0.9980 | 0.9988 | 0.9987 | 0.9987 |
| $CI_a$* | $\pm 8.75\times10^{-10}$ | $\pm 4.39\times10^{-10}$ | $\pm 1.03\times10^{-9}$ | $\pm 4.25\times10^{-10}$ |
| $CI_b$* | $\pm 8.96\times10^{-3}$ | $\pm 3.48\times10^{-4}$ | $\pm 5.09\times10^{-4}$ | $\pm 1.36\times10^{-4}$ |
| $SE_a$ (A) | $7.33\times10^{-11}$ | $5.78\times10^{-10}$ | $8.09\times10^{-10}$ | $7.66\times10^{-10}$ |
| $SE_b$ / (A $mol^{-1}$ L) | $5.33\times10^{-4}$ | $6.74\times10^{-4}$ | $9.42\times10^{-4}$ | $8.91\times10^{-4}$ |
| LOD / (mol $L^{-1}$) | $2.54\times10^{-9}$ | $1.03\times10^{-8}$ | $1.80\times10^{-8}$ | $7.47\times10^{-9}$ |
| LOQ / (mol $L^{-1}$) | $8.47\times10^{-9}$ | $3.46\times10^{-8}$ | $5.98\times10^{-8}$ | $2.49\times10^{-8}$ |
| RSD % (n = 10) (Repeatability) | 0.25 | 0.37 | 0.28 | 0.31 |
| RSD % (n = 5) (Reproducibility) | 1.33 | 0.84 | 0.75 | 1.13 |

* P = 0.05.

were different. The most probable explanation for this problem is the higher quantity of dissolved organic matter present in the aquatic environment that is adsorbed on the electrode surface, decreasing the active area, and competing with the DMZ molecules. Moreover, as can be seen in the Experimental section, these samples were collected in areas with a large presence of sediments, detritus rich in organic matter, where its mineralization is associated to environmental conditions, such as redox potential, dissolved oxygen, pH and temperature,[1] indicating the likely presence of humic acids. Studies with natural waters showed that these substances can interact with other dissolved compounds in the environment,[14,29] in this case DMZ molecules, which can reduce their concentration in the electrochemical cell. Recently, Botero *et al.*[7] showed that some drugs can interact with ionized oxygenated groups of aquatic humic substances, through hydrogen bonds, which can strongly influence the transport and reactivity of these contaminants in aquatic systems. Similar discussions can also justify the differences in the linear regression results obtained for purified water and raw natural water samples (Figure 6).

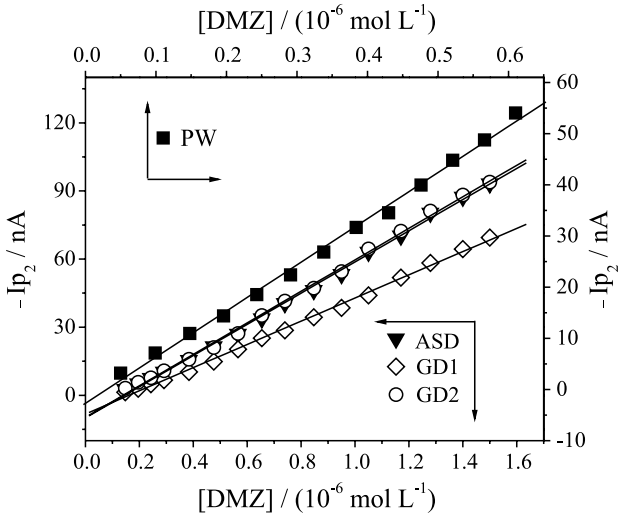


**Figure 6.** Response of peak currents as a function of corresponding concentration of DMZ, ranging from $4.98\times10^{-8}$ to $6.10\times10^{-7}$ mol $L^{-1}$ in purified water and $1.48\times10^{-7}$ to $1.50\times10^{-6}$ mol $L^{-1}$, on the HMDE in BR buffer (pH 2.0), employing $f = 100$ $s^{-1}$, $a = 15$ mV and $\Delta E_s = 2$ mV, $E_{acc} = -0.60$V, $t_{acc} = 15$ s. Purified water (■), Gavião dam 1 (◇), Gavião dam 2 (○) and Ayres de Souza dam (▼).

Table 3 reports data regarding physicochemical parameters used to evaluate the quality of the waters. Among these, chlorophyll A, $DBO_5$, dissolved total organic carbon and thermotolerant coliforms confirmed the negative impacts from untreated effluents in these waters. One of the major consequences observed *in loco*, it was the proliferation of the aquatic macrophytes, floating and submerged, considered bioindicators of organic matter in decomposition, and it represents a serious risk to aerobic animals, for the threat of hypoxia in the environment.[1] This phenomenon is triggered by nutrients derived from phosphorous and nitrogen, evidenced by total phosphorous and nitrogen results. Therefore, when a drug is determined directly in these waters, it is necessary that an analytical method is selective and particularly robust, because of the complexity of the environmental matrix.

As can also be seen in Figure 6, the linear regression equation presents a negative intercept. As such, the paired *t*-test was used, according to equation 6, where $\bar{d}$ and $s_d$ are the average and standard deviations respectively of d, the difference between the values obtained in pure electrolyte and in natural water samples, and n is the number of determinations. The calculated *t* values were 3.80, 4.06 and 4.10 for GD1, GD2 and ASD, respectively, which represent values lower than the theoretical critical value ($t_{critical} = 4.30$) at an assurance level of 95%.[28] This is confirmed by the inclinations obtained in all natural water samples, which

**Table 3.** Physicochemical parameters for the raw natural waters. GD1: Gavião dam 1; GD2: Gavião dam 2; ASD: Ayres de Souza dam

| Parameter | GD1 | GD2 | ASD |
|---|---|---|---|
| pH / 25 °C | 7.65 | 7.65 | 7.40 |
| Chlorophyll A / (μg $L^{-1}$) | 43 | 125 | ≤ 0.2 |
| $NO_3^-$ / (mg N *per* L) | 0.036 | ≤ 0.035 | ≤ 0.035 |
| $NO_2^-$ / (mg N *per* L) | ≤ 0.005 | ≤ 0.005 | 0.006 |
| $NH_3$ / (mg N *per* L) | ≤ 0.1 | ≤ 0.1 | ≤ 0.1 |
| Total Nitrogen / (μg $L^{-1}$) | 550 | 2127 | 446 |
| $PO_4^{3-}$ / (mg P *per* L) | ≤ 0.01 | ≤ 0.01 | 0.013 |
| Total Phosphorous / (μg $L^{-1}$) | 82 | 44 | 69 |
| Thermotolerant Coliform / NMP *per* 100 mL | 15.43 | 15.43 | 50.00 |
| $BOD_5$ / (mg $O_2$ *per* L) | 10.29 | 10.29 | 10.80 |
| Dissolved Total Organic Carbon / (μg $L^{-1}$) | 819 | 1169 | 1169 |

**Table 4.** DMZ recuperation in purified water and natural waters from dams in the State of Ceará, using SW-AdsV on HMDE. PW = purified water; GD1 = Gavião dam 1; GD2 = Gavião dam 2; ASD = Ayres de Souza dam

| Parameter | PW | GD1 | GD2 | ASD |
|---|---|---|---|---|
| $[DMZ]_{added}$ / (mol $L^{-1}$) | $9.90\times10^{-8}$ | $1.96\times10^{-7}$ | $1.96\times10^{-7}$ | $1.96\times10^{-7}$ |
| $[DMZ]_{found}$ / (mol $L^{-1}$) | $9.87\times10^{-8}$ | $1.95\times10^{-7}$ | $1.93\times10^{-7}$ | $1.93\times10^{-7}$ |
| Recuperation % | 99.75 | 99.69 | 98.52 | 98.36 |
| RSD % | 0.25 | 0.17 | 0.22 | 0.26 |
| BIAS % | –0.30 | –0.30 | –1.48 | –1.63 |

were similar to inclinations obtained in purified electrolyte, confirming the hypotheses that the analytical sensitivity in natural water samples and in purified water were practically equal, and that these experiments were free from random errors.

$$t = \frac{\bar{d}\sqrt{n}}{s_d} \quad (6)$$

On the other hand, a comparison of the various values obtained for LOD and LOQ in the different natural waters, in comparison to purified water, indicates that the impurities cause no discrepant influence on the final analytical result. Massaropi *et al.*[30] have reported that the lower slope value, compared to purified water, is compensated by a smaller variation for the blank responses, and this is an important finding as no clean-up step was included in the present study, which is imperative for chromatographic methods. However, although antropic and natural activities contribute to an increase in the concentration of organic matter, and consequently an increase in LOD and LOQ values, these values were sufficiently small, with orders of magnitude very close to that seen in purified water, indicating that this technique can be successfully used in the direct analysis of DMZ residues in raw natural waters. Moreover, despite the complexity of the samples, no other electrochemical process was detected, associated with several species dissolved in natural water, which gives selectivity and ruggedness to the developed procedure.

Finally, in artificially contaminated samples, recovery experiments were performed by the standard addition technique. The obtained results are presented in Table 4, showing that the recovery values in GD1 (99.69%), GD2 (98.52%) and ASD (98.36%) were very significant, in addition to showing considerable repeatability and reproducibility. The calculated BIAS values were –0.30%, –1.48% and –1.63% for GD1, GD2 and ASD, respectively, demonstrating the accuracy and precision of the method,[31] and confirming this methodology as an excellent alternative for the direct determination of DMZ residues in natural waters.

## Conclusions

This paper reports the success in the utilization of SW-AdsV for the direct determination of DMZ in environmental samples. An electrochemical study of $5\times10^{-6}$ mol $L^{-1}$ DMZ solution showed two reduction processes associated to C-20 and C-3, representing a quasi-reversible and irreversible mechanism, respectively, with a strong adsorptive character on the HMDE.

The very low LOD values and high levels of repeatability and reproducibility obtained in raw natural water allowed the direct application of this methodology in the electroanalysis of DMZ in trace concentrations, without any clean-up step. Standard addition experiments found recovery values ranging between 98.36 and 99.69%, indicating that matrix effects can be satisfactorily reduced.

Differences between the figures of merit in purified and raw water are due to the adsorption of organic matter and/or other possible dissolved contaminants in the environment. However, the order of magnitude of these values was quite similar, showing that such a procedure can be applied with success in the direct electroanalytical determination of DMZ in complex environmental samples, in addition to giving robustness and selectivity to the developed method.

## Acknowledgments

The authors wish to thank the Brazilian research funding institutions CNPq, CAPES, FINEP for their financial support and to Prof. David Lima Azevedo (DQ-UFMA) for the assistance in the theoretical calculations. T. M. B. F. Oliveira would also like to thank the UERN for the award of a fellowship.

## References

1. Oliveira, T. M. B. F.; Di Souza, L.; Castro, S. S. L.; *Ecl. Quim.* **2009**, *34*, 17.
2. Baird, C.; *Química Ambiental*, 2nd ed.; Bookman: Porto Alegre, 2002.

3. Fernandez, M. A.; Limaverde, A. M.; Castro, I. B.; Almeida, A. C. M.; Wagener, A. L. R.; *Cad. Saúde Pública* **2002**, *18*, 463.
4. Bila, D. M.; Dezotti, M.; *Quim. Nova* **2007**, *30*, 651.
5. http://www.srh.ce.gov.br/index.php/projetos-especiais/pacto-das-aguas, accessed in May 2011.
6. Ghiselli, G.; Jardim, W. F.; *Quim. Nova* **2007**, *30*, 695
7. Botero, W. G.; Oliveira, L. C.; Cunha, B. B.; Oliveira, L. K.; Goveia, D.; Rocha, J. C.; Fraceto, L. F.; Rosa, A. H.; *J. Braz. Chem. Soc.* **2011**, *22*, 1103.
8. Illera, J. C.; Silván, G.; Martínez, M. M.; Blass, A.; Peña, L.; *J. Physiol. Biochem.* **2005**, *61*, 429.
9. Botero, L. F.; Roberts Jr., C. T.; LeRoith, D.; Adashi, E. Y.; Hernández, E. R.; *Endocrinology* **1993**, *132*, 2703.
10. Huang, T. J.; Shirley Li, P.; *Biol. Reprod.* **2001**, *64*, 163.
11. Illera, J. C.; Silván, G.; Martínez-Mateos, M. M.; Blass, A.; Lorenzo, P. L.; Illera, M.; *Anal. Chim. Acta* **2003**, *483*, 225.
12. Skinner, M. K.; Manikkam, M.; Guerrero-Bosagna, C.; *Reprod. Toxicol.* 2011, *31*, 337.
13. Ghoneim, E. M.; El-Attar, A.; Ghoneim, M. M.; *J. AOAC Int.* 2009, *92*, 597.
14. Rezaei, B.; Zare, S. Z. M.; Ensafi, A. A.; *J. Braz. Chem. Soc.* **2011**, *22*, 897.
15. Gupta, V. K.; Jain, R.; Radhapyari, K.; Jadon, N.; Agarwal, S.; *Anal. Biochem.* **2011**, *408*, 179.
16. Oliveira, T. M. B. F.; Ribeiro, F. W. P.; Soares, J. E. S.; De Lima-Neto, P.; Correia, A. N.; *Anal. Biochem.* **2011**, *413*, 148.
17. Goyal, R. N.; Chatterjee, S.; Rana, A. R. S.; *Electroanalysis* **2010**, *22*, 2330.
18. De Lima-Neto, P.; Correia, A. N.; Portela, R. R.; Juliao, M. S.; Linhares-Junior, G. F.; Lima, J. E. S.; *Talanta* **2010**, *80*, 1730.
19. Britton, H. T. S.; Robinson, R. A.; *J. Chem. Soc.* 1931, *458*, 1456.
20. Mocak, J.; Bond, A. M.; Mitchell, S.; Scollary, G.; *Pure Appl. Chem.* **1997**, *69*, 297.
21. Skoog, D. A.; West, D. M.; Holler, F. J.; *Fundamentals of Analytical Chemistry*, 7th ed., Saunders College: Philadelphia, 1996.
22. APHA, *Standard Methods for the Examination of Water and Waste Water*, 20th ed., American Public Health Association: New York, 1998.
23. De Boer, H. S.; Den Hartigh, J.; Ploegmakers, H. H. J. L.; Van Oort, W. J.; *Anal. Chim. Acta* **1978**, *102*, 141.
24. Gosser Jr, D. K.; *Cyclic Voltammetry: Simulation and Analysis of Reaction Mechanisms*, VCH Publ.: New York, 1994.
25. Toledo, R. A.; Mazo, L. H.; Santos, M. C.; Honório, K. M.; Silva, A. B. F.; Cavalheiro, É. T. G.; *Quim. Nova* **2005**, *28*, 456.
26. Fry, A. J.; *Synthetic Organic Electrochemistry*, 2nd ed., John Wiley: New York, 1989.
27. De Boer, H. S.; Van Oort, W. J.; Zuman, P.; *Anal. Chim. Acta* **1981**, *130*, 111.
28. Miller, J. N.; Miller, J. C.; *Statistics and Chemometrics for Analytical Chemistry*, 5th ed., Pearson Prentice Hall: United Kingdom, 2005.
29. Sibley, S. D.; Pedersen, J. A.; *Environ. Sci. Technol.* **2008**, *42*, 422.
30. Massaroppi, M. R. C.; Machado, S. A. S.; Avaca, L. A.; *J. Braz. Chem. Soc.* **2003**, *14*, 113.
31. Taverniers, I.; Loose, M. D.; Bockstaele, E. V.; *Trends Anal. Chem.* **2004**, *23*, 535.

*Submitted: June 5, 2011*
*Published online: October 25, 2011*

*J. Braz. Chem. Soc.*, Vol. 23, No. 1, 120-123, 2012.
Printed in Brazil - ©2012 Sociedade Brasileira de Química
0103 - 5053 $6.00+0.00

Article

# Morphology, Microstructure and Electrocatalytic Properties of Activated Copper Surfaces

***Juan C. M. Gamboa, Denise F. S. Petri, Tânia M. Benedetti, Vinicius R. Gonçales and Mauro Bertotti****

*Instituto de Química, Universidade de São Paulo, 05508-900 São Paulo-SP, Brazil*

Alterações morfológicas em superfícies de cobre resultantes da aplicação de um protocolo definido de potencial foram examinadas por microscopia eletrônica de varredura (MEV) e microscopia de força atômica (AFM). Os resultados mostraram uma boa correlação entre o tempo empregado na ativação do eletrodo, microestrutura resultante e a atividade eletroquímica.

Morphologic changes on copper surfaces upon applying an established potential protocol were examined by scanning electron microscopy (SEM) and atomic force microscopy (AFM). The results showed a good correlation between the time employed in the electrode activation and the resulting microstructure and electrochemical activity.

**Keywords**: nitrite, copper electrode, activation process, SEM, AFM

## Introduction

The deliberate manipulation of electrodic surfaces consists of an area of continuing interest, because this approach leads to an improvement in the ability to recognize molecules and carry out electron transfer processes at higher rates. Hence, one of the dominant subjects in electrochemistry is the attempt to control the chemical composition and morphological structure of the electrode surface to gain advantages in electroanalytical determinations. It is well known that the electroactivity of copper surfaces depends strongly on their morphology, surface area and structure, which would in turn depend on the method employed to prepare the electrode prior to electrochemical measurements. Hence, several studies have been reported in the literature on the use of copper surfaces aiming for the quantification of different species such as glucose,[1] carbohydrates,[2] ethanol,[3] nitrate,[4,5] nitrite,[5] and sufite.[6]

The electrochemical determination of nitrate after deposition of copper from solutions containing Cu(II) has been reported by some authors,[7,8] who examined qualitatively the morphology of the copper deposit by scanning electron microscopy (SEM) and atomic force microscopy (AFM). The increased sensitivity for nitrate after the surface modification by deposition of the fresh copper layer was attributed to morphologic changes assessed through quantitative parameters such as roughness and porosity of the film. Our group reported a new procedure for the activation of copper surfaces using a potential protocol based on copper oxidation and subsequent reduction of generated copper ions.[9,10] Taking into account these findings and as an attempt to understand which surface parameters control the electrochemical activity, the present study aims to evaluate whether there is a quantitative correlation between the surface area of copper electrodes and their electrochemical properties. Accordingly, copper electrodes were activated for different periods of time to produce layers which were analyzed by SEM and AFM. Then, the electrochemical activity of each generated surface was evaluated towards the cathodic reduction of nitrite. To the best of our knowledge, this is the first time that such a quantitative approach is applied for copper electrodes.

## Experimental

### Chemicals and materials

All solid reagents were of analytical grade and were used without further purification. Sulfuric acid and sodium sulfate were obtained from Merck (Darmstadt, Germany).

*e-mail: mbertott@iq.usp.br

The supporting electrolyte was a 0.1 mol $L^{-1}$ $Na_2SO_4$ solution, pH 2.0 (adjusted with $H_2SO_4$).

### Electrodes and instrumentation

An Autolab PGSTAT 30 (Eco Chemie) bipotentiostat with data acquisition software made available by the manufacturer (GPES 4.8 version) was used for the electrochemical measurements. Experiments were done in a conventional electrochemical cell using a Ag/AgCl (saturated KCl) electrode and a platinum wire as reference and counter electrodes, respectively. The working electrode was a 1 $cm^2$ pure copper sheet (Pertech® of Brazil) supported on a phenolic resin plate. The copper electrode was activated by polarization at 0.50 V (copper dissolution) and then at –0.25 V (copper redeposition) for 10, 20 and 30 s. Solutions were deoxygenated with argon for 5 min prior to the experiments.

AFM topographic images were obtained for copper surfaces using a pico SPM-LE molecular imaging system with cantilevers operating in the intermittent-contact mode (AAC), slightly below their resonance frequency of approximately 305 kHz in air. Scan areas (25 × 25) $\mu m^2$ with a resolution of 512 × 512 pixels were obtained. Image processing and the determination of the root mean square (RMS) roughness values were performed using the Pico Scan software. At least three films of the same composition were analyzed at different topographic positions on the surface. The morphology of the copper surfaces was analyzed by using a field emission gun scanning electron microscope (FEG SEM) JEOL JSM-7401F. In order to estimate the copper film thickness, the electrodes were tilted at 90°, so that the electron beam scanned the interface copper/phenolic resin plate. Copper substrates were conveniently pre-treated with the established potential protocol and stored in plastic bottles purged with argon to prevent copper surfaces from oxidation prior to AFM and SEM analyses.

## Results and Discussion

The activation of the copper surface by the proposed procedure involves the application of positive and negative potential steps. AFM topographic images were obtained to evaluate the effect of the activation time on the morphology and the surface area of the copper layer. Figure 1 presents AFM images prior to polarization of the copper electrode and after 10, 20 and 30 s of activation according to the procedure described in the Experimental section. As it can be seen, the electrode surface presents a rather heterogeneous morphology upon activation and the appearing of protuberances is noticed to a large extent as the activation time increases from 10 to 30 s.

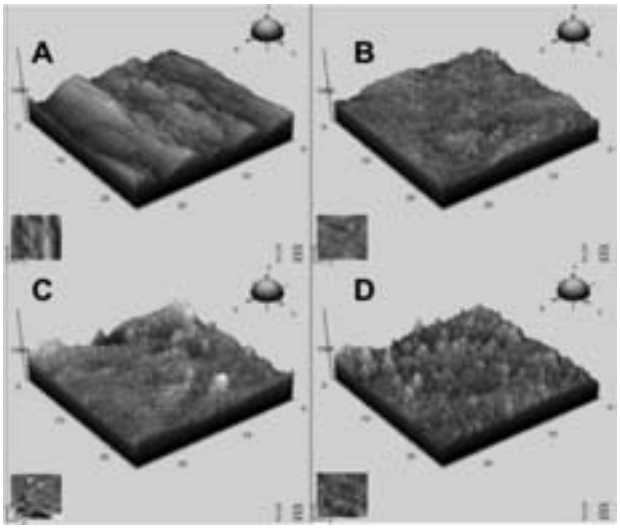


**Figure 1.** AFM topographic images for a copper electrode obtained before (A) and after pre-treatment of the surface using the proposed potential protocol for 10 (B), 20 (C) and 30 s (D). Scan areas (25 × 25) $\mu m^2$.

SEM images obtained for copper electrodes prior to activation presented a homogeneous surface (Figure 2A). After activation for 10 s (Figure 2B) the formation of well-defined filaments is noticed, evidencing the nucleation of electrodeposited copper. Longer activation times (Figure 2C and D) favors the formation of copper, pyramidal crystals and the complete surface modification.

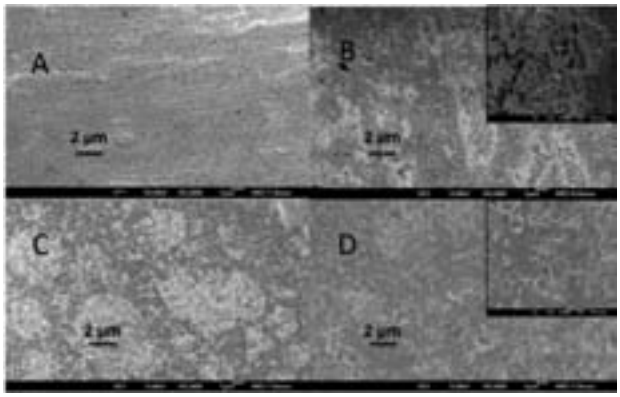


**Figure 2.** SEM images (secondary electron images) of a copper electrode obtained before (A) and after activation of the surface for 10 (B), 20 (C) and 30 s (D).

The influence of the activation procedure on the film thickness was evaluated by SEM by obtaining the images with a copper electrode placed in a vertical position. The bare unmodified copper layer presents a very smooth surface (Figure 3A), whereas a much rougher texture was obtained after the activation procedure and an increase of

*ca.* 10 μm in the film thickness was observed (Figure 3B). This open pore structure is attributable to the presence of pyramidal crystals and the possible adsorption of hydrogen bubbles on the electrode surface, which can explain the formation of the voids seen in Figure 3B. The evolution of hydrogen depends on the solution pH and this has been reported in the literature[11,12] to occur at negative potentials due to the interaction of H-atoms adsorbed in specific sites and diffusing protons, according to the following equation:

$$H^+ + H_{ads} + e^- \longrightarrow H_{2(g)} \quad (1)$$

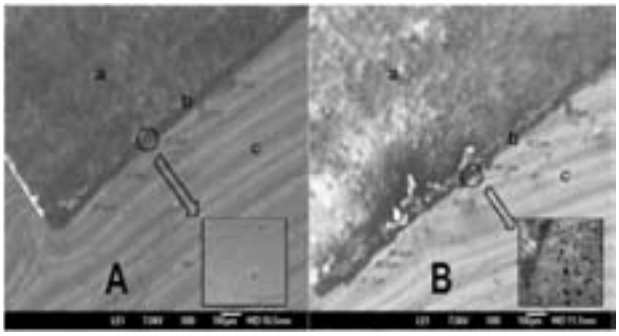


**Figure 3.** SEM images (secondary electron images) of a copper electrode obtained before (A) and after (B) pre-treatment of the surface for 30 s. a) Phenolic resin, b) copper layer and c) stub.

The images shown in Figures 1-3 reveal that the copper deposition process affects strongly the electrode surface morphology. In order to evaluate whether there is a correlation between surface morphology and the electrochemical response, mean roughness (RMS) values were determined for copper electrode surfaces after 10 s, 20 s and 30 s activation. Within the experimental error, RMS values presented no correlation with the activation time. This lack of correlation can be explained taking into account the RMS calculation, which considers the mean peak-to-valley distance and the deviations corresponding to all peak-to-valley distances measured for a given area. In this sense, RMS is a poor information about the surface because it is not regarded to the surface geometry. Hence, surfaces with different geometries might present similar peak-to-valley distances, yielding similar RMS values. Thus, RMS calculation is not a reliable tool to distinguish these surfaces (Table 1). On the other hand, calculations of surface fractal dimensions (FD) can also yield information about the surface roughness; for smooth surfaces FD = 2, whereas for extremely rough surfaces FD = 3. FD values were calculated as a function of activation time, using Gwyddion, a free software (www.gwyddion.net), and bilinear interpolation. As shown in Table 1, FD values increased with activation time up to 20 s and remained practically the same for 30 s.

**Table 1.** Influence of activation time on RMS and FD values

| Activation time / s | RMS / nm | FD |
|---|---|---|
| 0 | (249 ± 19) | 2.47 ± 0.02 |
| 10 | (384 ± 24) | 2.49 ± 0.01 |
| 20 | (360 ± 22) | 2.60 ± 0.02 |
| 30 | (280 ± 10) | 2.57 ± 0.03 |

The surface area was calculated by triangulation with the Gwyddion software and its dependence on the activation time is presented in Figure 4. Similarly to the dependence of FD on the activation time, there is an evident increase in the electrode surface area with increasing the activation time up to 20 s. The sigmoidal fit to the experimental data shows that for activation times longer than 20 s the surface area has already achieved a maximal magnitude or should increase modestly. The inset in Figure 4 shows the influence of the activation time towards nitrite sensing using a copper electrode. The electrochemical signal increases with the activation time up to 30 s, when the maximal current value seems to be achieved. This trend has also been noticed in a previous work.[13] The increased surface area, accompanied by a favorable adsorption of reactant molecules and hydrogen, facilitates the cathodic reduction of nitrite. Both behaviors indicate that there is an optimal activation time to obtain copper cathodes with maximal surface area and improved electrochemical response. This is in agreement with previous scanning electrochemical microscopy (SECM) experiments, which indicated the enhancement of the electrochemical reactivity of copper cathodes monitored with methyl viologen upon the potential activation protocol.[13]

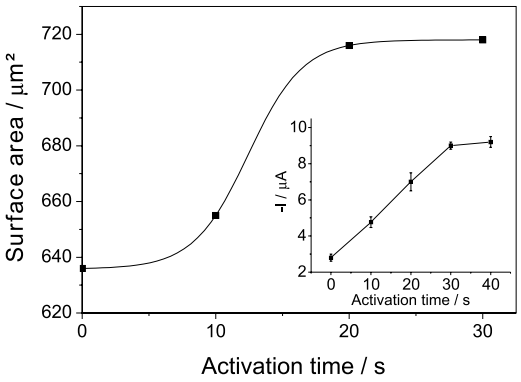


**Figure 4.** Dependence of surface area and current signal (inset) on the activation time. Current values were measured by differential pulse voltammetry in a 0.07 mmol $L^{-1}$ $NO_2^-$ + 0.1 mol $L^{-1}$ $Na_2SO_4$ solution (pH 2.0), (n = 3).

## Conclusions

By using an established activation protocol based on oxidative and reductive steps, the surface area of copper

electrodes can be greatly increased because of the rougher texture of the copper layer, generating very favorable platforms for cathodic reductions involving anions like nitrate and nitrite. A considerable increase in thickness (10 μm) was observed as a consequence of the formation of pyramidal crystals and probable adsorption of hydrogen bubbles on the structure. The rough texture produced by the electrochemical treatment is very similar to the one obtained by copper electrodeposition from solutions containing Cu(II), a procedure usually employed.[7,8,14]

However, the proposed activation protocol is advantageous as a plating solution is not required for the deposition of the catalytic layer and the surface can be easily renewed.

## Acknowledgments

Authors are thankful to FAPESP (Fundação de Amparo à Pesquisa do Estado de São Paulo), CAPES (Coordenação de Aperfeiçoamento de Pessoal de Nível Superior) and CNPq (Conselho Nacional de Desenvolvimento Científico e Tecnológico) for the financial support.

## References

1. Babu, T. G. S.; Ramachandran, T.; Bipin, N.; *Microchim. Acta* **2010**, *169*, 49.
2. Luo, M. Z.; Baldwin, R. P.; *J. Electroanal. Chem.* **1995**, *387*, 87.
3. Paixão, T. R. L. C.; Corbo, D.; Bertotti, M.; *Anal. Chim. Acta* **2002**, *472*, 123.
4. Fogg, A. G.; Scullion, S. P.; Edmonds, T. E.; Birch, B. J.; *Analyst* **1991**, *116*, 573.
5. Shovon, S. M.; Terou, H.; *Anal. Sci*. **2010**, *26*, 1173.
6. Corbo, D.; Bertotti, M.; *Anal. Bioanal. Chem*. **2002**, *374*, 476.
7. Davis, J.; Moorcroft, M. J.; Wilkins, S. J.; Compton, R. G.; Cardosi, M. F.; *Analyst* **2000**, *125*, 732.
8. Davis, J.; Moorcroft, M. J.; Wilkins, S. J.; Compton, R. G.; Cardosi, M. F.; *Electroanalysis* **2000**, *12*, 17.
9. Paixão, T. R. L. C.; Cardoso, J. L.; Bertotti, M.; *Talanta* **2007**, *186*, 191.
10. Gamboa, J. C. M.; Peña, R. C.; Paixão, T. R. L. C.; Bertotti, M.; *Talanta* **2009**, *80*, 58.
11. Simpson, B. K.; Johnson, D. C.; *Electroanalysis* **2004**, *16*, 532.
12. Wang, H. Y.; Huang, Y. G.; Tan, Z.; Hu, X. Y.; *Anal. Chim. Acta* **2004**, *526*, 13.
13. Gamboa, J. C. M.; Peña, R. C.; Paixão, T. R. L. C.; Lima, A. S.; Bertotti, M.; *Electroanalysis* **2010**, *22*, 2627.
14. Carpenter, N. G.; Pletcher, D.; *Anal. Chim. Acta* **1995**, *317*, 287.

*Submitted: June 30, 2011*
*Published online: October 27, 2011*

**FAPESP has sponsored the publication of this article.**

*J. Braz. Chem. Soc.*, Vol. 23, No. 1, 124-131, 2012.
Printed in Brazil - ©2012 Sociedade Brasileira de Química
0103 - 5053 $6.00+0.00

Article

# Total Synthesis and Allelopathic Activity of Cytosporones A-C

***Charles E. M. Zamberlam,[a] Alisson Meza,[a] Carla Braga Leite,[b] Maria Rita Marques,[b] Dênis P. de Lima[a] and Adilson Beatriz*,[a]***

[a]*Centro de Ciências Exatas e Tecnologia, Universidade Federal de Mato Grosso do Sul, Av. Senador Filinto Müller, 1555, 79074-460 Campo Grande-MS, Brazil*

[b]*Centro de Ciências Biológicas e da Saúde, Universidade Federal de Mato Grosso do Sul, Cidade Universitária s/n, 79070-900 Campo Grande-MS, Brazil*

A busca por herbicidas eficientes e ambientalmente corretos tem sido foco de numerosos estudos sobre a síntese de compostos isolados de fontes naturais. Citosporonas, as quais são lipídeos fenólicos isolados de fungos, apresentam notáveis propriedades biológicas. Este artigo relata a preparação das citosporonas A, B e C, através de uma rota sintética curta e com excelentes rendimentos. Os compostos sintetizados foram avaliados quanto às suas atividades alelopáticas em sementes de alface (*Lactuca sativa* L). Citosporona A e seu precursor metilado mostraram notável atividade alelopática, inibindo a germinação de sementes e crescimento das plântulas.

The search for efficient, environmentally friendly herbicides has been the focus of numerous studies on the organic synthesis of compounds isolated from natural sources. Cytosporones, which are phenolic lipids isolated from fungi, exhibit noteworthy biological properties. This paper reports the preparation of cytosporones A-C from the same starting material through a short synthetic route, with good yields. All compounds were tested for allelopathic activity on lettuce (*Lactuca sativa* L) seeds. Cytosporone A and its methylated precursor showed remarkable allelopathic activity, inhibiting seed germination and plantule growth.

**Keywords**: cytosporones, phenolic compounds, allelopathy, herbicides, Friedel-Crafts reaction

## Introduction

Phenolic compounds with long hydrophobic side chains have been isolated as secondary metabolites from plants, fungi, and bacteria since the beginning of the 20th century. Within the plant kingdom, these natural amphiphilic compounds, termed phenolic lipids, can be found in the Gramineae, Leguminosae, and Anacardiaceae. Resorcinolic lipids and their derivatives have drawn the interest of researchers, given their range of biological properties, which allows these compounds to be used as antibiotic, antifungal, molluscicidal, antitumoral, antiparasitic, and antioxidant agents.[1,2]

In 2000, Brady *et al*.[3] isolated five non-isoprenoid octaketide phenolic lipids from the endophytic fungi *Cytospora* sp. and *Diaporthe* sp., which were named cytosporones A-E (**1-5**, Figure 1). Cytosporones D and E (**4** and **5**) exhibited bactericidal activity against *Staphylococcus aureus*, *Enterococcus faecalis*, and *Escherichia coli* and fungicidal activity against *Candida albicans*. Cytosporone B (**2**) was later found to behave as a natural agonist ligand of the orphan nuclear receptor Nur77 of eukaryotic cells, which controls apoptosis in tumor cells and the metabolism of carbohydrates in mammals, properties that make it a potent and selective cytotoxic agent.[4]

Cytosporone A (**1**), also previously isolated from a phytoparasitic fungus (*Phoma* sp.), regulates seed germination factors at low concentrations, in addition to having herbicidal potential.[5]

Inhibition of plant growth and development by compounds released in the environment by other plants or microorganisms is known as allelopathy. The term applies both to beneficial or detrimental interactions, involving either direct or indirect mechanisms. Allelochemicals can be released in the substrate or volatilized.[6] The role of allelopathy in natural environments and agroecosystems has drawn attention to its potential use in weed biological

*e-mail: adilson.beatriz@ufms.br

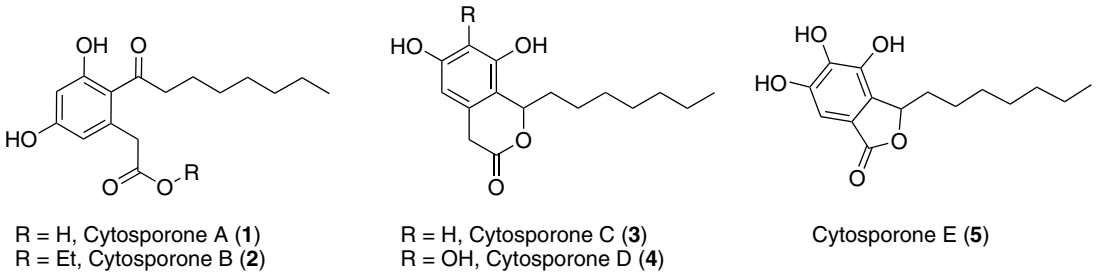


**Figure 1.** Cytosporones A-E.

control. The active participation of researchers from various areas has raised allelopathy to a multidisciplinary field of investigation, leading it to evolve from a basic to an applied science, owing to its applications in agriculture and forestry.[7]

Weeds compete for resources with food cultures, decreasing the productivity of the latter and contaminating subsequent cultivation through seed dispersal.[8] Of an estimated 7000 weed species, some 200 to 300 are considered pests, because of the considerable losses they inflict on producers, not only lowering productivity, but also increasing costs with herbicides. In 2004, the sector of agrochemicals in Brazil attained record sales, totaling US$ 4.495 billion. Herbicides alone are responsible for US$ 1.830 billion in sales, accounting for 54.1% of the market for agricultural defensives.[9] In the USA, expenses with herbicides have reached around US$ 6 billion since the late 1990s, as a consequence of acquired resistance to herbicides in target plant species. In addition, the abuse of synthetic herbicides takes its toll on human, animal and environmental health.[8,10,11] These concerns are drawing attention to alternative weed control technologies based on natural products.[8]

From an agronomic viewpoint, the research on allelophathy provides perspectives for reduction of the use of traditional herbicides. In a so-called organic production, the herbicides are totally suppressed and replaced by allelophatic compounds or extracts whose action mechanisms are generally very different.[12] Furthermore, the majority of allelophathic compounds are biodegradable and less poluents than the traditional herbicides.[13]

Herbicides based on natural products have demonstrated advantages over their classic counterparts, with lower ecological impact. Synthetic derivatives or semisynthetic compounds of these natural products can be more active, more selective, and longer-lasting agrochemicals. By acting through a different mechanism than conventional herbicides, many allelochemichals are a good choice as lead compounds to guide the discovery of new herbicides.[8] Besides, the continuing search for new agrochemical products has demonstrated that natural selection has been superior to combinatorial chemistry in developing bioactive compounds with varied biological activities.[14] These possibilities led our research group to focus on the development of new herbicides based on natural products obtained from microbial sources, and we have recently reported the synthesis of cytosporone analogues with promising allelopathic activity.[15] In the present article, we report the total synthesis of cytosporones A (**1**), B (**2**), and C (**3**) through a short, high-yield synthetic route. All natural products and intermediates involved were tested for their potential inhibition of seed germination and plantule development of lettuce (*Lactuca sativa* L., cv. Grand Rapids - Asteraceae).

## Results and Discussion

### Synthesis

Employing retrosynthetic analysis (Scheme 1), cytosporones A-C can be prepared through a single connection, followed by FGIs. 3,5-Dimethoxybenzoic acid (**7**) is commercially available at low cost. However, an additional step is required to homologate the carbon chain. For this purpose, phenylacetic acid **6** would be a more reliable (albeit more costly) reagent, allowing the reconnection of **6** with **9** to yield the advanced intermediate **8**. The subsequent steps would consist of simple FGIs leading to formation of target compounds.

Scheme 2 shows the sequence of reactions selected for direct synthesis of compounds **1**, **2**, and **3**, involving Friedel-Crafts acylation to form a C-C bond between the hydrophobic pendant and the hydrophilic aromatic ring. 3,5-Dimethoxyphenylacetic acid (**6**), used as the starting material, underwent acylation with octanoyl chloride in $CH_2Cl_2$ under reflux in the presence of $AlCl_3$ as the catalyst, giving the intermediate product 2-octanoyl-3,5-dimethoxyphenyl acetic acid (**8**), with 90% yield, and compound **10**, with 5% yield. The $^1$H NMR spectrum of **8** showed one triplet at $\delta_H$ 2.93 ppm (2H, *J* 7.0 Hz), which typically indicates homotopic methylenic hydrogens adjacent to the carbonyl of a ketone; two doublets at

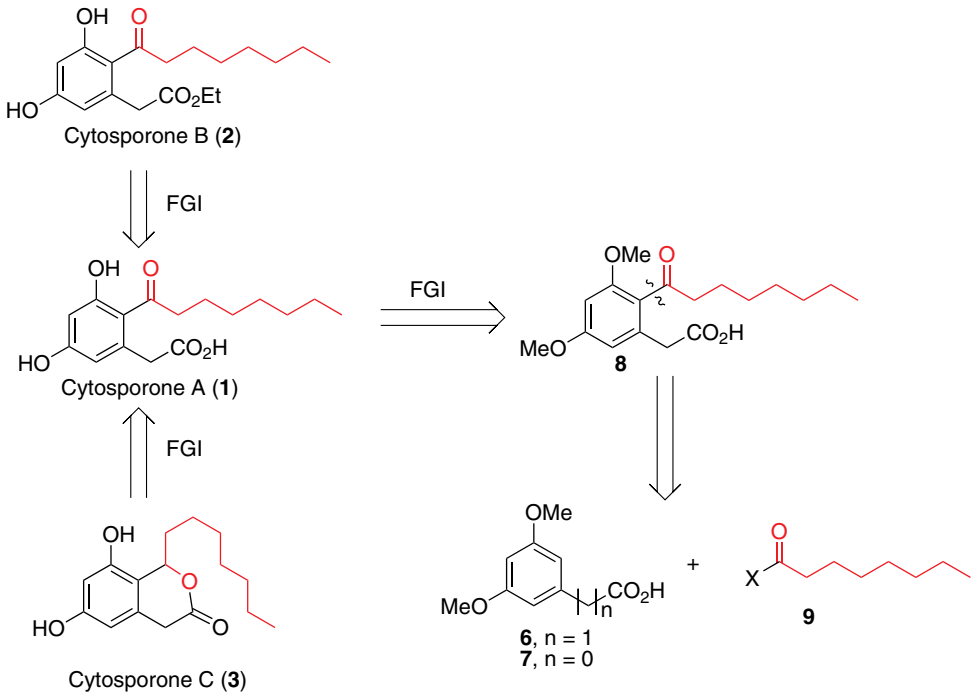


**Scheme 1.** Retrosynthetic analysis of cytosporones A-C.

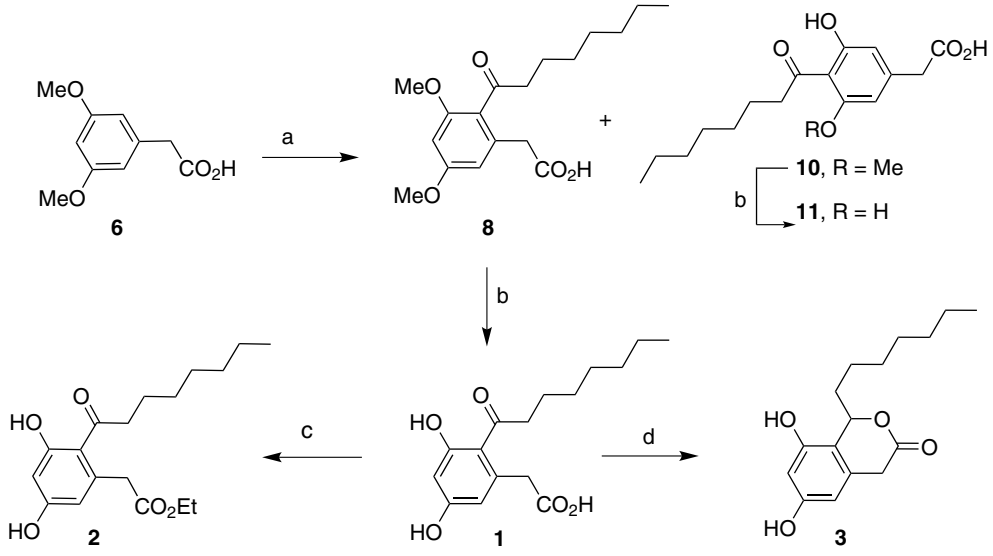


**Scheme 2.** Synthetic route to cytosporones A (**1**), B (**2**) and C (**3**). a) $Me(CH_2)_6COCl$, $AlCl_3$, $CH_2Cl_2$; b) $AlCl_3$, toluene; c) ethanol, $H_2SO_4$; d) $NaBH_4$, ethanol.

$\delta_H$ 6.50 ppm (1H) and 6.43 ppm (1H), *J* 2.0 Hz, which is consistent with aromatic hydrogens having a *meta* relationship. $^{13}C$ chemical shift and $^1H$-$^{13}C$ DEPT NMR data confirmed the presence of 3 methyl, 7 methylene, 6 aromatic, 1 carboxyl carbon (at 172.3 ppm), and 1 carbonyl carbon atom (at 210.1 ppm). The transformation of the compound **8** to the known cytosporone A (**1**), discussed below, confirmed its structure.

The $^1H$ NMR spectra of **10** had two aromatic hydrogen signals, at $\delta_H$ 6.50 (d, 1H) ppm and 6.30 ppm (d, 1H), *J* 2.0 Hz; a singlet at $\delta_H$ 13.35 ppm (1H), assigned to a phenolic hydroxyl in a hydrogen bond, and a singlet at $\delta_H$ 3.87 ppm (3H), in the region of aromatic methoxyls. The $^{13}C$ NMR spectra exhibited a signal at $\delta_C$ 207.6 ppm (C), related to a ketone carbonyl, and one single signal at $\delta_C$ 55.7 ppm ($OCH_3$). The presence of a phenolic hydroxyl in **10** is explained by the action of $AlCl_3$, which is a phenolic deprotection agent. Two-dimensional NMR experiments (HMBC, HSQC, and NOESY) corroborated the structure assignment of compound **10**. *O*-Demethylation of **10** using $AlCl_3$ in toluene under reflux furnished 60% yield of the regioisomer of cytosporone A (**11**).

Compound **8** was subsequently demethylated using $AlCl_3$ in toluene under reflux, to give cytosporone A (**1**) with a good yield (90%). Cytosporone A tautomerism, reported by Voblikova *et al*.,[5] was not detected in the $^1H$ NMR spectra using deuterated methanol as the solvent. Cytosporone B (**2**) was obtained in a quantitative yield from **1** after esterification in acid medium with ethanol. Reduction of cytosporone A (**1**) by $NaBH_4$ in ethanol was the method selected to produce cytosporone C (**3**). After this reaction, cyclization of the resulting alcohol produced the formation of the six-membered ring lactone, in 90% yield. Characterization data of cytosporones A-C were in complete agreement with the literature data reported by Brady *et al*.[3]

The total syntheses of cytosporones A and C have not been reported in the literature. As for cytosporone B, the synthesis was recently reported by Huang *et al*.[16] in a 44% global yield. The authors have prepared the intermediate **12** (Scheme 3) by esterification of the corresponding acid **6** followed by Friedel-Crafts reaction to connect the acyl group to the aromatic ring. However, since the deprotection procedures using $BBr_3$, HBr/AcOH and $AlCl_3$ were unsuccessful, a sequence of protection and deprotection reactions was carried out, increasing the synthetic route in three more steps.

In our procedure, the key step of demethylation of carboxylic acid **8** was performed by using $AlCl_3$ in toluene under reflux, outperforming the previously reported synthesis, where the same transformation was attempted in $CH_2Cl_2$ at 0 ºC to r.t. In conclusion, by using our procedure, it is possible to achieve cytosporone B with 81% global yield from the same starting material (compound **6**).

## Allelopathy

Allelochemical compounds modify plant physiological processes by acting as germination and growth inhibitors. The visible effect is only a secondary sign of the action of these compounds on germination and development, an action initially taking place at the molecular and cellular levels, involving a great number of molecules and plant hormones.[17,18]

Most of the known allelochemicals are secondary metabolites and multifunctional compounds.[19] Therefore, many studies are being carried out with organic solvents to extract pure bioactive compounds or for their homogeneization.[20,21] These *in vitro* assays are considered a first investigation approach of the allelophathic potential, following by tests in field or semi-field conditions, by using different types of formulations.[22] Among the widely accepted methods to test allelophathy reported in the literature, there are those on lettuce (*Lactuca sativa*) seeds since they are characterized by homogeneous germination and, are easy to manipulate. Providing the controls are correctly prepared, the results are recognized as a positive indication of allelophatic activity in tested extracts or pure compounds.[19,23]

The synthesized compounds **8**, **1**, **2**, and **3** were submitted to allelopathic assays on seeds of *L. sativa*[24] to evaluate inhibition of germination. The assay also served to evaluate the ability of these compounds to inhibit the development of hypocotyls and primary roots of *L. sativa* seedlings. Caffeine was used as a positive control because of its known inhibitory activity on seed germination and seedling growth. The negative controls were a buffer solution and the solvents (chloroform for compound **8** and methanol for the others) employed in the experiment.

The germination rates are shown in Table 1. A previous experiment carried out at a concentration of 5 mg $mL^{-1}$ to determine the allelopathic profile did not provide evidence of germination for three days, except when cytosporone C (**3**) was employed. Subsequently, the experiment was repeated at concentrations of 2.5 and 1.25 mg $mL^{-1}$, revealing satisfactory allelopathic activity for **1** and **8**, allowing these compounds to be further diluted to 0.625 mg $mL^{-1}$.

Cytosporone C (**3**) exhibited lower inhibitory activity than the other compounds or caffeine. Cytosporone A (**1**) and its precursor (**8**) fully inhibited seed germination at 2.5 mg $mL^{-1}$ for three days. Also, **1** and **8** were more active than caffeine at this concentration. At 1.25 mg $mL^{-1}$, cytosporone A (**1**) inhibited nearly all the seeds for the first day and was slightly inferior to compound **8** for the last

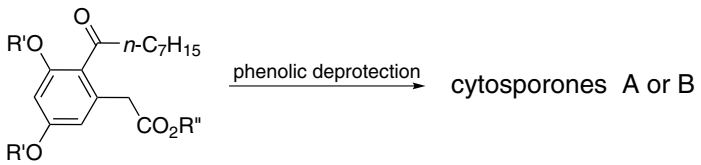


**8**, R' = Me, R" = H
**12**, R' = Me, R" = Et
**13**, R' = Bn, R" = Et

**Scheme 3.**

**Table 1.** Percentage of germination inhibition of *L. sativa* seeds for selected compounds over a three-day period

| Concentration / (mg mL$^{-1}$) | Percentage of inhibition | | | | |
|---|---|---|---|---|---|
| | Caffeine | Compounds | | | |
| | | **8** | **1** | **2** | **3** |
| 2.5 | d1 = 100<br>d2 = 67 ± 10<br>d3 = 52 ± 8 | d1 = 100<br>d2 = 100<br>d3 = 100 | d1 = 100<br>d2 = 100<br>d3 = 100 | d1 = 99 ± 23<br>d2 = 49 ± 18<br>d3 = 38 ± 16 | d1 = 76 ± 7<br>d2 = 36 ± 2<br>d3 = 25 ± 6 |
| 1.25 | d1 = 87 ± 9<br>d2 = 45 ± 10<br>d3 = 32 ± 18 | d1 = 69 ± 16<br>d2 = 71 ± 30<br>d3 = 63 ± 25 | d1 = 92 ± 4<br>d2 = 55 ± 10<br>d3 = 49 ± 4 | d1 = 84 ± 23<br>d2 = 42 ± 10<br>d3 = 34 ± 7 | d1 = 77 ± 7<br>d2 = 34 ± 8<br>d3 = 25 ± 9 |
| 0.625 | d1 = 79 ± 15<br>d2 = 42 ± 2<br>d3 = 25 ± 7 | d1 = 57 ± 14<br>d2 = 42 ± 12<br>d3 = 32 ± 8 | d1 = 85 ± 3<br>d2 = 46 ± 4<br>d3 = 32 ± 7 | - | - |

d1: day 1; d2: day 2; d3: day 3. Inhibition by buffer solution (%): d1 = 39 ± 12; d2 = 25 ± 7; d3 = 8 ± 5. Inhibition by solvent (%): d1 = 40 ± 4; d2 = 23 ± 6; d3 = 17 ± 8.

two days. Both **1** and **8**, however, were more active than caffeine. At the lowest concentration (0.625 mg mL$^{-1}$), these compounds inhibited germination more strongly than caffeine or the other compounds evaluated. At this concentration, cytosporone A (**1**) yielded superior results. Cytosporone B (**2**) showed reasonable inhibition ability, similar to that of caffeine.

On the fifth day of the experiment, hypocotyl and primary root length were measured in the surviving seedlings (Table 2). Primary root length was the feature most visibly affected by all compounds.

**Table 2.** Average length of primary root and hypocotyl in germinating seeds of *L. sativa* after treatment with synthesized compounds

| Sample | Concentration / (mg mL$^{-1}$) | Average length / mm | |
|---|---|---|---|
| | | Primary root | Hypocotyl |
| Buffer | - | 14.4 (± 1.4) | 4.0 (± 2.5) |
| Chloroform | - | 11.5 (± 2.1) | 4.2 (± 1.4) |
| Methanol | - | 17.2 (± 3.5) | 3.8 (± 3.4) |
| Caffeine | 2.5 | 1.0 (± 0.1) | 1.4 (± 0.2) |
| | 1.25 | 0.4 (± 0.2) | 2.4 (± 0.8) |
| | 0.625 | 1.2 (± 0.8) | 2.4 (± 0.1) |
| **8** | 2.5 | 0 | 0 |
| | 1.25 | 0.6 (± 1.6) | 0.4 (± 0.8) |
| | 0.625 | 6.0 (± 1.8) | 2.4 (± 0.4) |
| **1** | 2.5 | 0 | 0 |
| | 1.25 | 0.5 (± 0.1) | 0.8 (± 0.2) |
| | 0.625 | 2.0 (± 0.2) | 2.5 (± 0.1) |
| **2** | 2.5 | 0.8 (± 0.2) | 1.8 (± 0.1) |
| | 1.25 | 1 (± 0.2) | 2.4 (± 0.5) |
| **3** | 2.5 | 1.4 (± 2.4) | 6.8 (± 3.1) |
| | 1.25 | 3.5 (± 1.3) | 7.2 (± 1.4) |

Inhibition by chloroform (%): d1 = 40 (± 4); d2 = 23 (± 6); d3 = 17 (± 8). Inhibition by methanol (%): d1 = 40 (± 4); d2 = 23 (± 6); d3 = 17 (± 8).

Cytosporone C (**3**) interfered the least in initial tissue development of the seeds, but retarded primary root growth.

Of the compounds tested, cytosporone A (**1**) showed the best results, inhibiting 100% of seed germination at a concentration of 2.5 mg mL$^{-1}$ and drastically reducing primary root and hypocotyl growth at the evaluated concentrations (see Table 2). It also inhibited primary root development substantially more than caffeine, while its inhibiting effect on hypocotyl development was similar to that of caffeine.

Cytosporone B (**2**) also effectively inhibited seedling growth, to a similar degree as caffeine, but less strongly than cytosporone A (**1**) or its synthetic precursor (**8**). The latter failed to effectively inhibit primary root growth at a concentration of 0.625 mg mL$^{-1}$.

The results of seedling growth inhibition demonstrate the allelopathic properties of cytosporone A (**1**), its synthetic precursor (**8**), and cytosporone B (**2**).

The literature reports that phenolic compounds, especially phenolic acids, originating from the shikimic acid and polyketide routes, are potentially allelopathic. In natural environments and agroecosystems, these secondary metabolites interfere with growth and development of other plant species.[25,26] Cytosporones are generated through the same biosynthetic route as other phenolic lipids.[1,3] Their production by endophytic fungi is an aspect of the mutualistic interaction between these organisms and some plant species. Secondary compounds released in the environment by fungi can improve survival resources that allow plants to compete with other species. Phenolic compounds are also found in pre-cultivated soils of this class of compounds. These soils show allelopathic activity, probably indicating cumulative dispersal of phenols to the environment.[27]

Porter and Thimann[28] reported that some organic acids whose structures include a charge separation of

approximately 0.5 nm exhibit allelopathic activity, manifested as seed germination inhibition. These compounds include indoleacetic acid, phenylacetic acid, and the agrochemical 2,4-D (Figure 2). The same feature is found in the structure of cytosporone A (**1**) and its synthetic methylated precursor (**8**), allowing us to infer that this condition limits a more pronounced inhibitory activity on lettuce seeds by either compound. This ionic separation is not found in the structures of cytosporones B (**2**) or C (**3**), in which the acid group is esterified. The lactone ester renders cytosporone C (**3**) structurally more rigid in comparison to cytosporone B (**2**), suggesting substantial loss of activity in **3**.

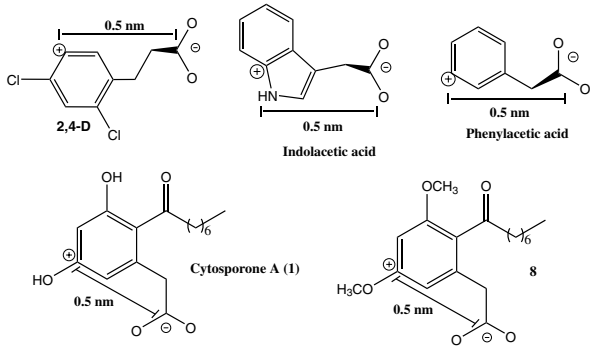


**Figure 2.** Structural separation of charges in allelochemicals.

## Experimental

### General

$^{1}H$ and $^{13}C$ NMR spectra were obtained at 300 and 75 MHz, respectively, using a Bruker Avance DPX-300 spectrometer. Chemical shifts are reported relative to TMS; coupling constants are given in hertz. IR spectra were recorded on a Bomen FT-IR-MB100 Spectrometer. Mass spectra (EI, 70 eV) were run on a Shimadzu CGMS QP2010 Plus gas chromatography mass spectrometer. Melting points were measured by a Uniscience do Brasil 498 apparatus. Purifications were carried out by means of flash chromatography using silica from Merck. All compounds and reagents were commercially acquired from Acros, Synth, and Merck. The allelopathy experiment was performed in BOD chambers (model MA 415/S Marconi).

### Synthesis

#### 3,5-Dimethoxy-2-octanoylphenylacetic acid (*8*)

Thionyl chloride (0.17 mL, 2.3 mmol) was added to a solution of octanoic acid (0.17 g, 1.2 mmol) in $CH_2Cl_2$ (3.5 mL) under nitrogen atmosphere. After reflux under stirring for 4 h, the solvent was evaporated by vacuum pump, followed by addition of dry $CH_2Cl_2$ (4.4 mL). The resulting solution was added dropwise to a solution of 3,5-dimethoxyphenylacetic acid (**6**) (0.15 g, 0.8 mmol) in $CH_2Cl_2$ (4 mL) under a nitrogen atmosphere in a crushed-ice bath. After complete addition of octanoyl chloride, the reaction was kept under reflux for 6 h. A solution of aqueous HCl 6 mol $L^{-1}$ (20 mL) was added to the reaction mixture, transferred to a separatory funnel, and extracted with ethyl acetate (3 × 20 mL). The organic phase was dried over $MgSO_4$ and filtered, and the solvent removed under reduced pressure. Products **8** and **10** and the starting material were purified by column chromatography (6:3:1, hexane:ethyl acetate:$CH_2Cl_2$). Product **8** (90% yield) is a white solid, mp 72-78 °C (recrystallized from $CHCl_3$). Compound **10** (5% yield) is a white solid, mp 122-126 °C.

#### 3,5-Dihydroxy-4-octanoylbenzoic acid (**11**)

A solution of compound **10** (0.04 g, 0.14 mmol) in toluene (15 mL) was added to a two-necked round bottom flask attached to a condenser connected to a silica gel drying tube. Next, dry $AlCl_3$ (0.26 g, 2.0 mmol) was added and the reaction was stirred and refluxed for 7 h. Subsequently, a cooled diluted solution of HCl 1 mol $L^{-1}$ (5 mL) was added dropwise. The reaction mixture was extracted with ethyl acetate (3 × 30 mL), washed with brine, and dried over $MgSO_4$. The product was purified by flash chromatography on silica gel (1:1, hexane:ethyl acetate). Compound **11** is a white solid (60% yield), mp 73-77 °C (recrystallized from ethyl acetate).

#### Cytosporone A (**1**)

Compound **8** (0.04 g, 0.12 mmol) was solubilized in anhydrous toluene (10 mL) and the solution was stirred. $AlCl_3$ was added (0.24 g, 1.8 mmol) to the solution and the reaction was kept under stirring and reflux for 7 h. After this period, a diluted solution of HCl 1 mol $L^{-1}$ (10 mL) was added. The reaction mixture was placed into a separatory funnel and extracted with ethyl acetate (3 × 20 mL). The organic phase was washed with brine, dried over $MgSO_4$ (3 × 20 mL), filtered, and the solvent was evaporated under reduced pressure. The product was purified by flash chromatography (1:1, hexane:ethyl acetate). Cytosporone A (**1**) was obtained as a white solid (90% yield); mp 109-113 °C (recrystallized from ethyl acetate).

#### Cytosporone B (**2**)

An anhydrous ethanol solution (10 mL) of cytosporone A (**1**) (0.02 g, 0.07 mmol) was prepared. 0.05 mL of concentrated sulfuric acid was added to this solution, and the reaction was kept under stirring for 1 h at room

temperature. After this period, $CH_2Cl_2$ (20 mL) was added and the organic phase was washed with a diluted solution of $NaHCO_3$ (4 × 10 mL), dried over $MgSO_4$ and filtered, and the solvent was evaporated under reduced pressure. Cytosporone B was obtained as a brown solid (95% yield); mp 35-40 °C (recrystallized from $CHCl_3$).

### Cytosporone C (**3**)

A solution of **1** (0.01 g, 0.034 mmol) and $NaBH_4$ (0.003 g, 0.06 mmol) in anhydrous ethanol (5 mL) was stirred at room temperature for 24 h. Next, about 0.15 mL of concentrated HCl and distilled water (10 mL) were added. The mixture was placed in a separatory funnel and the product was extracted with ethyl acetate (2 × 20 mL). The organic phase was dried over $MgSO_4$, filtered, and the solvent was evaporated under reduced pressure. The product was purified by flash chromatography (2:1, hexane:ethyl acetate). Cytosporone C (**3**) was obtained as colorless oil (90%).

### Allelopathy assay

The methodology applied is reported in the literature with modifications.[24] Filter papers, previously wet with the test solutions at selected concentrations (Table 1), were placed into Petri dishes. Solutions of caffeine at the same concentrations, also placed on filter papers, served as positive controls. Negative controls comprised of one filter paper wet with the solvent used (chloroform and methanol) and one with the buffer solution employed in the experiment. The Petri dishes were maintained at 45 °C, for 1 h, to evaporate the solvent, at a mild temperature, in order to keep the properties of the tested compounds. Next, 25 seeds of *L. sativa* were placed on each dish and wet with a solution of phosphate buffer (0.025 mol $L^{-1}$ pH 6.0) (day 0). The experiment was conducted in a chamber at 25 ºC ± 2 ºC with a photoperiod of 12 h for three days. The assay was carried out in triplicate and the number of germinated seeds from day 1 to day 3 was counted by sampling. Seeds exhibiting radicle protrusion greater than or equal to 2 mm were considered germinated. The total number of non-germinated seeds was expressed as percentage of inhibition.

## Conclusions

In summary, the total synthesis of cytosporones A-C has been achieved from same starting material (3,5-dimethoxyphenylacetic acid) through a short synthetic route, with good yields. The cytosporones and their intermediates were tested for allelopathic activity on lettuce (*Lactuca sativa*) seeds. Our results revealed that inhibitory allelopathic activity is considerably more pronounced in cytosporone A (**1**) and its precursor (**8**), followed by cytosporone B (**2**), indicating the potential of these compounds as herbicides and as templates for new defensives. Although the other synthesized natural products evaluated did not exhibit comparable allelopathic activity, their synthetic routes (Scheme 2) can feasibly be applied to the industrial development of this class of products, particularly in the case of cytosporone B (**2**), which can be of pharmaceutical interest.

## Supplementary Information

Analytical data and selected $^1$H NMR spectra of compounds **1**-**3** (cytosporones A-C), **8**, **10** and **11** are available free of charge at http://jbcs.sbq.org.br.

## Acknowledgments

The authors would like to thank Kardol Ind. Química Ltda., Fundação de Apoio ao Desenvolvimento do Ensino, Ciência e Tecnologia do Estado de Mato Grosso do Sul (FUNDECT) and CNPq (Brazil) for their financial support. They are also indebted to the UFMS technicians who participated in the experiments.

## References

1. Kozubek, A.; Tyman, J. H. P.; *J. Am. Chem. Soc*. **1999**, *99,* 1.
2. Zarnowski, R.; Suzuki, Y.; *J. Food Compos. Anal.* **2004**, *17*, 649.
3. Brady, S. F.; Wagenaar, M. M.; Singh, M. P.; Janso, J. E.; Clardy, J.; *Org. Lett*. **2000**, *2*, 4043.
4. Zhan, Y.; Du, Xi.; Chen, H.; Liu, J.; Zhao, B.; Huang, D.; Li, G.; Xu, Q.; Zhang, M.; Weimer, B. C.; Chen, D.; Cheng, Z.; Zhang, L.; Li, Q.; Li, S.; Zheng, Z.; Song, S.; Huang, Y.; Ye, Z.; Su, W.; Lin, S. C.; Shen, Y.;Wu, Q.; *Nat. Chem. Biol*. **2008**, *4*, 548.
5. Voblikova, V. D.; Kobrina, N. S.; Gerasimova, N. M.; Pavlova, Z. N.; Dem'yanova, G. F.; Murygina,V. P.; Volosova, L. I.; Muromtsev, G. S.; *Chem. Nat. Comp.* **1985**, *21*, 362.
6. Rizvi, S. J. H.; Haque, H.; Singh, U. K.; Rizvi, V. A. A. In *Allelopathy: Basics and Applied Aspects*; Rizvi, S. J. H.; Rizvi, H., eds.; Chapman & Hall: London, 1992, pp. 1-10.
7. Weston, L. A.; *HortTechnology* **2005**, *15*, 529.
8. Vyvyan, J. R; *Tetrahedron* **2002**, *58*, 1631.
9. http://www.iea.sp.gov.br/out/index.php, accessed in June 2010.
10. Macías, F. A.; Marín, D.; Oliveros-Bastidas, A.; Varela, R. M.; Simonet, A. M.; Carrera, C.; Molinillo, J. M. G.; *Biol. Sci. Space* **2003**, *17*, 18.

11. Macías, F. A.; Marín, D.; Oliveros-Bastidas, A.; Chinchilla, D.; Simonet, A. M.; Molinillo, J. M. G.; *J. Agric. Food Chem.* **2006**, *54*, 991.
12. Wink, M.; Latz-Bruning, B.; In *Allelopathy: Organisms, Processes and Applications*; Inderjit, S.; Dakshini, K. M. M.; Einhellig, F. A., eds.; American Chemical Society: Washington DC, 1995, pp. 117-126.
13. Macías, F. A.; Varela, R. M.; Torres, A.; Oliva, R. M.; Molinillo, J. M. G.; *Phytochemistry* **1998**, *48*, 631.
14. Gary, A.; *Microb. Infect.* **2003**, *5*, 535.
15. Dos Santos, E. A.; Beatriz, A.; De Lima, D. P.; Marques, M. R.; Leite, C. B.; *Quim. Nova* **2009**, *32*, 1856.
16. Huang, H.; Zhang, L.; Zhang, X.; Ji, X.; Ding, X.; Shen, X.; Jiang, H.; Liu, H.; *Chin. J. Chem.* **2010**, *28*, 1041.
17. Olofsdotter, M.; Malik, A. U.; *Agron. J.* **2001**, *93*, 1.
18. Ferreira, A. G.; Aquila, M. E. A.; *Rev. Bras. Fisiol. Veg.* **2000**, *12*, 175.
19. Kruse, M.; Strandberg, M.; Strandberg, B.; *Ecological Effects of Allelopathic Plants – a Review*, NERI Technical Report No. 315, National Environmental Research Institute: Silkevorb, 2000.
20. Lobo, L. T.; Castro, K. C. F.; Arruda, M. S. P.; Silva, M. N.; Arruda, A. C.; Müller, A. H.; Arruda, G. M. S. P.; Santos, A. S.; Souza Filho, A. P. S.; *Quim Nova* **2008**, *31*, 493.
21. Berger, J.; Schager, M.; *Biologia (Bratislava)* **2004**, *59*, 9.
22. Olofsdotter, M.; Navarez, D.; Rebulanan, M.; Streibig, J. C.; *Weed Res.* **1999**, *39*, 441.
23. Narwal, S. S.; Sampietro, D. A.; Catalán, C. A. N.; Vattuone, M. A.; Politycka, B.; *Plant Bioassays*, Studium Press LLC: New Delhi, India, 2009.
24. Macias, F. A.; Varela, R. M.; Torres, A.; Oliva, R. M.; Molinillo, J. M. G.; *Phytochemistry* **1998**, *48*, 631.
25. Chon, S. -U.; Jang, H. -G.; Kim, D. K.; Kim, Y. -M.; Boo, H. O.; Kim, Y. J.; *Scientia Horticulcurae* **2005**, *106*, 309.
26. Blum, U.; Wentworth, T. R.; Klein, K.; Worsham, A. D.; King, L. D.; Gerig, T. M.; Lyu, S. W.; *J. Chem. Ecol.* **1991**, *17*, 1045.
27. Inderjit, S.; Dakshini, K. M. M.; *Tropical Agriculture* **1998**, *75*, 396.
28. Porter, W. L.; Thimann, K. V.; *Phytochemistry* **1965**, *4*, 229.

*Submitted: July 25, 2011*
*Published online: November 1, 2011*

*J. Braz. Chem. Soc.*, Vol. 23, No. 1, 132-141, 2012.
Printed in Brazil - ©2012 Sociedade Brasileira de Química
0103 - 5053 $6.00+0.00

Article

# Determination of Polychlorinated Biphenyls in Seawater using Headspace Solid-Phase Microextraction Coupled with Gas Chromatography-Mass Spectrometry with the Aid of Experimental Design

***Xingliang Song,*[*,a,b,#] Jinhua Li,[b,#] Lingxin Chen,*[*,b] Zongwei Cai,[c] Chunyang Liao,[b] Hailong Peng[d] and Hua Xiong[d]***

[a]*Department of Chemistry, Linyi University, Linyi 276005, P. R. China*

[b]*Key Laboratory of Coastal Zone Environmental Processes, CAS, Shandong Provincial Key Laboratory of Coastal Zone Environmental Processes, Yantai Institute of Coastal Zone Research, Chinese Academy of Sciences, Yantai 264003, P. R. China*

[c]*Department of Chemistry, Hong Kong Baptist University, Hong Kong SAR, P. R. China*

[d]*State Key Laboratory of Food Science and Technology, Nanchang University, Nanchang 330047, P. R. China*

Uma abordagem de pré-tratamento simples e confiável em cromatografia gasosa acoplada à espectrometria de massa (GC-MS) foi desenvolvida para a limpeza simultânea da água do mar e concentração de bifenilas policloradas (PCBs), com 1 a 8 átomos de cloro, baseada na combinação da oxidação de $KMnO_4$ com amostragem de headspace e microextração em fase sólida (SPME). Os fatores que afetam o processo de extração foram estudados usando uma abordagem multivariada. Sob condições ótimas, tais como fibra de PDMS com 7 μm, 78 °C de temperatura de extração, 33 min de tempo de extração e 8 mL de volume, os limites de detecção do método variaram entre 0,3 e 7,5 ng $L^{-1}$ e os valores de precisão variaram entre 3,9 e 9,9%, para um nível de fortificação de 0,05 μg $L^{-1}$ de PCBs. Ácidos húmicos da água do mar exibiram efeitos negativos marcantes; as recuperações de PCBs foram significativamente melhoradas, especialmente para os mais lipofílicos, CB171 e CB201, de 35% e 49% para 78% e 89%, respectivamente, após o pré-tratamento das amostras da água do mar com $KMnO_4$ em pH 6. O método desenvolvido mostrou-se simples, rápido, confiável e aplicável para a determinação de diferentes PCBs em água do mar contendo grandes quantidades de substâncias húmicas.

A simple and reliable pretreatment approach in gas chromatography-mass spectrometry (GC-MS) was developed for concurrent clean-up of seawater and the concentration of lipophilic polychlorinated biphenyls (PCBs) with 1-8 chlorine atoms based on the combination of $KMnO_4$ oxidation with headspace sampling and solid-phase microextraction (SPME). Factors affecting the extraction process were studied using a multivariable approach. Under optimum conditions such as PDMS 7 μm of fiber, 78 °C of extraction temperature, 33 min of extraction time, 8 mL of volume, the limits of detection ranged from 0.3 to 7.5 ng $L^{-1}$ and precisions were between 3.9 and 9.9% at spiked 0.05 μg $L^{-1}$ PCBs. Humic acids in seawater exhibited remarkably negative effects; recoveries of PCBs were significantly improved, especially for more lipophilic CB171 and CB201 from 35% and 49% to 78% and 89%, respectively, after $KMnO_4$ pretreating seawater samples at pH 6. The developed method was demonstrated to be simple, rapid, reliable and applicable for determining different PCBs in seawater containing large amounts of humic substances.

**Keywords:** polychlorinated biphenyls, headspace solid-phase microextraction, humic substances, experimental design, gas chromatography-mass spectrometry, seawater

*e-mail: lxchen@yic.ac.cn, xlssong@yeah.net
[#] Equally contributed to this work

## Introduction

Polychlorinated biphenyls (PCBs) constitute ubiquitous persistent environmental pollutants of great concern owing to their high toxicity and thereby potential risks for ecosystems and human health.[1-4] However, concentration levels of PCBs in contaminated environment are typically low in complex matrices.[5,6] Proper sampling and enrichment methods have to be employed to recover sufficient targeted compounds from suspended particulate matter or water phase.[7] This has promoted rapid developments in sample preparation and chromatographic techniques in the analysis of PCBs.[8,9]

Extraction and preconcentration techniques, such as liquid-liquid extraction (LLE), solid-phase extraction (SPE) and solid-phase microextraction (SPME), have been widely used to determine PCBs.[1,10,11] LLE and SPE are mainly used, but they have some fundamental limitations. LLE is a laborious, time consuming process and usually requires large amounts of high-purity and toxic solvents.[10] SPE is usually faster and consumes less organic solvents than LLE, however, for extraction from high volumes of water samples, the entire analysis of SPE might be lengthy and expensive because of a series of stages.[11,12] Thus, a relatively simple, rapid, cost-effective, and virtually solvent-free sample preparation method, SPME, has been greatly developed and applied to the determination of PCBs in different matrices, *e.g.*, soil, sediments, water, urine and milk.[13-18] As for water samples, humic substances are major components of dissolved organic matter (DOM)[5,19] and aquatic humic substances have been excellently characterized.[20] Humic acids significantly reduce the retention of PCBs and might cause insufficient recoveries attained.[14,20,21] Coupling of SPME with non-contact (between probe and samples) headspace sampling could greatly reduce matrix interferences for volatile compounds.[22-24] To quickly and reliably attain the best headspace SPME efficiency, various types experimental designs have been employed,[25-27] which assisted to optimizing the extraction conditions from a small number of experiments.[25-28] Moreover, headspace SPME allows using aggressive treatments to reduce their affinity with the sample matrix, and therefore further increases extraction yield.[29,30]

In this work, the feasibility of combining $KMnO_4$ strong oxidation and headspace SPME was demonstrated for pretreating seawater matrices containing numerous humic substances, followed by simultaneous identification and quantification of eight congeners of PCBs using gas chromatography-mass spectrometry (GC-MS). Key parameters affecting headspace SPME efficiency of trace PCBs in aqueous solutions were thoroughly evaluated, such as extraction fiber, extraction temperature, extraction solution volume, humic substance level, sample treatment modes and so on. During the optimization process, a factorial design was run to simultaneously study the influences of main parameters. The developed method was validated and successfully applied to analyze several PCBs in seawater samples.

## Experimental

### Chemicals and reagents

Individual standards of poly- CB1, CB5, CB29, CB47, CB98, CB154, CB171 and CB201 (IUPAC nomenclature) at 500 μg $L^{-1}$ in hexane were purchased from Supelco (Bellefonte, PA, USA). Their physicochemical property parameters are listed in Table 1.[31,32] Analytical grade $KMnO_4$, $K_2CrO_4$, concentrated $H_2SO_4$ (98%), potassium hydrogen phthalate (KHP), HCl (38%) and $H_2O_2$ (30%) were all acquired from Shanghai Sinopharm Chemical Reagent Company (Shanghai, China). HPLC grade methanol (MeOH) was obtained from Merck (Mollet del Vallés, Barcelona, Spain). Technical grade humic substances namely humic acids in the form of salt were supplied from Tianjin Chemical Research Institute (Tianjin,

**Table 1.** Physicochemical property parameters of PCBs

| IUPAC N. | Congeners | $t_R$[a]/min | Qualifiers (*m/z*) | Henry coefficients[31] - H (Pa $m^3$ $mol^{-1}$) | log $K_{ow}$[31,32] |
|---|---|---|---|---|---|
| CB1 | 2-Chlorobiphenyl | 6.5 | 188[b], 152 | ≥ 42.56 | 4.56 |
| CB5 | 2,3-Dichlorobiphenyl | 8.94 | 222, 152 | ≥ 17.0 | 5.15 |
| CB29 | 2,4,5-Trichlorobiphenyl | 11.26 | 256, 258, 186 | ≥ 24.29 | 5.77 |
| CB47 | 2,2', 4,4'-Tetrachlorobiphenyl | 13.23 | 292, 220, 290 | ≥ 17.2 | 6.26 |
| CB98 | 2,2',3',4,6-Pentachlorobiphenyl | 15.11 | 326, 324, 328 | ≥ 24.8 | > 6.2 |
| CB154 | 2,2',4,4',5,6'-Hexachlorobiphenyl | 17.39 | 360, 362, 290 | ≥ 11.9 | > 6.7 |
| CB171 | 2,2',3,3',4,4',6-Heptachlorobiphenyl | 21.26 | 394, 396, 324 | 5.40 | 7.44 |
| CB201 | 2,2',3,3',4,5',6,6'-Octachlorobiphenyl | 21.44 | 430, 428, 358 | 38.08 | 8.42 |

[a]Retention time. [b]Quantifiers.

China), which were dissolved in water and centrifuged at 2500 rpm for 30 min to remove insoluble parts of the technical grade product. Then humic acids at 14 mg $L^{-1}$ were spiked into seawater samples for use.

### Preparation of standards and seawater samples

Mixed standard stock solutions of the eight PCBs were prepared by successive dilutions with MeOH. Working solutions were prepared by subsequently successive dilutions according to Seawater Preparation Manual written by Subow's Recipe.[33] Both stock and working solutions were stored at 4 °C. Manual SPME holders and commercially available fiber coatings including polydimethylsiloxane (PDMS) of 100 μm and 7 μm (bonded), and carbowax/divinylbenzene (CW/DVB) (65 μm, bonded) were obtained from Supelco (Bellefonte, PA, USA). Prior to use, fibers were conditioned in a helium atmosphere according to the manufacturer's instructions. PDMS fiber withstood nearly 100 extraction runs in the headspace mode under normal limits. Highly purified (HPLC-grade) water was obtained by ultra filtration of deionized water with a Milli-Q system (Millipore, Bedford, MA, USA). All analyses were performed in 22 mL glass SPME vials, and the solutions were stirred with a thermostatic magnetic stirrer (Shanghai Laboratory Instrument Works Co., Ltd. Shanghai, China) using PTFE-coated magnetic stir bars (10 mm × 3 mm O.D.).

Surface seawater samples were collected into amber glass containers free of air bubbles, and immediately stored at 4 °C. The samples were filtered through 0.45 μm pore size membrane filters (Phenomenex) and analyzed within 24 h. The dissolved total organic carbon (TOC) samples were analyzed by using a TOC-$V_{CPH}$ analyzer (Shimadzu, Japan). The samples were acidified with 2 mol $L^{-1}$ HCl (pH < 2) to remove the inorganic carbonate, then purged with high purity $O_2$ (99.999%) for 5 min to remove the $CO_2$. Then 100 μL of the sample was injected into the quartz combustion tube to combust at 680 °C using platinum coated aluminum beads as catalyst. The samples were then cooled and the chlorine was removed with a halogen scrubber. Finally, the samples were measured in the nondispersive infrared (NDIR) detector (Apollo Electronics Co., Ltd, Shenzhen, China). The calibration curve was done with KHP in water (6 concentration levels). The coefficient variation was less than 2% (n = 3) and the water as reference was 3-7 μMC (*i.e.*, TOC in the water as reference was 3-7 μg $L^{-1}$). As a result, TOC was calculated at 1.23 mg $L^{-1}$ in the seawater samples.

The studied surface seawater samples were collected from six sampling sites, respectively, including Shilaoren Beach, Zhanqiao Pier Beach and Zhanshan Beach, all in Qingdao (Qingdao, China), and Laishan Beach, Moon Bay Beach and Golden Sands Beach, all in Yantai (Yantai, China). Three replicates were carried out and finally the results were averaged.

### Headspace SPME procedure

Eight milliliter (8 mL) seawater samples spiked with 1 μg $L^{-1}$ of PCB standard mixtures and a PTFE-coated magnetic stir bar were put into a 22 mL SPME vial with a PTFE septum and acidified to pH ≤ 1. Then 0.01 mol $L^{-1}$ $KMnO_4$ was added dropwise until a persistent violet solution was observed. The solution was stirred for 10 min, followed by the adding of $H_2O_2$ (10%) to form a colorless solution. After adjusting the solution acidity to approximately pH 6, the vial was sealed.

The solution was stirred with a magnetic hot stirrer (78 °C) at 800 rpm for 5 min. Then the SPME needle was inserted into the sample vial and the fiber was exposed in the headspace above sample for 33 min. After the extraction, the fiber was retracted into the needle which was removed from the septum and then immediately inserted into the GC injection port. Desorption time was set at 5 min to avoid a possible carryover effect. Desorption temperatures were set at 260 °C for CW/DVB, and 300 °C for PDMS. The vials were immediately sealed with hole-caps and PTFE/silicone septa for GC-MS analysis.

### GC-MS analysis

GC-MS analysis was carried out by using GC-MS-QP2010 plus with GC-MS solution software-based data handling (Shimadzu, Japan). QP2010 gas chromatograph coupled with a quadrupole mass spectrometer was operated in the electron ionization mode at 70 eV and mass spectra were acquired with a selected ion-monitoring (SIM) mode. An Rtx-5MS (30 m × 0.25 mm × 0.25 μm film thickness) column (Shimadzu, Japan) was used. The GC oven temperature was programmed from 80 °C (hold for 2 min) to 150 °C (hold for 3 min) at 20 °C $min^{-1}$, and was increased to 280 °C (hold for 5 min) at 8 °C $min^{-1}$. The injector temperature was held at 300 °C, and the injection was performed in a splitless mode (5 min). Helium (purity 99.999%) was employed as carrier gas at constant column flow of 1 mL $min^{-1}$. The chromatographic run was completed in 23 min. A solvent delay of 4.0 min was set to protect the filament from oxidation.

Mass spectra were obtained by acquiring data from *m/z* 50-500. Qualitative and quantitative analysis was completed by using the quantifiers coupled with other characteristic ions as qualifiers (Table 1).

## Results and Discussion

### Headspace SPME condition optimization

Multivariate optimization of selected working conditions for headspace SPME preparation and GC-MS determination were very important for the analysis of those PCBs at low concentrations in water.[34] As seen from Table 1, different numbers of chloro substituents of the eight congeners lead to different degrees of volatility and lipophilicity, namely, volatile or semi-volatile PCBs containing 1-6 chlorine atoms and low volatile and more lipophilic PCBs with 7 or 8 ones.

### Fiber evaluation

Fiber coating type largely affects the recoveries of analytes. Many types of commercial fibers are available for determining PCBs.[14] In this study, three commercial fibers (PDMS of 100 μm and 7 μm, and CW/DVB) were chosen for evaluation. Figure 1 shows the relative extraction efficiencies of PCBs (expressed by peak area of each compound). The semi-polar CW/DVB (bonded) fiber presented remarkably elevated extraction efficiency for the most volatile and polar CBs (1, 5 and 29). The non-polar PDMS fiber of 100 μm displayed a slightly higher extraction capacity for CB98 than that of 7 μm. The highest extraction efficiencies were attained by using the non-polar PDMS of 7 μm bonded fiber for more liposoluble CBs (47, 154, 171 and 201) due to the strong interactions between PDMS and CBs. Moreover, the thinner coating of PDMS speeded up mass transfer and shortened equilibrium time. Thus, also as a compromise for all the eight PCBs, the PDMS of 7 μm fiber was chosen for further study.

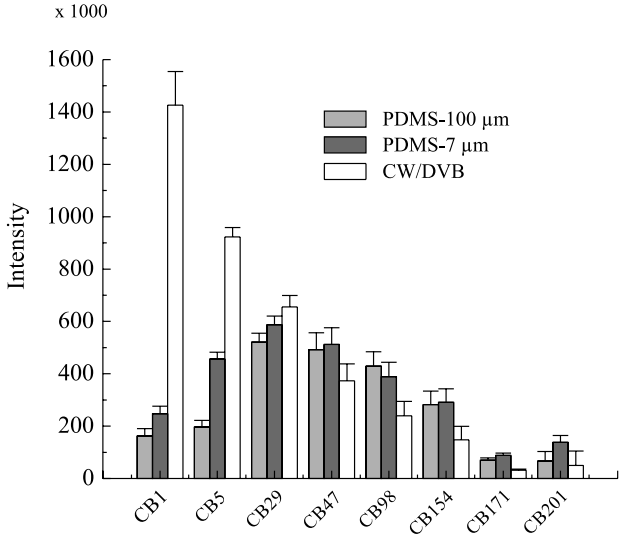


**Figure 1.** Headspace SPME efficiency obtained by using three different commercial fibers. Responses are the mean values for each fiber expressed as area counts, n = 80. Samples were maintained at 80 °C without the addition of humic substances, magnetically stirring at 800 rpm during extraction. These SPME parameters were optimized using 8 mL of manual seawater samples spiked with the eight PCBs individual at 1.0 μg $L^{-1}$ for each analysis.

### Factorial experimental design

A factorial design was run to simultaneously study the influences of main factors on micro-extraction process. The factors and levels included in the design were as follows: A, extraction temperature (60 and 80 °C); B, humic acid level (0 and 14 mg $L^{-1}$); C, extraction time (30 and 40 min); D, salinity (30 and 50%); and E, extraction solution volume (5 and 8 mL). Figure 2 shows the Pareto Charts.

As shown in Figure 2, extraction temperature was the most influential factor for the extraction of most PCBs. Extraction temperatures had negative effects on CBs (1, 5 and 29); this process could be explained by the slow diffusion of PCBs from sample to headspace phase, where excess PCBs present were to be sorbed on the SPME fiber.[35] This process differed for each PCB depending on difference in polarity, possible interaction with matrix components or volatility. Temperatures higher than 75 °C displayed positive effects on several CBs. At a higher temperature (80 °C), a marked decrease in the response for all the CBs was observed, possibly due to the displacement of equilibrium between fiber and headspace to the vapor phase, decreasing retention of compounds on the fiber surface. Therefore, 78 °C was selected.

The extraction time was also significant for most of the compounds. For CBs (1, 5 and 29), the negative effects played a relatively important role compared to that of the other four factors, while for other CBs, it was clear that the time factor was slightly significant (Figure 2). All the PCBs could be adsorbed into the stationary phase of the fiber coating, but the adsorption equilibrium time was different. Obviously, they increased with the decrease in the volatility of the PCBs. The limited stability of these 8 congeners was confirmed when long pre-heating periods were investigated. Very likely, the PCBs with a low degree of chlorination might also suffer a partial degradation when exposed, during prolonged time, to the strong oxidant conditions. The use of short equilibration time was also favorable to minimize the potential degradation of the PCBs.[14] Thus, the extraction time was finally set at 33 min.

The salting-out effect was not significant for all the compounds except CB201. As can be seen in Figure 2, the addition of salt was indicated to have only a very slight effect on the extraction of the seven PCBs. In case of CB201, the salinity factor predominated for extraction efficiency with negative effects. Such a decrease of

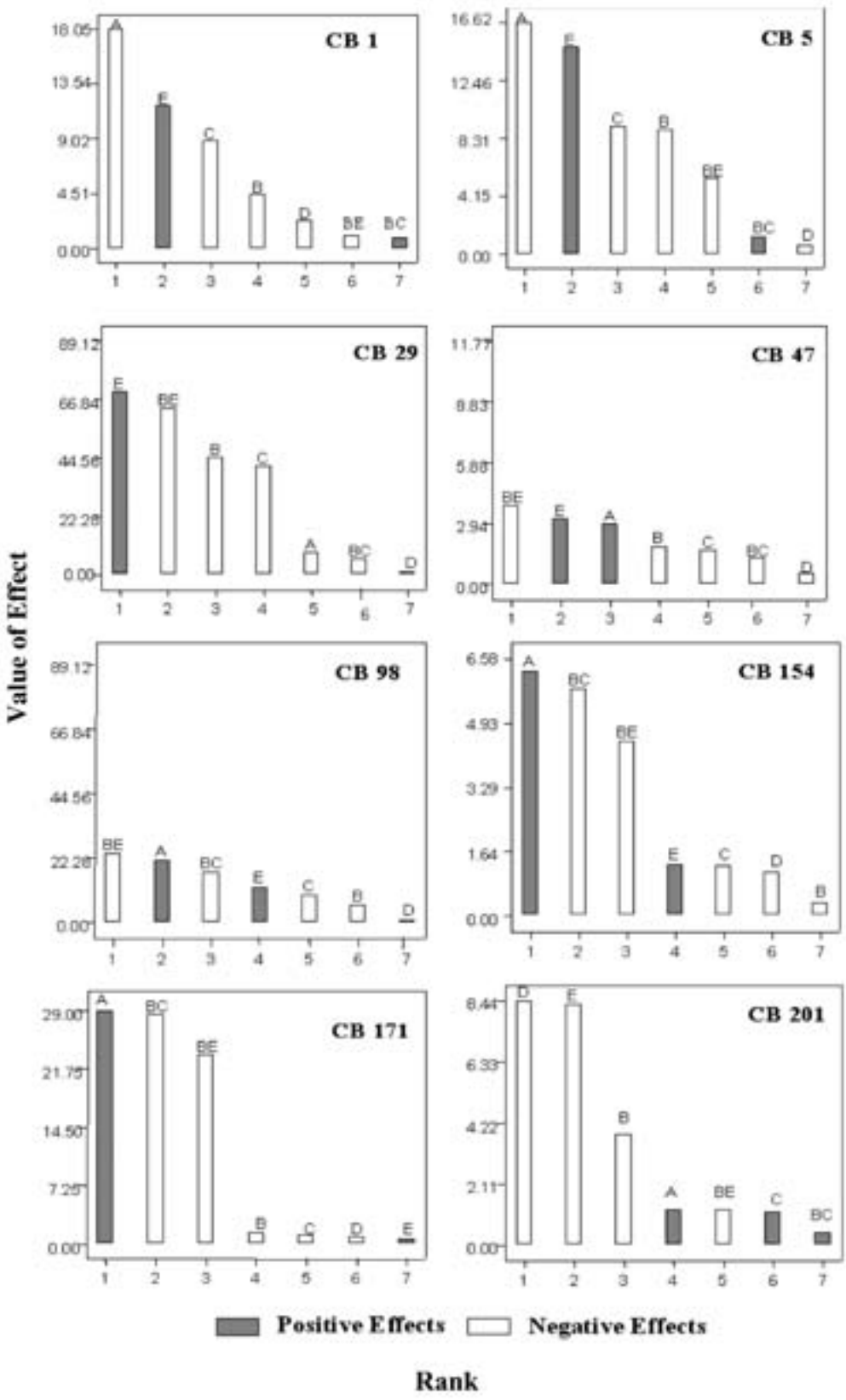


**Figure 2.** Standardized Pareto charts for the main effects and interactions. A: Temperature; B: humic acid; C: exaction time; D: salinity; and E: extraction solution volume. Factors and interactions that produced the lowest effects on the results obtained for each PCB have been removed except for the factor of humic acids. The length of each bar in the graphs is proportional to the absolute value of its associated standardized effect. The effects are displayed in decreasing order of importance, which assists to more easily identify the most important factors and the main effects.

extraction efficiency for high hydrophobic PCB might result from the increase of viscosity with the addition of salt, slowing down the extraction kinetics of the compound.[36] Therefore, for less volatile PCBs, it proved that removing the salts from seawater samples was very important.

As for the humic substance factor shown in Figure 2, extraction efficiencies for all the PCBs decreased with the concentration increasing of humic acids. The best results were attained at a very lower level or none of humic acids, meaning their negative effects were unavoidable during sampling seawater containing large amounts of humic substances. It can be attributed in part to the adsorption characteristics and binding phenomena of humic acids. Humic acids may affect the partition or adsorption processes of PCBs, since the association of PCBs with humic acids can lead to enhanced water solubility of the PCBs.[37] So, humic substances played a significantly negative role in extraction efficiency and their removal or decomposition became very imperative.

The effect of extraction solution volume on the response was also evaluated. As can be seen in Figure 2, the important variable presented positive influence for most congeners of the PCBs. Except for CB201, it was easily saturated into the fiber coating because of its smaller adsorption capacity. Since most compounds showed the higher extraction efficiency at 8 mL spiked samples volumes, it was selected. Higher volumes were not used to avoid the partial immersion of the fiber.

Regarding factor interactions, the most interesting one was the interaction between humic acids and extraction solution volume (BE), shown in Pareto Charts of Figure 2, indicating significant for most of the PCBs. The estimated response surfaces for the two factors were shown in Figure 3. A noticeable increase in headspace SPME efficiency was observed at an extraction volume of 8 mL for most PCBs. The efficiency improved when extraction volume increased with the amounts of humic acids decreasing (except CB201). At 8 mL, the two modes, with/without humic acids, were comparable for most of the analyzed PCBs. However, the fact that CB201 could be efficiently extracted at a lower extraction volume of 5 mL might appear unexpectedly, since the compound could be considered semi-volatile from the value of its Henry's law constant (Table 1). The same behavior had also been described for other compounds, such as polybrominated biphenyls and polybrominated diphenyl ethers.[38,39]

According to the above factorial design, the possible optimum conditions were obtained as follows: 78 °C of extraction temperature, 33 min of extraction time, 8 mL of extraction solution volume, and removing salts and humic substances from seawater samples.

### Effect of desorption temperature

The desorption temperature (250-310 °C) profile was studied. Peak areas of the PCBs increased with desorption temperature from 250 to 300 °C and remained constant from 300 to 310 °C. All the PCBs reached maximum response at 300 °C. The maximum endurable temperature of the 7 μm PDMS fiber was 320 °C. Hence, 300 °C as optimal desorption temperature was selected to avoid damage of the fiber.

The fiber coating indicated a quick adsorptions process. For a routine analysis, it is not necessary to reach complete adsorption equilibrium as long as sufficiently low detection limits were acquired. To prevent possible further damage from overusing the fiber, and thereby to increase its service life, 5 min desorption time was chosen.

### Sample treatment

Several seawater samples from six different beach sites were employed for comparisons of different treatment modes, spiked with the 8 PCBs individual at 0.1 μg $L^{-1}$ and humic acids at a total concentrations of 14 mg $L^{-1}$. The results gave identical comparison trends. Take seawater sample from Shilaoren Beach as an example. As shown in Figure 4, the most suitable seawater pretreatment mode prior to the extraction of PCBs was the use of $KMnO_4$. Addition of a small quantity of $KMnO_4$ remarkably improved the headspace SPME efficiency, particularly, for the more volatile PCBs (Figure 4). Perhaps the employment of these strong oxidative conditions reduced the DOM content in the extraction vessel and improved the kinetics and thermodynamics of the headspace SPME.[14] In some cases strong oxidant treatments by $K_2Cr_2O_7$ resulted in lower extraction recoveries as compared to untreated samples (Figure 4). This may be because the oxidizing potential of chromate is high enough to lead to decompositions of the PCBs. The lower responses for the untreated samples were attributed to the great capability of humic substances to enhance the solubility of the PCBs by adsorbing part of them or blocking the active sites of the adsorbents.[40] It is very necessary to preventively eliminate humic substances for accurate quantification of PCBs.[41] However, average responses for all compounds remained unaffected when pre-heating held for 5 min or were not assayed under the selected $KMnO_4$ treatment. It was evident that the oxidative action of $KMnO_4$ was relatively fast for PCBs, resulting in good determination stability. Thus, $KMnO_4$ was chosen for sample clean-up and removal of humic substances.

Also, the influence of pH value was investigated. As seen in Figure 5, best efficiency was achieved at pH 6,

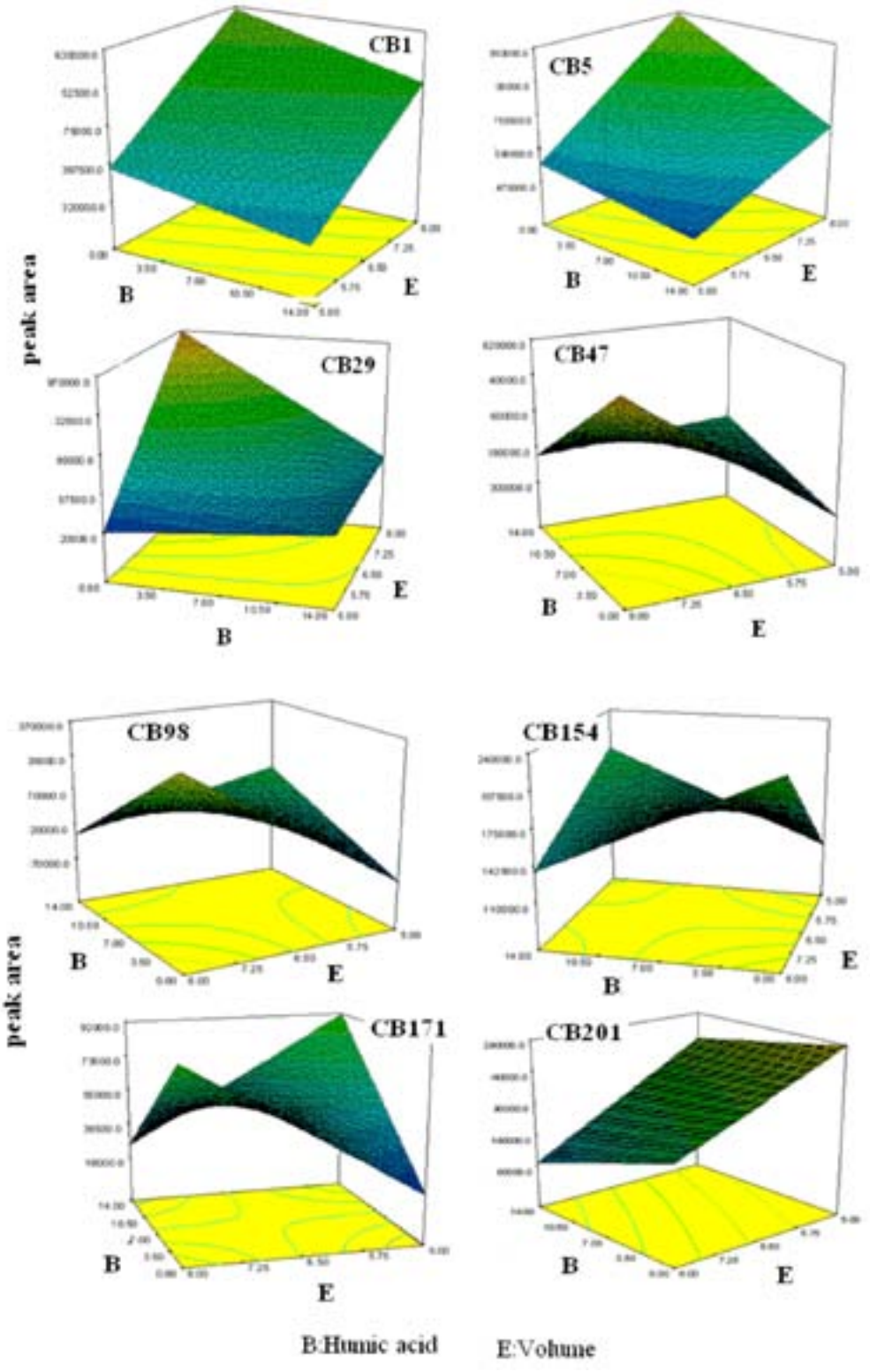


**Figure 3.** Estimated response surfaces (in area counts) for the factors of humic acid and extraction solution volume for the target PCBs.

which was reduced somewhat at pH 10, while much lower at pH 1. The liposoluble PCBs were volatile or semi-volatile; the acidity-basicity of targeted solution as a significant factor could affect the adsorption amounts of PCBs. The adverse acid effects on recovering PCBs were more obvious, probably, which would greatly decompose PCBs. Therefore, pH 6 was chosen as the optimal pH value for PCBs analysis from seawater samples.

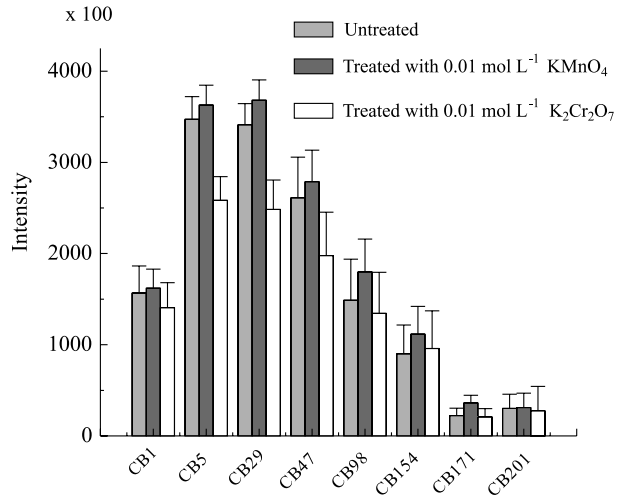


**Figure 4.** Comparison of the headspace SPME efficiency using three different pre-treatment modes on seawater spiked samples containing PCBs at 0.1 μg $L^{-1}$ and humic acids at a total concentration of 14 mg $L^{-1}$ (responses are the mean values for each mode expressed as area counts, n = 3 replicates).

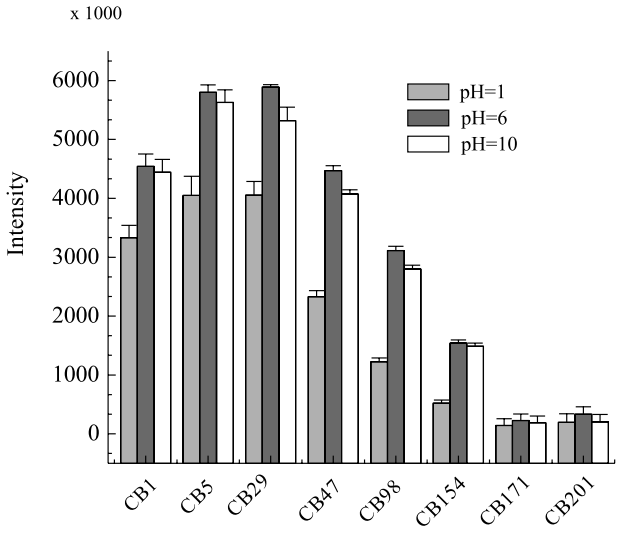


**Figure 5.** Headspace SPME efficiency at three different pH values for seawater spiked samples containing PCBs at 1.0 μg $L^{-1}$ and humic acids at a total concentration of 14 mg $L^{-1}$ (responses are the mean values for each mode expressed as area counts, n = 3 replicates).

## Method performance

The linearity of the developed method was evaluated using fractions of seawater spiked with increasing concentrations of the individual PCBs at five different concentration levels from 0.01-1.2 μg $L^{-1}$ for each congener except for CB171 and CB201 within 0.05-1.2 μg $L^{-1}$ (Table 2). Correlation coefficients of the obtained curves ranged from 0.974 to 0.998 showing an acceptable linearity within this interval of concentrations (Table 2). Carry-over effects were investigated by desorbing each 7 μm PDMS fiber twice, after being exposed to the seawater sample. When desorption conditions reported were employed, none of the considered PCBs were observed in the second injection with the exception of CB171 and CB201, which had only less than 3% residual quantities (data not shown). Precision was estimated by processing samples spiked at two levels (0.05 and 0.2 μg $L^{-1}$). Relative standard deviations (RSD) from 3.9 to 15% were obtained. Limits of detection (LODs) of the method, defined for a signal to noise (S/N) ratio of 3, were comprised between 0.3-7.5 ng $L^{-1}$ (Table 2). In spite of strong oxidative conditions of $KMnO_4$ in the SPME vessel for the removal of humic substances, PDMS fibers were used for around 70 extractions without noticeable changes in their efficiencies.

## Seawater sample analysis

To further demonstrate the feasibility of the developed method, it was applied to six surface seawater samples. The quantities of PCBs were calculated by the external standard method from an 8 mL seawater sample. It was observed that there was the similar detection result trends in spite of different values obtained from different sample matrices (Table 3). The endogenous PCBs in the seawater matrices were detected at higher levels when treated with $KMnO_4$ than without treatment; CB5 and CB201 were at too low levels to detect in all the samples; CB29 was not found in

**Table 2.** Analytical performances of PCBs obtained under the optimized headspace SPME conditions for spiked samples

| CB | Linear range / (μg $L^{-1}$) | Correlation coefficient (R) | RSD (%, n = 5) | | LOD / (ng $L^{-1}$) |
|---|---|---|---|---|---|
| | | | Added 0.05 μg $L^{-1}$ | Added 0.2 μg $L^{-1}$ | |
| 1 | 0.01-1.2 | 0.991 | 4.7 | 6.5 | 0.3 |
| 5 | 0.01-1.2 | 0.995 | 6.0 | 4.3 | 4.0 |
| 29 | 0.01-1.2 | 0.988 | 4.0 | 15.0 | 1.3 |
| 47 | 0.01-1.2 | 0.978 | 3.9 | 11.5 | 2.9 |
| 98 | 0.01-1.2 | 0.998 | 9.9 | 7.3 | 4.2 |
| 154 | 0.01-1.2 | 0.974 | 9.4 | 5.3 | 5.5 |
| 171 | 0.05-1.2 | 0.986 | 7.7 | 8.5 | 6.4 |
| 201 | 0.05-1.2 | 0.977 | 8.5 | 12.8 | 7.5 |

**Table 3.** Contents and recoveries of PCBs in 6 natural surface seawater samples determined by headspace SPME-GC-MS

| Source | Item | Modes | 1 | 5 | 29 | 47 | 98 | 154 | 171 | 201 |
|---|---|---|---|---|---|---|---|---|---|---|
| Shilaoren Beach | Found / (ng $L^{-1}$) | Untreated | 3.2 ± 0.23[a] | ND[b] | 3.8 ± 0.18 | 6.7 ± 0.15 | 7.1 ± 0.38 | 7.7 ± 0.39 | 9.1 ± 0.45 | ND |
| | | Treated | 7.1 ± 0.47 | ND | 4.4 ± 0.39 | 7.7 ± 0.39 | 8.2 ± 0.46 | 9.9 ± 0.42 | 12.6 ± 0.77 | ND |
| | Recovery / %[c] | Untreated | 92 ± 1.0 | 93 ± 2.2 | 91 ± 1.5 | 76 ± 1.5 | 65 ± 2.6 | 71 ± 4.2 | 36 ± 7.6 | 49 ± 4.2 |
| | | Treated | 95 ± 1.5 | 99 ± 1.6 | 97 ± 0.8 | 87 ± 2.0 | 76 ± 1.5 | 94 ± 2.5 | 69 ± 2.8 | 79 ± 4.2 |
| Zhanqiao Pier Beach | Found / (ng $L^{-1}$) | Untreated | 4.1 ± 0.34 | ND | 4.8 ± 0.25 | 5.6 ± 0.35 | 6.5 ± 0.32 | 8.7 ± 0.36 | 9.6 ± 0.41 | ND |
| | | Treated | 8.3 ± 0.55 | ND | 5.6 ± 0.41 | 6.7 ± 0.28 | 9.2 ± 0.51 | 9.6 ± 0.51 | 11.8 ± 0.84 | ND |
| | Recovery / % | Untreated | 93 ± 2.3 | 90 ± 1.6 | 92 ± 2.6 | 78 ± 2.5 | 68 ± 3.3 | 81 ± 5.2 | 38 ± 8.4 | 56 ± 5.2 |
| | | Treated | 97 ± 2.4 | 98 ± 1.3 | 99 ± 1.28 | 88 ± 2.6 | 79 ± 2.5 | 96 ± 3.7 | 78 ± 2.9 | 84 ± 3.2 |
| Zhanshan Beach | Found / (ng $L^{-1}$) | Untreated | 2.5 ± 0.43 | ND | 2.7 ± 0.16 | 5.7 ± 0.23 | 7.3 ± 0.48 | 6.7 ± 0.27 | 8.6 ± 0.53 | ND |
| | | Treated | 5.3 ± 0.32 | ND | 3.8 ± 0.22 | 8.3 ± 0.42 | 9.2 ± 0.55 | 8.5 ± 0.41 | 14.9 ± 0.91 | ND |
| | Recovery / % | Untreated | 90 ± 1.9 | 90 ± 3.2 | 90 ± 1.5 | 78 ± 2.1 | 70 ± 3.6 | 72 ± 4.3 | 45 ± 5.8 | 55 ± 5.1 |
| | | Treated | 92 ± 2.6 | 95 ± 1.5 | 95 ± 1.3 | 89 ± 2.3 | 81 ± 2.5 | 95 ± 2.7 | 79 ± 3.2 | 89 ± 5.7 |
| Laishan Beach | Found / (ng $L^{-1}$) | Untreated | 2.1 ± 0.15 | ND | ND | 5.8 ± 0.31 | 6.5 ± 0.47 | 7.5 ± 0.40 | 7.8 ± 0.51 | ND |
| | | Treated | 6.3 ± 0.36 | ND | ND | 7.4 ± 0.26 | 7.9 ± 0.26 | 9.6 ± 0.51 | 10.6 ± 0.54 | ND |
| | Recovery / % | Untreated | 90 ± 1.3 | 90 ± 2.6 | 89 ± 3.4 | 78 ± 2.3 | 72 ± 2.5 | 76 ± 5.2 | 45 ± 5.2 | 50 ± 5.1 |
| | | Treated | 95 ± 1.8 | 99 ± 2.5 | 94 ± 1.2 | 90 ± 2.0 | 80 ± 1.8 | 95 ± 2.4 | 70 ± 2.4 | 81 ± 3.6 |
| Moon Bay Beach | Found / (ng $L^{-1}$) | Untreated | 2.4 ± 0.16 | ND | ND | 4.5 ± 0.29 | 6.8 ± 0.51 | 6.9 ± 0.51 | 8.1 ± 0.35 | ND |
| | | Treated | 6.5 ± 0.51 | ND | ND | 6.3 ± 0.44 | 8.5 ± 0.55 | 9.5 ± 0.54 | 11.4 ± 0.69 | ND |
| | Recovery / % | Untreated | 90 ± 2.1 | 94 ± 3.5 | 90 ± 2.5 | 74 ± 2.5 | 60 ± 3.2 | 70 ± 3.2 | 35 ± 3.2 | 55 ± 5.2 |
| | | Treated | 97 ± 3.5 | 97 ± 2.7 | 95 ± 1.8 | 80 ± 2.3 | 75 ± 2.5 | 92 ± 2.1 | 70 ± 2.7 | 86 ± 5.7 |
| Golden Sands Beach | Found / (ng $L^{-1}$) | Untreated | 5.4 ± 0.64 | ND | ND | 5.8 ± 0.21 | 7.0 ± 0.56 | 7.4 ± 0.49 | 9.2 ± 0.62 | ND |
| | | Treated | 9.8 ± 0.75 | ND | ND | 7.3 ± 0.26 | 9.4 ± 0.66 | 9.6 ± 0.52 | 11.4 ± 0.81 | ND |
| | Recovery / % | Untreated | 93 ± 2.2 | 94 ± 2.8 | 90 ± 3.5 | 79 ± 2.3 | 68 ± 2.5 | 70 ± 4.1 | 39 ± 5.6 | 59 ± 3.2 |
| | | Treated | 97 ± 3.1 | 97 ± 2.7 | 96 ± 1.8 | 85 ± 3.1 | 79 ± 1.8 | 96 ± 2.7 | 70 ± 2.5 | 86 ± 5.6 |

[a]Averaged from three replicates. [b]Not detected. [c]Spiked each congener concentration at 0.1 μg $L^{-1}$.

the three beach sites of Yantai. Recoveries were calculated for the six spiked water samples with 0.1 μg $L^{-1}$ standards, respectively. Possibly due to the interferences of humic substances, poor recoveries for untreated seawater samples were relatively low, especially for CB171 and CB201 with only 35% and 49%, respectively (Table 3).

For the seawater samples treated with $KMnO_4$, the endogenous concentrations of PCBs were more sensitively determined and the recoveries were improved up to 69-99% (Table 3), which revealed that the strong oxidative activation of $KMnO_4$ reduced the content of humic substances and improved the kinetics and thermodynamics of the headspace SPME and therefore the extraction recoveries. The treated samples presented low DOM content and the recovery values were satisfactory.

## Conclusions

The addition of small amounts of $KMnO_4$ to seawater samples prior to headspace sampling with SPME extraction proved to be an effective, rapid, and convenient sample pretreatment approach to enhance the concentration detection sensitivity of PCBs using GC-MS. And the factorial design accelerated the gains of optimum headspace SPME conditions. The developed method provided acceptable linearity range, precision and LODs at ng $L^{-1}$ level. Sample treatment with $KMnO_4$ effectively minimized adverse effects of humic substances and presented high extraction efficiency and recoveries. The use of the headspace SPME device and the $KMnO_4$ treatment would allow the automation of the whole sample preparation step and increase the applicability of the developed method in screening studies. The method could be further improved by including other congeners and/or appropriate internal standards in order to minimize matrix effects during the extraction steps.

## Acknowledgments

This work was financially supported by the National Natural Science Foundation of China ((20975089, 21105117, 20907039), the Department of Science and Technology

of Shandong Province of China (2010GSF10222), the Natural Science Foundation of Shandong Province of China (Y2007B38, ZR2010BQ027), the Innovation Projects of the Chinese Academy of Sciences (KZCX2-EW-206), the Key Laboratory Foundation of Soil and Water Conservation and Environmental Conservation of Shandong Province of China (STKF201010), the Programs of State Key Laboratory of Food Science and Technology of Nanchang University of China (SKLF-KF-201006, SKLF-MB-201005), the Yantai Research and Development Program of China (2010158, 2007323), and the 100 Talents Program of the Chinese Academy of Sciences.

## References

1. Lambropoulou, D. A.; Konstantinou, I. K.; Albanis, T. A.; *J. Chromatogr., A* **2006**, *1124*, 97.
2. Liu, S. J.; Zhang, S. P.; Qu, C.; Liu, W.; Du, Y. G.; *Sci. Chin. Chem.* **2010**, *53*, 974.
3. Oberson, D; Lafon, D; *Arch. Mal. Prof. Environ.* **2010**, *71*, 141.
4. Matsui, T.; Uchimura, T.; Imasaka, T.; *Anal. Chim. Acta* **2011**, *684*, 108.
5. Botero, W. G.; de Oliveira, L. C.; Cunha, B. B.; de Oliveira, L. K.; Goveia, D.; Rocha, J. C.; Fraceto, L. F.; Rosa, A. H.; *J. Braz. Chem. Soc.* **2011**, *22*, 1103.
6. Wang, Y. H.; Li, Y. Q.; Zhang, J.; Xu, S. F.; Yang, S. G.; Sun, C.; *Anal. Chim. Acta* **2009**, *646*, 78.
7. Song, X. L.; Li, J. H.; Liao, C. Y.; Chen, L. X.; *Chromatographia* **2011**, 74, 89.
8. Quintanilla-Lopez, J. E.; Galindo-Iranzo, P.; Gomara, B.; Lebron-Aguilar, R.; *J. Chromatogr., A* **2010**, *1217*, 7231.
9. Liu, X. J.; Zhao, A. J.; Zhang, A. N.; Liu, H. Q.; Xiao, W. J.; Wang, C. J.; Wang, X. D.; *J. Sep. Sci.* **2011**, *34*, 1084.
10. Toledo, C.; Valle, L.; Narvaez, J.; Richter, P.; *J. Braz. Chem. Soc.* **2007**, *18*, 937.
11. Yang, F. X.; Jin, S. W.; Meng, D. Y.; Xu, Y.; *Chemosphere* **2010**, *81*, 1000.
12. Li, J. H.; Cai, Z. W.; Xu, S. F.; Liao, C. Y.; Song, X. L.; Chen, L. X.; *J. Liq. Chromatogr. Relat. Technol.* **2011**, *34*, 1578.
13. Poli, D.; Caglieri, A.; Goldoni, M.; Castoldi, A. F.; Coccini, T.; Rod, E.; Vitalone, A.; Ceccatelli, S.; Mutti, A.; *J. Chromatogr., B: Anal. Technol. Biomed. Life Sci.* **2009**, *877*, 773.
14. Montes, R.; Ramil, M.; Rodriguez, I.; Rubi, E.; Cela, R.; *J. Chromatogr., A* **2006**, *1124*, 43.
15. Hawthorne, S. B.; Grabanski, C. B.; Hageman, K. J.; Miller, D. J.; *J. Chromatogr., A* **1998**, *814*, 151.
16. Cortazar, E.; Zuloaga, O.; Sanz, J.; Raposo, J. C.; Etxebarria, N.; Fernandez, L. A.; *J. Chromatogr., A* **2002**, *978*, 165.
17. Hong, J. E.; Pyo, H.; Park, S. J.; Lee, W.; *Anal. Chim. Acta* **2005**, *539*, 55.
18. Kowalski, C. H.; Costa, J. G.; Godoy, H. T.; Augusto, F.; *J. Braz. Chem. Soc.* **2010**, *21*, 502.
19. Thurman, E. M. In *Organic Geochemistry of Natural Waters*; Martinus Nijhoff/Dr WJunk Publishers: Dordrecht, 1985.
20. Rodriguez, F. J.; Nunez, L. A.; *Water Environ. J.* **2011**, *25*, 163.
21. Otaka, H.; Shimono, H.; Hashimoto, S.; *Anal. Bioanal. Chem.* **2004**, *378*, 1854.
22. Ma, J. P.; Lu, W. H.; Li, J. H.; Song, Z. W.; Liu, D. Y.; Chen, L. X.; *Anal. Lett.* **2011**, *44*, 1544.
23. Vichi, S.; Castellote, A.; Pizzale, L.; Conte, L. S.; Buxaderas, S.; Lopez-Tamames, E.; *J. Chromatogr., A* **2003**, *983*, 19.
24. Ma, J. P.; Xiao, R. H.; Li, J. H.; Li, J.; Shi, B. Z.; Liang, Y. J.; Lu, W. H.; Chen, L. X.; *J. Sep. Sci.* **2011**, *34*, 1477.
25. Dron, J; Garcia, R; Millan, E.; *J. Chromatogr., A* **2002**, *963*, 259.
26. Larreta, J.; Vallejo, A.; Bilbao, U.; Alonso, A.; Arana, G.; Zuloaga, O.; *J. Chromatogr., A* **2006**, *1136*, 1.
27. Liorente, D. D.; Abrodo, P. A.; de la Fuente, F. D.; Alvarez, J. G.; Alvarez, M. D. G.; Gomis, D. B.; *J. Sep. Sci.* **2011**, *34*, 1293.
28. Wen, Y. Y.; Li, J. H.; Zhang, W. W.; Chen, L. X.; *Electrophoresis* **2011**, *32*, 2131.
29. Llompart, M.; Pazos, M.; Landin, P.; Cela, R.; *Anal. Chem.* **2001**, *73*, 5858.
30. Shu, Y. Y.; Wang S. S.; Tardif, M.; Huang, Y. P.; *J. Chromatogr., A* **2003**, *1008*, 1.
31. Wang, L. S.; Han, S. K.; *Organic Pollution Progress in Chemistry*, Chemical Industry Press: Beijing, 1998.
32. Mackay, D.; Shiu, W. Y.; Ma, K. C.; Lee, S. C.; *Handbook of Physical-Chemical Properties and Environmental Fate for Organic Chemicals*, 2nd ed., Lewis: Boca Raton, 2006.
33. Zhang, Z. B.; Liu, L. S.; *Marine Physical Chemistry*, Science Press: Beijing, 1989.
34. Mmualefe, L. C.; Torto, N.; Mapil, P. H.; Mbongwe, B.; *Microchem. J.* **2009**, *91*, 239.
35. Serrano, E.; Beltrán, J; Hernández, F.; *J. Chromatogr., A* **2009**, *1216*, 127.
36. Quintana, J. B.; Rodil, R.; Muniategui-Lorenzo, S.; Lopez-Mahia, P.; Prada-Rodriguez, D.; *J. Chromatogr., A* **2007**, *1174*, 27.
37. Knulst, J. C. C.; *Environ. Toxicol. Chem.* **1992**, *11*, 1209.
38. Landin, P.; Lompart, M.; Lourido, M.; Cela, R.; *J. MIcrocolumn Sep.* **2001**, *13*, 275.
39. Polo, M.; Gómez-Noya, G.; Quintana, J. B.; Lompart, M.; García-Jares, C. C. R.; *Anal. Chem.* **2004**, *76*, 1054.
40. Wu, J. X.; Cao, L.; Wang, H. Z.; *Metall. Anal.* **2006**, *26*, 1.
41. Christoforids, A.; Stamatis, N.; Schmieder, K.; Tsachalidis, E.; *Chemosphere* **2008**, *70*, 694.

*Submitted: September 22, 2010*
*Published online: November 3, 2011*

*J. Braz. Chem. Soc.*, Vol. 23, No. 1, 142-147, 2012.
Printed in Brazil - ©2012 Sociedade Brasileira de Química
0103 - 5053 $6.00+0.00

Article

# A Method for Determination of Ammonia in Air using Oxalic Acid-Impregnated Cellulose Filters and Fluorimetric Detection

***Erika P. Felix[a] and Arnaldo A. Cardoso*[*,b]***

*[a]Departamento de Química e Biologia, Universidade Tecnológica Federal do Paraná, Av. Sete de Setembro 3165, Rebouças, 80230-901 Curitiba-PR, Brazil*

*[b]Instituto de Química, Universidade Estadual Paulista, CP 355, 14800-900 Araraquara-SP, Brazil*

Um método fluorimétrico foi adaptado para determinação de amônia no ar ambiente. A coleta da amostra foi feita em filtros de celulose impregnados com ácido oxálico, seguida pela solubilização do íon amônio, adição dos reagentes e determinação fluorimétrica. Alguns parâmetros analíticos importantes foram avaliados, tais como tempo e vazão de amostragem. Formaldeído, dietilamina e sulfeto de hidrogênio não interferiram no método. A curva analítica apresentou linearidade até pelo menos 34 ppbv, em vazão e tempo de amostragem respectivos de 0,3 L $min^{-1}$ e 20 min. Nestas condições, o limite de detecção alcançado foi de 3 ppbv. O método proposto aqui apresentou resultados similares ao método colorimétrico do indofenol, porém necessitou de um tempo de amostragem menor. Mostrou ser de fácil aplicação, sendo útil para medir baixas concentrações de amônia e possíveis flutuações na sua concentração em intervalos de tempo curtos, como 20 min.

A fluorimetric method was developed for the determination of ammonia in ambient air. Samples were collected using cellulose filters impregnated with oxalic acid, followed by solubilization of the ammonium ion, addition of reagents and fluorimetric detection. Important analytical parameters that were evaluated included sampling time and flow rate. Formaldehyde, diethylamine and hydrogen sulfide did not interfere in the method. The analytical curve was linear up to at least 34 ppbv of ammonia, using a sample flow rate of 0.3 L $min^{-1}$ and a sampling time of 20 min. The limit of detection achieved under these conditions was 3 ppbv. The proposed method offers advantages compared to the indophenol colorimetric method, especially the ability to use a shorter sampling time. The method proved to be easy to apply, and should be useful in applications where measurements of low concentrations of ammonia are required, or where there are rapid fluctuations in ammonia concentrations over periods as short as 20 min.

**Keywords**: gaseous ammonia, acid-impregnated filter, fluorimetric detection, *o*-phthaldialdehyde, isoindole

## Introduction

Ammonia ($NH_3$) is found naturally in ambient air, as well as emitted from anthropogenic sources, and plays a role in atmospheric chemistry. It has many sources, including agriculture, fossil fuel combustion, industrial emissions and biochemical processes in natural soils.[1-4] Food production is a significant source of ammonia, with emissions occurring due to application of fertilizer or manure to soils and volatilization from animal waste.[5-7] Close to the source, $NH_3$ is deposited onto vegetation, soil and water, and consequently may both modify acidity and increase the availability of nitrogen, which can lead to eutrophication of surface waters.[8] $NH_3$ is considered an important pollutant due to its role as a precursor in fine particulate matter formation, in the formation of the greenhouse gas nitrous oxide ($N_2O$), and in the nitrogen balance of ecosystems.[9-11] The fine particulates formed in the atmosphere due to acid-base reactions of ammonia with acidic sulfur- and nitrogen-containing gases are responsible for long-range transport of nitrogen and sulfur.[12,13] In many regions, a large fraction of airborne fine particulate matter consists of ammonium salts formed during neutralization of atmospheric acid gases. The incorporation of ammonia in the aqueous phase of the aerosol enhances the solubility of $SO_2$, and increases its oxidation rate.[12] High levels of

*e-mail: acardoso@ iq.unesp.br

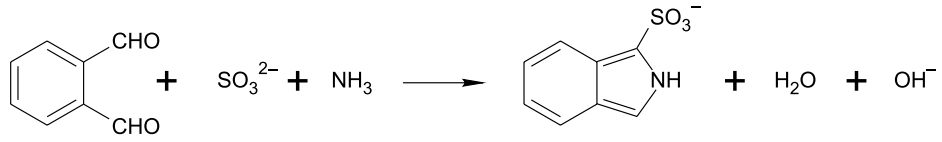


**Figure 1.** Schematic of the reaction between ammonia and *o*-phthaldialdehyde in the presence of sulfite.

ammonia are of concern in large-scale animal production, for reasons of hygiene and odor, since adequate indoor air quality in buildings housing animals is essential for the health of agricultural workers and livestock.[14]

Concentrations of ammonia in the lower troposphere are usually low. For example, in central São Paulo State levels of ammonia in the range 0.5-3.4 ppb have been found even close to sources such as agricultural areas and biomass burning.[15] This can be explained by the reactivity and solubility of ammonia, as well as its fairly rapid dry deposition close to emission sources, which results in a short atmospheric lifetime.[16]

Evaluation of the emission rates, transport and fate of ammonia requires information concerning its atmospheric concentration. Spectroscopic methods such as photofragmentation laser-induced fluorescence, differential optical absorption spectroscopy (DOAS), Fourier transform infrared (FTIR) spectroscopy are expensive, require a dedicated operator, and are not suitable for routine application.[1,17] The low atmospheric concentration of ammonia limits the applicability of many chemical measurement methods, which normally require a preconcentration step. Procedures involving absorption using acidic solutions,[18] coated-wall denuders[19] and acid-impregnated filters[20,21] have been reported in the literature for the collection of ammonia. Although methods using acid-impregnated filters generally require a long sampling time, the use of filters is highly practical for field measurements. After extraction into aqueous solution, detection of dissolved ammonium ions has been performed by photometry[22] and ion chromatography.[23]

An attraction of fluorescence-based techniques is their sensitivity, which is usually one to three orders of magnitude better than that of absorbance-based systems. A variety of fluorescence and chemiluminescence methods have been proposed as a result.[24-26] In the 1970s, Roth described a fluorescence reaction for ammonia with *o*-phthaldialdehyde and 2-mercaptoethanol.[27] Jacobs[25] suggested that sulfite offered advantages as a reducing agent, compared to 2-mercaptoethanol, and Genfa and Dasgupta[28] confirmed that the spectral characteristics of the OPA-sulfite reaction product are considerably more attractive for fluorimetric detection than the corresponding product obtained using 2-mercaptoethanol. The use of the OPA-sulfite reaction for the determination of ammonia has mainly focused on its measurement in water.[29,30] Westra *et al.*[31] employed a fluorimetric method for determination of ammonia in air and breath, although the collection of gaseous $NH_3$ into a nitrogen-cooled sample trap, equipped with Teflon inlet and outlet valves and a pressure sensor, limits its use in the field. Groves *et al.*[32] proposed the collection of ammonia in a sorbent tube containing 100 mg of acid-treated silica gel.

In this paper, we propose the use of oxalic acid-impregnated cellulose filters to collect gaseous ammonia, with analysis using fluorescence based on chemical reaction of ammonia with *o*-phthaldialdehyde and sodium sulfite (Figure 1). The advantages of this approach are the use of a sampling device that is low cost, easy to prepare and readily deployed for field measurements, together with a highly sensitive analytical technique.

## Experimental

### Ammonia-free water

Ammonia is highly soluble in water, so that it is difficult to store ammonia-free water in the laboratory without potential contamination from the ammonia present in indoor air. In the present work, ammonia-free water was prepared daily by further purifying distilled water by reverse osmosis. This water was used to prepare all solutions employed during the development of the proposed method.

### Reagent solutions

Six solutions of *o*-phthaldialdehyde (Aldrich) were prepared, at concentrations ranging from 0.0125 to 0.05 mol $L^{-1}$. Portions of *o*-phthaldialdehyde were dissolved in 2.5 mL of methanol, followed by addition of water to make up to a final volume of 10 mL. These solutions were stored refrigerated for up to 1 week. Four sodium sulfite (Merck) solutions were prepared by dissolving 0.0126 to 0.0630 g of the salt in phosphate buffer, made up to a final volume of 10 mL. The phosphate buffer was prepared by dissolution of 6.7 g of $Na_2HPO_4$ in 200 mL of water, adjusting the pH to 11 with 2 mol $L^{-1}$ NaOH, and diluting to 250 mL. These solutions were prepared daily. The coating

solution was prepared by dissolving 50 g of oxalic acid (Mallinckrodt) and 20 mL of glycerol (Merck) in water, with the volume made up to 1 L.

### Preparation of sampling filters

Whatman N. 41 cellulose filters were cut into 15 mm diameter circles. Any ammonium contamination was then removed by soaking the filter circles in deionized water for two days, changing the water four times daily. The filters were then immersed in oxalic acid solution for 4 h, and rinsed with water. Finally, the filter circles were immersed overnight in a 5% (m/v) oxalic acid/glycerol solution, and dried in a desiccator for at least 24 h. The dry filters were wrapped in oxalic acid-impregnated filter paper, and stored in a refrigerator prior to use.

### Sampler arrangement

The sampler arrangement used to house the impregnated filters was constructed as previously described by Felix *et al.*[33] The sampler was adapted from a 12 mL hypodermic syringe, from which part of the body had been removed (Figure 2). The impregnated filter was placed at the bottom of the sampler, and a plastic ferrule was used to seal the air inlet before and after sampling.

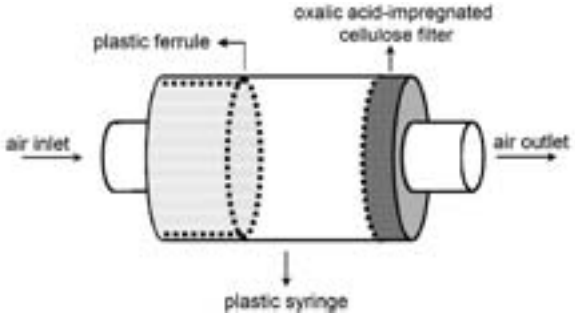


**Figure 2.** Sketch of the components of the ammonia sampler.

### Generation of ammonia standard gas mixture

The equipment used for ammonia standard gas generation is illustrated in Figure 3, and followed the same procedure described previously.[34] An ammonia permeation tube device (VICI Metronics, Santa Clara), certified to release $NH_3$ at a rate of 22.9 ng $min^{-1}$ (at 30 °C), was placed inside the permeation chamber and maintained at a constant temperature of 30.0 ± 0.1 °C. Air was purified by passage through three sequential columns (20 mm × 40 cm) containing silica gel (A1), activated carbon (A2) and oxalic acid solution supported on silica gel (A3). One portion of the flow of pure air was directed to the permeation chamber, at 1.0 L $min^{-1}$. This primary stream (FC2) could be diluted with a second pure air stream (FC3). A desired portion of the resultant total flow was sampled (FC5), and the remainder of the standard gas was discarded with the aid of a vacuum pump (P) controlled by a needle valve (NV3).

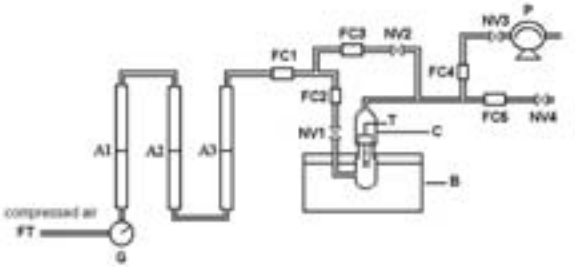


**Figure 3.** Ammonia gas generation system: FT, total flow rate; G, pressure gauge; A1-3, sequential columns for air purification; FC1-5, flowmeters; NV1-4, needle valves; C, permeation chamber; T, permeation tube; B, thermostatic bath; P, vacuum pump.

### Experimental protocol

The following experimental protocol was used: (*i*) a filter impregnated with oxalic acid was loaded into the sampler; (*ii*) after sampling, the filter was placed inside a hypodermic syringe (12 mL) without the piston. The filter was shaken with about 3.0 mL of water. This solution was forced out into a 5.0 mL volumetric flask with the aid of the piston; (*iii*) 1.0 mL of *o*-phthaldialdehyde solution was added, followed by 1.0 mL of sodium sulfite solution, with the final volume made up to 5.0 mL; (*iv*) after formation of the fluorescent product, the fluorescence of the solution was measured using a Shimadzu RF-1501 spectrofluorimeter ($\lambda_{ex}$ = 360 nm and $\lambda_{em}$ = 425 nm), with an optical length of 10 mm.

Measurements of blank were made following the same procedure of the samples, but without exposure of the filter system to generate ammonia. The difference signal between sample and blank was considered as analytical signal.

## Results and Discussion

### Optimum fluorescence

Initially, experiments were performed using three different sampling times (0, 30 and 60 min) and an ammonia concentration of 34 ppbv, at a sampling flow rate of 0.4 L $min^{-1}$ and reaction time of 30 min. After sampling, the ammonium collected in the filters was extracted with deionized water, and the reagents added as described previously. The excitation and emission spectra of the fluorescent product were investigated using the

spectrofluorimeter, and the results of the scans (Figure 4) showed that the greatest fluorescence response occurred at an excitation wavelength of 360 nm and an emission wavelength of 425 nm.

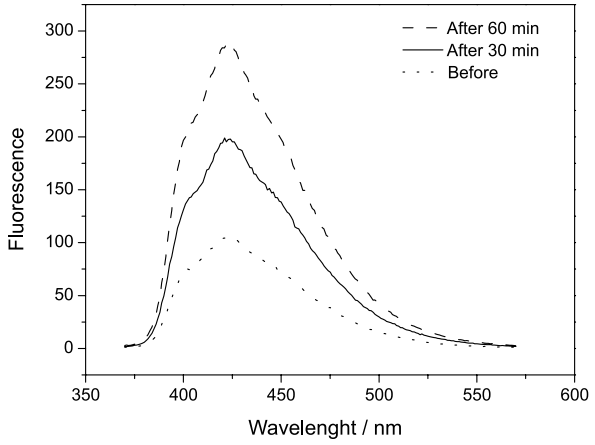


**Figure 4.** Fluorescence spectra of the product of the reaction between ammonia (34 ppbv), *o*-phthaldialdehyde and sulfite during three stages: before sampling of ammonia, after 30 min of sampling, and after 60 min of sampling. Excitation wavelength set at 360 nm, sampling flow rate of 0.4 L $min^{-1}$ and reaction time of 30 min.

## Influence of o-phthaldialdehyde and sodium sulfite concentrations

The influences of *o*-phthaldialdehyde and sodium sulfite concentrations on the fluorescent product were studied using an ammonia concentration of 34 ppbv, a sampling time of 20 min, sampling flow rate of 0.3 L $min^{-1}$ and reaction time of 15 min (Figure 5). The best analytical signal was obtained with an *o*-phthaldialdehyde concentration of 0.025 mol $L^{-1}$ and a sulfite concentration between 0.02 and 0.04 mol $L^{-1}$. In subsequent experiments, the concentrations of *o*-phthaldialdehyde and sodium sulfite used in all procedures were 0.025 mol $L^{-1}$ and 0.03 mol $L^{-1}$, respectively.

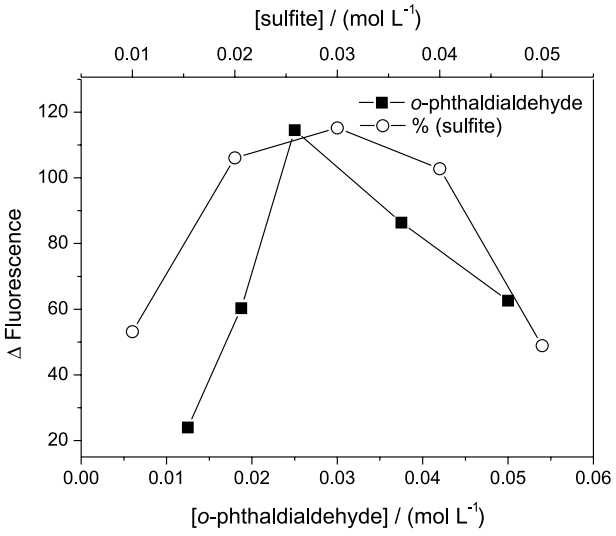


**Figure 5.** Analytical signals obtained as a function of *o*-phthaldialdehyde and sulfite concentrations. Conc. $NH_3$ = 34 ppbv, sampling flow rate = 0.3 L $min^{-1}$, sampling time = 20 min, reaction time = 15 min. Excitation ($\lambda_{exc}$) and emission ($\lambda_{em}$) wavelengths of 360 nm and 425 nm, respectively.

## Effect of sampling time

The duration of sampling is an important parameter in all atmospheric analyses that include a preconcentration step. The influence of sampling time was investigated using a sampling flow rate of 0.3 L $min^{-1}$ and an ammonia concentration of 34 ppbv. The results obtained are shown in Figure 6.

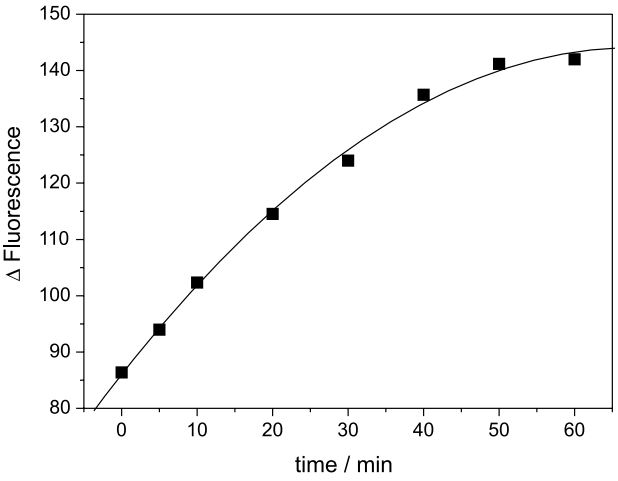


**Figure 6.** Analytical signal as a function of sampling time. Conc. $NH_3$ = 34 ppbv, sampling flow rate = 0.3 L $min^{-1}$, reaction time = 15 min, $\lambda_{exc}$ = 360 nm, $\lambda_{em}$ = 425 nm.

The analytical signal initially increased linearly with increasing sampling time, before reaching a maximum. The data points could be fitted by a second-degree polynomial as follows,

$$\Delta S = 86.04 + 1.703\ t - 0.01254\ t^2 \qquad R = 0.9970 \qquad (1)$$

where ΔS is the fluorescence signal and t is the sampling time in minutes. If the impregnated filter collected ammonia with no change in efficiency with time, the points would be expected to be connected by a straight line. However, linearity was only observed for short sampling times (*ca.* 20 min), when the quadratic term of the equation was insignificant compared with the other terms. In accordance with equation 1, a sampling time of 20 min was selected, which ensured good linearity (with a maximum deviation of only 4%) between the amount of ammonia and the fluorescence signal.

### Effect of sampling flow rate

For the same sampling time, an increased flow means that a greater number of molecules reach the impregnated filter, although increased breakthrough at higher flow rates results in the samplers being most efficient within a fairly narrow flow rate range. Here, 34 ppbv of ammonia was passed through the impregnated filter for 20 min, and the gas flow rate was varied from 0.1 to 0.5 L $min^{-1}$. The results are shown in Table 1.

**Table 1.** Analytical signal as a function of sampling flow rate. Conc. $NH_3$ = 34 ppbv, sampling and reaction times of 20 and 15 min, respectively. $\lambda_{exc}$ = 360 nm, $\lambda_{em}$ = 425 nm.

| Sampling flow rate / (L $min^{-1}$) | Δ Fluorescence |
|---|---|
| 0.1 | 34.06 |
| 0.2 | 92.14 |
| 0.3 | 114.53 |
| 0.4 | 115.97 |
| 0.5 | 114.26 |

The fluorescence signal increased with increasing sampling rate, reaching a maximum at 0.3 L $min^{-1}$, after which no further improvement in the signal was observed. This was the sampling flow rate chosen for subsequent experiments.

### Interferences

Possible interferences in the analytical signal due to the presence of other reactive molecules were investigated using the three gases diethylamine, formaldehyde and hydrogen sulfide. Air/ammonia standard gas mixtures were contaminated with these gases emitted from permeation tubes (VICI Metronics, Santa Clara, CA). The results showed that no interferences occurred, even when the gases were present at levels three times higher than the ammonia concentration.

The determination of N (−III) by reaction with *o*-phthaldialdehyde can be used for amines and amino acids, as well as ammonia.[25] However, in the present application the use of oxalic acid as the reagent for impregnation of filters to collect ammonia appears to be advantageous, since oxalic acid is shown to be highly inefficient for collection of diethylamine (and, by inference, other amines).

### Sensitivity and limits of detection

The response of the method was investigated using different ammonia concentrations. Here, the sampling flow rate was 0.3 L $min^{-1}$, the sampling time was 20 min and the reaction time was 15 min. The ammonia concentrations ranged from 0 to 34 ppbv (concentrations exceeding this range are not usually encountered in the outdoor atmosphere).[1,21] Three samples were collected at each concentration, and the averages calculated. The following linear relationship was obtained,

$$\Delta S = (71.65 \pm 0.25) + (1.30 \pm 0.02)\,[NH_3] \quad R = 0.9997 \quad (2)$$

where ΔS represents the fluorescence analytical signal, and $[NH_3]$ the ammonia concentration (in ppbv). Although the upper limit of linearity was not reached, the analytical signal increased linearly up to at least 34 ppbv of ammonia. The detection limit, considered to be three times the standard deviation of the blank signal, divided by the straight-line angular coefficient, was better than 3 ppbv. This limit depends on the ratio between the magnitude of the analytical signal and that of the fluctuations of the blank signal, and is usually higher because of contamination arising from the presence of ammonia in the environment. The major source of contamination in the laboratory is frequently the operator; the ammonia concentration in expired air can be as high as one hundred parts per billion.[35] Limits of detection can be improved by using a longer sampling time, which increases the analytical signal, albeit at the expense of sampling frequency. Nonetheless, the results obtained here demonstrate that environmental ammonia contamination can be successfully controlled and avoided. The relative standard deviation (RSD) for 10 replicates of 34 ppbv of ammonia determination was 5%, indicating a very reproducible response.

## Conclusions

The use of filters treated with oxalic acid, combined with an analytical technique based on the detection of fluorescence after reaction of ammonium with *o*-phthaldialdehyde in the presence of sodium sulfite, provides a sensitive method for the measurement of atmospheric ammonia. The analytical protocol employed is simple, and the system is compact, easily constructed and of low cost. The sensitivity of the method can be readily adjusted (upwards or downwards) by altering the sampling time, enabling deployment in environments with widely differing ammonia levels. Additionally, other solid supports may be tested and used in the development of new samplers.

Preliminary measurements were made in outdoor air, using the method developed here and the indophenol method (colorimetric determination at 600 nm).[1] The results were similar and the outdoor ammonia concentrations varied

from 0.5 to 5 ppbv during the daytime, with higher values at evening (8 ppbv). However, the indophenol method requires sampling times longer than 6 h in environments where the concentration of ammonia is only a few ppbv. The new procedure described here therefore affords the opportunity to readily obtain an improved understanding of the atmospheric ammonia cycle, involving both emission and consumption of the gas, during much shorter periods of an hour or less.

## Acknowledgments

We gratefully acknowledge the financial support of CNPq (Brazilian National Council for Scientific and Technological Development) and FAPESP (State of São Paulo Research Foundation).

## References

1. Felix, E. P.; Cardoso, A. A.; *Quim. Nova* **2004**, *27*, 123.
2. Da Rocha, G. O.; Allen, A.; Cardoso, A. A.; *Environ. Sci. Technol.* **2005**, *39*, 5293.
3. Livingston, C.; Rieger, P.; Winer, A.; *Atmos. Environ*. **2009**, *43*, 3326.
4. Rumburg, B.; Mount, G. H.; Filipy, J.; Lamb, B.; Westberg, H.; Yonge, D.; Kincaid, R.; Johnson, K.; *Atmos. Environ.* **2008**, *42*, 3364.
5. Zhang, Y.; Luan, S.; Chen, L.; Shao, M.; *J. Environ. Manage*. **2011**, *92*, 480.
6. Sommer, S. G.; Ostergard, H. S.; Lofstrom, P.; Andersen, H. V.; Jensen, L. S.; *Atmos. Environ*. **2009**, *43*, 915.
7. Harper, L. A.; Flesch, T. K.; Powell, J. M.; Coblentz, W. K.; Jokela, W. E.; Martin, N. P.; *J. Dairy Sci*. **2009**, *92*, 2326.
8. Baum, K. A.; Ham, J. M.; *Atmos. Environ.* **2009**, *43*, 1753.
9. Wu, S-Y.; Hu, J-L.; Zhang, Y.; Aneja, V. P.; *Atmos. Environ*. **2008**, *42*, 3437.
10. Plessow, K.; Spindler, G.; Zimmermann, F.; Matschullat, J.; *Atmos. Environ*. **2005**, *39*, 6995.
11. Allen, A. G.; Cardoso, A. A.; Wiatr A. G.; Machado, C. M. D.; Paterlini, W. C.; Baker, J.; *J. Braz. Chem. Soc.* **2010**, *21*, 87.
12. Tursic, J.; Berner, A.; Podkrajsek, B.; Grgic, I.; *Atmos. Environ*. **2004**, *38*, 2789.
13. Renner, E.; Wolke, R.; *Atmos. Environ*. **2010**, *44*, 1904.
14. Ni, J. Q.; Hendriks, J.; Vinckier, C.; Coenegrachts, J.; *Environ. Int.* **2000**, *26*, 97.
15. Machado, C. M. D.; Allen, A. G.; Cardoso, A. A.; *Environ. Sci. Technol*. **2008**, *42*, 381.
16. Theobald, M. R.; Bealey, W. J.; Tang, Y. S.; Vallejo, A.; Sutton, M. A.; *Sci. Total Environ*. **2009**, *407*, 6024.
17. Parrish, D. D.; Fehsenfeld, F. C.; *Atmos. Environ*. **2000**, *34*, 1921.
18. Lodge Jr., J. P.; *Methods of Air Sampling and Analysis*, 3rd ed., Lewis Publishers: Michigan, 1989.
19. Luo, Y.; Al-Othman, R.; Christian, G. D.; Ruzicka, J.; *Talanta* **1995**, *42*, 1545.
20. Kasper, A.; Puxbaum, H.; *Anal. Chim. Acta* **1998**, *32*, 3925.
21. Ugucione, C.; Felix, E. P.; Rocha, G. O.; Cardoso, A. A.; *Eclét. Quim*. **2002**, *27*, 103.
22. Searle, P. L.; *Analyst* **1984**, 109, 549.
23. Perrino, C.; Gherardi, M.; *Atmos. Environ*. **1999**, *33*, 4579.
24. Feigl, F.; *Spot Tests in Inorganic Analysis*, Elsevier: Amsterdam, 1972.
25. Jacobs, W. A.; *J. Chromatogr*. **1987**, *392*, 435.
26. Li, J. Z.; Dasgupta, P. K.; *Anal. Chim. Acta* **1999**, *398*, 33.
27. Roth, M.; *Anal. Chem.* **1971**, *43*, 880.
28. Genfa, Z.; Dasgupta, P. K.; *Anal. Chem.* **1989**, *61*, 408.
29. Kérouel, R.; Aminot, A.; *Mar. Chem.* **1997**, *57*, 265.
30. Aminot, A.; Kérouel, R.; Birot, D.; *Water Res.* **2001**, *35*, 1777.
31. Westra, H. G.; Van Doorn, J. E.; Tigchelaar, R. G.; Berden, J. A.; *Anal. Biochem.* **2001**, *296*, 225.
32. Groves, W. A.; Agarwal, D.; Chandra, M. J.; Reynolds, S. J.; *J. Environ. Monit*. **2005**, *7*, 163.
33. Felix, E. P.; de Souza, K. A. D.; Dias, C. M.; Cardoso, A. A.; *J. AOAC Int.* **2006**, *89*, 480.
34. Felix, E. P.; Cardoso, A. A.; *Instrum. Sci. Technol.* **2003**, *31*, 283.
35. Ugucione, C.; Cardoso, A. A.; *Anal. Bioanal. Chem*. **2007**, *389*, 1647.

*Submitted: March 3, 2011*
*Published online: November 3, 2011*

**FAPESP has sponsored the publication of this article.**

*J. Braz. Chem. Soc.*, Vol. 23, No. 1, 148-155, 2012.
Printed in Brazil - ©2012 Sociedade Brasileira de Química
0103 - 5053 $6.00+0.00

Article

# Ultra-Performance Liquid Chromatographic Method for Measurement of Voriconazole in Human Plasma and Oral Fluid

***Paula Boeira,[a] Marina V. Antunes,[a] Huander F. Andreolla,[b] Alessandro C. Pasqualotto[b] and Rafael Linden*[,a]***

*[a]Instituto de Ciências da Saúde, Universidade Feevale, Rodovia RS 239, No. 2755, 93352-000 Novo Hamburgo-RS, Brazil*

*[b]Laboratório de Biologia Molecular, Santa Casa de Porto Alegre, Porto Alegre-RS, Brazil*

Um método simples, sensível e seletivo para determinação de voriconazol em plasma e fluido oral empregando cromatografia líquida de ultra-eficiência foi desenvolvido e validado. Após extração líquido-líquido do plasma e fluido oral com metil-*tert*-butil éter, o analito e o padrão interno foram separados numa coluna Hypersil Gold C18 (2,1 × 100 mm, d.p. 1,9 µm), eluída isocraticamente com uma mistura de tampão fosfato trietilamônio pH 3,0 e acetonitrila (70:30, v/v). O tempo total da análise foi de 4 min, com consumo total de fase móvel de 2,2 mL. A determinação foi realizada com detector de arranjo de fotodiodos com quantificação em 256 nm. As concentrações de voriconazol no fluido oral foram, em média, 57,5% (± 5,3) daquelas determinadas em amostras pareadas de plasma.

A simple, sensitive and selective ultra-performance liquid chromatography method for the determination of voriconazole in plasma and oral fluid was developed and validated. After a liquid-liquid extraction with methyl-*tert*-butyl ether, the analyte and internal standard were separated on a Hypersil Gold C18 column (2.1 × 100 mm, p.d. 1.9 µm), eluted with a mobile phase composed of thietylammonium phosphate buffer and acetonitrile (70:30, v/v). Total run time was 4 min, total mobile phase consumption of 2.2 mL. Detection was performed with a photodiode array detector with quantitation at 256 nm. Voriconazole concentrations in oral fluid were on average 57.5% (± 5.3) of those measured in paired plasma samples.

**Keywords**: voriconazole, UPLC-PDA, oral fluid, drug monitoring

## Introduction

Voriconazole (VRC), designated chemically as (2*R*, 3*S*)-2-(2,4-difluorophenyl)-3-(5-fluoro-4-pyrimidinyl)-1-(1*H*-1,2,4-triazole-1-yl)-2-butanol (Figure 1), is currently the drug of choice for the treatment of invasive aspergillosis,[1] based on a large trial that showed a survival benefit for patients randomized to receive VRC instead of amphotericin B deoxycholate.[2] VRC is also approved for the treatment of invasive candidosis, as well as for less frequent fungal infections such as fusariosis and scedosporiosis.[3] Since VRC suffers extensive hepatic biotransformation, many drugs are known to interact with this antifungal agent, which has resulted in patients presenting a wide range of VRC plasma concentrations after fixed doses. Several studies have suggested that low VRC plasma concentrations may result in treatment failure, whereas high concentrations may be related to drug toxicity, especially visual disturbances, central nervous side effects and hepatotoxicity.[4-6] Pascual *et al*.[7] reported that lack of response was more frequently observed in patients with VRC levels below 1 µg mL$^{-1}$. Although there is no clear threshold for maximum acceptable VRC plasma concentrations, a cut-off of 6 µg mL$^{-1}$ has been recommended.[8] Recently, oral fluid was suggested as alternative sample for VRC therapeutic drug monitoring (TDM), especially by its easy collection characteristics, with a relatively constant relation to plasma levels.[9]

Several methods are available to measure VRC concentrations in biological fluids, mainly based on high performance liquid chromatography (HPLC), with either fluorimetric,[9] mass spectrometric[10-12] or spectrophotometric

*e-mail: rafael.linden@feevale.br

detection,[13-16] the former being advantageous by its robustness and lower instrumental and running costs. Moreover, VRC presents a strong absorption maximum at 256 nm at acidic pH, with UV detection being sensitive enough to measure clinically relevant concentration in plasma.[8] The specificity of the assay can be further improved with the use of a photodiode array detector (PDA), allowing spectral comparisons and peak purity evaluation, what is especially useful in the presence of other drugs.[17] Moreover, spectrophotometric detection is free from matrix ionization effects observed in liquid chromatography-mass spectrometry. Besides these advantages of PDA detection, the need of complete chromatographic separation of the analytes and matrix components usually results in long analytical runs, leading to low throughput and high consumption of solvents, together with a considerable production of chemical waste.

An alternative to conventional HPLC methods is ultra-performance liquid chromatography (UPLC), based on the use of columns with sub-2 μm diameter particles, that could render faster and high-resolution separations. Recently, an UPLC-tandem mass spectrometry method for the simultaneous quantitation of several antifungals was described.[18] However, the coupling of UPLC to PDA detection allows fast analysis while keeping the advantages and robustness of UV detection modes, at a moderate cost.[19] In the present work, we validated a novel and fast UPLC-PDA assay for TDM of VRC in human plasma and oral fluid samples, after a simple liquid-liquid extraction.

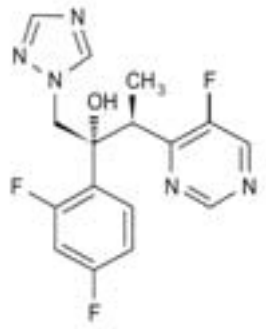


**Figure 1.** Chemical structure of voriconazole.

## Experimental

### Chemicals

VRC and its analogue UK 11579 (internal standard) were kindly donated by Pfizer (Croton, USA). Triethylammonium phosphate buffer 1 mol $L^{-1}$ pH 3.0 was purchased from Fluka (Buchs, Switzerland). Tris(hydroxymethyl)aminomethane was purchased from Nuclear (Diadema, Brazil). Sodium hydroxide, methanol, acetonitrile and methyl-*tert*-butyl ether (MTBE) were obtained from Merck (Darmstadt, Germany). Ultrapure water was obtained through an Elga Purelab Ultra® apparatus from Elga Labwater (High Wycombe, UK).

### Preparation of solutions and standards

Individual stock methanolic solutions of VRC and UK 11579 (IS) were prepared by powder dissolution in order to obtain a concentration of 1 mg $mL^{-1}$. VRC working solutions were prepared combining aliquots of each stock solution and proper volumes of methanol to obtain solutions containing 1.0, 2.5, 5.0, 10.0, 25.0, 50.0 and 100.0 μg $mL^{-1}$ of VRC. The working internal standard solution was prepared by dilution of stock with methanol to obtain a 20 μg $mL^{-1}$ concentration. Mobile phase buffer was prepared daily diluting 500 μL of triethylammonium phosphate buffer 1 mol $L^{-1}$ to 100 mL with ultrapure water to obtain a 5 mmol $L^{-1}$ concentration, followed by filtration with 0.2 μm cellulose acetate membranes from Sartorius (Göettingen, Germany). Tris buffer pH 10.0 was prepared dissolving 2.43 g of tris(hydroxymethyl)aminomethane in 100 mL of ultrapure water, and the pH was properly adjusted with NaOH 0.1 mol $L^{-1}$.

### Equipment and chromatographic conditions

The UPLC system consisted of an ACQUITY UPLC® coupled to an ACQUITY UPLC® photodiode array detector, both from Waters (Milford, USA). The separation was performed on a Hypersil Gold® C18 column (2.1 × 100 mm, particle diameter 1.9 μm), from Thermo Scientific (San Jose, USA). The system was controlled and data was managed by Empower® software, also from Waters. Mobile phase was a mixture of triethylammonium phosphate buffer 5 mmol $L^{-1}$ and acetonitrile (70:30, v/v), which was sonicated for 15 min before use. The flow rate was 0.55 mL $min^{-1}$, and total run time was 4 min. The column temperature was set at 55 °C. Spectra were acquired for all peaks in the range of 205 to 380 nm and the quantitation wavelength was 256 nm.

### Sample preparation

To 2 mL disposable polypropylene tubes, 500 μL of either calibration, quality control or patient's samples (plasma or oral fluid) were added, followed by 50 μL of working internal standard solution, 100 μL of Tris buffer pH 10.0 and 1,000 μL of methyl-*tert*-butyl ether. The tubes were capped and vortex mixed for 30 s and then

centrifuged at 10,000 × *g* for 10 min at 4 °C. An aliquot of 900 µL of the organic layer was evaporated to dryness at 50 °C, under a gentle stream of air. The dried extract was recovered with 150 µL of mobile phase, vortex mixed for 30 s and centrifuged at 10,000 × *g* for 10 min, at 4 °C. The supernatant was transferred to an autosampler vial and 10 µL were injected into the UPLC system.

### Selectivity

Blank plasma and oral fluid samples from 6 different sources were prepared as described above to check for peaks that might interfere with the detection of the analyte or the IS. In addition, the use of a photodiode array detector (PDA) permitted to check for the presence of spectral impurities in each chromatographic peak.

### Stability

For estimation of stability of processed samples under the conditions of analysis, control samples at 0.2 and 8.0 µg $mL^{-1}$ (n = 5 each) were extracted as described above. The extracts obtained at each concentration were pooled. Aliquots of these pooled extracts at each concentration were transferred to autosampler vials and injected under the conditions of a regular analytical run at time intervals of 1 h, during 12 h. Stability of VRC was tested by regression analysis plotting absolute peak areas corresponding to each compound at each concentration *vs*. injection time. Using the obtained linear regression, the concentration after 12 h was calculated. A decrease or increase of up to 10% in the measured peak areas was considered as acceptable. For evaluation of freeze-thaw stability, quality control samples at 3 levels (0.2; 2.0 and 8.0 µg $mL^{-1}$) were analyzed before (control samples, n = 3) and after 3 freeze-thaw cycles (stability samples, n = 9). For each freeze-thaw cycle, the samples were frozen at −20 °C for 48 h, thawed, and kept at ambient temperature for 3 h before extraction. The concentrations of the control and stability samples were calculated from daily calibration curves and the variance evaluated using ANOVA test. $P$ values of ≤ 0.05 were considered statistically significant.

### Linearity

Aliquots of blank plasma or oral fluid (450 µL) were enriched with 50 µL of the corresponding working solutions to obtain calibration samples containing 0.1, 0.25, 0.50 1.0, 2.5, 5.0, or 10.0 µg $mL^{-1}$ of VRC. Replicates (n = 6) at each concentration for both matrices were analyzed as described above. Calibration curves were constructed by calculating the ratios of the peak area of VRC to the peak area of the internal standard and relating these ratios with nominal concentrations of the calibration samples. Homoscedasticity of calibration data was evaluated with F-test at the confidence level of 95%. Curves were fitted by least-squares linear regression using several weighting factors ($1/x$, $1/x^{0.5}$, $1/x^2$, $1/y$, $1/y^{0.5}$, $1/y^2$). The calibration models were evaluated by their correlation coefficients (r) and cumulative percentage relative error ($\sum$%RE), according to Almeida *et al*.[20] The correlation between the calibration curves obtained from plasma and oral fluid was established by linear regression and evaluated through the coefficient of correlation. Daily calibration curves using the same concentrations (single measurements *per* concentration) were prepared with each batch of validation and authentic samples.

### Accuracy and precision

Aliquots of blank plasma and oral fluid (450 µL) were enriched with 50 µL of the corresponding working solutions to obtain quality control samples containing VRC at 0.20 (quality control low, QCL), 2.0 (quality control medium, QCM) and 8.0 µg $mL^{-1}$ (quality control high, QCH). The quality control samples were analyzed as described above in triplicate on each of 5 days. Within-assay precision and between-day precision were calculated by one-way ANOVA with the grouping variable "day" and were expressed as CV%. Accuracy was defined as the percentage of the nominal concentration represented by the concentration estimated with the calibration curve. The acceptance criterion for accuracy was mean values within ±15% of the theoretical value and for precision was a maximum CV of 15%.[21] Additionally, the method was applied to 2 plasma samples from the antifungal interlaboratorial quality control program of Kwaliteitsbewaking Klinische Geneesmiddelanalyse en Toxicologie, The Hague, The Netherlands, which contained VRC at the nominal concentrations of 4.4 (proficiency test low, PTL) and 8.0 µg $mL^{-1}$ (proficiency test high, PTH).

### Lower limit of quantitation

The lowest point of the calibration curve was 0.1 µg $mL^{-1}$. An independent quality control sample at this concentration was included in the accuracy and precision experiments (quality control at the lower limit of quantitation, QCLLOQ) and was tested in triplicate in three different days. The acceptance criteria established for the limit of quantification was accuracy within 100 ± 20% of the nominal value and a maximum CV of 20%.[21]

### Extraction efficiency

The extraction efficiency was determined by comparing the peak areas of the analytes obtained at the plasma QC samples of the accuracy and precision experiments to those obtained with methanolic solutions at levels corresponding to complete recovery, measured in triplicate at three different days, in the same analytical batch. Extraction efficiency was expressed as percentage of the concentration of the reference samples.

### Method application

The developed method was applied to 15 paired samples of plasma and oral fluid obtained from 9 patients, collected from March 2010 to January 2011. All patients were adults, over 18 year of age. Trough blood samples, collected at day 2 and 5 after initiation of VRC therapy, were collected by venipuncture to EDTA containing tubes. After collection, the tubes were centrifuged within 10 min and plasma was separated. The oral fluid samples were collected at the same times by chewing on the cotton wool swabs of a commercial saliva collecting device (Salivette®, Sarstedt, Germany) impregnated with citric acid. The chewing time was standardized in 2 min. Plasma and oral fluid samples were kept at −20 °C until analysis. Written informed consent was obtained from all patients. The study was approved by the Ethics Committee of the Irmandade da Santa Casa de Misericórdia de Porto Alegre (Porto Alegre, Brazil).

## Results and Discussion

### Chromatography and sample preparation

Most HPLC-UV methods for chromatographic determination of VRC have long run times or high consumption of mobile phases, reducing their applicability for routine analysis, along with high costs associated to the use of solvents and the disposal of chemical residues. In this study we described a fast LC-UV method for the measurement of VRC. This is the first description of the use of columns with sub-2 μm particle diameter to this drug. The combination of a narrow bore column with small diameter particles, allowed a rapid and efficient separation of the analytes, despite the higher linear velocity of mobile phase. As a consequence of these conditions, a high operating pressure of the system was observed, with typical run pressures over 7,000 psi, which are not supportable by conventional HPLC equipments, requiring special instrumentation. Retention times for VRC and IS were 3.05 and 3.65 min, respectively (Figure 2), with

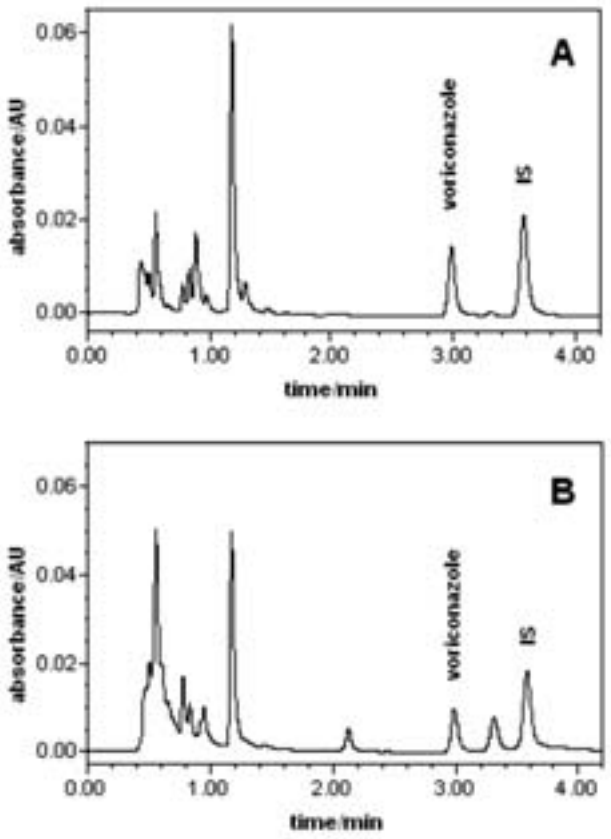


**Figure 2.** Chromatograms from samples of the same patient, obtained simultaneously 5 days after initiation of voriconazole therapy, monitored at 256 nm; A: Plasma sample with concentration of 1.1 μg $mL^{-1}$. B: Oral fluid sample plasma with concentration of 0.58 μg $mL^{-1}$.

a total run time of 4 min. There is only one report of a LC-UV method for VRC determination with a similar run time, from Chhun *et al.,*[15] that employed a monolithic column with high mobile phase flow rate, in the order of 3.5 mL $min^{-1}$, resulting in a total consumption of mobile phase of 14 mL for run. Other LC-UV published method had higher run times, in the order of 10-20 min, and higher mobile phase consumptions, from 8-15 mL.[10,13-16] Total use of mobile phase in our assay was only 2.2 mL *per* analysis, considerably lower than other published LC-UV methods.

Interfering endogenous plasma peaks were not observed in the blank plasma and oral fluid samples (Figure 3). Additionally, all analyte's peaks were evaluated with respect to their spectral purity and compared with library reference spectra, using the Empower® software. No spectral impurity was observed in identified peaks or in any patient's tested sample.

In the present work, by means of simplicity and cost, we choose a liquid-liquid extraction procedure with MTBE to extract the drugs from plasma and oral fluid. The small volume of solvent taken for evaporation (900 μL) allowed a fast concentration of the samples, in the order

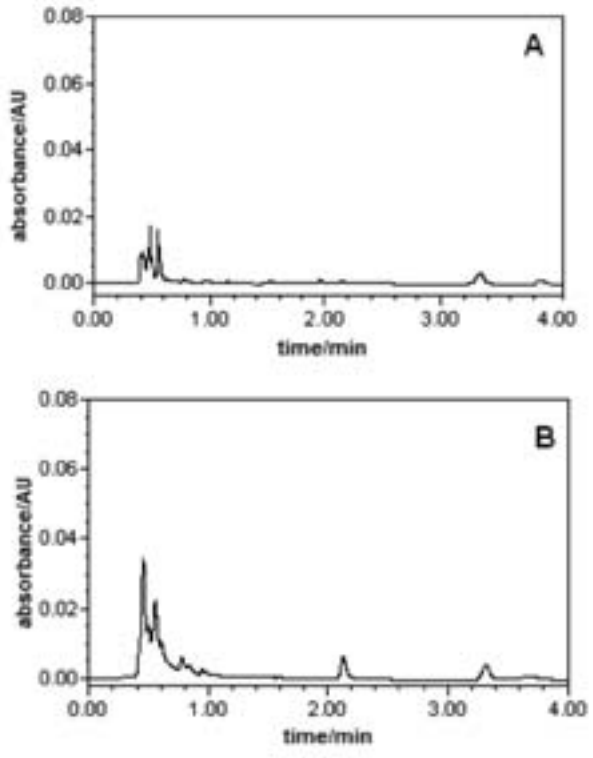


**Figure 3.** Chromatograms monitored at 256 nm; A: Blank plasma sample. B: Blank oral fluid sample.

of 5 min. Considering the possibility of clogging in the column, especially due to the small inter-particle spaces, an additional step of centrifugation was employed after recovery of the dried extract with mobile phase. However, the extraction procedure was rapid, simple and inexpensive, with consistent yields in the range of 80.6-81.8% in plasma and 82.5-86.2% in oral fluid.

## Method validation

There was no indication of instability of the analyte in any of the tested conditions. Regression analysis of absolute peak areas of the analytes plotted *vs*. injection time indicated no instability of processed samples during a time interval of 12 h, with concentration changes based on linear regression on the range of −4.3 to 5.9% for plasma and −3.8 to 4.5 in oral fluid. The time frame of 12 h was determined considering the maximum run time needed for analysis of a large batch of samples with the developed method, even considering its high throughput. The ratios of means (stability *vs*. control samples) of the freeze-thaw samples also fulfilled the acceptance criteria ($p = 0.05$) for both matrices (Table 1).

Calibration samples were prepared at 6 concentrations spread from 0.1 to 10 μg mL$^{-1}$ of VRC, covering concentrations that are to be expected for most authentic plasma and oral fluid samples. The slopes (b) and *y*-intercepts (a), including 95% confidence intervals of both variables, as well as the coefficients of correlation and cumulative percentage relative error (∑%RE), as obtained in the linearity experiments, are listed in Table 2. Several weighted regression models were evaluated in order to account to the significant heteroscedasticity of the calibration data. The best weighting factor was chosen according to the ∑%RE, defined as the sum of absolute percentage relative error, which compares the regressed concentration computed from the regression equation obtained for each weighting factor, with the nominal standard concentration. The inverse of the concentration (1/x) was selected as the best weighting factor, with maximum ∑%RE of $-5.3 \times 10^{-15}$ for plasma and ∑%RE of $9.77 \times 10^{-14}$ for oral fluid, contrasting to a maximum ∑%RE of 84.31 for plasma and ∑%RE of 27.55 for oral fluid when unweighted regression was applied. The coefficients of correlation were above 0.999 for all weighing factors. The back-calculated concentrations of all calibration samples fulfilled the criteria established by Shah *et al*.[21]

QC samples for accuracy and precision experiments were prepared at 3 concentrations (QCL, QCM, and CQH) covering the calibration range. The results of the

**Table 1.** Freeze and thaw stability

| VRC / (μg mL$^{-1}$) | Benchtop stability | Freeze and thaw stability | | | |
|---|---|---|---|---|---|
| | Concentration change after 12 h (based on regression) / % | Control concentration after each cycle (n = 3) | | | |
| | | First | Second | Third | *P* value (ANOVA) |
| Plasma | | | | | |
| 0.20 | -4.3 | 0.18 | 0.18 | 0.19 | 0.45 |
| 2.00 | - | 2.02 | 2.11 | 2.05 | 0.46 |
| 8.00 | 5.9 | 8.30 | 8.37 | 8.23 | 0.41 |
| Oral fluid | | | | | |
| 0.20 | -3.8 | 0.24 | 0.21 | 0.20 | 0.10 |
| 2.00 | - | 1.98 | 1.98 | 1.97 | 0.51 |
| 8.00 | 4.5 | 7.80 | 7.76 | 7.89 | 0.29 |

**Table 2.** Summary of the evaluation of the calibration models

| Weighting factor | Regression parameters | Plasma | Oral fluid |
|---|---|---|---|
| unweighted | b | 0.5390 | 0.5385 |
| | a | – 0.0363 | – 0.0213 |
| | r | 0.9999 | 0.9999 |
| | ∑%RE | 84.309 | 27.554 |
| 1/x | b | 0.5281 | 0.5350 |
| | a | – 0.0063 | – 0.0115 |
| | r | 0.9999 | 0.9999 |
| | ∑%RE | $-5.3 \times 10^{-15}$ | $9.7 \times 10^{-14}$ |
| $1/x^{0.5}$ | b | 0.5334 | 0.5371 |
| | a | – 0.0149 | – 0.0156 |
| | r | 0.9999 | 0.9999 |
| | ∑%RE | 21.563 | 10.535 |
| $1/x^2$ | b | 0.5150 | 0.5201 |
| | a | – 0.0011 | – 0.0057 |
| | r | 0.9999 | 0.9999 |
| | ∑%RE | $-1.2 \times 10^{-13}$ | $7.11 \times 10^{-14}$ |
| 1/y | b | 0.5277 | 0.5348 |
| | a | – 0.0062 | – 0.0116 |
| | r | 0.9999 | 0.9999 |
| | ∑%RE | 0.2644 | 0.3585 |
| $1/y^{0.5}$ | b | 0.5332 | 0.5371 |
| | a | – 0.0148 | – 0.0156 |
| | r | 0.9999 | 0.9999 |
| | ∑%RE | 21.447 | 10.563 |
| $1/y^2$ | b | 0.5142 | 0.5174 |
| | a | – 0.0010 | – 0.0054 |
| | r | 0.9999 | 0.9999 |
| | ∑%RE | 0.8495 | 2.828 |
| Test of homoscedasticity $F_{tab}$ (5.0 5.0 0.95) = 5.05 | $F_{exp}$ | 211.36 | 2881.64 |

accuracy and precision experiments are given in Table 3. All accuracy values fulfilled the acceptance criteria for this parameter, lying within the range 96.3-99.8% of the nominal concentrations for plasma and 99.3-103.4% for oral fluid samples. Within-assay precision was in the range of 2.8-4.5% for plasma and 2.5-4.9% for oral fluid, where between-assay precision was 1.4-4.9% for plasma and 1.3-3.8% for oral fluid, also being accepted. An additional evaluation of the method accuracy was done by analyzing two proficiency test samples (PTL and PTH). The measured values were in close agreement with target values, being 4.34 μg $mL^{-1}$ for PTL (target value 4.4 μg $mL^{-1}$, accuracy 98.6%) and 8.07 μg $mL^{-1}$ for PTH (target value 8.0 μg $mL^{-1}$, accuracy 100.9%).

Another QC sample containing VRC at a concentration equal to those of the lowest point of the calibration curve (QCLLOQ) was prepared to determine whether the criteria for analytical recovery and precision were fulfilled even at this concentration, which corresponded to the practical LOQ. The plasma QCLLOQ presented mean accuracy of 102.7%, within-assay precision of 6.8%, and between-assay of 4.5%, whereas the oral fluid QCLLOQ presented mean accuracy of 108.2%, within-assay precision of 7.2%, and between-assay of 5.9%, both fulfilling the acceptance criteria for the lower limit of quantification.

## Method application

The developed method was applied to 15 paired plasma and oral fluid samples, collected at trough conditions (Table 4). A wide range of concentrations were observed, with a 10 fold difference between the lower and the

**Table 3.** Precision, accuracy and extraction yield*

| QC sample / (μg $mL^{-1}$) | Nominal concentration / (μg $mL^{-1}$) | Precision / (CV%) | | Accuracy / % | Extraction yield / % |
|---|---|---|---|---|---|
| | | Within-assay | Between-assay | | |
| Plasma | | | | | |
| QCLLOQ | 0.1 | 6.8 | 4.5 | 102.1 | - |
| QCL | 0.2 | 2.8 | 1.4 | 96.3 | 80.6 |
| QCM | 2.0 | 4.5 | 4.9 | 97.3 | 81.8 |
| QCH | 8.0 | 3.2 | 4.3 | 99.8 | 81.7 |
| PTL | 4.4 | - | - | 98.6 | - |
| PTH | 8.0 | - | - | 100.9 | - |
| Oral Fluid | | | | | |
| QCLLOQ | 0.1 | 7.2 | 5.9 | 108.2 | - |
| QCL | 0.2 | 3.3 | 2.1 | 101.0 | 84.5 |
| QCM | 2.0 | 4.9 | 3.8 | 99.3 | 86.2 |
| QCH | 8.0 | 2.5 | 1.3 | 103.4 | 82.5 |

*n = 15 for QCL, QCM and QCH; n = 9 for QCLLOQ; n = 1 for PT samples.

**Table 4.** Plasma and oral fluid trough levels and OF/P ratios

| Patient | Days after initiation of VRC | Plasma trough level / (μg mL$^{-1}$) | Oral fluid trough level / (μg mL$^{-1}$) | OF/P (%) |
|---|---|---|---|---|
| 1 | 5 | 3.85 | 2.02 | 52.4 |
| 2 | 2 | 1.78 | 0.94 | 52.6 |
| 2 | 5 | 1.11 | 0.58 | 52.0 |
| 3 | 2 | 2.83 | 1.68 | 59.3 |
| 3 | 5 | 1.97 | 1.26 | 63.8 |
| 4 | 2 | 8.24 | 4.78 | 58.0 |
| 4 | 5 | 8.11 | 4.39 | 54.2 |
| 5 | 5 | 0.84 | 0.54 | 64.3 |
| 6 | 2 | 1.92 | 1.02 | 53.5 |
| 6 | 5 | 2.44 | 1.28 | 52.4 |
| 7 | 2 | 0.61 | 0.38 | 61.5 |
| 7 | 5 | 1.50 | 1.02 | 67.9 |
| 8 | 2 | 8.49 | 4.52 | 53.3 |
| 9 | 2 | 4.71 | 2.60 | 55.3 |
| 9 | 5 | 4.14 | 2.58 | 62.3 |
| Range | | 0.84-8.49 | 0.54-4.52 | 52.0-67.9 |
| Mean (± sd) | | 3.50 (± 2.7) | 1.97 (± 1.5) | 57.5 (± 5.3) |

OF: oral fluid; P: plasma; VRC: voriconazole.

higher plasma measured concentrations. In oral fluid, the concentration span was a little smaller, of 8.4 fold. In the 15 measured plasma concentrations, 3 were above the upper proposed threshold of 6 μg mL$^{-1}$ and 2 were below the lower expected concentration of 1 μg mL$^{-1}$, with one third of all measurement outside the expected therapeutic range. The use of oral fluid for VRC TDM was previously described by Michael *et al*.[9] and is supported by the physico-chemical characteristics of this drug, especially its pKa of 1.76[22] (with ionization being unaffected by usual mouth's pH) and its protein binding of 58%.[23] Interestingly, the percentage of oral fluid related to plasma concentration was relatively stable, ranging from 52.0-67.9%, with mean of 57.5%. However, these values were considerably different from those found by Michael *et al*.,[9] which were in the range of 14-56% with an overall mean of 40% in adult patients. The authors of the study did not mentioned the time expended by patients chewing the Salivette® cotton swab, and considering that we standardized this time in our procedure, this can be a possible source of variation. Considering that our sample size is limited, further studies are necessary to establish a clinically valid relation between VRC concentrations in plasma and oral fluid. However, oral fluid seems to be a useful alternative matrix for TDM of VRC.

## Conclusions

A fast, simple and fully validated method was developed for the measurement of VRC in human plasma and oral fluid samples, using ultra-performance liquid chromatography, with the smallest consumption of mobile phase published so far. The method was applied to 15 paired plasma and oral fluid samples, showing a consistent ratio of concentrations in both matrices, with oral fluid presenting a mean of 57.5% of the plasma levels.

## Acknowledgments

We thank Pfizer for the donation of reference samples of VRC and UK 11579, as well as Universidade Feevale for the financial support. Dr. Pasqualotto is thankful to CNPq (Conselho Nacional de Desenvolvimento Científico e Tecnológico), Brazilian Government Agency.

## References

1. Walsh, T. J.; Anaissie, E. J.; Denning, D. W.; Herbrecht, R.; Kontoyianniset, D. P.; Marr, K. A.; Morrison, V. A.; Segal, B. H.; Steinbach, W. J.; Stevens, D. A.; van Burik, J.; Wingard, J. R.; Patterson, T. F.; *Clin. Infect. Dis.* **2008**, *46*, 327.
2. Herbrecht, R.; Denning, D. W.; Patterson, T. F.; Bennett, J. E.; Greene, R. E.; Oestmann, J. W.; Kern, W. V.; Marr, K. A.; Ribaud, P.; Lortholary, O.; Sylvester, R.; Rubin, R. H.; Wingard, J. R.; Stark, P.; Durand, C.; Caillot, D.; Thiel, E.; Chandrasekar, P. H.; Hodges, M. R.; Schlamm, H. T.; Troke, P. F.; de Pauw, B.; *N. Engl. J. Med*. **2002**, *347*, 408.
3. http://www.accessdata.fda.gov/drugsatfda_docs/label/2010/021266s032lbl.pdf accessed in September 2011.
4. Trifilio, S.; Ortiz, R.; Pennick, G.; Verma, A.; Pi, J.; Stosor, V.; Zembower, T.; Mehta, J.; *Bone Marrow Transplant.* **2005**, *35*, 509.
5. Johnson L. B.; Kauffman C. A.; *Clin. Infect. Dis*. **2003**, *36*, 630.
6. Denning, D. W.; Ribaud, P.; Milpied, N.; Caillot, D.; Herbrecht, R.; Thiel, E.; Haas, A.; Ruhnke, M.; Lode, H.; *Clin. Infect. Dis*. **2002**, *34*, 563.
7. Pascual, A.; Calandra, T.; Bolay, S; Buclin, T.; Bille, J.; Marchetti, O.; *Clin. Infec. Dis.* **2008**, *46*, 201.
8. Pasqualotto, A. C.; Xavier, M. O.; Andreolla, H. F.; Linden, R.; *Expert Opin. Drug Saf*. **2010**, *9*, 125.
9. Michael, C.; Bierbach, U.; Frenzel, K.; Lange, T.; Basara, N.; Niederwieser, D.; Mauz-Körholz, C.; Preiss, R.; *Ther. Drug Monit*. **2010**, *32*, 194.
10. Zhou, L.; Glickman, R. D.; Chen, N.; Sponsel, W. E.; Graybill, J. R.; Lam, K. W.; *J. Chromatogr., B: Anal. Technol. Biomed. Life Sci.* **2002**, *776*, 213.
11. Keevil, B. G.; Newman, S.; Lockhart, S.; Howard, S. J.; Moore, C. B.; Denning, D. W.; *Ther. Drug Monit*. **2004**, *26*, 650.
12. Vogeser, M.; Schiel, X.; Spohrer, U.; *Clin. Chem. Lab. Med*. **2005**, *43*, 730.
13. Gage, R.; Stopher, D. A.; *J. Pharm. Biomed. Anal.* **1998**, *17*, 1449.

14. Pennick, G. J.; Clark, M.; Sutton, D. A.; Rinaldi, M. G.; *Antimicrob. Agents Chemother*. **2003**, *47*, 2348.
15. Chhun, S.; Rey, E.; Tran, A.; Lortholary, O.; Pons, G.; Jullien, V.; *J. Chromatogr., B: Anal. Technol. Biomed. Life Sci*. **2007**, *852*, 223.
16. Langman, L. J.; Boakye-Agyeman, F.; *Clin. Biochem*. **2007**, *40*, 1378.
17. Pragst, F.; Herzler, M.; Erxleben, B. T.; *Clin. Chem. Lab. Med*. **2004**, *42*, 1325.
18. Decosterd, L. A.; Rochat, B.; Pesse, B.; Mercier, T.; Tissot, F.; Widmer, N.; Bille, J.; Calandra, T.; Zanolari, B.; Marchetti, O.; *Antimicrob. Agents Chemother*. **2010**, *54*, 5303.
19. Antunes, M. V.; Poeta, J.; Ribeiro, J. P.; Sprinz, E.; Linden, R.; *J. Braz. Chem. Soc*. **2011**, *22*, 134.
20. Almeida, A. M.; Castel-Branco, M. M.; Falcão, A. C.; *J. Chromatogr., B: Anal. Technol. Biomed. Life Sci.* **2002**, *774*, 215.
21. Shah, V. P.; Midha, K. K.; Findlay, J. W. A.; Hill, H. M.; Hulse, J. D.; McGilveray, I. J.; McKay, G.; Miller, K. J.; Patnaik, R. N.; Powell, M. L.; Tonelli, A.; Viswanathan, C. T.; Yacobi, A.; *Pharm. Res.* **2000**, *17*, 1551.
22. Adams, A. I.; Morimoto, L. N.; Meneghini, L. Z.; Bergold, A. M.; *Braz. J. Infect. Dis*. **2008**, *12*, 400.
23. Drobitch, R. K.; Svensson, C. K.; *Clin. Pharmacokinet*. **1992**, *23*, 365.

*Submitted: March 25, 2011*
*Published online: November 8, 2011*

*J. Braz. Chem. Soc.*, Vol. 23, No. 1, 156-162, 2012.
Printed in Brazil - ©2012 Sociedade Brasileira de Química
0103 - 5053 $6.00+0.00

Article

# Cooking Effects on Iron and Proteins Content of Beans (*Phaseolus Vulgaris* L.) by GF AAS and MALDI-TOF MS

***Juliana Naozuka*,[a] and Pedro V. Oliveira[b]***

[a]*Universidade Federal de São Paulo, Diadema-SP, Brazil*

[b]*Departamento de Química Fundamental, Instituto de Química, Universidade de São Paulo, São Paulo-SP, Brazil*

Os efeitos do cozimento doméstico na distribuição de proteínas, compostos orgânicos e Fe em feijão (*Phaseolus vulgaris* L.) foram investigados. Extração seqüencial com diferentes agentes extratores (mistura de metanol e clorofórmio 1:2 v/v, água, NaCl, etanol e NaOH) foi usada para extrair lipídeos, albuminas, globulinas, prolaminas e glutelinas, respectivamente. A determinação de Fe por espectrometria de absorção atômica com forno de grafite (GF AAS), de proteínas pelo método de Bradford e compostos orgânicos por espectrometria de massas por tempo de vôo acoplada à ionização dessortiva de matriz por laser (MALDI-TOF MS) foram feitas nesse trabalho. Altas concentrações de albuminas, globulinas e glutelínas foram encontradas em feijão cru, enquanto que em grãos cozidos, albuminas e glutelínas foram os principais tipos de proteínas. Os espectros de MALDI-TOF MS do feijão cru e cozido revelaram que o cozimento doméstico alterou os pesos moleculares dos compostos orgânicos, uma vez que nos grãos cozidos foram encontrados compostos entre 2 e 3,5 kDa, os quais não estavam presentes no feijão cru. Além disso, no feijão cozido foi também observada a presença de quatro compostos de alto peso molecular (12-16 kDa), sendo que em grãos crus há somente um (*ca.*15,2 kDa). Nos grãos crus foi possível observar que Fe está principalmente associado a albuminas, globulinas e glutelínas. Para os grãos cozidos, Fe está presente em alta concentração em albuminas e globulinas.

The effects of domestic cooking on proteins, organic compounds and Fe distribution in beans (*Phaseolus vulgaris* L.) were investigated. Sequential extraction with different extractant solutions (mixture of methanol and chloroform 1:2 v/v, water, 0.5 mol $L^{-1}$ NaCl, 70% v/v ethanol and 0.5 mol $L^{-1}$ NaOH) were used for extracting lipids, albumins, globulins, prolamins and glutelins, respectively. Iron determination by graphite furnace atomic absorption spectrometry (GF AAS), proteins by Bradford method and organic compounds by matrix-assisted laser desorption ionization time-of-flight mass spectrometry (MALDI-TOF MS) were carried out in this work. High concentration of albumins, globulins and glutelins were found in raw beans, while in the cooked beans, albumins and glutelins are main proteins types. The MALDI-TOF MS spectra of raw and cooked beans revealed that the domestic cooking altered the molecular weight of the organic compounds, since that in the cooked beans were found compounds between 2 and 3.5 kDa, which were not presented in the raw beans. Besides this, in cooked beans were also observed the presence of four compounds of high molecular weight (12-16 kDa), being that in the raw grains there is only one (*ca.* 15.2 kDa). In raw grains is possible to observe that Fe is mainly associated to albumins, globulins and glutelins. For cooked grains, Fe is associated to albumins and globulins.

**Keywords**: iron, proteins, beans, GF AAS, MALDI-TOF MS

## Introduction

Beans (*Phaseolus vulgaris* L.) are a typical culture of tropical and subtropical weather. Brazil is the largest worldwide producer (2.2-2.5 million tons, in approximately 5 million hectares cultivated) and consumer (around 16 kg *per* capita). Beans is one of the richest foods in proteins consumed by the Brazilian population.[1] Normally, countryside population is responsible for the high consumption of this food.[1,2] However, consumption of beans is declining, due to the changes in traditional dietary habits of Brazilian population.[2]

Beans are a good source of vitamins, minerals (K, Ca, Mg, P and Fe salts), proteins (20-25%) and complex

*e-mail: jnaozuka@gmail.com

carbohydrates (50-60%).[2-4] Besides their nutritional importance, beans contain certain anti-nutritional constituents, such as trypsin inhibitors, tannins, phytic acid and oligosaccharides that limit protein and carbohydrate absorption.[5]

The heating of beans can increase the protein and starch digestibility from 25-60% (raw grains) to 85% (cooked grains), depending on the species and cooking procedure.[6] Futhermore, cooking promotes the production of desirable sensory properties in beans, such as sweet taste, cooked-bean flavor, and soft and mushy textures.[2] However, cooking causes considerable changes in the composition of numerous chemical constituents, including amino acids, vitamins and minerals.[3]

The effects of cooking in the distribution of soluble iron were evaluated for legumes, beans, chickpeas and lentils.[7] It was reported that cooking increases soluble iron contents presented in the cooking water. These studies are very important, because the heating can influence the iron bioavailability. It is generally accepted that only soluble non-heme iron can be absorbed. However, interactions with other compounds, such as anti-nutritional constituents, presented in the beans can also alter the iron bioavailability. Numerous studies have led to the conclusion that phytic acid and tannins may bind to proteins and some essential dietary minerals, making them unavailable or only partially available for absorption.[8]

Studies about heating effects in proteins and essential elements (*e.g.*, Fe) are still limited, especially for cultivars commonly consumed in Brazil, where beans are the staple food. Additionally, in Brazil there are some research aiming the enrichment of beans with essential elements, such as iron. Consequently, the elaboration of methodologies that allow the evaluation of the cooking effects in the distribution of proteins and elements is imperative, since cooking is required to eat beans. Considering the nutritional importance, the aim of this work was to evaluate the effects of domestic cooking in beans on proteins, organic compounds and Fe distribution. Sequential extraction with different extracting agents (*e.g.*, water, NaCl, ethanol and NaOH) and Fe, proteins and organic compounds determination by GF AAS, Bradford method[9] and MALDI-TOF-MS, respectively, were used in this investigation.

## Experimental

### Instrumental

A ZEEnit 60 model atomic absorption spectrometer (AnalytikjenaAG, Jena, Germany) equipped with a transversely heated graphite atomizer, pyrolytically coated graphite tube, transversal Zeeman-effect background corrector was used for Fe determination. The spectrometer was operated using hollow cathode lamp. All measurements were based on integrated absorbance values. The instrumental conditions for the spectrometer and the heating program are shown in Table 1. Argon 99.998%, v/v (Air Liquide Brasil, São Paulo, Brazil) was used as protective and purge gas.

**Table 1.** Instrumental parameters and heating program for Fe determination by GF AAS

| Instrumental parameters | Fe | | |
|---|---|---|---|
| λ / nm | 248.3 | | |
| slit / nm | 0.8 | | |
| I / mA | 4.0 | | |
| Heating program | | | |
| Step | T / ºC | Ramp / (ºC $s^{-1}$) | Hold / s |
| Dry I | 100 | 10 | 10 |
| Dry II | 130 | 10 | 15 |
| Pyrolysis | 1200 | 100 | 20 |
| Atomization | 2300 | 2300 | 5 |
| Cleaning | 2500 | 1200 | 2 |

An Ultrospec 2100 pro spectrophotometer (Biochrom LTD, Cambridge, UK), equipped with xenon lamp and wavelength ranged to 190 from 900 nm was used for protein determination at 590 nm.

The digestion of samples and reference certified material (CRM) were carried out in a closed vessel microwave oven, model Microwave 3000 (Anton Paar, Graz, Austria), equipped with 16 fluoropolymer vessels and a ceramic vessel jacket. They support a maximum temperature and pressure of 240 ºC and 4 MPa, respectively. The internal temperature and pressure are monitored in only one controlling vessel using a sensor-protecting glass tube that enters directly into contact with digested solution. The external temperature is controlled in all vessels using an IR sensor, which measures each digestion vessel through ports in the rotor base.

An orbital shaker (Quimis, São Paulo, Brazil) was used to mix the samples and extracting agents using rotation velocity of 250 rpm for 30 min.

A vacuum filtration system of borosilicate glass, model XX15 047 00 (Millipore, USA) and a 0.45 mm Nylon® membrane filter (Millipore, USA) and a model Q222TM centrifuge (Quimis, São Paulo, Brazil) were used to separate the supernatant of the solid material after extractions.

Matrix-assisted laser desorption ionization time-of-flight mass spectrometry (MALDI-TOF-MS), model Ettan

MALDI-TOF Pro MS (Amersham Biosciences, Uppsala, Sweden) was used for quantitative determination of organic species of beans after and before cooking.

### Reagents and samples

All solutions were prepared with analytical reagent grade chemicals using high-purity deionized water obtained by Milli-Q® water purification system (Millipore, Bedford, USA). Nitric acid 65% (m/v) (Merck, Darmstadt, Germany) distilled in a quartz sub-boiling still (Marconi, SP, Brazil) and $H_2O_2$ 30% (m/v) (Merck) were used for sample digestion. Tritisol® standard solution of 1000 mg $L^{-1}$ of Fe (Merck) was used to prepare the reference analytical solutions by serial dilution in 0.14 mol $L^{-1}$ $HNO_3$.

Analytical grade chloroform, ethanol, methanol, NaCl and NaOH (Merck) were used for solid-liquid extractions.

The total protein concentration in each extractant (water, NaCl, ethanol and NaOH) was determined using Bradford method.[9] The Bradford reagent was prepared using 10 mg of Coomassie Blue G-250, 5.0 mL of methanol and 10 mL of 85% (v/v) phosphoric acid (Sigma). The final volume (100 mL) was completed with deionized water. The protein standard was prepared dissolving 4.0 mg of ovoalbumin (BioAgency, São Paulo, Brazil) in 2.0 mL of deionized water, using Vortex stirring for 2 min. Afterward this solution was 10-fold diluted with deionized water.

For MALDI-TOF MS analysis, the dialyzed fractions (water fraction) were adequately diluted in saturated solution of sinapinic acid (LaserBio Labs, France) in 50% (v/v) acetronitrile (Merck, USA) and 0.5% (v/v) trifluoroacetic acid (TFA, Fluka, Switzerland).

The bean, called "carioca", used in this research was purchased at local markets. Before analysis, sample was washed with deionized water several times.

Corn (SRM 8433) as certified reference material from NIST (National Institute of Standards and Technology, Gaithersburg, Maryland, USA) was used to check the entire accuracy of the analytical method.

### Sample digestion

Sample mass ranging from 150 to 250 mg were digested using a diluted oxidant mixture (2 mL $HNO_3$ + 1 mL $H_2O_2$ + 3 mL $H_2O$).[10] This mixture was submitted to digestion in a closed-vessel microwave system. The heating program was performed in three steps (Temperature/ºC; ramp/min; hold/min): 1 (140; 5; 1); 2 (180, 4, 5); and 3 (220, 4, 10). There is a fourth step for cooling down the system through forced ventilation for a period of 20 min. After the digestion, samples (beans and corn bran) and analytical blank solutions were transferred to plastic flasks and made up to 10 mL with deionized water. Samples and CRM (corn) were digested in triplicate.

### Cooking procedure

After cleaned with deionized water the beans were separated in two parts. The first portion was ground in a household food grinder and dried in stove at 60 ºC until constant mass. The second portion (*ca.* 500 g) was cooked in stainless steel pressure cooker in 1.0 L of deionized water for 40 min. A mixture of cooked grains and water was ground and dried using the same procedure adopted for the raw beans.

### Sequential extraction

The sequential extraction procedure was described by Naozuka *et al.*[11] Masses around 5.0 g of dried raw and cooked grains were used to solid-liquid sequential extraction with 10 mL of different extractants: methanol and chloroform (1:2 v/v), deionized water, 0.5 mol $L^{-1}$ NaCl, 70 % (v/v) ethanol and 0.5 mol $L^{-1}$ NaOH. An orbital shaker was used for extraction for 30 min. The separation of solid phase was carried out after filtration with 0.45 μm membrane filter (methanol and chloroform phase) and centrifugation using rotation velocity of 350 rpm for 30 min (other phases). Proteins and Fe were determined in the supernatants, except in the methanol/chloroform fraction. This experiment was performed in triplicate.

### Total protein determination

The total protein concentration was determined in water, NaCl, ethanol, and NaOH fractions by the Bradford method. The spectrophotometer calibration was performed using analytical reference solutions of 4, 6, 8, 10, 12, 16 and 20 μg of ovoalbumin in 1.0 mL of Bradford reagent. Water and NaCl extracts were diluted 10-fold and NaOH fraction was diluted 20-fold. After dilution, a volume of 100 μL of these solutions was used for protein determination. The ethanol portion was not diluted.

### MALDI-TOF MS analyses

The aqueous supernatants of raw and cooked grains were analyzed by MALDI-TOF MS. Aqueous supernatants volumes of 5 mL were put in a cellulose tubing of 32 mm diameter (D0530, Sigma-Aldrich) for dialysis in 1.0 L of deionized water over agitation (100 rpm for 24 h).

The dialyzed aqueous fractions were mixed 1:1 (v/v) (raw grains) and 1:10 (v/v) (cooked grains) with a saturated solution of sinapinic acid in 50% (v/v) acetronitrile and 0.5% (v/v) trifluoroacetic acid. This mixture was agitated and subsequently centrifuged using rotation velocity of 5000 rpm for 10 s. An aliquot of 0.5 μL was spotted onto a MALDI plate and analyzed by MALDI-TOF MS.[11]

The analyses were performed in the linear mode using an acceleration voltage of 20 kV and a vacuum pressure of $1.5 \times 10^{-6}$ bar. Laser pulses were generated by a nitrogen laser (8 pulses *per* second). Each spot was analyzed twice, accumulating mass spectra composed of a total of approximately 200 laser shots.

### Fe determination by GF AAS

The digested samples and supernatants (water, NaCl, ethanol and NaOH) were analyzed by GF AAS. Appropriated dilution in deionized water, ranging from 2 to 50-fold, was performed, depending on the extractant. An aliquot of 10 μL was introduced into the graphite tube without chemical modifier and submitted to the heating program described in Table 1. The calibration was done using analytical reference solutions: 10-40 μg $L^{-1}$ of Fe.

Chemical interferences were verified by addition and recovery test. For this, it was added an analytical solution of 40 μg $L^{-1}$ Fe in all of the extractants, except in the methanol/chloroform fraction.

## Results and Discussion

### Cooking effects on protein concentration

The protein determination by Bradford method[9] was carried out in each extractant obtained after the sequential extraction (water, NaCl, ethanol and NaOH). The results are shown in the Table 2. It is well discussed in the literature[12,13] that the extractants water, NaCl, ethanol and NaOH promoted the separation of different groups of proteins: albumins, globulins, prolamins and glutelins, respectively.[12,13] The total protein concentration obtained by the masses sum of all extracts revealed that cooking promoted a sensible decrease in the protein content, mainly in the globulins fraction, when compared to the uncooked beans. Previous investigations showed that the total protein concentration ranged from 22.57 to 24.42 g *per* 100 g and from 23.25 to 26.29 g *per* 100 g for raw and cooked beans, respectively.[14] Comparing these protein value with obtained protein concentration (sum of each fraction), it is possible to observe that low quantity of protein was extracted (6.6-7.0% and 4.1-4.6% for raw and cooked beans, respectively). However, it is important to point out that the domestic cooking changed the albumins, prolamins, globulins and glutelins distribution, since high concentrations of albumins, globulins and glutelins were found in raw grains, while albumins and glutelins were the main groups of proteins determined in cooked grains. Such behavior can be associated to the association-dissociation properties of proteins that are expected to be changed by heating, resulting in a decrease of the protein solubility.[15]

### Cooking effects on organic compounds (MALDI-TOF MS)

In Figures 1 and 2 are shown the MALDI-TOF MS spectra of aqueous supernatant phases of raw and cooked grains, respectively. Comparing the results, it is possible to observe that the heating procedure decreased the number of compounds of molecular weights ranged from 2 to 17 kDa (1 Da = $1.661 \times 10^{-24}$ g).[16] The raw grains spectrum presented 32 compounds, while in the cooked grains results show only 22 compounds. Cooking resulted in a decrease of the molecular weights of the compounds in the beans. Compounds of molecular weight in the range of 2 and 3.5 kDa were only found in cooked grains. In the cooked beans, four high molecular weight compounds (12-16 kDa)

**Table 2.** Protein and Fe concentration in each protein fractions and digested samples

| | Raw grains | | | Cooked grains | | |
|---|---|---|---|---|---|---|
| | Proteins / (mg $g^{-1}$) | Fe / (μg $g^{-1}$) ± SD[b] | Fe/P (%)[a] | Proteins / (mg $g^{-1}$) | Fe / (μg $g^{-1}$) ± SD[b] | Fe/P (%)[a] |
| Albumins | 2.84 ± 0.02 | 7.8 ± 0.8 | 2.4 | 3.35 ± 0.03 | 14 ± 3 | 4.6 |
| Globulins | 3.50 ± 0.03 | 9.3 ± 0.7 | 2.8 | 0.37 ± 0.02 | 15 ± 2 | 4.9 |
| Prolamins | 0.541 ± 0.002 | 0.55 ± 0.02 | 0.17 | 0.797 ± 0.001 | 0.16 ± 0.04 | 0.052 |
| Glutelins | 9.3 ± 0.1 | 73 ± 5 | 22 | 6.14 ± 0.04 | 2.8 ± 1.3 | 0.92 |
| Sum[c] | 16.1 ± 0.1 | 90 ± 5 | - | 10.7 ± 0.1 | 32 ± 6 | - |
| Total[d] | - | 331 ± 21 | - | - | 305 ± 43 | - |

[a]Fe/P = Fe associated to proteins, calculated value considering the total Fe concentration. [b]SD = standard deviation (n = 3). [c]Sum = sum of masses of each protein fraction. [d]Total = concentration in digested samples.

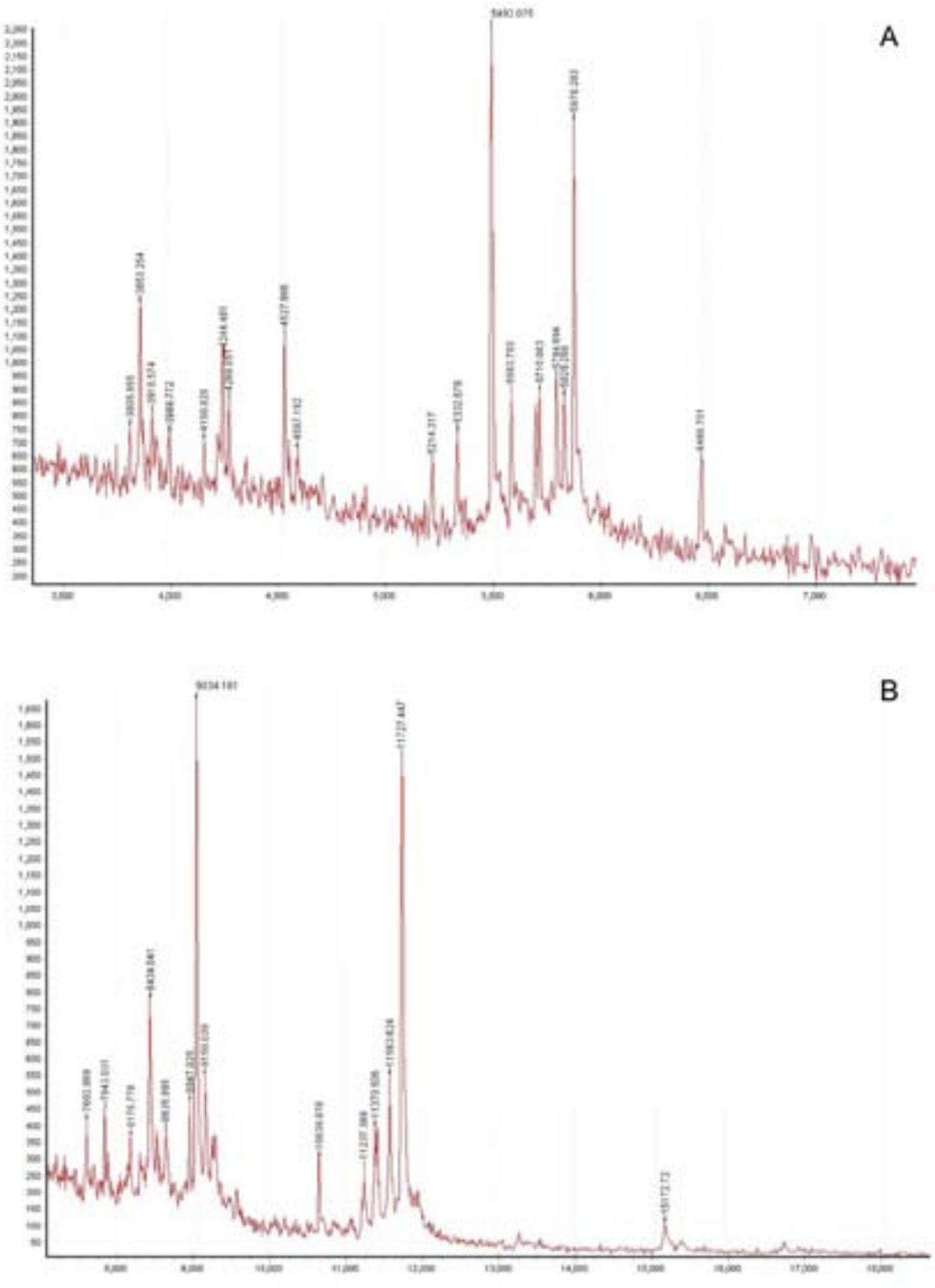


**Figure 1.** MALDI-TOF spectra of the water-soluble fraction of the raw grains: (A) 3.5-7.0 kDa and (B) 7.5-18 kDa.

were observed in the MALDI TOF MS spectrum (Figure 2). However, in the raw beans only one high molecular weight compound (*ca.* 15.2 kDa) is observed (Figure 1B). Even as the proteins, some organic compounds can be degraded with cooking procedure, such as tannins and phytate.[14] Additionally, the association and dissociation of proteins can explain the presence of new compounds of low and high molecular weights after the domestic cooking. In immature seeds of flageolet bean, the cooking improved the high protein quality by destroying or inactivating heat-labile anti-nutritional factors, such as trypsin inhibitors, phytic acid, tannins and oligosaccharides.[3,5]

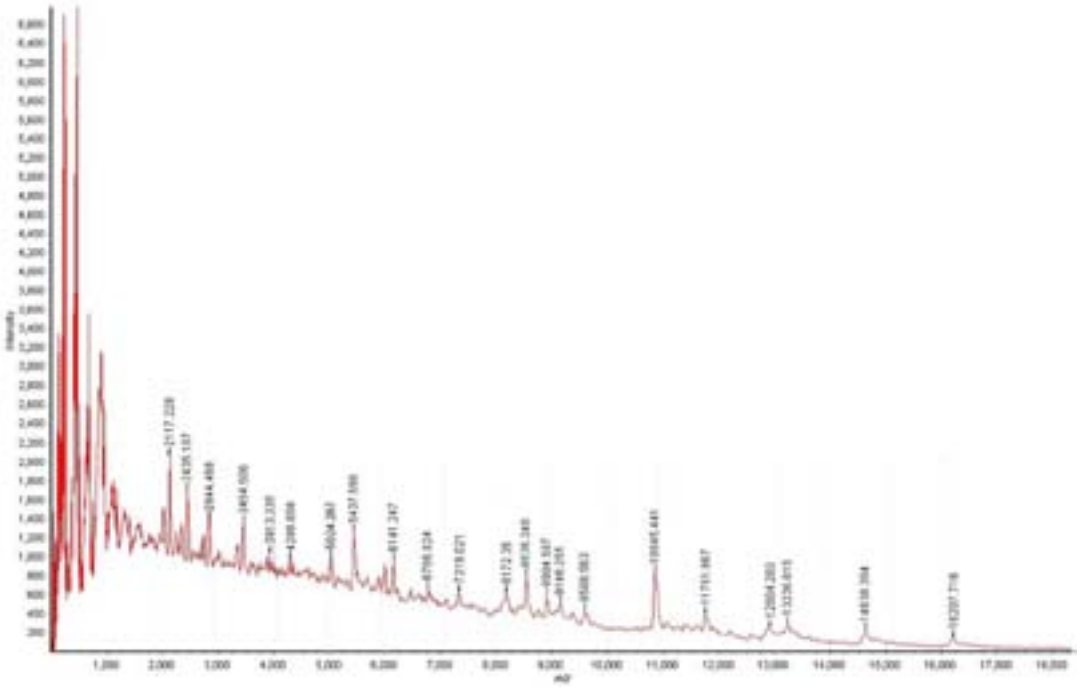

**Figure 2.** MALDI-TOF spectra of the water-soluble fraction of the cooked grains.

## Cooking effects on Fe distribution in different extracts

Comparing the certified (14.8 ± 1.8 mg $kg^{-1}$) with the obtained values (16.8 ± 3.8 mg $kg^{-1}$), it is possible to assure that they are coincident at 95% of confidence interval, according to Student *t* test. The addition of analytical solution of Fe (40 μg $L^{-1}$) in the water, NaCl, ethanol and NaOH extracts of the cooked grains showed recoveries of 89, 123, 96 and 100%, respectively, which indicate no interference during the Fe determination by GF AAS. According to NBR ISO/IEC 17025[17] the recovery tolerance ranges from 70 to 120%.

Table 2 shows total Fe concentration in the digestates and in each fraction (water, NaCl, ethanol and NaOH). These results indicate that cooking did not affect Fe concentration. Deionized water used for cooking was the blank.

Comparing the total Fe concentration (digestates) with the concentration resulting from the sum of masses of Fe associated to the different protein groups (albumins, globulins, prolamins and glutelins), Table 2, it is interesting to observe that 27 and 10% of the Fe is associated to proteins (albumins, globulins, prolamins and glutelins) in the raw and cooked beans, respectively. It is evident that the domestic cooking affected the Fe distribution in these protein types. Additionally the heating also altered the Fe percentage in each fraction (Table 2), distinguishing the lost of Fe mainly in the glutelin fraction. It is possible that the heating can release Fe of the active sites of proteins, since that the transition metal ions, such as $Fe^{2+}$, have the strongest coordinating interactions, thus being found in the majority of metalloproteins.[16] Studies showed that cooking may affect macro and micronutrients bioavailability. The digestibility and hence absorption of micronutrients, such as Fe, is improved upon heat processing; with the resultant softening of the food matrix, protein-bound elements is released, thus facilitating its absorption. In addition, heat processing of food also alters the inherent factors that inhibit mineral absorption, such as phytate and dietary fiber. In white beans, the traditional cooking had a positive effect on the bioavailability of Ca, Zn and Fe.[6,18]

In raw grains, it is possible to observe that Fe is mainly associated to albumins, globulins and glutelins (Table 2). For cooked grains, Fe is presented in high concentration in albumins and globulins. The cooking procedure altered the association of Fe with glutelins. The main amino acids constituents of albumins, globulins, prolamins and glutelins are rich in sulfur and charged groups such as methionine, cysteine, glutamic acid, arginine, aspartic acid and lysine.[11,19-21] The metal ions present high-affinity for these amino acids. The cooking effects in the elements distribution in these proteins types can be associated to alteration in the aminoacids content, since that heat procedure causes considerable changes in the composition of numerous chemical constituents, including amino acids, vitamins and minerals, depending on the temperature and time of thermal treatment.[3] Studies with pulses showed that the long cooking time reduces the nutritive value and the levels of some essential amino acids.[5]

## Conclusions

Cooking affected the chemical composition of beans. Total Fe concentration was constant after the heating. Total protein concentration was reduced, indicating the domestic cooking altered the protein structure and consequently their solubility in the different extractants (water, NaCl, ethanol and NaOH). Some organic compounds were changed, considering their molecular weights (< 3.5 and > 12 kDa). The cooking also affected the Fe distribution in the different protein types (albumins, globulins, prolamins and glutelins), mainly in the glutelin fraction. The heating is capable of promoting protein denaturation, association-dissociation of proteins, inactivation or destruction of anti-nutritional components and alteration of elemental bioavailability.

## Acknowledgments

The authors are grateful to the Conselho Nacional de Desenvolvimento Científico e Tecnológico (CNPq) and Fundacão de Amparo à Pesquisa do Estado de São Paulo (FAPESP) for financial support and fellowship provided. P.V.O. is thankful to CNPq for the research fellowship.

## References

1. Brigide, P.; Canniatti-Brazaca, S. G.; *Food Chem.* **2006**, *98*, 85.
2. Ranilla, L. G.; Genovese, M. I.; Lajolo, F. M.; *J. Agric. Food Chem.* **2009**, *57*, 5734.
3. Słupski, J.; *Food Chem.* **2010**, *121*, 1171.
4. Saha, S; Singh, G.; Mahajan, V.; Gupta, H. S.; *Plant Foods Hum. Nutr.* **2009**, *64*, 174.
5. Wang, N.; Hatcher, D. W.; Tyler, R. T.; Toews, R.; Gawalko, E. J.; *Food Res. Int.* **2010**, *43*, 589.
6. Bressani, R.; *Food Rev. Int.* **1993**, *9*, 237.
7. Quinteros, A.; Farre, R.; Lagarda, M. J.; *Food Chem.* **2001**, *75*, 365.
8. Ramírez-Cárdenas, L.; Leonel, A. J.; Costa, N. M. B.; Reis, F. P.; *Food Res. Int.* **2010**, *43*, 573.
9. Bradford, M. M.; *Anal. Biochem.* **1976**, *72*, 248
10. Naozuka, J.; Vieira, E. C.; Nascimento, A. N.; Oliveira, P. V.; *Food Chem.* **2011**, *124*, 1667.
11. Naozuka, J.; Marana, S. R.; Oliveira, P. V.; *J. Food Compos. Anal.* **2010**, *23*, 78.
12. Chunhieng, T.; Pétritis, K.; Elfakir, C.; Brochier, J.; Goli, T.; Montet, D.; *J. Agric. Food Chem.* **2004**, *52*, 4318.
13. Naozuka, J.; Oliveira, P. V.; *J. Braz. Chem. Soc.* **2007**, *18*, 1547.
14. Ramírez-Cárdenas; Leonel, A. J.; Costa, N. M. B.; *Cienc. Tecnol. Aliment.* **2008**, *28*, 200.
15. Carbonaro, M.; Vecchini, P.; Carnovale, E.; *J. Agric. Food Chem.* **1993**, *41*, 1169.
16. Garcia, J.S.; Magalhães, C. S.; Arruda, M. A. Z.; *Talanta* **2006**, *69*, 1.
17. Burin, R.; Burin, V. M.;Taha, P.; Bordignon-Luiz, M. T.; *Ciênc. Tecnol. Aliment.* **2008**, *28*, 973.
18. Lombardi-Boccia, G.; Santis, N.; Lullo, G. D.; Carnovale, E.; *Food Chem.* **1995**, *53*, 191.
19. Garcia, R. M.; Arocena, R. V.; Laurena, A. C.; Tecson-Mendoza, E. M.; *J. Agric. Food Chem.* **2005**, *53*, 1734.
20. Moreno, F. J.; Jenkins, J. A.; Mellon, F. A.; Rigby, N. M.; Robertson, J. A.; Wellner, N.; Mills, E. N. C.; *Biochim. Biophys. Acta* **2004**, *1698*, 175
21. Sun, S. S. M.; Leung, F. W.; Tomic, J. C.; *J. Agric. Food Chem.* **1987**, *35*, 232.

*Submitted: October 25, 2010*
*Published online: November 8, 2011*

**FAPESP has sponsored the publication of this article.**

Article

*J. Braz. Chem. Soc.*, Vol. 23, No. 1, 163-170, 2012.
Printed in Brazil - ©2012 Sociedade Brasileira de Química
0103 - 5053 $6.00+0.00

# Molecular Docking and Molecular Dynamic Studies of Semi-Synthetic Piperidine Alkaloids as Acetylcholinesterase Inhibitors

***Amanda Danuello,[a] Nelilma C. Romeiro,[b] Guilherme M. Giesel,[c] Marcos Pivatto,[a] Claudio Viegas Jr.,[d] Hugo Verli,[c,e] Eliezer J. Barreiro,[b] Carlos A. M. Fraga,[b] Newton G. Castro[f] and Vanderlan S. Bolzani*[,a]***

*[a]Núcleo de Bioensaios, Biossíntese e Ecofisiologia de Produtos Naturais (NuBBE), Departamento de Química Orgânica, Instituto de Química, Universidade Estadual Paulista 'Julio de Mesquita Filho', CP 355, 14801-970 Araraquara-SP, Brazil*

*[b]Laboratório de Avaliação e Síntese de Substâncias Bioativas (LASSBio), Faculdade de Farmácia, Universidade Federal do Rio de Janeiro, CP 68023, 21944-910 Rio de Janeiro-RJ, Brazil*

*[c]Centro de Biotecnologia, Universidade Federal do Rio Grande do Sul, Av. Bento Gonçalves 9500, CP 15005, 91500-970 Porto Alegre-RS, Brazil*

*[d]Laboratório de Fitoquímica e Química Medicinal (LFQM), Departamento de Ciências Exatas, Universidade Federal de Alfenas, 37130-000 Alfenas-MG, Brazil*

*[e]Faculdade de Farmácia, Universidade Federal do Rio Grande do Sul, Av. Ipiranga 2752, 90610-000 Porto Alegre- RS, Brazil*

*[f]Departamento de Farmacologia Básica e Clínica, Instituto de Ciências Biomédicas, Universidade Federal do Rio de Janeiro, CCS Bloco J Sala J1-029, 21941-902 Rio de Janeiro-RJ, Brazil*

A mistura dos derivados semissintéticos cloridrato da (–)-3-*O*-acetil-cassina e cloridrato da (–)-3-*O*-acetil-espectalina, preparada a partir da mistura dos alcalóides (–)-cassina e (–)-espectalina (4:1) obtida de *Senna spectabilis*, é um potente inibidor da acetilcolinesterase (AChE), assim justificando mais estudos moleculares. Neste sentido, estudos de *docking* e dinâmica moleculares foram conduzidos neste trabalho com o objetivo de adquirir uma compreensão mais profunda de todos os aspectos estruturais das moléculas cloridratos da (–)-3-O-acetil-cassina e (–)-3-O-acetil-espectalina, as quais diferem em seus potenciais inibidores de AChE. Os dois derivados em estudo apresentaram diversas interações com o sítio periférico aniônico dentro da cavidade catalítica de AChE de *Torpedo californica*. Entretanto, somente o composto majoritário (–)-3-*O*-acetil-cassina mostrou interação com a tríade catalítica de maneira significativa. As simulações de dinâmica molecular utilizando água como solvente foram importantes para compreender as interações hipotéticas entre cloridratos da (–)-3-O-acetil-cassina e (–)-3-O-acetil-espectalina com AChE. Os dados obtidos indicam que o composto (–)-3-*O*-acetil-cassina é o inibidor da enzima mais potente possivelmente devido às suas interações favoráveis com a proteína, com menor custo de dessolvatação. Estes resultados sugerem que o tamanho da cadeia lateral influencia no potencial inibitório das moléculas avaliadas e podem representar o ponto de partida para o desenvolvimento de novos derivados de (–)-3-*O*-acetil-cassina, objetivando a descoberta de inibidores de AChE mais eficazes.

The mixture of semi-synthetic derivatives (–)-3-*O*-acetyl-cassine hydrochloride and (–)-3-*O*-acetyl-spectaline hydrochloride, prepared from the mixture of natural alkaloids (–)-cassine and (–)-spectaline (4:1) isolated from *Senna spectabilis*, has been shown to be a potent acetylcholinesterase (AChE) inhibitor, thereby prompting further molecular studies. In this sense, docking and dynamic molecular studies were carried out in this work, aiming to acquire a deeper understanding about all the structural aspects of molecules (–)-3-*O*-acetyl-cassine and (–)-3-*O*-acetyl-spectaline hydrochlorides, which differ with respect to their AChE inhibitory potentials. Both molecules establish important interactions with the peripheral anionic site within the catalytic gorge of *Torpedo californica* AChE. However, only the major compound (–)-3-*O*-acetyl-cassine hydrochloride significantly interacts with the catalytic triad. Explicit-solvent molecular dynamic simulations were conducted in order to gain better understanding about the hypothetical interactions taking place between the semi-synthetic alkaloid molecules (–)-3-*O*-acetyl-cassine and (–)-3-*O*-acetyl-spectaline hydrochlorides and AChE. The data obtained in this study indicated that (–)-3-*O*-acetyl-cassine hydrochloride is the most potent inhibitor of AChE possibly due to the favorable interactions of this molecule with the target protein, with lower desolvation cost. These results suggested that the size of the side chain has an effect on the inhibitory potential of the evaluated molecules and may represent the starting point for the development of new derivatives of (–)-3-*O*-acetyl-cassine hydrochloride, with a view to the discovery of new effective AChE inhibitors.

**Keywords:** molecular docking, molecular dynamic, piperidine alkaloids, acetylcholinesterase inhibitors

*e-mail: bolzaniv@iq.unesp.br

## Introduction

Alzheimer's disease (AD) is a late-onset neurodegenerative pathology that affects the memory, motor coordination, and cognition in a progressive, and eventually lethal, manner.[1-3] It has been postulated that at least some of the cognitive impairment experienced by AD patients results from deficient acetylcholine levels and consequent reduction in cholinergic neurotransmission. Consequently, the key approach employed in the development of drugs for use in the symptomatic treatment of AD has targeted the cholinergic deficit. Currently, only five drugs have received approval in the USA and Europe for therapeutic use in AD, namely tacrine (**1**; Cognex™),[4] donepezil (**2**; Aricept™),[5] rivastigmine (**3**; Excelon™),[6] galantamine (**4**; Reminyl™)[7] and memantine (**5**; Ebixa™)[8] (Figure 1). All of these compounds are acetylcholinesterase inhibitors (AChEIs),[4-7] with the single exception of **5**, which acts by blocking the *N*-methyl-D-aspartate (NMDA) glutamate receptors. It is apparent, therefore, that inhibition of acetylcholinesterase remains an important therapeutic strategy to the palliate cognitive deficit in AD.

The screening of numerous plant species that were typically selected based on their ethnobotanical data or report of their popular uses has been carried out in order to discover anticholinesterasic compounds with novel structural entities.[9-18] In this context, flowers, fruits, leaves and seeds from the ornamental plant *Senna spectabilis* (syn. *Cassia spectabilis*) (Fabaceae) have been reported to be sources of biologically rare piperidine alkaloids.[19] A deep analysis of the structural features of the naturally-occurring (–)-3-*O*-acetyl-spectaline (**6**) identified that part of this compound contains a molecular fragment similar to acetylcholine (ACh) (Figure 2). This has led to the preparation of several semi-synthetic derivatives, including (–)-3-*O*-acetyl-spectaline hydrochloride (**10**), which was prepared from natural piperidine (–)-spectaline (**8**). This derivative has been shown to display both *in vitro* (inhibitory concentration ($IC_{50}$) = 7.32 μM) and *in vivo* cholinergic activity during the spatial memory test (water maze).[20] Aiming to elucidate the mechanism of cholinesterase inhibition followed by this derivative, kinetic studies have revealed noncompetitive cholinesterase inhibition and central nervous selectivity with few peripheral side effects.[21]

Considering these results, compound **10** was selected as a prototype for further studies aiming to achieve a lead molecule. Additional scale-up fractionation of *S. spectabilis* and further isolation of the natural alkaloid **8** were monitored by electrospray ionization mass spectrometry (ESI-MS). This investigation revealed that the previously published piperidine alkaloids were in fact mixtures of two homologous piperidine alkaloid isomers (–)-cassine (**7**) and (–)-spectaline (**8**) at a ratio of 4:1, respectively (Figure 2).[22] So, the cholinesterase inhibition properties identified in that study were due to the mixture of (–)-3-*O*-acetyl-cassine hydrochloride (**9**) and **10** instead of being due to only the latter compound.

In spite of this problem, the main aim of this study was to investigate the binding patterns of the derivatives **9** and **10** with AChE and to verify the possible differences in their inhibition profiles. Molecular modeling studies of complexes formed between *Torpedo californica* acetylcholinesterase (*Tc*AChE) and the target semi-synthetic AChE inhibitors were accomplished by the application of flexible docking methodologies. The docking complexes were also submitted to explicit-solvent molecular dynamic (MD) simulations in water in order to gain dynamic understanding of the hypothetic interactions taking place between the molecules and AChE.

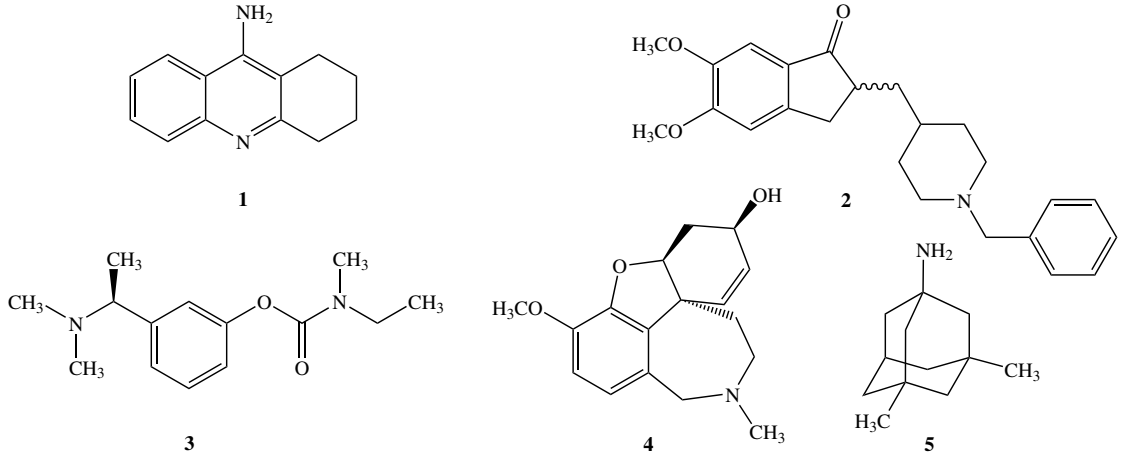


**Figure 1.** Marketed acetylcholinesterase inhibitors tacrine (**1**), donepezil (**2**), rivastigmine (**3**), galantamine (**4**) and NMDA/glutamate receptor blocker memantine (**5**).

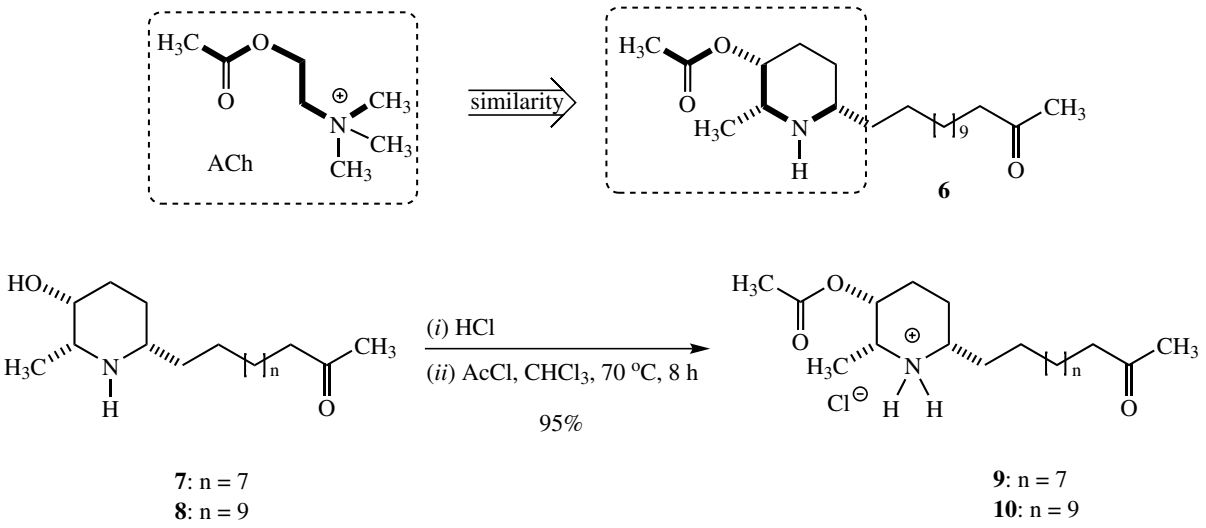


**Figure 2.** Molecular structures of (–)-3-*O*-acetyl-spectaline (**6**), (–)-cassine (**7**), (–)-spectaline (**8**), (–)-3-*O*-acetyl-cassine hydrochloride (**9**) and (–)-3-*O*-acetyl-spectaline hydrochloride (**10**).

A considerable amount of data related to the crystal structure of AChE and to various AChEI complexes is available.[23-25] With information, it is possible to apply molecular modeling methods to gain insight into the mechanism of action of the enzyme and to investigate the molecular determinants that modulate the molecular recognition of AChE inhibitors. Such knowledge can be exploited during the design of novel AChE inhibitors that might be more effective in the treatment of AD.[26-30]

## Methodology

### Molecular docking analyses

The accurate prediction of protein-ligand interaction geometries is essential for the success of the virtual-screening approaches employed during structure-based drug design. This procedure requires docking tools that are able to generate suitable conformations of a ligand within a protein-binding site and demands reliable energetic evaluations for the quality determination of the interaction. In this respect, the FlexX™ scoring function has been shown to be reliable in a variety of different cases, even when flexible ligands are concerned.[31] Thus, in the present study, docking with FlexE was performed using the default FlexX™ scoring function following the preparation of both the ligand and the protein.

Molecular docking analyses were accomplished by using the SYBYL 9 (Tripos Inc., St. Louis, MO, USA) version 7.2 software and the programs embedded therein. Formal charges were assigned, and the FlexX scoring function[31] was chosen for computation of the FlexE[32] docking poses.

### Preparation of ligands for the docking studies

Ligand coordinates were generated using the sketcher tool embedded in the SYBYL software suite, and the correct atom types (including hybridization states) and bond categories were defined. Hydrogen atoms were subsequently added, Gasteiger-Hückel charges[33] were assigned to each atom, and the final structures were energy-minimized. Carboxylic acid groups were modeled in their anionic form, whereas amino groups were considered in their protonated form.

### Preparation of protein structures for the docking studies

Three-dimensional crystal structures of *Tc*AChE complexed with huperzine, tacrine and donepezil were retrieved from the RCSB (Research Collaboratory for Structural Bioinformatics) protein data bank[34] under PDB IDs 1VOT, 1ACJ and 1EVE, respectively. The active site of *Tc*AChE was defined as the collection of residues within 15.0 Å of the bound inhibitor present in the reference structure 1ACJ. The bound inhibitors were not included in the docking runs.

For each structure, the description of an ensemble contains the definition of the protein atoms (via chain identifiers and hetero groups), the resolution of ambiguities in the PDB file (alternate location indicators etc.), the location of hydrogen atoms at the heteroatoms and the definition of the active site atoms. The first step in the generation of suitable protein structures for ensemble superimposition is the selection of one chain from the reference crystal structure (1ACJ). This process generally involves retention of chain A and deletion of other chains, if present.

Stepwise analysis and correction of the geometric parameters, including atom types, atom names, torsion angles, bump elimination and hydrogen addition, were carried out with the aid of the Biopolymer "protein preparation" tool embedded in the SYBYL software suite. The assignment of the hydrogen positions was based on default rules, except for the definition of the torsion angles at the hydroxyl groups of the amino acid residues serine, threonine and tyrosine, and the hydrogen position inside the histidine side chain. Charges were added according to the AmberF99 force field simulation.[35] The side-chains of lysine and arginine, and the carboxylate groups of aspartic and glutamic acids, were modeled in their ionized states. Water molecules contained in the PDB file were removed. After each docking run, thirty poses were saved in Mol2 files for further analysis.

### Ligand topologies

The structure of each compound was submitted to the PRODRG Server,[36] and the initial geometries and crude topologies were retrieved on the basis of the best ranking docking poses previously obtained by flexible docking with FlexE. The employed atomic charges were derived from the Löwdin scheme and were obtained at the HF/6-31G** level using the program GAMESS[37] in an appropriated form for molecular dynamic calculations. Analyses were carried out using the GROMACS simulation suite[38] and the GROMOS96 force field, as previously reported.[39-41]

### Molecular dynamic simulations

Three systems were submitted to molecular dynamic (MD) simulations: (*i*) uncomplexed AChE in solution, (*ii*) AChE complexed with **9** and (*iii*) AChE complexed with **10**. The GROMACS simulations suite and GROMOS96 force field were used by employing an MD protocol based on previous studies.[42] Briefly, these systems were solvated in triclinic boxes using periodic boundary conditions and the SPC water model.[43] Counter ions were added, so as to neutralize the charges of the systems. The LINCS method[44] was applied in order to constrain covalent bond lengths. This allowed for an integration step of 2 fs after an initial energy minimization step using the steepest descent algorithm. Electrostatic interactions were calculated with particle-mesh Ewald.[45] Temperature and pressure were kept constant by separately coupling protein, ligand, ions, and solvent to external temperature and pressure baths with constants of $\tau = 0.1$ and 0.5 ps, respectively.[46] The system was slowly heated from 50 to 310 K in steps of 5 ps, each one increasing the reference temperature by 50 K. After this thermalization, the reference temperature was maintained at 310 K. Interaction energies are presented as the sum of Coulomb and Lennard-Jones components over the entire MD trajectories. Ranked data were evaluated using Kruskal-Wallis one-way analysis of variance (ANOVA),[47] whereas pairwise multiple comparisons were assessed by the Tukey test.[48] Between-group comparisons were appraised with the Mann-Whitney rank sum test.[49,50]

## Results and Discussion

### Enzyme-inhibitor interactions at the bottom of the AChE gorge

The visual inspection of the ligand-*Tc*AChE complexes (Figures 3a-b) shows that the bottom of the active site gorge of AChE may be represented by amino acid residue Trp84. The evaluation of the best ranking docking poses obtained for **9** and **10** revealed that neither of these molecules was

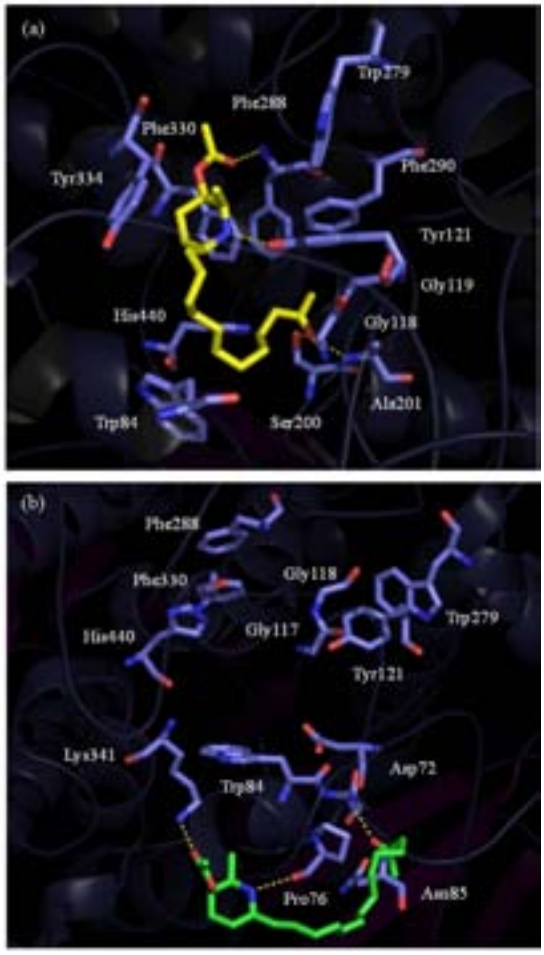


**Figure 3.** Top scored ligand-*Tc*AChE complexes obtained by flexible docking with FlexE for (a) **9** and (b) **10**. Non-polar hydrogen atoms were omitted for clarity. Only active site residues are shown. Hydrogen bonds are represented as green dashed lines.

able to penetrate deeply into the enzyme gorge. Presumably, this is a consequence of the volume of the long aliphatic side chains present in the two compounds. However, unlike its homologue **10**, acetyl hydrochloride derivative **9** was able to interact with one of the residues, hence forming the AChE catalytic triad (*i.e.*, Ser200, Glu327 and His440) through formation of a hydrogen bond linking the terminal oxygen atom of its acetyl group with Ser200.

### Enzyme-inhibitor interactions in the middle of the AChE gorge

A constriction is located within the region considered to be the middle of the AChE active site gorge and is represented by amino acid residue Phe330 (Figures 3a-b). However, neither **9** nor **10** appear to interact with Phe330, although a binding site with **9** is located relatively close to this residue (Figure 3a).

### Enzyme-inhibitor interactions at the entrance to the AChE gorge

Amino acid residues, including Tyr70, Tyr121 and Trp279, making up the peripheral anionic site of AChE are located close to the top of the active site gorge. The visual inspection of the top scoring pose of **9** reveals that the piperidine ring and the aromatic rings of Phe288 and Phe290 are within van der Waals contact distance (Figure 3a). Additionally, **9** is able to form hydrogen bonds with the –NH group of Phe288 via the ester function, with Gly118, Gly119 and Ala201 via the oxygen of the terminal acetyl group, and with Tyr121 via the hydrogen atom associated with the protonated amino group of the piperidine moiety (Figure 3a). In contrast, **10** can establish hydrogen bonds with Lys341 via the ester function, with Pro76 via the protonated nitrogen atom of the piperidine ring, and with Asn85 via the terminal acetyl group. It is noteworthy that, as compared to **9**, **10** binds to AChE in a perpendicular fashion, with an extended conformation (Figures 3a-b). Binding of compounds **9** and **10** to the peripheral anionic site of AChE is likely to generate a steric blockade of the enzyme gorge similar to that described for the anticholinesterasic drug donepezil, which presents analogous binding characteristics.[25]

### Molecular dynamics stimulations

In order to obtain further information regarding the dynamics of AChE inhibition by **9** and **10**, complexes between the enzyme and the semi-synthetic derivatives were submitted to MD simulations in water. Figures 4a-b show the docking-obtained orientations of each compound superimposed on the respective 5 ns MD simulations, while Figure 4c depicts the 5 ns MD simulations of **9** and

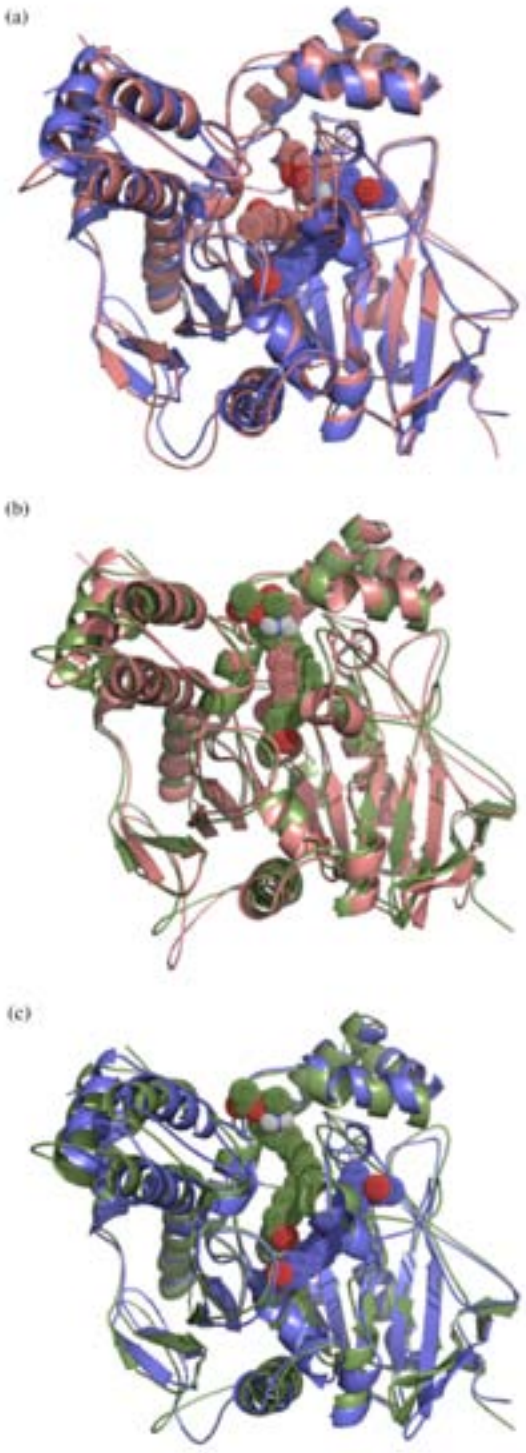


**Figure 4.** Superimposition of AChE complexed with **9** and **10**: (a) **9** in the docking-derived orientation (salmon) and after 5 ns MD (blue), (b) **10** in the docking-derived orientation (salmon) and after 5 ns MD (green) and (c) **9** (blue) and **10** (green) after 5 ns MD. Oxygen atoms are presented in red and polar hydrogen atoms in white.

**10** superimposed one upon the other. Both compounds underwent significant reorientations in the simulated time scale, indicating an important role for the solvent with respect to the flexibility and stabilization of the complexes. However, such conformational accommodations did not appear to induce major modification in AChE dynamics or secondary structural elements (Supplementary Information, data available).

MD simulation revealed interactions between both molecules **9** and **10** and the amino acid residue Trp84 at the bottom of the enzyme gorge, although the binding energy of **9** with this residue (–7.7 ± 6.5 kJ mol$^{-1}$) was more favorable than that of **10** (–1.9 ± 2.6 kJ mol$^{-1}$) (Table 1). In the middle of the gorge, both **9** and **10** interacted with Trp432, which lies in a region close to the amino acid residue Phe330. At the top of the gorge, **9** exhibited binding with Tyr70 and Asp72, and exhibited a very favorable interaction with the latter residue with a binding energy of –13.7 ± 10.0 kJ mol$^{-1}$. Close to this region of the gorge, derivative **9** also interacted with Tyr121 and Ser122. Although **10** did not bind with these residues, it interacts with residues Gln74, Asp285, Ser286, Arg289, Tyr334 and Gly335 (Table 1).

**Table 1.** Interaction energies between **9** and **10** and the amino acid residues of *Tc*AChE, together with the interaction energies of the unbound molecules with the solvent (water)

| Amino acid residues[a] | Energy / (kJ mol$^{-1}$)[b] | |
|---|---|---|
| | Compound **9** | Compound **10** |
| Tyr70 | –1.8 ± 1.5 | 0.0 ± 0.0 |
| Asp72 | –13.7 ± 10.0 | 0.0 ± 0.0 |
| Gln74 | 0.0 ± 0.0 | –3.6 ± 6.4 |
| Trp84 | –7.7 ± 6.5 | –1.9 ± 2.6 |
| Gly118 | 0.0 ± 0.0 | 0.0 ± 0.0 |
| Tyr121 | –5.0 ± 7.8 | 0.0 ± 0.0 |
| Ser122 | –2.1 ± 4.0 | 0.0 ± 0.0 |
| Asp285 | 0.0 ± 0.0 | –9.4 ± 8.1 |
| Ser286 | 0.0 ± 0.0 | –2.6 ± 2.5 |
| Arg289 | 0.0 ± 0.0 | –1.6 ± 2.5 |
| Tyr334 | 0.0 ± 0.0 | –4.0 ± 5.8 |
| Gly335 | 0.0 ± 0.0 | –2.0 ± 1.8 |
| Trp432 | –1.4 ± 2.9 | –1.3 ± 1.9 |
| $\Delta H_{AChE}$ | –34.0 ± 15.1[c] | –30.9 ± 17.7[c] |
| $\Delta H_{solvent}$ | –77.7 ± 15.4[c] | –92.6 ± 16.5[c] |

[a]Only the main interacting amino acid residues are shown; [b]fluctuation of each interaction along the performed simulations is presented in the Supplementary Information; [c]significant differences between values within a row (ANOVA; $p \leq 0.001$).

In view of the considerable flexibility shown by the AChE inhibitors, molecules **9** and **10** were also submitted to MD simulation on a 0.1 μs time scale in the presence of water but without the target protein (Figure 5). The data suggest that the increase in hydrophobicity of **10** as compared to **9** culminates in a greater entropic cost associated with the complexation of the former.

MD simulation of the AChE-inhibitor docking complexes AChE-9 and AChE-10 generated interaction energies of –34.0 ± 15.1 and –30.9 ± 17.7 kJ mol$^{-1}$, respectively (Table 1). The application of the Mann-Whitney rank sum test established that these values are statistically different ($p \leq 0.001$), a result that correlates with the observed differences in the biological activities of **9** and **10**. Similarly, the observed interaction energies between uncomplexed **9** and **10** and solvent water may be readily related to the enthalpic cost of desolvation associated with inhibition of AChE by these molecules. Therefore, the more active structure **9** may be seen as presenting a more favorable interaction with the target protein and as being held with lower intensity by the solvent. On the other hand, the less active compound **10** exhibits a less favorable interaction with the target receptor and a more intense interaction with the solvent.

## Conclusions

The molecular modeling study described herein was carried out with the aim of elucidating the molecular basis of the differential AChE inhibition profiles of two semi-synthetic acetyl derivatives of the piperidine alkaloids (–)-cassine and (–)-spectaline isolated from *S. spectabilis*. Flexible docking revealed different binding conformations and interaction patterns for (–)-3-*O*-acetyl-cassine hydrochloride (**9**) and (–)-3-*O*-acetyl-spectaline hydrochloride (**10**) with respect to AChE, especially in the peripheral anionic site. Explicit-solvent molecular dynamic simulations in water revealed that the more active compound **9** presents a more favorable interaction with the target protein, as anticipated by flexible docking, at a lower desolvation cost. On the other hand, the less active compound **10** exhibits a less favorable interaction with the enzyme along with a more intense interaction with the solvent. These results emphasize the importance of the shorter side chain of **9** for a better interaction with AChE. This is due to reduced steric limitations to the entry of the inhibitor into the active site gorge. This finding will be able to guide the design of new derivatives of **9**, *e.g.*, via shortening of the side chain bearing different functionalities, aiming at the synthesis of anti-Alzheimer lead compounds based on natural products from our Brazilian biodiversity.

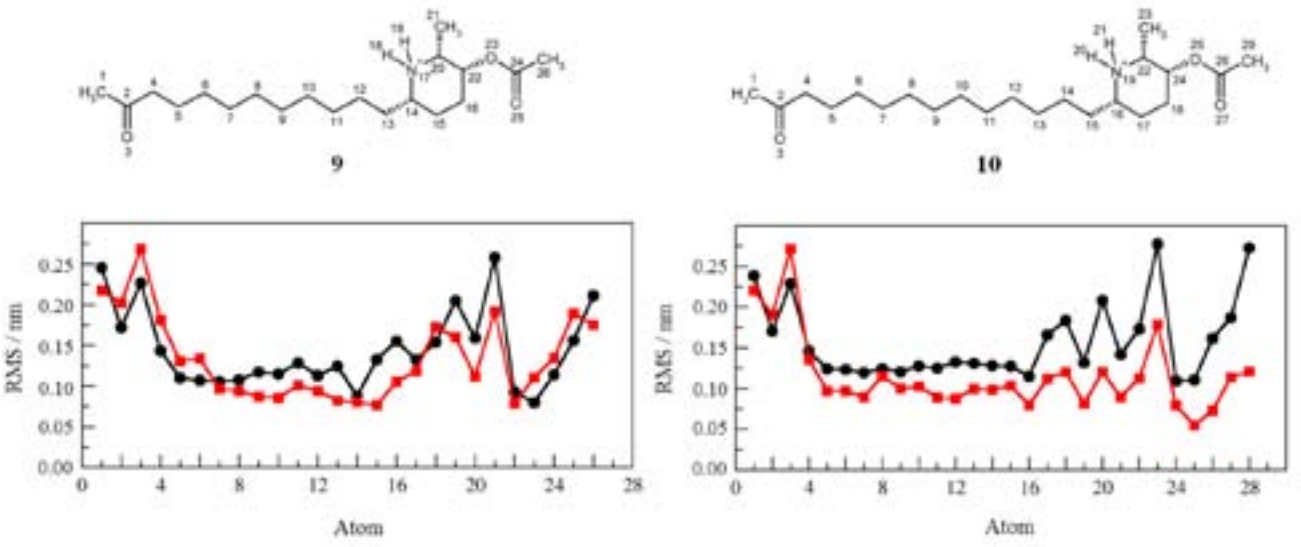


**Figure 5.** RMS fluctuation for **9** and **10** in uncomplexed (black curve) and complexed (red curve) forms.

## Supplementary Information

Supplementary information (Figures S1-S7) are available free of charge at http://jbcs.org.br as a PDF file.

## Acknowledgements

This research was supported by a grant (No. 03/02176-7) awarded to V. S. B. from Fundação de Amparo à Pesquisa do Estado de São Paulo (FAPESP) as part of the Biodiversity Virtual Institute Program (www.biota.org.br). A. D., H. V., E. J. B., C. A. M. F. and V. S. B. acknowledge FAPESP, Fundação de Amparo à Pesquisa do Estado do Rio de Janeiro (FAPERJ), Coordenação de Aperfeiçoamento de Pessoal de Nível Superior (CAPES) and Conselho Nacional de Desenvolvimento Científico e Tecnológico (CNPq), for PhD and research fellowships.

## References

1. Whitehouse, P. J.; Price, D. L.; Struble, R. G.; Clark, A. W.; Coyle, J. T.; DeLong, M. R.; *Science* **1982**, *215*, 1237.
2. Blennow, K.; de Leon, M. J.; Zetterberg, H.; *Lancet* **2006**, *368*, 387.
3. Ferri, C. P.; Prince, M.; Brayne, C.; Brodaty, H.; Fratiglioni, L.; Ganguli, M.; Hall, K.; Hasegawa, K.; Hendrie, H.; Huang, Y.; Jorm, A.; Mathers, C.; Menezes, P. R.; Rimmer, E.; Scazufca, M.; *Lancet* **2005**, *366*, 2112.
4. Brufani, M.; Filocampo, L.; Lappa, S.; Maggi, A.; *Drugs Future* **1997**, *22*, 397.
5. Sugimoto, H.; *Chem. Rec.* **2001**, *1*, 63.
6. Spencer, C. M.; Noble, S.; *Drugs Aging* **1998**, *13*, 391.
7. Sramek, J. J.; Franckiewicz, E. J.; Cutler, N. R.; *Expert Opin. Investig. Drugs* **2000**, *9*, 2393.
8. Robinson, D. M.; Keating, G. M.; *Drugs* **2006**, *66*, 1515.
9. Atta-ur-Rahman; Choudhary, M. I.; *Pure Appl. Chem.* **2001**, *73*, 555.
10. Ma, X.; Gang, D. R.; *Phytochemistry* **2008**, *69*, 2022.
11. Ge, H. M.; Zhu, C. H.; Shi, D. H.; Zhang, L. D.; Xie, D. Q.; Yang, J.; Ng, S. W.; Tan, R. X.; *Chem.-Eur. J.* **2008**, *14*, 376.
12. Mukherjee, P. K.; Kumar, V.; Mal, M.; Houghton, P. J.; *Planta Med.* **2007**, *73*, 283.
13. Rollinger, J. M.; Schuster, D.; Baier, E.; Ellmerer, E. P.; Langer, T.; Stuppner, H.; *J. Nat. Prod.* **2006**, *69*, 1341.
14. Oinonen, P. P.; Jokela, J. K.; Hatakka, A. I.; Vuorela, P. M.; *Fitoterapia* **2006**, *77*, 429.
15. Ingkaninan, K.; Temkitthawon, P.; Chuenchom, K.; Yuyaem, T.; Thongnoi, W.; *J. Ethnopharmacol.* **2003**, *89*, 261.
16. López, S.; Bastida, J.; Viladomat, F.; Codina, C.; *Life Sci.* **2002**, *71*, 2521.
17. Orhan, I.; Terzioglu, S.; Sener, B.; *Planta Med.* **2003**, *69*, 265.
18. Kim, D. K.; Lee, K.; *Arch. Pharm. Res.* **2003**, *26*, 735.
19. Viegas Jr., C.; Bolzani, V. S.; Barreiro, E. J.; Young, M. C.; Furlan, M.; Tomazela, D.; Eberlin, M. N.; *J. Nat. Prod.* **2004**, *67*, 908.
20. Viegas Jr., C.; Bolzani, V. S.; Pimentel, L. S.; Castro, N. G.; Cabral, R. F.; Costa, R. S.; Floyd, C.; Rocha, M. S.; Young, M. C.; Barreiro, E. J.; Fraga, C. A. M.; *Bioorg. Med. Chem.* **2005**, *13*, 4184.
21. Castro, N. G.; Costa, R. S.; Pimentel, L. S.; Danuello, A.; Romeiro, N. C.; Viegas Jr., C.; Barreiro, E. J.; Fraga, C. A. M.; Bolzani, V. S.; Rocha, M. S.; *Eur. J. Pharmacol.* **2008**, *580*, 339.
22. Pivatto, M.; Crotti, A. E. M.; Lopes, N. P.; Castro-Gamboa, I.; Rezende, A.; Viegas Jr., C.; Young, M. C. M.; Furlan, M.; Bolzani, V. S.; *J. Braz. Chem. Soc.* **2005**, *16*, 1431.

23. Raves, M. L.; Harel, M.; Pang, Y. P.; Silman, I.; Kozikowski, A. P.; Sussman, J. L.; *Nat. Struct. Biol.* **1997**, *4*, 57.
24. Harel, M.; Schalk, I.; Ehret-Sabatier, L.; Bouet, F.; Goeldner, M.; Hirth, C.; Axelsen, P. H.; Silman, I.; Sussman, J. L.; *Proc. Natl. Acad. Sci. U. S. A.* **1993**, *90*, 9031.
25. Kryger, G.; Silman, I.; Sussman, J. L.; *Struct. Fold. Des.* **1999**, *7*, 297.
26. Jia, P.; Sheng, R.; Zhang, J.; Fang, L.; He, Q.; Yang, B.; Hu, Y.; *Eur. J. Med. Chem.* **2009**, *44*, 772.
27. Bembenek, S. D.; Keith, J. M.; Letavic, M. A.; Apodaca, R.; Barbier, A. J.; Dvorak, L.; Aluisio, L.; Miller, K. L.; Lovenberg, T. W.; Carruthers, N. I.; *Bioorg. Med. Chem.* **2008**, *16*, 2968.
28. Sauvaître ,T.; Barlier, M.; Herlem, D.; Gresh, N.; Chiaroni, A.; Guenard, D.; Guillou, C.; *J. Med. Chem.* **2007**, *50*, 5311.
29. da Silva, C. H.; Carvalho, I.; Taft, C. A.; *J. Biomol. Struct. Dyn.* **2007**, *24*, 515.
30. Correa-Basurto, J.; Flores-Sandoval, C.; Marín-Cruz, J.; Rojo-Domínguez, A.; Espinoza-Fonseca, L. M.; Trujillo-Ferrara, J. G.; *Eur. J. Med. Chem.* **2007**, *42*, 10.
31. Rarey, M.; Kramer, B.; Lengauer, T.; Klebe, G.; *J. Mol. Biol.* **1996**, *261*, 470.
32. Clauben , H.; Buning, C.; Rarey, M.; Lengauer, T.; *J. Mol. Biol.* **2001**, *308*, 377.
33. Gasteiger , J.; Marsili, M.; *Tetrahedron* **1980**, *36*, 3219.
34. Berman, H. M.; Westbrook, J.; Feng, Z.; Gilliland, G.; Bhat, T. N.; Weissig, H.; Shindyalov, I. N.; Bourne, P. E.; *Nucleic Acids Res.* **2000**, *28*, 235.
35. Cornell, W. D.; Cieplak, P.; Bayly, C. I.; Gould, I. R.; Merz Jr., K. M.; Ferguson, D. M.; Spellmeyer, D. C.; Fox, T.; Caldwell, J. W.; Kollman, P. A.; *J. Am. Chem. Soc.* **1995**, *117*, 5179.
36. van Aalten, D. M. F.; Bywater, B.; Findlay, J. B. C.; Hendlich, M.; Hooft, R. W. W.; Vriend, G.; *J. Comput. Aided Mol. Des.* **1996**, *10*, 255.
37. Schmidt , M. W; Baldridge, K. K.; Boatz, J. A.; Elbert, S. T.; Gordon, M. S.; Jensen, J. H.; Koseki, S.; Matsunaga, N.; Nguyen, K. A.; Su, S. J.; Windus, T. L.; Dupuis, M.; Montgomery, J. A.; *J. Comput. Chem.* **1993**, *14*, 1347.
38. Berendsen, H. J. C.; van der Spoel, D.; van Drunen, R.; *Comput. Phys. Commun.* **1995**, *91*, 43.
39. Verli, H.; Guimarães, J. A.; *Carbohydr. Res.* **2004**, *339*, 281.
40. Becker, C. F.; Guimarães, J. A.; Mourão, P. A. S.; Verli, H.; *J. Mol. Graphics Modell.* **2007**, *26*, 391.
41. Verli, H.; Guimarães, J. A.; *J. Mol. Graphics Modell.* **2005**, *24*, 203.
42. Groot, B. L.; Grubmüller, H.; *Science* **2001**, *294*, 2353.
43. Berendsen, H. J. C.; Grigera, J. R.; Straatsma, T. P.; *J. Phys. Chem.* **1987**, *91*, 6269.
44. Hess, B.; Bekker, H.; Berendsen, H. J. C.; Fraaije, J. G. E. M.; *J. Comput. Chem.* **1997**, *18*, 1463.
45. Darden, T.; York, D.; Pedersen, L.; *J. Chem. Phys.* **1993**, *98*, 10089.
46. Berendsen, H. J. C.; Postma, J. P. M.; DiNola, A.; Haak, J. R.; *J. Chem. Phys.* **1984**, *81*, 3684.
47. Theodorsson-Norheim, E.; *Comput. Methods Programs Biomed.* **1986**, *23*, 57.
48. Tukey, J. W.; Ciminera, J. L.; Heyse, J. F.; *Biometrics* **1985**, *41*, 295.
49. Wilcoxon, F.; *J. Econ. Entomol.* **1946**, *39*, 269.
50. Mann, H. B.; Whitney, D. R.; *Ann. Math. Statist.* **1947**, *18*, 50.

*Submitted: May 5, 2011*
*Published online: December 1, 2011*

**FAPESP has sponsored the publication of this article.**

*J. Braz. Chem. Soc.*, Vol. 23, No. 1, 171-179, 2012.
Printed in Brazil - ©2012 Sociedade Brasileira de Química
0103 - 5053 $6.00+0.00

# Short Report

## Metal Chloride Hydrates as Lewis Acid Catalysts in Multicomponent Synthesis of 2,4,5-Triarylimidazoles or 2,4,5-Triaryloxazoles

***Marcelo V. Marques,[a,b] Marcelo M. Ruthner,[c] Luiz A. M. Fontoura*[a,c] and Dennis Russowsky*[b]***

[a]*Departamento de Engenharia de Processos, Fundação de Ciência e Tecnologia, 94930-230 Cachoeirinha-RS, Brazil*

[b]*Laboratório de Sínteses Orgânicas, Instituto de Química, Universidade Federal do Rio Grande do Sul, 91501-970 Porto Alegre-RS, Brazil*

[c]*Curso de Química, Universidade Luterana do Brasil, 92452-900 Canoas-RS, Brazil*

Uma série de nove hidratos de cloretos metálicos ($ZnCl_2 \cdot 2H_2O$, $SnCl_2 \cdot 2H_2O$, $CdCl_2 \cdot 2H_2O$, $MnCl_2 \cdot 4H_2O$, $CoCl_2 \cdot 6H_2O$, $SrCl_2 \cdot 6H_2O$, $NiCl_2 \cdot 6H_2O$, $CrCl_3 \cdot 6H_2O$ e $CeCl_3 \cdot 7H_2O$) foi investigada como catalisadores ácidos de Lewis brandos e baratos na síntese multicomponente de triarilimidazóis. O melhor catalisador para as reações com benzila foi o $SnCl_2 \cdot 2H_2O$, enquanto que para as reações com benzoína, o $CeCl_3 \cdot 7H_2O$ foi mais eficiente. Todas as reações foram efetuadas em EtOH como solvente. Estes catalisadores também foram empregados igualmente com sucesso na síntese de triariloxazóis.

A series of nine metal chloride hydrates ($ZnCl_2 \cdot 2H_2O$, $SnCl_2 \cdot 2H_2O$, $CdCl_2 \cdot 2H_2O$, $MnCl_2 \cdot 4H_2O$, $CoCl_2 \cdot 6H_2O$, $SrCl_2 \cdot 6H_2O$, $NiCl_2 \cdot 6H_2O$, $CrCl_3 \cdot 6H_2O$ and $CeCl_3 \cdot 7H_2O$) was investigated as mild and inexpensive Lewis acid catalysts to promote the multicomponent synthesis of triarylimidazoles. Reactions starting from benzil showed the best results when $SnCl_2 \cdot 2H_2O$ was used, while for benzoin as the starting material, $CeCl_3 \cdot 7H_2O$ was more efficient. All reactions were performed in EtOH as solvent. These catalysts were also successfully employed in the synthesis of triaryloxazoles.

**Keywords:** triarylimidazoles, triaryloxazoles, multicomponent reaction, metal halide hydrates, Lewis acids, Radziszewski reaction, benzil, benzoin

## Introduction

Imidazole is a five-membered ring heteroaromatic compound with two nitrogen atoms at 1 and 3 positions.[1] This type of compound is known to exhibit a broad range of pharmaceutical and industrial applications. For instance, the imidazole core unity is present in many compounds with pronounced biologic activities such as angiotensin inhibitors,[2] anti-inflammatory,[3] glucagon antagonist,[4] antiviral,[5] antimicrobial,[6] fungicidal[7] and high cytotoxicity, which has indicated them as new candidates in cancer therapy.[8]

A particular class of triarylimidazoles, the pyridinyl arylimidazoles 1, 2 and 3 have been recognized as a potent p38 mitogen-activated protein (MAP) kinase inhibitors and emerged as possible therapeutic drugs in the treatment of various diseases such as cancer and as anti-inflammatory agent, combating the associated pain with osteoarthritis (Figure 1).[9] Beyond the pharmacological applications, arylimidazoles have been used in the industry as chemiluminescent[10] and chromotropic materials[11] due to their optic and electronic properties.[12]

The synthesis of triarylimidazoles from the three-component reaction of 1,2-dicarbonyl compounds, aldehyde and ammonia was independently discovered by Japp and Robinson[13] in 1882 and Radziszewski.[14] However, long periods of time and harsh conditions were frequently associated with low yields of production. Davidson *et al.*[15] showed to be possible to reduce the reaction times using acetic acid as solvent and ammonium acetate instead of ammonia. This last protocol became usual and default procedure for the synthesis of triarylimidazoles.

Recently, Kamijo and Yamamoto[16] have reviewed the progress on the synthesis of imidazoles through catalyzed

*e-mail: dennis@iq.ufrgs.br

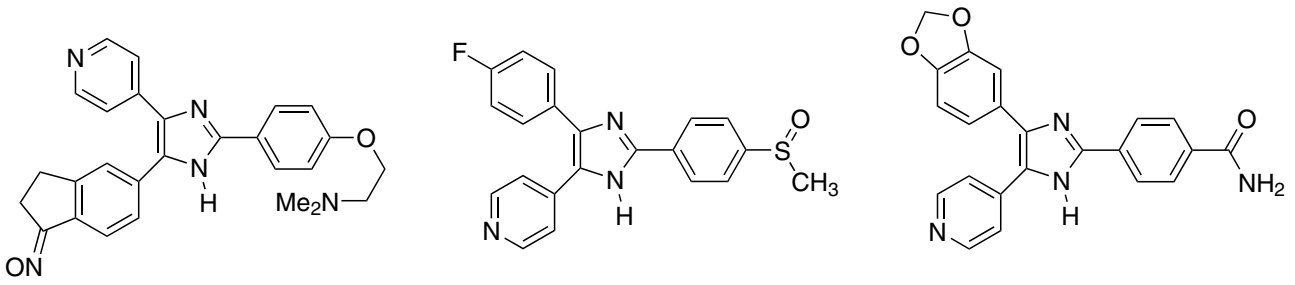


**1 - SB-590885**
Oncogenic B-Raf protein kinase inhibitor

**2 - SB-203580**
Anti-inflammatory

**3 - SB-431542**
Brain cancer therapy

**Figure 1.** Structures of some biologically active pyridinyl arylimmidazoles.

process. Besides other methods using Brønsted catalysis of *p*-toluenesulfonic acid (*p*-TSA),[17] heteropolyacids,[18] oxalic acid[19] and phosphomolybdic acid[20] were developed. Heterogeneous catalysts based on silica-supported Brønsted or Lewis acids, such as $HClO_4/SiO_2$,[21] $H_2SO_4/SiO_2$,[22] $BF_3/SiO_2$,[23] $NaHSO_4/SiO_2$[24] or zeolites HY-type,[25] were successfully employed. Microwave,[26] ultrasound irradiation[27] and ionic liquids[28] were also reported as efficient promoters to the synthesis of arylimidazoles. Other solid catalysts, such as $NaHSO_3$[29] or $I_2$[30] and proline[31] or tetrabutylammonium bromide (TBAB)[32] as organocatalysts, were also effective. Although many catalysts have been employed in the Radziszewski reaction, the use of Lewis acid catalysts such as metal triflates as $Yb(OTf)_3$,[33] metal halides as $ZrCl_4$,[34] $Zn(acac)_4$[27] or cerium ammonium nitrate[35] are rare. Additionally, few examples of metal halide hydrates like $InCl_3·3H_2O$[36] and $NiCl_2·6H_2O/Al_2O_3$[37] were reported for the synthesis of these compounds.

The previous experience of our research group on the use of highly moisture sensitive metal halides as Lewis acid catalysts in organic reactions[38] prompt us to investigate the similar ability of the metal halide hydrates, which are cheaper, easily handled and compatible moisture. Fortunately, our group discovered that $SnCl_2·2H_2O$ was successfully employed in the Biginelli reaction,[39] Friedlander condensation[40] and in conjugate Friedel-Crafts reaction.[41] In the present work, we explore the ability of a series of metal chloride hydrates ($SnCl_2·2H_2O$, $ZnCl_2·2H_2O$, $CdCl_2·2H_2O$, $MnCl_2·4H_2O$, $CoCl_2·6H_2O$, $SrCl_2·6H_2O$, $NiCl_2·6H_2O$, $CrCl_3·6H_2O$ and $CeCl_3·7H_2O$) as mild and inexpensive Lewis acid catalysts in the multicomponent Radziszewski reaction. Besides the search for catalyst efficiency, variables such as protic/aprotic solvents and molar ratio of reagents and catalyst were investigated towards the optimization of a general and useful protocol.

## Results and Discussion

### Catalysts

To investigate the abilities of metal chloride hydrates as Lewis acid catalysts, lophine (2,4,5-triphenyl-1*H*-imidazole) (**8a**) was chosen as the model compound. In a first example, the reaction of benzil (**4a**, 1.0 mmol), benzaldehyde (**6a**, 1.0 mmol ), $NH_4OAc$ (**7**, 4.0 mmol) and $SnCl_2·2H_2O$ (0.10 mmol) was carried out in gently refluxing EtOH. The course of the reaction was monitored by thin layer chromatography (TLC) and after a period of 4 h, the starting materials were consumed. After this time, the reaction was stopped and the crude product was isolated (Table 1, entry 2). Therefore, this time was chosen as default for comparison with other catalysts (Scheme 1).

**Table 1.** Different metal chloride hydrate catalysts for the synthesis of lophine (**8a**)

| entry | Catalyst | Amount / mmol | time / h | **8a** - Yield / % | |
|---|---|---|---|---|---|
| | | | | from **4a** | from **5** |
| 1 | – | – | 4 | 57 | 17 |
| 2 | $SnCl_2·2H_2O$ | 0.1 | 4 | 91 | 67 |
| 3 | $MnCl_2·4H_2O$ | 0.1 | 4 | 83 | 70 |
| 4 | $ZnCl_2·2H_2O$ | 0.1 | 4 | 73 | 72 |
| 5 | $CdCl_2·2H_2O$ | 0.1 | 4 | 76 | 61 |
| 6 | $CoCl_2·6H_2O$ | 0.1 | 4 | 79 | 63 |
| 7 | $SrCl_2·6H_2O$ | 0.1 | 4 | 78 | 63 |
| 8 | $NiCl_2·6H_2O$ | 0.1 | 4 | 76 | 63 |
| 9 | $CrCl_3·6H_2O$ | 0.1 | 4 | 73 | 65 |
| 10 | $CeCl_3·7H_2O$ | 0.1 | 4 | 77 | 88 |
| 11 | $SnCl_2·2H_2O$ | 0.05 | 4 | 82 | – |
| 12 | $CeCl_3·7H_2O$ | 0.05 | 4 | – | 68 |
| 13 | $CeCl_3·7H_2O$ | 0.1 | 2 | – | 55 |
| 14 | $CeCl_3·7H_2O$ | 0.1 | 6 | – | 92 |

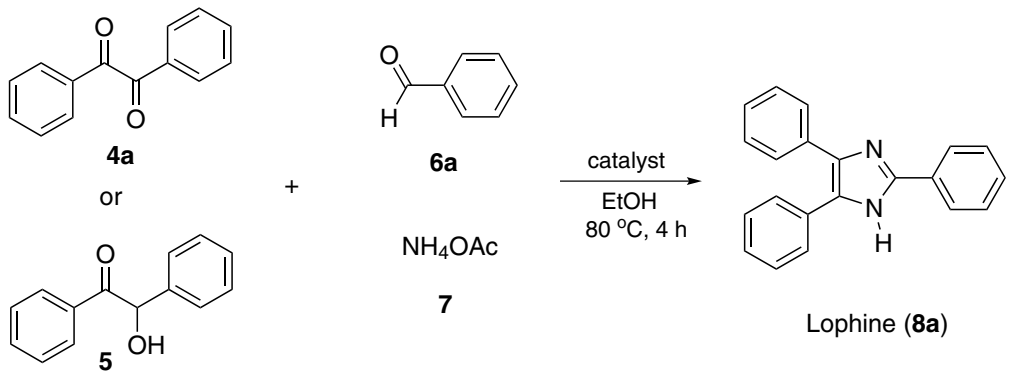


**Scheme 1.** The three-component Radziszewski reaction.

The same conditions were applied for the reactions with benzoin (**5**, 1.0 mmol) instead of benzil, and the results are shown in the Table 1. In all cases, the metal chloride hydrates showed catalytic activity affording lophine in variable yield. It should be noted that in the absence of the catalyst, the yield was drastically reduced, evidencing the metal halide activity (see Table 1, entry 1). The best results (higher than 80% yield) starting from benzil (**4**) were found in the presence of $SnCl_2{\cdot}2H_2O$ and $MnCl_2{\cdot}2H_2O$ (entries 2 and 3, respectively). On the other hand, the optimum result with benzoin (**5**) was achieved in the presence of $CeCl_3{\cdot}7H_2O$ (entry 10). The decrease in the catalyst amount from 0.10 to 0.05 mmol afforded worse results for both starting ketones (entries 11 and 12). Finally, the reactions that were carried out for 2 h caused a decrease in the yield of the product, while an increase of 6 h in the time of the reaction led only to a small improvement (*cf.* entries 10 and 14, respectively). Therefore, it was decided to explore the use of $SnCl_2{\cdot}2H_2O$ and $CeCl_3{\cdot}7H_2O$ (0.10 mmol) as the main catalysts and the time of 4 h as default.

Different mechanistic pathways have been proposed for this multicomponent reaction having the benzil or benzoin as starting materials.[15,28,33] The proposed rationale by Kokare *et al.*[19] seems to be in accordance with the results in Table 1 (Scheme 2). The authors suggested the initial formation of *N*,*N*-ketal (**9**) under Brønsted acidic catalysis from benzaldehyde (**6a**) and 2 equivalents of $NH_4OAc$ (**7**). It was assumed that the same activation occurs in the Lewis catalysis. Therefore, the condensation of **9** with benzil (**4a**) after losing 2 equivalents of water, leads to the conjugate intermediate **10** which rearranges via a [1,5]-sigmatropic proton shift to afford the corresponding lophine (**8a**).

On the other hand, starting from benzoin, the cyclization of intermediate imino-alcohol (**11**) should occur by an intramolecular attack of nitrogen in a more hindered and saturated carbon to afford the dihydroimidazole intermediate (**12**) (Scheme 3). Additionally, the needed oxidation step to produce the conjugated intermediate (**10**) could be corroborating to explain the minor reactivity that is observed in reactions starting from benzoin. The intermediate (**10**) is suggested as common specie in both mechanistic pathways.

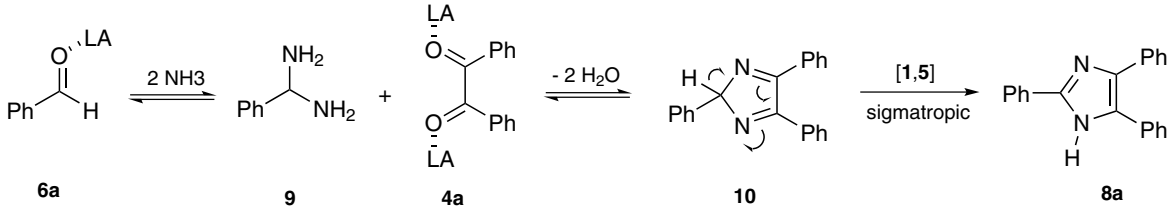


**Scheme 2.** Suggested mechanistic pathway starting from benzil (**4a**).

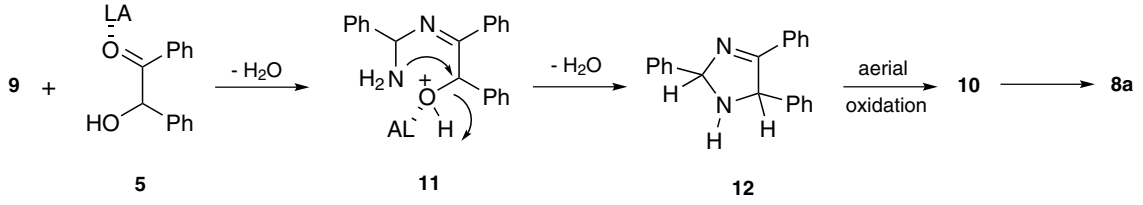


**Scheme 3.** Suggested mechanistic pathway starting from benzoin (**5**).

### Solvent

Despite the use of $H_2O$,[42] MeOH, EtOH, *i*-PrOH, $CH_2Cl_2$, THF, 1,4-dioxane[43] or $CH_3CN$[34] as solvents has already been reported in presence of different catalysts, the relative influence of alcoholic solvents in the Radziszewski reaction was not well studied. For this purpose, were investigated the reactions of benzil (**4a**, 1 mmol) or benzoin (**5**, 1 mmol), benzaldehyde (**6a**, 1.0 mmol), $NH_4OAc$ (**7**, 4.0 mmol) and the catalyst (0.10 mmol) carried out in MeOH, EtOH, *n*-PrOH, $CH_3CN$ and THF (tetrahydrofuran) promoted by $SnCl_2{\cdot}2H_2O$ or $CeCl_3{\cdot}7H_2O$ for the synthesis of lophine (**8a**, Scheme 4). The results are shown in the Table 2, bellow.

Table 2 shows the solvents, their dipole moments (μ) and relative dielectric constants (ε).[44] The reaction from benzyl in the presence of $SnCl_2{\cdot}2H_2O$ seems to be more influenced by the solvent (Table 2, entries 1-5). Aprotic solvents led to poorer yields. In the case of $CH_3CN$ (the most polar between them), the solvent might be associating to the catalyst in a stronger way than the other ones do, reducing more significantly the reaction rate (entry 4). On the other hand, from benzoin and $CeCl_3{\cdot}7H_2O$, the yields are essentially the same for all the solvents, protic or aprotic (entries 6-10). The effect of $CH_3CN$ is not observed, which might be attributed to the metal volume, making their association more difficult (entry 9). Besides the effects of polarity of the solvents, their ability in acting as "hydrogen bond donors" can be considered. This new principle can be evidenced in the activation process through the hydrogen bonding between the solvent and reactants on organocatalyzed reactions, as recently reviewed by Akiyama.[45] Therefore, based on the results above discussed and on economical and ambient sustainability reasons, lower toxicity and easy availability, ethanol becomes more advantageous solvent and was chosen as a default solvent in our present study.

### Molar ratio of $NH_4OAc$

Next, it was investigated the influence of the molar ratio of $NH_4OAc$ on the synthesis of lophine under catalysis of

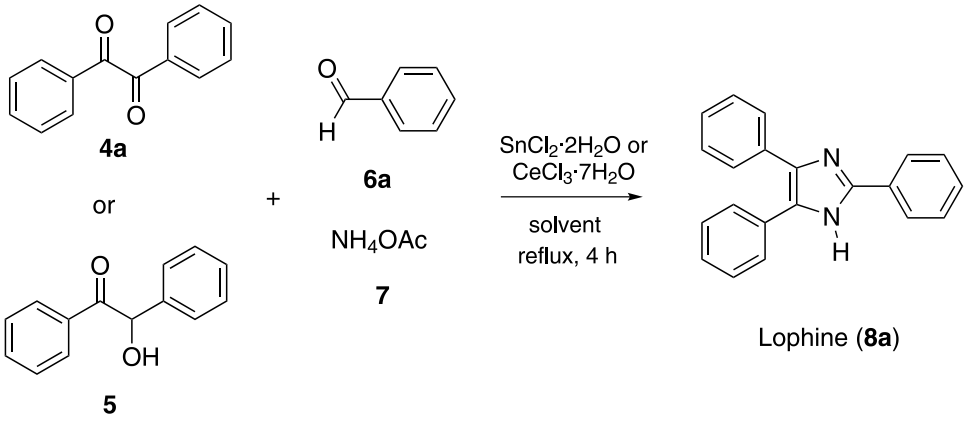


**Scheme 4.** Synthesis of lophine (**8a**) under different solvents.

**Table 2.** Synthesis of lophine via Scheme 4

| entry | Ketone[a] | Catalyst[b] | Solvent | μ / debye | $\varepsilon_R$ | **8a** - Yield / % |
|---|---|---|---|---|---|---|
| 1 | **4a** | $SnCl_2{\cdot}2H_2O$ | MeOH | 1.70 | 32.6 | 79 |
| 2 | **4a** | $SnCl_2{\cdot}2H_2O$ | EtOH | 1.69 | 24.3 | 89 |
| 3 | **4a** | $SnCl_2{\cdot}2H_2O$ | *n*-PrOH | 1.55 | 20.1 | 78 |
| 4 | **4a** | $SnCl_2{\cdot}2H_2O$ | $CH_3CN$ | 3.92 | 37.5 | 65 |
| 5 | **4a** | $SnCl_2{\cdot}2H_2O$ | THF | 1.75 | 7.6 | 75 |
| 6 | **5** | $CeCl_3{\cdot}7H_2O$ | MeOH | 1.70 | 32.6 | 88 |
| 7 | **5** | $CeCl_3{\cdot}7H_2O$ | EtOH | 1.69 | 24.3 | 88 |
| 8 | **5** | $CeCl_3{\cdot}7H_2O$ | *n*-PrOH | 1.55 | 20.1 | 85 |
| 9 | **5** | $CeCl_3{\cdot}7H_2O$ | $CH_3CN$ | 3.92 | 37.5 | 80 |
| 10 | **5** | $CeCl_3{\cdot}7H_2O$ | THF | 1.75 | 7.6 | 81 |

[a]1 mmol; [b]0.1 mmol.

$SnCl_2 \cdot 2H_2O$ and $CeCl_3 \cdot 7H_2O$. The molar ratio of benzil (**4a**, 1.0 mmol) or benzoin (**5**, 1.0 mmol), benzaldehyde (**6a**, 1.0 mmol) and catalyst (0.10 mmol) were the same for all performed assays. The results are shown in Table 3. From substrates, **4a** or **5**, the increase in the $NH_4OAc$ amount from 2 to 4 mmol was followed by an improvement on the reaction yield (*cf.* entries 1, 2 and 4, 5, respectively).

**Table 3.** Synthesis of lophine (**8a**) under different molar ratio of $NH_4OAc$

| entry | Ketone | Catalyst | $NH_4OAc$ / mmol | **8a** - Yield / % |
|---|---|---|---|---|
| 1 | **4a** | $SnCl_2 \cdot 2H_2O$ | 2 | 45 |
| 2 | **4a** | $SnCl_2 \cdot 2H_2O$ | 4 | 91 |
| 3 | **4a** | $SnCl_2 \cdot 2H_2O$ | 10 | 96 |
| 4 | **5** | $CeCl_3 \cdot 7H_2O$ | 2 | 38 |
| 5 | **5** | $CeCl_3 \cdot 7H_2O$ | 4 | 88 |
| 6 | **5** | $CeCl_3 \cdot 7H_2O$ | 10 | 64 |

From substrates, benzyl or benzoin, the increase in the $NH_4OAc$ amount from 2 to 4 mmol was followed of an improvement on the reaction yield (*cf.* entries 1, 2 and 4, 5, respectively). Using 10 mmol of $NH_4OAc$, a little improvement from benzyl was observed (entry 3). In contrast, a poorer yield from benzoin (entry 6) was achieved. In summary, 4 mmol (2 molar equivalents) were considered the optimum amount of this reagent. This developed protocol was applied to the reaction of benzils (**4a**-**c**) and benzoin (**5**) with aldehydes (**6a**-**k**) to afford a library of triarylimidazoles (**8a**-**p**) (Scheme 5). The results are show in the Table 4.

## Pyrazine and triaryloxazoles

The decrease in the yield when 10 mmol of $NH_4OAc$ was employed with benzoin (**5**, see Table 3, entry 6) was attributed to the formation of pyrazine (**13**) as a byproduct (identified by GC-MS analysis).

Similar observation was already reported in the literature.[15] Intending to confirm this hypothesis, it was performed the reaction of benzoin (**5**, 2.0 mmol), $NH_4OAc$ (**7**, 4.0 mmol) under refluxing of ethanol and $CeCl_3 \cdot 7H_2O$ (0.10 mmol) over 4 h in absence of the aldehyde. After this time, the pyrazine (**13**) was isolated in 87% yield (Scheme 6).

On the other hand, the reaction of benzil (**4a**, 2.0 mmol) with ammonium acetate (**7**, 4.0 mmol) under refluxing of ethanol and $SnCl_2.2H_2O$ (0.10 mmol) over 4 h afforded the triaryloxazole (**10a**) in 74% yield (Scheme 7).

Davidson *et al.*[15] early reported the formation of 2,4,5-trifenyloxazole as a lateral product in the Radziszewski reaction under acetic acid media. By the proposed mechanistic pathway suggested by Davidson *et al.*,[15] it is clear the aid of acetic acid as a Brønsted acid catalyst. Triaryloxazoles are structurally similar to triarylimidazoles and also have some of their properties, but have been less studied so far. Due to their broad application (for example, in nonlinear optical devices[46] or as biologically active compounds),[47] it was decided to investigate the ability of metal chloride hydrates such as $NiCl_2 \cdot 6H_2O$, $ZnCl_2 \cdot 2H_2O$, $MnCl_2 \cdot 4H_2O$ and $SnCl_2 \cdot 2H_2O$ to participate as Lewis acid catalysts in the synthesis of triaryloxazoles. The results are shown in Table 5.

The reactions were carried out as described in the synthesis of lophine (see Table 1). In the absence of the catalyst (Table 5, entry 1), **10a** was only isolated in a poor yield. The same result was observed when $NiCl_2 \cdot 6H_2O$ or $MnCl_2 \cdot 4H_2O$ was added (entries 2 and 3). Changing the catalyst to $ZnCl_2 \cdot 2H_2O$, an increase in the yield was observed. In the presence of $SnCl_2 \cdot 2H_2O$, a reasonable yield (78%) was achieved (entries 4 and 5, respectively). Other solvents were also investigated. The reactions were carried

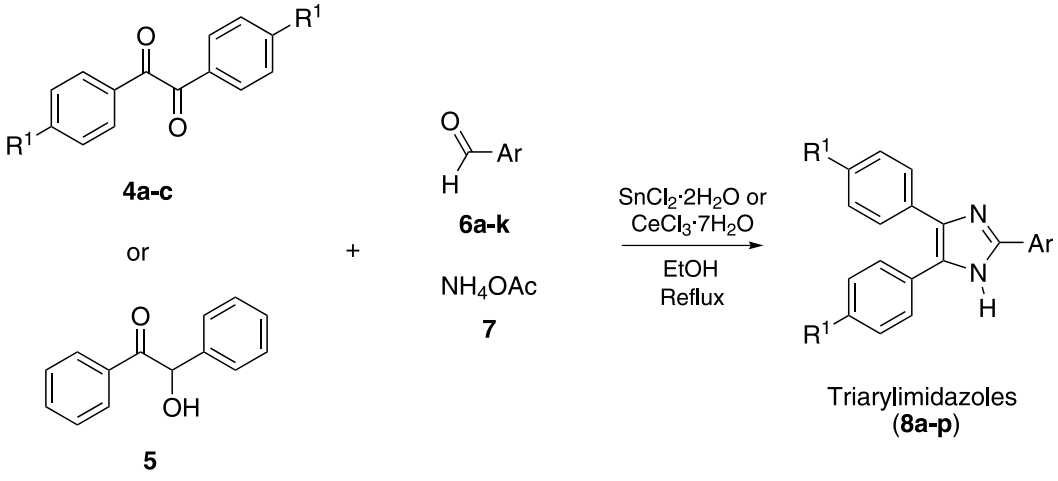


**Scheme 5.** Synthesis of a library of triarylimidazoles (**8a**-**p**).

**Table 4.** Triarylimidazoles from different aromatic aldehydes

| entry | Ketone (**4**, **5**) | Aldehyde (**6**) | Catalyst - yield / % | | Imidazoles (**8**) |
|---|---|---|---|---|---|
| | $R^1$ | Ar | $SnCl_2{\cdot}2H_2O$[a] | $CeCl_3{\cdot}7H_2O$[b] | |
| 1 | H (**4a**, **5**) | $C_6H_5$ (**6a**) | 94 | 81 | **8a** |
| 2 | H (**4a**, **5**) | 4-(HO)$C_6H_4$ (**6b**) | 96 | 81 | **8b** |
| 3 | H (**4a**, **5**) | 4-($CH_3O$)$C_6H_4$ (**6c**) | 95 | 91 | **8c** |
| 4 | H (**4a**, **5**) | 3,4-($CH_3O$)$_2C_6H_3$ (**6d**) | 92 | 62 | **8d** |
| 5 | H (**4a**, **5**) | 1-naphthyl (**6e**) | 61 | 85 | **8e** |
| 6 | H (**4a**, **5**) | 4-(CN)$C_6H_4$ (**6f**) | 71 | 83 | **8f** |
| 7 | H (**4a**, **5**) | 3-($NO_2$)$C_6H_4$ (**6g**) | 91 | 87 | **8g** |
| 8 | H (**4a, 5**) | 2-($NO_2$)$C_6H_4$ (**6h**) | 74 | 60 | **8h** |
| 9 | H (**4a**, **5**) | 2-furyl (**6i**) | 73 | 69 | **8i** |
| 10 | H (**4a**, **5**) | 2-thienyl (**6j**) | 75 | 82 | **8j** |
| 11 | H (**4a**, **5**) | 3-thienyl (**6k**) | 94 | 84 | **8k** |
| 12 | $CH_3O$ (**4b**) | 3-thienyl (**6k**) | 98 | - | **8l** |
| 13 | F (**4c**) | $C_6H_5$ (**6a**) | 87 | - | **8m** |
| 14 | F (**4c**) | 4-(CN)$C_6H_4$ (**6f**) | 64 | - | **8n** |
| 15 | F (**4c**) | 2-furyl (**6i**) | 71 | - | **8o** |
| 16 | F (**4c**) | 3-thienyl (**6k**) | 92 | - | 8p |

[a]In reactions from benzil (**4a**); [b]in reactions from benzoin (**5**).

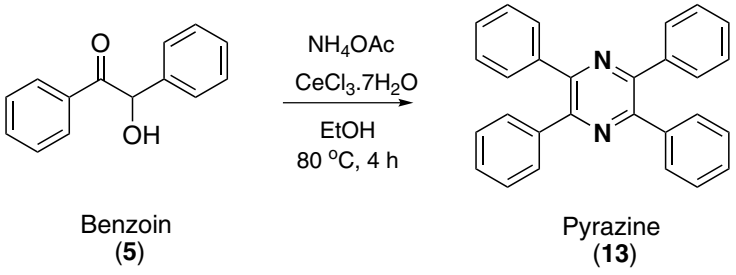


**Scheme 6.** Synthesis of pyrazine (**13**) from benzoin (**5**).

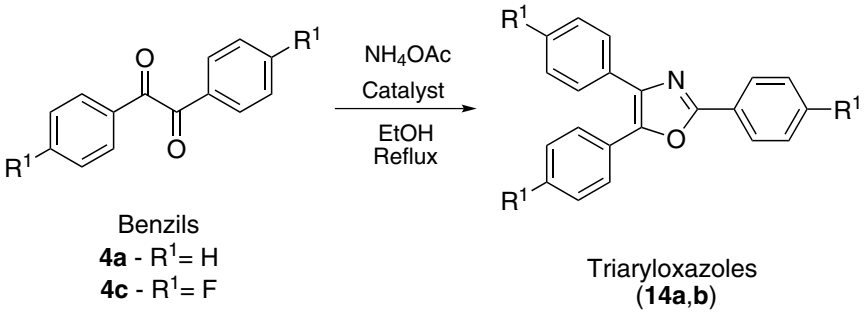


**Scheme 7.** Synthesis of triaryloxazoles (**14a,b**) from benzils (**4a**,**c**).

out under reflux. In MeOH, a decrease in the yield was observed, while the use of *n*-PrOH permitted to isolate the product in a yield of 73% (entries 6 and 7, respectively). On the other hand, in $CH_3CN$ and THF (aprotic polar solvents), benzyl was recovered after the work up (entries 8 and 9, respectively). So, EtOH was considered to be the best solvent. After that, the amount of catalyst was diminished from 10 to 5 mol% (*cf.* entries 5 and 10, respectively) and no significant decrease in the yield was observed, therefore, this new condition was set as default.

Finally, the increase in the reaction times also caused an increase in the yield of triaryloxazole (**14a**), 84 and 94% (entries 11 and 12, respectively). The use of benzyl (**4c**) under the optimized protocol afforded the triaryloxazole

**Table 5.** Synthesis of triaryloxazoles **14a** and **14b** from Scheme 7

| entry | Benzil | Catalyst / load[a] | Solvent | time / h | Oxazole | Yield / % |
|---|---|---|---|---|---|---|
| 1 | **4a** | – | EtOH | 4 | **14a** | 15 |
| 2 | **4a** | $NiCl_2·6H_2O$ / 0.10 | EtOH | 4 | **14a** | 15 |
| 3 | **4a** | $MnCl_2·4H_2O$ / 0.10 | EtOH | 4 | **14a** | 15 |
| 4 | **4a** | $ZnCl_2·2H_2O$ / 0.10 | EtOH | 4 | **14a** | 56 |
| 5 | **4a** | $SnCl_2·2H_2O$ / 0.10 | EtOH | 4 | **14a** | 78 |
| 6 | **4a** | $SnCl_2·2H_2O$ / 0.10 | MeOH | 4 | **14a** | 44 |
| 7 | **4a** | $SnCl_2·2H_2O$ / 0.10 | *n*-PrOH | 4 | **14a** | 73 |
| 8 | **4a** | $SnCl_2·2H_2O$ / 0.10 | $CH_3CN$ | 4 | **14a** | – |
| 9 | **4a** | $SnCl_2·2H_2O$ / 0.10 | THF | 4 | **14a** | – |
| 10 | **4a** | $SnCl_2·2H_2O$ / 0.05 | EtOH | 4 | **14a** | 74 |
| 11 | **4a** | $SnCl_2·2H_2O$ / 0.05 | EtOH | 6 | **14a** | 84 |
| 12 | **4a** | $SnCl_2·2H_2O$ / 0.05 | EtOH | 18 | **14a** | 94 |
| 13 | **4c** | $SnCl_2·2H_2O$ / 0.05 | EtOH | 18 | **14b** | 93 |

[a]The load of catalyst in mmol.

(**14b**) in good yield, confirming the applicability of this protocol.

## Conclusions

We found that the metal halide hydrates were active as Lewis acid catalyst to prepare 2,4,5-triarylimidazoles in reasonable to good yields through the Radziszewski multicomponent synthesis. These catalysts were effective starting from benzoin, as well as from benzils. The $SnCl_2·2H_2O$ showed the best results in reactions from benzyl, while $CeCl_3·7H_2O$ was more effective with benzoin. Additionally, we demonstrate that the molar ratio of $NH_4OAc$ is important to improve the yields of the products and the large excess of them can leads to the formation of 1,2,4,5-tetraarylpyrazines. The $SnCl_2·4H_2O$ was also effective to promote the reaction of benzils with $NH_4OAc$ to afford the respective triaryloxazoles in good yields.

## Experimental

### General considerations

The solvents and reagents were used without previous treatment, except for benzaldehyde, anisaldehyde and furfural, which were distilled prior to use. The reactions were monitored by thin layer chromatography (TLC) on ALUGRAM® SIL G/UV 254 Macherey-Nagel silicagel plates. A mixture $CH_2Cl_2$/AcOEt in 98:2 ratios was used as eluent. The plates were visualized in alcoholic solution of 2,4-dinitrofenilidrazine or under UV light (254 nm). The $^1H$ and $^{13}C$ nuclear magnetic resonance (NMR) spectra were recorded in DMSO-$d_6$ using a Varian VNMRS or a Varian Mercury spectrometers at 300/400 MHz and 75/100 MHz, respectively. The chemical shifts ($\delta$) are reported in parts *per* million (ppm) relative to DMSO-$d_6$ at $\delta$ 2.50 ppm for $^1H$ NMR and the line at $\delta$ 39.5 ppm for $^{13}C$ NMR. The coupling constants *J* are reported in Hz. The following abbreviations are used for the multiplicities: s (singlet), d (doublet), dd (double of doublets), t (triplet), q (quartet), m (multiplet) and br s (broad singlet). The infrared (IR) spectra were recorded on a Perkin-Elmer Spectrum One, between 4000 and 600 $cm^{-1}$ (Nujol). The melting points (mp) were measured on an Uniscience Brazil fusing equipment (model 498) and are uncorrected. The mass spectra (MS) were recorded on a GC-MS QP 2010 Shimadzu (EI, 70 eV).

### General procedures

#### Synthesis of 2,4,5-triarylimidazoles (***8a-p***) from benzyls (***4a-c***)

A 10 mL round-bottom flask equipped with magnetic stirrer was charged with benzyls (**4a**-**c**) (1.0 mmol), aldehydes (**6a**-**k**) (1.0 mmol), $NH_4OAc$ (**7**, 4.0 mmol) and $SnCl_2·2H_2O$ (0.10 mmol), followed by EtOH (4 mL). The reaction mixture was stirred and gently refluxed for 4 h. After the completion of the reaction with the monitoring of TLC, 4 mL of water were added. The solid was filtered under reduced pressure and washed with small portions of a mixture of cooled EtOH/$H_2O$ (1:1, v:v). The crude product was recrystallized from acetone/water 9:1 or toluene.

#### Synthesis of 2,4,5-triarylimidazoles (**8a-k**) from the benzoin (**5**)

A 10 mL round-bottom flask equipped with magnetic stirrer was charged with benzoin (**5**) (1.0 mmol),

aldehydes (**6a**-**k**) (1.0 mmol), $NH_4OAc$ (**7**, 4.0 mmol) and $CeCl_3.7H_2O$ (0.10 mmol), followed by EtOH (4 mL). The reaction mixture was stirred and gently refluxed for 4 h. After the completion of the reaction with the monitoring of TLC, 4 mL of water were added. The solid was filtered under reduced pressure and washed with small portions of a mixture of cooled EtOH/$H_2O$ (1:1, v:v). The crude product was recrystallized from acetone/water 9:1 or toluene.

Synthesis of 2,4,5-triaryloxazoles (**14a**,**b**) from benzyls (**4a**,**c**)

A 10 mL round-bottom flask equipped with magnetic stirrer was charged with benzyls (**4a,c**) (1.0 mmol), $NH_4OAc$ (**7**, 5.0 mmol) and $SnCl_2{\cdot}2H_2O$ (0.05 mmol), followed by EtOH (4 mL). The reaction mixture was stirred and gently refluxed for 4 h. After the completion of the reaction with the monitoring of TLC, 4 mL of water were added. The solid was filtered under reduced pressure and washed with small portions of a mixture of cooled EtOH/$H_2O$ (1:1, v:v). The crude product was recrystallized from acetone/water 9:1 or toluene.

## Supplementary Information

Supplementary data (spectral data of compounds **8a**-**p** and **10a**,**b** and spectra) are available free of charge at http://jbcs.org.br as PDF file.

## Acknowledgments

The authors would like to acknowledge FAPERGS (Fundação de Amparo à Pesquisa do Estado do Rio Grande do Sul) and CNPq (Conselho Nacional de Desenvolvimento Cientifico e Tecnológico, Grant 2007-6/484615) for financial support and graduate fellowship (M. V. M).

## References

1. For reviews on the chemistry of imidazoles, see: Grimmett, M. R. In *Comprehensive Heterocyclic Chemistry*, vol. 5; Katritzky, A. R.; Rees, C. W., eds.; Pergamon: Oxford, 1984; Grimmett, M. R. In *Science of Synthesis*, vol. 12; Neier R., ed.; Thieme: Stuttgart, 2002.
2. Palkowitz, A. D.; Steinberg, M. I.; Thrasher, K. J.; Reel, J. K.; Hauser, K. L.; Zimmerman, K. M.; Wiest, S. A.; Whitesitt, C. A.; Simon, R. L.; Pfeifer, W.; Lifer, S. L.; Boyd, D. B.; Barnett, D. J.; Wilson, T. M.; Deeter, J. B.; Kakeuchi, K.; Riley, R. E.; Miller, W. D.; Marshall, W. S.; *J. Med. Chem.* **1994**, *37*, 4508.
3. Trujillo, J. I.; Kiefer, J. R.; Huang, W.; Thorarensen, A.; Xing, L.; Caspers, N. L.; Day, J. E.; Mathis, K. J.; Kretzmer, K. K.; Reitz, B. A.; Weinberg, R. A.; Stegeman, R. A.; Wrightstone, A.; Christine, L.; Compton, R.; Li, X.; *Bioorg. Med. Chem. Lett.* **2009**, *19*, 908.
4. Linda, L.; Chang, L. L.; Sidler, K. L.; Cascieri, M. A.; Laszlo, S.; Koch, G.; Li, B.; MacCoss, M.; Mantlo, N.; O'Keefe, S.; Pang, M.; Rolandoc, A.; Hagmanna, W. K.; *Bioorg. Med. Chem. Lett.* **2001**, *11*, 2549.
5. Sharma, D.; Narasimhan, B.; Kumar, P.; Judge, V.; Narang, R.; Clercq, E.; Balzarini, J.; *Eur. J. Med. Chem.* **2009**, *44*, 2347.
6. Kumar, S.; Boehm, J.; Lee, J. C.; *Nat. Rev. Drug Disc.* **2003**, *2*, 717.
7. Laufer, S.; Koch, P.; *Org. Biomol. Chem.* **2008**, *6*, 437.
8. King, A. J.; Patrick, D. R.; Batorsky R. S.; Ho, M. L.; Do, H. T.; Zhang, S. Y.; Kumar, R.; Rusnak, A. K.; Wilson, D. M.; Hugger, E.; Wang, L.; Karreth, F.; Lougheed, J. C.; Lee, J.; Chau, D.; Stout, T. J.; May, E. W.; Rominger, C. M.; Schaber, M. D.; Luo, L.; Lakdawala, A. S.; Adams, J. L.; Contractor, R. G.; Smalley, K. S. M.; Herlyn, M.; Morrissey, M. M.; Tuveson, D. A.; Huang, P. S.; *Cancer Res.* **2006**, *66*, 11100.
9. Young, P. R; McLaughlin, M. M.; Kumari, S.; Kassisi, S.; Doyle, M. L.; McNulty, D.; Gallagher, T. F.; Fisher, S.; McDonnell, P. C.; Carr, S. A.; Huddleston, M. J.; Seibel, G.; Porter, T. G.; Livi, G. P.; Adams, J. L.; Leei, J. C.; *J. Biol. Chem.* **1997**, *272*, 12116.
10. Yagi, K.; Soong, C. F.; Irie, M.; *J. Org. Chem.* **2001**, *66*, 5419.
11. Fridman, N.; Speiser, S.; Kaftory, M.; *Cryst. Growth Des.* **2006**, *6*, 2281.
12. Santos, J.; Mintz, E. A.; Zehnder, O.; Bosshard, C.; Bu, X. R.; Gunter, P.; *Tetrahedron Lett.* **2001**, *42*, 805.
13. Japp, F. R.; Robinson, H. H.; *Ber. Dtsch. Chem. Ges.* **1882**, *15*, 1268.
14. Radziszewski, B.; *Ber. Dtsch. Chem. Ges.* **1882**, *15*, 1493.
15. Davidson, D.; Weiss, M.; Jelling, M.; *J. Org. Chem.* **1937**, *2*, 319; Davidson, D.; Weiss, M.; Jelling, M.; *J. Org. Chem.* **1937**, *2*, 328.
16. Kamijo, S.; Yamamoto, Y.; *Chem. Asian J.* **2007**, *2*, 568.
17. Khodaei, M. M.; Bahrami, K.; Kavianinia, I.; *J. Chin. Chem. Soc.* **2007**, *54*, 829.
18. Nagarapu, L.; Apuri, S.; Kantevari, S.; *J. Mol. Catal. A: Chem.* **2007**, *266*, 104.
19. Kokare, N. D.; Sangshetti, J. N.; Shinde, D. B.; *Synthesis* **2007**, 2829.
20. Yadhav, S. D.; Kokare, N. D.; Jadhav S. D.; *J. Heterocycl. Chem.* **2008**, *45*, 1461.
21. Kantevari, S.; Vuppalapati, S. V. N.; Biradar, D. O.; Nagarapu, L.; *J. Mol. Catal. A: Chem.* **2007**, *266*, 109.
22. Shaabani, A.; Rahmati, A.; *J. Mol. Catal. A: Chem.* **2006**, *249*, 246.
23. Sadeghi, B.; Mirjalili, B. B. F.; Hashemi, M. M.; *Tetrahedron Lett.* **2008**, *49*, 2575.
24. Karimi, A. R.; Alimohammadi, Z.; Azizian, J.; Mohammadi, A. A.; Mohammadizadeh, M. R.; *Catal. Commun.* **2006**, *7*, 728.

25. Sivakumar, K.; Kathirvel, A.; Lalitha, A.; *Tetrahedron Lett.* **2010**, *51*, 3018.
26. Shih, M.-H.; Tsai, C.-H.; Wang, Y.-C.; Shieh, M.-Y.; Lin, G.-L.; Wei, C.-Y.; *Tetrahedron* **2007**, *63*, 2990.
27. Khosropour, A. R.; *Ultrason. Sonochem.* **2008**, *15*, 659.
28. Siddiqui, S. A.; Narkhed, U. C.; Palimkar, S. S.; Daniel, T.; Lahoti, R. J.; Srinivasan, K. V.; *Tetrahedron* **2005**, *61*, 3539.
29. Sangshetti, J. N.; Kokare, N. D.; Kotharkar, S. A.; Shinde, D. B.; *Monatsh. Chem.* **2008**, *139*, 125.
30. Kidwai, M.; Mothsra, P.; Bansal, V.; Somvanshi, R. K.; Ethayathulla, A. S.; Dey, S.; Singh,T. P.; *J. Mol. Catal. A: Chem.* **2007**, *265*, 177.
31. Shitole, N. V.; Shelke, K. F.; Sonar, S. S.; Sadaphal, S. A.; Shingate, B. B.; Shingare, M. S.; *Bull. Korean Chem. Soc.* **2009**, *30*, 1963.
32. Chary, M. V.; Keerthysri, N. C.; Vupallapati, S. V. N.; Lingaiah, N.; Kantevari, S.; *Catal. Commun.* **2008**, *9*, 2013.
33. Wang, L.-M.; Wang, Y.-H.; Tian, H.; Yao, Y.-F.; Shao, J.-H.; Liu, B.; *J. Fluorine Chem.* **2006**, *127*, 1570.
34. Sharma, G. V. M.; Jyothi, Y.; Lakshmi, P. S.; *Synth. Commun.* **2006**, *36*, 2991.
35. Sun, Y.-F.; Huang, W.; Lu, C.-G.; Cui, Y.-P.; *Dyes Pigm.* **2009**, *81*, 10.
36. Sharma, S. D.; Hazarika, P.; Konwar, D.; *Tetrahedron Lett.* **2008**, *49*, 2216.
37. Heravi, M. M.; Bakhtiari, K.; Oskooie, H. A.; Taheri, S.; *J. Mol. Catal. A: Chem.* **2007**, *263*, 279.
38. Russowsky, D.; Petersen, R. Z.; Godoi, M. N.; Pilli, R. A.; *Tetrahedron Lett.* **2000**, *41*, 9939; Andrade, C. K. Z.; Rocha, R. O.; Russowsky, D.; Godoi, M. N.; *J. Braz. Chem. Soc.* **2005**, *16*, 535; Godoi, M. N.; Costenaro, H. S.; Kramer, E.; Machado, P. S.; D'Oca, M. G. M.; Russowsky, D.; *Quim. Nova* **2005**, *28*, 1010; Silveira, C. C.; Vieira, A. S.; Braga, A. L.; Russowsky, D.; *Tetrahedron* **2005**, *61*, 9312; Russowsky, D.; Canto, R. F. S.; Sanches, S. A. A.; D'Oca, M. G. M.; Fatima, A.; Pilli, R. A.; Kohn, L. K.; Antonio, M. A.; de Carvalho, J. E.; *Bioorg. Chem.* **2006**, *34*, 173.
39. Russowsky, D.; Lopes, F. A.; Silva, V. S. S.; Canto, K. F. S.; D'Oca, M. G. M.; Godoi, M. N.; *J. Braz. Chem. Soc.* **2004**, *15*, 165.
40. Costa, J. S.; Pisoni, D. S.; Silva, C. B.; Petzhold, C. L.; Russowsky, D.; Ceschi, M. A.; *J. Braz. Chem. Soc.* **2009**, *20*, 1448.
41. Schwalm, C. S.; Ceschi, M. A.; Russowsky, D.; *J. Braz. Chem. Soc.* **2011**, *22*, 623.
42. Chauveau, E.; Marestin, C.; Schiets, F.; Mercier, R.; *Green Chem.* **2010**, *12*, 1018.
43. Chary, M. V.; Keerthysri, N. C.; Vupallapati, S. V. N.; Lingaiah, N.; Kantevari, S.; *Catal. Commun.* **2008**, *9*, 2013.
44. Lide, D. R.; *Handbook of Chemistry and Physics*, 79th ed.; CRC Press: Boca Raton, 1993.
45. Akiyama, T. In *Hydrogen Bonding in Organic Synthesis*; Pihko, P. M., ed.; Wiley-VCH: Weinheim, 2009, chapter 2.
46. McCairn, M. C.; Culliford, S. J; Kozlowski, R. Z; Sutherland, A. J.; *Tetrahedron Lett.* **2004**, *45*, 2163.
47. Epple, R.; Cow, C.; Xie, Y.; Azimioara, M.; Russo, R.; Wang, X.; Wityak, J.; Karanewsky, D. S.; Tuntland, T.; Nguyen-Tran, V. T. B.; Ngo, C. C.; Huang, D.; Saez, E.; Spalding, T.; Gerken, A.; Iskandar, M.; Seidel, H. M.; Tian, S.-S.; *J. Med. Chem.* **2010**, *53*, 77.

*Submitted: July 6, 2011*
*Published online: October 11, 2011*

*J. Braz. Chem. Soc.*, Vol. 23, No. 1, 180-185, 2012.
Printed in Brazil - ©2012 Sociedade Brasileira de Química
0103 - 5053 $6.00+0.00

Short Report

# Effects of the Essential Oil from Fruits of *Schinus terebinthifolius* Raddi (Anacardiaceae) on Reproductive Functions in Male Rats

***Cristiano R. G. Affonso,[a] Rozeverter M. Fernandes,[a] Jamylla M. G. de Oliveira,[a] Maria do Carmo de Carvalho e Martins,[b] Sidney G. de Lima,*,[c] Gustavo R. de Sousa Júnior,[c] Maria Zenaide de Lima C. Moreno Fernandes*,[d] and Surama F. Zanini[e]***

*[a]Departamento de Morfofisiologia Veterinária, [b]Departamento de Biofísica e Fisiologia, [c]Departamento de Química and [d]Departamento de Bioquímica e Farmacologia, Universidade Federal do Piauí, 64049-550 Teresina-PI, Brazil*

*[e]Centro de Ciências Agrárias, Universidade Federal do Espírito Santo, Alegres-ES, Brazil*

O óleo essencial de *Schinus terebinthifolius* foi analisado por CG e CG-EM. α-Fencheno, limoneno, β-pineno, α-felandreno e β-isosilvestreno representam aproximadamente 80% da composição do óleo. A toxicidade na reprodução de ratos Wistar machos foi avaliada. Não foram observadas mudanças na massa dos órgãos reprodutivos, no número e morfologia dos espermatozoides, nas taxas de reprodução e na massa corporal dos ratos machos após tratamento com o óleo essencial de *S. terebinthifolius*.

The essential oil of *Schinus terebinthifolius* (Anacardiaceae) was analyzed by GC and GC-MS. α-Fenchene, limonene, β-pinene, α-phellandrene, and β-isosylvestrene represent about 80% of the oil composition. The reproductive toxicity of the essential oil in Wistar male rats was evaluated. No changes were observed in the mass of the reproductive organs, number and morphology of spermatozoa, reproductive rates, and the body mass of offspring of male rats after treatment with the essential oil of *S. terebinthifolius*.

**Keywords**: *Schinus terebinthifolius* Raddi, GC-MS, essential oil, male reproductive toxicity, Wistar male rats

## Introduction

*Schinus terebinthifolius*, also known as Brazilian pepper, aroeira-vermelha, Florida holly, pink pepper, or christmas-berry belongs to the Anacardiaceae family of plants.[1] It is native to South and Central America and it can also be found in semitropical and tropical regions of the United States and Africa.[2]

*S. terebinthifolius* has been reported to have antifungal,[3] healing[4] and anti-allergic effects,[5] among others. In Brazil, it is used in folk medicine for the treatment of inflammatory and hemostatic diseases,[6] as well venereal diseases, rheumatism, diarrhea, pain, gingivitis and fever.[7,8] The extract of stem bark is widely used as an anti-inflammatory, to heal over or cicatrize wounds, whereas fruits are used for colds, fungal and bacterial infections.[9]

The berries of *S. terebinthifolius* are rich in essential oil, which imparts a peppery flavor, and are used as a food seasoning that is highly sought after and of significant economic value. These fruits are also used in syrups, vinegar, and beverages in Peru as well as in Chilean wines. In some countries, dried and ground berries are used as a pepper substitute or as an adulterant of black pepper (*Piper nigrum*). They have also been used in the perfume industry.[10] The leaves and reddish fruits are also rich in essential oil, and earlier investigations have reported high concentrations of monoterpenes along with some sesquiterpene hydrocarbons. Despite the positive findings of the pharmacological properties of *S. terebinthifolius* and its growing use in cooking, little research has been carried out to ensure the safety of using this species. Since this plant is widely used for medicinal purposes, and mutagenic (cytotoxic) activity has been detected in stem bark extracts,[11] as well as hypersensitivity to the volatile oil, we decided to carry the analysis of the essential oil

*e-mail: sidney@ufpi.edu.br, zmoreno@ufpi.br

and evaluate its toxicity on the reproductive functions in Wistar male rats.

## Results and Discussion

### Analysis of the essential oil

Chromatographic analysis by GC-MS permitted the identification and quantification of 100% of the integrated components from the essential oil isolated from the fruits of *S. terebinthifolius*. Spectra were considered coincident if the similarity index was higher than 95%. Twenty two components, including mono-, and sesquiterpenes were identified, with a yield of about 2.6% (w/w) of dry fruit weight. The chemical composition of the essential oil is presented in Table 1.

When compared to literature data, our study evidenced some differences in the chromatographic profile as well as in quantitative composition.[12-17] The major constituents were α-fenchene (20.75%), β-pinene (10.11%), β-myrcene (9.30%), α-phellandrene (14.94%), limonene (20.81%) and isosylvestrene (13.87%). α-Fenchene and isosylvestrene were found only in our study (Table 1). α-Phellandrene and β-pinene were found at 14.94% and 10.11% in our study, while they represented an average of 7.0% and 1.5%, respectively, in the study by Barbosa *et al.*[12] Most of the oil samples from leaves, flowers and/or fruits of *S. terebinthifolius* collected at different locations revealed α-pinene (15.01-51.82%) as the major component, especially in those originating from India.[13,16,17] Sabinene was found at 40.66% in the study of Gundidza *et al.*[14] while it accounted for 3.49% in the study of Barbosa *et al.*[12] Other major components detected by Barbosa *et al.*[12] in the oil from unripe fruits of *S. terebinthifolius* were α-cadinol (20.60%), δ-cadinene (15.48%), β-pinene (10.21%) and epi-α-muurolol (9.89%). More recently Richter *et al.*[18] indicated that α-pinene (16.9%), α-phellandrene (21.1%), β-phellandrene (10.8%) and limonene (23.7%) were the major constituents of fruits of *S. terebinthifolius*.

**Table 1.** Chemical composition of the essential oil obtained by hydrodistillation from fruits of *S. terebinthifolius*

| Compounds | $IK_{Exp}$ [a] | Area / % |
|---|---|---|
| α-Thujene | 954 | 0.71 |
| α-Fenchene | 961 | 20.75 |
| Camphene | 962 | 0.24 |
| β-Pinene | 987 | 10.11 |
| β-Myrcene | 991 | 9.30 |
| Mentha-1(7),8-diene <meta> | 999 | 2.32 |
| α-Phellandrene | 1012 | 14.94 |
| Sylvestrene <iso> | 1018 | 13.87 |
| α-Terpinene | 1022 | 0.86 |
| *p*-Cymene | 1030 | 1.16 |
| Limonene | 1038 | 20.81 |
| γ-Terpinene | 1062 | 1.03 |
| Terpinolene | 1087 | 0.84 |
| Terpineol-4 | 1174 | 0.46 |
| δ-Elemene | 1332 | 0.12 |
| Unidentified | 1386 | 0.21 |
| *E*-Caryophyllene | 1408 | 0.78 |
| α-Humullene | 1450 | 0.12 |
| Germacrene-D | 1471 | 0.83 |
| γ-Cadinene | 1503 | 0.07 |
| δ-Cadinene | 1515 | 0.34 |
| Elemol | 1542 | 0.11 |
| | | Total: 100% |

[a]Retention indices relative to $C_8$-$C_{20}$ *n*-alkanes.

### Acute oral toxicity study

The toxicity study of the essential oil from *S. terebinthifolius* fruits showed that the oral dose of 5 g $kg^{-1}$ did not produce any signs of acute toxicity or death in mice during 14 days of observation. So possibly the LD50 would be greater than 5 g $kg^{-1}$. According to Kennedy *et al.*[19] substances with LD50 greater than 5 g $kg^{-1}$ can be considered nontoxic. These findings are in accordance with those described by Lima *et al.*,[20] using the extract from the bark of *S. terebinthifolius.*

### Reproductive toxicity study

Reproductive toxicity can be defined as the occurrence of adverse effects on the reproductive system, which can result from exposure to environmental agents, drugs and diseases in general. In this study we evaluated the effects of treatment with the essential oil of *S. terebinthifolius* fruits in reproductive performance and body mass of offspring. There was no statistically significant difference regarding the offspring/mother ratio and reproductive rates analyzed when the groups treated with essential oil were compared with the control group. Additionally there were no significant changes in litter mass and body mass on Day 1 and Day 21 of life of offspring from rats treated with essential oil when compared to the control group (Table 2).

Fertility studies evaluate the outcome of mating after pre-treatment in at least one of the sexes. Evaluation of fertility and subsequent pregnancy provides important information about the functional consequences of the

**Table 2.** Effects of the essential oil from fruits of *S. terebinthifolius* on reproductive performance and body mass of offspring

| Variables | Control | Essential oil/(mg kg$^{-1}$) | | |
|---|---|---|---|---|
| | | 375 | 750 | 1500 |
| Offsprin /mother ratio | 11.1 ± 0.7 | 10.2 ± 1.0 | 10.6 ± 1.0 | 9.7 ± 0.4 |
| Fertility rate/% | 44.4 | 61.1 | 58.3 | 57.1 |
| Birth rate/% | 94.68 | 99.1 | 93.67 | 95.12 |
| Viability rate/% | 100.00 | 99.1 | 98.65 | 97.43 |
| Lactation rate/% | 98.88 | 97.32 | 97.30 | 97.44 |
| Litter mass at 1 day of life/g | 67.96 ± 4.82 | 62.90 ± 5.33 | 61.84 ± 5.96 | 58.48 ± 1.54 |
| Litter mass at 21 days of life/g | 358.1 ± 19.70 | 363.5 ± 27.09 | 334.5 ± 25.85 | 326.5 ± 18.82 |
| Offspring body mass at 1 day of life/g | 6.199 ± 0.211 | 6.245 ± 0.294 | 5.857 ± 0.242 | 6.049 ± 0.225 |
| Offspring body mass at 21 days of life/g | 34.95 ± 1.29 | 39.43 ± 2.70 | 36.31 ± 2.44 | 37.85 ± 2.55 |

Mass data are presented as mean ± S.E.M.; number of females mated = 12-18 animals *per* group.

chemical agent on the reproductive system.[21] The results obtained demonstrated that treatment with the essential oil before mating did not affect the fertility of rats. Moreover, the measures of masses of reproductive organs like as the testes, epididymis and prostate, are useful for assessing male reproductive toxicity.[21] A reduction in testes and epididymis mass indicates reduced fertility or contraceptive activity because these organs are responsible for the formation and maturation of sperm.[22,23] The prostate is an accessory organ that secretes prostatic fluid, which is important to increase the motility and fertility of spermatozoa and its weight is androgen-dependent and may reflect changes in the endocrine and testicular function in animals.[21,24]

In this study, body mass at the end of treatment and the relative gain of body mass in the groups treated with essential oil did not change significantly when compared to controls except for the body mass at the end of the treatment in group T2 ($p < 0.05$). The relative mass (g *per* 100 g) of the testes, epididymis and prostate of the groups treated with the essential oil did not differ significantly from the control group (Table 3). Our results showed that treatment of rats with the essential oil from fruits of *S. terebinthifolius* at three different doses by oral gavage for 60 days did not significantly alter the mass of reproductive organs, which indicates the absence of contraceptive activity.

Toxic substances can lead to male contraception by decreasing sperm density and/or by changing the morphology and function of sperm.[25] The number and morphology of spermatozoa evaluation showed that treatment of rats with essential oil for 60 days at the three different doses by oral gavage did not significantly alter the number of spermatozoa in the epididymis tail or the percentage of spermatozoa with abnormal morphology when compared with the control group (Table 3). These data suggest the absence of adverse effects on the process of spermatogenesis. The values of reproductive variables analyzed in this study did not differ from the control group which confirms the absence of reproductive toxicity in male

**Table 3.** Effects of the essential oil from fruits of *S. terebinthifolius* on body weight and reproductive parameters of male rats

| Variables | Control | Essential oil/(mg kg$^{-1}$) | | |
|---|---|---|---|---|
| | | 375 | 750 | 1500 |
| Body mass day 0/g | 141.6 ± 7.74 | 140.6 ± 6.41 | 139.7 ± 5.88 | 137.1 ± 8.36 |
| Body mass day 60/g | 313.8 ± 13.58 | 272.3 ± 14.49 | 261.7 ± 10.82* | 284.8 ± 8.725 |
| Body mass relative gain/% | 124.5 ± 9.71 | 104.9 ± 8.16 | 96.24 ± 12.14 | 94.47 ± 12.05 |
| Sperm number (× $10^6$) | 144.2 ± 12.8 | 155.1 ± 8.5 | 135.5 ± 17.9 | 148.0 ± 23.84 |
| Abnormal sperm/% | 1.70 ± 0.35 | 1.88 ± 0.50 | 2.05 ± 0.60 | 1.93± 0.55 |
| Relative mass/(g *per* 100 g) | | | | |
| Testis | 0.775 ± 0.026 | 0.790 ± 0.050 | 0.776 ± 0.080 | 0.795 ± 0.031 |
| Epididymis | 0.359 ± 0.016 | 0.387 ± 0.024 | 0.382 ± 0.030 | 0.353 ± 0.013 |
| Prostate | 0.199 ± 0.015 | 0.192 ± 0.008 | 0.186 ± 0.012 | 0.181 ± 0.009 |

Data are presented as mean ± S.E.M. (n = 6-9 animals *per* group).

rats. However, this investigation should be pursued with plant material from different geographical areas, in order to relate variations in chemical composition of essential oils and extracts with the biological activity.

## Experimental

### Plant material

The botanical material was collected at Cia. Vale do Rio Doce (CVRD) Reserva Florestal Rio Doce S/A (Brazil) and the vegetable material and voucher specimen were deposited at herbarium of the Florestal Reserve of CVRD under the number 439144, collector No. 5734.

### Volatile constituent

The ripe fruits of *S. terebinthifolius* were ground and subjected to hydrodistillation for 1.5 h using in a Clevenger-type apparatus. The oil was collected and dried using anhydrous sodium sulfate and, after filtration, stored under low light conditions at < 10 °C until analysis.

### Essential oil analysis by GC and GC-MS

The gas chromatography-mass spectra (GC-MS) analyses were performed using a Shimadzu GC-17A/MS QP5050A-GC-MS system (EI mode 70 eV, source temperature 260 °C, scanned mass ranged 43-350 amu). The operating conditions were: DB-5HT column (J & W Scientific, 30 m × 0.25 mm i.d. × 0.1 μm film thickness); helium as carrier gas at a flow rate of 1.0 mL $min^{-1}$ with split ratio of 1:30; temperature program from 60 °C (2 min) to 180 °C at 2 °C $min^{-1}$ and then from 180 °C (4 min) to 260 °C at 10 °C $min^{-1}$, with a final hold of 10 min at 260 °C. The identification of the essential oil (EO) components was accomplished by matching their mass spectra with those recorded in the Wiley 275 L database.

The identity of each compound was confirmed by comparison of its retention index relative to $C_8$–$C_{20}$ n-alkanes (Fluka Analytical, 1.0 mL alkane standard solution). The retention indices were compared to those of the literature.[6,26,27] Samples of 1 μL of oil diluted in 5% dichloromethane were injected. These analyses were carried out by gas chromatography with flame ionization detection (GC-FID) using an Agilent 5975C instrument equipped with a capillary column coated with DB-5 (30 m × 0.25 mm i.d. × 0.25 μm film thickness; J & W Scientific, Folsom, CA, USA). GC oven temperature and conditions were as described above to GC-MS. The detector and injector temperatures were held at 260 °C and hydrogen used as carrier gas at a flow rate of 1.0 mL $min^{-1}$, and split mode (1:10). The GC-FID was also used for relative quantification using area percent.

### Animals

Wistar male rats were obtained from the Animal Facility for Maintenance of Animals for Experimentation of the Federal University of Piauí (UFPI). All animals were previously adapted to laboratory conditions for 14 days before the start of the experiment. The animals were maintained under standard conditions of temperature room (23 ± 1 ° C) and light cycle (12 h light/12 h dark). They were provided with a rodent-pellet diet and water *ad libitum*. All experimental procedures were approved by UFPI's Ethics Committee on Animal Experiments, protocol number 007/09.

### Doses and treatments

The animals were treated with essential oil and vehicle Tween 80 at a ratio of 1:1 in order to facilitate the administration and to reduce possible irritation (pure essential oil). Wistar male rats (120-150 g) were randomly divided into four groups (n = 10). A control group (Tween 80 1.5 g $kg^{-1}$) and three groups were treated with different doses (0.375 g $kg^{-1}$, 0.75 g $kg^{-1}$, and 1.5 g $kg^{-1}$) of essential oil from *S. terebinthifolius* fruits. All animals were treated daily for 60 days by oral gavage.

### Acute oral toxicity study

This assay was performed according to Brito in Swiss mice weighing 25 ± 5.0 g, randomly divided in 2 groups of 10 (5 males and 5 females) and housed individually.[28] The animals were fasted overnight (12 h) with free access to water prior to the oral administration of distilled water (10 mL $kg^{-1}$ for the control group) or single doses of essential oil (dosage of 5 g $kg^{-1}$), and observed continuously for 6 h, intermittently for 24 h and then once a day for the next 14 days for general behavioral changes, signs of toxicity and mortality.

### Reproductive performance and body mass of offspring

After treatment the male rats were placed together with females at a ratio of 1:2 for a period of seven days. Females have been previously examined to make sure they were fertile, the presence of sperm in the vaginal smear indicating successful mating. The female rats were then kept in individual cages, and after the birth of offspring

reproductive variables were determined: relationship of offspring/mother fertility rate (number of pregnant rats/number of mated females); birth rate (number of offspring born alive/total number of offspring born); viability rate (number of offspring alive on day 4 postnatal/number of offspring born alive); lactation rate (number of offspring alive at day 21 postnatal/number of offspring born); and offspring body mass and litter mass at 1 and 21 days of life.[29]

### Body mass and mass of the reproductive organs

The body mass was recorded weekly during the treatment period. After the mating period the male rats were euthanized by receiving a lethal dose of sodium thiopental (100 mg $kg^{-1}$) and the testes, epididymis and prostate were removed and weighed. The mass of organs was expressed in terms of mass per one hundred grams of body mass (g *per* 100 g).

### Number and morphology of spermatozoa

To quantify the number of spermatozoa the epididymis tails were fragmented into small pieces and homogenized for 1 min in 10 mL of 0.9% NaCl containing 0.5% Triton X-100. The spermatozoa count took place in a hemocytometer chamber and the value was the mean of four fields multiplied by the correction factor ($3 \times 0.520833$).[30] To evaluate sperm morphology the ducts deferens from each animal was sectioned in 5 mL of 0.9% NaCl and a sperm suspension was obtained. Smears prepared from each suspension were stained with 2% eosin and the samples were observed microscopically (400×) to evaluate the morphology of 200 spermatozoa per animal and to count the spermatozoa with abnormal heads and/or abnormal tails.[31]

### Statistics

Values are expressed as mean ± standard error of mean (SEM). Differences between groups were determined by analysis of (ANOVA) followed by the Tukey test. The rates of fertility, birth viability and lactation were analyzed using the chi-square test. The level of statistical significance was 5% ($p < 0.05$).

## Acknowledgments

We are grateful to PIBIC-UFPI for its financial support and research fellowships and to Lapetro - UFPI for the chromatographic analysis; Dr. Carol Collins for revising this manuscript, Prof. Dr. Pedro J. M. Abreu and an anonymous reviewer for thoughtful suggestions and corrections; and Agrorosa Ltda (export company of pink pepper) for botanical material.

## References

1. Lorenzi, H.; *Árvores Brasileiras - Manual de Identificação e Cultivo de Plantas Arbóreas Nativas do Brasil*, 1st ed.; Plantarum: Nova Odessa, SP, Brasil, 1992.
2. Ferriter, A.; *Brazilian Peppertree Management Plan for Florida. Florida Exotic Pest Plant Council, Brazilian Peppertree,* Task Force: Florida, 1997.
3. Siddiqui, R.; Ahmad, H.; Sultan, S.; Ehteshamuddin, A. F. M.; Shirrem, S.; *Pak. J. Sci. Ind. Res.* **1996**, *39*, 43.
4. Melo Jr., E. J. M.; Raposo, M. J.; Neto, J. A.; Diniz, M. F. A.; Marcelino, C. A. C.; Sant'ana, A. E. G.; *Phytomedicine* **2002**, *9*, 109.
5. Machado, S. C.; Rosas, E. C.; Brito, F. A.; Heringe, A. P.; Oliveira, R. R.; Kaplan, M. A. C.; Figueiredo, M. R.; Henriques, M. G. M. O.; *Int. Immunopharmacol.* **2008**, *8*, 1552.
6. De Lima, S. G.; Moita Neto, J. M.; Costa, J. G. M. D.; Citó, A. M. G. L.; Reis, F. A. M.; *J. Chil. Chem. Soc.* **2009**, *53*, 1718.
7. Balbach, A.; *A Flora Nacional na Medicina Doméstica*, 1a. ed.; M.V.P.: São Paulo, Brasil, 1984.
8. Stasi Di, L. C.; Oliveira, G. P.; Carvalhaes, M. A.; Queiroz Junior, M.; Tien, O. S.; Kakinami, S. H.; Reis, M. S.; *Fitoterapia* **2002**, *73*, 69.
9. Matos, F. J. A.; *O Formulário Fitoterápico do Professor Dias da Rocha*, 9a. ed.; UFC: Fortaleza, CE, Brasil, 1997.
10. Khaled, F.; El-Massry; El-Ghorab, A. H.; Shaaban, H. A.; Shibamoto, T.; *J. Agric. Food Chem.* **2009**, *57*, 5265.
11. Carvalho, M. C. R. D.; Barca, F. N. T. V.; Agnez-Lima, L. F.; Medeiros, S. R. B.; *Environ. Mol. Mutagen.* **2003**, *42*, 185.
12. Barbosa, L. C. A.; Demuner, A. J.; Clemente, A. D.; De Paula, V. F.; Ismail, F. M. D.; *Quim. Nova* **2007**, *30*, 1959.
13. Chowdhury, A. R.; Tripathi, S.; *Ind. Perfum* **2001**, *45*, 257.
14. Gundidza, M.; Gweru, N.; Magwa, M. L.; Mmbengwa, V.; Samie, A.; *Afr. J. Biotechnol.* **2009**, *8*, 7164.
15. Ibrahim, M.; Fobbe, R.; Nolte, J.; *Bull. Fac. Pharm.* **2004**, *42*, 289.
16. Jamal, Y.; Agusta, A.; *Majalah Farmasi Indonesia* **2001**, *12*, 135.
17. Singh, A. K.; Singh, J.; Gupta, K. C.; Brophy, J. J.; *J. Essent. Oil Res.* **1998**, *10*, 697.
18. Richter, R.; Von Reuß, S. H.; König, W. A.; *Phytochemistry* **2010**, *71*, 1371.
19. Kennedy, G. L.; Ferenz, R. L.; Burgees, B. A.; *J. Appl. Toxicol.* **1986**, *6*, 145.
20. Lima, L. B.; Vasconcelos, C. F. B.; Maranhão, H. M. L.; Leite, V. R.; Ferreira, P. A.; Andrade, B. A.; Araújo, E. L.; Xavier, H. S.; Lafayette, S. S. L.; Wanderley, A. G.; *J. Ethnopharmacol.* **2009**, *126*, 468.

21. U.S. Environmental Protection Agency; *Guidelines for Reproductive Toxicity Risk Assessment*, 1st ed.; Washington, DC, 1996.
22. Gupta, R. S.; Yadav, V. P.; Dixit, V. P.; Dobhal, M. P.; *Fitoterapia* **2001**, *72*, 236.
23. Moundipa, F. P.; Kamtchouing, P.; Koueta, N.; Tantchou, J.; Foyang, N. P. R.; Mbiapo, F. T.; *J. Ethnopharmacol.* **1999**, *65*, 133.
24. Ahlgren, G.; Rannevik, G.; Lilja, H.; *J. Androl.* **1995**, *16*, 491.
25. Sá, R. C. S.; Leite, M. N.; Reporedo, M. M.; Almeida, R. N.; *Contraception* **2003**, *67*, 327.
26. Adams, M.; Berset, C.; Kessler, M.; Hamburger, M.; *J. Ethnopharmacol.* **2009**, *121*, 343.
27. Alencar, J. W.; Craveiro, A. A.; Matos, F. J. A.; Machado, M. I. L.; *Quim. Nova* **1990**, *13*, 282.
28. Brito, A. S.; *Manual de Ensaios Toxicológicos in vivo*; Ed. Unicamp: Campinas, 1994.
29. Elbetieha, A.; Al-Hamood, M. H.; Alkofahi, A.; Bataineh, H.; *J. Ethnopharmacol.* **1998**, *61*, 67.
30. Robb, G. W.; Amann, R. P.; Killian, G. J.; *J. Reprod. Fertil.* **1978**, *54*, 103.
31. Seed, J.; Chapin, R. E.; Clegg, E. D.; Dostal, L. A.; Foote, R. H.; Hurtt, M. E.; Klinefelter, G. R.; Makris, S. L.; Perreault, S. D.; Schrader, S.; Seyler, D.; Sprando, R.; Treinen, K. A.; Veeramachaneni, D. N.; Wise, L. D.; *Reprod. Toxicol.* **1996**, *10*, 237.

*Submitted: May 2, 2011*
*Published online: November 1, 2011*

*J. Braz. Chem. Soc.*, Vol. 23, No. 1, 186-189, 2012.
Printed in Brazil - ©2012 Sociedade Brasileira de Química
0103 - 5053 $6.00+0.00

**Short Report**

# Biomimetic Hydrogen Generation Catalyzed by Triironnonacarbonyl Disulfide Cluster

***Charles A. Mebi,* Kyra E. Brigance and Robert B. Bowman***

*Department of Physical Sciences, College of Natural and Health Sciences, Arkansas Tech University, 1701 N. Boulder Ave, Russellville, Arkansas 72801 USA*

O "cluster" dissulfeto de triferrononacarbonila, um precursor sintético e estável para modelos do sítio ativo da enzima hidrogenase [Fe-Fe], foi avaliado como catalisador para a geração eletroquímica de hidrogênio por voltametria cíclica. Na presença de ácido acético, $Fe_3S_2(CO)_9$ catalisa a redução do próton para hidrogênio em – 2,24 V (*vs.* $Fc/Fc^+$) com um sobrepotencial de –0,78 V (acetonitrila como solvente). O sobrepotencial é comparável àqueles relatados para os modelos diferrocarbonila de hidrogenase [Fe-Fe].

Triironnonacarbonyl disulfide cluster, a stable and synthetic precursor for active site models of [Fe-Fe] hydrogenase enzyme, has been evaluated as catalyst for the electrochemical generation of hydrogen by cyclic voltammetry. In the presence of acetic acid, $Fe_3S_2(CO)_9$ catalyzes the reduction of proton to hydrogen at –2.24 V (*vs.* $Fc/Fc^+$) with an overpotential of –0.78 V (acetonitrile as solvent). The overpotential is comparable to those reported for diironcarbonyl models of [Fe-Fe] hydrogenase.

**Keywords**: electrocatalysis, hydrogen, iron-cluster, metalloenzyme, transition metal

## Introduction

Iron-sulfur clusters, diverse in composition (containing one to eight iron atoms) and structure, are ubiquitous in biological systems. These clusters are involved in electron transfer and biocatalytic processes. The chemistry of iron-sulfur clusters has been associated with the development of life on planet Earth.[1-3] Iron-sulfur clusters can be coordinated to organic ligands through iron-carbon bonds to form organometallic clusters. A typical example of an organometallic iron-sulfur cluster is triironnonacarbonyl disulfide [$Fe_3S_2(CO)_9$], Figure 1.[4]

The chemistry of $Fe_3S_2(CO)_9$ has drawn a lot of attention over the past few decades.[1] Triironnonacarbonyl disulfide was first prepared in 1958 by Hieber and Beck[5] by the reaction of $[HFe(CO)_4]^-$ and sulfite ion. However, $Fe_3S_2(CO)_9$ has been identified as a common product from reactions between iron-carbonyls and sulfur supplying agents.[1] Wei and Dahlz[6] structurally characterized $Fe_3S_2(CO)_9$ using X-ray crystallography revealing its *nido*-type square pyramidal or trigonal bipyramidal arrangement. $Fe_3S_2(CO)_9$ is stable and its electronic structure and electrochemical properties have been extensively investigated using photoelectron spectroscopy,[7] computational methods,[7,8] cyclic voltammetry,[9] and spectroelectrochemical technique.[10] The reactivity of $Fe_3S_2(CO)_9$ has been explored and continues to be of great interest.[1,11-14] Some important reactions of $Fe_3S_2(CO)_9$ are depicted in Scheme 1: (a) the reaction of $Fe_3S_2(CO)_9$ with formaldehyde and amines to form diiron clusters of the type, $Fe_2[(SCH_2)_2NR](CO)_6$, models for the active site of [Fe-Fe] hydrogenase enzyme (Figure 2)[14] and (b) the photochemical transformation of $Fe_3S_2(CO)_9$ in the presence of $Fe(CO)_5$ to the tetrairon cluster, $Fe_4S_2(CO)_{11}$.[13]

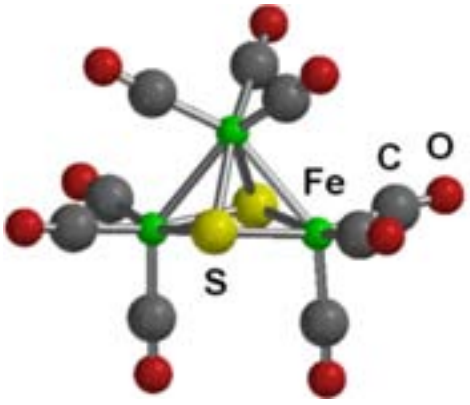


**Figure 1.** Triironnonacarbonyl disulfide, $[Fe_3S_2(CO)_9]$.

*e-mail: cmebi@atu.edu

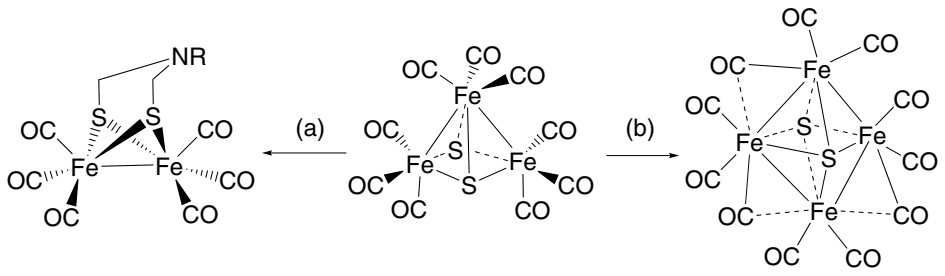


**Scheme 1.** Reactivity of $Fe_3S_2(CO)_9$: (a) $(CH_2O)_n/RNH_2$; (b) h$\nu$, $Fe(CO)_5$, cyclohexane.

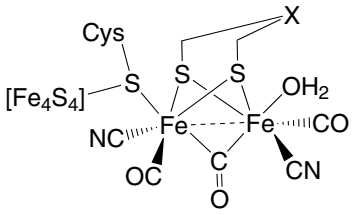


**Figure 2.** Active site of [Fe-Fe] hydrogenase enzyme ( X = NH or $CH_2$).

Although the reactivity, electrochemical properties, and electronic structure of $Fe_3S_2(CO)_9$ have been investigated, to the best of our knowledge, its catalytic properties remain unexplored. Giving the synthetic and structural relationship between $Fe_3S_2(CO)_9$ and models for the active site of [Fe-Fe] hydrogenase enzyme, it is important to examine the ability of $Fe_3S_2(CO)_9$ to mimic the enzyme. The hydrogenase enzyme efficiently catalyzes the evolution of hydrogen by proton reduction in aqueous media (TOF = 6000-9000 $s^{-1}$). The reduction potential of the $H^+/H_2$ couple for [Fe-Fe] hydrogenase has been determined to be –0.36 V *vs.* SCE at pH 6 and 30 °C.[14] Studies on the enzyme and its synthetic models are useful in the development of catalysts for the production of hydrogen, a clean alternative to fossil fuels. In this study, we report on the electrocatalytic reduction of proton to produce hydrogen by $Fe_3S_2(CO)_9$. The catalytic properties of $Fe_3S_2(CO)_9$ are compared to those of some diironcarbonyl models of the enzyme reported in the literature.

## Experimental

Electrocatalytic studies were conducted using an Epsilon BAS potentiostat. Cyclic voltammograms of $Fe_3S_2(CO)_9$ were obtained with increasing concentrations of acetic acid (0, 7, 21, 35, 42, 49, 56, 63 mmol $L^{-1}$) using a three-electrode cell. The electrodes used are glassy carbon working electrode, platinum auxiliary electrode, and Ag/AgCl reference electrode. The platinum and glassy carbon electrodes were polished with aluminum paste and rinsed with water and acetone. A 0.1 mol $L^{-1}$ $CH_3CN$ solution of $Bu_4NPF_4$ was used as supporting electrolyte. The concentration of $Fe_3S_2(CO)_9$ was 1 mmol $L^{-1}$ and the scan rate was 100 mV $s^{-1}$. We degassed the electrolyte solution by bubbling nitrogen at room temperature for 5 min before measurement. The potentials obtained with reference to Ag/AgCl electrode are quoted in this report against ferrocene/ferrocenium ($Fc/Fc^+$) potential except otherwise mentioned. The $Fc/Fc^+$ reference is used to allow for comparison with reported redox potential values of similar models. All reagents were obtained from commercial sources. Acetonitrile for electrochemical assay was purchased from Aldrich and used without any further purification. We obtained $Fe_3S_2(CO)_9$ as a byproduct from the reaction of $Fe_3(CO)_{12}$ and phenanthrene-4,5-disulfide.[15] The identify of $Fe_3S_2(CO)_9$ was confirmed by infrared and X-ray crystallography.

## Results and Discussion

The electrochemical properties of $Fe_3S_2(CO)_9$ have been previously investigated in benzonitrile by cyclic voltammetry.[9] $Fe_3S_2(CO)_9$ is reported to undergo two one-electron reduction processes at –0.43 V (reversible, $E_{1/2}$) and –1.38 V (irreversible, $E_{pc}$). An irreversible oxidation of $Fe_3S_2(CO)_9$ was observed at +1.30 V *vs.* Ag/AgCl. These results are similar to those obtained by us in acetonitrile (Table 1). We observe *ca.* 0.07 V shift in the electrochemical potentials with the change of solvent from benzonitrile to acetonitrile.

The electrocatalytic generation of hydrogen by $Fe_3S_2(CO)_9$ from acetic acid (a weak acid; $pK_a$ = 22.3 in acetonitrile) has been studied and the results are contained in Table 2 and Figure 3. Figure 3 contains cyclic voltammograms of $Fe_3S_2(CO)_9$ in the absence of acid and with increasing amounts of acetic acid. In the absence of acid, only the three redox events mentioned in Table 1 were observed. On addition of 7 mmol $L^{-1}$ of acetic acid, a new peak at –2.24 V (*vs.* $Fc/Fc^+$) appears and its current intensity increases with sequential increment of acid concentration (Figure 4). These observations are indicative of electrocatalytic reduction of proton to molecular hydrogen.[16] The overpotential was determined to be –0.78 V using the standard reduction ($E^o_{HA}$) of –1.46 V (*vs.* $Fc/Fc^+$) for acetic

**Table 1.** Electrochemical data for $Fe_3S_2(CO)_9$

| Electrochemical Process | | Benzonitrile (V *vs* Ag/AgCl)[a] | Acetonitrile (V *vs* Ag/AgCl)[b] | Acetonitrile (V *vs* $Fc/Fc^+$)[b] |
|---|---|---|---|---|
| $[Fe_3S_2(CO)_9] + e^- \rightleftharpoons [Fe_3S_2(CO)_9]^-$ | $E_{1/2}$ | –0.43 | –0.50 | –0.94 |
| $[Fe_3S_2(CO)_9]^- + e^- \longrightarrow [Fe_3S_2(CO)_9]^{2-}$ | $E_{pc}$ | –1.38 | –1.31 | –1.75 |
| $[Fe_3S_2(CO)_9] \longrightarrow [Fe_3S_2(CO)_9]^+ + e^-$ | $E_{pa}$ | +1.30 | +1.24 | +0.80 |

[a]Reference 9. [b]This work.

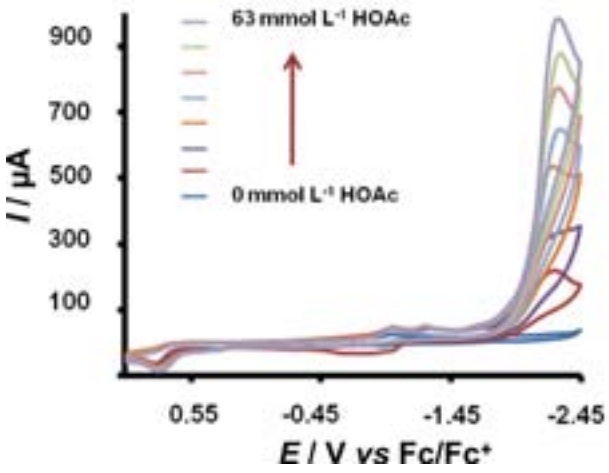


**Figure 3.** Cyclic voltammograms of $Fe_3S_2(CO)_9$ (1 mmol $L^{-1}$, 10 mL) with acetic acid (0, 7, 21, 35, 42, 49, 56, 63 mmol $L^{-1}$) in 0.1 mol $L^{-1}$ $BuN_4PF_6$/acetonitrile at a scan rate of 100 mV $s^{-1}$.

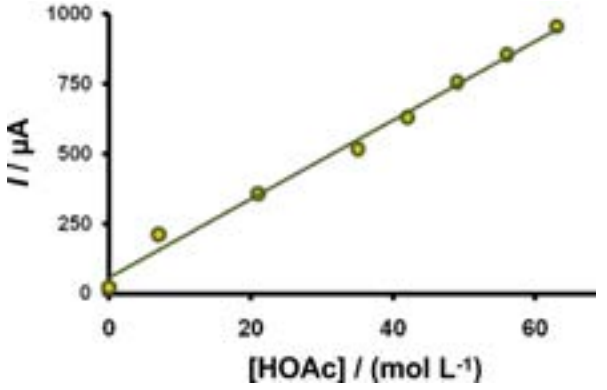


**Figure 4.** Dependence of current heights of the electrocatalytic peaks of $Fe_3S_2(CO)_9$ on concentration of acetic acid.

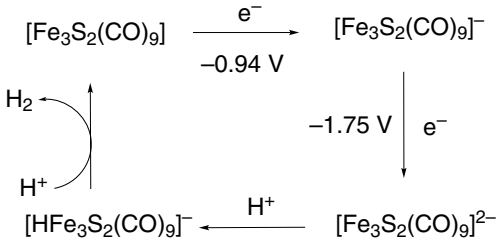


**Scheme 2.** Proposed mechanism for the electrocatalytic proton reduction of acetic acid to produce $H_2$ by $Fe_3S_2(CO)_9$.

acid.[17] The overpotential and potential for the reduction of acetic acid to hydrogen ($E_{cat}$) by $Fe_3S_2(CO)_9$ are contained in Table 2 alongside those of some diironcarbonyl models of [Fe-Fe] hydrogenase.[17,18] As observed in Table 2, the overpotential and $E_{cat}$ for $Fe_3S_2(CO)_9$ are comparable to those of the diironcarbonyl models.

Scheme 2 shows a tentative mechanism for the electrocatalytic hydrogen production by $Fe_3S_2(CO)_9$. The suggested electrochemical-electrochemical-chemical-chemical (EECC) mechanism is based on the results described above and similar reported examples.[16] As depicted in Scheme 2, $Fe_3S_2(CO)_9$ first undergoes successive one-electron reductions to produce $[Fe_3S_2(CO)_9]^{2-}$ which upon protonation affords $[HFe_3S_2(CO)_9]^-$. Subsequent protonation of $[HFe_3S_2(CO)_9]^-$ generates hydrogen.

**Table 2.** A comparison of electrocatalytic data for $Fe_3S_2(CO)_9$ and some diironcarbonyl models of [Fe-Fe] hydrogenase[a]

| | Models | | | | |
|---|---|---|---|---|---|
| Overpotential / V | | –0.54 | –0.65 | –0.78 | –0.89 |
| $E_{cat}$ / V | | –2.00 | –2.11 | –2.24 | –2.35 |

[a]Values for diironcarbonyl models were obtained from references 17 and 18.

## Conclusions

$Fe_3S_2(CO)_9$ has been shown to mimic [Fe-Fe] hydrogenase by catalyzing the electrochemical evolution of hydrogen with an overpotential of –0.78 V (*vs.* $Fc/Fc^+$). This overpotential is comparable to those of reported models of [Fe-Fe] hydrogenase. We have proposed an EECC catalytic cycle for the generation of $H_2$ by $Fe_3S_2(CO)_9$. However, more studies (computational, bulk electrolysis, and spectroelectrochemical) are required to characterize the species involved and ascertain the mechanism.

## Acknowledgments

Acknowledgment is made to the Donors of the American Chemical Society Petroleum Research Fund, for support of this research.

## References

1. Ogino, H.; Inomata, S.; Tobita, H.; *Chem. Rev.* **1998**, *98,* 2093.
2. Meyer, J.; *J. Biol. Inorg. Chem.* **2008**, *13*, 157.
3. Cody, G. D.; Boctor, N. Z.; Filley, T. R.; Hazen, R. M.; Scott, J. H.; Sharma, A.; Yoder, H. S. Jr.; *Science* **2000**, *289*, 1337; Koutsantonis, G. A. In *Concepts and Models in Bioinorganic Chemistry*; Heinz-Bernhard, K.; Nils, M-N., eds.; Wiley-VCH: Weinheim, 2006, ch. 13; Crichton, R. R.; *Biological Inorganic Chemistry*: *An Introduction*,1st ed., Elsevier: Oxford, 2008; Ei-Ichiro, O.; *Bioinorganic Chemistry: A Survey*, Elsevier: Burlington, 2008.
4. Figure 4 was generated using Spartan software. 1991-2009 by Wavefunction Inc. (www.wavefun.com).
5. Hieber, W.; Beck, W.; *Z. Anorg. Allg. Chem.* **1958**, *296*, 91.
6. Wei, C. H.; Dahlz, L. F.; *Inorg. Chem.* **1965**, *4*, 493.
7. Chesky, P. T.; Hall, M. B.; *Inorg. Chem.* **1983**, *22,* 2998; Hall, M. B.; Fenske, R. F.; *Inorg. Chem.* **1972**, *11*, 768; Rives, A. B.; Xiao-Zeng, Y.; Fenske, R. F.; *Inorg. Chem.* **1982**, *21,* 2286.
8. Eveland, J. R.; Saillard, J-Y.; Whitmire, K. H.; *Inorg. Chem.* **1997**, *36,* 330.
9. Madach, T.; Vahrenkamp, H.; *Chem. Ber.* **1981**, *114*, 505.
10. Best, S. P.; Borg, S. J.; Vincent, K. A. In *Spectroelectrochemistry*; Kaim, W.; Klein A., eds.; Royal Society of Chemistry: Cambridge, UK, 2008, ch. 1.
11. Adams, R. D.; Babin, J. E.; *Inorg. Chem.* **1986**, *25*, 3418.
12. Fang, Z-G.; Wen, Y-S.; Wong, R. K. L.; Ng, S-C.; Liu, L-K.; Hor, T. S. A.; *J. Cluster Sci.* **1994**, *5*, 327.
13. Adams, R. D.; Babin, J. E.; Estrada, J.; Wang, J-G.; Hall, M. B.; Low, A. A.; *Polyhedron* **1989**, *8*, 1885; Mathur, P. In *Advances in Organometallic Chemistry Vol. 41*; West, R.; Hill, A. F., eds.; Academic Press: California, USA, 1997, ch. 5.
14. Li, H.; Rauchfuss,T. B.; *J. Am. Chem. Soc.* **2002***, 124*, 727; Helm, M. L.; Stewart, M. P.; Bullock, R. M.; DiuBois, M. R.; DuBois, D. L.; *Science* **2011**, *333*, 863; Vincent, K. A.; Parkin, A.; Armstrong, F. A.; *Chem. Rev*. **2007**, *107*, 4366.
15. Mebi, C. A.; Noll, B. C.; Gao, R.; Karr, D. S.; *Z. Anorg. Allg. Chem.* **2010**, 2550.
16. Song, L-C.; Yang, Z-Y.; Bian, H-Z.; Liu, Y.; Wang, H.-T.; Liu, X-F.; Hu, Q-M.; *Organometallics* **2005**, *24*, 6126.
17. Felton, G. A.; Mebi, C. A.; Petro, B. J.; Vannucci, A. K.; Evans, D. H.; Glass, R. S.; Lichtenberger, D. L.; *J. Organomet. Chem*. **2009**, *694*, 2681; Mejia-Rodriguez, R.; Chong, D.; J. Reibenspies, H.; Soriaga, M. P.; Darensbourg, M. Y.; *J. Am. Chem. Soc*. **2004**, *126*, 12004.
18. Mebi, C. A.; Felton, C. M.; *J. Undergrad. Chem. Res.* **2011**, *10*, 111.

*Submitted: August 29, 2011*
*Published online: November 8, 2011*